Structural and Tectonic Evolution within the Envelope and Margins of the Volvi Complex, N.E. Greece.

STEVEN DOUGLAS BATTY

THESIS SUBMITTED FOR THE DEGREE OF

DOCTOR OF PHILOSOPHY

UNIVERSITY OF EDINBURGH

1993

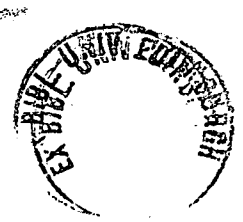

DECLARATION

This thesis has been composed by myself and except where specifically stated, is my own work.

Steven Douglas Batty

June 1993

Abstract

The Serbo-Macedonian Massif (SMM) is a complex metamorphic and tectonic terrane, possessing an early poorly constrained (Hercynian?) deformation history, extensively overprinted by several Mesozoic deformation events. This study has focused on part of the eastern margin of the SMM of NE Greece, covering an area approximately 400 km^2 to the north of Lake Volvi, 50 km east of Thessaloniki. This project has concentrated on determining the origin and geological setting of a large body of metamorphosed sheeted dykes and gabbros (the Volvi Complex) emplaced within this polymetamorphic massif, by focussing on the structural history of its marginal zone, envelope and off-shoots.

By this means a progressive polyphase strain-partitioned structural history (Mesozoic) has been determined, overprinting an older highly deformed (Hercynian?) migmatitic basement. The Mesozoic deformation provides the dominant structures within the area which have resulted in the development of low-strain pods wrapped in three dimensions by high-strain anastomosing shear zones. The high-strain zones are associated with extensively retrogressed greenschist-facies assemblages, whereas areas of low-strain preserve evidence for peak upper amphibolite-facies conditions and thermal perturbations into the granulite-facies.

Granulite-facies conditions are shown by the overprinting of cordierite bearing melt assemblages developed in association with early extensive mafic intrusions at low-P, high-T conditions. Evidence from local melting and geochemical studies have suggested a mechanism of crustal anatexis for the granitoids within the study area. Pseudomorphing of cordierite by kyanite-garnet-biotite assemblages and the development of garnet-bearing coronas in gabbros suggests that the initial P-T conditions were promoted to regional peak amphibolite-facies (high-P, medium-T) conditions. Evidence of a range of early to late intrusive basic bodies is provided by field observations of small medium- to coarse-grained gabbros intruding extensive areas of amphibolite and sheeted dykes which is indicative of continued intrusion during crustal thickening. Geochemical analysis of basic rocks show the Volvi mafic suite to be derived from a range of primitive sources, with possible arc components, which have been subjected to varying degrees of partial melting, subsequently modified by fractionation processes.

A model is proposed of a transtensional-transpressional regime, with the original initiation of a pull-apart basin at shallow levels accompanied by the intrusion of early Volvi Complex mafic lithologies. Subsequent rapid burial of the pull-apart

basin to achieve the transition to amphibolite-facies from lower P cordierite-bearing assemblages is inferred to have been caused by the arrival of a restraining bend from along the same strike-slip system. Consequently, locally thermally perturbed low-P, high-T rocks remained at high-T with increasing pressure as shown by the re-equilibration of cordierite + melt assemblages to kyanite-garnet-biotite.

During loading of the pull-apart basin, magmatic intrusions are envisaged as continuing to be emplaced. A present day analogue for the interpretation of the study area can be found in California, where a deep, sediment filled basin with magmatic activity at the base (the Salton Trough) has the potential to be overridden by a large crustal mass acting as a restraining bend (the Transverse Ranges) from along the same strike-slip system within a relatively rapid time period of approximately 4 Ma.

The study has also suggested that the Kerdilion and Vertsikos Groups, hitherto considered distinct, can be considered equivalents, and that the "Svoula Group" metasediments in the Volvi area are probably a Lower Jurassic sedimentary fill to this transtensional basin rather than displaced outcrops of the marginal Circum Rhodope sequences.

Acknowledgements

This thesis has been completed with the help and encouragement of numerous people to whom I am extremely grateful. I would like to thank my supervisors John Dixon and Mike Johnson for their invaluable assistance, time and effort throughout this thesis. I am especially obliged to John Dixon for his supervision, company and supplying the whiskey during my field work. This thesis has greatly benefited from John's help and advice in developing different models, and his extensive and detailed reviews of numerous earlier versions. Mike Johnson is thanked for his constructive reviews and encouragement which provided a light at the end of what appeared to be a very long tunnel.

Sarandis and Maria Dimitriadis are thanked for their hospitality on my initial visit to Greece. Sarandis also provided invaluable assistance whilst in Greece and is responsible along with JED of introducing me to Elsa (the famous landlords daughter) and Mikri Volvi. Nikos Sidiropoulos, Mina Sidiropoulos (formerly Kourou) and Agyro Asvesta are thanked for their friendship, hospitality and numerous discussions which I always enjoyed during my visits to Thessaloniki.

My time in Greece would never have been as memorable if it had not been for the inhabitants of Mikri Volvi, all of which made me exceptionally welcome, although I was not allowed to play for the football team. I would particularly like to thank Elsa for being a good friend and for many evenings acting as my translator. Byron and Katina Mavroudha provided lodgings, food, friendship and a genuine warm welcome into their home throughout my time in Greece.

George and Soula Aletras and family are thanked for introducing me to village life and inviting me to their sons christening. I would like to thank George for his constant companionship during many evening meals and for his help in resolving the occasional problem. Lucas is thanked for what I considered to be excellent and plentiful, although limited culinary delights and numerous free beers.

Life in Greece would not have been the same without my numerous friends in Mikri Volvi, Dalgleish, George, Tim, Yanis, Paneotis, Themis, Soula, Ria and Maria to name but a few, who provided a wide range of entertainment. I would like to thank George especially for the numerous late night snacks, drinks and long conversations.

It is impossible to thank all the people who have made my time in Edinburgh so enjoyable, and I apologise to any I have not named, Lorna Boyd, Debbie Carr, Pete Clift, Paul Degnan, Karen Dobbie, Adrian Finch, Ian Fitzsimons, Ed Follows, Yvette Hague, Greg Jones, Stuart Kearns, Pete Kinny, Nana Kolocotroni, Dave Latin, Claire

Linklater, Fotini Liakopolou, Neil Melville, Tony Morris, Owen O'Brian, Andrew Patience, Ian Sharp, Timur Ustaomer, Trischi Ward, Dave Walker, Dave Whitmarsh and loads of others.

Pete Clift, Stuart Kearns and Ian Fitzsimons are thanked for reviewing earlier versions of this thesis. Fitz is especially thanked for his time, effort, help and advice when reviewing some of the more arduous chapters, and for drinking lots of my whiskey. Nana Kolocotroni and Fotini Liakopolou are thanked for making a number of often time consuming translations.

Technical assistance and expertise in Edinburgh was provided by Peder Aspen, Diana Baty, Yvonne Cooper, Jane Foster, Godfrey Fitton, Dodie James, Stuart Kearns and Shane Voss.

NERC are thanked for funding the first three years in Edinburgh and the DSS are thanked for the last year and a half. I would also like to thank my parents for their financial assistance throughout my time at Edinburgh and especially for supplying the infamous Landrovers.

Last, but far from least, I thank Michelle for typing parts of this thesis (usually under duress), for colouring the maps (a tedious task!) and for keeping me sane (?) during its final stages. I am especially grateful to my parents William and Mavis Batty, to whom I dedicate this thesis, for their considerable support and encouragement throughout my academic career and who made it possible for me to undertake and successfully complete this work.

Table of Contents

CHAPTER 3: Structural Evolution and Intrusive History

CHAPTER 4: Petrography and P-T-t History

CHAPTER 5: Geochemistry of Igneous Lithologies

Part I: Mafic (Basaltic) Geochemistry

List of Figures

CHAPTER 1

CHAPTER 2

CHAPTER 3

CHAPTER 4

CHAPTER 5

CHAPTER 6

List of Plates

CHAPTER 2

CHAPTER 3

CHAPTER 4

List of Tables

CHAPTER 1

INTRODUCTION AND GEOLOGICAL SETTING

CHAPTER 1

PART I: Objectives and Rationale

1.1 Introduction to the Study Area

The Serbo-Macedonian Massif (SMM) is a complex metamorphic terrane, over 600 km in length and up to 50 km in width, outcropping in Greece, Yugoslavia and Bulgaria (Insert, Map A; Sections 1.5, 1.6). The Massif is extremely heterogeneous and poorly understood preventing reliable correlations along-strike into Yugoslavia and Bulgaria being made at the present time. Published isotopic ages range from 300 Ma in the west to <30 Ma in the east (Appendix II). The SMM contains several kilometre-scale igneous bodies of granitic, basic and ultrabasic composition in a predominantly metasedimentary host. One of these, the 40 km^2 Volvi Complex, was shown by Dixon and Dimitriadis (1984) to contain gabbros, amphibolites and large tracts of sheeted dyke complex with a high-grade amphibolite-facies metamorphic imprint. Evidence of local melting around this complex suggested an in situ origin rather than the more customary attribution in East Mediterranean terranes to an emplaced ophiolite slab. Reconnaissance within the SMM approximately 30 km to the N of Lake Volvi revealed an early migmatite basement locally remelted in a clearly later event (Thessaloniki-Serres road, Dixon and Dimitriadis, pers comm.). Cordierites associated with these melts were pseudomorphed by higher pressure assemblages of garnet-kyanite-phlogopite. These findings suggested some intense but localised thermal event, perhaps also associated with basic magmatism at depth.

The initial objective of this study was to attempt to establish first a local, and then a regional structural framework for the metamorphosed basic bodies such as Volvi and to attempt to link the structural and metamorphic events across a wider area. No regional correlations existed and no study clarifying the relationship between the intrusive events recorded in the Volvi body and the deformational events in the envelope had been undertaken. A potentially important time marker was the suite of variably deformed and metamorphosed basic dykes within envelope metasediments. Besides the regional objective, the tectonic setting of this extensional basic magmatism was not clear and merited study. It will be argued in this thesis that Volvi is most probably the mid- to upper crustal expression of a magma injected pull-apart or transtensional zone. The documentation of the complex structural, metamorphic

and magmatic events characterising the Volvi envelope became the main subject of this study. Regional correlation is hampered by poor exposure and difficult terrain and remains a future goal. Hence, the research and subsequent models developed during this study are based on the southernmost part of the SMM (Kroussia Block; see review by Aleksic *et al.,* 1984) outcropping in NE Greece. The Kroussia Block occupies the eastern part of the Halkidiki Peninsula, incorporating the top of the Sithonia Peninsula in the west, across to the Strimon Valley in the east and as far north as the Yugoslav/Bulgarian border.

This thesis is based on data derived from extensive field mapping of an area approximately 400 km^2, towards the eastern boundary of the SMM around Lake Volvi, approximately 50 km east of Thessaloniki (Insert, Map A). The topography within the area is a contrast between 800 m high, gently undulating hills deeply incised by N-S trending river valleys, and low-level E-W trending plains (filled with Neogene to Recent sedimentary deposits and lakes) produced by Neotectonic graben development (Section 1.11). The best exposures throughout the area are found at, or near to the bottom of, the numerous generally *dry* river valleys and along the two approximately N-S trending roads which traverse the Besikon Hills from both ends of Lake Volvi (Insert, Map A). Exposure on the sides of the river valleys and on the tops of the hills is variable but generally poor, particularly on the densely vegetated more pelitic outcrops.

The area is sparsely populated. The inhabitants of the scattered small towns and villages (Insert, Map A) depend on either farming or fishing. Tobacco, olives and wheat are the main crops: sheep, goats and pigs are raised. Fishing in Lake Volvi supports a handful of families, while the coastal town of Stavros is supported by sea-fishing, boat construction and repair activities. Asprovalta and Stavros are also semi-dependant upon the summer tourist trade, which was formerly dominated by Yugoslavs.

1.2 Previous Work

The SMM was originally recognised and defined in its present form in Yugoslavia by Arsovski (1961; see review by Aleksic *et al.,* 1984), and was later extended into Greece by Kockel and Walther, (1965, 1968). However, the southern most Greek part of the SMM, (the Kroussia block), has as a whole remained a poorly understood area. The most comprehensive work with respect to the SMM consists of collaborative mapping by the B.G.R. Hannover, and I.G.M.E. Greece, resulting in the publication of a 1: 100 000 scale map and explanatory memoir (Kockel *et al.,* 1977),

followed by a series of 1: 50 000 sheets published by I.G.M.E. in Athens (the maps relevant to the research area consist of the Stavros, Zangliverion, Sitochorion and Sochos sheets). These large-scale maps provide useful although limited information on the complex geology of the area. The stratigraphic sequences and tectonic models produced in the memoir for the SMM (Kockel *et al.*, 1977) were the most comprehensive to have been made and have remained generally accepted up to the present. Information for the Greek SMM on a regional or even local-scale predating Kockel *et al.*, (1971, 1977) is negligible. Research within the SMM since Kockel *et al.*, (1971, 1977) has tended to be of a specialised nature and was not concerned with upgrading or reassessing earlier work.

Specialised studies have included K/Ar, Ar/Ar isotope age determinations, (Borsi *et al.*, 1965; Harre *et al.*, 1968; De Wet and Miller, 1987; Section 1.9); geochemical analyses and interpretations of various lithological groups, e.g. amphibolites (Kassoli-Fournaraki, 1981; Sapountzis *et al.*, 1990), and extensive Neotectonic investigations (Section 1.11).

Dixon and Dimitriadis, (1982, 1984, and current unpublished work), worked on the "Volvi Complex" which lies within the central zone of the study area, concentrating mainly on its petrology and geochemistry. Further work by the same authors has consisted of an intensive study of a road section traversing the SMM from Thessaloniki to Serres to the north of this research area. The road section exposes excellent sections through the eastern margin of the SMM, displaying high-grade (upper-amphibolite) assemblages and complex deep-level structures (Dixon and Dimitriadis, 1982, 1984, pers. comm.).

Papadopoulos and Kilias (1985), mapped the gneissic and metasedimentary (envelope) lithologies to the west of the Volvi Complex. They distinguished a series of lithological sub-divisions for the Vertiskos Group and proposed a structural sequence using fold styles and orientations present within the area (Table 3.1). It is now apparent that this conventional approach may not be appropriate.

Dimitriadis (1974, 1980) worked on various aspects of the SMM and has a joint active ongoing research programme with Dixon. Three Greek students have now completed Ph.D. theses involving detailed mapping, geochemical, petrographical, structural and tectonic based projects within the SMM and are now briefly described:

Sidiropoulos (1991) studied an area along the NW margin of the SMM towards the Yugoslav border to the west of the Kroussia Mountain. The area consists predominantly of semi-pelitic schists which have been partially melted to produce augen and stromatic migmatites. Psammitic, pelitic, some marbles and calc-silicate

rocks are also found in the stratigraphic sequence. Intrusive rocks consist of amphibolite bodies, retrogressed eclogites and two deformed and metamorphosed granites (Theodorio and Myriophyton), some augen gneisses and tectonically intercalated serpentinised ultramafic bodies. A complex metamorphic and structural history has been determined from this area. From comparison of results with geological data of the wider area and some available isotopic ages, Sidiropoulos (1991) attributed a pre-Hercynian age to the high pressure M_1 event, an Hercynian age to the M_2 anatectic event and the formation of the Theodorio granite, a Permo-Triassic age to the M_3 event, a Late Jurassic age to the M_4 event related to the intrusion of the Myriophyton granite and finally, a post Jurassic age for the M_5, D_4, D_5 events.

Kourou (1991) studied an area immediately west of the Arnaea granite, N of Lake Koronia. The area consists predominantly of metasedimentary gneisses and semi-pelitic and psammitic schists many of which have been partially melted to produce stromatic and augen migmatites. Amphibolite bodies, serpentinised ultramafics and rare extensively retrogressed ex-eclogite bodies, have been tectonically intercalated into the metasedimentary sequence. The area has been intruded by numerous small acidic lithologies associated with the Polydendri granite. The latest magmatic event consists of relatively undeformed doleritic dykes which cross-cut all the previous lithologies and structures. A complex metamorphic and structural history has been determined from this area. From comparison of results with geological data of the wider area and some available isotopic ages, Kourou (1991) attributed a pre-Hercynian age for the high-P (eclogite) M_1 event, while a Hercynian age is proposed for the M_2 anatectic event, the M_3 event is interpreted to be Permo-Triassic in age, and a Late Jurassic age is suggested for the M_4 event during which the Polydendri granite and most of the pegmatites were formed and emplaced, finally a post-Jurassic age is proposed for the M_5 and D_4 events.

Asvesta (1992) studied an area to the west of the Arnaea granite incorporating most of the rifted margin of the SMM, north of Thessaloniki. The area consists predominantly of volcanosedimentary sequences alternating with Triassic psammites, pelites and carbonates. Geochemistry of the basic volcanics define a transitional mid ocean ridge basaltic suite indicative of an extensional setting in a continental environment, predating continental rifting and the opening of an oceanic basin. The majority of the acidic volcanics are interpreted as products of extensive (nearly complete) melting of the base of thinned continental crust caused by basaltic underplating prior to rifting. The final interpretation and model for the area proposes a passive continental margin progressively forming to the west of the present-day

western margin of the Vertiskos Group. Prior to rifting the future continental shelf was covered by a shallow epicontinental sea. The sea floor was uneven and unstable due to active extension. Coral reefs were forming on top of tectonic highs (horsts), while argillaceous pelagic sediments and carbonate olistholiths and olisthostromes were deposited in intra-platform basins (grabens). Acidic volcanics were extruded on to the continental margin, partly subaerially, partly in deep water at the base of slopes below carbonate build ups. Pelagic sedimentation covered all the neritic formations during the Late Triassic-Early Jurassic, while volcanism ceased. At this stage lithospheric extension by rifting probably ceased and one or more oceanic basins opened to the west of the SMM.

Another closely related Ph.D. study is that of Sakellariou (1988, 1990) a Mainz University student under Durr, who carried out a general field-based project directly south of Lake Volvi. Part of Sakellariou's area has been remapped to test his proposed tectonic sequence and its wider applicability (Chapter 3; Table 3.2).

Unpublished and uncompleted work by Echtler (1985) on the eastern margin of the SMM directly north of the Athos and Sithonia peninsulas was interpreted in terms of a ductile deep-level shearing event. This work has been of particular interest to this study as it suggests that ductile deformation may be found on a regional scale along the eastern margin of the SMM. Unfortunately, the Ph.D. programme for which this work was done had to be abandoned and the details of Echtler's findings remain largely inaccessible.

All of these more regional field-based studies have succeeded in highlighting some of the inadequacies of the regional mapping and interpretations of Kockel *et al.,* (1971, 1977). This study has added to the detailed remapping and understanding of the region. Furthermore, the structural and tectonic framework produced in this study provides a new insight into the evolution of the area, along with a general interpretation for deep-level crustal processes.

1.3 Objectives of this Study

The foremost objective of this thesis has been to determine the origin of the Volvi Complex, a previously poorly understood large mafic body. The initial work was undertaken by Dixon and Dimitriadis (1982; 1984; 1989; pers. comm.) who proposed several interpretations for the origin of the Volvi Complex (Section 1.12). These models were based on work undertaken within the complex, and limited observations from the "country rock" gneisses directly to the west. In order to

understand the relevance of these models (Section 1.12) they are introduced after a general review of the geotectonic setting of the SMM (Part II).

In order to improve the three models proposed by Dixon and Dimitriadis (1984; Section 1.12), it was apparent that mapping on a regional scale would be necessary. The subsequent fieldwork involved a comprehensive specimen collection, measurement of structural data and geological mapping, with the scale and detail differing throughout the area depending on its importance. This has been the main undertaking of this study and the observations and results compose the bulk of this thesis. Previous regional mapping by Kockel *et al.*, (1971, 1977) provided a good base from which to start, (although too large a scale to provide enough detail for reinterpreting the origin of the Volvi Complex). The initial objectives were to map the main lithological units in detail and to determine the relationships between them. The main units included the margins of the Volvi Complex and the envelope lithologies, Vertiskos and Kerdilion Groups, Vertiskos and Volvi Metasedimentary (re: Svoula) Groups and the Vertiskos Group and Arnaea Granite. All of these lithological units were previously mapped by Kockel *et al.*, (1971, 1977) but were poorly constrained and understood in terms of a consistent structural and tectonic history. Thus the development of such a history for the area was of prime importance and constitutes the main component of this study.

In order to determine the metamorphic evolution of the SMM detailed thin-section petrographic studies were used to identify mineral assemblages and correlate microstructures with the outcrop-scale structural scheme developed in the field. Areas of particular interest have been recognised. However, the lithologies from these areas have at present only been subjected to limited analysis by electron microprobe. Therefore, more extensive thermobarometric studies are suggested as an important objective for future work (Section 6.9). Constraints on the P-T-t paths for the Volvi Complex and the surrounding area in this study are mainly qualitative. These results have been combined with limited quantitative data from Dixon and Dimitriadis (pers. comm.) to determine the P-T-t regime during peak and retrograde metamorphism.

Isotopic age dating was beyond the scope of this thesis. However, the available data for the SMM (Section 1.9; Appendix II) are incorporated into the final models presented in Chapter 6. New dates are expected for the Volvi Complex in the near future (Dixon, pers. comm.).

Geochemical analyses of whole rock specimens have been employed to determine the origin and tectonic setting of the Volvi Complex. Analyses were made of dykes and amphibolites from within the envelope, as well as from the margins of

the Volvi Complex. This data set has been supplemented with data from within the Volvi Complex (*s.s.*) from Dixon and Dimitriadis (1984; pers. comm.). Whole rock geochemical analysis has also been applied to granitic lithologies found throughout the area. Analyses of the granitic suite has been used to determine possible origins and evolution of the various granitic bodies present within the area.

1.4 Methodology

The thesis discusses in turn, the background to this study, field relationships, structural framework, detailed petrographic studies, and geochemical investigations of basic and acidic intrusives. The interpretations from this study are then summarised in a tectonic model and regional framework for the SMM. Superposed onto this bulk division is a two-fold division reflecting the main lithological groups (gneissic-metasedimentary lithologies and igneous lithologies) within the study area.

Chapter 1; part one outlines the scope and layout of the thesis. Part two, is a summary of previous geological investigations and provides a broad geological setting to this study. A review of the initial interpretations for the origin of the Volvi Complex prior to this study are presented at the end of the chapter.

Chapter 2; part one presents the geological units (gneissic and metasedimentary) and their relationship to one another. The initial stratigraphic sequence follows that of Kockel *et al.*, (1971, 1977). Due to the observations and conclusions made during this study, a revised stratigraphic sequence is proposed in the chapter summary. Part two presents the basic and acidic igneous units and their relationship to other units within the study area.

Chapter 3; is introduced with the methods and structural style applied to this study. Part one determines the evolution of structures and fabrics within a time framework related to shear zone development. The structural history is summarised at the end of the section. Part two determines the development of intrusions and their relationship to the deformation history.

Chapter 4; is introduced with a review of previous petrographic and metamorphic investigations. Each major lithological group is described in terms of mineral assemblages and textures from low- to high-strain and summarised by schematic qualitative P-T-t models. The chapter is concluded by a schematic qualitative P-T-t model determined from a combination of the lithology summaries.

Chapter 5; discusses the igneous geochemistry. Part one concentrates on the mafic lithologies and determines the validity of geochemical studies on amphibolite-grade lithologies and the fractional crystallisation and partial-melting history on the

understanding that the Volvi Complex is intruded into a within plate setting as determined from field observations. Part two discusses the evolution of granitoids and proposes a partial-melting and fractionation history for crustal anatexites.

Chapter 6; reviews the observations made during this study and determines the evolution of the SMM in a strike-slip transtensional-transpressional regime. A tectonic model is proposed and comparisons to modern analogues are made. Interpretations from this thesis are used to propose the role of the SMM within the Internal Hellenides. At the end of the thesis suggestions are made for further lines of research.

PART II: Characteristics and Geotectonics of the Internal Hellenides

1.5 Introduction

Greece can be divided into a series of well defined, predominantly NW-SE trending tectonic units (Aubouin, 1959; Aubouin *et al.*, 1970; Figs. 1.1, 1.2). These units are characterised by their internal consistency, with marked differences of sedimentary facies and tectonic (structural and metamorphic) histories between them. They are separated from one another by major tectonic contacts. This phenomenon was arguably first noted by Mojsisovics (1877; see review by Aleksic *et al.*, 1984), who termed these units "isopic zones" (literally, "similar looking"). Subsequent research has led to the isopic zones being accepted as individual palaeogeographical entities (Renz, 1955; Brunn, 1956; Aubouin, 1959; Aubouin *et al.*, 1970, 1977; Smith and Moores, 1974; Smith *et al.*, 1975, 1979), though the precise status of each zone has remained contentious.

Geologically Greece is situated predominantly within the Alpine orogenic system, a zone of continental collision between the African and Eurasian continents, represented in Greece by the Hellenide mountain chain (Section 1.10). The Hellenides have been divided into two major groups, (a) The Internal Hellenides (Fig. 1.1), which have been interpreted as representing part of the European crystalline basement, and (b) The External Hellenides (Fig. 1.1), which are interpreted as representing rifted segments off the African continent (Section 1.10). The Internal Hellenides of NE Greece were initially interpreted as a single crystalline basement Massif, the Rhodope Massif *s.l.* (c.f. Cvijic, 1908; Kossmat, 1924; and others as reviewed by Aleksic *et al.*, 1984). Later research highlighted differences within the Massif (Jaranoff, 1938, 1960; Dimitrijevic, 1963; Kockel and Walther, 1965; Mercier, 1966; see review by Aleksic *et al.*, 1984). These differences eventually led to the area being divided into two metamorphic tectonic units, the Rhodope Massif (Section 1.7) and Serbo-Macedonian Massif (Section 1.6). Depending on interpretation (Section 1.8) two metasedimentary tectonic units the Circum-Rhodope Massif and the Vardar Zone, (Kalenic, 1966; Dimitrijevic and Ciric, 1967; Kockel *et al.*, 1971, 1977; Kauffmann, 1976) are also recognised as zones of the Internal Hellenides. The External Hellenides are represented by the remaining isopic zones to the west of the Vardar Zone, namely the Pelagonian, Othris, Pindos, Gavrovo-Tripolitza, Ionian and Pre-Apulian Zones (Figs. 1.1, 1.2).

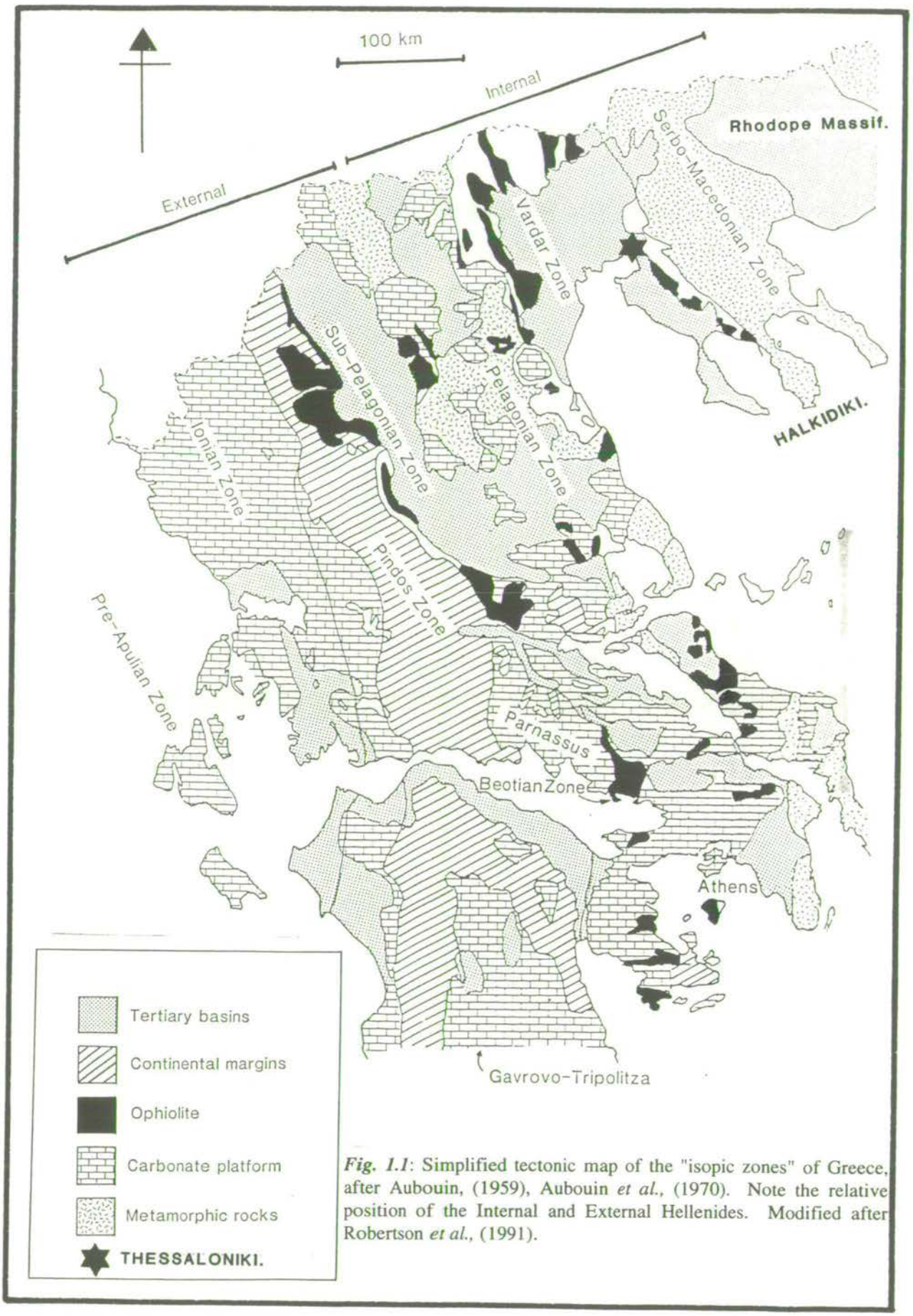

Fig. 1.1: Simplified tectonic map of the "isopic zones" of Greece, after Aubouin, (1959), Aubouin *et al.*, (1970). Note the relative position of the Internal and External Hellenides. Modified after Robertson *et al.*, (1991).

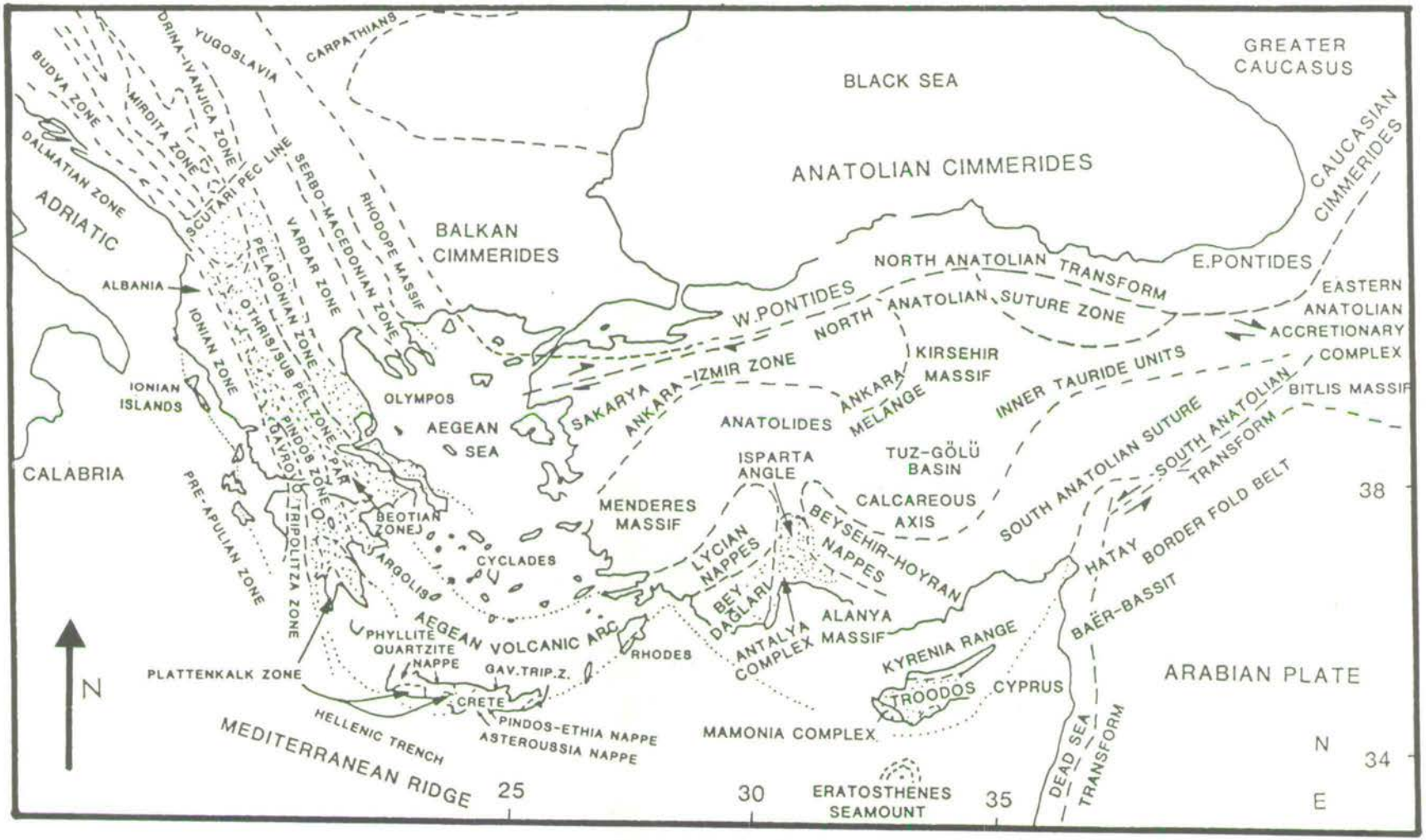

Fig. 1.2: Tectonic elements of the Eastern Mediterranean, based on Robertson and Dixon (1984). Note the trends of the isopic zones and their continuation to the NW and SE.

In order to place the SMM within a regional context comparisons have to be made with the adjacent isopic zones. The following sections provide a brief review (based on a recent study by De Wet, 1989) of the isopic zones which comprise the Internal Hellenides and detailed descriptions of the geology within the study area and Halkidiki Peninsula (Figs. 1.3, 1.4; Table 1.1). The Halkidiki Peninsula includes parts of the Vardar-Axios Zone and the SMM (Fig. 1.3).

The conventional interpretation of the SMM and Vardar-Axios Zone is that the SMM represents Palaeozoic or older stable basement which was only superficially involved in the complex Mesozoic and Cenozoic evolution of the Hellenides, whereas the Vardar-Axios Zone was formed primarily during the Mesozoic from oceanic and continental margin deposits which were assembled, deformed and metamorphosed during tectonic events throughout the Mesozoic and Cenozoic (Mercier, 1966; Kockel *et al.*, 1977).

This simplified view is somewhat misleading as the geology of the area is extremely complex. The subdivision into a Palaeozoic or older SMM and Mesozoic and younger Vardar-Axios Zone is no longer certain. Although the SMM undoubtedly includes some Palaeozoic or even older components, it has been affected by Mesozoic and Cenozoic events (Dixon and Dimitriadis, 1984). In addition, ages of many of the Halkidiki granites have been shown to be younger than previously suggested (De Wet *et al.*, 1989; De Wet, 1989).

The final aim of this study has been to distinguish local and regional similarities and differences in the geology and tectonic history developed between the SMM and the adjoining zones of the Internal Hellenides. The SMM (Section 1.6) is discussed in detail in order to provide a suitable background and therefore enable an understanding of the tectonic models and stratigraphic sequences proposed by Kockel *et al.*, (1971, 1977).

1.6 The Serbo-Macedonian Massif

The Serbo-Macedonian Massif (SMM) borders the Vardar-Axios Zone along an unconformity/structural contact trending NNW-SSE from Sithonia in the south to Guevgueli on the Yugoslavian border (Figs. 1.3, 1.4). By convention, the eastern border has been tectonically juxtaposed against the Rhodope Massif in the Strimon Valley (e.g. thrust faults: Kockel and Walther, 1965; strike-slip faults: e.g. Lyberis, 1984), however, Dixon (pers. comm., in De Wet, 1989) questions this geotectonic boundary and suggests that the SMM can be traced across the "Strimon line" with no break in metamorphic or tectonic elements. Dixon (pers. comm., in De Wet, 1989)

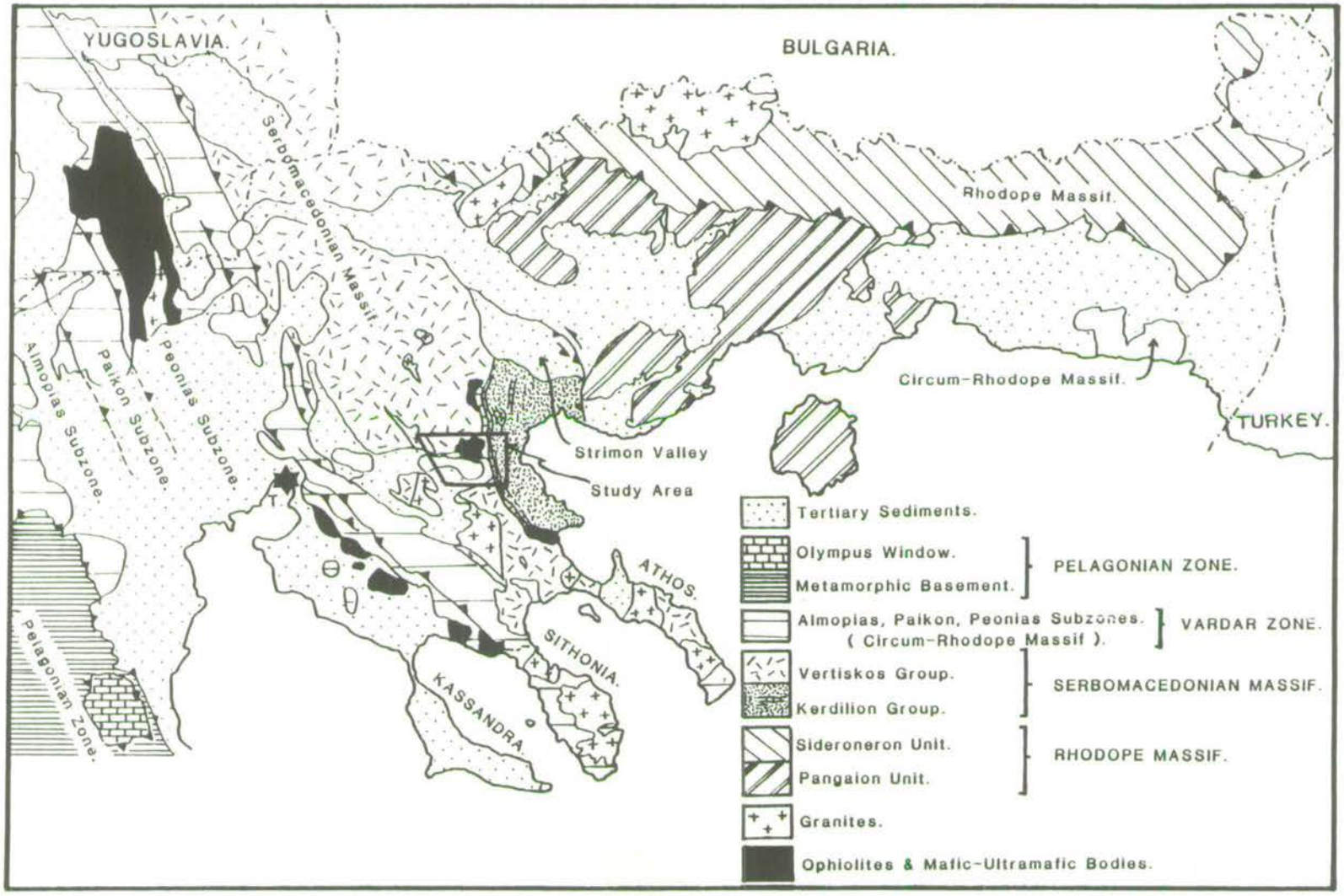

Fig. 1.3: Simplified geological map of the Internal Hellenides, distinguishing between the main lithological subdivisions. Modified after Kockel *et al.*, (1971, 1977); Papanikolaou and Panagopoulos, (1981); Aleksic *et al.*, (1984); Baroz *et al.*, (1987); De Wet *et al.*, (1989); Patras *et al.*, (1989).

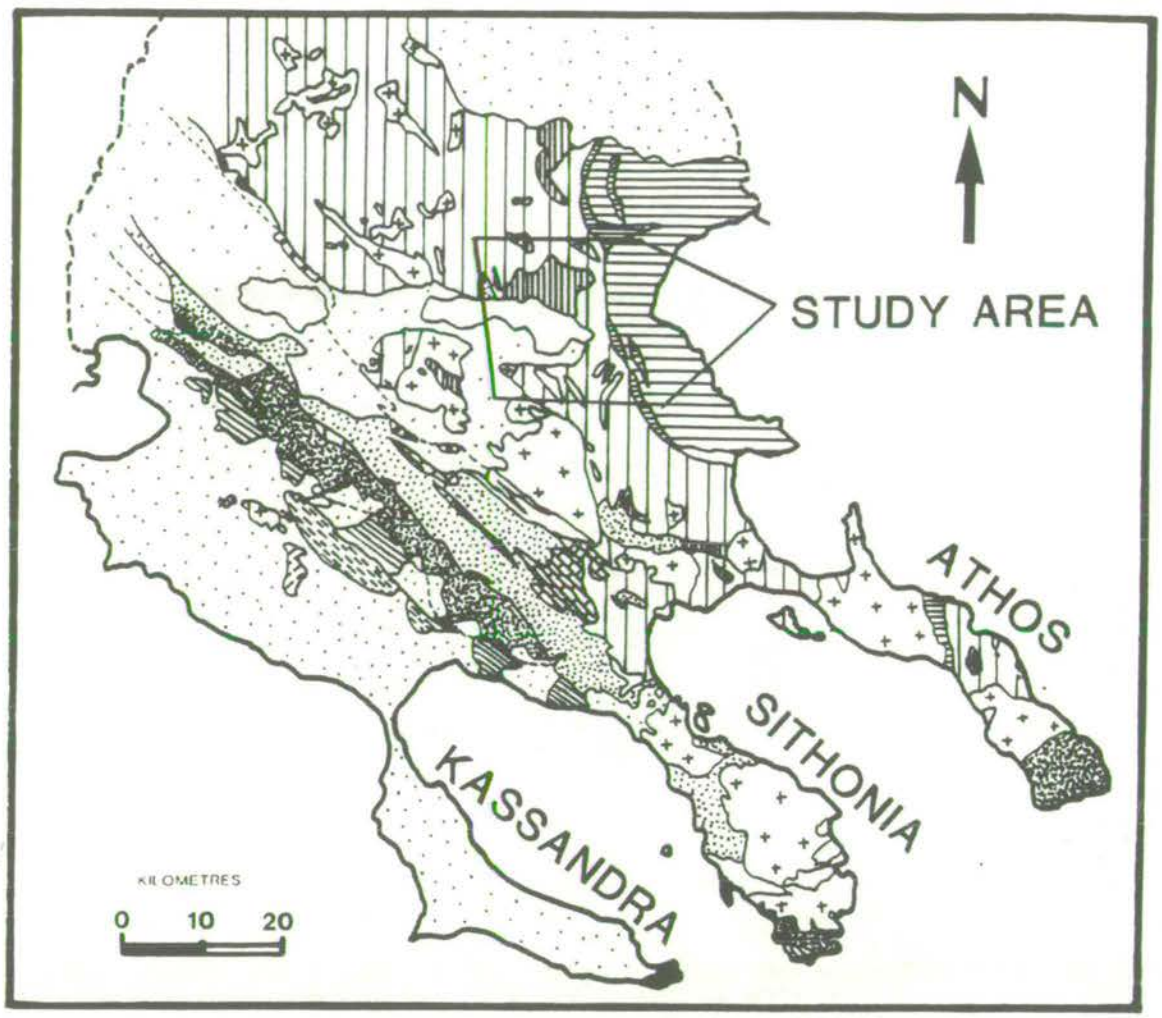

The Main Lithological Units of the Halkidki Peninsula

- Neogene
- Vasiliki Unit
- Chortiatis Unit
- Upper Ophiolite (Sithonia)
- Stip-Axios Unit
- Clastics
- Carbonate
  (Svoula Group)
- Granites
- Thessaloniki-Metamorphosis Ophiolite
  Ultrabasic and basic Lithologies
- Deve Koran-Doubia Unit
  Volcanics, Clastics, Carbonates

Lithologies of the Serbo-Macedonian Massif

- Vertiskos Group
- Carbonate
- Gniess and Schist
  (Kerdilion Group)
- Basic and Ultrabasic rocks
  Therma-Volvi-Gomati Complexes

Fig. 1.4: A detailed geological map of the Halkidiki Peninsula and surrounding areas, showing the main geological units.

GEOTECTONIC UNITS OF THE INTERNAL HELLENIDES

PELAGONIAN ZONE				
VARDAR ZONE OR VARDAR-AXIOS ZONE	ALMOPIAS ZONE			Ophiolites
	PAIKON ZONE		Upper Khromini Formation Livadia Formation Lower Gandatch Formation	Spillitic and Keratophyric Series Marbles and Greenschists
	PEONIAS ZONE	Peonias Subzone	Guevgueli Unit Vasilika Unit Stip-Axios Unit	Ophiolites, Granite Carbonate, Clastic Sediments, Granite Mylonites, Greenschists, Amphibolite-facies rocks
		Circum-Rhodope Belt (Kauffmann *et al.*, 1976)	Aspro Vrisi-Chortiatis Unit Melissochori-Cholomon Unit Deve Koran- Doubia Unit	Ophiolites, Chortiatis Series Svoula Carbonates, Clastics Examili Fm, Clastics, Volcanics, Carbonates
SERBOMACEDONIAN MASSIF	Vertiskos Group Kerdilion Group		Volvi Metasedimentary Group Vertiskos=Kerdilion Group Basement Migmatite Group	Marbles, Carbonates Gneiss, Schist Amphibolites, Granites, TVG Migmatites
RHODOPE MASSIF	Sideroneron Unit Pangaion Unit			

Table 1.1: Geotectonic units of the Internal Hellenides. The detailed subdivisions of Kockel *et al.*, (1971, 1977) and Kauffmann, (1976) for the Vardar-Axios Zone and the SMM are shown. The right hand column gives a very simplified summary of the main lithologies of each subdivision. Note TVG=Therma-Volvi-Gomati Complexes. Amended after De Wet, (1989).

argues that recent features such as small grabens and topographic highs have been misinterpreted as being part of a major ancient structural break, when they are actually Recent features. If this is the case then the relationship between the SMM and the Rhodope Massif warrants re-interpretation. The most recent interpretation of the Strimon Valley (Dinter and Royden, 1993) proposes a detachment surface exposed as a gently dipping low-angle normal fault which can be traced along strike for more than 150 km. Extensional deformation is interpreted to have characterised this boundary since at least the Middle Miocene. However, until the precise nature of this boundary is resolved, this study considers the Strimon line to represent the eastern boundary of the SMM. To the south, the SMM is strongly disrupted by Mesozoic and Cenozoic tectonism and plutonism. The boundary between the Vardar-Axios Zone and the SMM is highly irregular in the area between the Arnaea granite and Sithonia Peninsula.

The geology of the SMM as a whole is complex and varied (Figs. 1.3, 1.4). The most extensive unit found towards the eastern boundary of the SMM consists of a series of polymetamorphic gneissic formations. Using criteria based on textures, the percentage of lithologies present or absent and metamorphic assemblages, but not always in agreement with isotopic data (Section 1.9), the gneissic formations have been divided into a lower (older) *Kerdilion Group* to the east and an upper (younger) *Vertiskos Group* to the west (Kockel and Walther, 1965, 1968; Kockel *et al.,* 1971, 1977).

1) The Kerdilion Group consists predominantly of migmatites, leucocratic gneisses, schists and amphibolites with interlayered marbles. Minor intercalations or intrusions of granitic material and extensive pegmatitic veining are also commonly found.
2) The Vertiskos Group consists of leucocratic augen ortho- and para-gneisses, mica schists and amphibolites, with intercalations of meta-ophiolites and ultrabasic rocks. A variety of basic to evolved dykes are also found throughout the group (Kockel and Walther, 1965, 1968; Kockel *et al.,* 1971, 1977).

This traditional subdivision between the Kerdilion and Vertiskos Groups was based predominantly on the abundance of amphibolites, presence or absence of ultramafic rocks and minor petrographic/textural dissimilarities, as recognised originally by Kockel *et al.,* (1971, 1977). More recent work within the area usually brings this original subdivision into question. The mafic components of these two groups have been the basis of more recent geochemical investigations and shown to be consistently indistinguishable (Kassoli-Founaraki, 1981; Sapountzis *et al.,* 1990; and this study).

Hence, the subdivision of these two groups on the basis of mafic bodies is distinctly questionable. Dimitriadis (1974) recognised two distinct migmatisation events within the Kerdilion Group, separated by a major deformational event. In contrast no clear distinction was possible with the migmatites of the Vertiskos Group. This would suggest a good basis for separating the two groups, but this study has found similar evidence for migmatite evolution in both groups (Chapters 2 and 3). Dimitriadis (1974) also recognised that the first metamorphic event (M_1) appears to be different in the two groups, the Kerdilion Group (500-600°C, 3-4 kb) being slightly higher in grade than the Vertiskos Group. Both Groups are observed to be extensively retrogressed in a second apparently coeval event (M_2) to the greenschist-facies (Dimitriadis, 1974). However, these differences are only minor and reinterpretations of the metamorphic and P-T histories have been made in Chapters 4 and 6.

There is no direct structural or tectonic evidence available which can help constrain the subdivision between the Kerdilion and Vertiskos groups. This has resulted in a number of interpretations being proposed. Neubauer (1957), suggested there was a true tectonic or stratigraphic discontinuity between the two groups. However, Kockel and Walther (1965, 1968) claimed the divisions were simply concordant. Dimitriadis (1980) proposed that although the divisions now appear tectonically concordant, a primary discontinuity did exist, which has since been obliterated by a common style of reworking on both sides of it. The evidence and models developed in this study, tend to favour the models of Dimitriadis (1980), although the extent of the proposed primary discontinuity remains questionable.

Three mafic and ultramafic complexes occur within the Vertiskos Group along the boundary with the Kerdilion Group. The Therma and Gomati Complexes consist of ultramafic rocks, while the Volvi Complex consists of gabbros and sheeted dykes. Collectively the complexes are referred to as the "TVG Complex", (Kockel *et al.*, 1971, 1977). The complexes have been interpreted as Palaeotethyan ophiolites (Dimitriadis, pers. comm., in Sengor, 1984). However, more detailed work by Dixon and Dimitriadis (1984) suggests that they represent an in situ Mesozoic rift complex, rather than a Palaeotethyan remnant (Section 1.12). Due to its distinct characteristics the Volvi Complex can be considered as a third major lithological group within the study area.

A fourth lithological group within the study area is represented by a series of micaceous schists, marbles, carbonate and quartzitic gneiss formations which are found intercalated within the gneissic formations of the Vertiskos and Kerdilion Groups. The metasediments within the Vertiskos Group have tentatively been

correlated with the Svoula marble and flysch members of the Peonias Zone (Circum-Rhodope Massif) by a number of workers including Kockel *et al.*, (1971, 1977), and Kauffmann, (1976). The metasediments in the Kerdilion Group were assigned to a completely different source and origin and have been interpreted as an integral part of the basement (Kockel *et al.*, 1971, 1977; Kauffmann, 1976). However, actual field relationships within the Volvi area are obscure, which brings into question the validity of the original correlation by Kockel *et al.*, (1971, 1977) and Kauffmann, (1976). The origin and evolution of these metasediments are therefore reviewed in Chapters 2 and 6. The last distinctive lithological group recognised within the study area is represented by the Arnaea granite and various granitoid suites. Deformation of the main body of granite has resulted in a series of variably deformed ortho-augen to mylonitic ortho-gneisses. Associated apophyses, veinlets and sheets of "Arnaea-type" origin are found within the adjacent gneissic formations of the Vertiskos Group.

1.6.1 Stratigraphic Arguments

Ages for the various lithological components which make up the SMM are poorly constrained and therefore dependent on stratigraphic arguments. Recent reviews have been made by Dixon and Dimitriadis, (1984) and De Wet (1989) and are summarised in this section.

The most highly deformed, migmatitic lithologies found within the SMM have traditionally been regarded as a pre-Mesozoic, possibly pre-Hercynian metamorphic basement complex. The original argument was based on the tectonic contact between the SMM and the low-grade, north-easterly dipping thrust units (Late-Permian to Early-Jurassic) of the Vardar-Axios Zone (e.g. Dimitrijevic and Ciric, 1967). Support for these ideas was supplied by the recognition of a pre-Tremadocian unconformity on SMM rocks in Yugoslavia (Dimitrijevic and Ciric, 1967), and by an unconformity between the Examili Formation (believed to be Permian) and the schists of the SMM in the Halkidiki Peninsula. Further north, in eastern Serbia, the eastern boundary of the SMM with the Rhodope-Moesian Platform is marked by a complex series of Mesozoic sutures and associated basins and volcanic arcs (Getic Suture; Timok and Luznica zones: Grubic, 1980). In Bulgaria, the SMM is considered to be Precambrian (Zagorchev, 1974).

The western border of the SMM in Greece is characterised by a series of mainly NE-dipping, tectonically bounded slices of weakly metamorphosed sediments and igneous rocks. These constitute the Circum-Rhodope belt of Kauffmann *et al.*, (1976) and are well established as having been formed from at least Early Triassic to

Early Jurassic times. The stratigraphically lowest unit in this belt is the Examili Formation, composed of weakly deformed and recrystallised arkosic clastics which rest with recognisable unconformity on schists of the SMM proper in a series of discontinuous, fault-bounded outcrops (Mercier, 1973a; Kockel *et al.,* 1977; Dixon and Dimitriadis, 1984). They are unfossiliferous but are attributed to the Permian or Lower Triassic because of the time constraints imposed by the overlying "Volcano-Sedimentary Series" (rhyolitic lavas and tuffs etc.). This series is always in tectonic contact with the Examili Formation, and passes conformably up into fossiliferous Upper Skythian limestones (Kockel *et al.,* 1977). The overlying neritic carbonates of the Deve Koran-Doubia Unit (Mercier, 1973a) contain fossils of Upper Skythian, Ladinian, and Carnian age, with the highest horizons near Metaliko and Aspro Vrisi being assigned to the Rhaetian (Kockel *et al., op. cit.*). Along-strike to the SE in the Halkidiki Peninsula the neritic carbonates give way to increasingly deformed and recrystallised thin-bedded limestones of the Svoula Marble Formation. Upper Norian conodonts and foramanifera are known from the northern, low-grade, end of the outcrop (Kauffmann *et al.,* 1976). The Svoula marbles apparently pass up into phyllites and then into the thick sequence of unfossiliferous turbiditic sandstones, shales and conglomerates of the Svoula Flysch, inferred to be of Lower Jurassic age from their apparent stratigraphic position. This attribution is consistent with the occurrence of Upper Triassic limestone clasts in conglomerates within the formation (Kockel *et al.,* 1977). Locally, in the NW part of the belt, rare tectonic intercalations of Lower Jurassic carbonates also occur which may be lateral stratigraphic equivalents. At the structurally lowest, western-most part of this belt, immediately to the SE of Thessaloniki, lies the Chortiatis magmatic suite (gabbros, diorites and more evolved granitic rocks), and the mafic and ultramafic plutonics of the Halkidiki ophiolites. This association lies SE along-strike from the ophiolites of Guevgueli on the Yugoslavian border. These are cut by the 150 Ma Fanos granite (Spray *et al.,* 1984). The Circum-Rhodope Belt includes important thrust-bounded sheets of SMM-type schists and gneisses, which show a metamorphic discontinuity with the intersliced Mesozoic units. In summary, it seems clear that a pre-Triassic, possibly pre-Permian, metamorphic complex existed in this area during the Early Mesozoic on which a sequence of Permian to Lower Jurassic clastic, volcanic and carbonate rocks were deposited, followed by a thick sequence of turbiditic sandstones and shales. Whether this sequence represents the development of a rifted, passive continental margin is not clear, although parallels between the Pteleon Formation and Strimbes Limestone Formation which crop out within the succession of the Othris "margin"

with the Examili Formation and Deve Koran Formation are present (Smith *et al.*, 1975; Dixon and Dimitriadis, 1984). This margin was evidently involved in at least one SW-vergent imbricate thrusting event in the Mid Jurassic, which introduced ophiolitic components and slices of SMM basement into the structural succession. Stratigraphic control on this event is provided by the Fanos granite and by the Doubcon Molasse, a conglomeratic formation with Upper Jurassic-Lowermost Cretaceous coral-bearing interbeds, which unconformably overlies thrust-sheets of gabbros north of Thessaloniki (Mercier, 1973a).

It is apparent from the 1: 100 000 map of the Halkidiki Peninsula, and from the accompanying explanatory memoir Kockel *et al.*, (1977) that later deformation must also have affected the area (Dixon and Dimitriadis, 1984). For example, the Doubcon Molasse itself is involved in SW-vergent imbricate thrusting with the Svoula Flysch immediately to the SW of Deve Koran (Kockel *et al.*, 1971, 1977).

The most critical observation for the tectonic overview of the SMM has been the recognition of an extensive and complex (possibly Mesozoic-Tertiary) structural and metamorphic deformation history (Dixon and Dimitriadis, 1984; Vergely, 1984; Papadopoulos and Kilias, 1985; Mussallem and Jung, 1986). This tectonic event has overprinted what has traditionally been regarded as the main (pre-Mesozoic, or possibly pre-Hercynian) tectonic event (Kockel *et al.*, 1971, 1977). Dixon and Dimitriadis (1984) suggest that at least part of the SMM, within the western Vertiskos Group (Kockel *et al.*, 1971, 1977), underwent major Mid-Mesozoic metamorphic, plutonic and deformational events. To the SE, Dixon and Dimitriadis (1984), following Kockel *et al.*, (1977), suggested that the Svoula Limestone and Flysch deposits can be followed into a marble and phyllite sequence which can be traced into the SMM. Dixon and Dimitriadis (1984) argue that both the marble and surrounding phyllite/schist within the SMM have been subjected to the same deformation event and staurolite grade regional metamorphism. The metasediments are intruded by the Arnaea granite, which exhibits substantial deformation and recrystallisation.

The post-Jurassic evolution of the area includes intrusion of a suite of Eocene granites with limited associated deformation and metamorphism, and a suite of post-tectonic (possibly Oligocene) granites (De Wet, 1989). The area is cut by a series of Holocene-Recent, mainly NW-trending, active normal faults (e.g. Mercier *et al.*, 1979; Section 1.11). This younger tectonic episode is regarded as being responsible for the emplacement of the (possibly Mesozoic) ophiolitic complexes and granitic intrusions found throughout the SMM.

From this preliminary re-interpretation of the SMM, several authors have pointed out similarities between this Massif and the high-grade basement rocks of the Pelagonian Zone (Smith and Woodcock, 1982; Mountrakis, 1986). This could be the result of:

1) Coincidence. Both are Hercynian basement areas but were never closely associated (e.g. Robertson and Dixon, 1984).
2) Both were part of the same continental area separated during the Mesozoic by strike-slip motion (Smith and Woodcock, 1982; Mountrakis, 1986), or by Neotethyan oceanic spreading (Baroz *et al.,* 1987).

Structural, metamorphic and stratigraphic evidence indicate that the second hypothesis is probably the most correct.

1.6.2 Summary

The geology of the Halkidiki Peninsula and adjacent areas is summarised in Fig. 1.5, following a recent review by De Wet (1989). The complexities of the SMM are not depicted. Each sedimentary rock unit is plotted in its approximate stratigraphic position. Igneous rocks are plotted so that the top in the column shows their approximate age of crystallisation. For example, the lithologies of the Thessaloniki-Metamorphosis ophiolite are obviously contemporaneous and do not span Middle Triassic to Middle Jurassic time. However, due to the uncertainty in the age of the ophiolite, it may actually span this time period. The left hand column shows the alternative tectonic interpretations of Kockel *et al.,* (1977) and Vergely (1984). Both interpretations suggest a major tectonic phase during the Jurassic (180 Ma) upper greenschist orogenesis of Kockel *et al.,* (1977) and the Late Jurassic JE1 tectonic phase of Vergely (1984). The exact timing of the second, less intense deformation is different in the two interpretations. Kockel *et al.,* (1977), attributes the lower greenschist orogenesis to be an Aptian-Albian (Mid Cretaceous) event, whereas the CT1 event of Vergely (1984) is attributed to be either Palaeocene or Eocene. The simplified geological evolution of the area is:

1) Consolidation of the SMM (and the Stip-Axios Zone) in the Palaeozoic.
2) Rifting and the deposition of continental marginal sediments and volcanics in the Permo-Triassic.
3) Deposition of stable continental marginal sediments and neritic carbonates during the Upper Triassic.
4) Increasing instability, flysch deposition and oceanic basin formation within the IMHOB during the Jurassic.

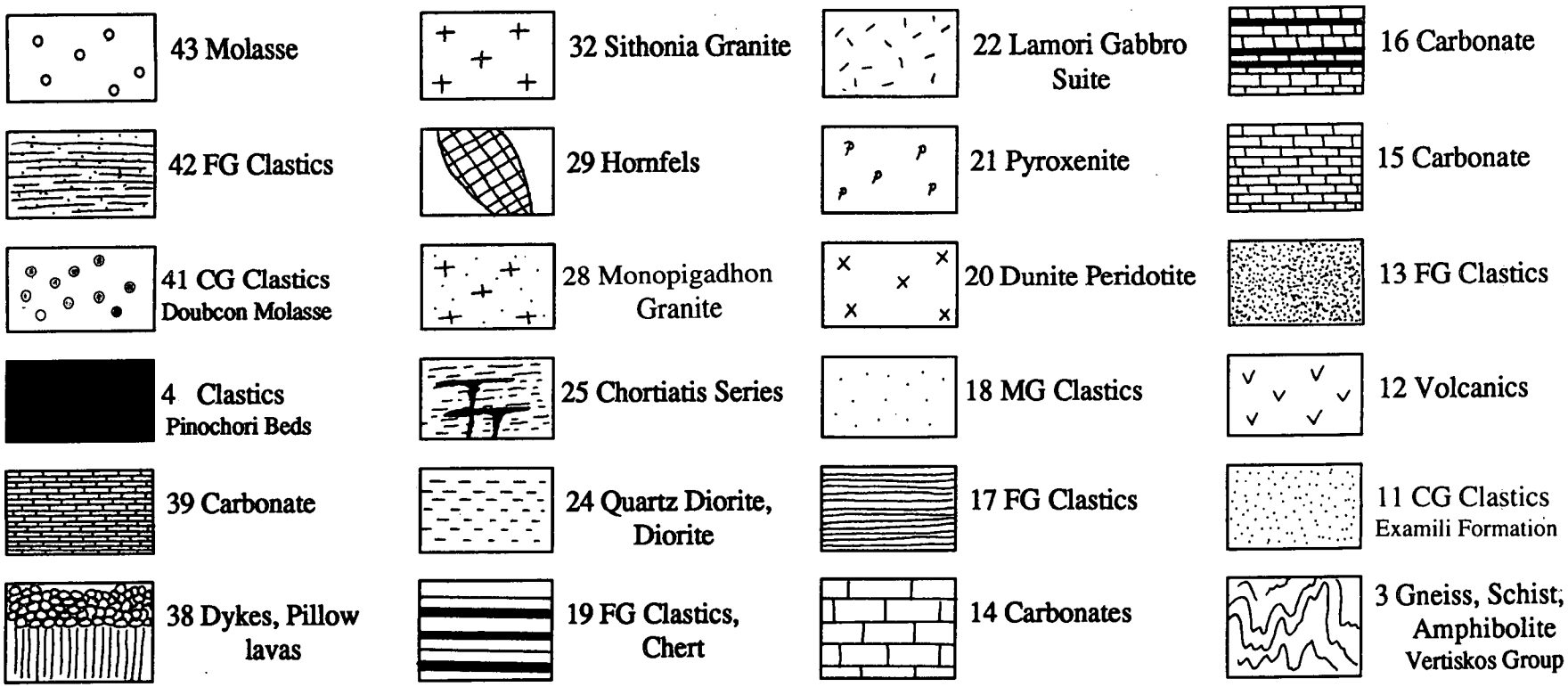

Legend for Fig. 1.5. CG=Coarse-grained, MB=Medium-grained, FG=Fine grained. Numbers are taken from Kockel and Mollat, (1976).

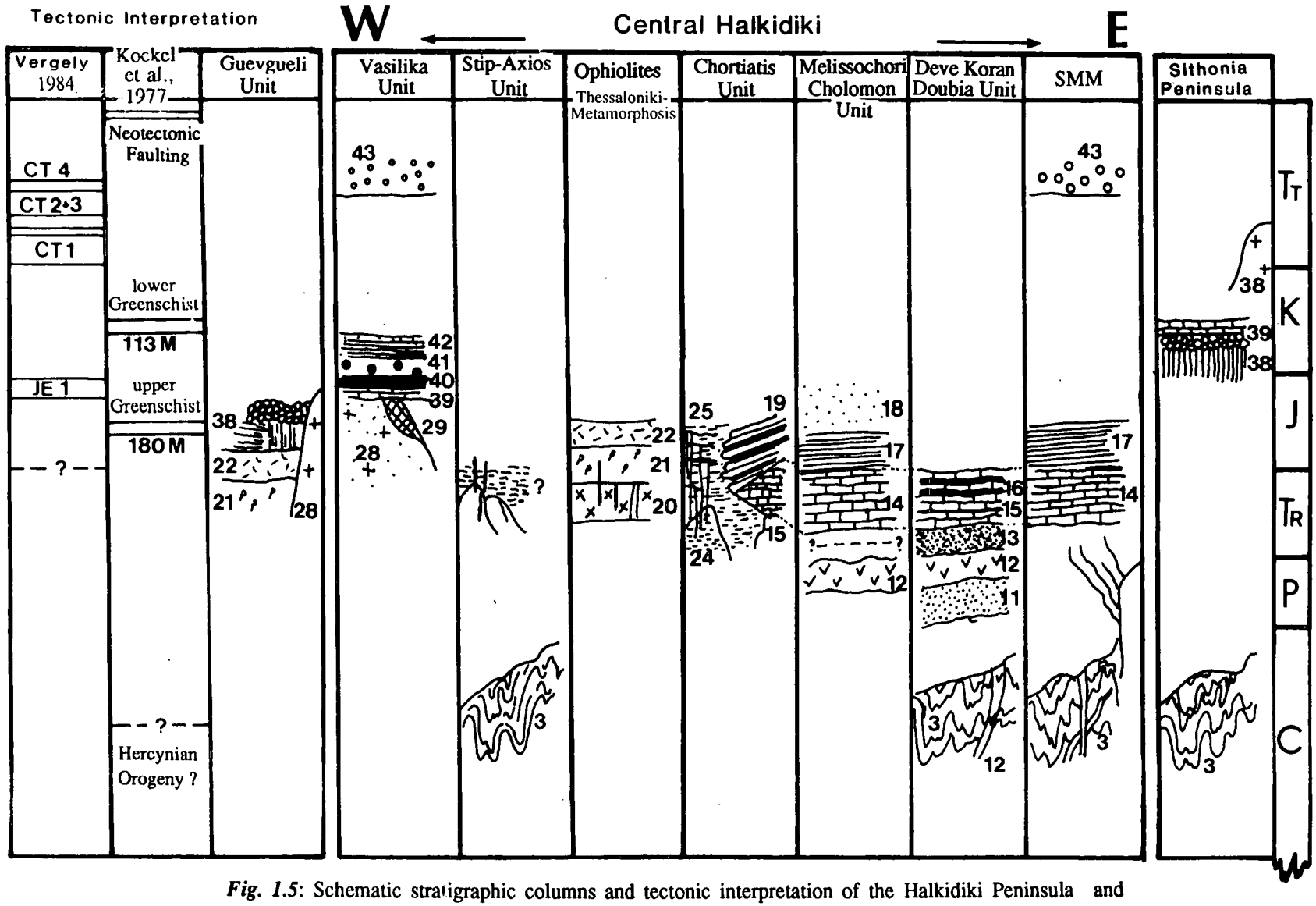

Fig. 1.5: Schematic stratigraphic columns and tectonic interpretation of the Halkidiki Peninsula and surrounding area. See Fig. 1.4 for the distribution of the units shown in this diagram.

5) Granite intrusion (Fanos, Arnaea and possibly Monopigadhon), ophiolite emplacement and orogenesis in the Late Jurassic.
6) Deposition of the Doubcon Molasse and carbonates of the Vasilika Unit during the Late Jurassic-Early Cretaceous. Formation of the Sithonia-Kassandra ophiolite.
7) Thrusting and low grade metamorphism during the Late Cretaceous, and possibly Tertiary.
8) Intrusion of the Sithonia, Ouranopolis, Chiliandariou and possibly Gregoriou granitoids in the Eocene, with associated deformation and shearing.
9) Molasse deposition, intrusion of granitoids (Stratoni, Megali Panagia) and faulting in the Oligocene.
10) Neogene sedimentation and faulting.

1.7 The Rhodope Massif

The crystalline basement lithologies of the Rhodope Massif lie to the east of, and are separated from, the SMM by the Struma-Strimon fault zone, which runs approximately NW-SE along the Strimon Valley (Figs. 1.1, 1.3). In two areas along the fault zone it is reported that the SMM is thrust over the Rhodope Massif (Kockel and Walther, 1965; Schenk, 1970; Koukouzas, 1972). The Massif extends to the east as far as the east Thracian Fault and to the north into Bulgaria, where it is again bounded by a steep fault, the Marcia deep fault (Boyanov and Kozhoukharov, 1968). The Rhodope Massif (*s.s.*) was regarded as a single homogeneous crystalline basement unit. This model has subsequently been modified, with the area being divided into three major supergroups, the Pre-Rhodopian (Ograzdenian, lower complex, of Archean age), the Rhodopian (upper complex, of Proterozoic age) and the Kulidzik Supergroup (cover complex, Circum-Rhodope Massif), as defined by Kozhoukharov, (1968, 1978); Kozhoukharov *et al.,* (1978). Within Greece the Rhodope Massif (*s.s.*) corresponds entirely to the Rhodopian Supergroup with only very minor outcrops of lithologies associated with the Pre-Rhodopian Supergroup.

Detailed structural and metamorphic analysis of the Rhodope Massif within NE Greece has highlighted a complex deformational sequence, which has resulted in the Massif being divided into two tectonic horizons, the *Sideroneron* and *Pangaion Units.*

1) The *Sideroneron Unit* (Fig. 1.3; Table 1.1), appears as an upper tectonic unit, as the result of thrusting upon the Pangaion Unit from N to S, along a long

tectonic line, generally orientated NW-SE (Papanikolaou *et al.*, 1982). This unit has been affected by two metamorphic events, the first of upper amphibolite/granulite facies, and the second a retrograde event of the greenschist-facies. These events affect a series of augen and leucocratic ortho-gneisses, migmatites, mica schists, amphibolites, thin intercalations of marbles, abundant pegmatite and aplite veins and a number of granitic bodies.

2) The *Pangaion Unit* (Fig. 1.3; Table 1.1), appears as a lower tectonic unit. This unit has only been affected by medium to low grade greenschist-facies metamorphism, which has affected a sequence of augen-gneisses, mica and hornblende schists, amphibolites and marbles (Osswald, 1938; Meyer and Pilger, 1963; Kronberg, 1966, 1969; Meyer, 1969; Kronberg *et al.*, 1970; Kronberg and Raith, 1977; Papanikolaou and Panagopoulos, 1981; Patras *et al.*, 1989).

Application of modern structural techniques and re-mapping of the Rhodope Massif led to significant advances in the interpretation of the deformation history. As a result, it is possible to consider the Rhodope Massif in NE Greece as a series of E-W trending tectonic units with southward directed movement (Ivanov *et al.*, 1978, 1979; Burg *et al.*, 1990). Within Bulgaria similar tectonic units have also now been recognised (Ivanov *et al.*, 1980, 1984; Ivanov 1988), with further syn-metamorphic thrusting events in both Bulgaria and Greece recognised and expanded upon by Burg *et al.*, (1990). Therefore, from a tectonic point of view, the Rhodope Massif can no longer be regarded as a single Precambrian tectonic block, which throughout its Phanerozoic evolution has been subjected only to vertical movements with minor internal deformation and granitic intrusions. Instead, it has been a very active segment during the Alpine orogeny. However, its precise geotectonic role remains uncertain (Ivanov *et al.*, 1978, 1979; Papanikolaou and Panagopoulos, 1981; Patras *et al.*, 1989). The Massif within Greece has also been subjected to major fault zones with essentially vertical movement. This has created a "block structure" of post-Oligocene age, which has been active throughout the Neogene and Quaternary periods (Fig. 1.8).

Extensive age dating within the Rhodope Massif has been derived via numerous methods and techniques. Due to the poor tectonic understanding of the Massif, it has often proved difficult to correlate and interpret these ages. Regionally the Rhodope Massif has been considered to be a Precambrian to Hercynian continental block, surrounded by two branches of the Alpine Himalayan collisional system; the Balkan belt to the north, and the Dinaride-Hellenide belt to the south, (see Section 1.10; e.g. Boncev, 1978, 1987, 1988; Dewey *et al.*, 1973; Hsu *et al.*, 1977).

However, from specific age data tighter constraints can be applied to the Massif, especially in areas where the tectonic history has been reinterpreted.

1) Palaeontological constraints were derived by a number of workers including Meyer and Pilger (1963), who derived a Palaeozoic or even Mesozoic age from coral data. Ancirev *et al.,* (1980) discovered molluscs indicating a Middle Ordovician to Lower Carboniferous age. Kozhoukharov and Timofeev (1980) proposed a Middle to Upper Proterozoic age on the basis of microphytofossils; whereas Late Cretaceous foraminifera bearing sediments, are found to lie unconformably on high grade metamorphic rocks (Boyanov *et al.,* 1982).

2) Radiochronological data have been determined by a number of researchers. Kokkinakis (1977), proposed an upper Palaeozoic age from intrusives within the region of Symvolon mountain and Kavala. Lilov (1981) proposed an age of 570-665 Ma (K/Ar method) for the Struma Diorite Formation, and also identified an Hercynian anatexis event. The zircons associated with this event were dated at 335 ± 40 Ma (therefore indicating at least the magmatic origin, if not the true origin of the intrusion). Boccaletti *et al.,* (1974) and Boncev (1987, 1988) recorded a Cretaceous age for a series of thrusts within the crystalline axis of the Balkan belt. Zagorchev and Moorbath (1986) proposed an approximate 100 Ma Rb/Sr errorchron on a metamorphosed granitoid, reflecting a major resetting of the Rb/Sr system during a widespread metamorphic event. Soldatos and Christofides (1986) defined a 90 Ma isochron from whole rock samples, and recognise the existence of a low grade Alpine metamorphism, which is defined by the foliation of the external parts of the granitoid bodies and the K/Ar mica ages in the range 38 to 14 Ma. The use of better tectonic interpretations has therefore resolved some of the regional interpretation problems, although others still remain contentious. It is proposed that similar tectonic reinterpretation of the SMM will resolve at least some of the dating anomalies proposed for the SMM.

1.8 The Vardar-Axios Zone

The Vardar Zone is a NW-SE trending isopic zone (Aubouin, 1959), which lies to the west of the SMM (Figs. 1.1, 1.2, 1.3). It was originally recognised in its present form by Kossmat (1924) and since the advent of plate tectonics has generally been interpreted as the suture zone of a Neotethyan "Vardar" ocean (Figs. 1.6, 1.7; e.g. Brunn, 1956; Mercier, 1966, 1973a, b; Aleksic *et al.,* 1974; Karamata, 1974; Karamata *et al.,* 1980; Vergely, 1984). From the recognition of distinctive facies variations, the Vardar Zone has been subdivided into three subzones, from west to

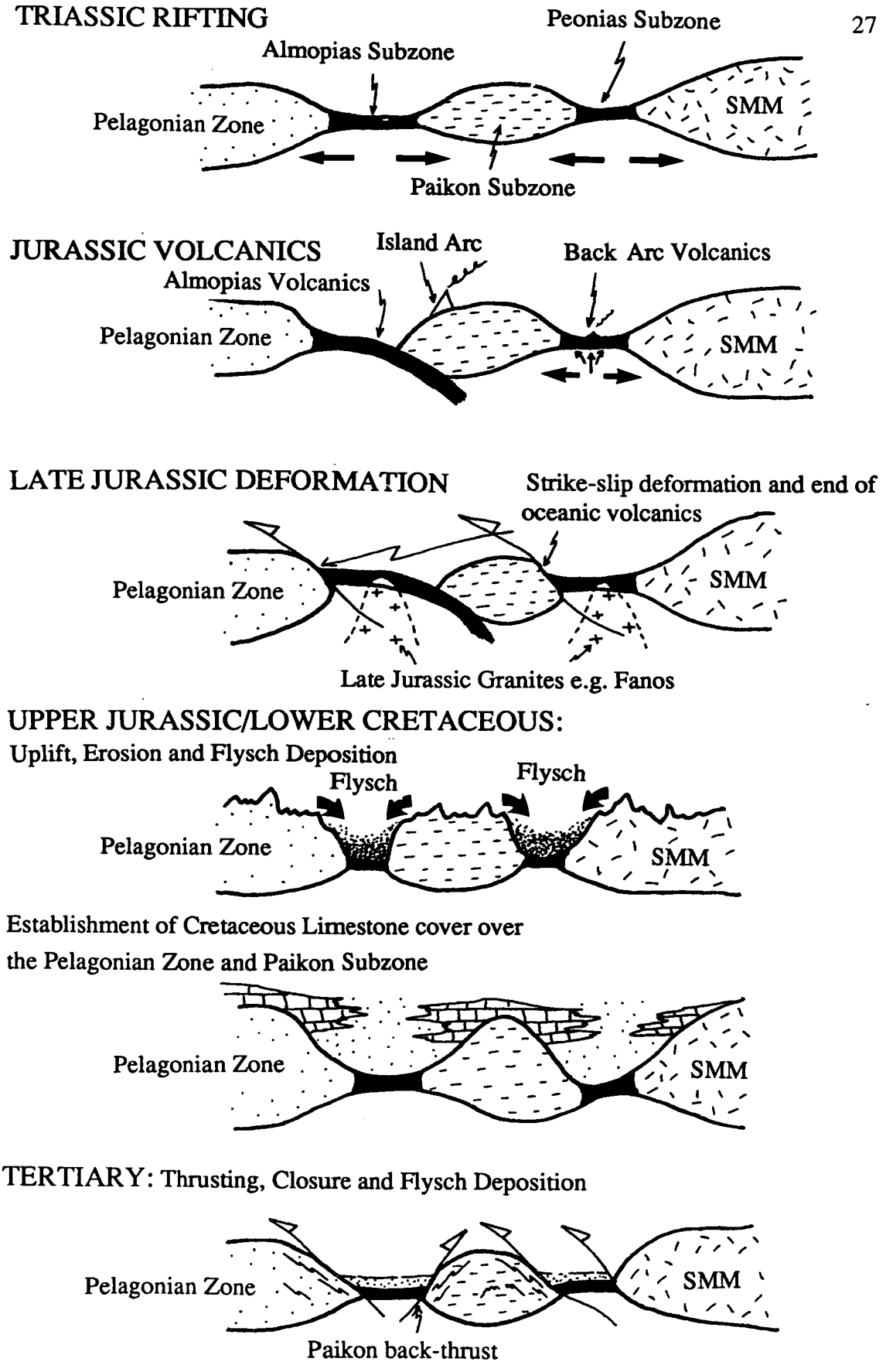

Fig. 1.6: Schematic cross-sections for the evolution of Greece, and the development of the Internal Hellenides. Modified after Boccaletti *et al.*, (1974); Hsu *et al.*, (1977); Jacobshagen *et al.*, (1978); Bebien *et al.*, (1980); Vergely, (1984); Mountrakis *et al.*, (1987); Sharp, (pers. comm.).

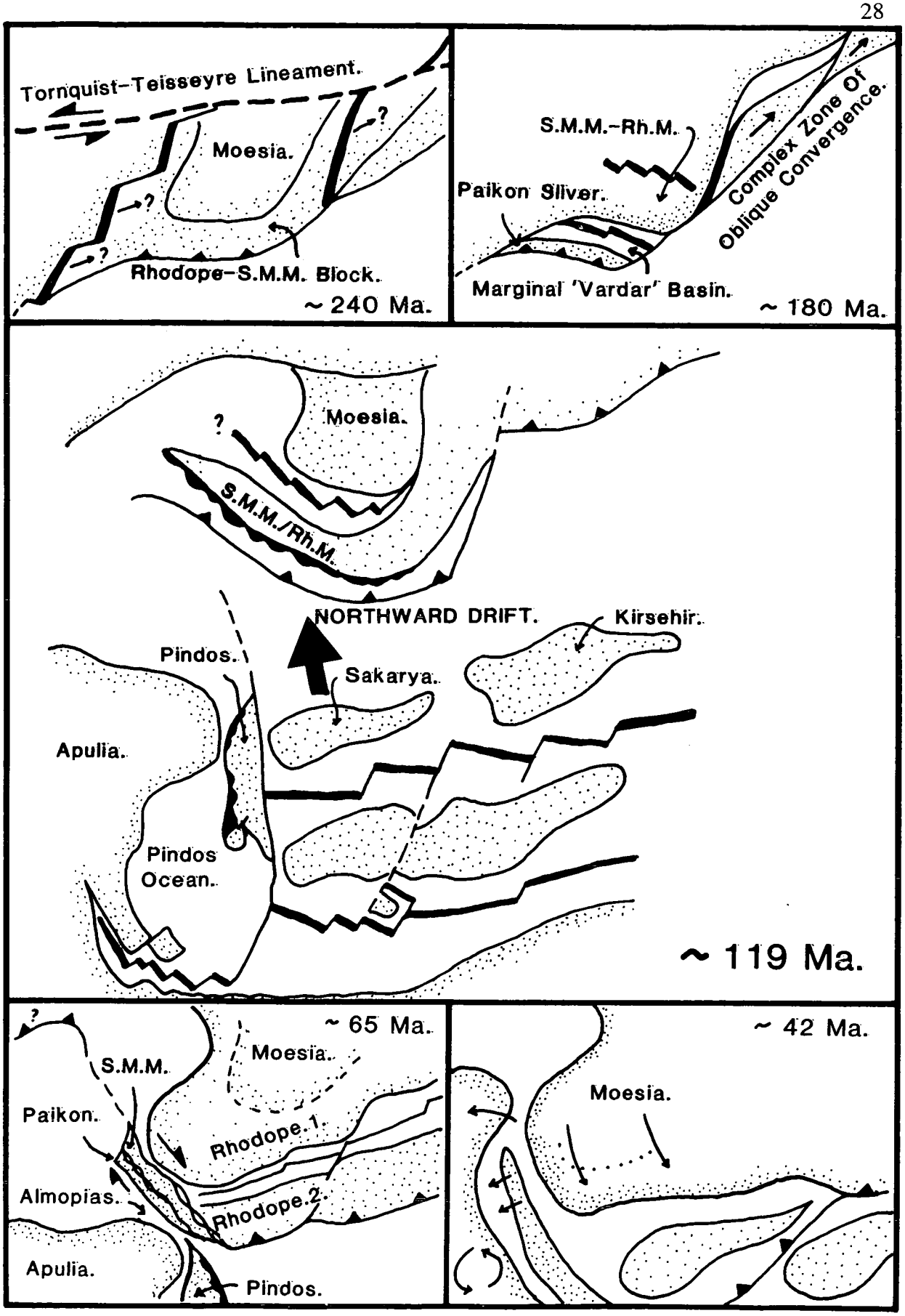

Fig. 1.7: Schematic plate reconstructions for Greece and the Aegean region, with emphasis on the Northern Internal Hellenic margin, after Robertson and Dixon, (1984).

east, the *Almopias*, *Paikon* and *Peonias Subzones* (Mercier, 1966a, 1973a; Mercier *et al.*, 1975). Only the Peonias Subzone is exposed on the Halkidiki Peninsula. However, the Almopias and Paikon Subzones are also important in the evolution of the Halkidiki Peninsula.

The boundary of the most easterly of these subzones (the Peonias Zone) with the SMM is structurally complex. This boundary is represented by a sequence of generally NE-dipping, discontinuous fault-bounded outcrops. As a result of the faulting Mesozoic Vardar lithologies are unconformably deposited over the gneissic lithologies of the SMM.

1.8.1 The Peonias Subzone

This subzone is represented by a lithological sequence of limestones with intercalations of conglomerates, rhyolites and pyroclastics, interbanded with dolerites and gabbros, and intruded by microgranites. Along the boundary with the SMM there are also a number of dismembered ophiolitic bodies (Mercier, 1960, 1966a, b, 1973a; Kockel *et al.*, 1971, 1977; Smith and Moores, 1974; Bebien *et al.*, 1980; Dimitriadis, 1980; Jung *et al.*, 1981; Mussallam and Jung, 1984; Dixon and Dimitriadis, 1984).

Kauffmann *et al.*, (1976) suggested that a new geotectonic element, the Circum-Rhodope Belt, be included within the framework of the Hellenides. This belt corresponds to the eastern part of the Peonias Subzone. On the east it is bounded by the SMM and on the west by the Stip-Axios Unit. The Circum-Rhodope Belt has been used to describe the ophiolites (Oreokastron, Thessaloniki-Metamorphosis and Sithonia-Kassandra) and related continental marginal sequences, which occur between the continental basement rocks of the Stip-Axios Unit and the SMM (Kauffmann *et al.*, 1976; Kockel *et al.*, 1977). These ophiolitic complexes, together with the Guevgueli Complex, are also referred to as the Innermost Hellenic Ophiolite Belt (IMHOB) to distinguish them from the ophiolite complexes of the Almopias Subzone (Bebien *et al.*, 1986). A similar unit, which is readily correlated with this subzone, is the Circum-Rhodope Zone. This zone lies to the SE of the Rhodope Massif in the area of Alexandropoulis (Fig. 1.3), where it is represented by a thick series of phyllites with intercalations of conglomerates and crystalline limestones of Triassic to Lower Cretaceous age (Maratos and Andronopoulos, 1964; Kauffmann *et al.*, 1976).

The Circum-Rhodope Belt in the Halkidiki Peninsula is sub-divided into several tectonic units based on sedimentological depositional facies, metamorphic grade and structural differences (Kockel *et al.*, 1977). The units, from the NE to SW are (Fig. 1.4):

Deve Koran-Doubia Unit: The lowermost parts of the Upper Palaeozoic-Mesozoic sequence are preserved within this subunit and include the Examili Formation (quartzites, arkoses and conglomerates), volcano-sedimentary lithologies and neritic limestones.

Melissochori-Cholomon Unit: This unit includes the Svoula Group which consists of Middle and Upper Triassic pelagic carbonates and Lower and Middle Jurassic continental marginal sediments, turbidites and olistostromes. Tectonic slices of supposed highly retrogressed basement occur within this sequence.

The main and continuous outcrop of the Svoula Group forms a faulted and sheared contact with the Arnaea Granite. Scattered infolded inliers of the Svoula Group occur in the high-grade basement rocks of the SMM.

The Svoula Group metasediments represent Permo-Triassic marine carbonates and shales in the east and Middle Jurassic geosynclinal flysch deposits (Svoula Flysch) in the west (Kockel *et al.,* 1977; Mussallam and Jung, 1986). The change from carbonate platform deposits to coarse-grained clastic facies probably represents continental margin instability and degradation during the Early and Middle Jurassic (Kockel *et al.,* 1977).

Aspro Vrisi-Chortiatis Unit: The unit includes deeper water equivalents of the sediments in the Melissochori-Cholomon unit, as well as igneous rocks ranging from ultramafics, diorites, dykes, volcanics and metagranitoids. Collectively they comprise the Thessaloniki-Metamorphosis Ophiolite Complex and the Chortiatis Magmatic Suite. The Chortiatis Group trends NW-SE and is bounded on the W by the mafic and ultramafic rocks of the Thessaloniki-Metamorphosis ophiolite and on the E by the Svoula Group. The western boundary of the Chortiatis Group is a linear, strongly sheared contact while the eastern boundary is more complex, in places being represented by a fault, but more commonly the contact with the Svoula Group is gradational and folded. The metasedimentary parts of the Chortiatis Group are presumed to be the deeper-water equivalents of the Svoula Group sediments (Kockel *et al.,* 1977).

Mussallam and Jung (1986) suggest that the Chortiatis Group rocks represent a volcanic arc formed above a subduction zone, which lay a few hundred kilometres to the west in the Subpelagonian Zone (Smith and Spray, 1984). Mussallam and Jung (1986) do not specifically suggest that transcurrent motion occurred along the subduction zone, but instead document lateral variations within the Chortiatis Magmatic Suite. They report a hypabyssal tonalite-trondjemite sequence in the NW of the area which grades into granophyres and submarine volcanic rocks into the SE.

They attribute this lateral variation to progressive attenuation of the continental crust towards the SE. The Halkidiki Ophiolite Complex exhibits similar lateral lithological and chemical variations and may have a similar history.

The Peonias Subzone is subdivided into two parts, the Peonias (revised) Subzone, which includes the Stip-Axios Unit and the Vasilika Unit, and the Circum-Rhodope Belt, comprising the eastern parts of the original Peonias Subzone. The Peonias (revised) Subzone is bounded on the west by the Paikon Subzone and on the east by the SMM. The Vasilika Unit includes the limestones near Petralona village and the Prinochori Beds. The Monopigadhon granite intrudes into the Vasiliki Unit.

The Stip-Axios Unit is defined here as including the rocks between the mafic and ultramafic lithologies of the Thessaloniki-Metamorphosis ophiolite and the limestone and metasediments (Prinochori Beds) of the Vasiliki Unit (Ricou, 1965).

The Stip-Axios Unit consists of amphibolite grade "basement" rocks and greenschist rocks which outcrop SW of the Aspro Vrisi-Chortiatis Unit. The amphibolite-facies rocks of the Stip-Axios Unit are traditionally regarded as thrust slices of the Vertiskos Group from the SMM (Kockel and Mollat, 1976; Kockel *et al.*, 1977; Greek 1: 50 000 geological map - Vasiliki sheet).

1.8.2 The Paikon Subzone

This subzone lies to the west of the Peonias Subzone and is separated from it by the Paikon Thrust (Figs. 1.3, 1.6). This subzone is represented by limestones, dolomites and shales, which are subsequently overlain by a variety of detrital sediments containing intercalations of shallow marine to sub-aerial volcanic debris. Finally, the sequence is intruded by a series of minor granitic intrusions (Mercier, 1960, 1966a, b, 1973a; Smith and Moores, 1974; Bebien *et al.*, 1980).

The Paikon Subzone represents an island arc system characterised by neritic marine sediments and volcanic rocks (Mercier *et al.*, 1975; Bebien *et al.*, 1987). Pre-Cretaceous, bimodal magmatic rocks (mafic submarine lavas and acidic tuffs or lavas) are intercalated with calcareous and siliciclastic sedimentary rocks. The volcanics yield a low K-tholeiitic affinity, but in the upper parts of the sequence subordinate tholeiites with MORB affinities also occur (Bebien *et al.*, 1987). During the Alpine orogeny the 8000 m-thick sequence suffered metamorphic recrystallisation but little deformation. The rocks contain a weak greenschist metamorphic overprint (Baroz *et al.*, 1987). In most of the lithologies the structural and textural features are those of the primary igneous or sedimentary protoliths. Where metamorphic recrystallisation was more dynamic, new mineral growth has partially replaced the primary textures.

1.8.3 The Almopias Subzone

The Almopias Subzone is geologically complex and is not well understood. It is bounded on the west by high-grade basement rocks of the Pelagonian Zone and on the east by the Paikon Subzone. The Almopias Subzone contains numerous ophiolite outcrops. Robertson and Dixon (1984) regarded this subzone as the main site of the Palaeotethys while others regard it as a Neotetethyan ocean basin remnant. At this time evidence suggests a Neotethyan age for the preserved ophiolites. Robertson and Dixon (1984) note, however, that Neotethyan oceanic crust does not preclude the possibility of Mesozoic spreading as a ridge system within a Palaeotethyan basin.

Baroz *et al.,* (1987) suggest that ocean floor spreading occurred during the Early and Middle Jurassic within the Almopias basin, and that an east-dipping oblique subduction zone was initiated during the Middle Jurassic. The subduction of the Almopias Subzone basin led to the creation of small oceanic back arc basins in the Peonias Subzone. Subduction was terminated with the emplacement of the Hellenic ophiolitic nappes thrust eastward on to the Paikon platform during a major pre-Tithonian tectonic phase (JE1 of Vergely, 1976; Sharp, pers. comm.).

1.8.4 Summary

Various structural sequences and debatable interpretations have been proposed for the Vardar Zone (e.g. Mountrakis, 1984, 1986; Vergely, 1977, 1984; Patras *et al.,* 1989; Sharp, pers. comm.). The metamorphism throughout all three subzones is accepted as being dominated by a regional greenschist event of Late Cretaceous age (Mercier, 1973a). Age constraints on the ophiolites within the Almopias Subzone have been defined as pre-Upper Jurassic from evidence derived from overlying sediments (Mercier, 1973a; Pichon, 1979). In contrast data from whole rock radiometric analyses for the igneous crystallisation of the ophiolites, suggest a Middle Jurassic spreading age (Roddick *et al.,* 1979; Spray and Roddick, 1980; Spray *et al.,* 1984; Section 1.9).

The final phase of all models for the evolution of the Vardar Zone involves the closure of the Vardar Ocean. This is considered by one group of authors to have resulted in the emplacement of the Subpelagonian ophiolites (derived from the Vardar Ocean) across the Pelagonian Zone, i.e. emplacement from east to west (Aubouin *et al.,* 1970; Bernoulli and Laubscher, 1972; Vergely, 1976, 1977, 1984). Others (e.g. Robertson and Dixon, 1984) consider the Subpelagonian ophiolites to have been derived from the Pindos Ocean basin to the west. Final closure of the Vardar Ocean is considered to be of Upper-Jurassic Lower-Cretaceous age (Jacobshagen *et al.,* 1976;

Vergely, 1984) and characterised by a number of granite intrusions and thrusting episodes (Figs. 1.5, 1.6). From the derived or inferred dates of major events within the Vardar Zone, broad constraints on the history of the SMM can be developed. This is particularly helpful when attempting to model the role of the SMM within the evolution of the Eastern Mediterranean (Chapter 6).

1.9 Radiogenic Constraints for the SMM

The determination of radiogenic ages was beyond the scope of this study, but are considered to be important in dating the evolution and subsequent models of the SMM. This review is based predominantly on two recent studies, a review by Dixon and Dimitriadis, (1984), and new data and further review by De Wet, (1989). The majority of the examples have been used either directly or indirectly to delimit the evolution of the SMM in a regional setting (Chapter 6). The presently available radiogenic data for the Internal Hellenides, and specifically the SMM, are presented in Appendix II.

Isotopic ages from the SMM (in Greece) published to date have been K/Ar determinations on muscovites, biotites and hornblendes, as well as Rb/Sr model ages determined on muscovites and biotites (Borsi *et al.*, 1965; Harre *et al.*, 1968; De Wet and Miller, 1985). Ages for the SMM fall into several groups. Near the western contact with the Circum-Rhodope Belt, but well to the north of Thessaloniki, Borsi *et al.*, (1965) obtained ages from white micas by both methods in the range 280-300 Ma. This range is suggestive of a slightly reset pre-Triassic, Late Hercynian, metamorphic age (Dixon and Dimitriadis, 1984). The implication is that the Jurassic deformation and recrystallisation event in the north was not sufficiently intense to fully reset the isotopic systems in white mica in a metamorphic basement last re-crystallised in Late Carboniferous times. Further to the SE, away from the contact, Harre *et al.*, (1968) obtained ages of 138 ± 2 Ma and 195 ± 3 Ma (ages calculated using the constants of Steiger and Jager, 1977) from different size fractions of white mica from a schistose pegmatite within the Vertiskos Group. This sample was taken from a region close to the boundary between "Jurassic" fabric trends and "pre-Mesozoic" fabric trends (Dixon and Dimitriadis, 1984). Further east two amphibolites from just within the eastern and northern margins of the Volvi Complex yielded late Lower Cretaceous ages in the range 116 to 111 ± 3 Ma. A schistose pegmatite at the eastern side of the Vertiskos outcrop, NE of Lachanas, yielded a K/Ar age of 107 ± 1.6 Ma from muscovite. Ages in the higher-grade migmatitic gneisses of the Kerdilion Group east of the Vertiskos Group are all much younger. These K/Ar muscovite ages are closely

grouped from 36 to 43 Ma (all ± <1 Ma) with biotite ages 32 to 38.5 Ma. A single K/Ar determination on hornblende from an amphibolite within the Kerdilion Group yielded 79.5 ± 1 Ma.

Therefore existing K/Ar and Rb/Sr isotopic ages provide a 300 Ma age at the western boundary of the Massif, which progressively decreases to a minimum age of 36-40 Ma at the eastern boundary (Borsi *et al.,* 1965; Harre *et al.,* 1968; De Wet and Miller, 1985).

In order to explain the younging of isotopic ages from west to east several models have been proposed. Harre *et al.,* (1968) and Kockel *et al.,* (1977) interpreted this phenomenon as "rejuvenation" of an earlier pre-Hercynian basement and relegated the associated metamorphic effects to retrograde metamorphism. Alternatively, Dixon and Dimitriadis (1982, 1984) suggested that the ages represent cooling, from a Late Jurassic regional metamorphism event which was followed by uplift progressively later and greater towards the east (Chapter 6).

1.9.1 The Stip-Axios Unit

Radiometric age data are extremely limited for the rocks of this unit. The greenschist-facies rocks maybe correlated with the Chortiatis Unit and thus are probably Triassic-Jurassic in age. The amphibolite-facies rocks (Galarinos Subunit) have been tentatively correlated with the SMM (Kockel *et al.,* 1977; Schunemann, 1985). This correlation implies a Late Palaeozoic age for the peak of metamorphism, as this is the generally accepted age of the main metamorphism of the SMM (Borsi *et al.,* 1965; Kockel *et al.,* 1977). This interpretation of the SMM has been challenged by Dixon and Dimitriadis (1984) who suggested a substantial overprinting event during the Mesozoic. De Wet (1989) dated biotite from a highly deformed granitic lithology with a distinct biotite/garnet chemistry using the Ar/Ar stepwise heating technique. The Ar/Ar results yielded a well-developed isotopic plateau of 160 ± 1.7 Ma. Ideally many more determinations on various minerals from different lithologies are needed in order to interpret the timing of geological events confidently (De Wet, 1989). However, the following are possible interpretations (De Wet, 1989):

1) The plateau dates the crystallisation of the biotite from a magma (assuming the granite gneiss was a granite).
2) The plateau dates the peak of metamorphism.
3) The plateau dates greenschist overprinting associated with late deformation.
4) It is an intermediate age.

Considering the alteration and extensive deformation that the rock has undergone it is unlikely to represent the primary (igneous) or the peak metamorphic event. If it does represent the timing of the peak metamorphic event, then this event is not Late Palaeozoic but rather Jurassic (De Wet, 1989). This would result in a complete re-evaluation of the Stip-Axios Unit's evolution and geotectonic origin. However, other evidence, including structural and metamorphic evidence, appear to support a pre-Mesozoic age for the main metamorphic and deformational event. Thus the 160 ± 1.7 Ma may represent the timing of the greenschist event or be intermediate.

1.9.2 The Thessaloniki-Metamorphosis Ophiolite Complex

Isotopic age data for the ophiolitic lithologies are limited. This is partly due to the difficulties in dating metamorphosed and altered mafic and ultramafic lithologies. There are two groups of age dates from the ophiolite, one group from the basic lithologies and another from later cross-cutting pegmatites.

Sapountzis (1969) determined a whole rock K/Ar age of 1400 to 1300 Ma on a hypersthene gabbro from Panorama to the east of Thessaloniki. Sapountzis (1980) determined ages using the whole rock K/Ar technique on gabbros from the major outcrops of the ophiolite (Vasilika-Galatista, Vavdos, Gerakini and Metamorphosis) which give ages between 42 ± 8 and 311 ± 30 Ma. K/Ar whole rock age dates are difficult to interpret because this technique is susceptible to resetting and excess argon (De Wet, 1989). This is especially true of deformed mafic rocks from ophiolites. The wide scatter of ages obtained by Sapountzis (1980) also suggests uncertainties. New data presented by Jung *et al.,* (1981) and De Wet (1989) confirm the presence of excess argon.

Jung *et al.,* (1981) referred to a K/Ar age on a hornblende from the youngest unit of the Halkidiki ophiolite which gave an approximate age of 160 Ma. Mussallam and Jung (1986) referred to a K/Ar igneous hornblende age of 172 ± 4.8 Ma from a gabbro dyke in dunite from the Halkidiki ophiolite.

De Wet (1989) determined several Ar/Ar total fusion ages for hornblende from amphibolites within the ophiolite near Vavdos village. These results yielded inconsistent ages (Appendix II). Numerous pegmatites cross-cut the ultramafic and mafic parts of the ophiolite near Vavdos and Metamorphosis. The pegmatites at least partly predate the deformation of the host rocks, and are strongly sheared. Burgath *et al.,* (1979) recorded K/Ar muscovite model ages of 155.6 ± 1.1, 154 ± 2.5 and 125 ± 1.4 Ma from these pegmatites (see also Mussallam and Jung, 1986).

It is probable that these pegmatites formed after the emplacement of the ophiolite (Mussallam and Jung, 1986), and the time of their intrusion potentially determines a minimum age of the ophiolite (De Wet, 1989).

Burgath *et al.,* (1979) interpreted the fabric present in the pegmatites as the result of syn-intrusive cataclasis including folding and boudinage accompanied by albitisation of the microclines and syn-genetic healing.

Muscovite from a pegmatite within the ophiolite SW of Vavdos was dated using the Ar/Ar total fusion technique. It gave an age of 117 ± 2 Ma, which is significantly younger than the 155 Ma ages obtained by Burgath *et al.,* (1979). The pegmatites contain two generations of muscovite, coarse-grained, primary muscovite and finer-grained, secondary muscovite associated with the deformational fabric. The older ages probably represent the age of intrusion of the pegmatites and the younger ages reflect later deformation. The ophiolite must therefore have been emplaced before 150 Ma.

1.9.3 The Chortiatis and Svoula Groups

There are only very limited isotopic data for the Chortiatis Series and the Svoula Group. Sapountzis (1969) recorded a K/Ar age of 113 ± 4 Ma for muscovite from a chlorite-epidote-sericite-albite gneiss from the Chortiatis Magmatic Suite. This date probably reflects the deformation of these rocks and not their primary crystallisation age.

De Wet (1989) determined two whole rock Ar/Ar total fusion ages on phyllites from the Svoula Group. These determinations gave ages of 108 ± 2 and 109 ± 2 Ma, very similar to the above age on the sericite from the Chortiatis Group. These rocks contained two fabrics, a dominant axial planar cleavage and later crenulation cleavage. Whether these ages reflect either of these fabric forming events is uncertain (De Wet, 1989).

1.9.4 Jurassic Granitoids

Late Jurassic sediments occur in association with the Monopigadhon granite. This association is important as it may help in determining the age of the granite (De Wet, 1989). Ricou (1965) interpreted the metamorphic rocks adjacent to the Monopigadhon granite, as representing remnants of the country rock into which the granite was intruded. These rocks must have been eroded off before the deposition of the Late Jurassic limestones and Pinochori Beds. An alternative hypothesis holds that the contact metamorphic rocks represent the contact aureole between the granite and

the Late Jurassic sediments, indicating that the granite is younger than the Late Jurassic. The distribution of the contact metamorphic rocks, the unconformity between the overlying sediments and the granite (Kockel *et al.,* 1977), as well as the limited isotopic geochronology do not support this hypothesis, but it cannot completely be ruled out (De Wet, 1989).

The age of the granite is isotopically poorly constrained. Ricou (1965) recorded a K/Ar biotite age of approximately 180 Ma. This date may, however, be unreliable (Ricou, pers. comm., in De Wet, 1989). More recently Kreuzer (pers. comm., in Mussallam and Jung, 1986), has reported a K/Ar biotite date of 149 Ma. This date is probably more reliable but represents at best a cooling age and at worst, a meaningless intermediate date between the age of crystallisation and later metamorphic events. If so it may be too young to be useful.

According to Kockel *et al.,* (1977) the granite is unconformably overlain by fine-grained, recrystallised, bedded and reefal limestones with a basal horizon of sandstone. Upper parts of the limestones contain weakly metamorphosed iron-rich layers of bauxite. Conformably above the limestones lie the Prinochori Beds comprising alternating sandy phyllite, sandstone and "Hornsteinbanken" with one layer of limestone. The total thickness exceeds 600 m. These sediments are only very weakly metamorphosed with a poorly developed spaced cleavage. These beds are correlated with the phyllites near Neachoroundha and with the phyllites and calci-turbidites on Kelifos Island (Kockel *et al.,* 1977). The limestones are supposed to be of Kimmeridgian to Portlandian age (156 to 144 Ma; Ricou, 1965). The Prinochori Beds are Tithonian (Kockel *et al.,* 1977). This indicates that the granite must be somewhat older than Kimmeridgian in order for the granite's cover to have been eroded and the granite exposed by the formation of a Kimmeridgian (>155 Ma) unconformity (De Wet, 1989).

1.9.4 Tertiary Granitoids

Kockel *et al.,* (1977) suggested that the Sithonia Granitoid was related to the Arnaea Granite and was a Jurassic syn- or late-orogenic intrusion. Recently several attempts have been made to isotopically date the Sithonia intrusion. Using the K/Ar technique, Kondopoulou and Lauer (1984) obtained whole rock/mineral pair Rb/Sr dates of approximately 40 Ma. Christofides *et al.,* (1986) determined a Rb/Sr whole rock isochron date of 50.9 ± 0.5 Ma, with an initial ratio of 0.7072 ± 1. Muscovite Rb/Sr dates from two mica granites ranged from 54.5 ± 3.1 Ma to 45.6 ± 1.3 Ma and biotite dates ranged from 47.7 ± 0.8 Ma to 28.9 ± 1.1 Ma. Whereas Rb/Sr biotite ages

from the granodiorites ranged from 46.5 ± 0.9 Ma to 41.3 ± 0.7 Ma (Christofides *et al.*, 1986)

It is apparent that the isotopic age data contradict the intrusive age assigned by Kockel *et al.*, (1977) on the basis of field relationships and structure. De Wet (1989) obtained isotopic evidence from biotite and coarse-grained muscovite separates from an undeformed sample of biotite-hornblende granodiorite, as well as coarse-grained muscovites from pegmatites which cross-cut the intrusion to indicate an Eocene age. Previous studies have suggested that coarse-grained muscovite is more likely to reflect the igneous cooling age of the sample rather than a resetting age caused by subsequent deformational events (De Wet, 1989).

Muscovite samples from the Sithonia intrusion have similar, slightly saddle-shaped, step heating spectra. These saddle-shaped spectra are regarded as being indicative of excess argon-40, which in general tends to be associated with the crystallisation of igneous rocks rather than metamorphic events (Lanphere and Dalrymple, 1971; Lanphere, 1976; Roddick *et al.*, 1980). Plateau ages of approximately 49 Ma were determined by De Wet (1989). The integrated ages are 52.2 ± 0.5 and 51.2 ± 0.7 Ma respectively. The closest approximation to the true age can be considered as the minimum age reached at the low point of the saddles, which in this case gives ages of 50 ± 1 Ma and 49.4 ± 5.9 Ma.

It is noteworthy that as the cooling age of biotite depends on factors such as the rate of heat dissipation from the hot intrusion and erosion rates, it may be several million years younger than the crystallisation age of the granitoid. As the ages of the granitoid intrusion and pegmatites are probably very similar, the age of the intrusion probably falls between the biotite age and the minimum age reached at the low-point of the muscovite saddles, yielding an age of approximately 50 Ma.

Whole rock Rb/Sr analyses of the Sithonia intrusion by De Wet (1989) failed to yield any meaningful results. This failure was probably the result of initial Sr isotopic heterogeneiity in these young granites. The two clusters of points which were developed correspond to different parts of the granite. De Wet (1989) concluded that:

1) The Sithonia granitoid is unrelated to the Arnaea granite (c.f. Kockel *et al.*, 1977).
2) The Rb/Sr isotopic age data are inconclusive, perhaps due to initial Sr isotopic heterogeneiity.
3) The Sithonia intrusion may be divided into two plutons, each with slightly different initial Sr isotopic compositions.

4) The ^{40}Ar-^{39}Ar data show that the muscovites contain excess argon. This may result in a slight overestimate of the crystallisation age of the pegmatites. The biotite date from the well-defined plateau is younger than the muscovite dates and represents the biotite cooling age. The age of the granite intrusion probably lies in between these dates, namely approximately 50 Ma (Eocene).

1.10 Previous Tectonic Models

The classic reconstructions for Greece and the Eastern Mediterranean envisaged the closure of a single ocean basin, "Tethys". The Tethyan ocean was originally modelled as a large "V" shaped ocean widening towards the east (e.g. Argand, 1924; Wegener, 1924; Bullard *et al.,* 1965; Smith and Briden, 1977). Subsequent closure of the Tethys Ocean resulted in the development of the Hellenic-mountain chain and a suture zone interpreted to lie in eastern Greece and the present day Aegean sea, (Figs. 1.6, 1.7), the Vardar Zone (Aubouin *et al.,* 1970; Bernoulli and Laubscher, 1972).

This simple model has subsequently been improved, initially by the recognition of a second oceanic suture in western Greece (Pindos Zone, Smith, 1971; Robertson *et al.,* 1991), leading to the realisation that the continental collision within the Hellenides area consisted of a more complex series of events than was originally suspected. The generally accepted model for the tectonic evolution of the Hellenides now incorporates an older Palaeozoic ocean, "Palaeotethys", (Smith, 1971; Dewey *et al.,* 1973) dating from Permo-Carboniferous times and a younger Mesozoic to Early Tertiary ocean "Neotethys" (Sengor *et al.,* 1984; Robertson and Dixon, 1984; Dercourt *et al.,* 1986; for a summary of models published up to 1977 see Brunn *et al.,* 1977). The Neotethyan ocean developed by rifting of blocks off the northern margin of Gondwana during the Middle Triassic, creating a collage of microcontinents, which were subsequently transported to the north and progressively accreted to the active margin of Eurasia, (Figs. 1.6, 1.7; see Robertson and Dixon, 1984). This model requires the development of numerous minor Neotethyan oceans (possibly interconnected), separated by rifted continental blocks. Due to extensive research, the External Hellenides are now accepted as having developed by collision and accretion of these rifted blocks to the European continent. However, the Internal Hellenides of NE Greece are less well understood, with their initial origin and subsequent development poorly constrained. The Internal Hellenides are far more complex than originally envisaged (Section 1.5), having been subjected to major thrusting and

strike-slip events. However, much of the literature indicates that the SMM is in fact a late derived sliver off the Rhodope Massif.

Considering the SMM and Rhodope Massif to have acted as a single unit until fairly late in their history has resulted in a variety of different origins being proposed. Hadzi *et al.*, (1974) suggested that the SMM was a fragment of the Scythian platform displaced to the W-SW, whereas e.g. Janev *et al.*, (1979), Kozhoukharov *et al.*, (1980), believe that the SMM was a stable crustal unit closely linked to the northern Eurasian continent.

Dewey *et al.*, (1973) suggested that the SMM was actually part of NE Africa and was progressively transported N-NW (similar to the units of the external Hellenides), where it was accreted to the Moesian platform. This particular suggestion is disputed by Hsu *et al.*, (1977) due to the lack of a major suture zone in Bulgaria. All these arguments and others are discussed by a number of workers (e.g. Ivanov *et al.*, 1979; Ivanov, 1981), with the final scenario remaining contentious.

Although the origin of the SMM remains in question, the general opinion is to group the Internal Hellenides within the European margin. Robertson and Dixon (1984) made a series of palaeogeographical reconstructions involving strike-slip movement along the Eurasian margin (Fig. 1.7), showing stages of the evolution of the Eastern Mediterranean through time. Models derived from the work undertaken during this study are presented and described in Chapter 6.

1.11 Neotectonics

Greece lies within a zone of intracontinental extension and strike-slip Neotectonics (Fig. 1.8), the effects of which are particularly intense in northern Greece (Fig. 1.9). Hence, the geology and topography of NE Greece is characterised by the development of numerous major Neotectonic structures (Mercier, 1981; Lyberis, 1984; Pavlides, 1985; Mercier *et al.*, 1988; Pavlides and Kilias, 1987; Rousos and Lyssimachou, 1988). These structures are typified by the development of horsts and grabens, major basins and extensive normal and strike-slip faults, (Figs. 1.9a, b). Along the entire length of the SMM three distinct Neotectonic zones can be recognised. However it is the southern-most section of the SMM within Greece (Kroussia Block) which has been affected most strongly by the Neotectonic activity (Psilovikos, 1984). Of particular relevance to this thesis is the development of the Mygdonia Graben, highlighted by the Langadha and Volvi Lakes, (Fig. 1.9b). This graben dominates the area and has been formed recently (Miocene-Quaternary) in two distinct phases (Psilovikos, 1977; Fountoulis, 1980; Mercier *et al.*, 1983).

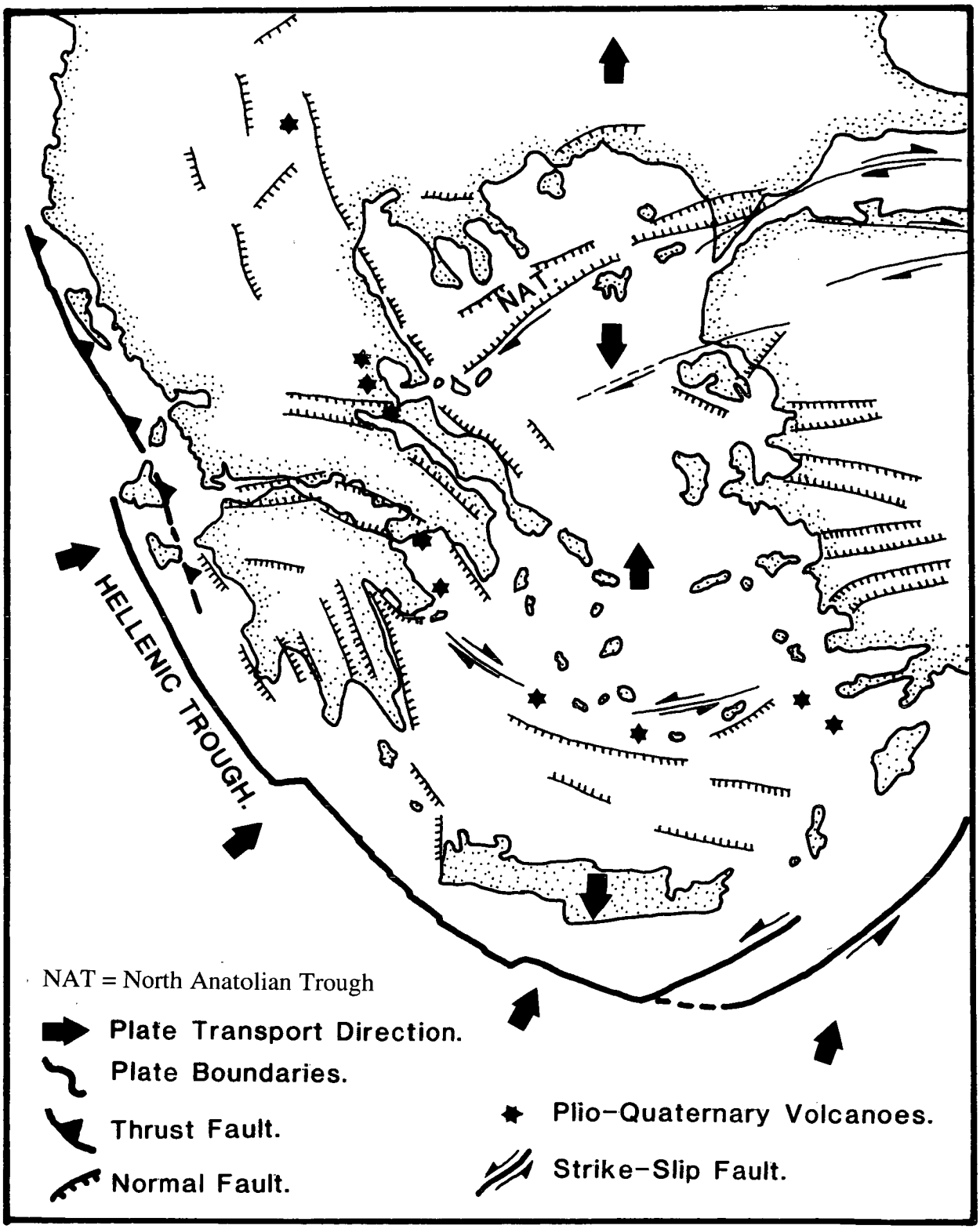

Fig. 1.8: Schematic Neotectonic reconstruction of the Aegean region, after Boccaletti *et al.*, (1974); McKenzie, (1978); Dewey and Sengor, (1979); Mercier *et al.*, (1979); Le Pichon and Angelier, (1981); Papazachos *et al.*, (1984) and Mountrakis *et al.*, (1987).

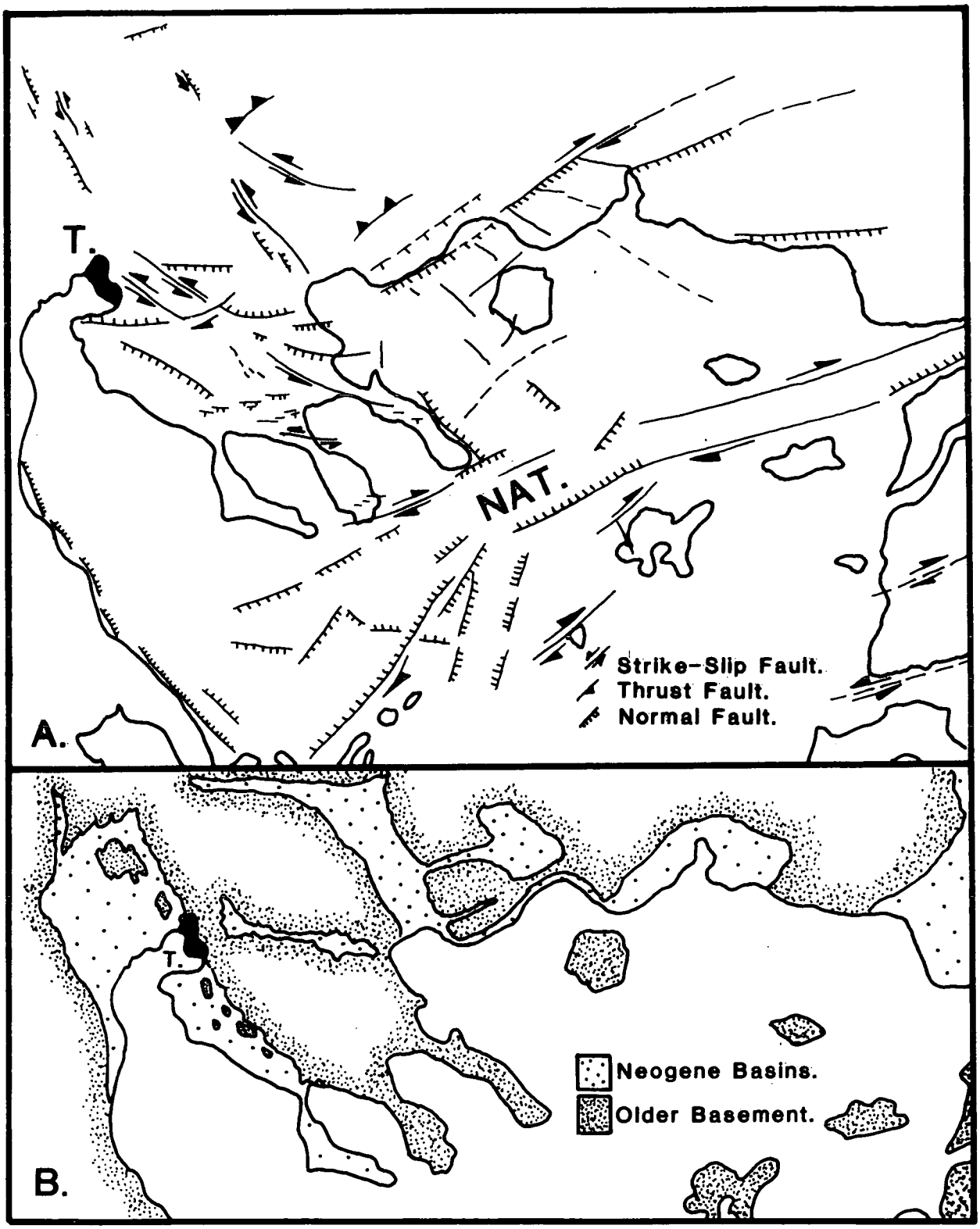

Fig. 1.9: Neotectonics of the Internal Hellenides of NE Greece, a) The main tectonic features active within NE Greece and the Aegean (NAT=North Anatolian Trough), b) Basin development as the result of Neotectonics. Modified after Psilovikos, (1984) and Pavlides and Kilias, (1987).

The Neotectonics of northern Greece can be categorised into three primarily extensional tectonic regimes (Fig. 1.8), (a) Late Miocene (NW-SE extension), with the NE-SW trending faults showing normal, pure, dip-slip displacements; (b) Pliocene to Early Pleistocene (NE-SW extension), with the NW-SE trending normal faults showing a distinct sinistral strike-slip component; and (c) Middle to Late Pleistocene (N-S extension) with the E-W trending fault planes again showing normal, pure, dip-slip movement, this stage of the Neotectonic evolution is also believed to be responsible for the North Anatolian Trough (NAT) and surrounding basins, (Lyberis, 1984; Mercier *et al.,* 1988).

The SMM is bounded by two NW-SE trending Neotectonic basins, the Struma-Strimon basin to the east and the Vardar-Axios basin to the west (Fig. 1.9b). Both of these basins are closely associated with major fault zones (Fig. 1.9a). Better understanding of these fault zones has enabled a re-interpretation of the boundary between the SMM-Rhodope Massif to be made. The boundary is now interpreted as a zone of left lateral wrenching (Karistineos and Sotiriadis, 1987), rather than the previous model of a major thrust emplacing the SMM over the Rhodope Massif (Kockel and Walther, 1965; Aubouin *et al.,* 1977; Jacobshagen *et al.,* 1978; I.G.M.E., 1983). It is questionable whether a similar interpretation can be derived for the fault/thrust zones for the western SMM-Vardar (Peonias) Zone boundary. However, left-lateral wrench faults do occur along the west side of the Vardar (Almopias) Zone (Jacobshagen *et al.,* 1976, 1978).

Studies of the Neotectonic activity and palaeomagnetic data have indicated that the SMM has undergone a clockwise rotation of about 25°-30° since the Oligocene (Kondopoulou, 1982; Kondopoulou and Westphal, 1986). Evidence from rotation has been detected in palaeomagnetic studies on Oligocene intrusives, and is the result of extensive Neotectonic faulting, combined with the strike-slip movements along the North Aegean Trough (Kondopoulou, 1982; Kondopoulou and Westphal, 1986). Neotectonic activity has clearly disrupted and reduced the coherence of structures and outcrop patterns within the study area (Inserts, Maps A to G). Numerous minor faults associated with the major Neotectonic structures reduce the lateral continuity of the earlier regional structures. However, the Neotectonics were not regarded as an initial objective of the thesis and therefore faults and recent sedimentation are only noted when clearly disrupting or obscuring the earlier structures and lithologies which form the basis of this thesis. It is also important to consider the rotation of the SMM when attempting to apply regional structures in the SMM with those of the Rhodope Massif in regional reconstructions. The angle of

relative rotation between the two massifs is approximately 25°-30° and would reduce the approximate NW-SE trend of the SMM, nearer to the E-W regional trend of the Rhodope Massif. The Neotectonic rotation may possibly be associated with the development of the 25-40 Ma isotopic ages found at the eastern margin of the SMM (within the Kerdilion Group). However, when reconstructing models for the evolution of the SMM the rotation should be considered as an important factor in the latest stages only (Chapter 6).

1.12 A Review of the Initial Interpretations for the Study Area

A review of the models produced by Dixon and Dimitriadis (1982, 1984, pers. comm.) for the origin of the Volvi Complex are presented below. At the start of this study these models represented the most recent interpretations for the origin of the Volvi Complex since Kockel *et al.,* (1971. 1977). The three models consisted of:

(A) *A Pre-Mesozoic Basement Model:* In this scenario the Volvi Complex belongs to the pre-Mesozoic basement of the SMM and was either tectonically or magmatically emplaced within it prior to the deposition of the Triassic cover and the last pre-Jurassic deformational event (Dixon and Dimitriadis, 1984). The metamorphic equilibration temperatures within the Volvi Complex, which are markedly higher than the envelope, appear to rule out the Volvi Complex being part of the basement. For the Volvi Complex to be a pre-Jurassic "basement" complex it would have to be argued that its metamorphism was synchronous with a very high-grade event in the "true" pre-Mesozoic basement of the envelope (not seen by Dixon and Dimitriadis, 1984). In addition the syn-tectonic staurolite grade event, found in the envelope would have to be represented by very localised recrystallisation in shear zones within the complex (again so far not recognised as important by Dixon and Dimitriadis, 1984). Limited observations by Dixon and Dimitriadis (1984) at the contact of the Volvi Complex did not eliminate this model, but tended to favour an in-situ rift origin (B). The link between magmatism and the main deformation event in the Volvi Complex would not be expected if the igneous rocks were Palaeozoic or older and the deformation post-Triassic and continuous into the "cover" (Dixon and Dimitriadis, 1984).

(B) *An In Situ Mesozoic Rift Model:* This model involves the Volvi Complex being an essentially in situ syn-/or late-orogenic intrusive complex of Mesozoic age, developed during a deep-level extensional event occurring within the SMM during active deformation (Dixon and Dimitriadis, 1984). This model accounts for the higher temperatures of equilibration within the Volvi Complex compared to the envelope,

and for the link between magmatism and deformation. This model would be substantiated further if granitic melts (local melting of the country rock) were developed in the marginal zone of the complex as a direct result of intrusions related to the complex. If the original contacts are preserved a sharp rise in regional metamorphic grade to silliminite- or kyanite-bearing migmatites might be expected within the envelope gneisses. The staurolite-garnet-schists found by Dixon and Dimitriadis (1984), may themselves be in a syn-tectonic thermal aureole. Systematic isotopic age progressions should occur, related to prolonged cooling in the high-temperature complex and its aureole, if uplift was uniform over the area during cooling. Geobarometry should provide a vital constraint on the consistency of depth inside and outside the complex (Dixon and Dimitriadis, 1984).

(C) *An Ophiolitic Suture Zone Model:* This option interprets the Volvi Complex (and the associated ultramafic bodies found within the study area) as being originally emplaced as a high-level ophiolite complex during the Mesozoic and subsequently metamorphosed at deeper levels during micro-continental collision. Jurassic metamorphism and deformation would then be superimposed on low-pressure igneous or sub-sea floor metamorphic assemblages (Dixon and Dimitriadis, 1984). Most of the objections to the pre-Mesozoic basement model (A) also apply to this model, particularly the metamorphic grade discontinuity and the absence (not recognised so far by Dixon and Dimitriadis, 1984) of any lower-grade precursor assemblages. This could be explained by final re-thrusting and stacking together of slices from different parts of one deeply buried suture zone. As before the early syn- to late-magmatic character of the deformation and mineral assemblage formation go against this. Dixon and Dimitriadis (1984) have not yet shown conclusively that the syn-magmatic fabrics are all related kinematically to the main post-magmatic fabric even though their initial field and thin-section data point that way. Metasedimentary screens in the dyke-complex are not likely in an idealised oceanic setting but not impossible. An aureole in the envelope would rule out a simple, originally allochthonous, ophiolite model.

The in situ rift and suture models (B and C) are clearly not completely mutually exclusive. Dixon and Dimitriadis (1982; 1984; pers. comm.) proposed that the Volvi Complex could be a fragment of an original continent-ocean boundary zone of Jurassic or Early Cretaceous age. It is important to note that these models developed by Dixon and Dimitriadis (1982; 1984; pers. comm.) were intended simply as a preliminary interpretation of their exploratory studies of the Volvi Complex and limited observations from the envelope.

CHAPTER 2

LITHOSTRATIGRAPHIC RELATIONSHIPS AND MAJOR IGNEOUS INTRUSIONS

CHAPTER 2

2.1 Introduction

The area of study around Lake Volvi historically contains five lithological groups; the Kerdilion, Vertiskos and Volvi Metasedimentary (re: Svoula) Groups, the Volvi Complex, and Granitoids, after Kockel *et al.*, (1971, 1977), Kauffmann *et al.*, (1976); *see* review in Chapter 1. However, a number of distinctive formations identified during this study have enabled a better determination of the overall structure of the area to be made. Consequently, a reappraisal of the lithostratigraphic sequence is made in Section 2.7.

However, the distinctive style and character of deformation within the Lake Volvi area (Chapter 3), has posed acute problems for describing the pre-deformational lithostratigraphic succession. The rocks in the area studied have been deformed in a series of anastomosing shear zones which have an inherently variable attitude in three dimensions. Strain has been partitioned amongst the zones in a complex way in space, and time, so that no single surface, let alone one of a constant orientation in space, can be identified as dominating the deformation at any stage. The best analogue of the bulk deformation is of a pile of flattened, low-strain, lozenge shaped cores, or "halibuts" (following John Dewey, oral presentation Edinburgh, 1991), with deformation concentrated at the margins of individual "fish", in the form of anastomosing high-strain shear zones (Chapter 3).

In some areas, e.g. the Vamvakia river (Section 2.3.2), a structural sequence is identifiable in that the "halibuts" are flatter and are on top of or beneath adjacent "fish", as found at the present time. The sequence however, is not necessarily restorable in a simple way as "out-of-sequence" is not distinguishable from "in-sequence" or normal tectonic juxtaposition. The area is further complicated by extensive arrays of Neotectonic faulting, which disrupt the continuity of the exposure (Section 1.11). The lithostratigraphic sequences are based on the spatial arrangement of lithological formations at the present time, supported by structural, metamorphic and geochemical data (Chapters 3, 4 and 5 respectively). It must therefore be accepted that the proposed lithostratigraphy (Section 2.7) is neither in general nor often in detail a sedimentary succession. Due to the complexity of the area there is no single locality where the entire lithostratigraphic sequence is present. Hence the aim of the mapping during this study has been to identify coherent components of a pre-shear zone succession within individual "fish", to look for consistent sequences between "fish" and to extract a "best-fit" pre-shearing lithostratigraphic sequence.

2.1.1 Terminology

Precise definitions of certain terms used in this Chapter have been matters of intense debate in the past. With respect to the Lake Volvi area, the literature is full of terms used in unconventional and contradictory ways, partly because of translation problems. Therefore the definitions of potentially contentious terms which are used in this Chapter, are described in order to reduce any ambiguity which may arise.

Most of the medium to high-grade lithologies are described either as "gneiss" or "migmatite", with an additional compositional qualification. "Gneiss" is used to denote medium- to coarse-grained rock with a pervasive fabric in hand specimen. The pervasive fabric need not include a compositional layering (commonly called "gneissic layering", e.g. Hobbs *et al.*, 1976; Yardley, 1989). "Orthogneiss" and "paragneiss" are used to describe gneiss of inferred igneous and sedimentary parentage respectively.

"Migmatite", following the non-genetic definitions of Mehnert (1968) and Ashworth (1985), is a composite rock comprising quartzofeldspathic or feldspathic portions of plutonic appearance and portions of metamorphic appearance. The pale-coloured, quartzofeldspathic component is described as "leucosome", and the part resembling a gneissic metamorphic rock is termed "mesosome". A third component, commonly dark in colour, is referred to as "melanosome". Melanosome generally occurs between leucosome and mesosome, and is depleted in quartzofeldspathic material compared to the mesosome. Most of the low grade lithologies are described as "schists", with an additional prefix according to their most prominent minerals. "Schist" is distinguished from "phyllite" by having a coarser grain size and a tendency towards an undulose cleavage.

The term "amphibolite" is used to describe a lithology with an approximate, basic igneous composition and an amphibolite-facies or epidote-amphibolite facies assemblage. No allowance is made for distinguishing the identity of the parental rock, e.g. fine-grained basalt, dolerite, gabbro or metasediment, which often cannot be determined. All the lithologies observed and studied within this area have been metamorphosed to at least the greenschist-facies. Consequently the terminology used for describing the lithologies should reflect their metamorphic status, e.g. terms such as gabbro and dolerite should have a "meta-" prefix. However, in order to simplify some of the terminology, this prefix has been dropped.

"Formation" is used as an informal term to describe a mappable lithology or series of lithologies. Descriptions of the formations are based on a series of correlatable local type-sections, rather than a single type-section. The term "group" is used for a series of adjacent formations.

PART I: Lithostratigraphic Relationships

2.2 The Kerdilion Group

2.2.1 Introduction

Exposure of this group is generally poor due to dense tree cover over the hill-sides, and overgrown streams and gullies. However, four traverses have been made into the Kerdilion Group, along a series of roads and tracks (Rendina to Stavros, Section 2.2.2; east of Modhi, Section 2.2.3; Arethousa to Vrasna [Vamvakia to Vrasna], Section 2.2.4; east of Stefanina, Section 2.2.5) *see* Inserts, Maps F and G. Displacement of formations along large km-scale anastomosing shear zones have disrupted the stratigraphic sequence (Fig. 2.1). However, best-fit lithostratigraphic sequences can be compiled for each traverse (Fig. 2.2). The sequences have been correlated to develop a composite lithostratigraphic sequence for the Kerdilion Group (Fig. 2.4; Section 2.2.6). The traverses, sample localities and areas of specific interest can be located on Maps F and G (Inserts). Traverses 1 and 2 lie along and south of a major fault zone (Kockel *et al.*, 1971, 1977) which runs along the line of traverse 1. Traverses 3 and 4 lie to the north of this fault zone, but are cross-cut by smaller fault arrays. Although in certain areas faulting is severe, a degree of continuity of lithological sequences is always preserved.

The formations of the Kerdilion Group generally dip towards the west. The lithostratigraphic sequence consists of metasediments in the west (upper part of the sequence) which are juxtaposed and apparently overlie a series of migmatites and gneisses (possibly basement) in the east (Fig. 2.1). This sequence has been interpreted as representing progressive younging (structurally up section) towards the west. The main objective of studying the Kerdilion Group was to understand its structural relationship to the Vertiskos Group. As the contact is poorly exposed, a broader comparative study of the lithologies, structure and metamorphic evolution of the two groups was made, and the contact relations have been re-interpreted in the light of this comparison (Section 2.7).

2.2.2 The Rendina-Stavros Traverse

This traverse consists of a series of road-cuttings along the main Thessaloniki to Asprovalta road. Additional key localities occur around the ancient ruins at Rendina, the World War II gun emplacement opposite the T-Junction to Stavros and road-cuttings along the road to the east of Stavros. Outcrops are grouped into sections approximately 200-300 m long, separated by areas with no exposure. Contact relationships between the formations are rare, and when present are mostly obscured by the strong regional foliation (S_2). Along this traverse the regional S_2 foliation

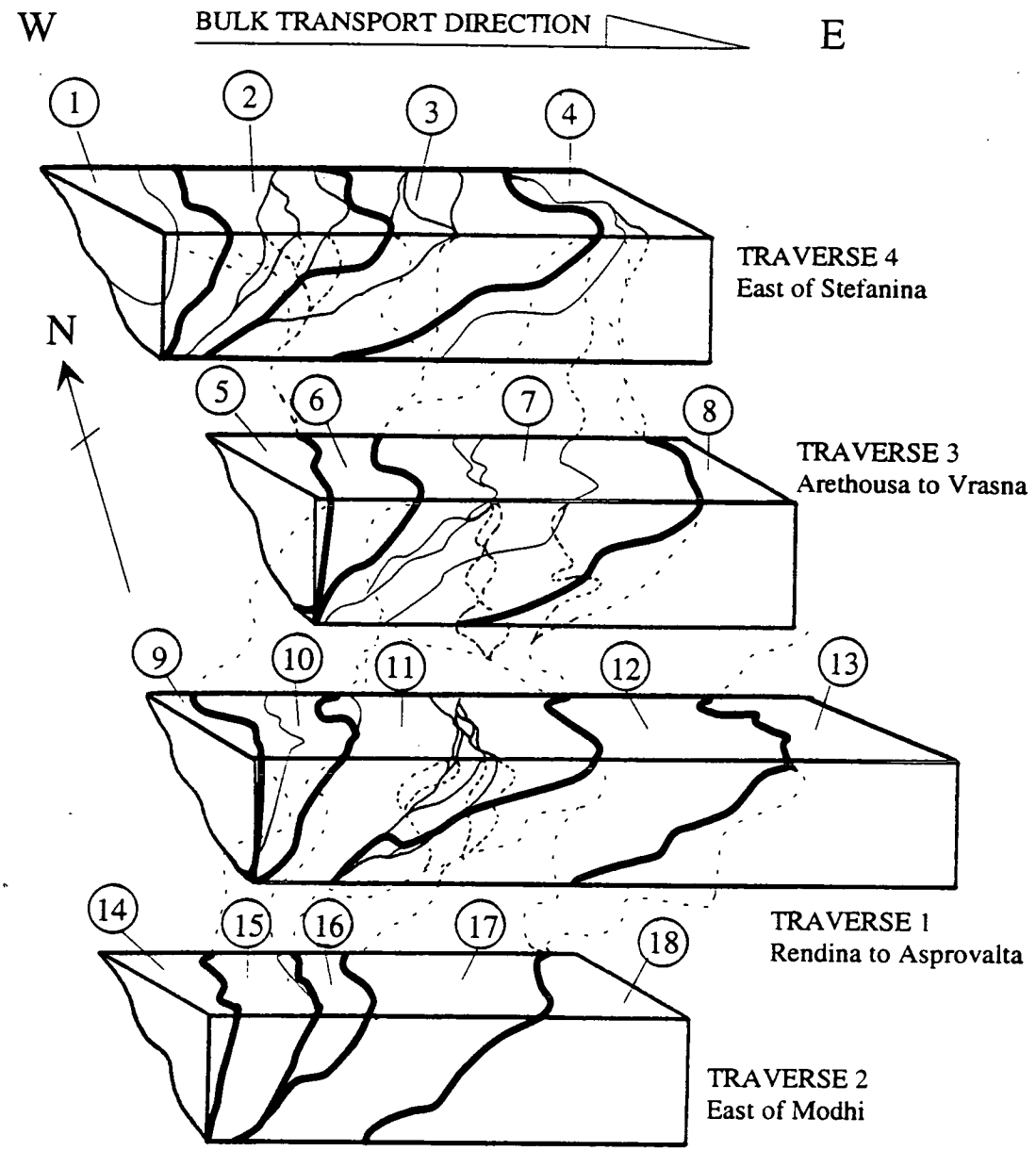

1. Arethousa Ultramafic Member
2. Stefanina marble Formation
3. Limni Amphibolite Formation
4. Stefanina Amphibolite Formation
5. Vamvakia Mafic Formation
6. Vrasna Marble Formation
7. Vrasna Feldspathic Gneiss Formation
8. Vrasna Amphibolite Formation
9. Vamvakia Mafic Formation
10. Rendina Marble Formation
11. Rendina Ruins Banded Gneiss Formation
12. Rendina Amphibolite Formation
13. Gun-emplacement Gneiss Formation
14. Askos Garnet Mica Schist Formation
15. Modhi Marble Formation
16. Modhi Granitoid Formation
17. Modhi Leucocratic Gneiss Formation
18. East Modhi Amphibolite Formation

Fig. 2.1: Schematic block diagrams representing the four traverses into the Kerdilion Group. The main features to note are the large (km-scale), anastomosing shear boundaries between formations. Circled numbers refer to the different formations (*see* Fig. 2.2).

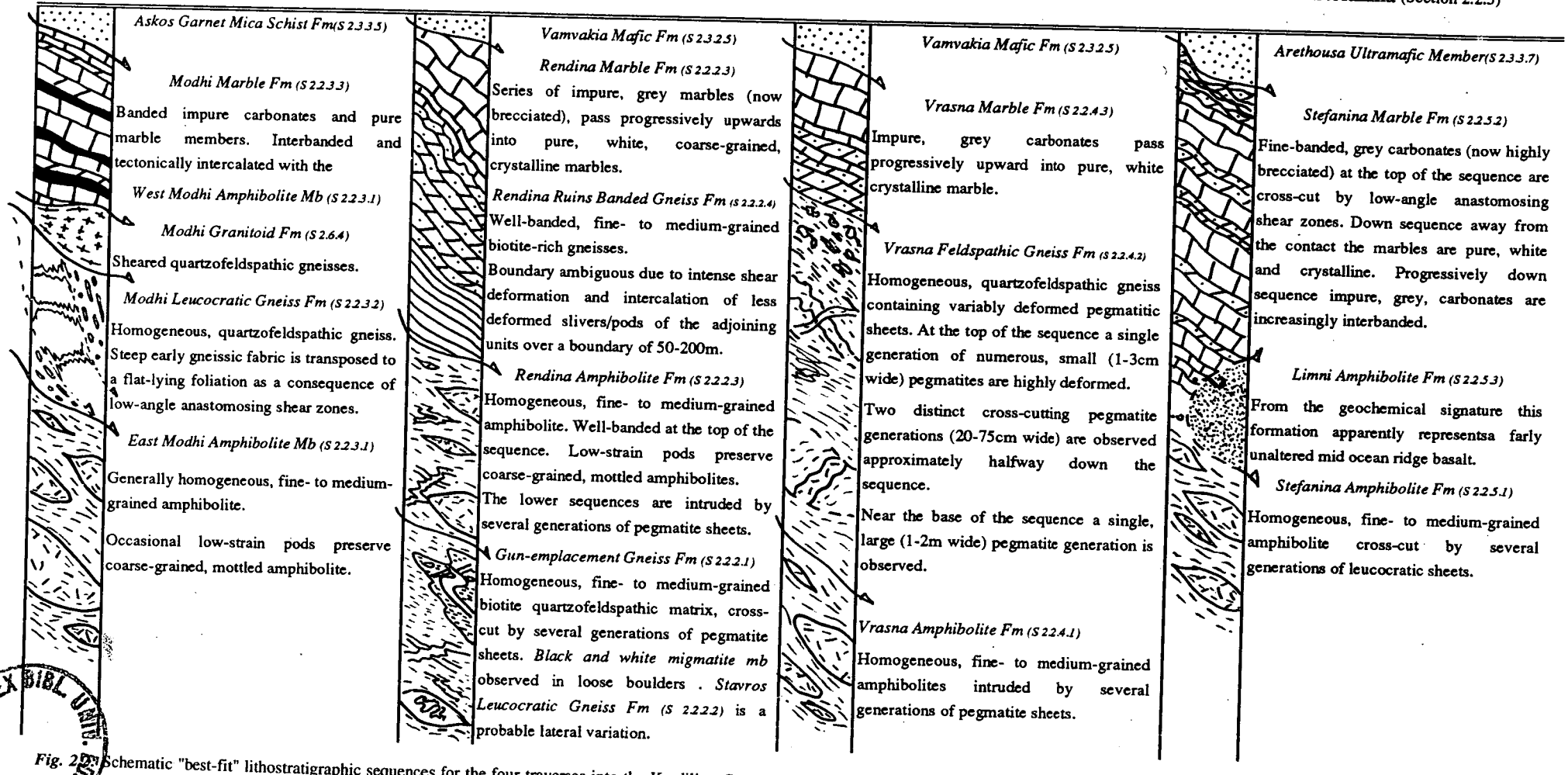

Fig. 2.2: Schematic "best-fit" lithostratigraphic sequences for the four traverses into the Kerdilion Group (*see* Fig. 2.1). The columns represent a generalised sequence of the formations in their present positions. However, it must be noted that these do not truly represent an original sequence due to displacement along anastomosing shear zones.

maintains a relatively consistent strike (from 007° to 027°), but has an extremely variable dip, (from 55°W to horizontal). This is interpreted as an effect of, km-scale, anastomosing shear zones affecting the Kerdilion Group (Fig. 2.1; Chapters 3 and 6).

2.2.2.1 The Gun-emplacement Gneiss Formation

This formation crops out at the World War II gun-emplacement opposite the T-Junction to Stavros (Fig. 2.3). Contact relationships with the adjacent formations to the east and west are not exposed. From a study of fabric development a small yet significant outcrop of black and white migmatite (c.f. Mehnert, 1968; Ashworth, 1985) appears to constitute the earliest lithological member. This migmatitic member has only been observed in a couple of large, loose, locally derived, fallen blocks. The actual outcrop is likely to occur further up the hill-side, obscured by vegetation and badly weathered. The migmatite (Plate 2.1) shows well-developed 1-3 cm thick leucosomes of quartz and plagioclase. The leucosomes are bounded by thin (1-4 mm thick) melanosomes of black predominantly biotite-rich material. The leucosome and melanosome are contained within a mottled, medium- to coarse-grained gneissic matrix (the mesosome), composed predominantly of quartz, plagioclase and biotite. The leucosomes appear slightly flattened and close to tightly folded, sub-parallel with a weak axial planar foliation contained within the mesosome. The foliation in the mesosome is caused by segregation of the quartzofeldspathic and biotite components. This weak foliation is cross-cut by a large 10-50 cm thick pegmatitic/aplitic sheet. A possible explanation for the lack of extensive migmatitic outcrops within the area is that the strong regional foliation completely transposed the migmatitic fabric, however, local pegmatite intrusions prevented intensification of the originally weak regional foliation preserving minor pods containing the original migmatite fabric.

The main lithological member present within the area is a largely monotonous medium- to fine-grained, homogeneous, quartz-plagioclase-biotite gneiss. However, this gneiss member is occasionally banded on a cm-scale, with the gneissic banding showing tight to isoclinal folds. Within the more homogeneous quartzofeldspathic biotite matrix no fold structures are observed unless pegmatites are present. This unit contains a variable gneissic foliation, the nature of which apparently depends on the degree of deformation, e.g. when low degree of deformation, well-defined leucocratic gneissic banding is preserved. It is possible that the gneiss is a highly deformed (high-strain) variation of the migmatite member, with the migmatite precursor preserved in low-strain pods/screens. However, no intermediate stage between migmatite and homogeneous quartzofeldspathic biotite gneiss has been observed. A regional continuous foliation (S_2), runs throughout this formation with a generally

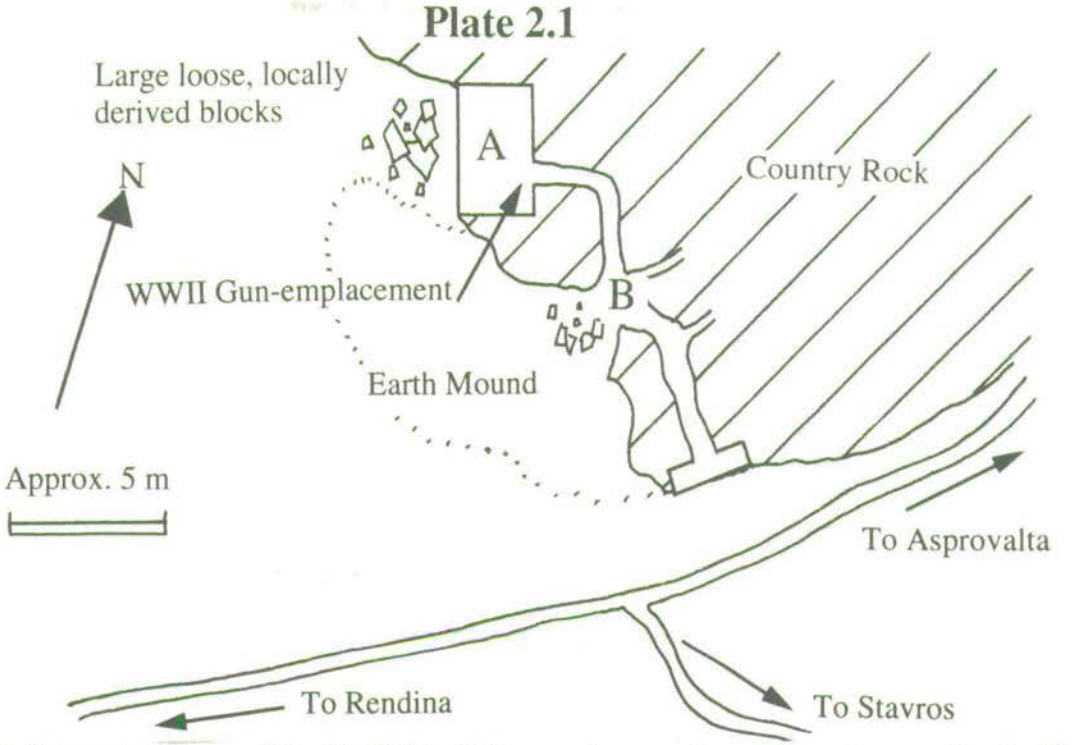

Fig. 2.3: Schematic diagram of the World War II Gun-emplacement (Insert, Map G), opposite the T-Junction to Stavros, immediately N of the Rendina to Asprovalta road. Several cross-cutting generations of pegmatite are well-exposed at the entrances A and B (Section 3.9.1).

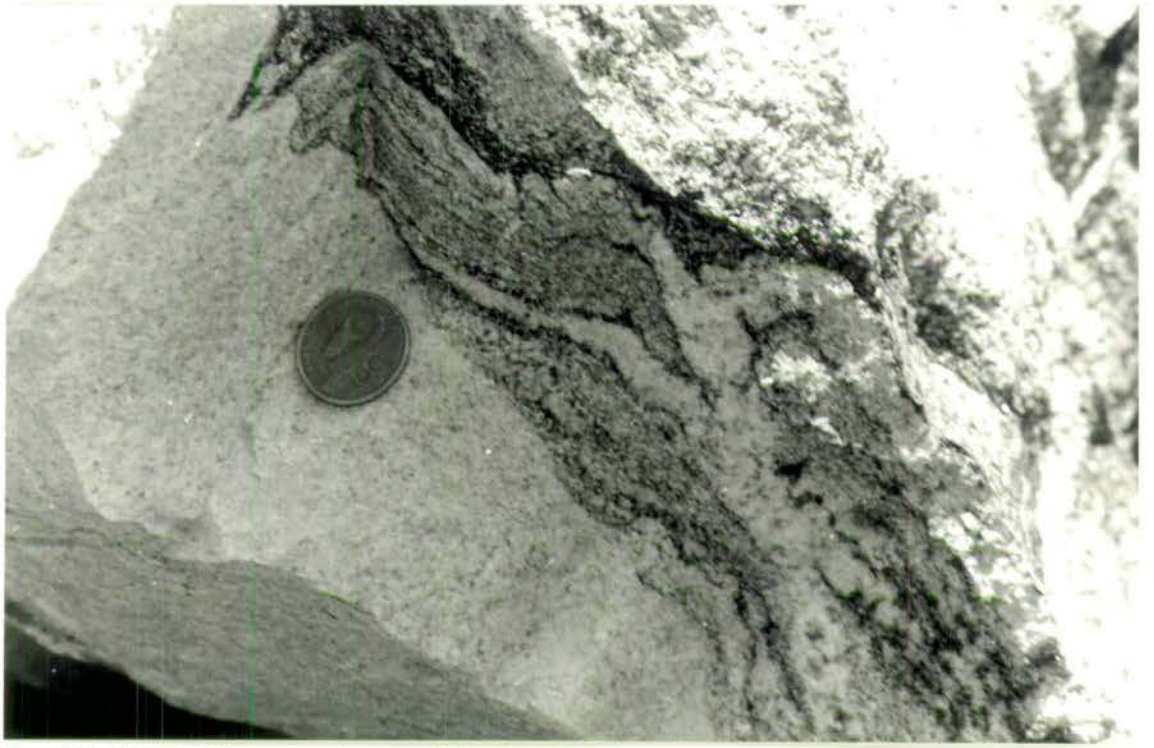

Plate 2.1: View looking approximately NE at the Gun-emplacement Migmatite Member (Section 2.2.2.1), observed in a large (2-4 m wide) loose block in front of entrance A (Fig. 2.3). The migmatite has well-developed 1-3 cm thick leucosomes, bounded by thin (1-4 mm thick) black biotite-rich melanosomes. These leucosomes are close to tightly folded and aligned parallel to the axial planar foliation which is developed in the mesosome. These migmatitic fabrics and structures are cross-cut by a 10-50 cm thick leucocratic (pegmatitic/aplitic) sheet. The coin is 28 mm in diameter.

horizontal dip and variable strike.

The gneiss member is shot through by at least three generations of pegmatitic sheets which are recognised as the only intrusive event within this formation. Distribution of the large volume of pegmatitic material (20-30% of the rock) is variable. These pegmatite generations are characterised by variations in the degree of deformation, thickness and composition (Section 3.9.1).

2.2.2.2 The Stavros Leucocratic Gneiss Formation

This formation crops out in a series of large road-cuttings, east of Stavros (Section 3.9.3). The main lithological member is represented by a medium- to fine-grained quartz-plagioclase-biotite gneiss, similar to the gneissic member which crops out at the gun-emplacement (Section 2.2.2.1). Contained within the gneissic matrix are at least four generations of leucocratic (pegmatitic/aplitic) sheets (Section 3.9.3). The leucocratic sheets are composed of an homogeneous, medium- to fine-grained, predominantly quartzofeldspathic matrix, and make up 20% of the outcrop. These leucocratic sheets are considered to be analogous to the pegmatite/aplitic sheets at the gun-emplacement (Section 2.2.2.1), and give the formation a distinctive character in the field. This formation is considered to be simply a lateral variation of the Gun-emplacement Gneiss Formation (Section 2.2.2.1), although described as a different formation here due to the lack of continuous outcrop between the two formations.

2.2.2.3 The Rendina Amphibolite Formation

This formation crops out either side of the road, approximately half-way between Rendina and the WW II gun-emplacement. The formation is exposed in dispersed (10-50 m long) road-cuttings, which are variably covered in vegetation. Contact relationships with the Gun-emplacement Gneiss Formation (Section 2.2.2.1) to the east are not exposed. The formation consists of a series of amphibolites with grain sizes varying from 0.2-1.5 mm. The medium- to coarse-grained varieties appear homogeneous and mottled (Plate 2.2a), whereas banding occurs on a mm- to cm-scale in the medium- to fine-grained varieties (Plate 2.2b). A progressively well-banded, fine-grained and foliated/sheared sequence is observed towards the inferred western contact with the Rendina Ruins Banded Gneiss Formation (Section 2.2.2.4).

The coarse-grained amphibolites are unfoliated, and represent either late intrusions or low-strain cores wrapped by fine-grained amphibolites. Medium- to fine-grained amphibolites always contain at least one strong (S_2) foliation and occasionally a minor sub-parallel (S_1 or early S_2) foliation (Chapter 3). Foliations dip between 25° and 45°W, with an approximate NNW-SSE to NNE-SSW trend. Intersection lineations produced by the foliations, plunge approximately 33°/286°.

Plate 2.2

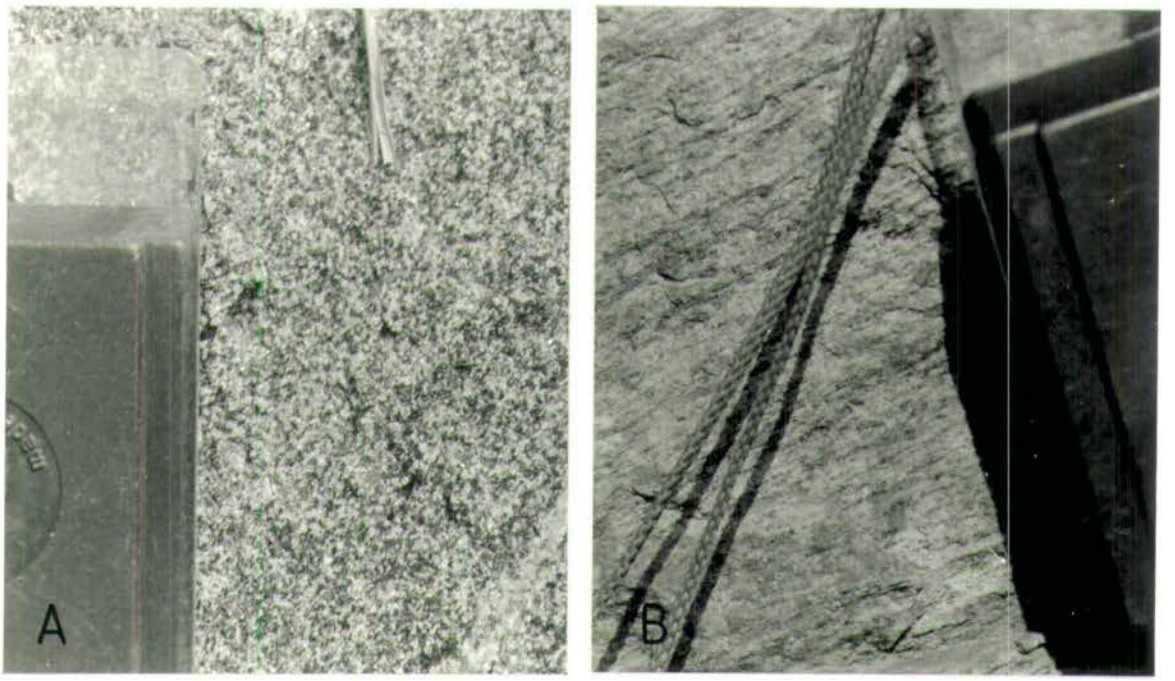

Plates 2.2a and b: Typical fabrics of the Rendina Amphibolite Formation (Section 2.2.2.3), compass clinometer is 10 cm long. (A) Low-strain member from a road-cutting, south of the Rendina to Asprovalta road, showing an homogeneous, mottled, medium- to fine-grained (0.2-1.5 mm) fabric. (B) High-strain member from a road-cutting north of the Rendina to Asprovalta road, showing a banded, fine- to medium-grained fabric.

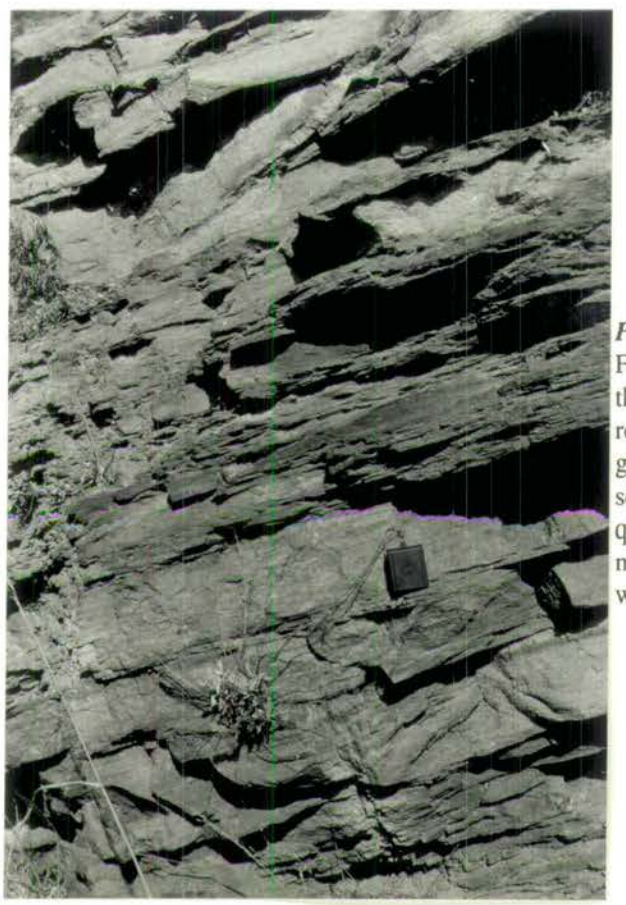

Plate 2.2c: The Rendina Ruins Banded Gneiss Formation (Section 2.2.2.4), immediately north of the Rendina to Asprovalta road. This formation is represented by well-banded, medium- to fine-grained quartzofeldspathic metasedimentary sequences. The thickest layers are predominantly quartzofeldspathic, whereas the thinner layers are more micaceous and exhibit fine-scale banding within them. Compass clinometer is 10 cm long.

Minor localised melting within the well-banded sequence is represented by discordant leucosome segregations (Section 3.12.4). Within the amphibolites are four generations of pegmatitic intrusions, with a quartz-plagioclase-K-feldspar assemblage. These pegmatites vary in size and their present style is due to their orientation with respect to progressive deformation within a shear zone regime (Section 3.9.2).

The main uncertainty for this formation concerns the nature of the western contact and the origin of the well-banded amphibolite sequence. The simplest conclusion is that the banded amphibolites are a highly sheared version of the mottled, coarse-grained amphibolite. The western contact is likely to represent a mixture of banded amphibolites (this section) and banded gneiss (Section 2.2.2.4) with the contact obscured by juxtaposition and out of sequence displacement along an anastomosing shear zone. The shear zone hypothesis is supported by the dip and strike of the regional (S_2) foliation, which steepens from 20°-30°W in the west, to sub-vertical at the inferred lithological boundary and progressively decreases back to 25°-30°W in the east (Fig. 2.1).

2.2.2.4 The Rendina Ruins Banded Gneiss Formation

This formation crops out around and to the east of the ancient ruins at Rendina, and can be traced laterally via small exposures, for 500 m to the N and 1.5 km to the S. The formation in the east consists of a coarse-grained banded gneiss member juxtaposed against the Rendina Amphibolite Formation (Section 2.2.2.3). The precise contact is obscured by the intense steep to vertical, NNW-SSE trending, regional (S_2) foliation. This gneissic member passes progressively into a series of well-banded, medium- to fine-grained quartzofeldspathic metasediments (Plate 2.2c). Individual bands (possibly transposed bedding) are parallel to the regional (S_2) foliation and range from 5-20 cm in thickness. The thickest bands are composed predominantly of quartz and plagioclase, whereas thinner layers are more micaceous and exhibit finer-scale banding within them.

From below the ancient ruins at Rendina, to the Rendina Marble Formation (Section 2.2.2.5), the formation consists of intensely-banded (0.5-3 cm thick), fine-grained quartzofeldspathic micaceous schists. This formation is extremely fissile and cut by flat-lying faults and shear zones. The formation is interpreted as a metasedimentary sequence with coarse quartzofeldspathic metaclastics at the base passing up via more pelitic, finer-grained lithologies, into a carbonate dominated sequence (Stefanina and Rendina Marble Formations, Section 2.2.5.2 and Section 2.2.2.5 respectively).

2.2.2.5 The Rendina Marble Formation

This formation is divided by an inferred major fault along the line of the Rendina-Asprovalta road (Kockel *et al.*, 1971, 1977; Insert, Map G). To the north of the road around the military range at Rendina is a large outcrop of pure, white, coarse-crystalline marble. The east contact of the marble is juxtaposed against the Rendina Ruins Banded Gneiss Formation (Section 2.2.2.4). The contact in the west is obscure although several minor exposures of Vertiskos type gneisses have been observed in gullies at the edge of some of the rough tracks. The nature of the west contact therefore remains uncertain.

To the south of the road, directly west of the ancient ruins at Rendina are a series of highly deformed marbles which outcrop in a laterally continuous sequence with a NNW-SSE strike. These marbles are predominantly grey, with an indication of strong original banding and are now highly brecciated (Plate 3.16a). The marble is shot through by quartz and carbonate veins and has a well-developed stylolitic cleavage. In several areas these impure, grey marbles (in the east) pass into purer, white, coarse-crystalline marbles (in the west) which are now also highly brecciated. The contact of the marble formation to the east is interpreted as being transitional with the Rendina Banded Gneiss Formation (Section 2.2.2.4). The contact to the west of the marble formation is made with a series of lithologies from the Vertiskos Group. The west contact is interpreted as being tectonic with initial ductile and finally brittle deformation (Chapters 3 and 6).

2.2.3 East of the Village of Modhi

This 3 to 4 km traverse is the most southerly into the Kerdilion Group and consists of relatively continuous (approximately 80%) outcrops along-side a rough track, east of Modhi (Insert, Map G). Weathered 1-3 m high cuttings and dense tree cover to the N and S precludes exposure. Changes in structural style are extreme with regional (S_2) foliations varying in intensity, orientation and trend. The S_2 foliations range from a weak spaced cleavage to well-developed mylonitic fabrics (Chapter 3). Variations of the S_2 foliation are attributed to large (km-scale) anastomosing shear zones (Fig. 2.1; Chapter 3). Within low-strain areas between shear zones, earlier structures are preserved. All contact relationships between the formations are obscured either by badly weathered outcrop or because they are sub-parallel with the intense regional S_2 foliation and/or shear zones. Three formations in all are distinguished along this traverse (Fig. 2.2).

2.2.3.1 The Modhi Amphibolite Formation

This formation consists of two amphibolite members which crop out, i) as a

massive (possibly continuous) sequence at the end of the track, 3 to 3.5 km east of Modhi, and ii) as a series of 5 to 25 m wide, approximately NNW-SSE trending exposures 0.5 to 1 km east of Modhi. Orientation of the foliations within both these members vary progressively from steep to flat-lying with a general NW-SE trend.

i) The *East Amphibolite Member* is pooly exposed, although the inferred outcrop is extensive. Contact relationships are difficult to constrain as the eastern boundary was not exposed and the western contact is juxtaposed with the Modhi Leucocratic Gneiss Formation (Section 2.2.3.2) via a sub-vertical, NNW-SSE trending, anastomosing shear zone. This member is composed of homogeneous, fine- to coarse-grained amphibolites. Variation in grain-size is attributed to either, original textural variations created by different modes of intrusion, or varying degrees of deformation developed across the area. This member has an igneous geochemical signature compatible with the Volvi Complex (Chapter 5) and represents either an early amphibolitic basement on which the remaining Kerdilion Group formations have been deposited/emplaced, an intrusive extension of the Complex or a tectonic intercalation of the Complex (Section 2.2.6).

ii) *The West Amphibolite Member* is intercalated with members of the Modhi Marble Formation (Section 2.2.3.3). The composition of this member is extremely variable and consists of a series of coarse- to fine-grained amphibolites down to retrogressed (possibly metasomatised) biotite-rich lithologies (Chapter 4). Within the core of a large (15-25 m wide), asymmetric N-S trending synformal structure within this member are a series of boudined exposures (0.5-1 m long) of a garnet-kyanite schist. Contact relationships between the schist and amphibolite are obscure with the main S_2 foliation wrapping the schistose exposures. Discontinuous pegmatitic intrusions within this member occur on various scales (5-10 cm to 1-1.5 m thick), and have been subjected to variable degrees of deformation. The smaller intrusions are homogeneous in composition and are highly deformed, discontinuous quartz-rich pods, whereas the largest pegmatitic intrusion exhibits a composite growth sequence (Section 3.9.4).

This member has no clear geochemical signature (Chapter 5) and hence the precursor of the amphibolites could have been marls, volcaniclastics or basic tectonic intercalations, within a carbonate/pelite sequence.

2.2.3.2 The Modhi Leucocratic Gneiss Formation

This formation crops out in a series of exposures 500 m to 1 km long either side of the track, approximately 2.5 km east of Modhi. Contact relationships to both the east and west are made across steep shear zones with members of the Modhi

Amphibolite Formation (Section 2.2.3.1). The formation consists of an homogeneous fine- to medium-grained, leucocratic gneiss, with grain-size variations reflecting degrees of deformation. In low-strain areas an early sub-vertical leucocratic banding (S_0) is discernible. The leucosomes consist of continuous 0.3-0.7 mm wide quartz-plagioclase-K-feldspar rich bands. The matrix (mesosome) consists of narrow (0.2-0.4 mm wide) bands of biotite which are intensely folded (Chapter 3; Plate 3.5).

2.2.3.3 The Modhi Marble Formation

This formation consists of two members (based on their mappable position in the field and physical characteristics) which crop out along the track east of Modhi, approximately 1 km and 2 km respectively.

The *West Marble Member* consists of a series of exposures (5 to 10 m wide), intercalated with the West Amphibolite Member (Section 2.2.3.1). Contacts are sub-vertical with a NNW-SSE trend. This member is composed of homogeneous, coarse-crystalline carbonate. Variations occur in colour and grain-size from a grey, fine-grained, homogeneous, crystalline marble early in the sequence (east), progressively changing to a white/orange, medium- to coarse-grained, homogeneous, crystalline marble in the west.

The *East Marble Member* consists of two almost continuous 10-30 m wide exposures, intercalated with the East Amphibolite Member (Section 2.2.3.1). Contacts vary from steep to flat-lying with a NNW-SSE trend. This member is composed of a series of impure carbonates. These carbonates contain distinctive bands (1-15 cm wide) of slightly different composition, which form fine- to coarse-grained, crystalline marbles showing a range of colour variations from blue-grey to white. Weathering of the weaker bands highlight well-developed interference patterns and cm- to m-scale tight parasitic folds (Plates 2.3a, 3.10).

The two marble members are interpreted as an originally continuous formation displaying lateral variations in composition. The marbles are now severely disrupted due to intense deformation, with shearing and faulting dominant in the west and folding dominant in the east. The marbles can be inferred to represent a sequence younging stratigraphically towards the west, reflecting a progression towards increasingly pure carbonate deposition.

2.2.4 The Arethousa-Vrasna Traverse (Vamvakia-Vrasna Traverse)

Two traverses cover essentially the same lithological sequence. (A) *The Arethousa-Vrasna Traverse* is an approximately NW-SE traverse consisting of a series of dispersed road-cuttings along a rough unmetalled road between Arethousa in

Plate 2.3

***Plate 2.3a*:** View of the Impure Modhi Carbonate Member, approximately 1.5 to 2 km east of Modhi. Weathering of less competent layers highlights well-developed close to tight parasitic folding. Field of view is approximately 2.5 m across.

***Plate 2.3b*:** View of the Vrasna Feldspathic Gneiss Formation from halfway along the Arethousa to Vrasna road. The homogeneous well-foliated gneissic matrix is cross-cut by two generations of pegmatite. Coin is approximately 2 cm across.

the northwest and Vrasna to the southeast. (B) *The Vamvakia-Vrasna Traverse* is an approximately W-E traverse along a very rough track between Vamvakia in the west and Vrasna in the east.

Exposure is intermittent, and contact relationships between formations are obscure. Due to the arrangement of these traverses, lateral variations with respect to lithological, structural and metamorphic characteristics can be observed within the formations. The structural style observed along both these traverses remains relatively constant, with the area subject to the main regional S_2 foliation with variations in its intensity associated with anastomosing shear zones. Along the first 2-3 km of road from Arethousa are a number of outcrops which provide evidence for W to E thrusting of units from the Vertiskos Group and Volvi Complex on to the Kerdilion Group (these are referred to more appropriately in Sections 2.3 and 2.5). Three distinct lithological formations are recognised (Fig. 2.2).

2.2.4.1 The Vrasna Amphibolite Formation

This formation crops out around Vrasna, and was only briefly studied. The east contact was not exposed and the west contact with the Vrasna Feldspathic Gneiss Formation (Section 2.2.4.2) only poorly exposed. However, from the sub-vertical orientation of the regional (S_2) foliations within the formations either side of the west contact, a sub-vertical, N-S trending boundary is inferred. The main continuous (S_2) foliation within this formation however, has a range of dips between 23-60°W and a general NW-SE trend. Within this formation are a number of highly deformed discontinuous pegmatite sheets which are interpreted as variants of the pegmatites within the Vrasna Feldspathic Gneiss Formation (Section 2.2.4.2). The amphibolites exhibit minor changes in colour and composition (e.g. the percentage of biotite). Similarity to amphibolites along the Rendina to Asprovalta road (Section 2.2.2.3), east of Modhi (Section 2.2.3.1) and Stefanina (Section 2.2.5.1) have been noted.

2.2.4.2 The Vrasna Feldspathic Gneiss Formation

This formation crops out in discontinuous exposures from about half-way along the Arethousa to Vrasna road towards Vrasna, and in fairly continuous exposures from about half-way along the track between Vamvakia to Vrasna (Insert, Map F). Contact relationships for the eastern boundary are uncertain due to lack of exposure, whereas the western boundary is represented by a variably orientated shear zone (Section 3.2.3). Along the Arethousa to Vrasna road the western contact of this formation is juxtaposed with the Vrasna Marble Formation (Section 2.2.4.3). Along the track between Vamvakia and Vrasna and stream sections between the two main

traverses the formation is in contact with amphibolite members of the Vamvakia Mafic Formation (Section 2.3.2.5). A large WNW-ESE trending fault is inferred to lie immediately to the south of the Arethousa to Vrasna road. This fault has the effect (along with the shear zone) of truncating the N-S trending outcrops of the Vrasna Marble Formation (Section 2.2.4.3).

The formation consists of homogeneous, fine- to medium-grained, quartzofeldspathic gneiss with gradational changes in grain-size over distances of at least 5 to 10 m. The coarse-grained gneisses commonly exhibit randomly orientated (0.5-1 cm long) stringers and blebs of quartz and plagioclase (possibly a remnant early S_0 fabric) within a micaceous matrix. The fine- to medium-grained varieties exhibit a generally homogeneous (0.1-0.5 mm), crystalline matrix. However, a distinctive transposed quartzofeldspathic banding (either S_1 or early S_2) is well-developed in many of the fine- and medium-grained gneisses. At least one and often two penetrative foliations are developed throughout the formation, sub-parallel with the main S_2 foliation. All the foliations have a NW-SE to NNW-SSE trend and variable dip (25°E, vertical to 39°W).

The formation contains several generations of intrusive pegmatite sheets. The style and number of recognisable pegmatite intrusions varies along a traverse into the formation, from the high-strain western boundary to areas of low-strain in the east (Chapter 3). At the western boundary of the formation, along the Vamvakia to Vrasna road, pegmatites occur as small (0.3-0.7 mm wide), highly deformed, discontinuous veinlets. Continuity of these pegmatites is poor due to the well-developed S_2 foliations and only one pegmatite suite is identified. Within this area pegmatites are so abundant they comprise approximately 20-25% of the rock. At the western boundary along the track between Arethousa and Vrasna, recognisable individual, small-scale pegmatites are less abundant, but a coarse quartzofeldspathic gneiss is common. Hence, many if not all the early (S_0) stringers and pods of the coarse-grained variety of quartzofeldspathic gneiss may actually represent areas of highly deformed pegmatite veinlets.

Away from the western boundary into the formation the number of individual pegmatite veinlets and overall volume of pegmatite material decreases to 5-10% of the rock. However, the individual pegmatite intrusions increase in size and variety of composition, with two distinctive continuous cross-cutting pegmatite sheets 8 to 10 cm wide identified (Plate 2.3b; Chapter 3; Plate 3.26). Further east, only one suite of pegmatites is identified, represented by single sheets (1-3 m wide) and represents approximately 2-4% of the rock. These pegmatites are coarse-grained and composed

predominantly of crystalline, quartz-plagioclase-K-feldspar, with occasional large (2-3 cm wide) books of muscovite. The characteristics and interpretations for these pegmatite generations are reviewed in Chapter 3.

2.2.4.3 The Vrasna Marble Formation

Outcrops of this formation occur in two (10-30 m wide) exposures along the Arethousa to Vrasna road and a 20-30 m wide exposure to the east of Vrasna. There are no marble exposures along the track between Vamvakia and Vrasna. Contact relationships between this formation and adjacent lithologies are either not exposed or obscured by intensification of the regional (S_2) foliation and narrow shear zones.

The first outcrop lies approximately halfway along the Arethousa to Vrasna road and consists of two marble members; a white to orange marble (to the west) and a grey to black marble (to the east), with no distinct boundary between the two. Both members are massive, coarse-crystalline and generally featureless, although ghost folding is seen in the white marble member. The colour change represents a transition from a pure limestone to an impure carbonate with a graphite component. The entire outcrop is severely brecciated, with the impure, grey carbonate appearing similar to the Rendina Marble Formation (Section 2.2.2.5). Lateral continuity of this outcrop to the north is obscured by dense tree cover and to the south it is truncated by an inferred large fault. The second and third outcrops to the east of the Vrasna Feldspathic Gneiss Formation (Section 2.2.4.2), west of the Vrasna Amphibolite Formation (Section 2.2.4.1) and to the east of Vrasna respectively consist of featureless, coarse-crystalline white marble. Both these outcrops maintain an approximate N-S trend.

The relationship between the individual outcrops of marble along this traverse and between these marbles and adjacent formations remain uncertain. An interpretation such as infolded inliers and/or intercalated sheared blocks with the formations of the Kerdilion Group may be inferred by comparison with the marble formations from the other traverses. However, no original contact relationships have been observed.

2.2.5 East of the Village of Stefanina

The most northerly traverse (Fig. 2.1) into the Kerdilion Group (apart from a minor reconnaissance into a series of amphibolites to the east of Limni, Section 2.2.5.3) followed a rough track to the east of Stefanina (Insert, Map F). Outcrops consist of small (1-3 m high), discontinuous, variably weathered road-cuttings. The structural style is variable however, with several areas only gently deformed. Within these areas of low-deformation, open to tight folds with a WNW-ESE to NW-SE fold

axial trend are developed. This trend is significantly different to the NNW-SSE trend exhibited by the regional (F_2) folds and (S_2) foliations. However, on an E to W traverse towards the thrust zone with the Arethousa Ultramafic Member (Section 2.3.3.6) the folds progressively tighten and rotate, becoming sub-parallel with the thrust and regional NNW-SSE foliation trend. Only minor shear zone deformation is developed to the east of the Arethousa Ultramafic Member (affecting the Stefanina Marble Formation, Section 2.2.5.2; Chapter 3), compared to equivalent traverses to the south. Hence it is proposed that a major slip plane developed within and along the boundary of the Arethousa Ultramafic Member (Section 2.3.3.6) absorbed the shear zone deformation and reduced its effect in the adjacent formations.

2.2.5.1 The Stefanina Amphibolite Formation

This formation was poorly exposed and only briefly studied. The amphibolite contained at least one penetrative foliation with a regional NW-NNW to SE-SSE trend, the dip of which ranged from steep to flat-lying. The amphibolite is generally homogeneous with a fine- to medium-grained matrix and contains several sets of leucocratic sheets. The leucocratic sheets ranged from cm- to m-wide layers and were variably deformed and folded. Contact relationships of this formation to the east were not exposed, however to the west is a sub-vertical, intensely foliated boundary with a well-banded member of the Stefanina Marble Formation (Section 2.2.5.2).

2.2.5.2 The Stefanina Marble Formation

This formation crops out as a series of discontinuous road-cuttings (1-5 m high) east of Stefanina. The formation is represented by a gradational series of carbonate lithologies; to the east, by medium- to coarse-grained banded marbles; to the west, by fine- to medium-grained impure carbonates.

The marbles consist of variably (1-30 cm thick) inter-banded sequences of white, crystalline marble and grey, fine-grained, impure carbonate. In the east, banding is predominantly of fine- to medium-grained impure carbonates, with the volume of white crystalline marble bands increasing progressively towards the west. There is also a general decrease in the thickness of the impure grey carbonate banding progressively from east to west. However, the massive, thickly banded, white crystalline marbles pass abruptly via a series of shear zones into a thick sequence (50-100 m thick) of homogeneous, fine-grained, impure, grey carbonates.

The wavelength of folds developed along this traverse decreases from east to west, reflecting the change in thickness of the more competent bands within this member. The banding foliation and fold axes in the east have an approximate NW-SE

The eastern boundary of this formation is juxtaposed with the Stefanina Amphibolite Formation (Section 2.2.5.1). The western boundary is juxtaposed with the Vamvakia Mafic Formation (Section 2.3.2.5) and Arethousa Ultramafic Member (Section 2.3.3.6), with the contact represented by a complex array of well-developed variable steep to flat-lying shear zones. Within low-strain pods and towards the eastern boundary of this impure carbonate member 1-3 cm thick (either original or transposed) compositional layers are well-developed. Within these fine-grained units quartz-filled veinlets/fractures and stylolitic cleavage are abundant.

2.2.5.3 The Limni Amphibolite Formation

This formation crops out to the north of Stefanina, and to the east of Limni (Insert, Map A) and consists of a series of variably deformed amphibolites. The contacts of this formation are not exposed. However, the formation is interpreted to be bounded by a number of inferred faults with large displacement. Hence the origin and setting of this suite of amphibolites remains uncertain. From geochemical analyses (Chapter 5) this amphibolite appears to lack both the large ion lithophile element enrichment and the typical relative depletion in Nb compared to large rare earth elements of most of the Volvi amphibolites. The samples are remarkably uniform with a flat rare earth element chondrite normalised pattern and are closest as a suite to mid ocean ridge basalts, compared to the other analysed samples (Chapter 5). Hence it may have a different origin from the Volvi Complex but its composition can nevertheless be matched by individual dykes within the Complex.

2.2.6 Compilation and Summary

By correlating the available information for the four traverses into the Kerdilion Group (Figs. 2.1, 2.2) it is possible to derive a schematic composite lithostratigraphy (Fig. 2.4). The earliest formation within the Kerdilion Group consists of a migmatitic, gneissic basement (the Gun-emplacement Gneiss Formation, Section 2.2.2.1; the Stavros Leucocratic Gneiss Formation, Section 2.2.2.2). These formations are considered to represent lateral variations of one another.

The migmatite/gneissic basement preserves evidence of an early (S_0) fabric-forming event and a related melt phase (S_{0B}), with no earlier fabrics preserved. The precursors for these basement lithologies are indeterminable as the original characteristics have been obliterated during deformation and metamorphic (D_1) events which developed the migmatites. The basement lithologies have been modified (i.e. flattened, folded, attenuated, etc.) by a series of later deformational events.

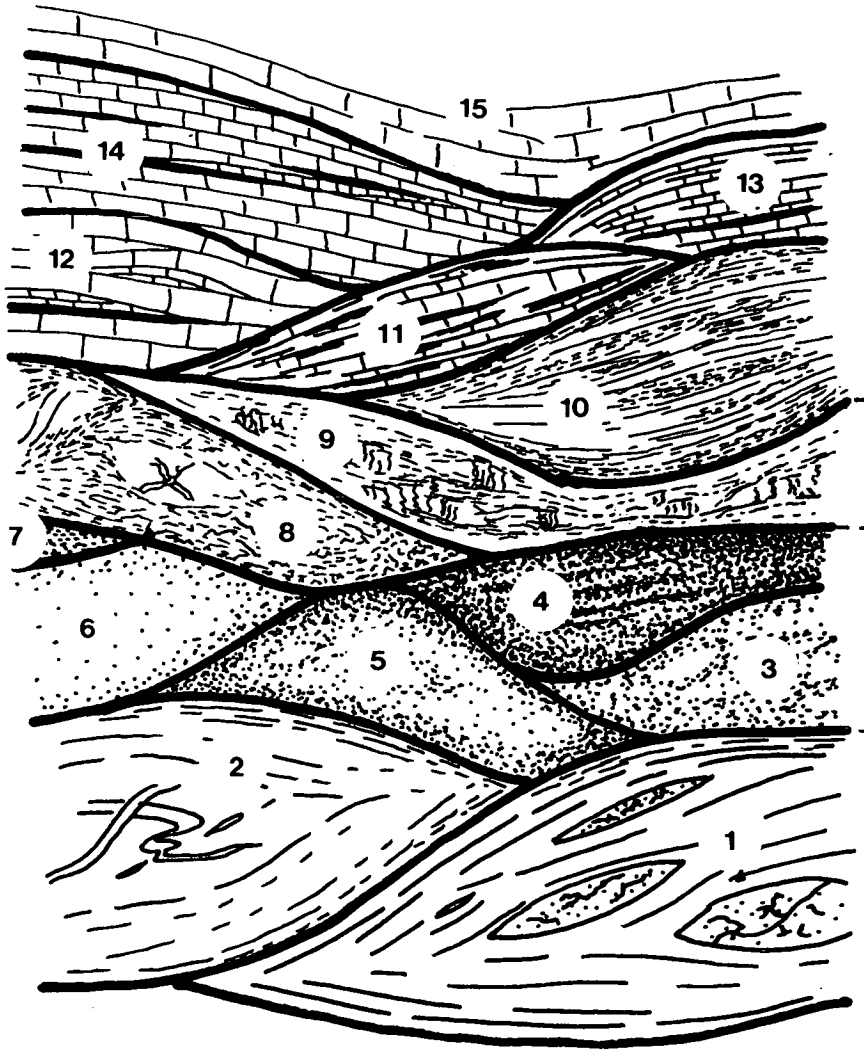

15 Marble Formation
14 The Vrasna Marble Formation
13 The Modhi Marble Formation
12 The Stefanina Marble Formation
11 The Rendina Marble Formation
10 The Rendina Ruins Banded Gneiss Formation
9 The Modhi Leucocratic Gneiss Formation
8 The Vrasna Feldspathic Gneiss Formation
7 The Limni Amphibolite Formation
6 The Stefanina Amphibolite Formation
5 The Rendina Amphibolite Formation
4 The Vrasna Amphibolite Formation
3 The Modhi Amphibolite Formation
2 The Stavros Leucocratic Gneiss Formation
1 The Gun-emplacement Gneiss Formation

↑ Volvi Metasedimentary Group

Volvi Complex — Gneiss → — Migmatite

Kerdilion & Vertiskos Group

Fig. 2.4: Schematic summary diagram representing the lithostratigraphic sequence for the Kerdilion Group. This sequence has been derived from relationships within and between a series of anastomosing pods. The lithostratigraphic sequence follows the reinterpretated lithostratigraphic sequence proposed in section 2.7.

The migmatitic/gneissic basement is juxtaposed with and now overlain by a number of ortho-amphibolitic units (Rendina Amphibolite Formation, Section 2.2.2.3; East Modhi Amphibolite Member, Section 2.2.3.1; Vrasna Amphibolite Formation, Section 2.2.4.1; Stefanina Amphibolite Formation, Section 2.2.5.1 and possibly the Limni Amphibolite Formation, Section 2.2.5.3). Geochemical signatures of these formations do not vary significantly (except for the Limni amphibolite) from that of the Volvi Complex (Chapter 5).

Bulk composition of these amphibolite formations remains constant, however, fabrics and textures which characterise these formations are varied. *Deformation:* the fabrics developed within each amphibolite formation consists of a dominant continuous (S_2) foliation, and occasionally earlier (S_1 or early S_2) foliations are preserved in low-strain pods (Chapter 3). Within each formation the dominant regional (S_2) foliations from steep to flat-lying are developed (Chapter 3). These dominant composite or shear (S_2) foliations wrap low-strain pods which preserve either mottled coarse-grained assemblages or medium- to fine-grained assemblages. The changes in foliation are attributed to large (km-scale) anastomosing shear zones (Chapter 3). *Intrusions:* All the amphibolite formations contain varying proportions (0-30% of the rock) of leucocratic (pegmatitic/aplitic) material. Within each formation the relative percentage of leucocratic material generally decreases progressively from east to west. Two possibilities arise which could affect the amphibolites which comprise the individual formations, (a) they are actually of different ages, with those containing pegmatites older than those which do not, and (b) the intrusion of the leucocratic (pegmatitic/aplitic) sheets was of variable local extent (greater to the east and hence, lower in the inferred lithostratigraphic sequence). However, an unequivocal interpretation of these sequences is not possible.

The amphibolites are juxtaposed with and now overlain by two leucocratic gneisses, the Vrasna Feldspathic Gneiss Formation (Section 2.2.4.2) and Modhi Leucocratic Gneiss Formation (Section 2.2.3.2). These formations have been correlated due to the similarity between their bulk composition and overall structural history. However, as these formations show a range of structural fabrics and have outcrops which vary in width from S to N, it is uncertain whether they represent lateral variations of the same formation or completely different formations. Due to the large volume of pegmatite sheets within the Vrasna Feldspathic Gneiss Formation (Section 2.2.4.2), it is considered to underlie the Modhi Leucocratic Gneiss Formation (Section 2.2.3.2). Contacts between these formations are not exposed, but are inferred to be juxtaposed via anastomosing shear zones.

The leucocratic gneisses are juxtaposed and apparently overlain by a series of (either transposed or compositionally layered) banded metasedimentary schists and gneisses (Rendina Ruins Banded Gneiss Formation, Section 2.2.2.4). The contact between these formations is obscured by intensification of the S_2 foliation and the development of shear zones. From the lack of continuity of pegmatitic/aplitic sheets and no evidence for the earliest structures across this contact, an original basement-cover discontinuity is inferred. However, the original contact relationship is obscured by tectonic (either D_2 or D_3) reworking.

The Rendina Ruins Banded Gneiss Formation (Section 2.2.2.4) apparently passes progressively and conformably upwards into impure carbonates, which in turn grade upwards into pure, white, coarse-crystalline marbles (Rendina Marble Formation, Section 2.2.2.5). A similar, less deformed sequence crops out to the east of Stefanina (Stefanina Marble Formation, Section 2.2.5.2). However, the uniformity of this sequence is dependent on the varying degrees of tectonic reworking. The Modhi Marble Formation (Section 2.2.3.3) in particular shows extreme tectonic intercalation and/or interbanding with the West Modhi Amphibolite Member (Section 2.2.3.1). A clear igneous or sedimentary precursor for this amphibolite member cannot be determined from geochemical analysis (Chapter 5). Comparison with the less deformed sequences however, favours a sedimentary origin.

The marble horizons within the Kerdilion Group were interpreted by Kockel *et al.*, (1971, 1977) as different formations due to the spatial arrangement of their outcrop at the present time. However, the marble horizons can be correlated laterally to the N and S, from areas of low- to high-deformation. From the continuity of outcrop along E-W traverses within areas of low-deformation, a progressive, banded gneiss → impure carbonate → pure marble sequence is identified. A similar sequence can be inferred for the areas of high deformation, which are now obscured by tectonic reworking. By accepting the marble horizons to originally have been continuous (though laterally variable), large scale folding and/or intercalation of marble horizons via anastomosing shear zones can be inferred. Evidence for large scale folding is preserved within some impure marble horizons (Sections 2.2.3.3; 2.2.5.2). A model of anastomosing shear zones is supported by structural data throughout the area studied (Chapter 3). However, specific evidence within the Kerdilion Group is provided by the transposition of foliations (Modhi Leucocratic Gneiss Formation, Section 2.2.3.2), and by progressive changes in the attitude of the main S_2 foliations from steep to flat-lying throughout the area.

2.3 The Vertiskos Group

2.3.1 Introduction

The formations which comprise the Vertiskos Group are the most extensive in the research area. Exposure of this group is variable, with the best exposures found at the bottom of the numerous N-S trending streams. Within the Vertiskos Group is a major complex body of basic sheeted dykes and gabbros, the Volvi Complex, which is interpreted as an *in situ* extensional phenomenon (Section 2.5). To establish the setting of the Volvi Complex with respect to the Vertiskos Group is the single most important aim of this thesis (Section 1.3). Contact relationships between the Vertiskos Group and the Kerdilion, Volvi Metasedimentary (re: Svoula) and Granitoid (Arnaea Granite) Groups have also been studied and subjected to small-scale mapping.

The Volvi Complex and Lake Volvi, divide the Vertiskos Group into three tracts, east (Section 2.3.2) and west (Section 2.3.3) of the Volvi Complex, and south (Section 2.3.4) of the lake. Exposure immediately north of the Volvi Complex is extremely poor. Lithostratigraphic sequences compiled for the three tracts (Fig. 2.5) are correlated to develop a composite lithostratigraphic sequence (Fig. 2.10; Section 2.2.6).

The three sequences from the Vertiskos Group exhibit a number of differing characteristics, as they coincide with changes in both structural and metamorphic regimes around the Volvi Complex (Chapters 3 and 4 respectively). Geochemistry of dykes, mafic bodies, amphibolites etc., within the Vertiskos Group, has also been particularly useful in constraining the origin of the Volvi Complex (Chapter 5).

2.3.2 East: The Vamvakia River

The Vamvakia river flows south from Arethousa in the north, past Vamvakia and finally enters the eastern end of Lake Volvi (Inserts, Maps A, C and F). Exposure along the bottom of the river is excellent ranging from 50-100% for the majority of its length, with the exception of the first 1-2 km from Arethousa and from Vamvakia to Lake Volvi where the exposure ranges from 0 to 5%. Exposure along tributaries of the Vamvakia river is generally poor with exposure ranging from 0 to 40%. The dominant structure along the river consists of low-angle anastomosing shear zones which intercalate the metasedimentary formations of the Vertiskos Group with a number of amphibolitic, doleritic and gabbroic units (the Vamvakia Mafic Formation; Section 2.3.2.5) *see* Insert, Map C and Fig. 2.6. Original contact relationships are mostly lost when crossing or approaching shear zone boundaries due to the increased intensity of the S_2 foliations (Chapter 3). However, within low-strain cores between

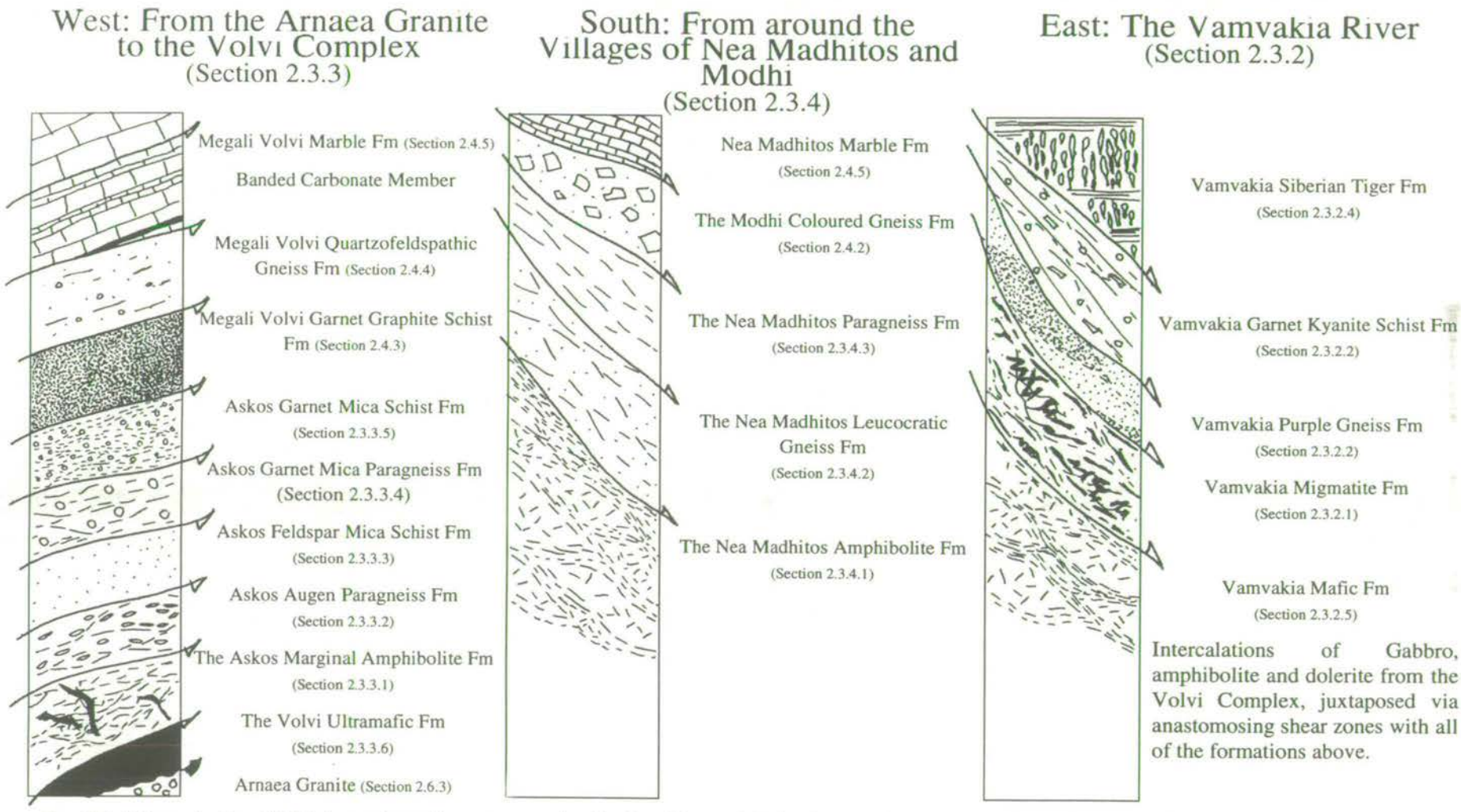

Fig. 2.5: Schematic "best-fit" lithostratigraphic sequences for the Vertiskos and Volvi Metasedimentary (re: Svoula) Groups, from around the Volvi Complex and Lake Volvi. Derived from a series of pods banded by anastomosing shear zones.

Fig. 2.6: Schematic representation of the spatial arrangement of the formations within the northern section of the Vamvakia river. Changes in formations are contained within a series of sheared pods, or "halibuts".

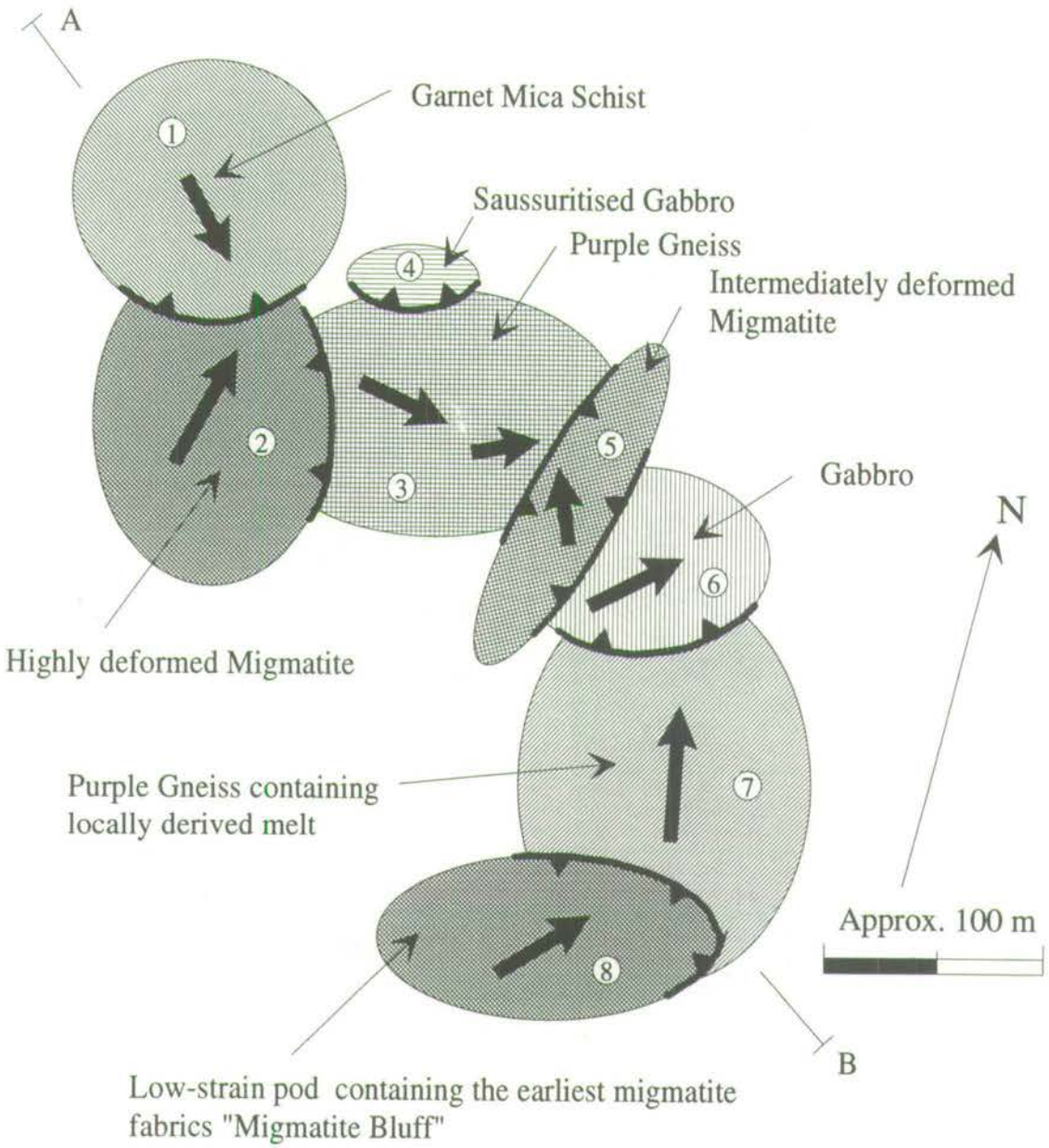

Schematic cross-section of the sequence from A to B.

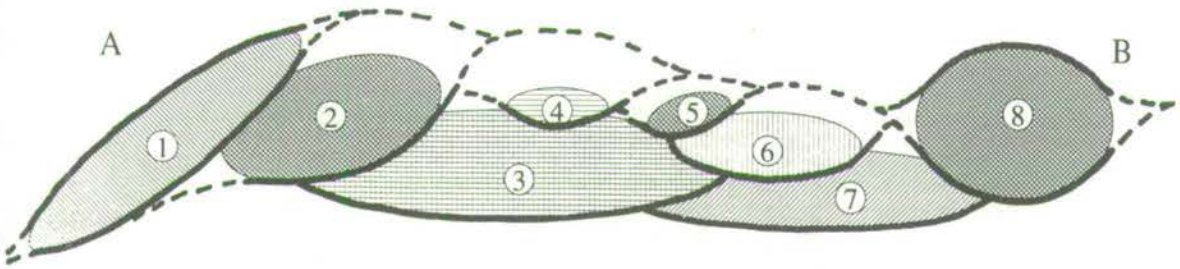

the anastomosing shear zones, early fabrics and structures are partially preserved. From the interpretation of these structures at least part of the early history of the Vertiskos Group can be determined.

Based on the spatial arrangement of lithological formations at the present time the river can be sub-divided into three sections, i) the first 2 to 3 km from the northern end of the river (Insert, Map C; Fig. 2.6). This section contains a range of lithologies which are interpreted as the oldest preserved in the Vertiskos Group, within the study area (Vamvakia Migmatite Formation; Section 2.3.2.1), ii) the central part of the Vamvakia river (Insert, Map F) consists entirely of amphibolitic gneisses and gabbros. On petrographic and geochemical grounds these mafic units are interpreted as part of the Volvi Complex (Chapter 5), iii) the southern 2-3 km of the river north of Vamvakia (Insert, Map F). This section is again predominantly amphibolite, however, minor exposures of the Vamvakia Garnet Kyanite Schist Formation (Section 2.3.2.3), and metasedimentary carbonates (Vamvakia Siberian Tiger Formation, Section 2.3.2.4) also crop out. These schist and carbonate formations show excellent examples of metasomatic reactions with the Volvi Complex amphibolites. Five distinct lithological formations in all are recognised along this traverse (Fig. 2.5).

2.3.2.1 The Vamvakia Migmatite Formation

This formation only crops out within the northern section of the Vamvakia river (Insert, Map C), in a series of (1-10 m wide) exposures. The least deformed exposure crops out as a large (10 m diameter), low-strain core exposed on a sheer NE-SW cliff-face "Migmatite Bluff" (Plate 2.4a). Within the centre of this low-strain core two sets of quartzofeldspathic leucosomes are preserved which represent the earliest (S_{0A}, S_{0B}) fabrics present in the studied area (Chapter 3; Plate 3.6), i) the first set of leucosomes are 0.2-1 cm thick and finely banded on a 0.5-1 cm scale. The mesosome consists of homogeneous, mottled, medium- to fine-grained biotite, plagioclase, K-feldspar and quartz (Section 3.3), ii) the second set of leucosomes are 2-5 cm thick, with narrow melanosomes of biotite 0.1-0.5 cm thick. These leucosomes cross-cut the first set and are randomly distributed and weakly banded (20-40 cm; Section 3.3).

Exposures representative of intermediate shear zone deformation crop out at the margin to Migmatite Bluff, as numerous discrete (1-4 m wide) exposures, and as loose blocks (Plates 2.4b, 3.6). Continued progressive disruption of these migmatites has produced coarse, banded gneisses with scattered augen and ultimately a mylonitic fabric. In migmatites showing an intermediate state of shear zone deformation, the earlier, fine-banded, (S_{0A}) fabric may be disrupted and "homogenised" to a mottled,

Plate 2.4

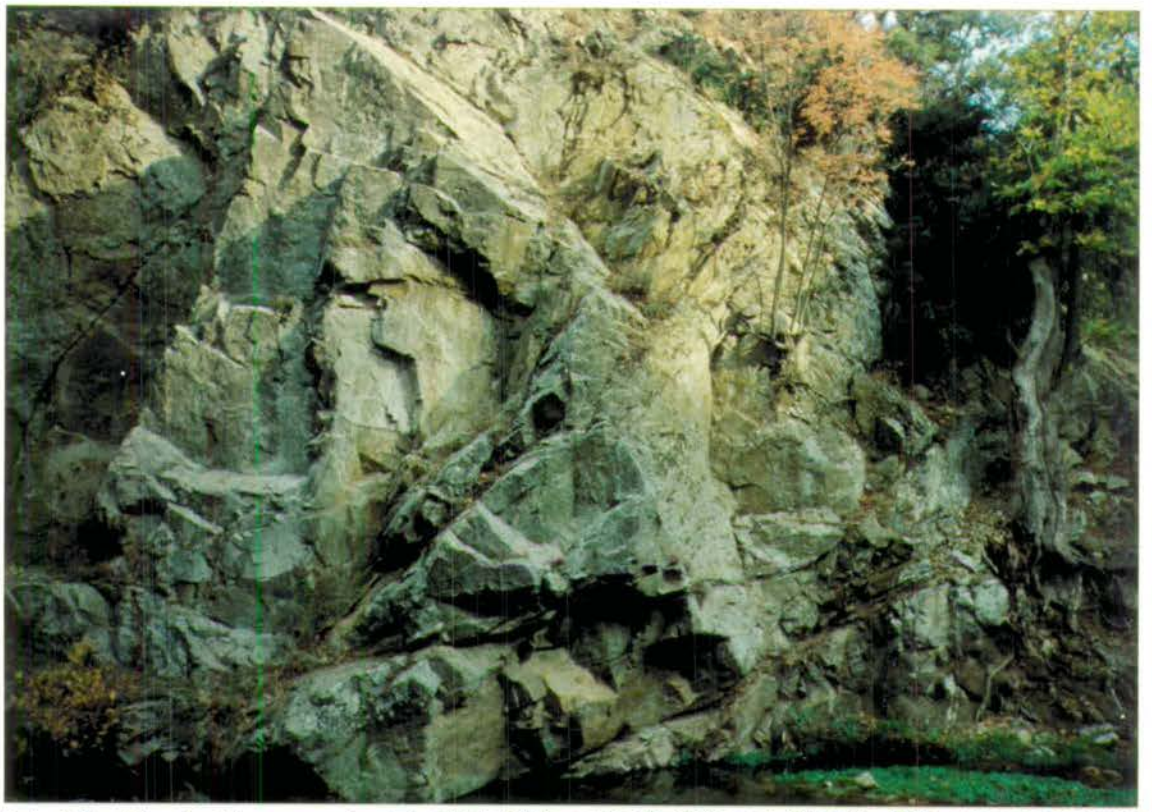

Plate 2.4a: View looking approximately ESE of Migmatite Bluff (Insert, Map C). This outcrop represents a large low-strain core (approximately 30 m wide) preserving the earliest migmatite fabrics within the study area. Intensification of fabrics from the low-strain core (left), to the high-strain rim (right) results in the progressive development of later shear zone structures and fabrics (Plate 2.3b). The low-strain pod has been reduced in size by the progressive encroachment of shear zones (centre).

Plate 2.4b: Typical intermediately-strained black and white migmatite within close proximity to "Migmatite Bluff", see Plate 3.6 for a description of the fabrics. Pen is 14 cm long.

biotite-plagioclase-k-feldspar-quartz matrix. However, the broader second phase leucosomes (S_{0B}) are still recognisable. As deformation intensifies towards the sheared margins of low-strain pods a range of folded, refolded and sheared fabrics are developed and finally result in banded porphyroblastic mylonites (Plate 2.5a).

A progressive increase in deformation related to shear zone development is well displayed (over 3 metres) from the centre to the base of Migmatite Bluff leading to the development of a mylonite with porphyroclasts of plagioclase and k-feldspar. Similar mylonitic gneisses derived by analogy from a migmatite precursor occur over a large part of the northern Vamvakia river section (Insert, Map C). Kinematic indicators provided by the porphyroclasts within the mylonites are poorly developed and often contradictory over short distances (1-5 m) towards the shear contact. However, an overall shear direction top to the NW is inferred for this outcrop.

2.3.2.2 The Vamvakia Purple Gneiss Formation

Outcrops of this formation are found in the northern part of the Vamvakia river (Insert, Map C), east of the Arethousa to Vrasna road and adjacent to a quartz-diorite intrusion west of Lefkoudha (Insert, Map H). Contact relationships are obscure with the formation juxtaposed with mafic bodies via low-angle shear zones.

The formation has a primary migmatitic fabric but with evidence of re-melting (not shown by the previous formation; Section 2.3.2.1) and in addition shows the development of abundant fine-grained kyanite and second generation garnet. These two minerals give the distinctive purplish aspect to the rock (Plate 2.5b). They are interpreted as post-re-melting cordierite break-down products (Chapter 4). The secondary melts show a range of segregation textures, from irregular blebs to well-defined net-veins, or may be absent altogether in restitic varieties. The complete range of secondary melt segregation textures is also subject to the complete range of shear zone deformation towards the margins of purple gneiss pods. Textural evidence (Chapter 4) suggests that this deformation was in part synchronous with the second garnet-kyanite overprint of earlier cordierite.

From NW to SE, the first outcrop of purple gneiss encountered (Insert, Map C; Section A^{I}-A^{II}) shows progressively earlier, less deformed sequences of gneissic fabrics, from a high-strain rim to low-strain core of a large sheared pod. At A^{I} the gneiss passes up into a complex sheared contact (2-7 m wide). This anastomosing shear zone places highly deformed Vamvakia Migmatites (Section 2.3.2.1) over the purple gneiss. The shear zone contains numerous variably deformed and compositionally different (e.g. dolerites, gabbros, garnet-kyanite schists) elongate pods (1-3 m long), separated by shear surfaces (Fig. 2.7, *see* Insert, Map C for the

Plate 2.5

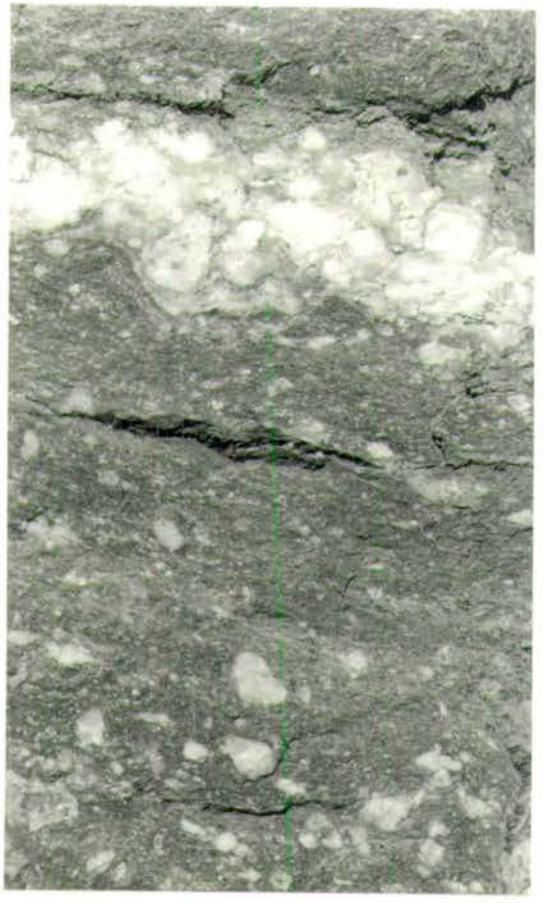

Plate 2.5b: A typical example of a high-strain banded porphyroblastic mylonitic to ultramylonitic lithology from the northern section of the Vamvakia river (Insert, Map C). The majority of these lithologies are interpreted to have had a migmatite precursor. However, when bands are ultramylonitic with few if any porphyroclasts an amphibolite precursor may be proposed. Field of view is approximately 15 cm across

Plate 2.5b: View of the Vamvakia Purple Gneiss (migmatite) showing a typical gneissic fabric cross-cut by a late melt sheet (*see* Plate 3.38 for a description of the fabrics). Pen is 14 cm long.

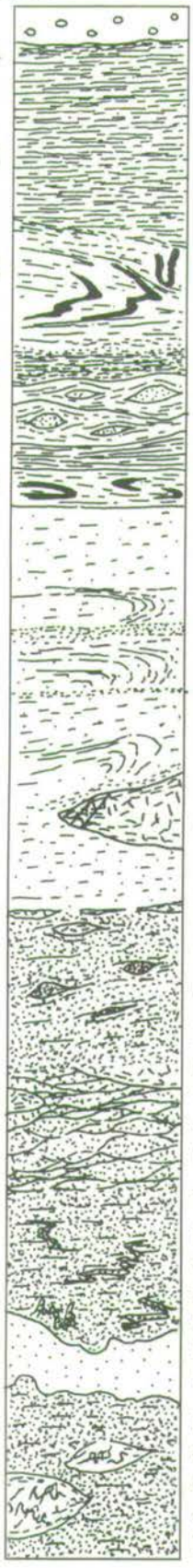

Volvi gabbro, characteristic saussuritised green and white, coarse-grained fabric.

Biotite-rich amphibolites (low-strain areas appear migmatitic). Quartzofeldspathic veins are disjointed. Tight folds are preserved in low-strain areas and progressively orientated into parallelism with the shear zone. Two amphibolites have been juxtaposed and a boundary inferred between them, as truncations in the banded sequences and the overall volume of feldspathic material are shown.

Banded amphibolites with continuous and semi-continuous feldspathic layers.

Biotite-rich matrix, containing 10-15 cm wide pods of garnet-rich schist.

Well-banded amphibolites (fabric parallel to the sheared margin).

Biotite-rich amphibolite with numerous tightly folded quartzofeldspathic veins.

Quartz-biotite-garnet gneiss. Lithology is homogeneous, possibly due to the high state of strain.

Garnet-mica schist (approximately 20 cm thick) with a strong foliation.
Homogeneous quartz-biotite-garnet gneiss. Flecks of k-feldspar appear throughout.
Muscovite-rich layer (6 cm thick), following the top of a large boudin of quartz-biotite-garnet gneiss over several metres.
Remnant fold with the lower limb obliterated along the shear zone.

Large (1.23 m long) pod of amphibolite wrapped by continuous layers of a quartzofeldspathic lithology, with garnet porphyroblasts (potential melt lithology).

Sharp boundary between purple gneiss and biotite-feldspar-rich amphibolite lithologies. Occasionally discrete pods of garnet-mica schist, within a fine-grained homogeneous matrix and pods of amphibolite 25-50 cm long are intercalated along the contact.. Purple gneisses with a well-defined leucocratic S2 foliation, are cross-cut by quartzofeldspathic sheets (possibly local melts).

Pods of garnet-k-feldspar-rich purple gneiss, are preserved within a highly deformed purple gneiss matrix. At the top of the zone is a block predominantly of feldspar and garnet (there is no purple colouration). Discrete (30-60 cm long) amphibolite pods are intercalated within this sequence. The entire zone is cut through by minor, small-scale anastomosing shear zones.

Well-banded purple gneiss with minor melt sheets (1-3 cm thick). Assymetric augen indicate shear top to the W. Within high-strain zones augen appear symmetric or are completely obliterated. Late pegmatites, cut the dominant foliation highlighted by quartzofeldspathic veins. Remnant isoclinal folds of the main fabric are also preserved.
Homogeneous, quartzofeldspathic sheet (laterally variable in thickness), parallel to the main S2 foliation with no evidence for cross-cutting relationships.

Early fabrics preserved in low-strain zones. In high-strain zones, folding is obliterated and quartzofeldspathic veins attenuated into the surrounding matrix.
Glassy (mylonitic) matrix, with augen (0.4-1 cm long) of K-feldspar. Stringers of quartz (up to 0.5 cm thick) are found throughout this unit.
Homogeneous purple gneiss containing disrupted quartzofeldspathic stringers.

Fig. 2.7: Log C-C′ (Insert, Map C), through a series of stacked/intercalated sheared pods recording a "pod-list", and associated fabrics. The log was made across the sheared boundary between the Vamvakia Purple Gneiss Formation and overlying Vamvakia Migmatites.

locality). Contact relationships between the different pods are uncertain due to the intense shear (S_2) fabrics.

At A^I the purple gneiss contains narrow (0.2-0.4 cm thick) leucosomes closely banded (1-3 cm wide), and tight to isoclinally folded with horizontal axial planes. Folds are attenuated by the shear related S_2 foliation creating an augen texture, with augen often preserving isolated fold closures. Leucocratic quartzofeldspathic sheets (possibly late melt) both cross-cut and are aligned with the S_2 augen foliation (Chapter 3; Plate 3.38). From A^I to A^{II} the earliest purple gneiss fabrics are preserved and exhibit two distinct sets of quartzofeldspathic leucosomes, similar in character to the Vamvakia Migmatite Formation (Section 2.3.2.1). At A^{II} the purple gneiss is inferred to lie beneath a large gabbroic pod (Section 2.3.2.5) with the contact obscured by a narrow (1-3 m wide) exposure of intermediately deformed Vamvakia Migmatites (Section 2.3.2.1).

Contacts between the pods consist of narrow shear zones (1-2 m wide). Half-way along section A^{II}-A^{III} the gabbroic pod (Section 2.3.2.5) overlies purple gneiss containing extensive local melts (Section 3.12.4.2). There is no continuity of purple gneiss exposure between sections A^I-A^{II} and A^{II}-A^{III}. However, the gneiss is either laterally continuous and connected beneath the gabbroic pod, with the gneiss and melts representing a structurally lower member, or the gneiss is present in discrete pods and these have moved into their present position from either different parts of the same precursor body (possibly ex-migmatite) or they have different source-bodies and P-T-t histories. Variations of angular purple gneiss blocks (5 cm to 1 m long) surrounded by local melts also crop out half-way along section A^{IV}-A^V (Section 3.12.4.2).

2.3.2.3 The Vamvakia Garnet Kyanite Schist Formation

This formation crops out predominantly in the northern section of the Vamvakia river within three distinct series of exposures (Insert, Map C), i) over 40 to 60 m; Section A-A^I, ii) over 20-30 m; to the south of Section A^{IV}-A^V, and iii) over 5 to 10 m; half-way along Section A^V-A^{VI}. The NW contact of the first set of exposures is poorly exposed but is inferred to be a sheared contact beneath a narrow ultramylonitic layer (5-30 cm thick), in turn beneath a series of gabbros, amphibolites and dolerites (Section 2.3.2.5). The SE contact is represented by a broad shear zone (2-6 m wide) which emplaced the formation over the highly deformed Vamvakia Migmatite Formation (Section 2.3.2.1). The migmatite is considered to have acted as a semi-rigid body, as the usual low-angle of dip (0-25°NW) of the shear zone increases to 45-60°NW, and ramps over the underlying formations (Fig. 2.8).

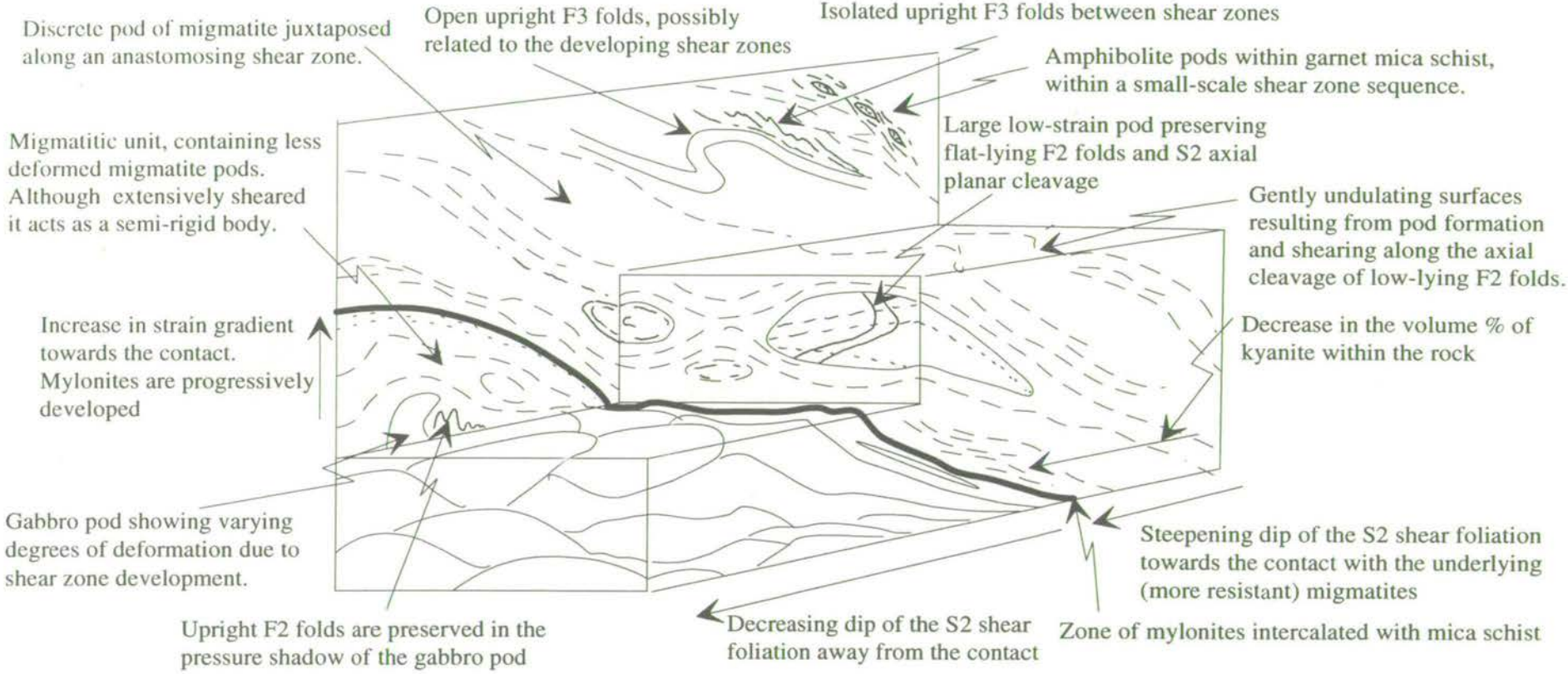

Fig. 2.8: Schematic block diagram for part of the Vamvakia river. Garnet mica schists are sheared over variably deformed migmatites, which are in turn juxtaposed via anastomosing shear zones over a range of purple gneisses.

The second main exposures crop out within a large sheared pod, intercalated between a series of gabbros and dolerites (towards the SE end of Section A^{IV}-A^{V}). Both the bottom and top contacts are composed of sharp flat-lying shear zones (0.5-1 m wide). The formation is emplaced above a mixture of gabbros and dolerites and below a sequence of amphibolites and ultramylonites.

A third small exposure crops out halfway along section A^{V}-A^{VI} and may be considered a part of the larger southern outcrop, as the contacts and lithologies with which it is juxtaposed are similar to the second main exposure.

The formation consists of distinctive garnet, muscovite schist with a variable content of plagioclase and kyanite. The northerly of the two outcrops is rich in muscovite (20-40% of the rock), finely banded (0.5-1.5 cm wide), and contains 1-3 mm diameter garnet porphyroblasts. Early isoclinal (F_1) fold cores are preserved in plagioclase augen. Shear zones which transect the formation intercalate a number of lithologies (e.g. amphibolites, dolerites) as elongate pods and cause a range of textural variations and fabrics to be developed within the formation over short distances (Fig. 2.9; *see* Insert, Map C for the locality). The southerly outcrop is richer in quartz and plagioclase and includes a distinctive coarse porphyroblastic garnet-kyanite schist with 1-1.5 cm diameter garnets and 1-2 cm long kyanites. This porphyroblastic lithology forms the cores of several recumbent tight to isoclinal F_2 folds. At least two well-developed continuous schistosities (probably early- to late- S_2 foliations) are developed throughout this formation related to the shear zones.

2.3.2.4 The Vamvakia Siberian Tiger Formation

This formation crops out in a number of exposures (4-27 m wide) within the southern section of the Vamvakia river (Insert, Map F). It is considered to be a metasomatised metasedimentary lithology, which now has a hornblende-diopside-epidote assemblage. The formation is mostly in faulted contact with a range of amphibolites and occasionally schists. However, at one locality approximately 500 to 800 m north of Vamvakia the formation has a progressively sheared contact (2-4 m wide) with well-banded amphibolites. The banding within the amphibolites dips between 40-47°NW in contrast to the sub-horizontal fabric of the Siberian Tiger Formation (Chapter 3; Plate 3.30). The compositional variation and banding within these amphibolites possibly represents a series of sheeted dykes. Differences in the dip of fabrics between the formations could be interpreted as originally inclined dykes, now amphibolites intruding and cross-cutting the sub-horizontal bedding now a metasedimentary fabric.

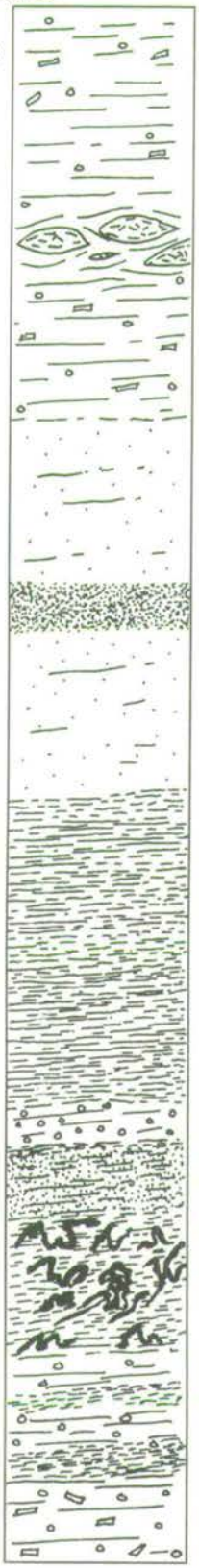

Well-banded sequence (2-6 cm thick) of garnet-kyanite-muscovite schists and gniesses.

Large amphibolite pods (≤ 1 m long, 60 cm wide), with garnet porphyroblasts up to 1.5 cm in diameter.

Garnet-muscovite-kyanite schist.

Minor reddish-brown carbonate contamination along faults and fractures.

Very fine-grained "glassy" (mylonitised) purple gneiss.

45 cm thick band of very fine-grained homogeneous garnet-K-feldspar-biotite gneiss. Weak development of a quartzofeldspathic layering.

Very fine-grained "glassy" (mylonitised) biotite-rich amphibolite.

Banded amphibolites with variable proportions of k-feldspar and garnet. Quartzofeldspathic-rich bands are fairly continuous highlighting the main S_2 foliation.

30 cm thick band of garnet-muscovite schist.

40 cm thick band of biotite-rich amphibolite with wispy feldspathic bands highlighting the main foliation.

Highly-deformed biotite-rich migmatite gneiss. Large porphyroclasts of k-feldspar are preserved in a biotite-rich matrix. The feldspathic porphyroclasts are progressively attenuated up sequence.

Interbanded garnet, muscovite Schist and a feldspathic, garnet-rich amphibolite. Close to tight upright F_2 folds are highlighted by the feldspathic banding.

Massively banded garnet-mica-kyanite-schist. A range of foliations are developed due to the high mica content of the rock.

Fig. 2.9: Log B-B′ (Insert, Map C), through a series of stacked/intercalated sheared pods recording a "pod-list", and associated fabrics. The log was made across the sheared boundary between the Vamvakia Garnet Kyanite Schist Formation and overlying amphibolites. All boundaries (contacts) are gradational across variably thick high-strain shear zones.

The formation consists of vaguely banded light green- to red, discontinuous pods and bands (0.2-1.5 cm thick and 3-40 cm long) within a quartzofeldspathic matrix. Continuity of the coloured bands is variable resulting in an overall appearance of "tiger-stripes" (Chapter 3; Plate 3.30). The striping generally remains uniform throughout the outcrop and is interpreted as remnant sedimentary bedding, much transformed by reaction during metamorphism. It is tentatively proposed that this formation represents a sequence of sediments caught up within a sheeted dyke complex. This interpretation is the same as that proposed by Dixon and Dimitriadis (1984) from study of screens of a similar looking tiger-striped lithology (which are composed of dark-green and black stripes within a quartzofeldspathic matrix) within the Volvi Complex, towards its western margin (Section 2.5). The only variation between the two lithologies is the colour of the discontinuous pods.

2.3.2.5 *The Vamvakia Mafic Formation*

This formation is the most extensive along the Vamvakia river. Petrography and geochemistry of the formation indicates a close comparison to the Volvi Complex (Chapter 5). Contact relationships between different mafic members and other formations are usually obscure, with juxtaposition of the various lithologies via flat-lying shear zones (Plate 2.6). Low-strain pods between shear zones preserve a number of intrusive, cross-cutting relationships usually between mafic lithologies, however, occasionally dykes cross-cutting country rock are seen (Chapter 3).

Gabbros: are common throughout the river (Insert, Map C) and occur as relatively undeformed medium- to coarse-grained (Plate 2.7a; Section A^{II}-A^{III}), and saussuritised gabbroic pods (Section A^{I}-A^{II}). Medium- to coarse-grained gabbros crop out as continuous large (up to 40 m long) pods, bounded by and cut through by anastomosing shear zones. Along section A^{II}-A^{III} the gabbro lies above a range of purple gneisses (Section 2.3.2.2) and beneath Vamvakia Migmatites (Section 2.3.2.1). Within this outcrop coarse-grained gabbroic pegmatitic pods (5 cm in diameter) and veinlets are common (Plates 2.7b). Occasionally, networks of gabbroic pegmatite are developed and constitute 20-40% of the rock (Plate 2.7c). The gabbroic pegmatite pods and veinlets usually have gradational boundaries with the medium-grained gabbroic host, however, sharp cross-cutting contacts are also observed (Plate 2.7d). Shear zones develop a progressive range of fabrics with gabbroic pods from low-strain cores, to high-strain rims (Chapter 3; Plate 3.29). Variations in the fabrics and petrography of a gabbroic pod (1.5-2 m in diameter) contained within the highly deformed Vamvakia Migmatite (Section A-A^{I}) are described in Chapters 3 and 4 respectively.

Plate 2.6

Large boudin of gabbro wrapped by anastomosing shear zones. Main pod to the left of the photograph overlaps a highly sheared/talc matrix. To the left of the photograph the main fine-grained pod overlies a series of small shear zone bounded pods and passes into a thick sequence of mylonitised and ultramylonitised lithologies (possibly ex-migmatite). Horizontal field of view is about 12 m across, looking approximately South.

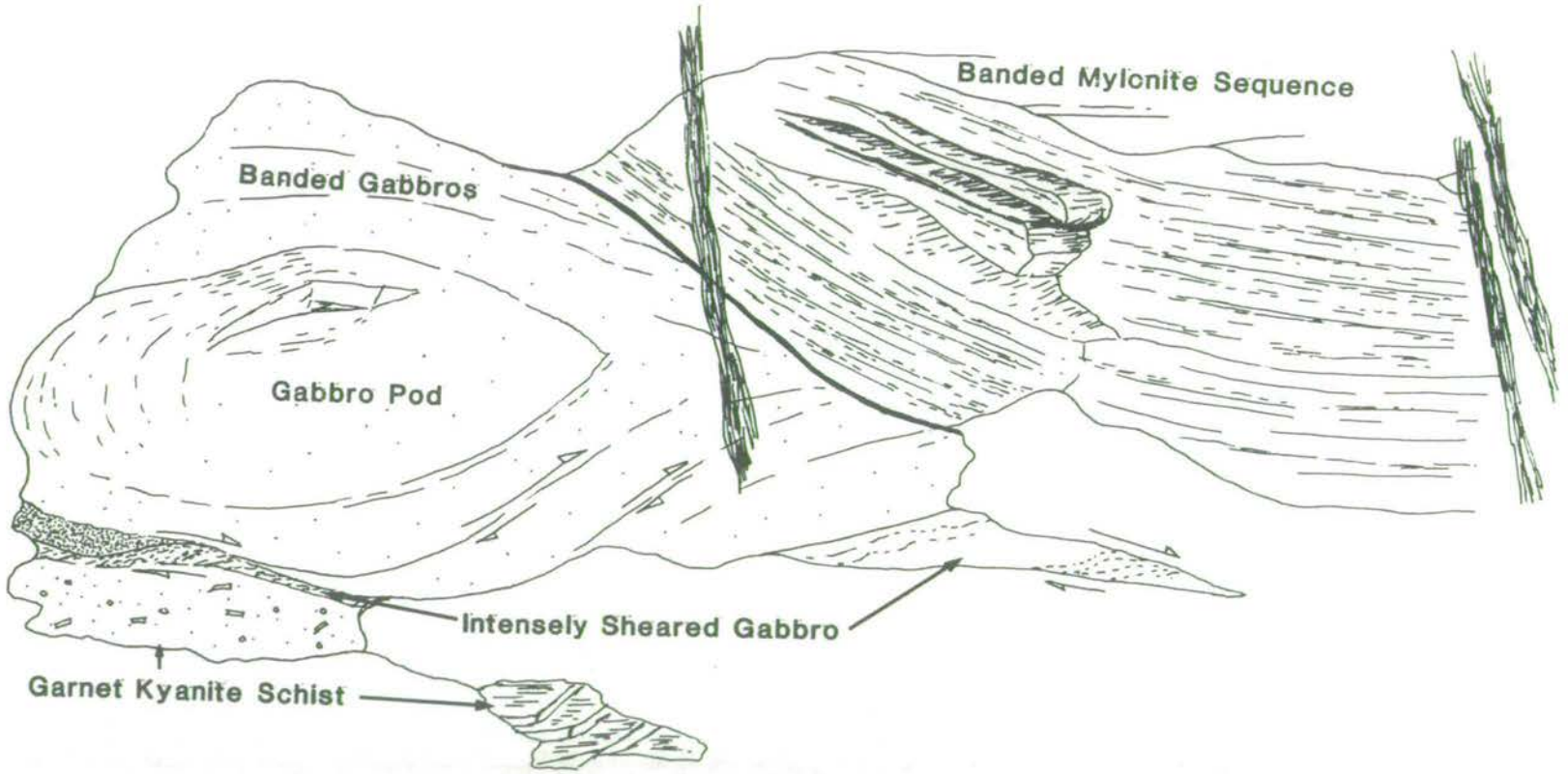

Plate 2.6

Plate 2.7

Typical gabbroic lithologies and fabrics from the northern section of the Vamvakia river. Coin is 27 mm in diameter.

Plate 2.7a: A typical medium- to coarse-grained gabbro, with no tectonic fabric developed.

Plate 2.7b: Discrete pod of a coarse-grained pegmatite within an homogeneous medium-grained gabbro. The pod may actually show an isolated fold hinge which has had its limbs completely attenuated.

Plate 2.7c: Network of pegmatitic veins within a medium-grained gabbro.

Plate 2.7d: Sharp contact between a coarse- and fine-grained gabbro. No chilled or baked margins are seen, suggesting that both gabbro bodies were at an equivalent temperature during intrusion,

Plate 2.7

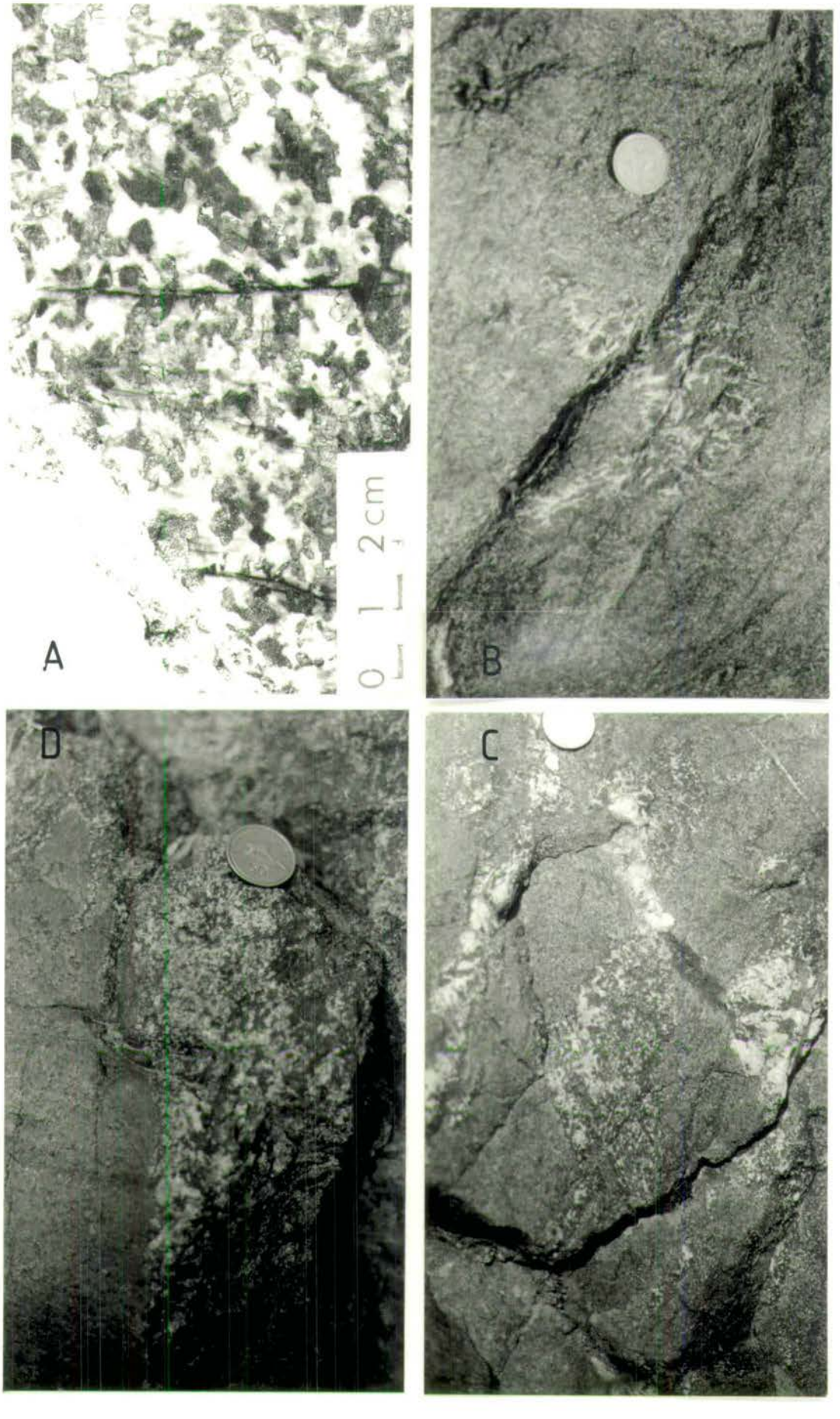

Dolerite: occurs in large laterally continuous bodies throughout the Vamvakia river and within the northern section (Insert, Map C) along sections A^{IV}-A^{V} and A^{V}-A^{VI}. Minor discontinuous, elongate (1-3 m long) pods are intercalated along shear zones with other formations and possibly represent attenuated/sheared dykes. It is possible that shear zones utilise and propagate along dyke-country rock boundaries, hence obscuring the original intrusive, cross-cutting relationship. At the end of section A^{V}-A^{VI}, a low-strain body containing large, angular, dolerite blocks (0.2-1.5 m in diameter) within a quartzofeldspathic matrix is interpreted to represent original magmatic mixing (Chapter 3; Plate 3.28). Similar outcrops are also found within the Volvi Complex (Section 2.5.2).

Amphibolite: crops out intermittently along the entire length of the river as generally homogeneous masses (1 to 40 m long), however, occasionally foliations highlighted by wispy, quartzofeldspathic blebs, or more continuous quartz-plagioclase leucocratic layers are developed. The amphibolites are often biotite-rich and an igneous parentage is occasionally uncertain. However, the petrography and geochemistry (Chapter 5) does not vary from that of the ortho-amphibolites found elsewhere around Lake Volvi (e.g. Section 2.5.4.1).

2.3.3 West: From the Arnaea Granite to the Volvi Complex

Vertiskos Group lithologies (Fig. 2.5) crop out from the Arnaea granite (the contact is approximately along the N-S trending road between Vaiohorion and Askos) in the west, to the western boundary of the Volvi Complex (approximately 3 km east of Megali Volvi) in the east (Inserts, Maps B, D and E). The best exposure occurs along the bottom of the numerous N-S trending streams (incising the south facing flank of the Besikon Hills), with the exposure on the hill-sides generally poor, restricting detailed correlation between stream sections. Extensive Neotectonic faulting, anastomosing sub-vertical shear zones and well-developed pervasive (S_2) foliations are common within the area (Chapter 3). These structures mostly obscure the contact relationships and original spatial arrangements of the Vertiskos Group formations. Consequently, the formations west of the Volvi Complex appear to be discontinuous and/or laterally variable in thickness, with an approximate NNW-SSE outcrop trend.

2.3.3.1 The Askos Marginal Amphibolite Formation

This formation crops out as a laterally continuous body from immediately north of Vaiohorion, to Askos, with an approximate NNW-SSE trend (Insert, Map B). Contact relationships between this formation and the Arnaea Granite to the west are

complex, obscured by two stages of shearing and extensive Neotectonic faulting (Section 2.6.3). The eastern contact can be divided into two sections; to the north, with the Askos Augen Orthogneiss Member (Section 2.6.3); to the south, with the Askos Augen Paragneiss Formation (Section 2.3.3.2). The SE contact is obscured by strong NNW-SSE trending (S_2) foliations which vary in dip from sub-vertical to 35° W, and by a series of shear zones (Chapter 3).

The formation consists of a dark, homogeneous, fine- to medium-grained amphibolite containing numerous leucocratic and augen granitic sheets and pods (approximately 20-40% of the rock). Mineral assemblages of the leucocratic sheets are similar to the Askos Augen Orthogneiss Member (Section 2.6.3) and Arnaea Granite (Section 2.6.3), *see* Chapter 4 for a review of the petrography. The large (0.5-1.5 m thick) leucocratic sheets have a distinctive medium- to coarse-grained, quartzofeldspathic augen fabric (Section 2.6.3), whereas the small (0.5-25 cm thick), leucocratic sheets are homogeneous and fine- to medium-grained. The leucocratic sheets are commonly in an intermediate state of strain, and tight to isoclinally folded. In low-strain zones the leucocratic sheets are open to tightly folded, whereas, in high-strain zones the leucocratic sheets are attenuated and wrapped by the amphibolite host resulting in discrete pods. The origin of this formation is uncertain and consequently several questions arise:

i) Does the amphibolite have an ortho- or para-origin?

ii) Does the amphibolite represent an "old" basement amphibolite with well-developed leucocratic segregations, injected by a series of later sheets and apophyses related to the intrusion of the Arnaea granite?

iii) Does the amphibolite formation simply represent a mafic intrusion related to the emplacement of the Volvi Complex, which has been intruded by a series of granitic sheets from the Arnaea granite?

iv) As the amphibolite formation creates an effective boundary between the Arnaea granite and the Vertiskos gneisses, is it an early marginal facies to the granite?

From the homogeneity and geochemistry (Chapter 5) of the amphibolite matrix the formation is identified as an ortho-amphibolite, with a geochemical signature comparable to the Volvi Complex. From field observations and petrographic studies the leucocratic sheets are considered to represent numerous stages of intrusion from the Arnaea granite. The Askos Marginal Amphibolite Formation is therefore considered to be an extensive mafic formation associated with the Volvi Complex (Section 2.5)

2.3.3.2 The Askos Augen Paragneiss Formation

This formation crops out in a continuous NNW-SSE trending sequence from immediately NW of Megali Volvi to Askos (Inserts, Maps B and D). The formation is laterally variable in thickness and contains numerous intercalations of other formations along anastomosing shear zones. These intercalated lithologies are contained within elongate pods, aligned parallel to the dominant (S_2) foliation, with a NW-NNW to SE-SSE trend. Contacts with the Askos Marginal Amphibolite Formation (Section 2.3.3.1) and Askos Augen Orthogneiss Member (Section 2.6.3) to the west, are complex as they are intercalated along anastomosing shear zones and define a broad contact zone. The actual contacts between individual pods are obscured by well-developed (S_2) foliations.

The formation consists of an intensely deformed quartzofeldspathic component within a micaceous matrix. The formation has usually been subjected to intense deformation and appears as a quartzofeldspathic augen gneiss, with the augen ranging from 0.5-1.5 cm in length. However, in low-strain areas the augen are observed as highly disrupted leucocratic sheets, occasionally preserving rootless isoclinal fold closures, wrapped and disrupted by at least two strong foliations. This formation is interpreted as a remnant highly deformed migmatite.

2.3.3.3 The Askos Feldspar Mica Schist Formation

This formation crops out to the west of Megali Volvi, intercalated with the Askos Garnet Mica Paragneiss Formation (Section 2.3.3.4), amphibolites and the formations of the Volvi Metasedimentary (re: Svoula) Group (Section 2.4). The formation consists of banded (cm- to m-scale) quartz-plagioclase and biotite-rich layers. Due to changes in the ratio of quartz and plagioclase to biotite a variety of schists are developed. Intense deformation has obliterated early S_1 foliations and developed a range of early to late S_2 foliations and structures from rootless isoclinal folds to kink bands (Chapter 3).

2.3.3.4 The Askos Garnet Mica Paragneiss Formation

This formation has the most extensive outcrop within the Vertiskos Group, west of the Volvi Complex. The formation crops out to the north of Megali Volvi and to the south of Askos, and is inferred to follow a continuous NNW-SSE trend between the two (Inserts, Maps B and D). This formation also crops out along the Askos to Anoixia road and around Xiropotamos. Variations of composition and states of strain in this formation make it too complex to be subdivided effectively with the amount of exposure available.

The formation is highly sheared and generally well-banded on a mm-, cm- and m-scale creating a distinctive stripy appearance. The major gneissic foliation (large m-scale banding) is well-preserved and consists of laterally continuous layers. Discontinuous leucocratic blebs with remnant fold closures are commonly preserved intercalated with the gneissic foliation on a cm-scale. A range of lithologies are preserved in discrete elongate pods, which have been attenuated or intercalated along the strong gneissic foliation during shearing. Within a number of bands, discontinuous leucocratic quartzofeldspathic stringers are intensely folded and refolded with often only the fold closures preserved. From the relatively large percentage of leucocratic layers/stringers within these bands, a migmatitic precursor is inferred. The formation as a whole is interpreted as an intensely folded and sheared migmatitic/gneissic sequence, and potential precursors are found throughout the area.

2.3.3.5 The Askos Garnet Mica Schist Formation

This formation outcrops predominantly to the NE of Vaiohorion, NW of Megali Volvi and S of Askos (Inserts, Maps B and D). Contact relationships with the adjacent lithologies are obscured by the regional (S_2) foliations, anastomosing shear zones and Neotectonic faulting.

The formation is composed of a variety of garnetiferous quartzofeldspathic mica schists. Staurolite is found within some of the more pelitic members (Chapter 4). From the structures preserved within this formation (Chapter 3) the entire outcrop is considered to be a low-strain core wrapped by high-strain anastomosing shear zones. Tectonic reactivation along the main foliation via shear zones is considered to have resulted in the intercalation of this formation with the adjacent lithologies.

2.3.3.6 The Volvi Ultramafic Formation

This formation crops out in three main areas around the Volvi Complex.

To the east of the Volvi Complex: the Arethousa Ultramafic Member is a large serpentinised body (2.5-3.5 km long, 1-1.5 km wide), to the east of Arethousa (Insert, Map F). The western contact is inferred to be juxtaposed against a major normal fault. Along several streams south of Arethousa, eastwards into this unit, distinctive low-angle shear fabrics are developed (Chapter 3; Plate 3.19). Between these fabrics are small (0.5-1 m diameter) pods of dense, dark, ultramafic material within a light-green, poorly consolidated, fissile matrix. This unit lies above garnetiferous schists similar to the Vamvakia Garnet Kyanite Schist Formation (Section 2.3.2.3). Near the source of the streams in the east, the dip of the low-angle shear fabrics and related foliations steepen (from 5° to 50°SW), which obscures the contact with the underlying

formations. This unit overlies an amphibolite formation to the north and the Stefanaina Marble Formation (Section 2.2.5.2) to the east. From its position close to the eastern margin of the Vamvakia river, it is inferred to be a tectonically displaced sliver of the Volvi Complex.

To the NW of the Volvi Complex: the Askos Ultramafic Member is a large serpentinised body (0.5-1 km diameter), 1 km to the east of Askos, and predominantly north of the Askos to Anoixia road. Contacts with the adjacent Vertiskos gneisses are sheared with a variable, steep to inclined dip and WNW to ENE trend, typical of the regional (S_2) foliation. Fabrics developed within this unit range from massive serpentinite, with a finely-spaced (0.2-0.5 mm wide) penetrative (S_2) foliation at the core, to a talc schist at the rim immediately adjacent to the sheared contact. The presence of talc schist implies SiO_2 infiltration has occured along the sheared contact.

To the W of the Volvi Complex and to the north of Vaiohorion: the Vaiohorion Ultramafic Member crops out between the Askos Marginal Amphibolite Formation (Section 2.3.3.1) and the Askos Augen Paragneiss Formation (Section 2.3.3.2) as sheared pods and boudins (1-5 m long, 0.5-3 m wide) with little if any lateral continuity. Original contact relationships are obscured by the well-developed regional (S_2) foliation and tectonic intercalation via anastomosing shear zones.

From the proximity of the Vaiohorion and Askos Ultramafic Members, a tentative correlation is made. Due to the spatial arrangement of these ultramafic members with the Askos Marginal Amphibolite Formation (Section 2.3.3.1), a further possible correlatable association is proposed. This correlation is supported by the less ambiguous, although tentative association between the Arethousa Ultramafic Member and the Volvi Complex. Hence, as the Askos Marginal Amphibolite Formation (Section 2.3.3.1) is assigned as an outlying sliver of the Volvi Complex, these Ultramafic members are in turn considered to have a possible origin related to the Volvi Complex.

2.3.4 South: From Around the Villages of Nea Madhitos and Modhi

Only a brief reconnaissance of the area south of Lake Volvi was undertaken consisting of, i) a stream section 1 km to the SE of Nea Madhitos (near the football ground), and ii) exposures in and around Modhi. Both areas revealed only minor exposures of Vertiskos lithologies, below more extensive units of the Volvi Metasedimentary (re: Svoula) Group (Section 2.4). The structural style is dominated by a series of late low-angle shear zones. Intercalation of the Vertiskos Group and metasedimentary cover units is widespread, and as elsewhere, has a tendency to disrupt the continuity of the lithostratigraphic sequence (Fig. 2.5), which consists of:

2.3.4.1 The Nea Madhitos Amphibolite Formation

This formation crops out as minor (1-5 m wide) bodies within the ortho- and para-gneiss formations from the Nea Madhitos area. Contact relationships with the gneissic host are always obscure, due to intercalation parallel with the dominant (S_2) foliation. The amphibolite bodies tend to be irregular in shape and laterally discontinuous, due to a mixture of late anastomosing shear zones and brittle faulting. The amphibolite bodies tend to be heterogeneous in composition, even over small outcrops, although there is minor variation in the quantity of plagioclase-feldspar (5 to 15% of the rock). The plagioclase component appears as a speckled (0.2-0.5 mm porphyroblasts) and occasionally banded texture (0.5-1 mm thick). Dark amphibolites with no or little plagioclase component occur as (1-10 cm long) enclaves within the more quartzofeldspathic lithologies. Geochemistry of these amphibolites reveals a typical Volvi Complex pattern (Chapter 5). However, the majority of the samples from the Nea Madhitos data set are either evolved or too altered to be used in the main geochemical analysis of the area (Chapter 5).

2.3.4.2 The Nea Madhitos Leucocratic Gneiss Formation

This formation crops out in fairly continuous exposures along the bottom of the stream section to the SE of Nea Madhitos. Contacts with the Nea Madhitos Paragneiss Formation (Section 2.3.4.3) appear to be gradational, whereas contacts with the overlying metasedimentary lithologies (Section 2.4) occur by juxtaposition along low-angle shear zones (Chapter 3; Plate 3.3) and across zones of chaotic mixing. A reddish-brown colouration is often developed throughout the outcrop, and particularly along fractures creating veinlets due to deposition of dolomite.

In general the formation consists of dark, homogeneous, biotite-rich amphibolite, containing numerous (0.2-15 cm thick) quartzofeldspathic sheets (5-30% of the rock). The leucocratic sheets are folded into close to isoclinal (F_2) folds. From the common occurrence of pairs of parallel leucocratic sheets, an earlier tight to isoclinal fold stage (either F_1 or early F_2) is inferred (Chapter 3). However, field evidence for refolded folds is extremely rare. The main (S_2) foliations change progressively from finely-spaced crenulation cleavages (0.2-0.4 mm wide), to intense blocky spaced cleavages (0.5-1 cm wide) towards the shear contact. The decollement surface (Chapter 3; Plate 3.3) suggests shear movement top to the left (west). However, there is no apparent consistency of kinematic indicators for these brittle shear zones. Minor (1-4 m long), homogeneous, fine-grained amphibolite bodies contained within this formation are intercalated along the (S_2) foliations (Section 2.3.4.1).

2.3.4.3 The Nea Madhitos Paragneiss Formation

This formation crops out throughout the area south of Lake Volvi. Contact relationships with the Nea Madhitos Leucocratic Gneiss Formation (Section 2.3.4.2), Modhi Coloured Gneiss Formation (Section 2.4.2) and the Nea Madhitos Marble Member (Section 2.4.5) are obscure due to tectonic displacements and poor exposure.

There are two distinct end members of the paragneiss formation, an essentially quartzofeldspathic gneiss with a variable but low-percentage of white-mica and a more micaceous end member containing garnet. From the composition of this formation it is interpreted as a psammitic to semi-pelitic sequence.

This formation is highly deformed exhibiting chaotic tight to isoclinal folding, and refolded folds (Chapter 3). The garnet-mica end member generally exhibits a finely spaced (0.2-0.6 mm wide) crenulation cleavage. However, variations of cleavage also include examples of spaced and S-C cleavages (Chapter 3).

2.3.5 Compilation and Summary

By correlating the available information it is possible to derive a schematic composite lithostratigraphy (Fig. 2.10). The earliest rocks within the Vertiskos Group consists of a migmatitic basement. The best examples are preserved in low-strain pods to the east of the Volvi Complex (Vamvakia Migmatite Formation, Section 2.3.2.1; Vamvakia Purple Gneiss Formation, Section 2.3.2.2). Equivalent, although more highly deformed and less extensive formations also crop out to the west of the Volvi Complex (Askos Augen Paragneiss Formation, Section 2.3.3.2; and certain horizons within the Askos Garnet Mica Paragneiss Formation, Section 2.3.3.4).

This migmatite basement (especially along the Vamvakia river) preserves evidence for an early, progressive deformation event (D_1), prior to the development of S_2 fabrics and shear zone development (Chapter 3). However, the majority of the early migmatite fabrics are subjected to later (D_2) deformation (folding and shearing) which partially or completely transposes the early migmatite fabrics. This is particularly true of the migmatites to the west of the Volvi Complex. The majority of the migmatites within the Vertiskos Group have a general quartz-plagioclase-biotite composition and are relatively useless for constraining the early P-T history. However, the Vamvakia Purple Gneiss Formation (Section 2.3.2.2) has a more varied assemblage and is reviewed in greater detail in Chapter 4. A tentative correlation can be made between these migmatites and the migmatite basement of the Kerdilion Group (Section 2.2.6), *see* Section 2.7.

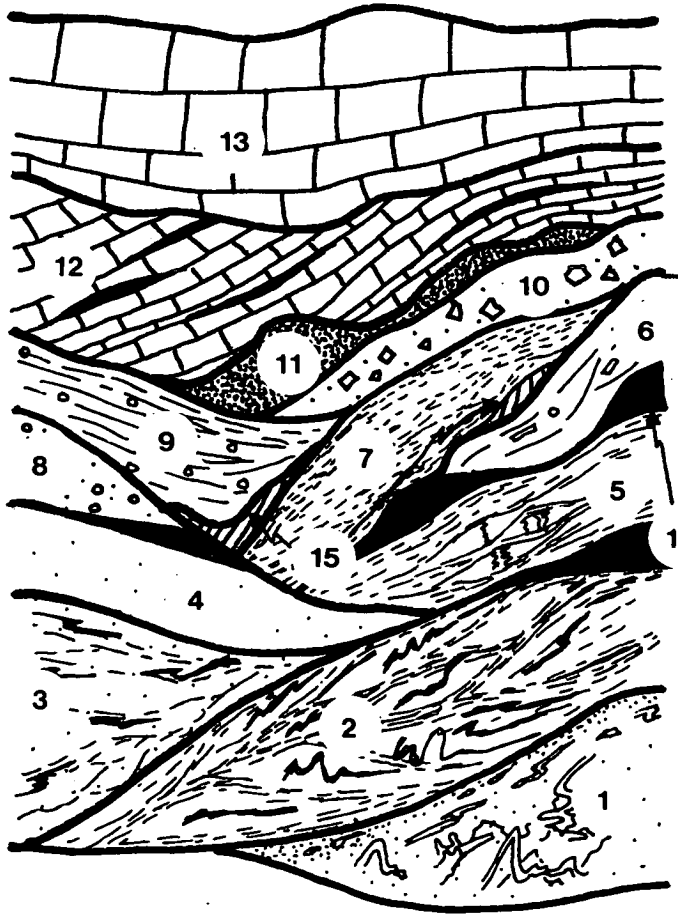

15 The Volvi Ultramafic Formation
The Nea Madhitos Amphibolite Formation
14 The Askos Marginal Amphibolite Formation
The Vamvakia Mafic Formation

Volvi Complex

13 The Megali Volvi Marble Formation
12 The Megali Volvi Quartzofeldspathic Gneiss Formation
11 The Megali Volvi Garnet Graphite Schist Formation
10 The Modhi Coloured Gneiss Formation
The Vamvakia Siberian Tiger Formation

Volvi Metasedimentary Group

9 The Askos Garnet Mica Schist Formation
8 The Nea Madhitos Paragneiss Formation
7 The Vamvakia Garnet Kyanite Schist Formation
6 The Askos Garnet Mica Paragneiss Formation
5 The Nea Madhitos Leucocratic Gneiss Formation
4 The Askos Feldspar Mica Schist Formation

Kerdilion

Vertiskos Group

3 The Askos Augen Paragneiss Formation
2 The Vamvakia Purple Gneiss Formation
1 The Vamvakia Migmatite Formation

Fig. 2.10: Schematic summary diagram representing the lithostratigraphic sequence for the Vertiskos and Volvi Metasedimentary Groups. This sequence has been derived from relationships within and between a series of anastomosing pods. The lithostratigraphic sequence follows the reinterpretated lithostratigraphic sequence proposed in section 2.7

The precursors for these basement lithologies are indeterminable as the original characteristics have been obliterated during the early deformation and metamorphic (D_1) events which developed the migmatites. The original position and stratigraphic arrangement of the migmatite formations with respect to adjacent gneissic formations has been obscured by movement and juxtaposition along steep (to the west of the Volvi Complex) and flat-lying (to the east of the Volvi Complex) shear zones (Chapter 3). Hence, the spatial arrangements of the formations at present are complex. However, the migmatites are inferred to be stratigraphically overlain by a series of paragneiss and schistose formations (Askos Garnet Mica Schist Formation, Section 2.3.3.5; Nea Madhitos Paragneiss Formation, Section 2.3.4.3 and the Vamvakia Garnet Kyanite Schist Formation, Section 2.3.2.3). These formations only contain evidence of deformation during the later (D_2) deformation event and hence, are considered to be a cover to the migmatite basement. The Askos Garnet Mica Paragneiss Formation (Section 2.3.3.4) may possibly represent one of the stratigraphically lowest gneissic units, due to the extensive inclusion of migmatitic bands and pods. This interbanding may have resulted from tight interfolding and/or shearing of an (possibly irregular) original contact surface, resulting in a more heterogeneous composite lithology.

The spatial relationship between the gneissic and schistose formations are complex and there is no locality where an original stratigraphic sequence is present. However, by accepting a progressively folded sequence prior to shearing (Chapter 3) of a generally layered gneissic/schistose sequence (the simplest model), a schematic stratigraphic sequence can be compiled. The Askos Garnet Mica Paragneiss Formation (Section 2.3.3.3) is inferred to be the lowest stratigraphic unit, immediately adjacent to the migmatite basement (which to the west of the Volvi Complex is composed of the Askos Augen Paragneiss Formation, Section 2.3.3.2). This is supported by the fact this formation has the most extensive outcrop within the area, which would be expected with increasing levels of erosion. This formation is in turn inferred to lie beneath the Askos Feldspar Mica Schist Formation (Section 2.3.3.3). This formation has a limited outcrop and appears to border or surround the Askos Garnet Mica Schist Formation (Section 2.3.3.5), which has the smallest outcrop and shows the clearest fold structures, as it is preserved in low-strain cores. Due to the garnet-staurolite assemblages found within this pelite formation, it is tentatively correlated with the Vamvakia Garnet Kyanite Schist Formation (Section 2.3.2.3), and the Nea Madhitos Paragneiss Formation (Section 2.3.4.3). The stratigraphic position

of the Nea Madhitos Leucocratic Gneiss Formation (Section 2.3.4.2) is uncertain but can be inferred to have a position somewhere near the basement-cover boundary.

Intercalated with these gneissic/schistose formations along anastomosing shear zones are a number of variably sized mafic/amphibolite formations (Askos Marginal Amphibolite Formation, Section 2.3.3.1; Nea Madhitos Amphibolite Formation, Section 2.3.4.1; Vamvakia Mafic Formation, Section 2.3.2.5 and the Volvi Ultramafic Formation, Section 2.3.3.6). Geochemical signatures of these formations do not vary significantly from the Volvi Complex (Chapter 5). Hence, all these formations are considered to be tectonically intercalated into the gneissic/schistose sequence rather than para-amphibolites conformably interbanded. However, due to the extensive alteration of some of the samples, this cannot be completely dismissed. The leucocratic sheets and veinlets within the Askos Marginal Amphibolite Formation (Section 2.3.3.1) have been derived from the Arnaea granite (Section 2.6.3), hence this amphibolite at least had been tectonically intercalated prior to granite emplacement (Section 2.7). The Vamvakia Mafic Formation (Section 2.3.2.5), is considered to represent the eastern boundary of the Volvi Complex. The stratigraphic sequence along this boundary is obscure due to the complex podded, anastomosing shear zone arrangement.

Also cross-cutting and intercalated with the gneissic/schistose lithologies are numerous mafic dykes (Section 3.11). From geochemical signatures these dykes are unequivocally linked with the Volvi Complex and help to constrain the complex as an *in situ* intrusion. Timing of dyke emplacement is difficult to constrain but is inferred to have been active during the progressive F_2 folding event and possibly during shear zone development (Chapter 3). The main timing constraints are based on the lack of dykes intruding and therefore older than the Volvi Metasedimentary (re: Svoula) Group (Section 2.4) and the Arnaea granite (Section 2.6.3).

2.4 The Volvi Metasedimentary (re: Svoula) Group

2.4.1 Introduction

A brief introduction to the "Svoula" Group is presented in Chapter 1. The metasedimentary formations of this Group were historically considered to be a lateral extension of the true Svoula Group (Kockel *et al.*, 1971, 1977; Kauffmann *et al.*, 1976). The importance of these metasedimentary sequences arises from the identification by Kauffmann *et al.*, (1976) of the Upper Triassic age of the Svoula marble. This Late Triassic age is critically important in establishing the conventional view of the internal history of the SMM in the vicinity of the Volvi Complex. SE of Thessaloniki the border of the SMM is a region of steeply dipping elongate strips of Svoula marble, metamorphosed Svoula flysch and Serbo-Macedonian schists. The Svoula marble strips appear to merge to the south with a north-south trending series of marble and phyllite horizons which strike up into the SMM proper, to the east of the Arnaea mass. These marble and relatively minor phyllite horizons within the massif are interpreted by Kockel *et al.*, (1977) as infolded and/or tectonically intercalated, *outliers* of Triassic and Lower Jurassic Svoula marble and flysch. Significantly, they are mapped outcropping immediately adjacent to the western margin of the Volvi body. If this stratigraphic correlation is correct then the deformation and metamorphic state of these intercalations in relation to that of the Vertiskos Schists and the neighbouring Volvi Complex, should provide a valuable reference point in a relative and absolute chronology of events.

However, the field evidence for this correlation is extremely tenuous, and the lithological and petrographic comparisons on which it is based are not very convincing. Because of this uncertain correlation, the term "Svoula Group" is abandoned for this sequence and the term "*Volvi Metasedimentary Group*" is adopted. This project aimed to clarify this point of contention by detailed mapping of contact areas in order to determine the areal extent of the Volvi Metasedimentary Group and its contact relationships with the underlying Vertiskos Group. The project also aimed to develop a lithostratigraphic sequence which could be used to correlate similar metasedimentary sequences elsewhere in the SMM. Although historically the Volvi Metasedimentary and Svoula Groups have been correlated, this study proposes a correlation between the outcrops of the Volvi Metasedimentary Group west of the Volvi Complex, with the Kerdilion and/or Modhi Marbles and their associated formations, east of the Complex (Section 2.7). Alternative models for the origin of the Volvi Metasedimentary Group are presented in Chapter 6.

To the north of Lake Volvi the Volvi Metasedimentary Group crops out in a series of discontinuous NW-SE trending outcrops predominantly to the west of the

Volvi Complex (Insert, Map E), from Megali Volvi in the south, to Filadelphi in the north. Minor exposures also occur in the southern section of the Vamvakia river (Vamvakia Siberian Tiger Formation, Section 2.3.2.4). The best exposures are generally found along the bottom of the N-S trending rivers. However, a number of marble horizons can be easily traced across the hill-sides. Field evidence indicates that the outcrop pattern of this group is related to laterally discontinuous, infolded sequences (Chapter 3), which have been modified and intercalated along major anastomosing shear zones.

To the south of Lake Volvi (Insert, Map G) the Volvi Metasedimentary Group crops out in an arcuate fashion (Kockel *et al.*, 1971, 1977; Sakellariou, 1990; and my own observations). Field evidence for the original relationships of the Volvi Metasedimentary Group with the Vertiskos Group are obscured by, (a) late shear zones and the associated intensification of foliations towards the contacts, (b) intercalation and discontinuity of units along shear zones, (c) normal Neotectonic faulting, which appears to utilise the contact between the two Groups as a plane of weakness.

There are only slight variations in lithology and structural style north and south of Lake Volvi. The formations comprising the group (Fig. 2.5) are described with reference to their northern outcrop and variations south of the lake are noted where appropriate.

2.4.2 The Modhi Coloured Gneiss Formation

This formation crops out throughout the area south of Lake Volvi. In reality it is not a true lithological formation, but simply a commonly occurring composite lithology representing a mixed series of gneisses (Nea Madhitos Leucocratic Gneiss, Section 2.3.4.2 and Paragneiss Formations, Section 2.3.4.3) and metasediments (the Megali Volvi Quartzofeldspathic Gneiss Formation, Section 2.4.4 and Marble Formation, Section 2.4.5). This formation has diffuse transitional boundaries (5-15 m wide) with the adjacent formations. The formation is characterised by being chaotic and highly deformed. Any continuity of outcrop is obscured by intense arrays of brittle fractures and low-angle shear zones. The formation is interpreted as a tectonic melange between large-scale, late, anastomosing shear zones.

2.4.3 The Megali Volvi Garnet Graphite Schist Formation

This formation crops out at the mouth of two stream sections about 1 km east of Megali Volvi and represents the western most outcrops of the metasedimentary group north of the lake. Minor exposures are also found to the south of Lake Volvi

(the Graphit-reiche Granat-gneise of Sakellariou, 1990; and supported by this study). As the exposures are close to the boundary with the Vertiskos gneisses, this formation could actually be a member of the gneissic/schistose Vertiskos Group (Section 2.3), now sheared and tectonically intercalated into sequence with the Volvi Metasedimentary Group. The exposure is discontinuous and occurs in a series of minor bodies (2-10 m long). The formation is easily deformed due to the high percentage of white-mica and graphite (40-60% of the rock). Contacts with the adjacent metasediments are obscured by the development of the strong regional (S_2) foliations.

The rock consists predominantly of a fine-grained quartzofeldspathic matrix, interbanded with layers of mica and graphite. A large phase of garnet porphyroblasts (1-2 cm in diameter) have overgrown early folded foliations and been wrapped by late foliations which are now at right angles to the original foliation trend (Chapter 3). The garnet porphyroblasts are common and contain fine graphite inclusion trails. A second clear garnet phase overprints the cores of the first garnet porphyroblasts.

2.4.4 The Megali Volvi Quartzofeldspathic Gneiss Formation

Outcrops of this formation are extensive within the metasedimentary group. The formation crops out predominantly between Megali Volvi and the Volvi Complex immediately north of Lake Volvi. Minor outcrops can be traced within stream sections and are inferred to follow a NW-SE trend. The formation is complexly folded, with tight to isoclinal (late F_2) folds overprinting an earlier F_2 or possibly F_1 fold stage (Chapter 3). Contact relationships with the adjacent formations are obscure but appear to be conformable and interfolded with the overlying impure carbonates and pure, white marbles of the Volvi Marble Formation (Section 2.4.5). The formation consists predominantly of quartz and plagioclase, with varieties containing minor quantities of white-mica.

2.4.5 The Megali Volvi Marble Formation

This formation crops out in a series of NW-SE trending exposures, from between Megali Volvi and the Volvi Complex in the south and past Filadelphi in the north. The main formation within the Volvi Metasedimentary Group consists of an impure, dolomitised carbonate member and a pure, white, coarse-grained, crystalline marble member. The lowest stratrgraphic unit is the medium- to coarse-grained reddish-brown carbonate member which generally exhibits well preserved F_2 folds and/or shear zones. This member is inferred to lie above the Megali Volvi Quartzofeldspathic Gneiss Formation (Section 2.4.4) and Garnet Graphite Schist

Formation (Section 2.4.3). The lower contact consists of a mixture of inter-banded, sheared and faulted formations. To the north of Lake Volvi the upper contact of the impure carbonate member is inferred to be gradational into the pure, white, crystalline marble member. This sequence is supported by the impure carbonate, to pure marble sequences exposed to the south of the lake around Nea Madhitos. The sequences to the south of the lake are less ambiguous than those north of the lake, as contacts are usually made across brittle, low-angle, shear zones. Late arrays of brittle fractures are also evident within some of the pure, crystalline marble horizons north of the lake.

2.4.6 Compilation and Summary

A correlation of metasedimentary sequences immediately to the north and south of Lake Volvi has already been proposed by Kockel *et al.*, (1971, 1977); Sakellariou (1990); and is supported by this work. The proposed stratigraphically younging sequence of the Modhi Coloured Gneiss Formation (Section 2.4.2), Megali Volvi Garnet Graphite Schist Formation (Section 2.4.3), Megali Volvi Quartzofeldspathic Formation (Section 2.4.4) and Megali Volvi Marble Formation (Section 2.4.5) is relatively unambiguous south of the lake where flat-lying extensional shear zones preserve an almost complete stratigraphic sequence, although always with some minor tectonic displacement.

The Modhi Coloured Gneiss Formation (Section 2.4.2) is interpreted as a tectonic melange developed during a late-ductile to brittle stage of shear zone development. Hence, contact relationships between Vertiskos gneisses and overlying metasediments are always across a tectonic boundary. North of the lake the sequences are not as clearly defined, as the formations are steeply inclined, laterally discontinuous and tectonically juxtaposed along anastomosing shear zones. The Megali Volvi Garnet Graphite Schist Formation (Section 2.4.3) south of the lake lies above the coloured gneiss (the Graphite-reiche Granat-Gneise of Sakellariou; and supported in this study), and can therefore be interpreted as a member of the Volvi Metasedimentary Group. From the inclusion trails within the garnet porphyroblasts and external fabrics this formation provides evidence for progressive deformation and transposition of the main foliation (Chapters 3) which cannot be observed in most of the more homogeneous or crystalline metasedimentary units. However, impure carbonates within the Kerdilion marbles (Modhi Marble Formation, Section 2.2.3.3) preserve interference structures indicative of a progressive deformation history. From a comparative study based predominantly on field relationships and supported by the tectonic history developed for the area (Chapters 3 and 6), the marbles and metasediments of the Kerdilion Group (Sections 2.2.2.4, 2.2.2.5, 2.2.3.3, 2.2.4.3,

2.2.5.2) are correlated with the metasedimentary sequences contained within the Vertsiskos Group and together comprise the Volvi Metasedimentary Group.

The formations of the metasedimentary group have been subjected to the same D_2 deformation and metamorphic events as the Vertiskos Group gneisses and schists. The main differences between the Volvi Metasedimentary Group and Vertiskos Group gneisses and schists are the lack of any pre-D_2 fabrics or structures and the lack of dykes (with the exception of the Vamvakia Siberian Tiger Formation, Section 2.3.2.4) within the metasediments. However, due to the similarity in structural history between the Volvi Metasedimentary Group and the Vertiskos Group the division between the most pelitic metasediments and the most pelitic gneisses is ambiguous. The division between gneissic basement and metasedimentary cover units is further obscured by the possibility of dykes intruding the earliest (lower) metasedimentary units but either being no longer active or unable to penetrate into higher (later) metasedimentary levels. The division between these units consists of lithologies which are unequivocally related to the Volvi Metasedimentary Group (e.g. the carbonate melange to pure, crystalline marble) and anything which is dubious (although possibly early formations of the metasedimentary group) attributed to the gneissic basement.

PART II: Major Igneous Intrusions

2.5 The Volvi Complex

2.5.1 Introduction

The Volvi Complex is a complex body of ophiolitic rocks approximately 120 km^2 in extent, composed mainly of a variety of deformed dykes and gabbros with amphibolite-facies metamorphic assemblages. The Volvi Complex lies immediately north of the eastern half of Lake Volvi and forms a rugged mass rising to 627 m. From the outset of the project it was determined that a detailed study of the Volvi Complex (*s.s.*) was not required, and consequently reference to the work of Dixon and Dimitriadis (1982, 1984, and work in progress) has been invaluable. The origin and emplacement of the Volvi Complex is the foremost aim of the project (Section 1.3). In order to satisfy the aims of the project, detailed mapping of the boundaries to the Volvi Complex was undertaken to determine the tectonic or intrusive relationships of the contact with the Vertiskos Group. Three areas provided the bulk of the field data:

i) *The eastern margin of the Volvi Complex*; along the Vamvakia river and road-cuttings along the Vamvakia to Arethousa road. The bulk of these lithologies have been reviewed (Section 2.3.1) in context with the local stratigraphic sequence.

ii) *The western margin of the Volvi Complex*; here they were studied in a couple of stream sections to the east of the proposed boundary with the Vertiskos gneisses with which they appeared to be partially intercalated.

iii) *The northern margin of the Volvi Complex*; this was the most extensive area studied, and was based around Lefkoudha.

2.5.2 A Review: The Volvi Complex *(Dixon and Dimitriadis, 1984; current work)*

The Volvi Complex is dominated by lithologies with a basaltic composition, but also has important intermediate basaltic andesitic or andesitic components. Minor outcrops of more evolved dioritic or granitic lithologies have been observed. Locally screens and angular blocks of highly metasomatised metasediments are found within dyke swarms (for comparisons of similar lithologies *see* Section 2.3.2.4, the Vamvakia Siberian Tiger Formation). Undeformed original igneous textures generally pseudomorphed by amphibolite-facies minerals, are preserved in rocks varying from fine-grained (1 mm) aphyric or micro-porphyritic (feldspar-phyric) dykes to very coarse pegmatitic gabbros with amphibolitised pyroxenes 10 cm long. The range of textural varieties within the Volvi Complex is the result of:

i) The extremely wide variation in the ratio of mafic to felsic components in original plutonic rocks 25:75 to 75:25 respectively.

ii) Superimposed on the range of primary mafic/felsic ratios and grain-sizes is a wide range of strain-states. Consequently a range of lithologies has been developed, e.g. schistose fine-grained homogeneous amphibolites, amphibolites finely striped on a 1-2 mm scale, to coarse striped amphibolites with a recognisable medium grained gabbroic parentage. Sheared, flaser- or banded mylonitic gabbros are inferred to have been derived from coarser parent material.

The textural progression of the lithologies of the Volvi Complex can be followed in shear zones from undeformed into deformed rock. However, it has also been observed that a similar final texture of, e.g. a medium-grained striped amphibolite, has been generated by more than one combination of original texture and state of strain. Dykes, gabbros and net-vein complexes, and their mutual contact relations, provide the primary field evidence of the intrusive history of the Volvi Complex.

a) *Dykes*: A high state of strain within fine-grained amphibolites has the tendency to obscure evidence of igneous contact relations and primary magmatic variations. However, areas composed of 100% dykes approaching 1 km in cross-strike length have been observed, with the original chilled contacts preserved. It is possible that other, slightly more sheared regions of fine-grained homogeneous amphibolite are also sheeted dyke-complex. Examples of the variability of original texture observed both within and between dykes are;

i) Dykes which are mildly feldspar-phyric, with feldspars concentrated and flow-aligned in the central regions.

ii) Dykes which show pseudomorphs of mafic micro-phenocrysts, possibly after olivine.

All the dykes are now composed of a finer-grained generally isotropic textured hornblende-garnet-plagioclase-(epidote-group mineral)-oxide assemblage. Clear one-way chilling has been observed, but is not usable as a statistical indication of spreading. Dykes occasionally show sheared micro-porphyritic centres strongly suggesting deformation occurred during intrusion while the centre of the dyke was still hot. In undeformed parts of the southern and central area, the mafic dykes are generally observed with a steep to vertical dip, and a NE strike. Isolated leucocratic aplitic sheets (0.5 to 2 m thick) are more variably inclined and often flat-lying.

A spectacular "tiger-striped" lithology has been observed occurring as screens and angular blocks preserved between dykes (also see Section 2.3.2.4). This rock is composed of laterally discontinuous 1 cm thick plagioclase-rich bands, interlayered

with similarly discontinuous mafic layers made up of garnet, diopside, hornblende and plagioclase. This lithology has been interpreted provisionally as a highly modified hornfelsed and metasomatised calcareous sediment, and if so is important evidence of a pre-existing "country-rock" into which the dyke components of the Complex were intruded. The preserved fine layering in several outcrops appears inconsistent with the parent rock having been deformed and metamorphosed prior to dyke intrusion.

b) *Gabbros:* The large bodies of gabbro appear to be relatively homogeneous masses, which preserve a primary igneous grain-size variation. However, in regions of transition to dyke complex which are observed to occur over 1-200 m the relationship becomes more complicated; pegmatoid patches and veins in gabbro become more abundant; transition through fine-grained dolerite to homogeneous amphibolite appears to be gradational via a nebulous "hybrid" with discontinuous diffuse boundaries between gabbroic veins and finer-grained doleritic rocks.

Gabbro-pegmatite sheets (varying from 1-2 cm to 1-2 m in thickness) apparently emanating from the upper part of the homogeneous mass and cutting fine-grained amphibolite provide textures suggestive of very high country rock temperatures at the time of intrusion. Fine-grained dykes cut coarse-grained gabbros in these transitional regions. Variably resorbed, often angular, small gabbroic patches in dykes are generally quite common, implying that assimilation of earlier crystallised material was an important process. Cumulate gabbros within the Volvi Complex are of two main types:

i) Those with plagioclase as the main cumulus phase.

ii) Those with prominent rod-like clinopyroxenes lying randomly in the plane of layering, accompanying plagioclase and scattered olivine or ex-olivine euhedra.

Layering tends to have a shallow dip, suggesting that undeformed parts of the body, even if bounded by faults and shear zones, have not rotated far from their original attitude at least about flat-lying axes.

c) *Net-veining:* angular, fracture-controlled intrusive relations occur on a cm- to m-scale. Prominent net-veining occurs with basic dyke blocks in a granitic (or possibly trondjemitic) vein matrix, "dioritic" hybrids between block and matrix also occur.

Dixon and Dimitriadis (1984) draw attention to the strong similarities between the Volvi structures and high-level gabbro and lower sheeted-dyke parts of ophiolite complexes (e.g. Oman: Pallister, 1981; Pallister and Hopson, 1981). Complex relationships between gabbro bodies and dykes have been observed. Gabbro bodies have been emplaced into regions already occupied by dykes while elsewhere late

basic injections appear as fine-grained dykes in gabbro. The inferred metasedimentary screens are difficult to explain as they imply the existence of a floor on which they were deposited. If this was continental crust, it would have to have been virtually completely displaced to both sides of the invading Volvi Complex. If oceanic crust, it might suggest that older pillow-lava screens, as yet unrecognised, lie at lower levels between dykes. This would imply a very complex two stage spreading history.

Conclusions from these observations are that crustal extension of a continental terrane approached 100% during intrusion. The Complex is ophiolitic in character in that it represents a mafic extensional phenomenon. No volcanic component has yet been identified and none might exist above the immediate levels seen.

d) *Deformation:* The dominant structure on an outcrop scale is a planar shear foliation of very variable intensity with a general dip towards the W or SW in the central and southern part of the complex. This foliation is affected locally by close to tight folds on a scale of 100's of metres with a generally consistent sense of overturn down the dip of the main fabric. Parasitic tight to isoclinal folds on scales of 10's of centimetres are abundant near the large folds but are generally rare overall. The Volvi Complex is cut by late, narrow shear zones affecting early fabrics and folds. Shear zones which cut the early fabrics are observed to be associated with chlorite and actinolite formation.

The Volvi Complex is dissected by several sets of late faults, some associated with intense hydrothermal alteration. Consequently the Volvi Complex is divided into blocks on a 1-2 km scale, hampering the process of correlation between river sections. The preliminary interpretation from the attitude of dykes and cumulate layering is that deformation has not completely destroyed an irregular, but possibly gently NE dipping, contact or transition zone between gabbro below and dykes above. Observed movement along NW-SE trending fault planes indicates a down-dip sense of displacement to the SW. A probable, but not yet proved, sense of motion on E-W faults suggests downthrow southwards towards Lake Volvi. This would have the effect of exposing progressively deeper levels of the Volvi Complex towards the north.

Relationships between early ductile deformation and magmatism are shown by schistose fabrics developed preferentially in the central regions of dykes, implying some magmatic temperature control on the mechanical properties of the dyke. The clearest evidence of an overlap in time between intrusive activity and deformation comes from the transition zones between gabbro and dykes. The 0.5 m scale

pegmatitic gabbro sheets which have been observed emanating from a homogeneous gabbro mass into fine-grained amphibolite, cut already deformed (and undeformed) dykes. The dykes contain strongly flattened feldspar microphenocrysts and mm scale isoclinally folded leucocratic veinlets. The cross-cutting gabbro sheets show a very weak fabric but have an essentially unstrained coarse igneous texture quite inconsistent with the implied strain suffered by the dykes. Elsewhere in the complex the reverse relationship can be found.

Further evidence of active deformation occurring between mafic and felsic dyke injection events has been observed where leucocratic "meta-trondjemite" sheets are not displaced by sinuous faults which offset the mafic dyke contact. The great majority of shear deformation occurred after emplacement as it clearly deforms an igneous texture. Trondjemite net-veining associations, which are late magmatic-events, are cut by shear zones which convert undeformed angular textures into striped heterogeneous amphibolites in the space of 1-2 m. Nevertheless from preliminary work on the metamorphic textures and mineral assemblages it is considered much of the deformation probably occurred before the present mineral assemblages had fully developed (Dixon and Dimitriadis, 1984).

The contact of the Volvi Complex was not comprehensively mapped by Dixon and Dimitriadis (1984) in the course of their work, consequently observations were limited to one river section, crossing the boundary of the Volvi Complex in the SW corner. Along this transect, amphibolites in the complex are increasingly interlayered with schistose garnet- and magnetite-bearing aplitic sheets over a distance of several hundred metres towards the contact. Dixon and Dimitriadis tentatively interpreted these as the products of partial melting of (meta)sediments in the envelope. Geochemically these aplites do not fall on magmatic evolution trends consistent with fractional crystallisation (Dixon, pers. comm.)

2.5.3 The western margin of the Volvi Complex

The western margin of the Volvi Complex is poorly exposed. However, from mapping a series of stream sections across the inferred boundary, approximately 1-2 km east of Megali Volvi, it is possible to provide an approximate limit to the extent of the complex (Insert, Map E). The western boundary is transitional over a distance of 0.25 to 0.75 km from east to west (Insert, Map E). Lithologies which are exposed across this boundary range from gabbros, immediately within the "undisputed" boundary of the Volvi Complex, through a progressively banded sequence of amphibolites to mafic gneisses, which represent the "ambiguous" boundary (Section 3.10.3). The exact position of the western boundary is considered to be ambiguous, as

rare bodies (5-20 m long) of quartzofeldspathic gneisses are juxtaposed along shear zones and surrounded by the banded amphibolites and mafic gneisses. The boundary has also been subjected to extensive Neotectonic faulting, disrupting the continuity of the outcrop. Good examples of the transition from banded amphibolites to orthogneisses are exposed adjacent to the east margin of large outcrops of the Volvi Metasedimentary Group.

Further, large outcrops of amphibolites and mafic gneisses are exposed to the north and west of the Volvi Metasedimentary Group (Inserts, Maps B, D and E). There is no direct field evidence to relate these outcrops with the Volvi Complex (*s.s.*). However, geochemical signatures of these outcrops are comparable with the Volvi Complex. These outcrops of mafic gneisses and amphibolites are interpreted as intercalated slivers of the Volvi Complex, juxtaposed along shear zones or by Neotectonic faulting. They can also be tentatively correlated by composition and intrusive history with the Askos Marginal Amphibolite Formation (Section 2.3.3.1).

2.5.4 The Northern Margin of the Volvi Complex

The northern margin of the Volvi Complex is located close to Lefkoudha (Insert, Map H). Exposure is generally intermittent with the best exposures along a series of NE-SW trending stream sections to the W and NW of the village. These stream sections are particularly useful as they are orientated perpendicular to the main regional (structural and intrusive) trends, which vary from NW-SE to N-S. Contact relationships between different mafic igneous formations are often obscure, as the intrusive contacts are either sub-parallel with the regional S_2 foliation, or consist of badly weathered or overgrown outcrop. Only minor outcrops of possible metasedimentary mica schists are found in the area. The exposures show a series of complex gabbro/dyke intrusions which are interpreted as being emplaced into an actively deforming area.

Structures developed in this area are similar to those found in the Volvi Metasedimentary Group and gneisses and schists of the Vertiskos Group (Chapter 3). Hence, the majority of the mafic lithologies are interpreted as being in place prior to the (D_2) deformation event, with the remainder associated with shear zone development. However, further local structural variations occur in the formations which are in close proximity to late granitic intrusions (Chapter 3). The nearest unambiguous igneous-gneissic contacts crop out along the Vamvakia river to the east of Lefkoudha (Section 2.3.2) and around Xiropotamos to the west. The exposure to the west of Lefkoudha is very poor due to dense vegetation.

2.5.4.1 The Lefkoudha Amphibolite Formation

This formation crops out in a series of elongate strips of variable thickness (10-300 m wide), throughout the area and as a margin between the gabbro (Section 2.5.4.2) and dolerite formation (Section 2.5.4.3). This formation is interpreted as the initial basic lithology within the area, into which the remaining igneous lithologies have been intruded. Due to the orientation of the later intrusions this formation maintains a general NW-SE trend. The contacts with the gabbro and dolerite formations are equally gradational (5 to 20 m wide). This formation has been subject to extensive alteration and deformation, however, from field observations a dolerite precursor is inferred.

Generally the amphibolite appears to be heterogeneous but maintains a homogeneous character for individual stream sections. The formation is typified by biotite-rich amphibolites and a minor series of coarse- to fine-grained amphibolites.

Often within the biotite-rich amphibolites are "kernels" (undeformed pods) of dolerite, ranging from 10 cm to 1.5 m in diameter. These doleritic kernels are interpreted as preserving a possible relict precursor to this formation. Commonly found in areas of biotite-rich amphibolites are extensive arrays of quartzofeldspathic net-veining. These net-veins are interpreted as the cause of "biotitisation" of otherwise K-poor amphibolite, by syn-metamorphic metasomatism (Chapter 4). In the river directly west of Lefkoudha, dolerite kernels and a single set of net-veins are well-developed (Section 3.10.2). Within stream sections further north, two sets of veining are developed; the first is representative of extensive net-veining, which maintains a consistent N-S trend; the second is represented by short discontinuous (10-20 cm long) felsic veins, with a general E-W trend.

The biotite-rich amphibolites are further characterised by the development of large (up to 6 mm in diameter), euhedral, almandine porphyroblasts. Where kernels of dolerite are contained within garnet-biotite-rich amphibolites, a variably developed purple colouration is developed. The purple colouration occurs in a range of forms from discrete speckles (0.5-1 cm in diameter), to complex clusters which appear like "snowflakes" (2-5 cm in diameter) and at the extreme, the whole kernel may develop a purple colouration (also see the Vamvakia Mafic Formation, Section 2.3.2.5).

Contained within the amphibolite to the west of Lefkoudha are a series of ultramafic pods (0.5 to 1 km in diameter). These pods are surrounded by a fibrous actinolite-talc rim, 5 to 10 cm thick and a quartzofeldspathic component probably related to the local granitic intrusions (Chapter 3; Plate 3.37). These ultramafic pods are interpreted as either relicts of early intrusions into the amphibolite, which have

subsequently been obliterated or possibly as relicts of an ultramafic host into which the amphibolite (dolerite) was intruded. Within the stream sections to the NW of Lefkoudha, evidence for both late ductile and brittle deformational events are developed (Chapter 3).

2.5.4.2 The Lefkoudha Gabbro Formation

This formation crops out to the NW of Lefkoudha as an elongate NW-SE trending, ellipsoidal shaped body (approximately 0.75-1 km long and 500 m wide). The NW contact of the gabbro is poorly exposed, however, the remaining contacts are transitional over a range of 5-20 m with members of the amphibolite formation (Section 2.5.4.1). The gabbro is a generally homogeneous, coarse-grained, basic, crystalline rock. However, minor locally developed leucocratic gabbroic bodies occur within the main gabbroic host along with pegmatitic patches with large (3 cm long) skeletal pyroxenes and plagioclase-feldspar phenocrysts. In general the gabbro is composed of plagioclase and pyroxene, locally enriched in biotite, and only minor quantities of amphibole.

2.5.4.3 The Dolerite Formation

Elements of this formation crop out within all the stream sections around Lefkoudha and is representative of the latest mafic igneous component within the area. Contacts of this formation with the amphibolite formation (Section 2.5.4.1) are consistently transitional over a range of 2-20 m. The dolerites are generally represented by homogeneous, fine- to medium-grained, dark (black to green), banded, crystalline rock. The dolerite is composed of a pyroxene-amphibole groundmass, and contains varying proportions of plagioclase-feldspar (0.1-0.3 cm long) phenocrysts in areas of low deformation. With increased deformation the feldspar phenocrysts become wispy and foliated and eventually in areas of high deformation continuous leucocratic layers are developed and the dolerite approaches a gneiss in appearance.

2.5.5 Compilation and Summary

The area has undergone a complex history of intrusion and deformation in which precise timing relationships are difficult to unravel, however, a few general conclusions can be made:

i) Two broad fabric forming trends are present within the area, a) the NW-SE trend of primary undeformed igneous features (including the gabbro, whose shape does not appear to be associated with deformation, i.e. it is not parallel to the

metamorphic foliation, and b) a NNW-SSE structural trend of antiforms and synforms (and metamorphic fabric).

ii) Little evidence is available to determine the relationship of the gabbro and dolerite complex to the SW. However, at its NE boundary a transition zone represented by a biotite-rich amphibolite has been developed mainly by the intrusion of the gabbro into a doleritic host. Further "biotitisation" of the doleritic host has developed due to the intrusion of dykes which clearly post-date the gabbro.

iii) Evidence for the unequivocal metasedimentary origin of rare mica schist horizons was not found, however, evidence which may suggest a metasomatic origin through alteration of striped amphibolite by granitic fluids has been found.

iv) Igneous activity and deformation appear to have overlapped in time, from the relationships of minor doleritic pods and cross-cutting doleritic sheets within the gabbro, some of which are affected by deformation and some of which clearly post-date it.

v) Deformation takes the form of a series of asymmetrical tight to open folds similar to the regional structure found in the country rock. These structures appear to have developed synchronously within local thermal and regional metamorphic episodes.

From the conclusions listed above, the area does not fit neatly into any of the three scenarios proposed by Dixon and Dimitriadis (1984), *see* Chapter 1. From this study two alternative models for the intrusive history for the area are proposed.

A) The amphibolite formation (Section 2.5.4.1) is inferred to be the oldest igneous formation around Lefkoudha and acts as the country rock into which the remaining igneous formations have been intruded. There are only minor exposures of a metasedimentary mica schist lithology within the area to indicate a possible country rock into which this amphibolite was originally intruded. This interpretation is based on the extensive alteration and deformation episodes which are developed within the formation and which are not obviously developed within the other intrusions.

The gabbro formation (Section 2.5.4.1) is inferred to be the earliest intrusion into the amphibolite. This is based on transitional boundary characteristics produced in the amphibolite out cropping on all the exposed margins of the gabbro. Part of the "biotitisation", and possibly some of the net-veining which are common within the amphibolite formation may be attributed to the intrusion of the gabbro. This is proposed as the granite intrusions within the area are of only minor extent while the biotitisation phenomenon occurs in a zone completely surrounding the gabbro.

However, it is more probable that an original syn-metamorphic event related to the intrusion of the gabbro has been utilised and thoroughly overprinted by the later granitic net-veining. The gabbro is in turn cross-cut by a number of dolerite dykes which show a range of deformation states, suggesting dyke intrusion was an actively on going process. Extensive undisrupted sequences of sheeted dykes are well-developed directly to the west of Lefkoudha. Outcrops of amphibolite are intercalated parallel with the dykes, yet contain an earlier fabric. The Lefkoudha Granite Formation (Section 2.5.5.4) is the youngest intrusive event as it shows several sharp cross-cutting contacts with the amphibolite and dolerite formations (Sections 2.5.4.1, 2.5.4.3). Net-veining derived from the granites causes biotitisation of the amphibolite.

Alternatively, B) The dolerite formation (Section 2.5.4.1) is inferred to be the oldest igneous formation around Lefkoudha and acts as the original basement lithology into which the remaining igneous formations have been intruded. This model proposes that the amphibolite formation represents an extensive syn-metamorphic margin, developed around the gabbro during its intrusion. The amphibolite intercalations with the sheared dykes could be interpreted as altered early dykes or simply the site of a preferred fluid path for later metamorphic events. Remnant doleritic kernels within areas of highly altered amphibolite suggest a doleritic precursor. Dolerite dykes which cross-cut the gabbro and altered amphibolite may represent, a) late Volvi dykes, or b) a synchronous dolerite-gabbro intrusive sequence, with gabbro intruding marginally later into an active doleritic dyke sequence.

A number of refinements can be made to these models, however, the main interpretation of the amphibolite formation acting as an old intrusive formation subsequently intruded by a number of younger igneous bodies, i.e. model (A) is preferred.The Lefkoudha Granite Formation (Section 2.5.5.4) is the youngest intrusive event as it shows several sharp cross-cutting contacts with the amphibolite and dolerite formations (Sections 2.5.4.1, 2.5.4.3). Net-veining derived from the granites causes biotisation of the amphibolite.

2.6 The Granitoid Group

2.6.1 Introduction

Within the area studied outcrops with a granitic composition have been widely observed, the most extensive and important of which is the Arnaea granite (Section 2.6.3; Chapter 3). Smaller outcrops of granitic composition are exposed throughout the Vertiskos Group to the west of the Volvi Complex and to the east of Modhi. Minor locally derived granitic melts are found along the Vamvakia river and along the Rendina to Asprovalta road (Section 3.12.4.1). For a more detailed assessment of the granitic lithologies studied during this work and their geochemistry, *see* Chapter 5, Part II. However, the field observations, lithological variations and the spatial extent of the outcropping granitoid material pose a problem, i.e. what is the relationship between outcrops of minor granitoid bodies and the Arnaea granite in time and/or origin? Several questions arise:

a) Are the granitoids older than the Arnaea body, e.g. are they associated with the early migmatites observed within the Vertiskos Group?

b) Are the granitoids, near the boundary between the Vertiskos and Kerdilion Groups, the product of local crustal melting by the Volvi Complex or are they acid differentiates of Volvi basaltic parent magmas or both ?

c) Are the granitoid bodies (especially those which crop out near the boundary between the Vertiskos and Kerdilion Groups), derived from continental crust thickened and melted in a collisional event (Chapter 5) ?

d) Are the granitoids coeval with the later granitoid intrusions which are known to occur throughout the Halkidiki Peninsula.

Further aims of this work have been to determine the relative ages, the origin and the subsequent development history for the different granitoid bodies. However, in a poorly dated polymetamorphic terrane such as the SMM (within Greece), granitoid intrusions can be useful absolute as well as relative time markers with respect to deformation events. This section therefore provides a review of the age constraints for the Arnaea granite (Section 2.6.2; also see Chapter 1), and hence provides a relative time scale in which to organise the minor granitoids within the area. The most significant granitoids are then reviewed concentrating on field observations and petrographic descriptions (Arnaea Granite Member (*s.s.*), Askos Augen Orthogneiss Member and a range of associated apophyses and veinlets, Section 2.6.3; Modhi Granitoid Suite, Section 2.6.4). Minor, yet significant granitoids found within the Volvi area, e.g. melts in the Vamvakia Purple Gneiss Formation (Section 2.3.2.2) and the Rendina Amphibolite Formation (Section 2.2.2.3), and leucocratic sheets within the Stavros Leucocratic Gneiss Formation (Section 2.2.2.2) and Askos Marginal

Amphibolite Formation (Section 2.3.3.1) etc., are referred to and described more appropriately with their host lithology and in Chapter 3.

2.6.2 A Review: Age Constraints For The Arnaea Granite

The spatial arrangement and characteristics of the Arnaea granite are presented in Section 2.6.3. Age constraints for the granite can be divided into two categories, i) field observations and, ii) radiometric dating.

(A) *Age Constraints From Field Observations:* To the SW of the Arnaea granite a thin sliver of Vertiskos schists and gneisses of the SMM, and a sequence of Triassic and lowermost Jurassic Svoula marbles and flysch of the Vardar zone are apparently intruded by apophyses, veins and sheets from the granite body (Kockel *et al.*, 1977). Along the SW margin of the granite body a dominant set of fold structures and the effects of a greenschist metamorphic event are also observed. Kockel *et al.*, (1977) concluded that this metamorphic event predated the undeformed overlying Upper Jurassic-Lowermost Cretaceous Doubcon Molasse sequence. A post-Lower Jurassic but pre-Upper Jurassic/Lower Cretaceous age for the Arnaea granite was therefore suggested (Kockel *et al.*, 1977). However, De Wet (1989) observed the SW contact of the granite body to be linear and strongly deformed, containing well-developed mylonitic fabrics. Consequently, the schists and gneisses described by Kockel *et al.*, (1977) are reinterpreted by De Wet (1989) to be the result of intense shearing and possibly contact metamorphism of the Svoula Formation by the Arnaea granite along this contact. De Wet (1989) also observed the Doubcon Molasse to be deformed, weakly metamorphosed and involved in imbricate thrusting with the Svoula flysch. From field observations and isotopic work, the granite was considered by De Wet (1989) to have a Late Jurassic intrusion age and an Early Cretaceous age for the metamorphic event (De Wet, 1989).

Contact relationships between the Volvi Complex and gneisses of the Vertiskos Group are complex and are partially obscured by the variably developed regional foliation. In several areas highly sheared quartzofeldspathic augen granitic gneisses (Askos Augen Orthogneiss Member, Section 2.6.3) are observed sub-parallel to the contact and regional foliation. However, immediately to the south of Lake Volvi, the contact of the Arnaea granite is observed to be strongly oblique to the dominant regional foliation (De Wet, 1989; 1: 50 000 Zangliverion Sheet, 1978). These variations in the structural observations suggest that the Arnaea granite essentially post-dates the dominant fabric-forming event in the SMM (De Wet, 1989).

North of Lake Volvi the Arnaea granite is parallel to the regional NW trending foliation (Section 2.6.3). According to Kockel *et al.*, (1977) this foliation resulted

from an Upper-Jurassic, pervasive, NE dipping, fabric forming event related to the imbrication event in the Circum-Rhodope belt. These structural observations suggest that the Arnaea granite pre-dates the dominant fabric forming event in the SMM.

By implication the original pre-Mesozoic fabric in this area was either fortuitously NW-SE or was completely overprinted or rotated into this orientation (Dixon and Dimitriadis, 1984). Further north, extensive parts of the SMM appear to have original pre-Mesozoic foliation elements intact. In these areas the granite cross-cuts the foliation obliquely and must therefore post-date this fabric forming event (Kockel *et al.*, 1977). Questions arising from the field observations of De Wet (1989) and this work are:

i) What is the relationship between the Arnaea granite and shear zones?

ii) Could the Arnaea granite at least in part have been emplaced along such a shear zone (Section 2.6.3)?

iii) From the implication of emplacement along shear zones, does this suggest a far more intense Late Jurassic/Early Cretaceous deformation event than previously suggested (particularly in terms of large scale anastomosing shear zones; Section 2.6.3 and Chapter 3)?

(B) *Age Constraints From Radiometric Dating:* Until recently (i.e. De Wet, 1989) the Arnaea granite was undated isotopically. Consequently ages for the SMM in the Volvi area had been inferred solely from field relationships. Kockel *et al.*, (1977) had originally proposed a post-Lower Jurassic age for the Arnaea granite, suggesting that the granite had been subjected to an upper greenschist-facies metamorphic event at approximately 180 Ma followed by a low-grade minor event at approximately 110 Ma. However, this was based on the assumption that the Arnaea body was related to the Monopigadhon granite and therefore intruded at 180 Ma. The Monopigadhon granite however, is itself poorly constrained. Ferrara (pers. comm., in Ricou, 1965) determined a single K/Ar biotite age of approximately 180 Ma. More recently Kreuzer (pers. comm., in Mussallam and Jung, 1986) determined a K/Ar biotite age of approximately 149 Ma. However, at best this age only represents a cooling age, therefore giving a minimum age for the timing of intrusion.

Dixon and Dimitriadis (1984), from observations made within the Volvi area, questioned the original interpretation of Kockel *et al.*, (1977), and proposed a major regional metamorphic and deformational event during the Late Jurassic (possibly to Early Cretaceous).

Papadopoulos and Kilias (1985) dated muscovite and biotite separated from an augen gneiss from the sheared boundary of the Arnaea granite, north of Lake Volvi

(Section 2.6.3, the Askos Augen Orthogneiss Member). Muscovite K/Ar and Rb/Sr model ages were 108 ± 4.7 and 131 ± 10 Ma respectively and biotite K/Ar and Rb/Sr ages were 124 ± 5.2 and 102 ± 10 Ma respectively. These results were considered to reflect a Early Cretaceous syntectonic, greenschist-facies metamorphic and deformational event, and therefore an Upper Jurassic/Lower Cretaceous age for the intrusion.

The most extensive isotopic dating of the Arnaea granite was undertaken by De Wet (1989), using Ar/Ar and Rb/Sr techniques. Ar/Ar analysis of phlogopite provided an age of 136 ± 1.3 Ma from which De Wet (1989) made several possible interpretations:

a) The age is geologically meaningless resulting from partial resetting by a later event. This interpretation appears to be disproved by the well developed plateau but there is evidence that even partially reset biotites (and thus potentially phlogopite) may give rise to a well developed plateau, e.g. as a result of analytical techniques (Hanson *et al.*, 1975)

b) The age is geologically meaningful and gives the age of crystallisation of the phlogopite (or at least the age at which the phlogopite passed through its closure temperature).

c) The age is geologically meaningful and gives the age of the main fabric forming event, i.e. Phengite formation.

d) The age may reflect the latest deformation event which led to the formation of the crenulation cleavage.

The Arnaea granite is observed to have been involved in a complex deformational history. Consequently the isotopic age data must be interpreted with caution. The Ar/Ar age of the phlogopite is interpreted as indicating a very simple thermal history and may reflect the youngest event (De Wet, 1989). In an attempt to avoid the effects of the later deformation and to obtain a crystallisation age for the granite, whole rock Rb/Sr isotopic dating was undertaken. Results scatter about a best fit line indicating an age of 155 ± 11 Ma. However, due to the scatter, the data can be broadly divided into two groups, which results in better fitting regressions indicating ages of 153 ± 3 Ma (IR=0.7225 ± 9, MSWD=4.3) and 144 ± 1 Ma (IR=0.7177 ± 1, MSWD=2.2). There is no obvious petrographic or geographical reason for the scatter of data and therefore for separating these sample suites. There are several possible interpretations for these results:

a) The data obtained indicate the approximate age of crystallisation of the granite, while the scatter reflects post emplacement alteration processes.

b) The data obtained represent the age of deformation and metamorphism of the granite, the scatter reflecting variations in resetting.

c) It is possible that the Arnaea granite is a composite body in which there were small but significant differences in initial Sr isotope ratio. Most of the samples were, however, collected from a limited area of the granite and showed similar chemical and petrographic characteristics.

Whole rock systems are generally resilient to metamorphic disturbance (Cliff, 1985), and therefore the Upper Jurassic age obtained probably reflects the true crystallisation age of the granite. However, given the susceptibility of Rb/Sr systematics to alteration and the post-intrusive metamorphic and deformational history of the body, the scatter may reflect post-emplacement alteration processes. The petrography suggests that these processes were unlikely to have resulted in the complete resetting of the Rb/Sr isotopic system. Nevertheless Yarwood and Aftalion (1976) and Yarwood and Dixon (1979) obtained a Cretaceous Rb-Sr whole rock/mineral isochron from a Pelagonian deformed granite with a 300 Ma zircon age.

In conclusion, data from the Rb-Sr analysis seems to confirm a minimum Upper Jurassic age for the Arnaea body, which is consistent with its intrusion in the Lower Jurassic Svoula Formation (Kockel *et al.*, 1977). A wider interpretation of the ages of the Arnaea granite can be used when compared to several other granites in the area, including the Fanos and Monopigadhon granites which are also attributed to the Upper Jurassic. The Arnaea granite may therefore be part of the same intrusive episode. Unlike the Fanos granite, the Arnaea granite does not intrude any of the ophiolitic complexes of the Vardar-Axios Zone (De Wet, 1989). Similar ages to De Wet, (1989); De Wet and Miller, (1987) and De Wet *et al.*, (1989) which have also been obtained in the SMM, have been produced by Borsi *et al.*, (1965) and Harre *et al.*, (1968).

2.6.3 The Arnaea Granite

The Arnaea granite crops out along the western margin of the SMM near the boundary with the Vardar zone. The main body of the granite lies to the south of Lake Volvi and crops out as a large approximately 35 km by 10 km sigmoidal shaped intrusion strongly suggestive of intrusion into a dextral rhombochasm. The granite body to the north of Lake Volvi (to the west of Vaiohorion and Askos) was studied during the course of this thesis. Due to the distinctive change in lithological characteristics between the granitic lithologies and the gneisses which comprise the local country rock, the Arnaea granite was used to delimit the western boundary of the

research area (Insert, Map B). A further brief reconnaissance was made within and to the west of the main body of the Arnaea granite (*s.s.*) north of Lake Volvi.

The main aim of studying the Arnaea granite was to establish criteria (i.e. geochemical, petrological and deformational) by which deformed granites and orthogneisses within the area studied could be identified as being of Arnaea type or not. The granitoids from the Volvi area could then subsequently be placed in a relative time scale with respect to the Arnaea granite (Section 2.6.2). The determination of the contact relations of the Arnaea granite with the country rock gneisses was necessary to further constrain the intrusion of the granite within the local deformational sequence and to try and resolve the origin and tectonic setting of the granite body (Chapter 3).

The Arnaea granite is variably deformed and can be broadly subdivided into a Main Granite (*s.s.*) Member and a progressively sheared Augen Orthogneiss Member (*s.l.*). An extensive array of veinlets and apophyses associated with the Arnaea granite are observed intruding the country rock gneisses and are variably deformed. The Arnaea granite (*s.s.*) has suffered extensive deformation, especially by anastomosing shear zones which occur in a continuous weak form, progressively over .1 km into the granite body from the boundary with the Askos Marginal Amphibolite Formation (Section 2.3.3.1). At this distance from the contact the Arnaea granite (*s.s.*) is represented by homogeneous, fine- to medium-grained, euhedral, porphyroblastic quartzofeldspathic lithologies. A poorly developed foliation is defined by parallel flakes of biotite and muscovite which are present in low quantities (5-25% of the rock) and by recrystallised and flattened stringers of quartz wrapping augen of plagioclase and K-feldspar (Chapter 3). Towards the margin of the granite (*s.l.*) and the contact with the Askos Marginal Amphibolite Formation, the granite progressively develops a distinctive feldspathic-augen texture and the percentage of white-mica increases from 5 to 25 % of the rock. The augen granite occurs in large outcrops in areas which are separated from the main granite body and hence interpreted as a separate member (the Askos Augen Orthogneiss Member). As the main body of the Arnaea granite (*s.s.*) is generally homogeneous, investigations within the granite (*s.s.*) were restricted to a brief reconnaissance and limited sampling (N=8) to provide:

i) Observations of the range of deformation styles and their effects on the granite.

ii) Data on the effects of deformation on the chemical composition.

iii) Evidence on the variations in geochemistry between the Arnaea granite and other granitoids within the area.

It was soon recognised that the main interest lay at the boundary between the Askos Augen Orthogneiss Member and the Askos Marginal Amphibolite Formation (Section 2.3.3.1). The main observations made during the course of this study therefore involved the Askos Augen Orthogneiss Member, and the relationship with the country rock gneisses. The Askos Augen Orthogneiss crops out primarily as a laterally continuous NNW-SSE trending margin to the Arnaea granite, varying in thickness from 100-500 m. The contact of the western margin of the augen orthogneiss member is transitional (over 5 to 20 m wide) with the main granite (*s.s.*). The distinction between the granite (*s.s.*) and the Askos Orthogneiss Member is based on the degree of deformation the rock has suffered, i.e. when greater than 50% of the rock has an augen fabric developed it is considered part of the augen orthogneiss member. The eastern boundary of the augen orthogneiss member with the Askos Marginal Amphibolite Formation (Section 2.3.3.1) is complex (Chapter 3). Numerous intercalations are developed between the two units, with the contact between the two units approximately following the Vaiohorion to Askos road (Insert, Map B). The Askos Augen Orthogneiss Member was sampled (N=22) along with a number of apophyses and veinlets which were considered to be offshoots of the Arnaea granite (Chapter 5).

Juxtaposition along shear zones has complicated the original intrusive relationships within the granite body (Chapter 3). Granites showing minor variations in composition are displaced over one another with a W to E sense of shear. Similar effects are observed in the sliver of the Askos Augen Orthogneiss Member which crops out with a NW-SE trend from NNE of Vaiohorion to Askos. This series of outcrops appears to be laterally continuous (although exposure is poor) and varies in thickness from 2-50 m. Intrusive effects are obscured by intense NNW-SSE trending vertical to steep anastomosing shear zones (dipping 65°W to vertical). The eastern margin of this sliver of the Askos Augen Orthogneiss Member shows interbanding along sub-vertical shears with the Askos Augen Paragneiss Formation (Section 2.3.3.2). Within the larger outcrops, minor late aplitic intrusions or possibly locally derived melts have been observed intruding the granite bodies. The western margin of this sliver with the adjacent Askos Marginal Amphibolite Formation (Section 2.3.3.1) remains sharp. Any intrusive or contact relationships are obscured by the intensity of the regional steep foliation.

Minor granitic intrusions, aligned parallel or sub-parallel to the regional foliation and up to 4-5 m across, are found within a number of the Vertiskos Gneisses to the east of Vaiohorion. Due to the intense foliation, contact relationships are

always obscured and the intrusions simply appear intercalated with the country rock gneisses. The assemblages of this suite of acidic intrusions are closely comparable to those of the Askos Augen Orthogneiss Formation. The whole area is further complicated by extensive brittle deformation and Neotectonic faulting.

2.6.4 The Modhi Granitoid Formation

The Modhi Granitoid Formation crops out approximately 1 to 1.5 km along the track to the east of Modhi (Insert, Map G). This formation is exposed along a continuous series of outcrops 1 to 4 m high and 100-150 m long and variably weathered. Lateral continuity to the N and S is obscured due to poor exposure. To the west of this series of outcrops the unit is bounded by a varied sequence of marbles and amphibolites (Modhi Marble Formation, Section 2.2.3.3; West Modhi Amphibolite Member, Section 2.2.3.1). The actual boundary is represented by an apparently reactivated shear zone, as ductile characteristics are observed in lithologies approaching the contact with a brittle "shatter" zone occurring at the contact. To the east of the formation there is a gradational boundary with a sequence of well-banded biotite-rich amphibolites (West Modhi Amphibolite Member, Section 2.2.3.1) which form a highly folded and sheared zone and which in turn pass into refolded marbles (Section 2.2.3.3). However, the precise boundary is obscured by well-developed shear fabrics. Lack of igneous texture or preserved intrusive relations in this highly sheared unit make its origin as granite or metasediment uncertain. Textural and geochemical data do not point clearly to a specific parent.

2.6.5 The Lefkoudha Granites

This formation crops out as a series of minor (1 to 10 m wide) ovoid bodies in the stream sections to the W and SW of Lefkoudha (Section 3.12.3). Intrusive contacts of the granite are predominantly sharp and cross-cut foliations within the amphibolite formation and to a lesser extent the sheeted dolerite complex. However, contacts are also obscured by truncated, sheared or faulted zones.

The granites are coarse-grained, quartz-plagioclase-muscovite-biotite bodies. The more micaceous members are extremely fissile. Within the least deformed granites are large (2-3 cm) euhedral plagioclase feldspar phenocrysts (Chapter 3; Plate 3.36). From the proximity of large plagioclase crystals within 0.5 m of the contact with its mafic host, it can be concluded that the mafic country rock must have been close to the granite solidus temperature. The net-veining within the amphibolite formation (Section 2.5.4.1) and the extensive syn-metamorphic metasomatism of the amphibolite formation is attributed predominantly to the granites (Section 2.5.4.2).

2.6.6 Summary

In summary the Arnaea granite is regarded as a complex quartz-rich granitoid which has been intruded into a region of actively deforming country rock gneisses. The nature of emplacement remains problematic, but there is evidence of intrusion pre-, syn-, and post- the development of anastomosing shear zones. Granite emplacement and shear zone development therefore appear to be linked. For a review of the possible mechanisms of intrusion for the Arnaea granite, *see* Chapter 6.

From the age constraints on the Arnaea granite, an Upper Jurassic/Lower Cretaceous age for the main recognised deformation is proposed. The subsequent scatter of age data being the result of minor deformation and metamorphic events.

The precursor of the Modhi Granitoid Formation remains unresolved (a detailed study of the local area is ideally required, however, the exposure is poor and the chances of improving the constraints are minimal). A granitoid origin is proposed because of the similarities with lithologies found within the Arnaea granite. The main support for an igneous precursor for the Modhi Granitoid Formation is based on geochemical evidence (Chapter 5), although from the data a metasedimentary origin remains a possibility. The original mechanism of emplacement for the Modhi Granitoid Formation remains a problem. From the geochemistry the formation is inferred to originate from local melting (anatexis) of the gneissic country rock. The mechanism of emplacement remains ambiguous, the only certain observation is that the formation was tectonically emplaced into its present position via anastomosing shear zones induced by the emplacement of the Volvi Complex

It is not totally unrealistic to consider granite emplacement to be closely associated with shear zone development. As noted earlier, the rhombic outcrop pattern of the Arnea granite is suggestive of emplacement into a rhombochasm or dextral pull-apart space. Other granitoid lithologies recognised in the area (with the exception of the melts within the Vamvakia Purple Gneiss Formation, Section 2.3.2.2), are regarded as being older than the Arnaea granite intrusion. These remaining granitoid lithologies are predominantly leucocratic sheets and veinlets within, e.g. the Stavros Leucocratic Gneiss Formation (Section 2.2.2.2), which represent either early intrusions or gneissic/migmatitic segregations. Within the Vamvakia river the melts within the Vamvakia Purple Gneiss Formation (Section 2.3.2.2) are unequivocally caused by the emplacement of the Volvi Complex. Hence the melts are inferred to be older than the Arnaea granite but younger than the gneissic/migmatitic segregations within the country rock gneisses.

PART III: Reappraisal of the Lithostratigraphic Sequence

2.7 A Proposed Lithostratigraphy

Field relationships between the different formations of the Lake Volvi area are usually obscured by the tectonic reworking and juxtaposition along anastomosing shear zones (Chapter 3). Therefore, by determining the structural evolution and tectonic style of the area (Chapter 3), in conjunction with the metamorphic history and geochemistry of the rocks (Chapters 4 and 5 respectively), the relationship between formations can be constrained. From the field relationships and structural history new interpretative models for the area can be put forward (Chapter 6). If these are correct then a reinterpretation of the present stratigraphic sequence is required. The relationships between each group determined from this study have been summarised at the end of the relevant sections. This section simply correlates these summaries.

The study area has a migmatitic basement with original fabric largely obliterated by the main D_2 deformation events (Chapter 3). No reason has been found during this study to separate the migmatites of the Kerdilion Group (Section 2.2) from those of the Vertiskos Group (Section 2.3). Most of the variations which have been observed can be simply attributed to differences in strain and deformation throughout the area.

This migmatitic basement is "overlain" by a series of gneisses and schists, which only contain evidence for D_2 structures and fabrics. The exact boundary between the basement and gneissic cover is obscured due to the intense regional deformation. An inferred upwards transition from psammitic to dominantly pelitic lithologies can be recognised within the gneissic lithologies which may reflect a proximal to distal sedimentary evolution. The gneisses and schists are intruded by the Volvi Complex and Arnaea Granite. A model is developed in Chapter 6 of a narrow, deep, strike-slip generated basin in which deposition of a sedimentary cover (the Volvi Metasedimentary Group) took place during intrusion with the deepest levels of the sedimentary sequence being intruded by a dyke and sill complex analogous to the present Gulf of California. This may also explain the complex, ill defined boundary between the gneiss/schist sequence representing the pre-dyke crust and metasedimentary cover.

From field relationships and lithological comparisons the metasedimentary sequences of the Kerdilion Group, east of Lake Volvi should be considered part of the Volvi Metasedimentary Group. The Kerdilion marbles are infolded with gneisses and amphibolites and modified by late anastomosing shear zones. The variations in

composition from impure carbonate to pure marble sequences can be explained by a stratigraphically younging sequence from E to W (Section 2.2.6) similar to the Volvi Metasedimentary Group. Refolded folds within the impure carbonates (Section 2.2.3.3) suggest a history for the metasediments comparable to the Megali Volvi Garnet Graphite Schist Formation (Section 2.4.3). Pods of garnet-kyanite schist within the West Modhi Amphibolite Member (Section 2.2.3.1) could be a possible equivalent to the Megali Volvi Garnet Graphite Schist Formation (Section 2.4.3) to the west. All these metasedimentary lithologies are considered to represent a rapidly filled basin sequence (Chapter 6). If this interpretation is correct then there is no neccessity to correlate these lithologies with the Svoula Group in the sense that they are a single stratigraphic unit. Similarities in the lithological sequences between the Volvi Metasedimentary Group and Svoula Group can be attributed to similar environments of deposition and source of material (Chapter 6) in basins which may not have been connected nor have been of exactly the same age.

CHAPTER 3

STRUCTURAL EVOLUTION AND INTRUSIVE HISTORY

CHAPTER 3

3.1 Introduction

The specific aim of this work was to establish the structural setting of the Volvi Complex within the SMM. Hence, a clear understanding of the full structural history of the envelope to the Volvi Complex was required. I believe that this has not been satisfactorily established in either of the two recent studies undertaken specifically within the area around Lake Volvi by Papadopoulos and Kilias (1985) and Sakellariou (1990) *see* Section 3.1.1. These previous workers have not taken a wide enough view of the whole area. Hence, they have generally attempted to impose a rigid, conventional system of fold and cleavage phases (*see* Tables 3.1 and 3.2) on what is in fact a complex system of anastomosing shear zones. In addition, the role of the igneous intrusive events in modifying the structural evolution has not previously been recognised.

The identification of cm-, m- and km-scale anastomosing shear zones, their effects on the local structures and fabrics and a series of igneous rocks progressively intruded into an actively deforming environment warrants a different approach and interpretation. Hence, this chapter interprets the structural and tectonic history from an approach based on the notions of progressive deformation and strain-partitioning (*see* Sections 3.1.3 and 3.1.4 respectively).

The area in general is structurally complex. Different generations of structures (e.g. folds, cleavages) from around the Volvi Complex display a range of structural styles caused by competence differences across the broad range of lithologies within the area. Changes in the structural regime over very short distances (e.g. original continuous cleavage → crenulation cleavage → new continuous cleavage) are caused by strain partitioning which again results in a range of structural styles being developed. Rapid changes in the structural morphology are also attributed to anastomosing shear zones which occur as an integral part of a progressive deformational event (D_2), *see* Sections 3.4 and 3.5. Hence, correlation of structural elements between exposures within the studied area is a problem (c.f. Park, 1969; Williams and Zwart, 1977; Williams, 1985). Recognition and correlation of large scale "late" regional structures and comparisons between local variations of "early" structures have been further hindered by extensive arrays of normal and strike-slip Neotectonic faults (Section 1.11). However, the minor variations in the trends and displacements on fault planes suggests only minor localised rotation of fault blocks has occurred. This is supported by the continuity and locally constant orientation of

the regional (S_2) foliations across individual faulted boundaries. In order to establish the overall structural sequence summarised in Table 3.3 the effects of Neotectonic faulting have been overlooked

Part I of this chapter describes the development of structures and fabrics which are considered in relation to a structural framework defined by pervasive shear zones. Part II presents evidence for the relationships between intrusions and deformation. The structural and intrusive data are used in conjunction with the metamorphic history (Chapter 4) and geochemical evolution (Chapter 5) to develop an overall structural and tectonic history for the Lake Volvi area (Chapter 6).

3.1.1 Previous Work

The most recent work to include a structural review of the area of interest is a brief study between the western margin of the Volvi Complex and the Arnaea granite by Papadopoulos and Kilias (1985) [*see* Table 3.1] and a more comprehensive study of an area immediately south of Lake Volvi by Sakellariou (1990) [*see* Table 3.2]. The structural sequence proposed by Papadopoulos and Kilias (1985) was developed for a limited area with a restricted structural style, and is therefore generally incomplete for the Lake Volvi area as a whole. From the description of Papadopoulos and Kilias (1985), it is clear that they have completely overlooked the development of the migmatites, and the deformation of these metamorphic fabrics in an earlier event. They have also described the range of progressively developed D_2 structures identified in this study (Chapter 3) as their S_1-S_2.

Table 3.1 A scheme proposed by Papadopoulos and Kilias (1985) for the structural, metamorphic and time framework of an area between the western margin of the Volvi Complex and the Arnaea granite. All comments and qualifying remarks are taken from Papadopoulos and Kilias (1985).

Structures	Metamorphism	Age
S_1: Axial planar. T_1: Sub-vertical isoclinal folds associated with shear. L_1: Elongation of hornblende and feldspar parallel to the fold axial plane. Plastic Deformation Field.	Amphibolite-facies (Kr_1) Syn- to post-tectonic with respect to T_1. Prograde Event	Pre-Cretaceous?[1]
S_2: Axial planar crenulation and spaced cleavages with respect to an earlier S_1 fabric. T_2: Inclined fractured folds, trend NNW-SSE/NNE-SSW.	Greenschist-facies (Kr_2) Syn-tectonic with respect to T_2. Retrograde Event	Early to Mid-Cretaceous[2]
No significant formation of structural features.	Low-grade retrogression (Kr_3). Possibly the final stage of the Kr_2 event	Late-Cretaceous-Tertiary?[3]

[1] Based on regional stratigraphic arguments, and comparison to similar styles of dated structures within the SMM by Chatzidimitriadis and Kilias (1984), and inferred from radiometric data determined by Papadopoulos and Kilias (1985)

[2] Determined from K/Ar and Rb/Sr radiometric dating by Papadopoulos and Kilias (1985)

[3] Inferred from structural and petrographic relationships, determined by Papadopoulos and Kilias (1985)

Furthermore there is no indication by Papadopoulos and Kilias (1985) that they recognised the later, open to close fold episode perpendicular to the main NW-SE trending F_{1-2} folds, or even late kink bands. The sequence proposed by Sakellariou (1990) is based on a more extensive and detailed field-study and contains the main structural elements found in this study (Chapter 3). However, the interpretation by Sakellariou (1990) for the S_0 fabrics is admittedly restricted by lack of suitable exposure. But the recognition and separation of F_2 and F_3 structures by Sakellariou (1990) into separate episodes is arguably too strict.

Table 3.2 A scheme proposed by Sakellariou (1990) for the structural, metamorphic and time framework, for an area immediately to the south of Lake Volvi. All comments and qualifying remarks are taken from Sakellariou (1990).

Structures	Metamorphism	Ages*
S_o: Earliest foliation/metamorphic layering. B_o: Isoclinal, intrafolial folds. (Evidence for this event is extremely rare).	Maximum metamorphic grade is not known. Assemblages are completely overprinted by the later events	Hercynian Orogeny? Only affects the basement gneisses of the SMM.
S_1: Axial planar foliation. B_1: Isoclinal folds, mean axial direction N120° L_1: Plunge direction parallel to fold hinges. Alignment of micas and hornblende	Prograde Event. middle-Amphibolite facies.	
S_2: Initially a crenulation cleavage relative to S_1, and subsequently a schistosity where S_1 is overprinted and obliterated. B_2: Isoclinal to tight similar folds, mean axial direction N150° L_2: Alignment of micas and hornblende. Plunge direction parallel to the fold hinge. Occasionally amphibolite lineations are perpendicular to fold hinges. (S_2 and L_2 are well developed in the Arnaea granite).	Retrograde Event. lower-Amphibolite facies.	Mid-Jurassic Cimmerian Orogeny
S_3: Crenulated to spaced cleavage with parallel alignment of micas. B_3: Similar, tight or open folds, mean axial planar direction N190°. L_3: Alignment of the syn-deformational micas, or "rodding" of quartzofeldspathic lithologies.	Continued Retrogression upper-Greenschist Almandine facies.	Late-Jurassic to Early-Cretaceous palaeo-Hellenic phase of the Alpine Orogeny.
S_4: Crenulation cleavage with or without parallel development of new minerals, or as a spaced cleavage. Locally develops as a fracture cleavage. B_4. Open to tight similar folds, mean axial planar direction N270° ± 40°. L_4: Rodding parallel with B_4 fold axial planes. Alignment of sheet-silicates locally developed and rarely observed.	Weak locally developed continued retrogression. lower-Greenschist facies.	Eocene meso-Hellenic phase of the Alpine Orogeny.

*Ages are based on stratigraphic arguments proposed by Kockel *et al.*, (1977) and radiogenic ages from the Arnaea granite determined by De Wet and Miller (1987).

Table 3.3 A brief summary of the structural and metamorphic evolution within an inferred time framework developed for the Lake Volvi region. This structural and metamorphic evolution was determined completely from this study.

Structures (see Chapter 3)	Metamorphism (see Chapter 4)	Ages*
S_o: Development of an early migmatitic fabric (S_{0A}), gently deformed and cross-cut by a second migmatitic fabric (S_{0B}). Commonly distinguished as a remant fabric related to gneissic or migmatitic banding now represented as a transposed foliation. Evidence for deformation of this fabric is not observed until the F_1 folding events	Uncertain ? High enough for migmatite development.	Hercynian orogeny? Only affects the basement gneisses
S_1: Axial planar spaced foliations, and crenulation cleavages with respect to early S_1 foliations. Variations depending on lithology and state of strain. **F_1**: Tight to close folds, upright to gently plunging, coaxial refolding of early by late F_1 structures. Usually tightened into more commonly observed intrafolial isoclinal folds, aligned sub-parallel to the main S_2 foliation, resulting in steeply plunging structures with an approximately NNW-SSE trend. **L_1**: Mica (biotite) alignment parallel to fold axis.		
S_2: Crenulation cleavages with respect to S_1 or earlier S_2 foliations. When well-developed, spaced cleavage obliterates $S_1$and early S_2. When in close proximity to shear zones S_2 foliations are overprinted by S-C fabrics (sub-vertical to sub-horizontal). A general composite fabric of this generation would be classed as S_{2T}. This foliation usually has a NNW trend dipping to the WSW.	Prograde Event. middle-upper Amphibolite facies	Mid- to Late-Jurassic/Early -Cretaceous
F_2: Isoclinal, tight or close folds, upright to gently plunging. Coaxial refolding of a range of early to late F_2, trending approximately NNW-SSE. Due to the progressive deformation a number of local variations have been observed. **L_2**: Rodding of feldspar parallel to the F_2 fold axes. Alignment of mica parallel to the F_2 axial plane. Locally S_1-S_2 or early to late S_2 intersection lineations are well-developed.	Retrograde Event. Greenschist-facies	
SZ: Steep to flat-lying anastomosing shear zones. Progressive development of S-C fabrics. Shear zones are observed tightening folds and intensifying foliations. Where shear zones are the dominant structure an intense foliation (S_{2S}) is developed. A range of these structures are well-developed and variable in their intensity within the Arnaea granite.		
S_3: Rare locally developed, weak, spaced cleavage, verging on jointing, axial planar to F_3 folds. Usually no foliation observed with F_3 folds. **F_3**: Open (very occasionally tight) folds, with axial planes trending approximately N270°.	Greenschist facies	Early- to Mid-Cretaceous ?
F_4: Kink bands, possibly the effects of the latest stage of the F_3 folding event. However, they are distinctive and common and therefore regarded as a separate fold stage.		Post Mid-Cretaceous ?
Neotectonic Faulting.		Recent ?

*Ages are based on stratigraphic arguments and radiometric dates from previous work. See reviews in Part II of Chapter 1, and Appendix II.

By far the most important omission in both studies is their failure to recognise and discuss the anastomosing shear zones. Papadopoulos and Kilias (1985) refer to a plastic deformation and deformation restricted to particular horizons. This seems to indicate at least some recognition of the (anastomosing) shear zones, which admittedly are best developed east of the Volvi Complex. However, Sakellariou (1990) made no recognition of shear zone development, even though south of the lake, ductile and more distinctly ductile-brittle extensional duplexes in particular are common. Hence, both studies have resorted to a formal fold and cleavage sequence approach which is clearly inadequate to describe the structures within the Volvi area.

3.1.2 Terminology

Orientations of planar structures are presented throughout this work as individual components or a combination of strike and dip (strike 132°; dip 27°SE; 137°/27°SE) respectively. Fabrics and structures are labelled using standard symbols; S, is used for planar fabrics (compositional banding, foliations etc.); SZ, for a fabric which is clearly associated with discrete shear zones; F and L refer to folds and lineations respectively. A subscripted numeral is used to indicate association with a particular deformational event. When local variations to a fabric or structure occur, an area identifier may be added, e.g. S_{2A}= S_2 in the Askos area. If several structures occur an additional subscript may be used to indicate their character; L_R= rodding; L_I= intersection.

The use of a subscripted numeral although useful, assumes that the rock mass has deformed more or less homogeneously and simultaneously over large areas. However, it is apparent that the nature of deformation of large rock masses is commonly heterogeneous and often diachronous (e.g. Chadwick, 1968). In areas such as the Lake Volvi region where progressive deformation occurs, an alternative nomenclature is required e.g. designating certain planar structures as a "transposition" or "composite" foliation (e.g. Turner and Weiss, 1963; S_T of Williams and Compagnoni, 1983; S_{1-2} of Lagarde and Michard, 1986) or referring to successive deformations using alphabetical subscripts (e.g. D_S, D_I, etc.) while describing the details of the structures in non-chronological terms (e.g. Platt and Behrmann, 1986). The assignment of fabrics and structures to different deformational events within the studied area is made principally to aid description and is based on temporal relationships observed in the field rather than the processes responsible for their formation. No implication of synchronous development in the three sub-areas is implied by a structure having the same number in each, because of the possibility of continuous, progressive deformation.

3.1.2.1 Foliations (S) Terminology

Existing classifications of rock fabrics and cleavages are confused, with many overlapping terms and genetic connotations. In order to reduce any possible ambiguity in the terms used in this thesis, the classification proposed by Powell (1979) is applied where possible to the following descriptions.

In order to accommodate and provide a reference point with respect to previous work, the general regional foliation (NNW-SSE trend, variable steep to flat-lying dip) of Kockel *et al.,* (1971, 1977) can be referred to as S_{2T} with respect to the structural sequence developed for this thesis, *see* Table 3.3 (S_T = A composite foliation, represented by a planar surface or group of surfaces whose components share similar morphological features and orientations; Tobisch and Paterson, 1988). This continuous foliation of Kockel *et al.,* (1971, 1977) consists of domains of successive, morphologically similar, parallel foliations in which it is not always possible to separate out the different components. In similar domains, the concept of a composite foliation has been usefully applied (c.f. Turner and Weiss, 1963; Williams and Compagnoni, 1983; Lagarde and Michard, 1986) and interpreted as a function of the partitioning of progressive deformation (c.f. Tobisch and Paterson, 1988). Earlier foliations than this pervasive S_{2T} are confined to the cores of low-strain pods bounded by shear zones..

3.1.3 Progressive Deformation

The term progressive deformation was first used by Flinn (1962), who suggested that a rock undergoing progressive irrotational deformation will pass through a continuous series of shape changes "until the deformation ceases" (c.f. Means, 1976). It is also commonly defined in a more general sense, for example, without the constraints of "continuous" or "irrotational" (e.g. Ramsay, 1967) or, in more specific cases, where the term has been applied in the context of different degrees of (non-) coaxiality (Means *et al.,* 1980). However, the term is always used to imply a sequence of related structural events that give rise to a final fabric. In ductile shear zones, where movement or transport directions may change orientation over relatively short time intervals, the progressive deformation may be expressed by development of multiple sets of structures. In this study progressive deformation is used to imply:

i) A close relationship between the various sets of structures in terms of orientation, sense of movement, style and prevailing metamorphic conditions.
ii) A relatively constant orientation of the regional stress field.
iii) The various sets of structures developing as a relatively continuous sequence of events within a geologically short period of time.

3.1.4 Partitioning of Deformation

The basic concept of deformation partitioning has been well established and is recognised on a large variety of scales (e.g. Turner and Weiss, 1963; Bell, 1981, 1985, 1986; Williams and Schoneveld, 1981; Bell *et al.,* 1986). Tobisch and Paterson (1988) provide a review of deformation partitioning. In the most general case, deformation partitioning refers to the concentration of deformation in discrete domains in a rock mass. These domains can reflect variations in rock type, temperature-pressure conditions, presence of fluids, strain rate etc. Strain partitioning has also been used to represent different processes active in each domain, such as simple shear, pure shear and no strain (e.g. Bell, 1985). In more rigorous mathematical language, deformation partitioning has been analysed in terms of the two components of vorticity active in a flowing rock mass expressed as spin and internal (shear-induced) vorticity (Means *et al.,* 1980; Lister and Williams, 1983). These two terms refer to the relation between the angular velocity of the instantaneous stretch directions and, respectively, the external co-ordinate system and material lines. The degree to which these two components are partitioned during deformation influences the manner and type of geologic structures which develop (Lister and Williams, 1983).

Deformation on a large scale within orogenic belts is commonly heterogeneous and/or diachronous, so that sequences of structures may have irregular spatial or temporal distributions (e.g. Williams, 1985; Tobisch and Paterson, 1988).

In most rock masses, structures of a given "generation" will probably not develop simultaneously in all parts of the area, but will be strongly influenced by the larger-scale partitioning of the deformation. That is, structures will develop in that part of the rock mass in which stress or movement is concentrated at any given time. In this model, continuous cleavage (Powell, 1979) in different parts of the rock mass may represent entirely different times of formation given a heterogeneous movement pattern, e.g. in a thrust zone, the different parts of the thrust sheet will move at different times (e.g. Butler, 1982; Coward and Potts, 1983), as the deformation is sequentially partitioned to different parts of the sheet. It is entirely conceivable that in one domain (A), continuous cleavage may develop as that part of the sheet moves. With a shift in movement direction of the rock mass, however, crenulations of the initial continuous cleavage foliation begin forming in domain (A), while in a contiguous domain (B), the new movement and/or relocalised high stress there has now initiated the development of a continuous cleavage. Under such conditions, continuous cleavage and crenulation cleavage are forming simultaneously in contiguous domains. Similar observations have been made with respect to mylonite zones (e.g. Bell, 1978; Bell and Hammond, 1984) and accretionary prisms (e.g. Knipe

and Needham, 1985) and have demonstrated that local polyphase sequences of structures can form during single, progressive deformational phases. For these reasons, traditional chronological notations such as S_1, S_2 etc., tend to create a regional picture which is misleading. They greatly oversimplify the timing and partitioning of deformation in a heterogeneously deforming body, and this inhibits the construction of models which can realistically depict the manner by which rock masses deform.

Consequently, in heterogeneous rock masses undergoing progressive deformation, the following are likely to hold true: (a) each part of the mass will have its own unique deformation path, (b) there is likely to be contemporaneous development of foliations showing different morphologies (e.g. continuous cleavage forming in domain B while crenulations are forming in domain A), and (c) because of the common occurrence of crenulation cleavages being transposed into continuous cleavages which are then subsequently crenulated, continuous cleavages in different parts of an area undergoing progressive deformation may be of different ages. The same concept applies to the age of crenulations. While placing structures in time categories (S_1, S_2 etc) may be valid for any given point, conceptually there is often no justification to extend the correlation beyond the scale of the exposure or thin section.

An alternative nomenclature may be used to distinguish the morphology of the different fabrics, (i) S_0, migmatitic banding, (ii) S_C, continuous cleavage, (iii) S_{CC}, crenulation cleavage with or without differentiated layers, (iv) S_T transposed and/or composite foliation which includes at least some domains of new continuous cleavage (c.f. Williams and Compagnoni, 1983). The process of generating a composite foliation can involve various mechanisms:

i) Simple rotation of early foliation into a new direction without an intervening crenulation cleavage phase.

ii) Complex rotation of early foliation passing through a crenulation cleavage phase, accompanied by transposition of layers or pre-existing cleavages with or without differentiation.

iii) Recrystallisation and formation of neoblasts in the new direction.

In addition, the composite foliation can include remnants of early isoclinal folds with other early or later structural elements parallel or nearly parallel to each other. In most cases, it is difficult to distinguish when the various components were formed. Individual structures or structural associations may display complex geometric arrangements such as folds with highly curvilinear hinges (Cobbold and Quinquis, 1980), or cleavages that transect broadly contemporaneous folds (e.g. Powell, 1974).

PART I: Development of Structures and Fabrics

3.2 Structural Framework

The dominant structures within the area are anastomosing shear zones which are variably developed in scale and orientation around Lake Volvi and the Volvi Complex (Fig. 3.1). These shear zones are particularly well exposed in an unambiguous form along the Vamvakia river (Insert, Map C; Section 2.3). The shear zone structures are associated with the development of the dominant S_2 foliations throughout the area and generally obscure the evidence for any earlier structures. However, within the low-strain cores between the shear zones, early structures are preserved. These cores have a broadly "flat-fish" shape and as they have behaved much as a stack of such "fish" would, they are referred to as "halibuts", following John Dewey (oral presentation, Edinburgh, 1991). Three distinct deformational sequences (D_{1-3}) can be identified. D_1 is related to deformation of a high-grade migmatite basement preserved within the low-strain cores (Section 3.3), D_2 is related to a range of pre-shear to syn-shear deformational events (Sections 3.4 and 3.5) and D_3 to ductile-brittle post-shear deformation (Section 3.6). Due to the variations in style and orientation of the shear zones the structural sequences within the studied area have been divided into three main sub-areas, to facilitate description. These are:

i) From the eastern margin of the Volvi Complex eastwards into the Kerdilion Group.

ii) From the western margin of the Volvi Complex westwards towards the boundary with the Arnaea granite.

iii) To the south of Lake Volvi.

3.2.1 Shear Zones (SZ)

As the shear zones and structures and fabrics which are developed with them are the dominant structures within the area, they are reviewed at this point so that the following structural sequences and observations can be viewed in their true context.

The shear zones distributed around Lake Volvi are composed of a network of anastomosing high-strain zones wrapping variably elongate low-strain pods, or "halibuts" (Fig. 3.2). Each of the individual low-strain pods contain evidence for only part of the regional structural history. The shear zones are most clearly visible on a scale of 1 to 10 metres throughout the area (Plates 3.1, 3.2, 3.3). However, depending on the different lithologies and thin-section observations, similar structures occur on a mm- and cm-scale and have also been identified (inferred) on a km-scale by regional mapping (Inserts, Maps B to H). It is proposed that the same models,

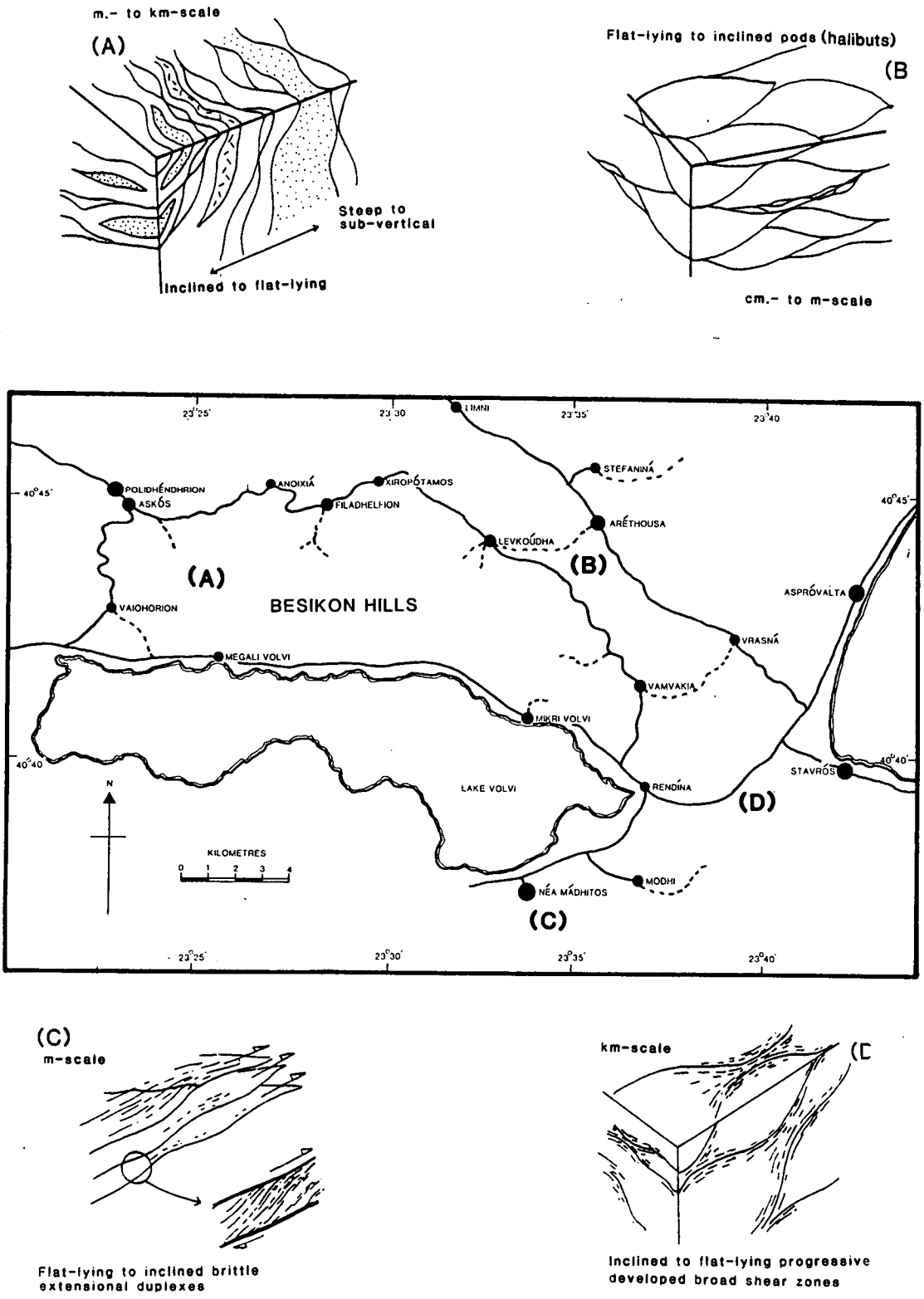

Fig. 3.1: Variations in style and orientation of anastomosing shear zones around Lake Volvi.

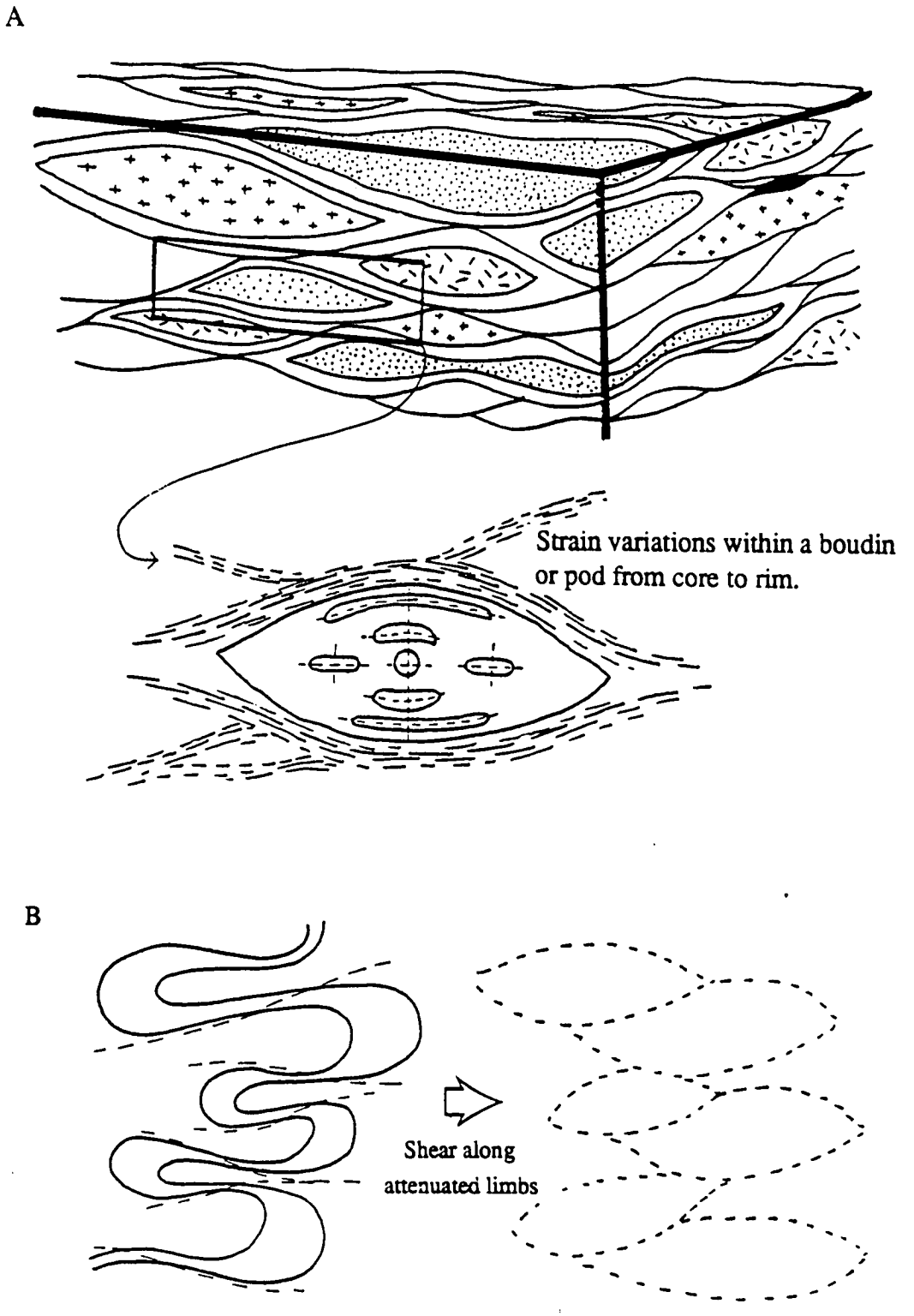

Fig. 3.2: Geometry of anastomosing shear zones with, "halibut" development. (A) Strain variations from low-strain core to high-strain rim. (B) Extreme attenuation of fold limbs maybe considered one possible cause for the initiation of anastomosing shears.

Plate 3.1

Shear zones are found throughout the area and within all the lithologies, however, their character (size, style, orientation, etc.) is strongly related to the individual lithologies. The lens cap within all the plates is 52 mm in diameter.

Plate 3.1a: Narrow (1-2 cm wide) shear zone within a coarse gabbroic unit, from inside the western margin of the Volvi Complex.

Plate 3.1b: Gabbroic unit from inside the western margin of the Volvi Complex displaying broad (cm- to m-scale) shear zones. A clear distinction can be made between the original coarse-grained member (A) and progressively sheared flaser gabbros (B) and banded amphibolitic (ex-gabbroic) members (C).

Plate 3.1c: Quartzofeldspathic unit approximately 1 to 1.5 km along a stream section to the NE of Megali Volvi. The shear zone is highlighted by the attenuation of the mafic component (centre) into an intense fabric, from an otherwise homogeneous mottled mtrix (top).

Plate 3.1d: A 15 cm wide shear zone with shear displacement top to the NW, within the Askos Garnet Mica Paragneiss Formation. The shear zone overprints and tightens upright F_2 folds. Within the centre of the picture a quartz vein has been tightened into an isoclinal fold with its limbs completely sheared.

Plate 3.1

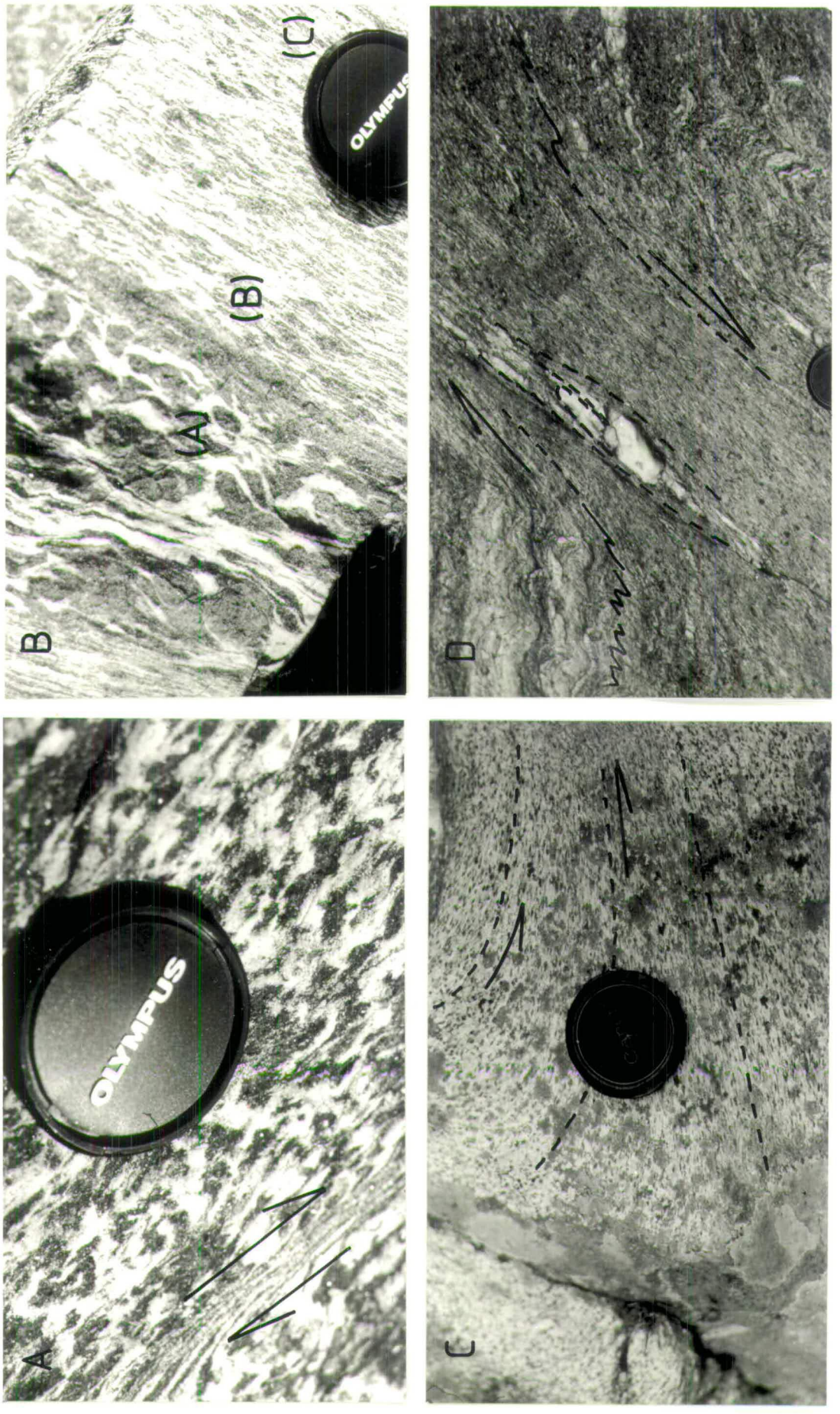

Plate 3.2

Plate 3.2a: Ductile shearing within impure carbonates and graphitic schists to the NE of Megali Volvi. Lens cap is 52 mm in diameter.

Plate 3.2b: Ductile-brittle shearing of granites along the Askos to Vaiohorion road. View looking N to NW with shear direction top to E to NE. Horizontal field of view is approximately 30 m across.

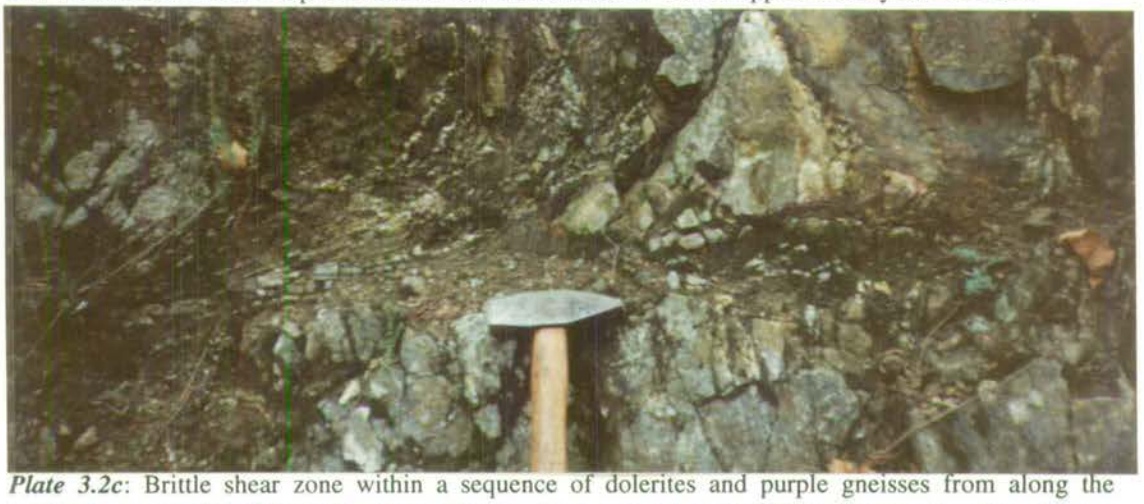

Plate 3.2c: Brittle shear zone within a sequence of dolerites and purple gneisses from along the northern section of the Vamvakia river. View looking approximately NNE with the shear direction top to E. Head of hammer is 16 cm long.

Plate 3.3

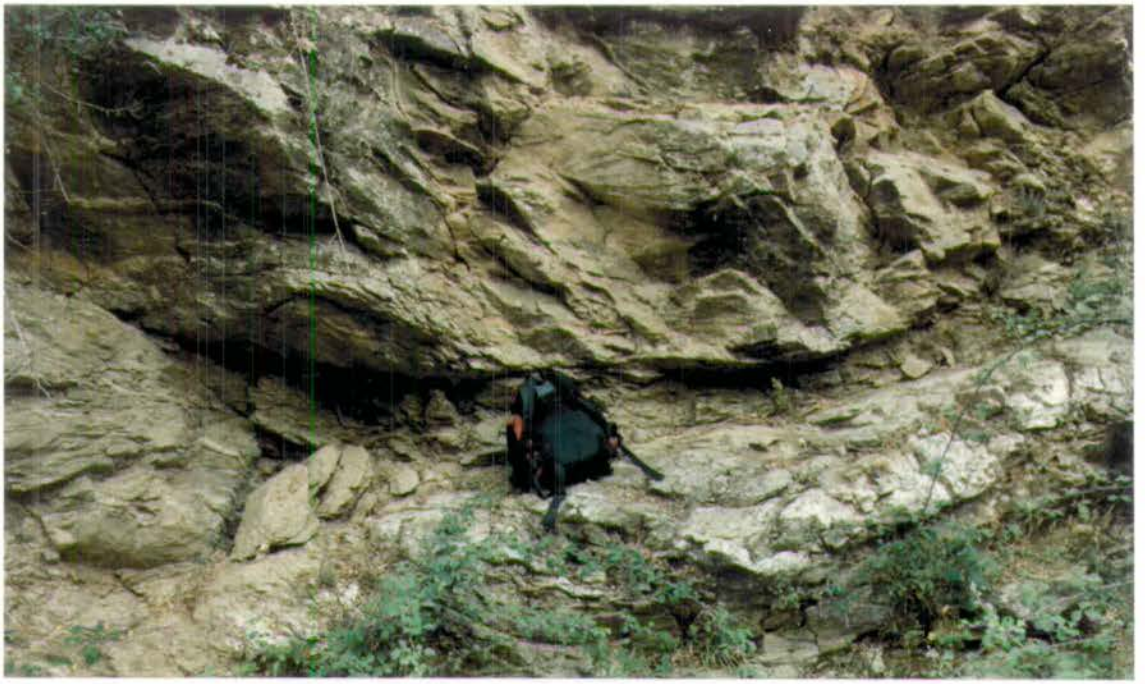

Plate 3.3a: Brittle, extensional shear zones within carbonate lithologies to the SE of Nea Madhitos. View looking approximately SSE with shear direction top to ENE. The shear zone has a flat-lying, gently undulating attitude, with a weakly anastomosing character caused by extension along the S_2 foliation and late brittle fractures. Rucksack is approximately 1 m long.

Plate 3.3b: Close view of a typical brittle, extensional shear zone south of Lake Volvi. The displacement along the shear zone is concentrated into an area approximately 30 cm to 40 cm wide. This zone is typified by intensely foliated and steeply dipping fabrics, grading progressively downwards into a fine-grained (fault-gouge) matrix. Immediately adjacent to the shear zone the dominant fabrics are inclined to flat-lying with a weak anastomosing character. View looking approximately NNE with shear displacement top to NNW. Lens cap is 52 mm in diameter.

processes and mechanisms observed for well-defined small-scale (cm- and m-scale) structures within the area can be proposed for the larger, km-scale regional features.

Generally shear zones intensify or obliterate earlier structures, however, the characteristic outcrop pattern of low-strain pods wrapped by anastomosing high-strain zones preserve a range of progressively developed and deformed structural and igneous relationships. Consequently, fabrics associated with shear zone development are complex (Section 3.2.3), as slightly shifting movement directions along shear zones can produce multiple generations of contemporaneous structures (Tobisch and Paterson, 1988). Comparable examples of the progressive evolution of mesoscopic shear zone structures have been described in recent years by a number of authors (Ramsay and Graham, 1970; Coward, 1976; Berthé *et al.,* 1979; Berthé and Brun, 1980; Simpson, 1982; Choukroune and Gapais, 1983; Ghosh and Sengupta, 1987).

3.2.2 West of the Volvi Complex (SZ_W)

The main shear zones (SZ_{1W}) to the west of the Volvi Complex tend to have a diffuse character and occur as steep to sub-vertical, m- to km-scale anastomosing complexes (Fig. 3.1a; Insert, Map B). The general NNW-SSE trends for these regional shear zones (SZ_{1W}) are marked by the progressive intensification of the regional S_2 foliation (Section 3.4.1). Identification of this characteristic intense S_2 foliation has been used to locate the (SZ_{1W}) shear zones. A particularly well-defined shear zone boundary occurs to the NE of Vaiohorion. The Askos Augen Orthogneiss Member (Section 2.6.3) crops out to the W of the boundary and the Askos Augen Paragneiss Formation (Section 2.3.3.2) and Askos Marginal Amphibolite Formation (Section 2.3.3.1) crop out to the SE and NE of the boundary respectively, *see* Insert, Map B. Shear zones within the Askos Augen Paragneiss Formation (Section 2.3.3.2), become progressively more diffuse further to the east. Within the various paragneiss and schist formations of the Vertiskos Group the (SZ_{1W}) shear zones are developed as narrow zones (1-5 m wide) of intense shear, with variable dip and strike (dip, 35°W-vertical-75°E, and strike, 178° to 147°).

The effects of the anastomosing (SZ_{1W}) shear zones are most intense along the boundary between the Askos Marginal Amphibolite Formation (Section 2.3.3.1) and the Askos Augen Paragneiss Formation (Section 2.3.3.2). The styles of structures along this boundary are characterised by numerous small, elongate (0.5 to 5 m long) pods, wrapped by an intense S_2 foliation, and by the development of numerous boudins (Fig. 3.3; Plates 3.4a, b). Pods and boudins along this boundary are considered to have developed by layer parallel extension during intense shear. Localised S-C fabrics with a variable sense of shear are developed due to the intensity

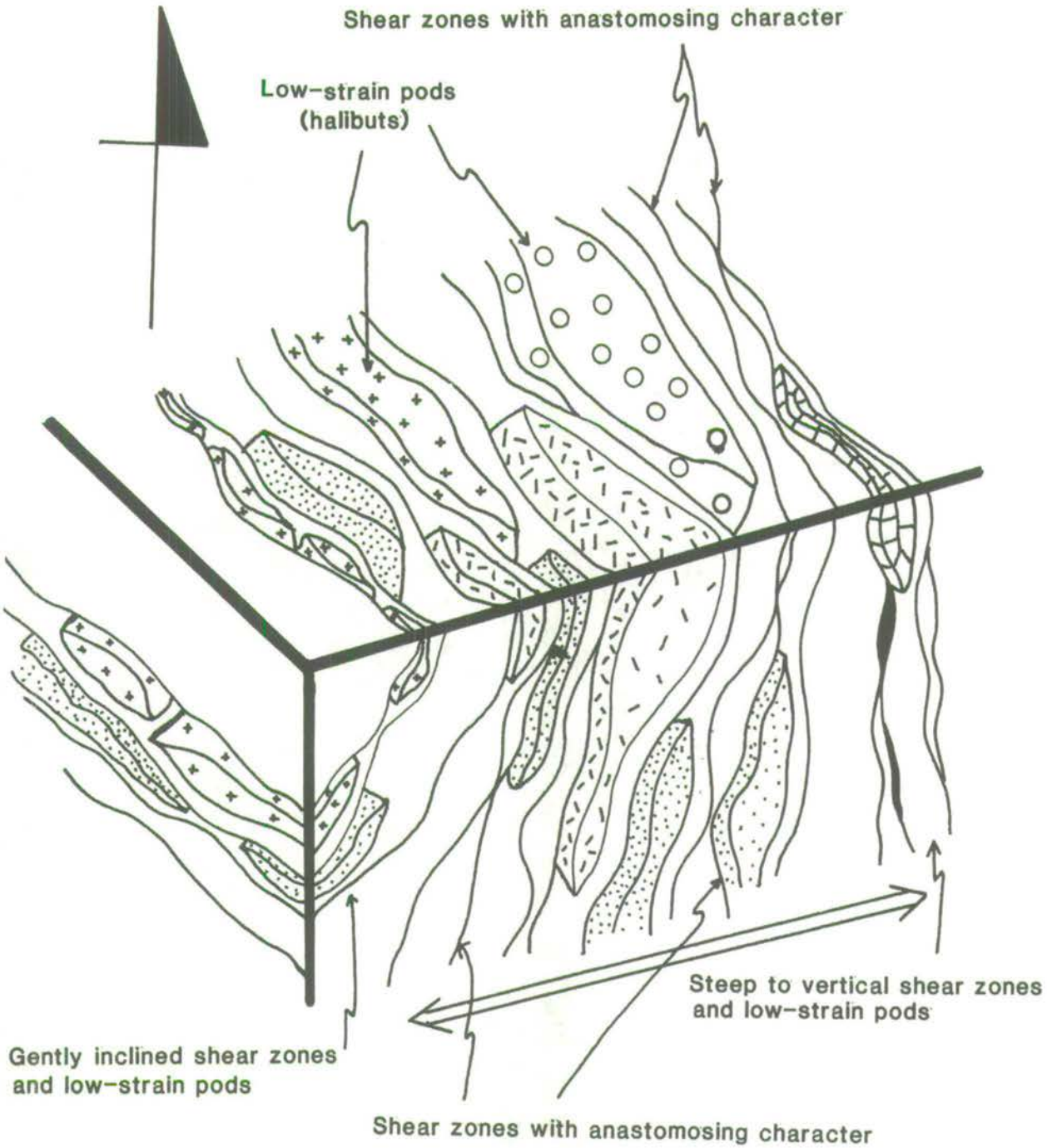

Fig. 3.3: Schematic interpretation for the area west of the Volvi Complex. Displacement of formations along anastomosing shears is considered partially responsible for the discontinuity of formations and structures throughout the area. Low-strain bodies, or "halibuts" range from m- to km-scale. The m-scale pods (halibuts) show a distinctive low- to high-strain gradient from core to rim respectively. Similar relationships are inferred for the km-scale structures.

Plate 3.4

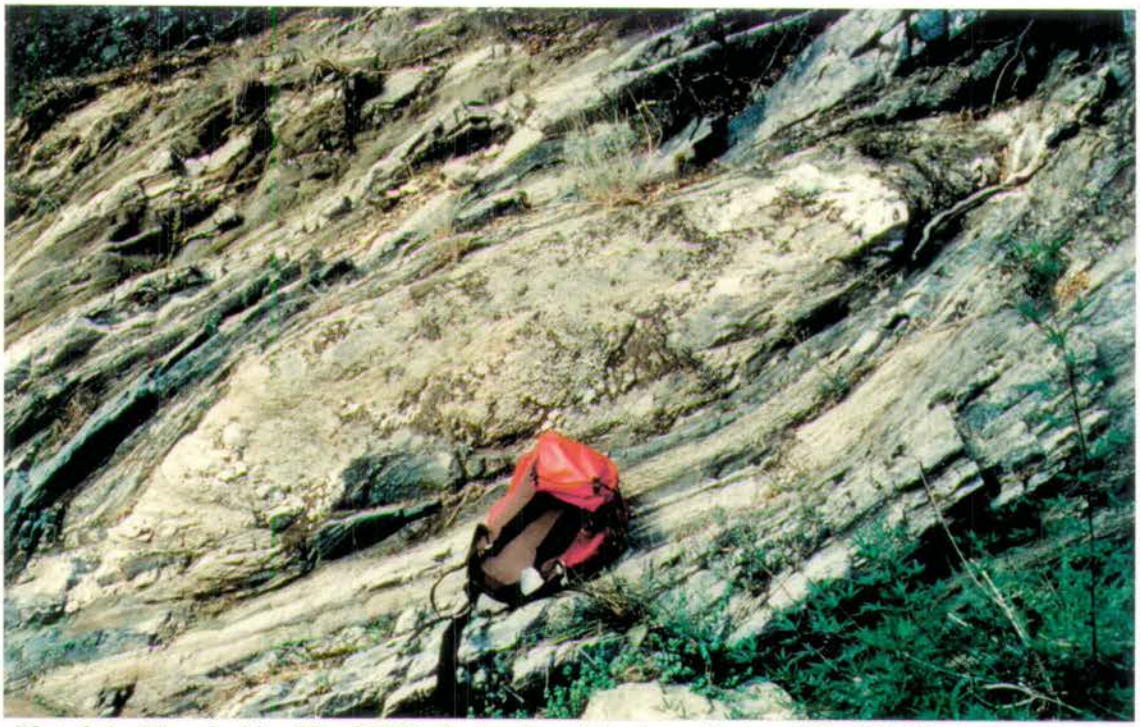

Plate 3.4a: View looking N to NNW of a boudin within the main river NE of Vaiohorion, *see* Insert, Map B. Well-banded amphibolite and quartzofeldspathic augen orthogneiss lithologies have been subjected to layer parallel extension with a shear component indicating top to N to NE. Rucksack is approximately 1 m long.

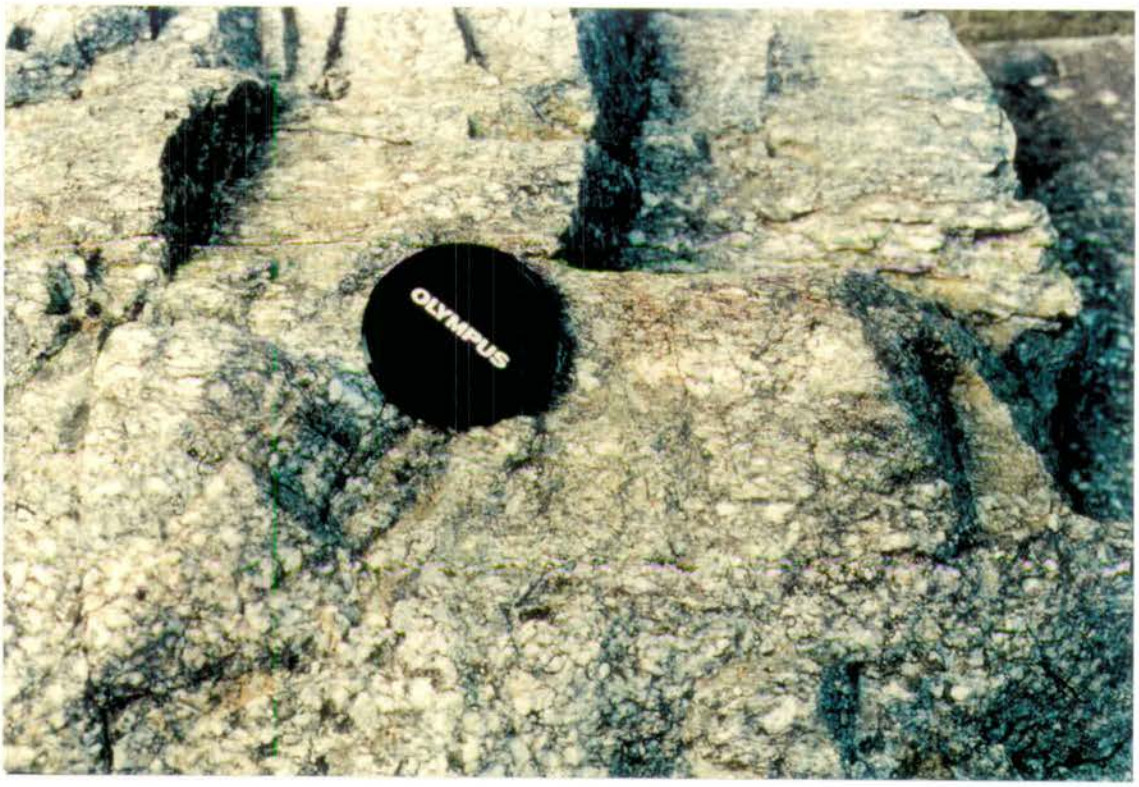

Plate 3.4b: View of a boudin within the main river NE of Vaiohorion, *see* Insert, Map B. Progressive intensification of strain, depicted by euhedral plagioclase porphyroblasts within the core, through an intermediate augen-rich section and finally into a mylonitic quartzofeldspathic rim. Lens cap is 52 mm in diameter.

of the S_2 foliation (Section 3.4.2). Within the Askos Marginal Amphibolite Formation (Section 2.3.3.1), boudins of the Askos Augen Orthogneiss Member (Section 2.6.3) occur with a marked strain gradient from the core to rim (Plate 3.4b). The low-strain core preserves euhedral, plagioclase phenocrysts with a fairly random orientation. These phenocrysts are progressively aligned, flattened and rounded towards the margin of the pod, developing a porphyroclastic mylonitic fabric at the rim. Similar progressive strain indicators occur along the Vaiohorion to Askos Road (Section 3.12.1), with evidence for the progressive tightening of folds abundant within some of the larger pods along this sheared boundary (Section 3.4.2).

The effects of the steep to sub-vertical regional shear are gradually reduced from the east boundary of the Askos Marginal Amphibolite Formation (Section 2.3.3.1) to the west boundary with the Arnaea granite (Section 2.6.3). The dip of the S_2 foliations are reduced from 80-90°W to 30-40°W, and become less intense, reverting to more typical combinations of composite S_2 (e.g. S_{2C}, S_{2CC}, S_{2T}) foliations.

A second series of minor flat-lying shear zones (SZ_{2W}) is locally developed along the Vaiohorion to Askos road. These flat-lying shear zones (SZ_{2W}) have a general SW-NE trend and locally tighten and boudinage a number of F_2 structures (Section 3.4.2). From the orientation and attitude of the SZ_{2W} shear zones they appear to be related to and a possible cause of, at least some if not all of the gentle to open, upright F_3 folds during ductile to brittle shear zone development (Section 3.2.1).

3.2.3 East of the Volvi Complex (SZ_E)

The styles and orientations of anastomosing shear zones are more variable to the east of the Volvi Complex. Immediately adjacent to the eastern margin of the Volvi Complex along the Vamvakia river there is an intense network of approximately NNW-SSE trending flat-lying to horizontal anastomosing shear zones (SZ_{1E}) wrapping 3 to 8 m long low-strain pods (Fig. 3.1b; Section 2.3.2). The (SZ_{1E}) shear zones locally intensify the regional S_2 foliation.

Along this river the low-strain pods are juxtaposed and apparently transported in a random fashion although with an overall top to the NE shear sense (Section 2.3.2). Further east, along the inferred boundary between the Vertiskos and Kerdilion Groups (Section 2.7; Insert, Map F), the shear contact takes on a ductile-brittle character. To the east and south of Arethousa, the Arethousa Ultramafic Member (Section 2.3.3.7) is sheared over the underlying units with a steep trend to the east and flat-lying trend to the south of Arethousa. The ductility of this lithological unit is considered to be the main factor in shear zone development along this contact.

Further south along the Arethousa to Vrasna road, the regional (S_2) foliation is intensified and a narrow (1-5m wide), sub-vertical shear zone with an approximate N-S trend and dip 79-85°E is developed. Along the track between Vamvakia and Vrasna the contact is again represented by intensification of the regional (S_2) foliation, however, a broad (5-20 m wide) steep to gently inclined shear zone with a N-S trend and dip 39-67°W is developed. Along stream sections between these two traverses, the shear zone contact of the western boundary has an approximate NW-SE trend and dips between 25-35°E. The shear zone also decreases progressively in width towards the north. The projected extension of this shear zone to the south of Lake Volvi takes on a more brittle character (Section 3.2.4). Further east into the Kerdilion Group the formations are inferred to be juxtaposed along large km-scale, variably orientated (NW-NNW to SE-SSE trend and steep to flat-lying) anastomosing shear zones (Fig. 3.1d).

3.2.4 South of Lake Volvi (SZ_S)

To the south of Lake Volvi, shear zones (SZ_S) have a predominantly flat-lying to horizontal attitude. Within this area they appear to be relatively brittle in character and associated with extensional structures. The anastomosing appearance typical of the shear zones (SZ_W) north of the lake is now extremely vague (Section 3.2.1). These extensional, brittle shear zones south of the lake, may be representative of higher structural levels compared to the ductile shear zones north of the lake and may therefore preserve different deformation histories. This theory is supported by the presence of a major Neotectonic fault trending E-W along the Lake Volvi basin, with downthrow to the S, which juxtaposes the areas N and S of the lake (Section 1.11). However, evidence from east of Modhi indicates a fairly continuous transition from a ductile to brittle-ductile regime. Evidence for the shear history south of Lake Volvi is therefore complex and preserves evidence for a wide range of deformation regimes. This structural evolution has been determined from three main areas.

(1) To the south of Nea Madhitos (Insert, Map G), shear zones are characterised by flat-lying extensional duplexes (Plate 3.3), with variable sense of shear. These shear zones are interpreted as structures representing deformation around a ductile-brittle transition. This type of shear zone development indicates a different history for the areas N and S of the lake. However, there is a strong possibility that the shear zones N and S of the lake were synchronous in their development. Hence, the present configuration simply shows different structural levels of the regional evolution.

(2) To the east of Modhi and Rendina, the lateral continuity of the ductile shear zone from NE of the lake (Section 3.2.3), takes on a more brittle characteristic.

This is particularly well displayed by the Rendina Marble Formation (Section 2.2.2.5) which is now highly brecciated. This change in deformation style may indicate either tectonic juxtaposition of deep and shallow level structures N and S of the lake respectively, or they may indicate relative timing of their development early- to late N and S of the lake respectively in the regional evolution.

(3) Along the track east of Modhi there are a range of transitions between ductile to ductile-brittle shear zone development. These ductile shear zones are typified by progressive deformation and transposition of early structures. Isoclinal folding (F_1) of early leucosomes (rarely preserved), is obscured by an intense sub-vertical spaced cleavage (S_1), parallel or sub-parallel to the leucocratic banding. The spaced cleavage is expressed by alignment of biotite. The leucocratic banding is progressively disrupted towards areas of more intense strain, where it is transposed into discontinuous stringers and augen of quartzofeldspathic-rich material (Plates 3.5; Fig. 3.4). These stringers and progressively flattened augen are orientated perpendicular to the leucocratic (S_0) trend. Progressive transposition of sub-parallel S_0/S_1 fabrics within the Modhi Leucocratic Gneiss Formation (Section 2.2.3.2) is interpreted as being caused by overprinting of flat-lying continuous (S_2) foliations initiated and progressively intensified by flat-lying shear zones (Plate 3.5; Fig. 3.4). The style and nature of development of these ductile shear zones are similar to structures N of the lake.

3.2.5 Summary

Shear zones are characterised by a range of styles, orientations and scales which are variably distributed and developed around the Volvi Complex and Lake Volvi. The most distinctive character of the shear zones is their well-developed anastomosing geometry. A clear distinction can be made between "early" ductile SZ_1 and "late" ductile-brittle SZ_2 phases of shear zone development. These different phases of shear zones are developed both synchronously at different structural levels in the regional structural regime, and overprinted by later deformation after juxtaposition along late faults.

One of the main conclusions for the structural history is that the coaxial folding of early F_2 by late F_2 folds is directly related to the progressive development of the shear zones. Hence, the local trends and orientations of the shear zones and fold structures are closely related. Therefore apart from migmatitic (D_1) structures preserved within low-strain cores, most D_1 structures and coaxially refolded F_2 folds and the associated foliations to these structures are rotated into parallelism during the development of D_2 shear zones.

Plate 3.5

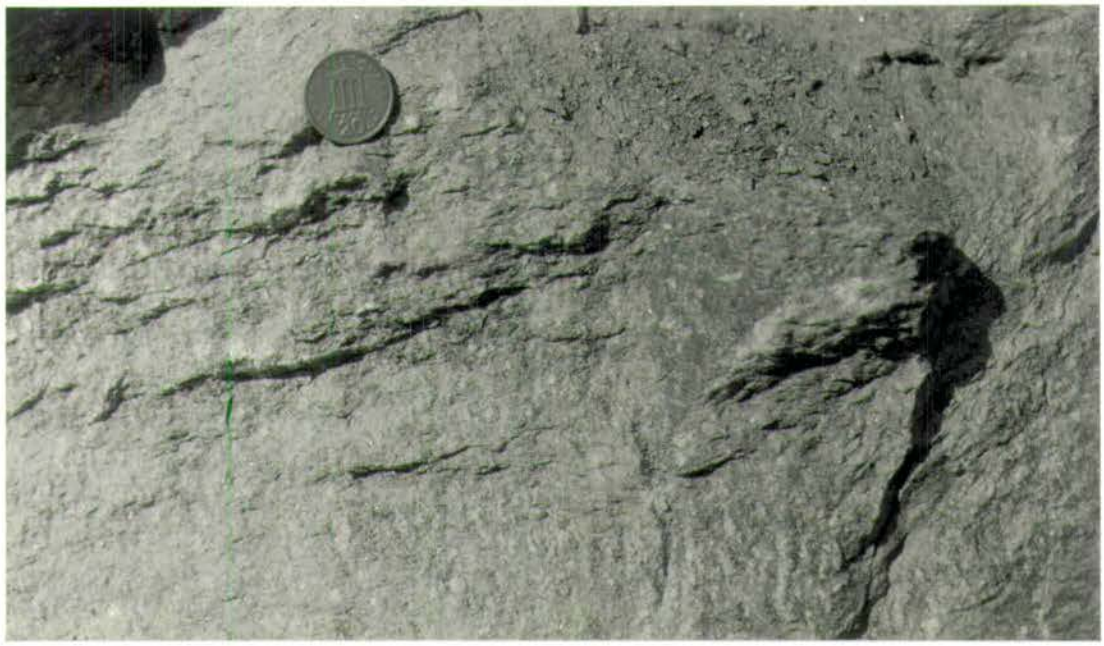

Plate 3.5: Transposition of early upright fabrics by the progressive development and intensification of flat-lying to inclined (S_2) shear foliations. View looking approximately N to NW of the Modhi Leucocratic Gneiss Formation. Sense of shear displacement is top to NE. Coin is 28 mm in diameter.

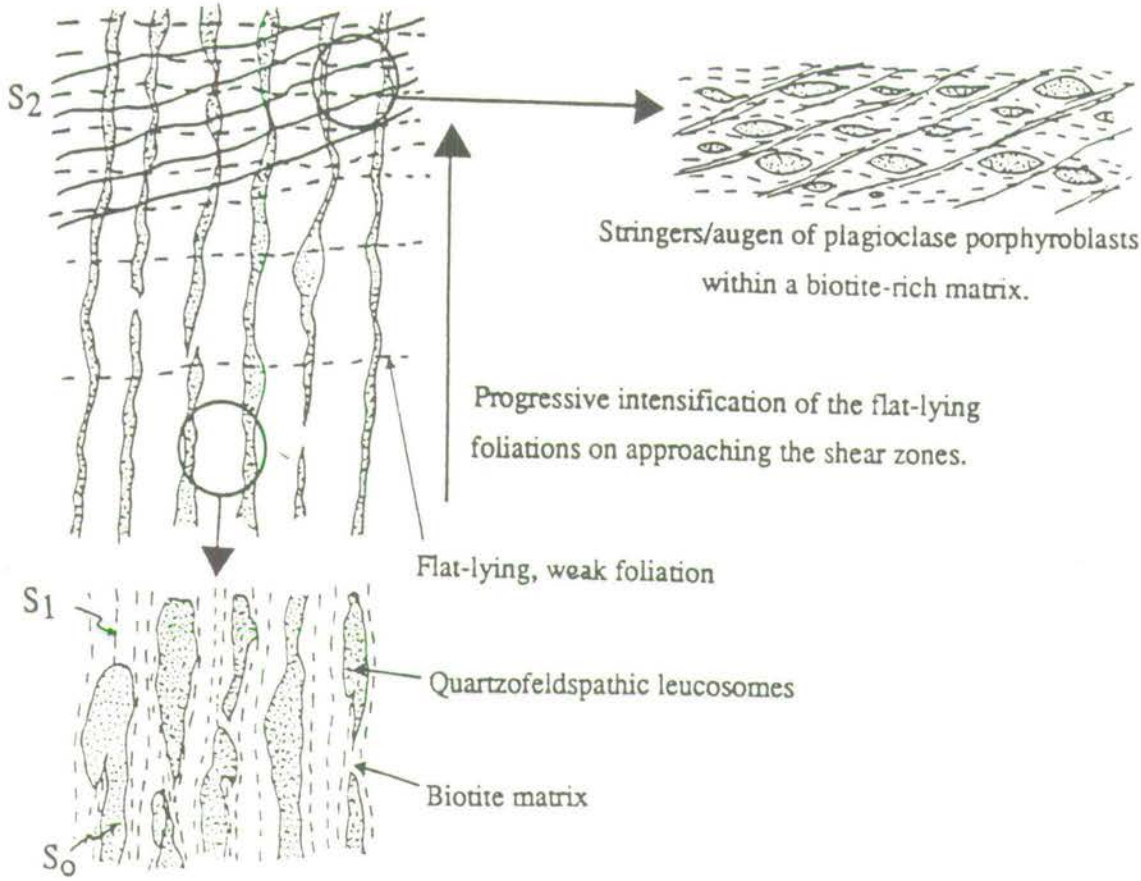

Fig. 3.4: Transposition of an early upright (S_0) fabric, (F_1) fold and associated (S_1) cleavage phase, by two flat lying shear related (S_2) foliations

3.3 D_1: Original Basement Structures and Fabrics

3.3.1 The Earliest Fabrics (S_0)

The S_0 fabrics are of metamorphic origin and composed of discontinuous mm- to cm-scaled leucocratic banding created by a migmatite event (Figs. 3.5, 3.6; Plates 3.6a to d; Insert, Map C). Development of the S_0 fabrics within this migmatite event is of an undetermined age, possibly associated with an Hercynian orogenic event (Chapter 1). No earlier "original" fabrics have been found, therefore the migmatite leucosomes are denoted as the earliest fabrics, with all subsequent structures and foliations which are developed numbered accordingly. The migmatitic S_0 fabrics are particularly well-preserved in two units to the east of the Volvi Complex; the Gun-emplacement Migmatite Member (S_0; Section 2.2.2.1) and especially the Vamvakia Migmatite Formation (S_{0A}, S_{0B}; Section 2.3.2.1). Within these two units the well-preserved S_0 fabrics are limited to low-strain areas (generally pods), wrapped by high-strain anastomosing shear zones.

Gneisses to the west of the Volvi Complex, e.g. the Askos Augen Paragneiss Formation (Section 2.3.3.2) and bands within the Askos Garnet Mica Paragneiss Formation (Section 2.3.3.4) also have a "migmatitic" precursor, although less well preserved (Plates 3.7a to e). These gneisses contain pinched and swelled refolded leucosomes with biotite selvedges present. Even when extensively overprinted by later schistosity a migmatite precursor can still be inferred.

3.3.2 The First Phase Foliations (S_1)

The range of progressively developed S_1 foliations (Fig. 3.5) are particularly well preserved in the low-strain pods associated with S_0 fabrics (Section 3.3.2) of the Vamvakia Migmatite Formation (Section 2.3.3.1). The earliest S_1 foliations consist of an early continuous S_{1C} foliation axial planar to early F_1 (F_{1A}) folds, which are created by folding the S_{0A} migmatite fabric (Section 3.3.5). The S_{1C} foliation is either crenulated into an S_{1CC} foliation or is intensified into a composite (S_{1T}) foliation by a later continuous $S_{1C'}$ foliation (the $S_{1C'}$ foliation is axial planar to late F_1 (F_{1B}) folds associated with the S_{0B} migmatite fabric; Section 3.3.5). Rarely, two equally well-developed cross-cutting and sub-parallel continuous foliations are preserved (S_{1C} and $S_{1C'}$).

Within the Modhi Leucocratic Gneiss Formation (Section 2.2.3.2) to the east of Modhi, an original leucocratic banding (S_0) preserves rare isoclinal folds with a continuous sub-vertical axial planar foliation (S_{1C}). The folded leucocratic layers are

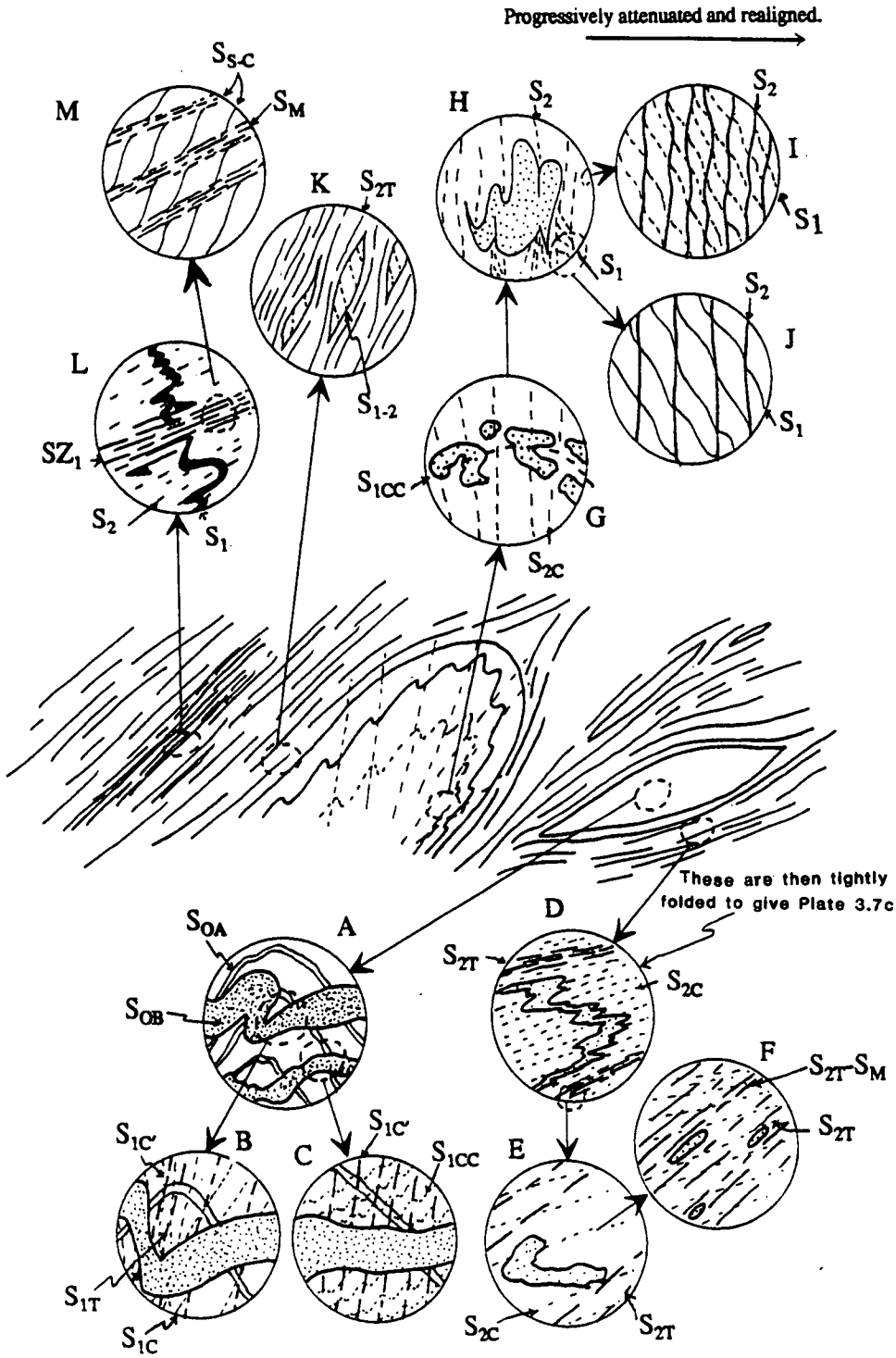

Fig. 3.5: Schematic representation of the diverse range of foliations, developed relative to major structures. A, B, C depict migmatitic(S_0) fabrics and early (S_1) cleavages found within the cores of low-strain pods. D, E, F depict rotated (S_0) leucocratic fabrics and the development of shear related (S_2) foliations. G, H, I, J depict (S_1) and (S_2) foliations related to fold development. K, represents partially sheared and intensified (S_1) and (S_2) foliations, resulting in a composite fabric. L, M represent mylonitic and S-C (S_2) fabrics related to shear zone development.

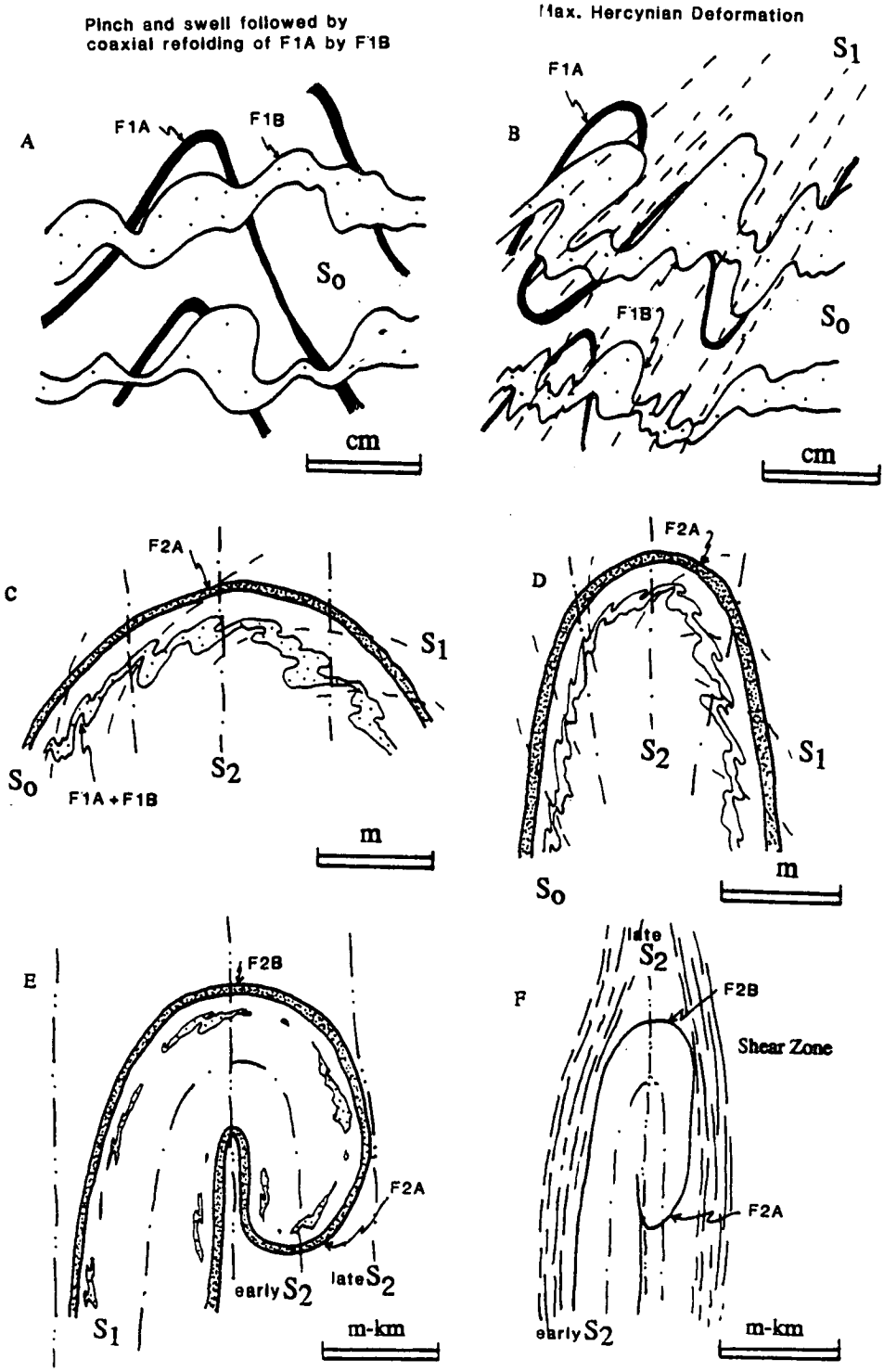

Fig. 3.6: Simplistic interpretation for the development of the main structures and fabrics within the studied area. Progressive, often coaxial development of structures results in a complex array of overprinted fabrics: (a) to (b) folding and cleavage development in a migmatite; (c) second phase folding and cleavage development (m-scale); (d) progressive tightening and intensification of foliations; (e) coaxially refolded second phase fold with a new cleavage; (f) shear zone with a shear related foliation wrapping the low-strain pod, or "halibut", containing preserved early structures.

Plate 3.6

Low- to medium-strain migmatites from the northern section of the Vamvakia river, *see* Insert, Map C. The hammer is 52 cm long and the pen is 14 cm long.

Plate 3.6a: Migmatites within the low-strain core of "Migmatite Bluff", with well-preserved S_{0A} and S_{0B} leucocratic fabrics. The pegmatite/leucocratic bands (S_{0B}) cross-cut the primary migmatitic pinch and swell fabric (S_{0A}). The S_{0B} fabric was in turn subjected to a stage of pinch and swell development. Both fabrics are subsequently close to tightly folded along a coaxial axial plane in progressively developed upright (F_1) structures.

Plate 3.6b: Typical intermediately-strained black and white migmatite within close proximity to "Migmatite Bluff". Ductile extension of the S_{0B} leucosomes has resulted in a sub-parallel orientation with the S_{0A} migmatite fabric. A new set of S_2 foliations have been developed in association with the development of F_2 structures. The F_2 structures re-fold the tight to isoclinal F_1 folds. Fabrics are now flat-lying and folded into a series of close, tight and isoclinal F_2 folds. Within the low-strain zone (bottom of plate) close F_2 folds refold what are possibly earlier F_1 structures. Isoclinal F_2 folds in areas of high-strain (centre of plate) reflect the progressive tightening of the tight parasitic F_2 folds on the limb of the close F_2 fold.

***Plate 3.6c*:** A large loose block possibly from the core of "Migmatite Bluff". The pegmatite/leucocratic bands (S_{0B}) cross-cut the primary migmatitic pinch and swell fabric (S_{0A}). The S_{0B} fabric was in turn subjected to a stage of pinch and swell development. Progressive tightening of the F_1 folds, has resulted in the partial alignment of the S_{0A} and S_{0B} fabrics.

Plate 3.6d: Medium- to high-strained migmatite with only poorly preserved cross-cutting relations between the pegmatite/leucocratic bands (S_{0B}) and the primary migmatitic pinch and swell fabric (S_{0A}). This plate shows the effects of extreme tightening of the F_1 folds, resulting in the alignment of the S_{0A} and S_{0B} fabrics. The rock now has a banded appearance which is in turn subjected to a stage of pinch and swell development.

Plate 3.6

Plate 3.7

Migmatitic lithologies within various formations of the Vertiskos Group west of the Volvi Complex showing more intense deformation of "shear zone" age. Lens cap within all the plates is 52 mm in diameter.

Plate 3.7a: Well-banded migmatitic fabrics (probably S_{0B} which has been subjected to a similar deformation history to Plate 3.6d) with pinch and swelling of the leucosomes. Tight to isoclinal folding of the migmatitic fabric and attenuation of fold limbs helps to create the bleb-like character of this lithology. Possibly has a complex early deformation based on the similarity to Plate 3.6d. The rock is also cross-cut by a late stage of broad crenulation (top left to bottom right).

Plate 3.7b: Close to tight refolded probably F_2 folds with a type 3 interference pattern are contained within a fine-grained pelitic host (bottom of plate).

Plate 3.7c: Close to tight steeply inclined harmonic coaxial refolding of early F_2 folds by later F_2 structures, with type 3 interference patterns developed. Shearing along F_2 fold limbs has obscured the F_2 interference structures and obliterating any possible remnant F_1 migmatite folds.

Plate 3.7d: Intensely sheared quartzofeldspathic (migmatitic) fabric with pinch and swelled leucosomes (potentially isoclinally folded). Foliations (due to shear) are so intense at least two cleavages are well-developed.

Plate 3.7e: A slightly more pelitic lithology than Plate 3.7d. However, a discontinuous pinch and swelled leucocratic fabric can still be determined. Due to the higher modal proportion of mica within this rock, S-C shear fabrics are more clearly defined.

Plate 3.7

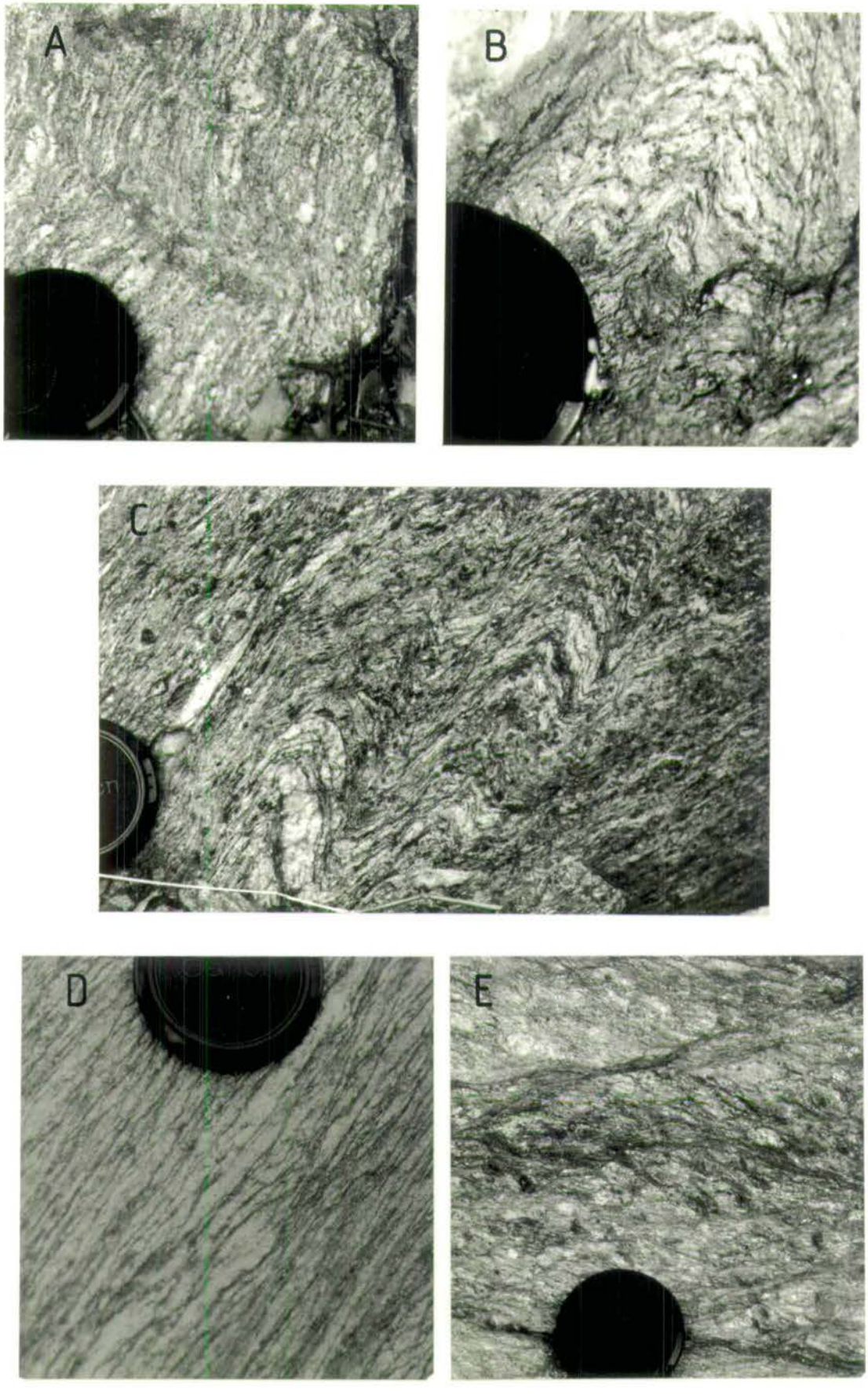

discontinuous, truncated by a later continuous sub-vertical ($S_{1C'}$) foliation, sub-parallel to S_{1C}. Depending on the angle between the S_{1C} and $S_{1C'}$ foliations the S_{1C} foliation develops a range of morphologies; an original continuous foliation (S_{1C}) → crenulated foliation (S_{1CC}) → composite foliation (S_T), in which it can no longer be separated from $S_{1C'}$. This range of early to late sub-vertical S_1 foliations are subsequently transposed into a series of sub-horizontal early to late S_2 foliations (Section 3.4.1; Fig. 3.4, Plate 3.5).

To the west of the Volvi Complex and south of Lake Volvi, S_1 foliations are difficult to determine as they are usually orientated parallel to sub-parallel with later S_2 foliations. However, in low-strain zones the S_1 foliations often appear as low-angle crenulated (S_{1CC}) foliations at high angles to the later sub-vertical (S_2) foliations (Figs. 3.5, 3.6). Throughout the area studied it is commonly observed that as "strain" increases, the angle between the different generations of S_1 and S_2 foliations progressively decreases (Figs 3.5, 3.6; Plates 3.5, 3.6, 3.7).

3.3.3 Folds (F)

Stages and classification of fold evolution have been decided by overprinting relationships, style, trends of the axial planes, and where possible metamorphic fabrics. Within the area there are at least three main sets of fold structures (Table 3.3; *see* Inserts, Maps B to G).

3.3.4 The First Phase Folds (F_1)

The best examples are preserved along the Vamvakia river at Migmatite Bluff (Section 2.3.2.1). The first set of leucosomes have been folded into upright, close to tight similar folds early F_1 (F_{1A}) folds with a wavelength of 2-30 cm and have a well-developed axial planar cleavage early S_1 foliation. A second set of leucosomes were intruded during late F_1 (F_{1B}) fold development and coaxially folded into less regular, upright, open to tight folds, while F_{1A} folds are tightened. The F_{1B} folds are often asymmetric and exhibit irregular thickening and thinning of fold limbs. Axial planar cleavages (late S_1) with respect to the F_{1B} folds were developed parallel to sub-parallel with the early S_1 cleavage. An equivalent foliation and fold sequence occurs in the Vamvakia Purple Gneiss Formation (Section 2.3.2.2) establishing that the recrystallisation to garnet-kyanite bearing assemblages post-dates the early S_0 migmatite events. The first fabric (S_0) consists of leucosomes (0.4-0.6 cm thick), separated by mesosomes (0.4-0.7 cm thick), producing a fine-banded migmatitic lithology. This fabric is tight to isoclinally folded with horizontal axial planes. The second set of leucosomes (1-2.5 cm thick) cross-cut the first set and show close to

tight folds (coaxial to the tightened folds of the first set of leucosomes), again with a sub-horizontal axial plane. Further along the section from A^I to A^{II} (Insert, Map C) the degree of folding decreases with folds becoming progressively more open and the first set of leucosomes shows a sub-vertical trend. These folded leucosomes represent a pre-shear zone folding event comparable to the S_{0A}, S_{0B} fabrics of the Vamvakia Migmatite (Section 2.3.2.1). The sub-vertical leucosomes are cross-cut by minor low-angle shear zones (2 to 10 cm wide) which reorientate the gneissic fabric into parallelism. Approximately half-way from A^I to A^{II} a narrow shear zone (0.4-1 m wide) separates the gneiss into two members. These are marked by a change in the style of the fabric from S_0 to S_1 or early S_2 and also in the trend of the foliation from approximately N-S representative of S_0 and S_1 to NW-SE typical of the range of S_2 foliations (Insert, Map C).

The first phase of folding (F_1) recognised throughout the remaining area especially to the west and south of the Volvi Complex, is generally rare. The examples of F_1 folds which have been observed, occur as isolated isoclinal fold hinges and intrafolial isoclinal folds on a 1 mm to 0.1 m scale. These F_1 folds are best preserved within the more leucocratic micaceous gneisses, e.g. the Askos Augen Paragneiss Formation (Section 2.3.3.2) and the Askos Garnet Mica Gneiss Formation (Section 2.3.3.4) etc. Evidence of F_1 fold structures are rarely found in the more homogeneous lithologies, due mainly to overprinting by later structures. However, within the low-strain zones throughout the area, F_1 folds occur in a progressive tight to isoclinal fold sequence, dependent on the extent of later strain (low to high respectively).

The F_1 folds within the gneissic formations to the west of the Volvi Complex are steeply plunging with fold axial planes parallel to sub-parallel with the main (S_2) foliation. One possible explanation for this is fold reorientation by the intense shearing common throughout the area.

3.4 Early D_2: Pre- to Syn-Shear Zone Structures and Fabrics

3.4.1 The Second Phase Foliations (S_2)

The S_2 foliations are the most common and widespread foliations observed around Lake Volvi. This foliation phase is correlated with the (S_{2T}) foliation proposed by Kockel *et al.*, (1971, 1977). On close inspection the S_2 foliations can be divided into three broad subgroups:

i) Axial planar cleavages to minor (cm- to m-scaled) F_2 folds.

ii) Axial planar cleavages to major (10 m to km-scaled) inferred regional F_2 folds. In this case it is particularly difficult to differentiate between different S_2

foliations, and assign them to a particular phase in the development of this fold stage as they are mostly rotated into sub-parallelism.

iii) Intense regional-scale cleavages associated with the development of shear zones.

A range of second phase foliations (S_2) are synchronously developed within a progressively deforming regime, with structural styles dependent on proximity to local major structures and changes in lithological composition (Figs. 3.5, 3.6). The S_2 foliation also displays a distinctive change in orientation around the Volvi Complex, i.e. immediately to the east of the complex the S_2 foliations are essentially sub-horizontal, progressively steepening in attitude to the east; to the west and south of Lake Volvi, the S_2 foliations are essentially steep to sub-vertical. The orientation of the S_2 foliations are attributed to initiation and/or rotation during shear zone development (Section 3.2).

To the east of the Volvi Complex D_1 fabrics within the Vamvakia Migmatite Formation (Section 2.3.2.1), Vamvakia Purple Gneiss Formation (Section 2.3.2.2) and the Modhi Leucocratic Gneiss Formation (Section 2.2.3.2) are transposed from a steep (70° to 90°W) to low-angled (0° to 35°W) trend (Section 3.2.5). A progressive sequence of low- to high-strain fabrics and structures are developed in these formations on approaching shear zones (Figs. 3.5, 3.7). Within the Vamvakia migmatites, the leucocratic fabric is refolded into sub-horizontal F_2 folds (Section 3.4.2) with a continuous axial planar cleavage (S_{2C}). As strain increases the leucocratic fabric is attenuated, folds tighten, and a new continuous cleavage (S_{2CC}) truncates the leucocratic fabric and crenulates the original continuous S_{2C} cleavage. Increase in strain causes the S_{2CC} and S_{2C} foliations to approach parallelism, with the ultimate development of a composite (S_{2T}) foliation. At the highest strain, the rock develops a mylonitic fabric (S_{2M}) wrapping porphyroclasts of rounded plagioclase and epidote (Fig. 3.5; Plate 3.8).

To the west of Lefkoudha, a composite S_{2T} fabric is further rotated and transposed from the local well-developed flat-lying trend into a steep to sub-vertical attitude (Section 3.10.2). This transposition is interpreted as a local phenomenon caused by a minor late intrusion (Section 2.5.4).

The S_2 foliations to the west of the Volvi Complex and to the south of Lake Volvi are predominantly sub-vertical and spatially associated with sub-vertical shear zones (Section 3.3). However, a range of early to late S_2 foliations preserved in low-strain zones were developed in association with a progressive, multiple, coaxial folding episode (Section 3.4.2). Hence, a range of cleavage morphologies are developed depending on the position with respect to the overprinting structures (Figs. 3.6, 3.7). Within several horizons, e.g. the Askos Augen Paragneiss Formation

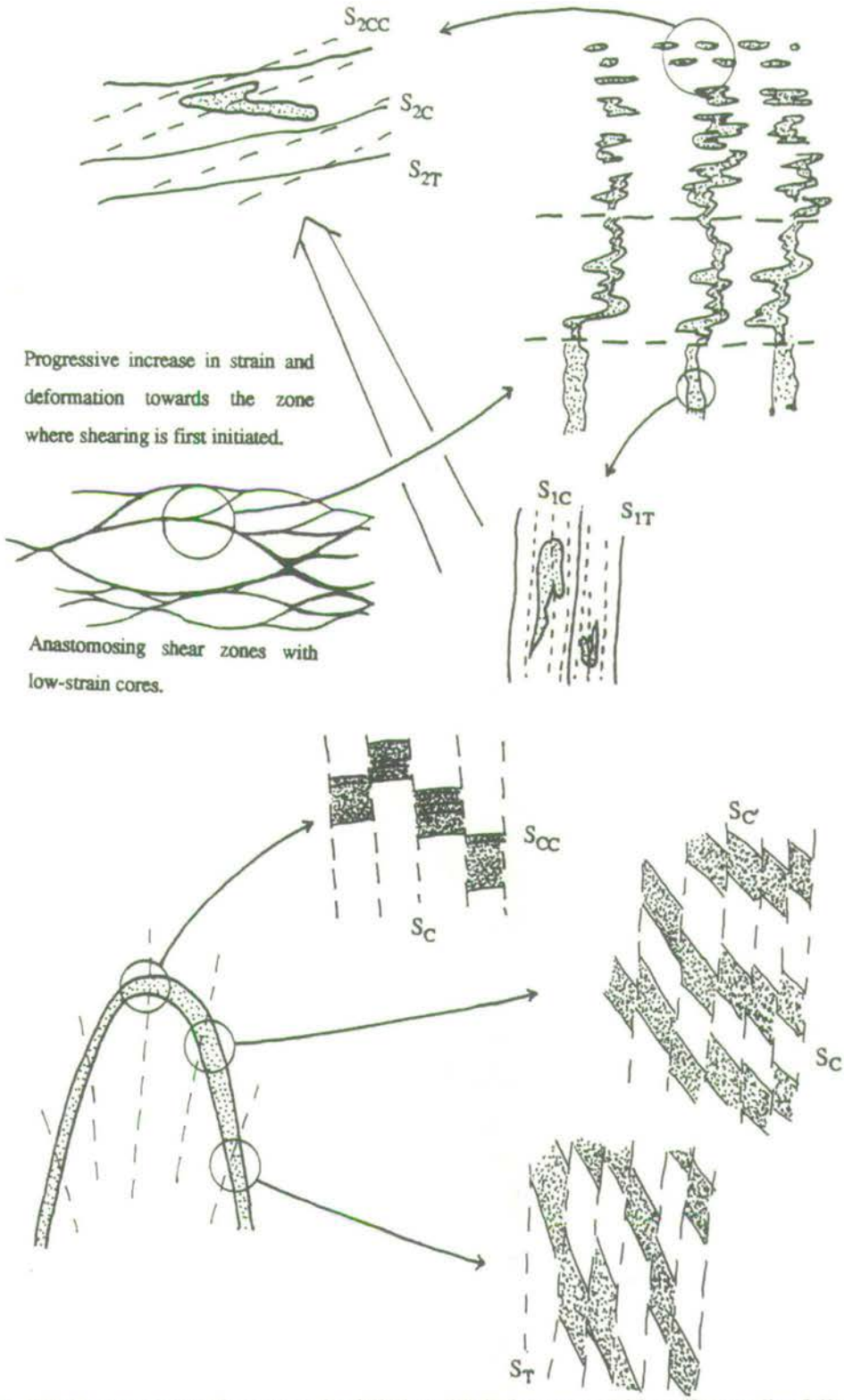

Fig. 3.7: Development of a composite foliation, (a) during transposition of an earlier foliation due to a component of shear, (b) during generations of progressive folding and refolding.

Plate 3.8

Progressively increasing strain from A to E within a closely related set of biotite-rich migmatitic lithologies. Outcrops are seen along the northern section of the Vamvakia river (see Insert Map C). The development of a wide range and intensity of S_2 foliations are assisted by the abundance of boitite in this rock. Horizontal field of view in Plate 3.8a is about 2.5 m across, the pen is 14 cm long and the coin is 28 mm in diameter.

Plate 3.8a: Low-strain pod of moderately deformed migmatite (predominantly early S_2 and F_2 structures) contained within and wrapped by a high-strain, highly deformed migmatite matrix (late D_2).

Plates 3.8b, c: Tight to isoclinally folded leucocratic layers are truncated by low-angle shear (S_2) foliations, creating a quartzofeldspathic porphyroblastic texture. In (C), intensification of the S_2 foliation approaches an S-C fabric in character.

Plate 3.8d: The intensity of shear increases from bottom to top, towards the margin of this highly deformed migmatite member. The S_2 foliation ranges from porphyroblastic (bottom) to mylonitic (top) in character.

Plate 3.8e: Mylonitised migmatite matrix containing rounded porphyroclasts of feldspar.

Plate 3.8

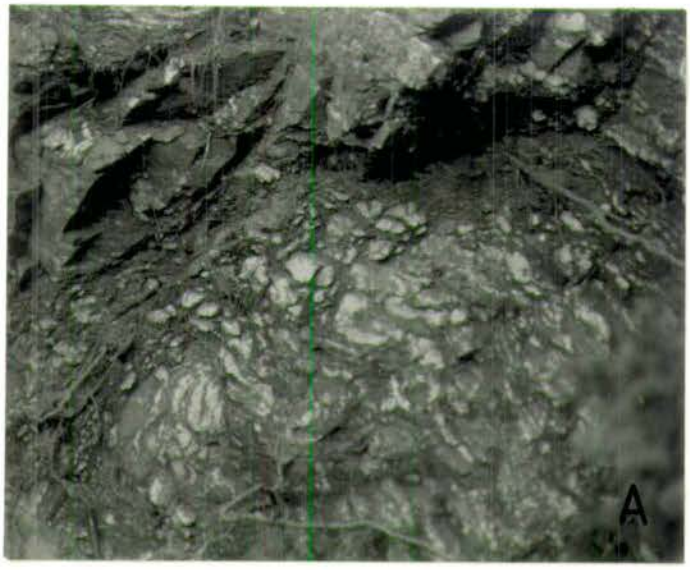

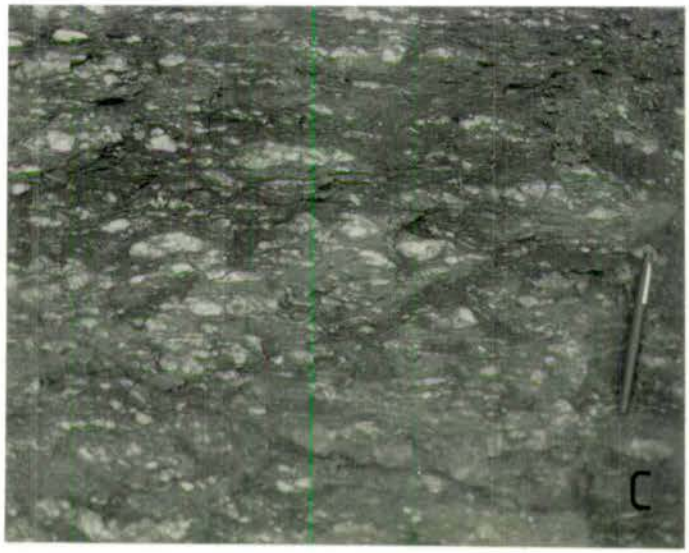

(Sections 2.3, 3.3), a possible original migmatite (S_{0A} or S_{0B}) fabric preserves isolated isoclinal F_1 or early F_2 fold closures (Sections 3.3.4; 3.4.2). The relationship of the S_0 fabric to the shear zone is unknown. Hence, an accurate correlation with the migmatites of the Vamvakia river is not possible. To minimise the nomenclature the fabric is simply attributed the lowest number used in a local structural sequence (S_0).

The (S_0) fabric is cut by an S_1 cleavage axial planar to the F_1 folds and is cross-cut by the continuous cleavage (S_{2C}) associated with the F_2 folds. The effect of the continuous S_{2C} cleavage on the earlier cleavage is dependent on the position with respect to the F_2 fold (Fig. 3.7). On the fold hinge, S_1 and S_{2C} are perpendicular and S_1 is crenulated by S_2, whereas on the limb, S_1 and S_{2C} are sub-parallel and S_1 either remains as a continuous S_{1C} cleavage or develops into a composite S_{2T} cleavage. However, due to the tightening of the F_2 folds, S_1 and S_{2C} cannot readily be separated (Fig. 3.6). A continuous array of cleavage morphologies are developed between the S_C, S_{CC} and S_{2C} end members (Fig. 3.7).

The matter is further complicated as the early F_2 (F_{2A}) folds are coaxially refolded by a late F_2 (F_{2B}) fold episode (Section 3.4.2) and an axial planar cleavage is developed (Fig. 3.6). Hence, a repeat of the dilemma created between F_1 and F_2 fold cleavages is developed. The sequence is complicated still further by the development and intensification of fabrics related to shear zones (Section 3.2), which actually simplifies the fabric by obliterating early structural relics. Approaching the shear zones the S_2 fabrics are intensified and a range of shear related S-C and mylonitic fabrics are developed (Fig. 3.5; Section 3.2).

3.4.2 The Second Phase Folds (F_2)

F_2 fold structures are the dominant fold phase within the Lake Volvi area (Inserts, Maps B to G). A range of coaxially refolded early F_2 (F_{2A}) by late F_2 (F_{2B}) are found as 1 mm to m-scale folds with well-developed vergence. In turn these small-scale folds indicate large (10 m to 100 m scale) upright F_2 structures. The majority of the second phase (F_2) folds are approximately NNW-SSE trending isoclinal, tight to close structures plunging predominantly to the SE with a sub-vertical axial plane. The fold styles are varied, and appear to be dependent on their position with respect to areas of intense strain. Within the high-strain zones the (F_2) fold limbs are normally sheared out and fold hinges are tightened. The extent of shearing of the (F_2) fold limbs is dependent upon the intensity and scale of the local anastomosing shear zones. However, it is difficult and usually impossible to determine whether a local F_1 fold is really an early F_2 (F_{2A}) structure or a tightened true F_1 structure refolded during shear zone generation. These shear-zone-generated, refolded and tightened folds usually completely overprint the range of earlier F_1

structures, and are associated with a strong axial planar S_2 foliation (which is possibly a composite of an earlier S_1 foliation). The (F_2) folds are associated with a variable shearing component, which also resulted in rotation of F_1 fold axial planes, and the creation of a strong rodding-stretching lineation (L_{2S}). Attenuation of F_1 and early F_2 fold limbs has produced an augen structure by boudinage and isolation of fold hinges (Section 3.2.1).

Homogeneiity of the F_2 fold structures decreases close to shear zones. Within the Askos Marginal Amphibolite Formation (Section 2.3.3.1), F_2 folds have been altered by the late SZ_2 shear zones, resulting in complex fold geometries (Plate 3.9; Fig 3.8). This variation of F_2 fold geometries is attributed to tightening, refolding and re-orientation of F_2 folds, by the sub-vertical to steep SZ_1 and predominantly flat-lying SZ_2 shear zones. However, by intensifying or broadening the shear zones, the preserved F_2 folds are reduced in size and eventually obliterated.

As the axial planes of the F_2 fold structures are always parallel or sub-parallel to the dominant local shear zones (steep: west of the Volvi Complex; flat-lying: east of the Volvi Complex), potential mechanisms for the continued development of F_2 folds can tentatively be attributed to shear zone development. Hence, the initiation of the shear zones could have occurred by attenuation of isoclinal to tight early F_2 folds (Fig 3.2) while late F_2 folds are considered to have partially developed by a combination of compression between the main shear zones and simple shear parallel to these shear zones. Variations of F_2 fold structures could have developed by a similar combination of pure and simple shear with the shear component dominated by the later (SZ_2) shear event.

A range of (F_2) fold styles dependent on the local state of strain and lithology is developed throughout the area. Within the East Modhi Marble Member (Section 2.2.3.3), two dominant fold styles are apparent. The most common are tight to close cm- to m-scale parallel, similar and harmonic parasitic folds ranging from recumbent to upright in attitude. The vergence of these fold structures can be used to identify folds on a scale of tens of metres. These large-scale folds are a series of recumbent to gently inclined asymmetric antiformal and synformal structures with a sub-horizontal axial plane (trend NNW-SSE). The extensive flat-lying limbs (dip: 3° to 15°W) are disrupted and discontinuous, whereas the short steep limbs (dip: 65°W to 10°E) are often intact and well exposed (Fig. 3.17).

Within the East Modhi Marble Member (Section 2.2.3.3), several small 4-8 m wide outcrops of impure carbonate display excellent interference structures (Ramsay, 1967), which range from well-defined type 2 to variations of type 1 interference patterns (Plates 3.10a, b and c; Fig 3.9).

Plate 3.9

Plate 3.9: Buckle folding of a competent quartzofeldspathic layer within an amphibolite host. View looking W to NW from approximately halfway along the disused road section between Askos and Vaiohorion (Insert, Map B). Lens cap is 52mm in diameter.

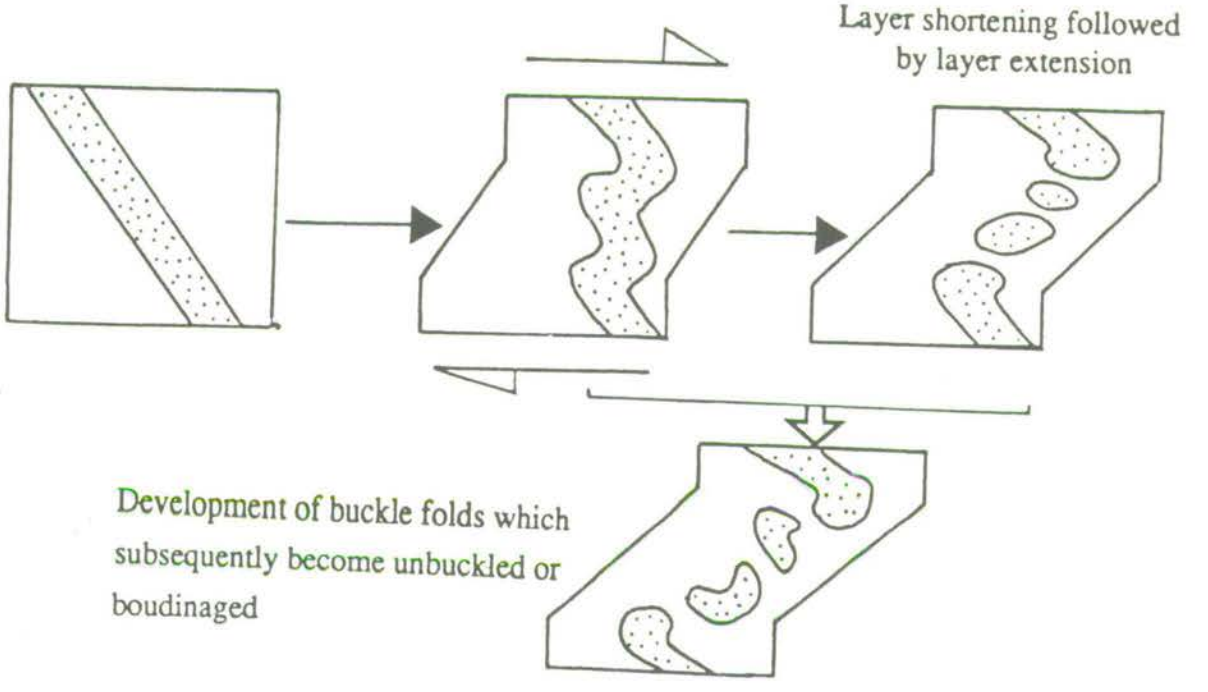

Fig. 3.8: Development of buckle folds from a process of simple followed by pure shear. Original orientation of the leucocratic sheet was arranged at an angle oblique to a shear zone and progressively sheared. A change in shear regime from simple to pure shear caused flattening of the boudinaged structure (c.f. Ramsay, 1979).

Plate 3.10a: View of the Impure Modhi Carbonate Member, approximately 1.5 to 2 km east of Modhi. Weathering of less competent layers highlights well-developed type 1 and type 2 interference patterns. Hammer is 52 cm long.

Plate 3.10b: Type 1 (1→2) interference pattern.

Plate 3.10c: Type 2 interference pattern.

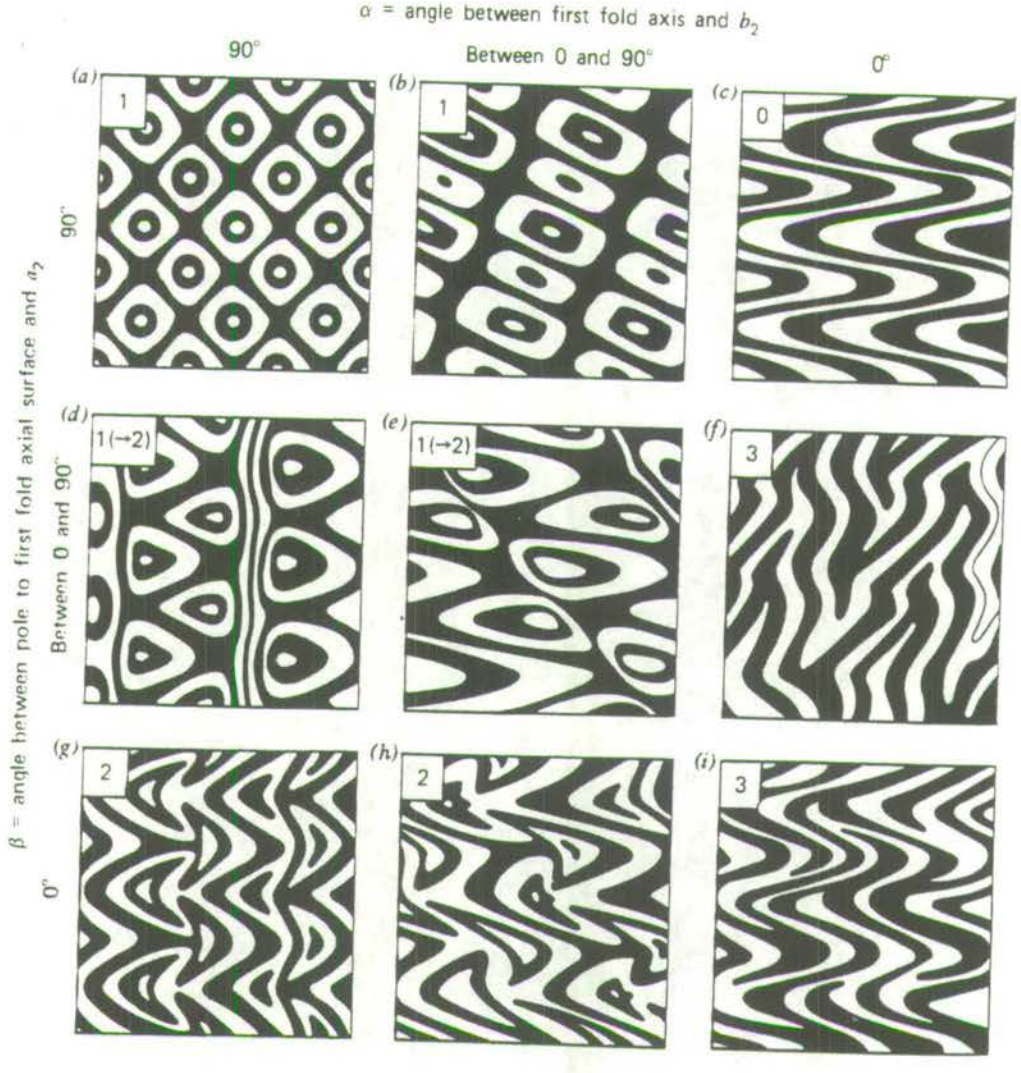

Fig. 3.9: Development of interference structures, after Ramsay (1967).

However, these particular interference structures are rare throughout the study area, with the common interference pattern being type 3 structures created by coaxial refolding of an inclined early F_2 fold (coaxial refolding of an early by late F_1 structure may rarely be preserved in low strain-cores with only a weak F_2 structure developed) by an upright late F_2 fold (Plates 3.11a, b).

F_2 folds are often truncated by or modified between distinct shear surfaces. This is particularly common along the Vamvakia river (Insert, Map C). Tight to close, gently inclined to recumbent F_2 folds with an E-W axial trend are found within the Vamvakia Garnet Kyanite Schist Formation (Section 2.3.2.3), *see* Plate 3.12; Fig. 3.10. These F_2 folds are considered to be synchronous with F_2 shear related folds within the Vamvakia Migmatite Formation (Plate 3.6).

However, the overall early to late F_2 structural style appears to indicate a coaxial refolding of progressively developed upright to recumbent structures. To the west of the Volvi complex (and to a lesser degree east of the Volvi Complex) these structures are compressed and sheared between large-scale anastomosing shear zones which appear to exploit and propagate along fold limbs, resulting in tight to isoclinal intrafolial fold closures (Plates 3.13a to c)

3.4.3 Lineations (L)

Lineations within the area consist of three main types, stretching-rodding, foliation intersection and mineral lineations (Table 3.3; *See* Inserts, Maps B to G).

3.4.3.1 Stretching-rodding Lineations (L_S)

Stretching-rodding lineations occur in numerous localities throughout the Lake Volvi area. One of the best examples occurs at the boundary between the Askos Marginal Amphibolite Formation (Section 2.3.3.1) and the Askos Augen Paragneiss Formation (Section 2.3.3.2). The stretching-lineation along this boundary appears to be the result of tightening of F_1 fold hinges, with attenuation of fold limbs and boudinage of the overall fabric, leaving isolated, discontinuous asymmetric fold closures. Further stretching of these isolated F_1 folds creates an L to L-S tectonite fabric (Plates 3.14, 3.15). The lineation tends to have a S to SE plunge when seen on the foliation plane (Fig 3.15), suggesting that an oblique shear direction was in operation (with movement of shear planes either upwards towards the N to NW or downwards towards the S to SE). It is not possible to determine an unequivocal strain path due to the lack of asymmetry of augen and boudinaged fold hinges which are elongated along this lineation. However, a strain history incorporating both pure and simple shear mechanisms may be the simplest solution.

Plate 3.11

Interference structures within migmatitic and quartzofeldspathic lithologies outcropping to the west of the Volvi Complex. Fold structures are developed by the refolding of early F_2 folds by late F_2 folds developed during the same deformation episode, possibly related to the development of shear zones. The lens cap is 52 mm in diameter.

Plate 3.11a: Intensely folded and refolded quartzofeldspathic layers are developed into type 3 interference patterns. Narrow (5-10 cm wide) shear bands attenuate the fold limbs obscuring the early deformation history.

Plate 3.11b: Sample EMV22, from N of Megali Volvi shows a series of predominantly harmonic (in some areas disharmonic) refolded semi-continuous quartzofeldspathic layers (migmatite fabric). These refolded folds form close to tight, upright, type 3 interference patterns, but in areas of high-strain these are tightened and progressively sheared.

Plate 3.11c: The Askos Quartzofeldspathic Gneiss Formation, NE of Megali Volvi. View shows a series of intensely refolded leucocratic layers displaying type 3 and type 1 interference patterns.

Plate 3.11

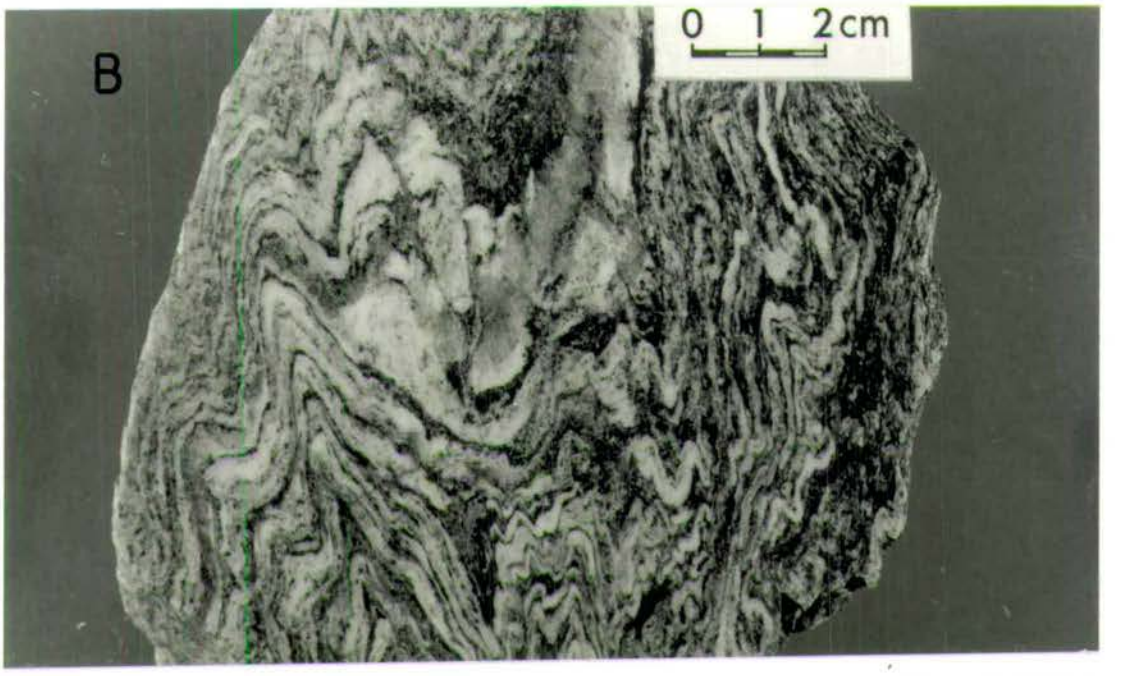

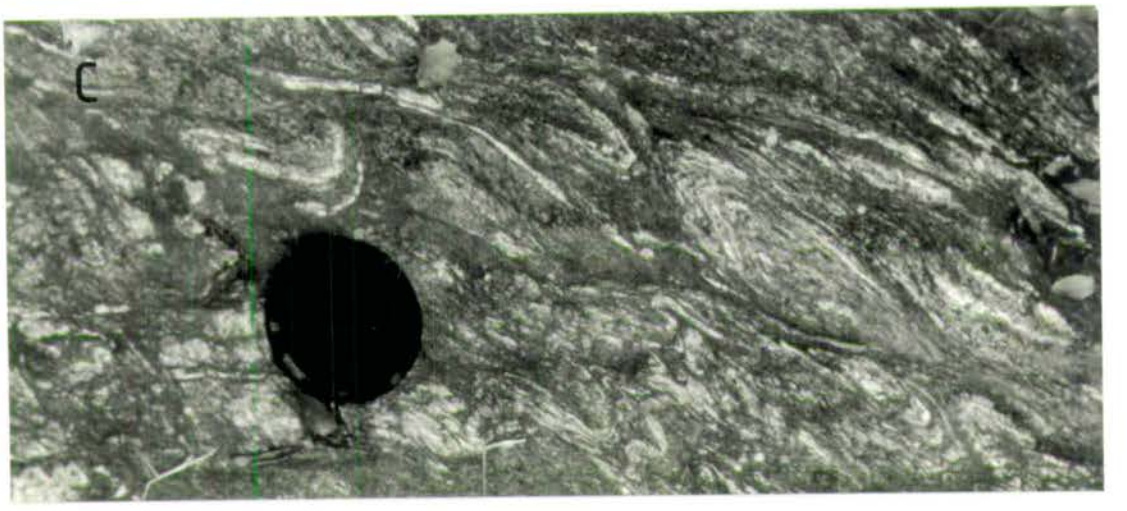

Plate 3.12

Plate 3.12: View (looking approximately N) of an isolated, close to tight inclined (F_2) fold outcropping along the northern section of the Vamvakia river. Continuity of the fold is obscured by flat-lying shear zones which have propogated along the fold limbs. A well-developed fanning (S_2) cleavage is preserved in the core but overprinted towards the surrounding shear zone.

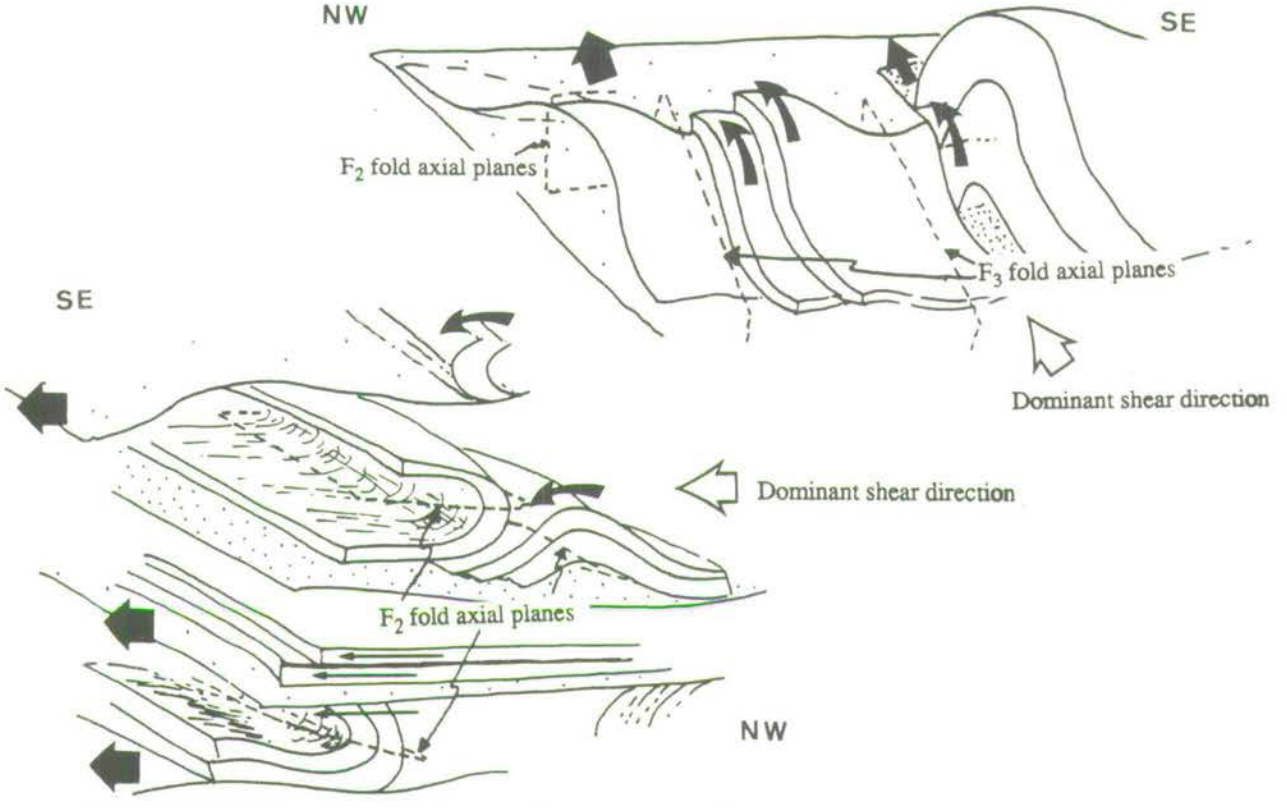

Fig. 3.10: Recumbent, tight (F_2) folds, with partially sheared fold limbs and refolded by gentle to open (F_3) upright folds perpendicular to F_2. Outcrop from along the northern section of the Vamvakia river (Insert, Map C).

Plate 3.13

Plate 3.13a: Tight F_2 fold with a complex sequence of cm-scale parasitic folds with pinch and swell structures (possibly a result of earlier folding). There is a progressive increase in strain towards shear zones where folds are tightened and limbs attenuated A→B. Lens cap is 52 mm in diameter.

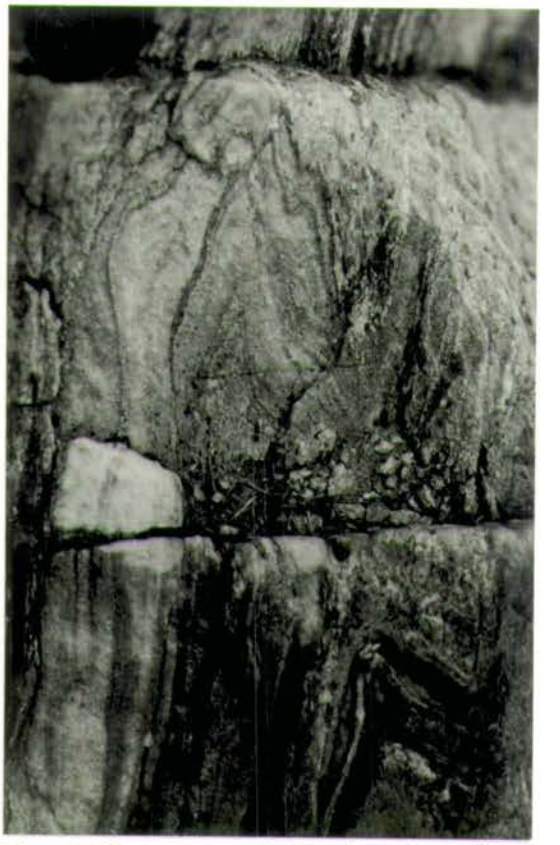

Plate 3.13b: Impure carbonate from immediately N of Megali Volvi, with tight, upright, steeply plunging folds. Field of view is approximately 30 cm across.

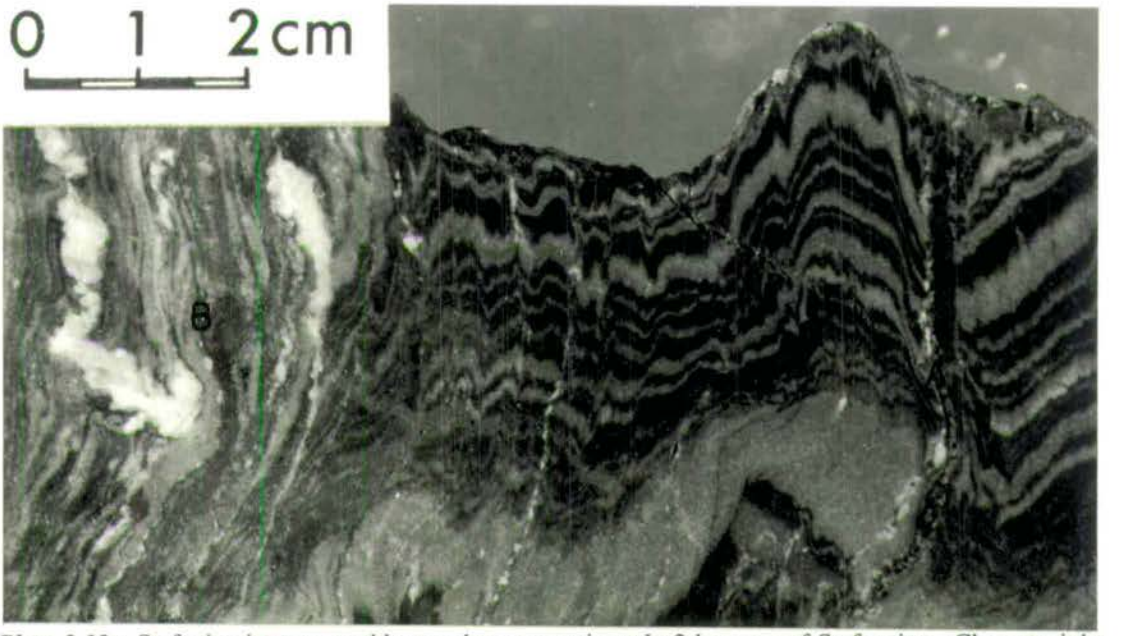

Plate 3.13c: Stefanina impure marble member, approximately 2 km east of Stefanaina. Close to tight harmonic folds are disrupted by a series of narrow (A) and broad (B) shear zones.

Plate 3.14

Lineations within augen orthogneisses and Vertiskos lithologies west of the Volvi Complex. All these particular examples are taken from the main river immediately N of Vaiohorion, although similar examples are found throughout the area. Lens cap is 52 mm in diameter, coin is 28 mm in diameter and the pen is 14 cm long.

Plate 3.14a: Mineral stretching lineation within a porphyroblastic augen orthogneiss.

Plate 3.14b: Banding cleavage intersection lineation within a homogeneous fine-grained schist.

Plate 3.14c: L-S tectonite fabric and intersection lineations developed within an augen orthogneiss. The flat-lying surface contains subhedral porphyroblasts whereas the steep surface displays elongate augen and intersection lineations.

Plate 3.14d: Crenulation lineation developed on the schistosity surface (or S_1 surface) of crenulated psammitic schists.

Plate 3.14

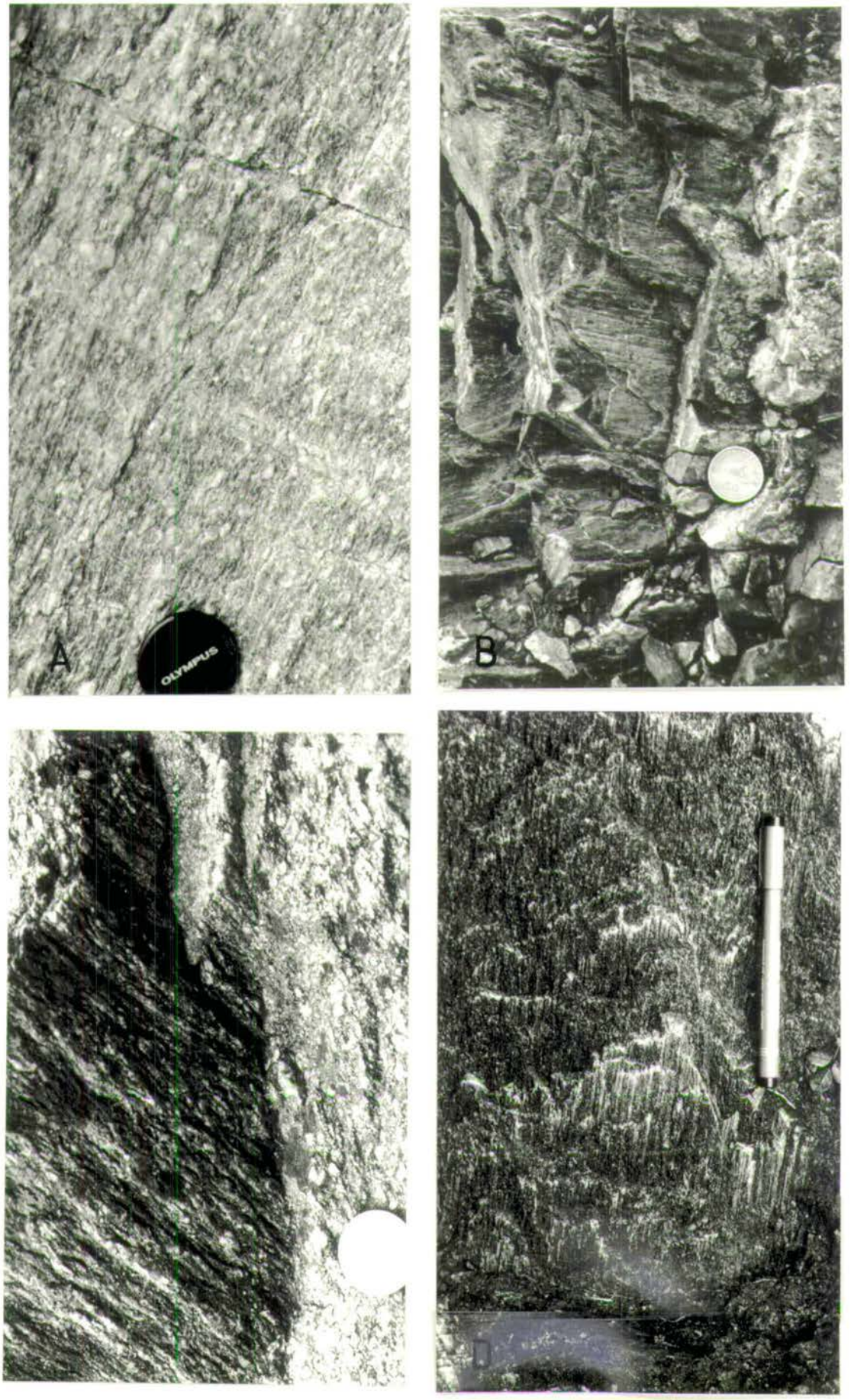

Plate 3.15

Plate 3.15a: Augen orthogneiss N of Vaiohorion with an L-S tectonite fabric defined by a mineral stretching lineation developed along cleavage surfaces (parallel to the pen). Pen is 14 cm long.

Plate 3.15b: Garnet mica schist showing a well-developed mineral lineation highlighted by laths of biotite.

Due to the apparent relationship of the lineation to the shear event it has been classed as an L_{2S} lineation (i.e. a stretching lineation developed during the second deformational event and possibly associated with sheaar zone development).

All the stretching-rodding lineations (L_S) throughout the area are interpreted as being developed during similar stages of the D_2 deformational event, with the variations caused simply by changes in lithology and proximity to shear zones. To the west of the Volvi Complex, the L_{2S} lineation is strongly developed, plunging 10-35° SE. To the east of the Volvi Complex the L_{2S} is also well developed, plunging 0-15° E to SE/NE or W to SW/NW.

3.4.3.2 Foliation Intersection Lineations (L_I)

Intersection lineations occur throughout the area and have a general S to SE plunge (Plate 3.15). Within the low-strain pods they define the mean intersection of the S_1 and S_2 foliations related to the F_1, F_2 folds respectively. The F_1 and F_2 folds have been variably rotated or developed, sub-parallel or parallel to the main intense S_2 foliation (Section 3.2.1). Hence, the intersection lineation L_{2I} has been rotated along with the F_1 and F_2 folds. Within the more intensely sheared areas, there is an S-C fabric intersection lineation which lies within the main regional S_2 foliation. Consequently it is difficult to separate the lineation into sub-categories (related to folding or shear) and it is therefore referred to in terms of a general L_{2I} lineation.

The appearance of the intersection lineation (L_I) remains fairly constant throughout the area. The main variations consist of:

a) Spacing and abundance of the lineations: this is generally a reflection of variable foliation development between lithologies.
b) Orientation of the lineation: this is variable but appears to be a reflection of the reorientation of foliations into parallelism with the regional shear foliation S_2.

3.4.3.3 Mineral Lineations (L_{ML})

Mineral lineations are generally rare throughout the Lake Volvi area. When present they are predominantly defined by the alignment of biotite laths (Plate 3.15b). Within some of the more amphibolitic lithologies, alignment of hornblende laths also occur. Although mineral lineations are generally rare, alignment of biotite in areas of well-developed intersection lineations is common. However, biotite lineations in these areas must be treated with some caution, as it is possible that biotite laths are arranged in a planar manner, and that the lineation is an artefact of the intersection lineation. The L_{ML} lineation has an approximate plunge between 10-45°S to SE.

3.5 Late D_2 to Early D_3: Syn- to Post-Shear Zone Structures and Fabrics

3.5.1 The Third Phase Foliations (S_3)

A poorly developed S_3 foliation (along the road from Vaiohorion to Askos) is represented by the local development of a weak spaced cleavage. In some areas the S_{3V} (where V signifies the area around Vaiohorion) foliation may be considered the equivalent of well-developed jointing. This foliation does not appear to be directly associated with the gentle to open (F_3) folds. However, it is possible that it represents a phase of brittle fracture related to large scale warping, and is axial planar to the F_3 folds. Within the Rendina Marble Formation (Section 2.2.2.5), a complex sequence of brittle deformation structures have been developed. Layer parallel stylolitic foliations overprint an earlier (possibly original) banded carbonate fabric (Plate 3.16a). This structure is indicative of volume loss and contractional strains in a brittle regime, which may imply deformation of this unit to have been a relatively late event. Brittle fracturing has resulted in displacement of the carbonate fabric and stylolitic foliation. Later extensional fractures within these carbonates are infilled by composite vein growth, which is particularly well-displayed using cathodoluminesence (Plate 3.16b). This composite vein structure is interpreted to be the result of the last, low-grade metamorphic event to affect this unit, as the veins are not recrystallised.

3.5.2 The Third Phase Folds (F_3)

The third phase (F_3) folds are different from the previous structures in that the axial planes of this fold phase usually have an approximately E-W trend, almost perpendicular to the trends of F_1 and F_2 folds. The F_3 folds are mostly upright, gentle to open, but occasionally tight, with amplitudes from 1 to 10 m. F_3 folds with a wavelength on a km-scale can be inferred from regional mapping, but rarely identified with certainty. Development of the small-scale (1-10 m) F_3 folds appear to be closely associated with the low-angled (SZ_2) shear zones (Section 3.3.1), e.g. within the margin of the Arnaea granite and the Askos Marginal Amphibolite Formation (Section 2.3.3.1), and along the Vamvakia river (Insert, Map C).

3.5.3 Mylonites

The term "mylonite" was originally used and defined (from the Greek, mylon: a mill) by Lapworth (1885). Translation of the term is misleading when considering the mechanism of development, as Lapworth (1885) actually used the term "mylonite" to describe rocks deformed in an essentially ductile manner (Bell and Etheridge, 1973). However, it is recognised that in some environments mylonitic

Plate 3.16

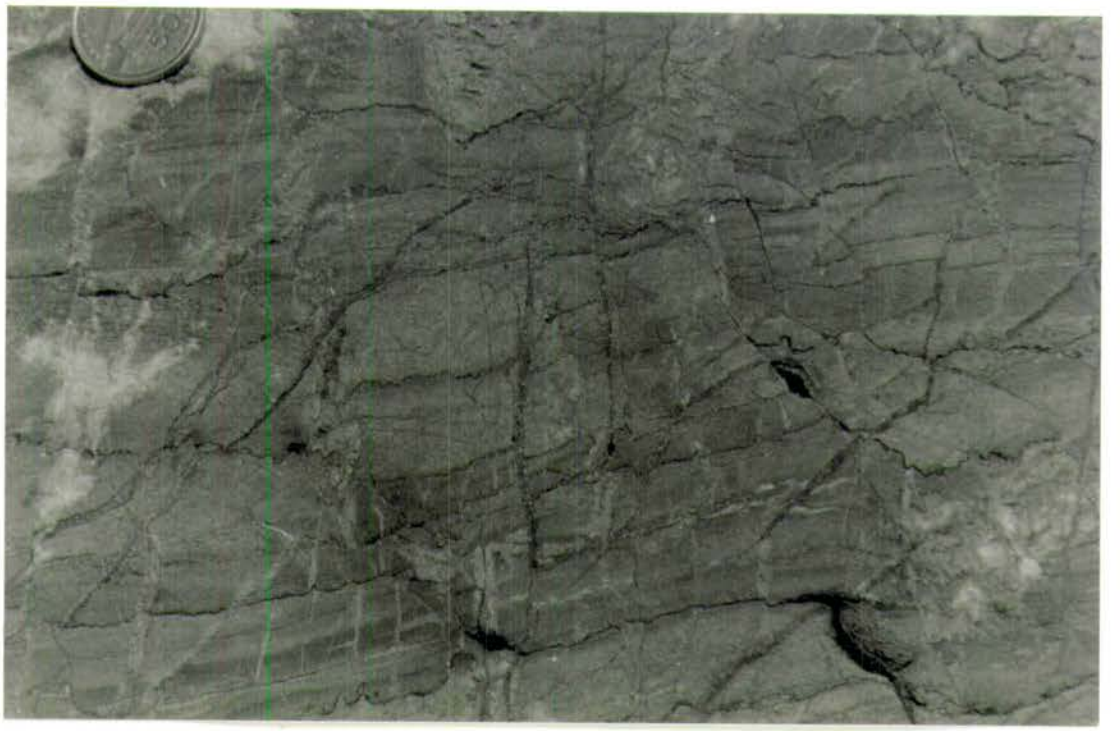

Plate 3.16a: View of the impure Rendina Marble Member immediately S of the ancient ruins at Rendina, *see* Insert, Map G. This lithology shows well-developed stylolitic cleavages disrupted by late brittle fractures. Coin is 28 mm in diameter.

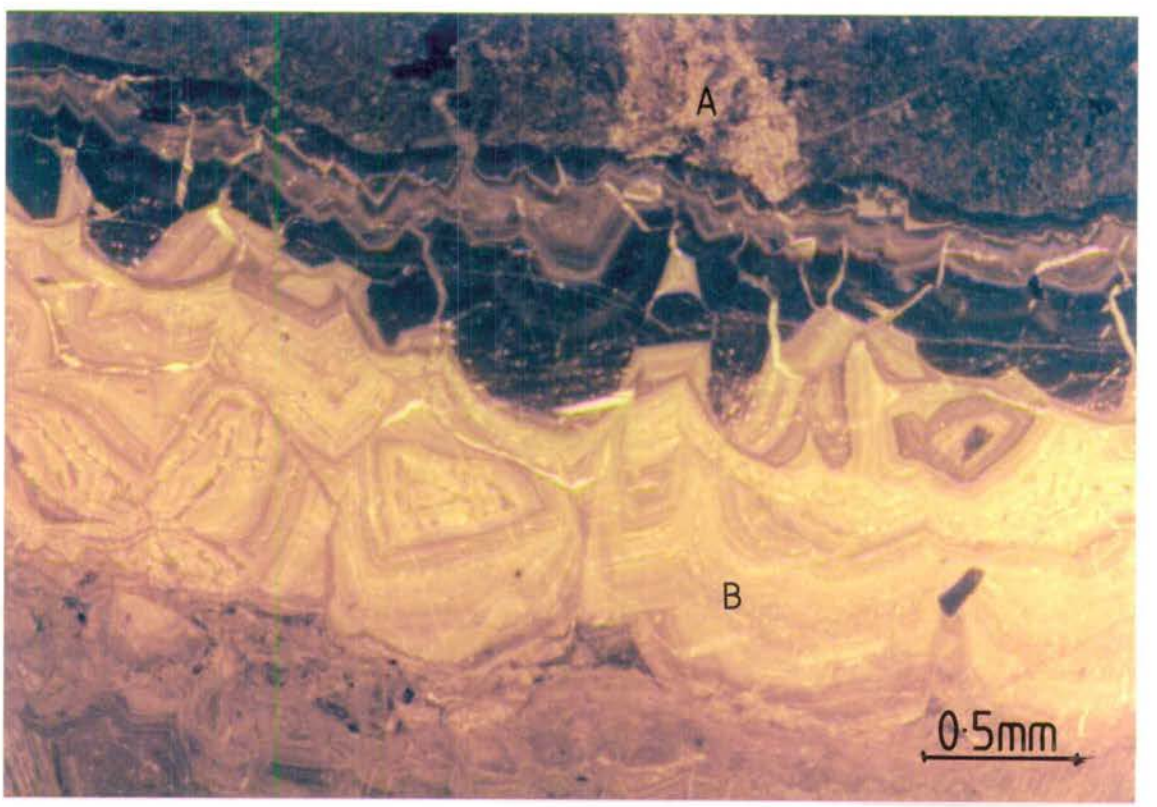

Plate 3.16b: Veins within the impure Rendina Marble Member are characterised by early veins (A) being recrystallised while comparatively late veins are typified by composite, multilayered veins with well-preserved growth fabrics (B). View using cathodoluminesence, approximately 3 mm across.

rocks contain structures genuinely attributable to brittle deformation (Scott and Drever, 1953).

A more general definition of a mylonite is: a foliated rock commonly lineated and containing megacrysts, in narrow, planar zones of intense deformation. It is often finer grained than the surrounding rocks, into which it grades (Bell and Etheridge, 1973). The terminology for describing mylonitic lithologies has been the subject of much debate with the descriptive terms applied to "mylonitic" rocks resulting in numerous fault rock classifications (e.g. Spry, 1969; Higgins, 1971; Bell and Etheridge, 1973; Zeck, 1974; Sibson, 1977; Tullis *et al.*, 1982; Wise *et al.*, 1984 and others). The definition of a mylonite used in this thesis follows the fault rock classification proposed by Sibson (1977; *see* Table 3.4). This considers foliated and random-fabric fault rocks to indicate generation in ductile (quasi-plastic) and brittle (elastico-frictional) regimes respectively (Table 3.5).

A wide range of fault rocks is developed within the Lake Volvi area. These fault rocks include members of the mylonite and cataclasite series, pseudotachylites and incohesive fault gouge. Throughout the area these fault rock lithologies are associated with localised shear and fault zones, which are in turn associated with large (km-scale) anastomosing shear zones (Section 3.2.1). It is proposed that the wide range of fault rocks generated in specific environments are each developed under specific conditions of temperature and pressure, *see* Fig. 3.11 and Table 3.5 (Sibson, 1977; Grocott, 1977*b*; Watts and Williams, 1979). Hence, the different fault rock textures within the shear zones provide evidence for progressive development during continuous evolution down temperature and down pressure.

3.5.3.1 The Mylonite Series

To generate a member of the mylonite series, a dominant mineral constituent, e.g. quartz in a granitoid rock, must deform in a plastic manner. This is achieved when deformation takes place at >250-350°C which represents a depth in the crust of 10-15 km at normal geothermal gradients (Sibson, 1977). At temperatures of 250 to 350°C a relatively high strain rate (approximately 10^{-12} S^{-1}, White, 1975) is necessary for mylonite generation. Blastomylonite is likely to be formed under conditions of slightly lower strain rate or higher temperatures. Protomylonite, mylonites and ultramylonites are developed within a range of lithologies which have been subjected to high-strain in the regional shear zones.

Compositional banding of felsic and mafic layers often occurs within the mylonites. However, it is difficult to assess to what extent this is a relict gneissic

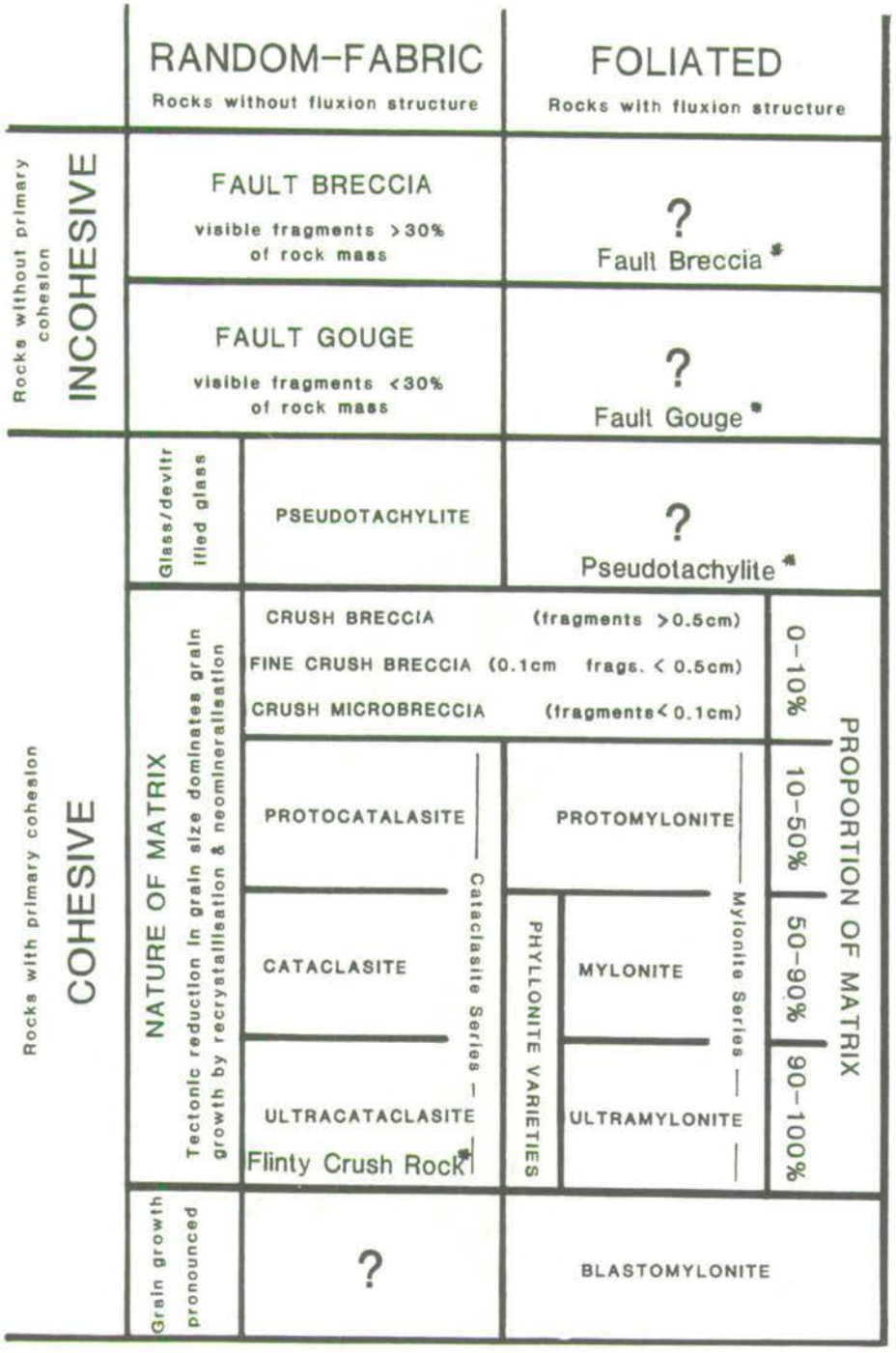

* Additional terms used by McClay (1987)

Table 3.4: Textural classification of fault rocks, after Sibson (1977).

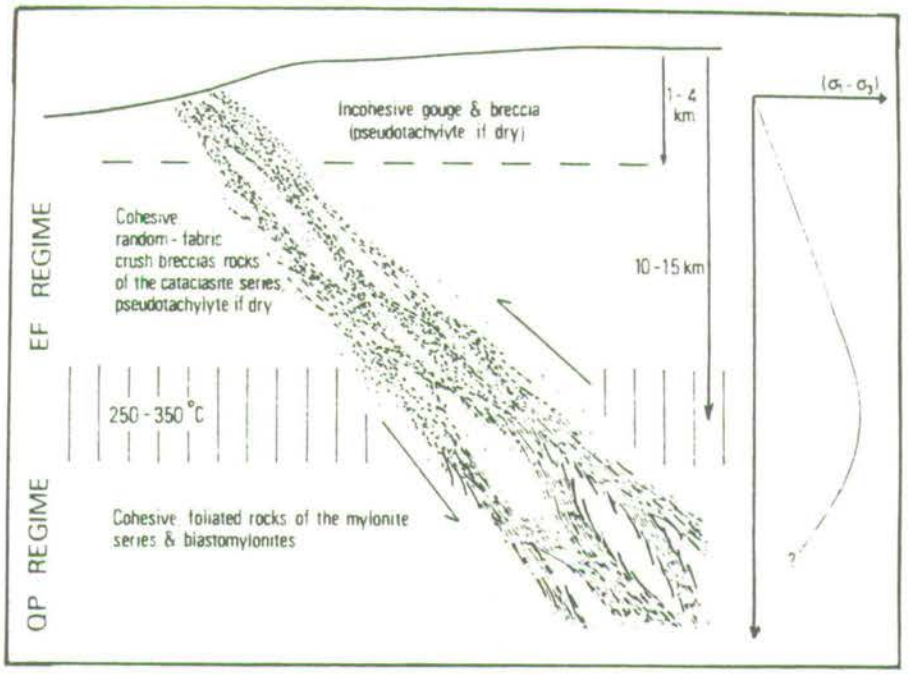

Fig. 3.11: Conceptual model of a major fault zone, after Sibson (1977).

REGIME	DEFORMATION MODE	DEFORMATION PRODUCT	FABRIC	GENERATION DEPTH	STRAIN RATE
ELASTICO FRICTIONAL	Brittle Fracture	Fault Gouge	Incohesive, random	1 — 4km	?
	Polyphase Cataclasis & Frictional Melting	Cataclasite Series Pseudotachylite	Cohesive, random	4 — 10km	$>10^{-1}$ s^{-1}
TRANSIT-IONAL	Frictional Melting	Transition Pseudotachylite	Deformed pseudo-tachylite Aligned Qu., Fp. clasts	10 — 15km ?	Sliding rate 10–100 cm s^{-1}
QUASI PLASTIC	Mylonitization	Mylonite Series Blastomylonite	L–S & S	15 — 20km	-10^{-4} s^{-1}
	Homogeneous Deformation	Schistose Amphibolites & Granitoids	Schistosity	20km+	10^{-14} s^{-1}
	Metatexis	Migmatitic Gneiss	Metatexite banding	?	?

DOMINANTLY SEISMIC

DOMINANTLY ASEISMIC

HETEROGENEOUS BEHAVIOUR

Defm Trend

HOMOGENEOUS BEHAVIOUR

Table 3.5: Synoptic diagram of fault rock time sequence and conditions for their formation, after Watts and Williams (1979). The strain rates given are those typically used in discussions dealing with the formation of fault rocks (White, 1975, 1976; Sibson, 1975) and generation depths are taken from Sibson (1977).

banding or an induced banding formed from ductile deformation of a polymineralic rock with accompanying grain-size reduction (Vernon, 1974). The main mylonitic zone along the Vamvakia river (Insert, Map C) has two potential precursors, the Vamvakia Migmatite Formation (Section 2.3.2.1) and Vamvakia Amphibolite Member (Section 2.3.2.5). Both of these formations already contain a well-developed element of an earlier banding. However, the variable development and intensity of deformation may result in the banding being obscured with the layering now preserved apparently due entirely to ductile deformation (Plates 3.17a, b).

Grain size reduction, characteristic of long-lived ductile shear zones (Watterson, 1975) is accomplished by the dynamic recovery and recrystallisation of strained quartz whose behaviour as a plastically flowing matrix leads to the brittle fragmentation and comminution of feldspar.

Almost the entire range of lithologies which crop out within high-strain zones contain quartz exhibiting microstructural evidence for plastic behaviour. This is shown by undulose extinction, deformation bands, sub-grains, elongate and ribbon quartz textures (Plate 3.18). The presence of new grains indicates that recrystallisation has taken place, and using the criteria of Green *et al.*, (1970), and White (1977), dynamically recrystallised grains can be distinguished from statically recrystallised grains. Large (0.5-1.5 cm diameter) porphyroclasts are commonly preserved within a uniformly fine-grained (0.5 mm diameter) matrix. However, within one particularly distinctive suite of mylonites along the Vamvakia river there are usually no pressure shadows and associated tails to indicate sense of shear and hence bulk shear direction. This lack of pressure shadow and tail development may be explained by a multiply directed shear mechanism, with the porphyroclasts behaving as randomly rotating rolling marbles (Fig. 3.12). The preservation of the spherical to elliptical porphyroclast geometry is either a result of a complex array of alternating shear directions, or more likely a result of competency contrasts between porphyroclast and matrix.

Following Ramsay and Graham (1970), the mylonite foliation is thought to lie along the XY plane of the finite strain ellipsoid. A stretching lineation developed with the shear zones, traces out the X-direction. Hence, the main ductile transport direction has been in a strike-slip sense.

Although the dominant mode of deformation of feldspars is a brittle fracture, evidence of plastically deformed feldspar such as kinks and sub-grains (Bell and Etheridge, 1973; Nicolas and Poirier, 1976) also occurs (Plates 3.17, 3.18). The fracture of feldspar porphyroclasts is usually cleavage controlled (c.f. Wakefield, 1977), and antithetic internal movement of feldspars is seen.

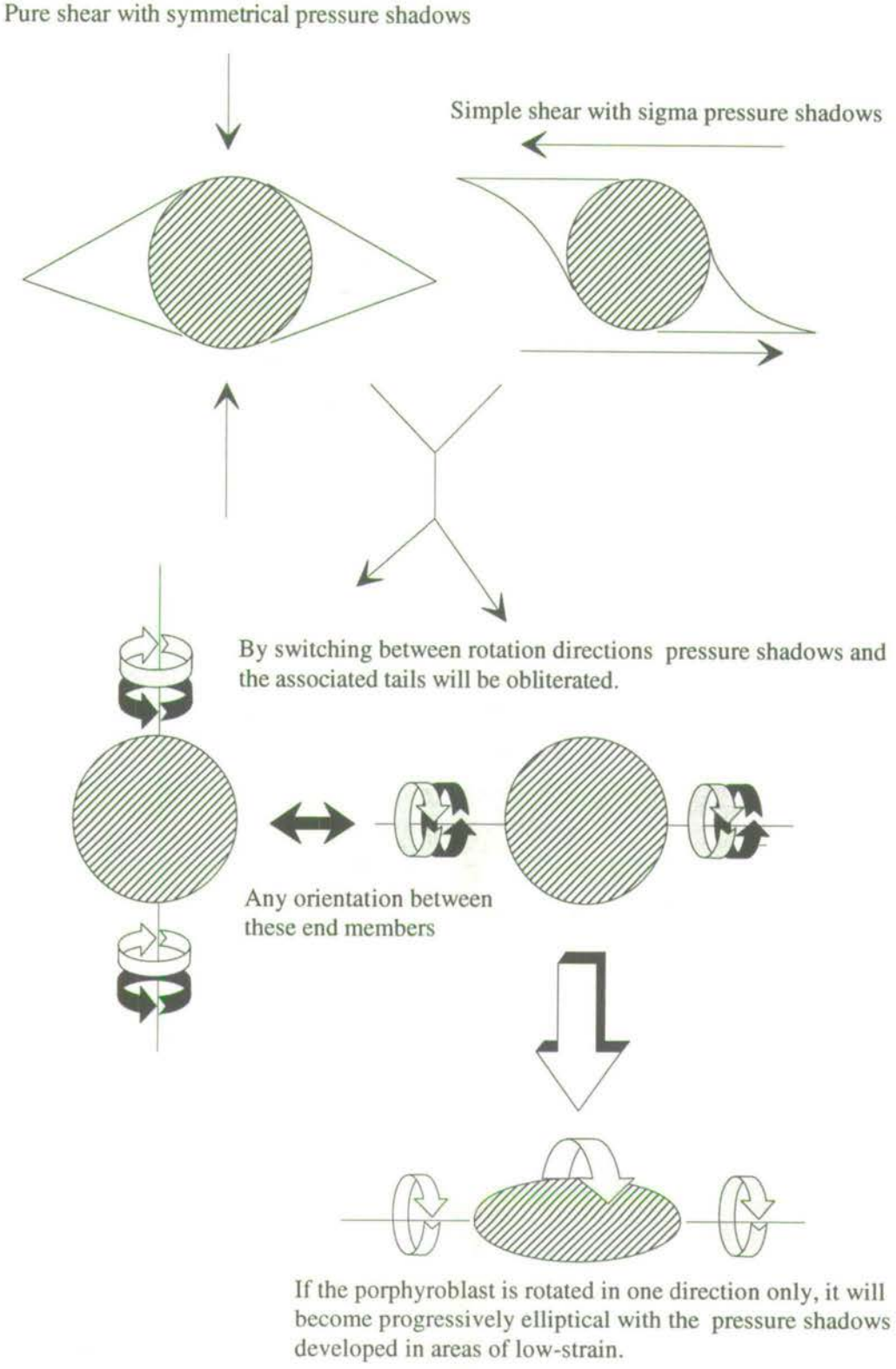

Fig. 3.12: Synoptic diagram for the development of rounded porphyroblasts with no prevalent pressure shadows.

Plate 3.17

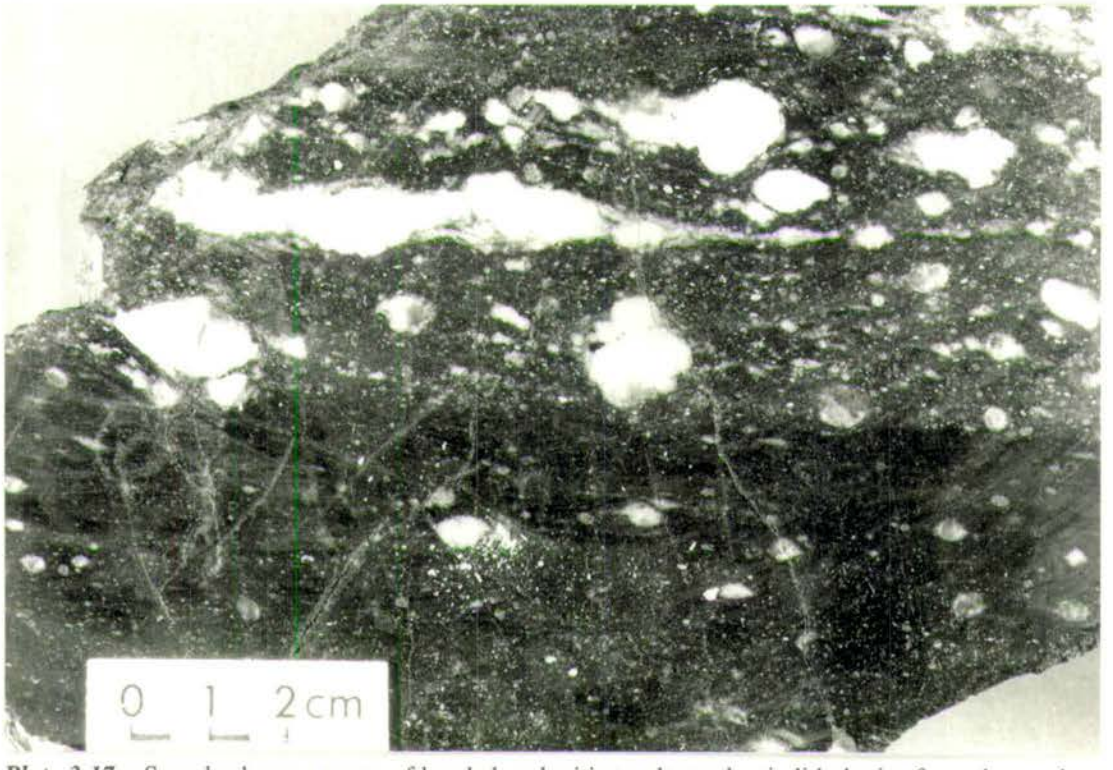

Plate 3.17a: Sample shows a range of banded mylonitic to ultramylontic lithologies from the northern section of the Vamvakia river. The precursor for these mylonites is considered to be the Vamvakia Migmatite Formation, from the numerous semi-continuous leucocratic layers (centre). The finer-grained ultramylonitic matrix is developed within areas of increased strain, and the plagioclase porphyroblasts are increasingly rounded with few if any pressure shadows.

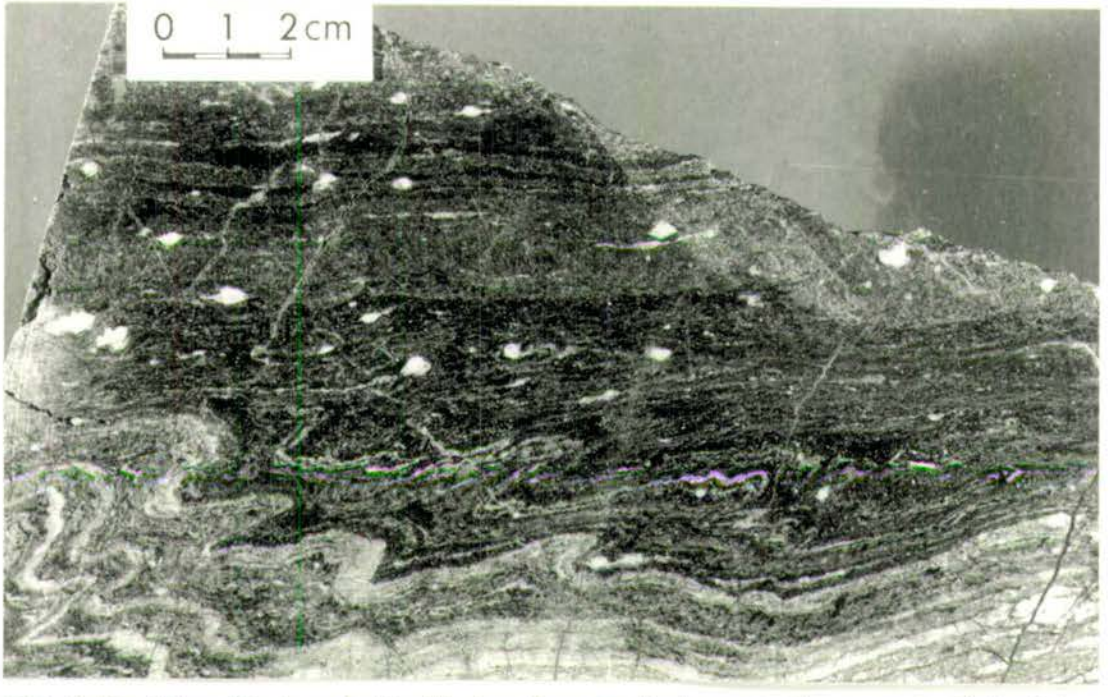

Plate 3.17b: Migmatitic to mylonitic lithology from the Arethousa to Vrasna road. Both of these fabrics are folded into asymmetrical, inclined, close to tight folds in the centre of the sample. However, shearing is more intense at the top of the specimen with a strong unfolded mylonitic fabric developed. This may suggest either a pulsed phase of shearing within this area or local variations in the total shear strain.

Plate 3.18

Photomicrographs of quartzofeldspathic textures and fabrics within a range of mylonites.

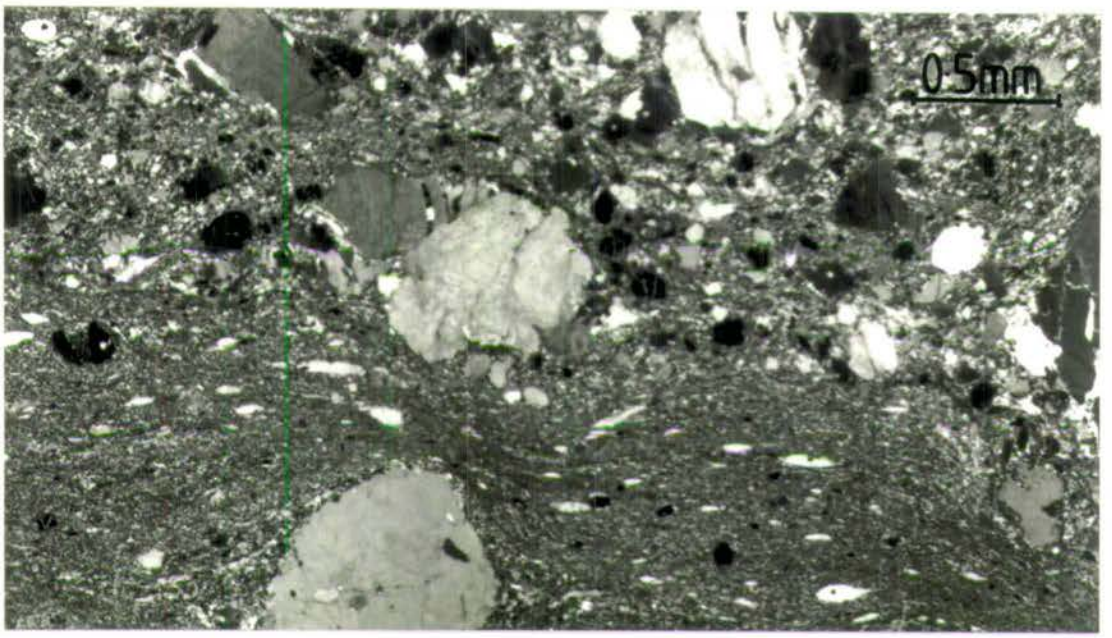

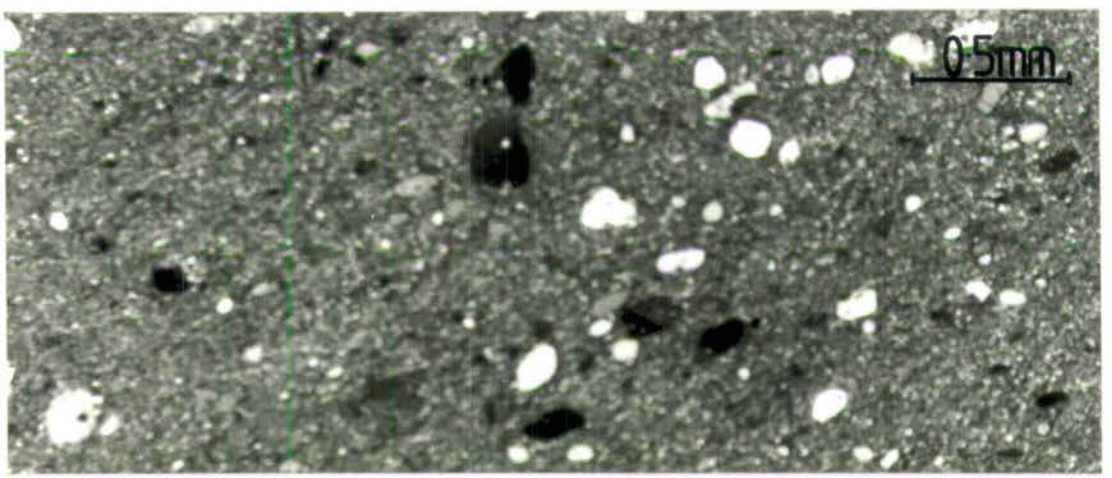

The following order of deformation can be deduced from the way minerals have responded to changes in the deformational environment:

i) Plastic deformation of quartz and feldspar
ii) Cleavage controlled fracture of feldspar with plastic flow of quartz/mica into tensional feldspar fractures
iii) Continued cyclic plastic deformation of quartz
iv) Temperature reduction and "freezing-in" of the microstructures

3.5.3.2 Cataclasite Series

Cataclasite series rocks are by definition random fabric fault rocks which are thought to be generated by brittle fragmentation in fault zones (Sibson, 1977). Cataclasites are formed by cataclastic flow when temperatures are sufficiently low to prevent plastic deformation of minerals in the parent rocks, and deformation proceeds by brittle fragmentation and comminution of particles. In quartzofeldspathic rocks this takes place at temperatures below 250°C.

The best examples of cataclasites have been found in outcrops along the Arethousa to Vrasna road and Vaiohorion to Askos road. These samples are distinctive in that all the porphyroclasts are typically angular, which suggests brittle comminution and fragmentation (Plate 3.19). As these textures overprint earlier fabrics attributable to ductile mylonitic behaviour, it is proposed that the effects are the result of a regional decrease in pressure and temperature conditions.

The best examples of ultracataclasites occur along the sheared base of the Arethousa Ultramafic Member (Plate 3.19b; Section 2.3.3.6; Insert, Map F).

3.5.3.3 Pseudotachylites

Pseudotachylite has been defined as a rock formed by melting of already hot rocks because of frictional fusion during faulting near igneous intrusions (Higgins, 1971), or a rock formed by the generation of molten material on a dry fault surface by frictional processes (Philpotts, 1964; Sibson, 1975, 1977). Frictional melting may reasonably be expected to occur at typical seismic slip rates of 10-100 cm s^{-1} (Sibson, 1975, 1977). Restriction to a specific zone for the generation of pseudotachylite may not be necessary as Sibson (1975) regards deformed pseudotachylite associated with the Outer Hebrides as a representation of transient discontinuities within ductile shear zones. However, Wenk (1978) has shown that some rocks which have been classified as pseudotachylites reveal textures which support an origin by extensive cataclasis. These rocks are in fact represented by fine-grained aggregates of strongly strained quartz and feldspar particles.

Plate 3.19

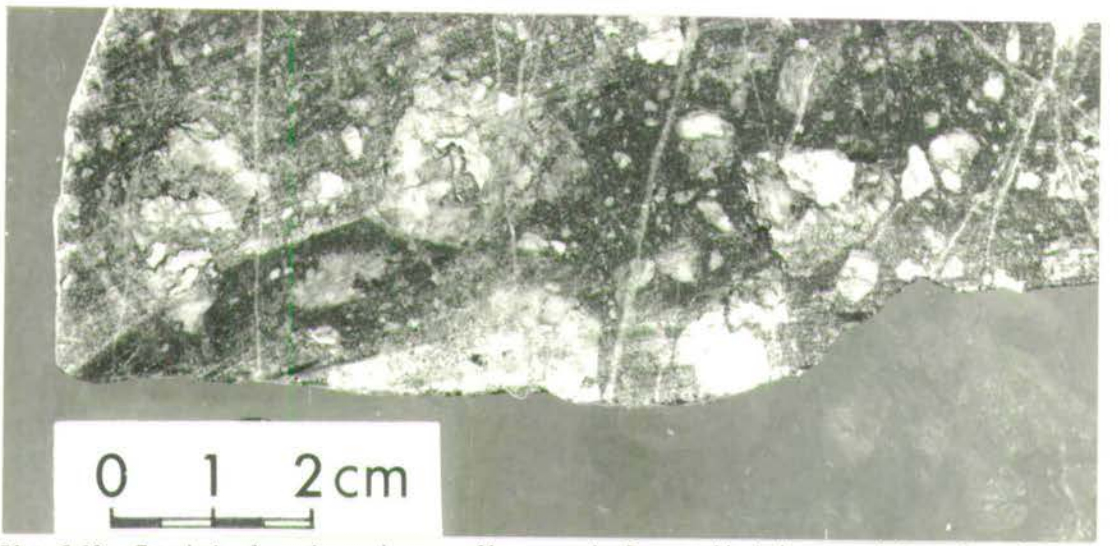

Plate 3.19a: Cataclasite from the arethousa to Vrasna road. Large subhedral to rounded porphyroclasts are preserved within a fine-grained, mylonitic (blastomylonitic) matrix.

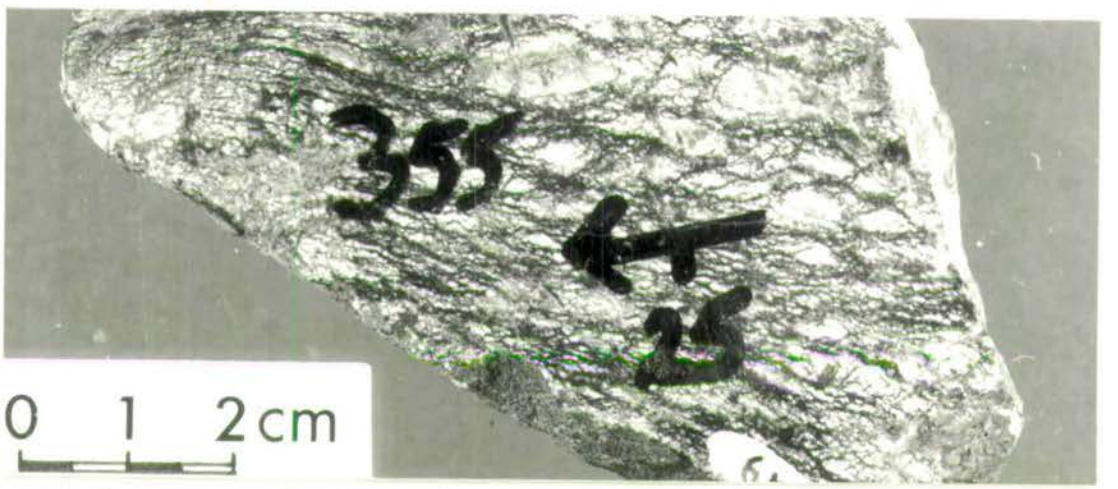

Plate 3.19b: Ultracataclasite from the base of the Arethousa Ultramafic Member. The actual outcrop indicates a shear component top to the NNW, while the sample shows a complex anastomosing texture around kernels of bright green mafic material (serpentinite).

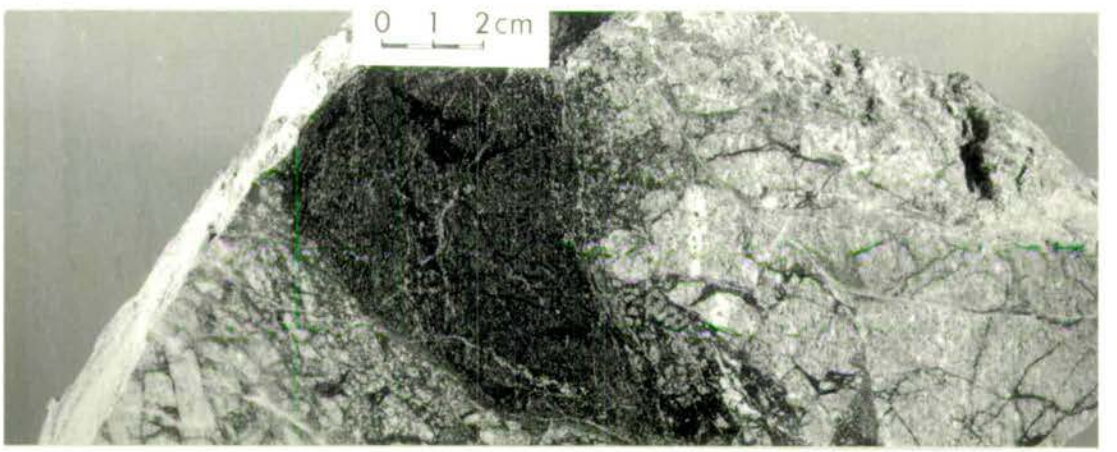

Plate 3.19c: Ultracataclasite or possibly pseudotachylite from the main stream section NNE of Megali Volvi. Extensive brittle fracturing of the quartzofeldspathic contry rock with fine-grained "glassy" pseudotachylite or ultracataclasite propagating and infilling fractures. A multiple intrusive-fracturing model is proposed to account for the progressively later and inclusion free (darker) intrusives.

Minor exposures which show a possible pseudotachylite character have been found in streams to the north of Megali Volvi (Plate 3.19c; Insert, Map D). However, these rocks are also associated with dyke intrusions. Therefore, it must be noted that the glassy appearance of the pseudotachylite veinlets may in fact be minor magmatic melts injected along cataclasite-ultracataclasite fractures.

3.6 Middle to Late D_3: Post-Shear Zone Structures and Fabrics

3.6.1 The Fourth Phase Folds (F_4)

The F_4 folds are characterised by well-defined, individual and conjugate sets of kink bands. These are found throughout the area, with the intensity of F_4 folds apparently dependent on lithology. The F_4 folds are interpreted as the last stages of the deformation episode which created the F_3 fold structures. Consequently they could be recorded as late F_3 (F_{3A}) folds, however as they occur as common regional fold structures, and for clarity and ease of comparison with other areas they are recorded and referred to as a separate F_4 fold phase (Plate 3.20).

3.6.2 Incohesive Fault Gouge-Late Fractures

Incohesive fault gouge is thought to form at depths of approximately 1-4 km (Sibson, 1977), although Wu *et al.*, (1975) have predicted that clay gouge can exist down to depths of 10 km. The best examples occur along the Vaiohorion to Askos road and associated with the extensive Neotectonic faulting which affects the entire area. These numerous late fractures show only minor (1-5 m) displacements and cut the mylonitic and cataclastic lithologies. Hence, these incohesive fault gouge-late fractures are interpreted as the final brittle movements of the original shear zones. Fracture planes are often characterised by a distinctive iron-red stain with large fractures or fault zones occasionally containing blue-grey, incohesive fault gouge.

3.6.3 Summary and Conclusions

The entire range of fault rocks preserved within the Lake Volvi area are thought to represent polyphase movements along a series of strain softened zones. For all these products to be preserved at one level, fault movements must have taken place over a long period of time during which there was continued uplift and erosion of the area. Therefore, the fault rocks represent a sequence in time (from ductile to brittle rock products). This transition reflects either a passage of the area from deep level through the brittle/ductile transition to the present day level, or a cooling history. This model is analogous to that of Grocott (1977b) for the Ikertoq Shear Belt of West

Plate 3.20

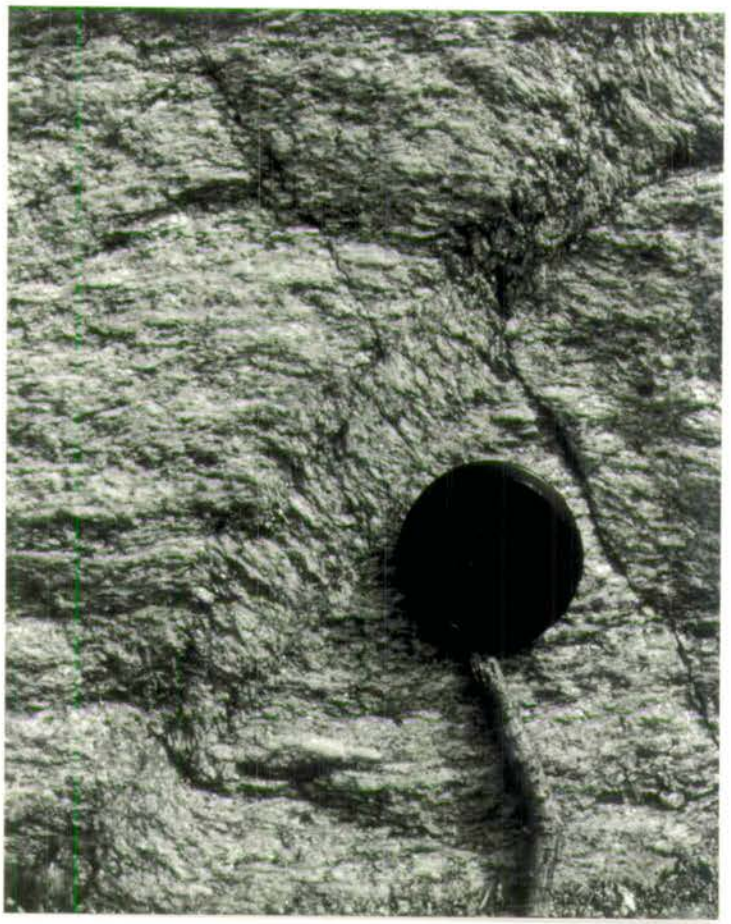

Plate 3.20a: The latest brittle fold structures are typified by well-developed kink folds. The lens cap is 52 mm in diameter.

Greenland which preserves both brittle and ductile products at present day level. However, it must be noted that the overall sequence of ductile to brittle fault rocks is not complete over the entire area, but is instead comprised of partial sequences, which together indicate the overall transition. Although they have a widespread distribution, the ductile to ductile-brittle effects have been concentrated in preferred localities (shear zones). The positions of these shear zones are related to regional shear strain (Section 6.3), rather than a particular geometry for an individual unroofing scenario.

3.7 Mechanisms for Structural Development

3.7.1 Transposition of Foliations

The transposition of foliations from a steep to flat-lying trend occurs throughout the area. This transposition has developed on scales of a thin-section to several metres, and if the process is scale invariant could also be developed on a km-scale. Bell (1986), describes a mechanism which could be suitable for this transposition based on the development of crenulation cleavage.

Reactivation of foliations during deformation partitioning occurs when zones of progressive shearing switch from anastomosing around the axial planes of actively developing folds, to anastomosing around an earlier discordant foliation that is being deformed (folded) by these folds. The foliation is thus reactivated with a sense of shear that is always antithetic relative to the fold, and shearing parallel to the axial plane of the contemporaneous folds ceases locally (Fig. 3.13; Bell, 1986). During this transposition the foliation is likely to pass through several (though not necessarily all) stages of crenulation cleavage development (Fig. 3.14).

One of the best examples of this transposition occurs in the Modhi Leucocratic Gneiss Formation (Section 2.2.3.2), where a progressive sequence of S_1 and S_2 fabrics developed (Figs. 3.4; Section 3.2, 3.1). The full extent of this transposition series is obscured due to lack of continuous exposure. However, to the east of the Volvi Complex, the Vamvakia Purple Gneiss Formation (Section 2.3.2.2) shows a similar phenomenon over more continuous outcrop.

Probably the most complete examples of foliation transposition within the studied area are preserved in thin-sections of garnet-graphite schist (Samples L65a, b; Plate 3.21). Within these thin sections large (1-3 cm diameter) garnet porphyroblasts preserve well-defined inclusion trails highlighted by graphite. These inclusion trails maintain a consistent orientation within the cores of the garnet porphyroblasts and progressively rotate into alignment with the external fabrics which have been transposed. One of the initial problems with these porphyroblasts and their inclusion

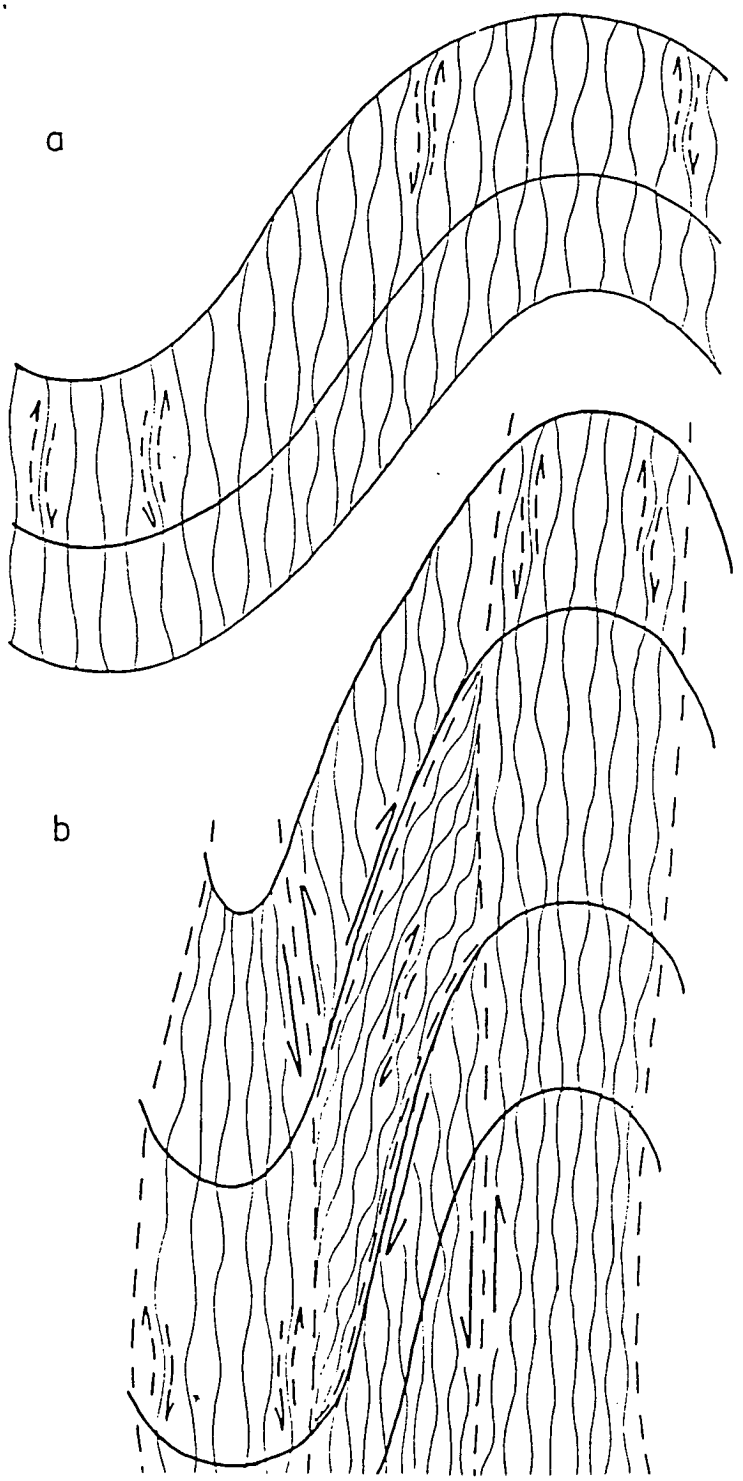

Fig. 3.13: Schematic diagrams showing a shift in the pattern of deformation partitioning (fine and coarse spaced lines represent lines of shearing anastomosing around zones of shortening) during the formation of a fold limb, such that the folded foliation locally becomes reactivated. Progressive shearing (dashed arrows) is synthetic everywhere relative to the developing fold in(a), but locally antithetic in the zone undergoing reactivation in (b). Solid arrows in (b) show the sense of shearing at the coarser scale of deformation partitioning defined by the dashed lines, after Bell (1986).

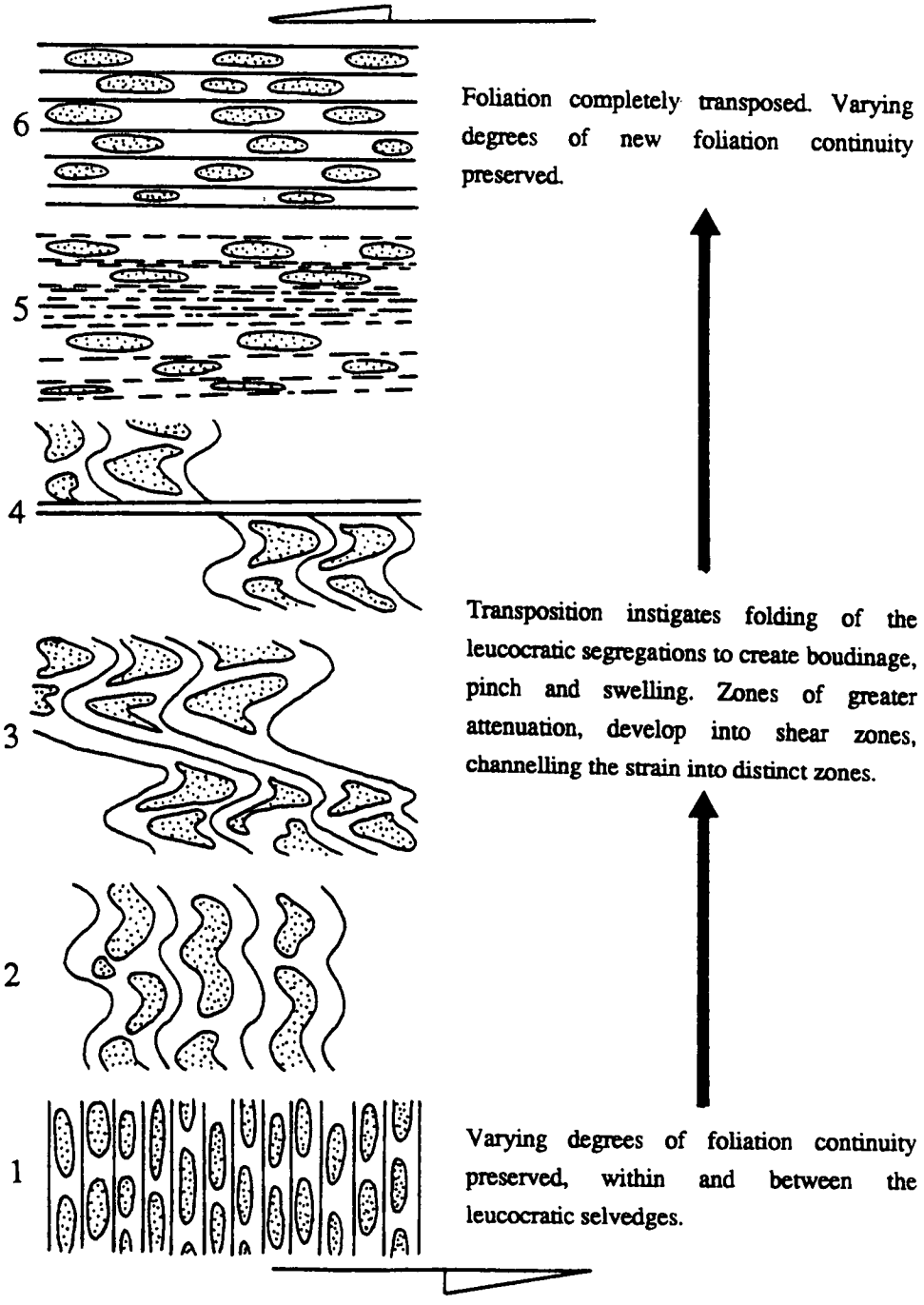

Fig. 3.14: Six types of foliation transposition, modified after Bell and Rubenach (1983); Bell (1986). (1) Uncrenulated original foliation, (2) Crenulations, (3) Differentiated crenulation cleavage with continuity across the crenulation cleavage, (4) Differentiated crenulation cleavage, (5) Differentiated layering due to destruction of crenulation hinges by further deformation, (6) homogenised cleavage through penetrative deformation and crystallisation/ recrystallisation on the grain scale.

Plate 3.21

Fabrics within garnet porphyroblasts showing the transposition of the matrix fabrics rather than a marked rotation of the porphyroblast.

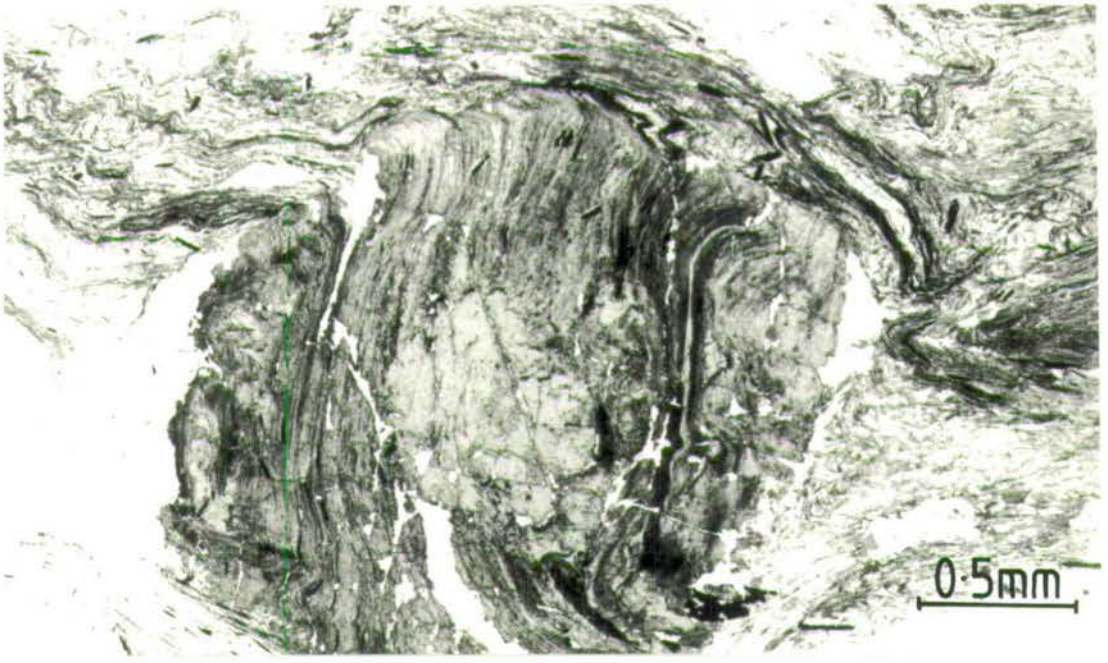

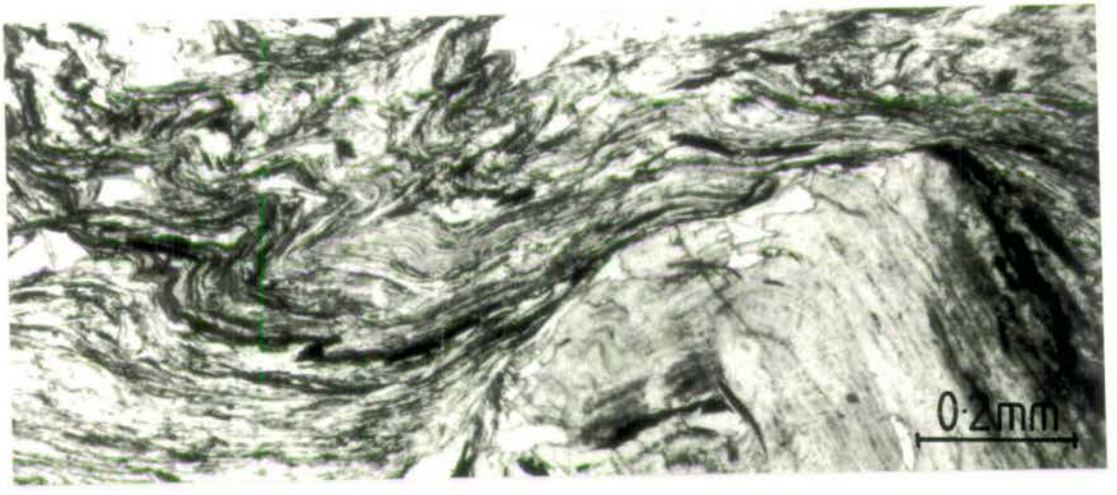

trails concerns the matter of whether or not rotation has occurred (Section 3.7.2).

If this mechanism is scale invariant then it could explain the preservation of folds within the Vamvakia river wrapped by anastomosing shear zones (Section 3.3), and possibly the arrangement of the lithologies to the west of the Volvi Complex (Section 3.7). It would also support the evidence for a complex history which has subsequently been obliterated (apparently simplified) as a result of extensive late overprinting.

3.7.2 Porphyroblast Development

Rotation of S_i in porphyroblasts relative to S_e has been attributed to a number of processes, all of which probably do occur in some rocks. From the two thin-sections (Sample L65a; Plate 3.21) S_i and S_e are interpreted as being generated by the same deformational event (c.f. Olesen, 1978). However, the relationship between S_i and S_e may be due to rotation of pre-existing S_i relative to pre-existing S_e or newly formed S_i relative to newly formed S_e, which could be a result of:

i) Rotation of the porphyroblasts (Cox, 1969; Spry, 1969; Powell and Treagus, 1970; Schoneveld, 1977; Powell and Vernon, 1979; Williams and Schoneveld, 1981; Lister and Williams, 1983), or

ii) Rotation of the matrix (Ramsay, 1962; Powell and Treagus, 1970; Wilson, 1971; Olesen, 1978; Bell and Rubenach, 1983), or

iii) Differential rotation of the porphyroblast and matrix (Ramsay, 1962; Wilson, 1971; Olesen, 1978; Bell and Rubenach, 1983), or a combination of both.

The frequent argument for porphyroblast rotation is that the inclusion trails are commonly oblique, and partially or completely continuous with the external foliation, and therefore appear to have been generated in a single deformation event. However, Bell (1985) considers many foliations to have developed by reactivation of earlier ones. Even after the development of a differential crenulation cleavage (Fig. 3.14, stages 3 and 4; Bell and Rubenach, 1983), the earlier foliation can still be reactivated as the strain becomes more highly non-coaxial and the earlier crenulations unfold (Bell, 1985). Consequently, in these examples the external schistosity is a product of deformation subsequent to that which generated the foliation preserved as inclusion trails inside the porphyroblasts. Depending on the timing of porphyroblast growth, the foliation may have undergone some rotation due to subsequent deformation, although porphyroblasts commonly overgrow and preserve unrotated relics of the earlier foliation because of the control of deformation partitioning on porphyroblast nucleation and growth sites (Bell *et al.*, 1986).

Correlation of foliation sequences from one exposure to the next is difficult within the area. However, an overall structural sequence can be developed by considering the range of foliations as a series of cycles (e.g. original continuous foliation → crenulation cleavage → new continuous cleavage foliation) which can be assigned to a particular deformational event. However, it is noted that some mis-correlation of individual foliations is inevitable and may result in an over simplification of the regional structure. Individual examples displaying evidence for the mechanisms of strain-partitioning and progressive deformation are readily observed throughout the area studied.

3.7.3 Summary

A number of problems have been encountered when attempting to assign specific foliations to particular events. This problem is particularly relevant to the correlation of foliations developed within the Arnaea granite to foliations developed in the country rock. The difficulty in correlating internal and external foliations of the Arnaea granite is typical of many other granite bodies. The development of foliations in granites has been studied by Vernon and Flood (1988), who have shown that quartz-mica rich granitoids in the Lachlan belt, Australia (usually S-type), have undergone ductile deformation and foliation development to a greater degree than quartz-mica poor granitoids (usually I-type) of similar age in that belt. However, discrete zones of granitoid have remained weakly or non-foliated, despite the common occurrence of quartz and biotite. A very similar case has been reported by Choukroune and Gapais (1983). This preferential development of ductile strain within particular zones has been attributed to fluid activity and associated strain softening mechanisms in these preferred zones which promote continued deformation *there*, rather than initiate deformation in non-foliated domains (White *et al.*, 1980; Passchier, 1982; Vernon *et al.*, 1983).

The number of tectonic foliations developed within granitoids, are therefore likely to be variable in the number of generations and their intensity of development (Choukroune and Gapais, 1983; Castro, 1986; Paterson *et al.*, 1987). There is also a problem of differentiating between foliations which were developed during and after emplacement. Hence there is a danger of misusing the presence or absence of tectonic foliation in granitoids to determine their time of emplacement relative to comparative cleavage generations. However, if the mineral assemblages defining a foliation in the granitoid indicates low- to moderate-temperatures, a tectonic origin is supported (Vernon *et al.*, 1983).

An unambiguous interpretation for the evolution of foliations in the Arnaea granite is not possible as they cannot be modified in terms of distinct deformation phases. This is due to the development and local superposition of structures within a progressive deformation event (c.f. Brun and Choukroune, 1981; Harris, 1985).

3.8 Structural Evolution: Summary

This section summarises the structural evolution for the area determined during this study. Detailed observations and descriptions are presented in the earlier sections of this chapter. A brief summary is presented in Table 3.3.

The early basement (D_1) structures and fabrics are described in Section 3.3. Migmatitic (S_0) fabrics were developed during a metamorphic event of uncertain age, which obliterated any earlier structures and fabrics. These migmatitic fabrics are used as a reference point for the regional structural history, and subsequent structures and related fabrics are labelled with respect to this initial metamorphic fabric.

Early migmatitic fabrics (S_{0A}) are defined by narrow leucosomes, attenuated to develop a pinch and swell fabric. This S_{0A} fabric was gently folded (F_1) with a weak axial planar cleavage developed. At an early stage in the deformation history the S_{0A} leucosomes were cross-cut by thicker leucocratic (pegmatitic) sheets which define a S_{0B} fabric. The S_{0B} fabric was also attenuated to develop a pinch and swell fabric which probably formed during early folding of the S_{0A} fabric. The S_{0B} fabric was folded into structures which are coaxial with the early F_1 folds. This continuous development of coaxial early to late F_1 folds resulted in progressive tightening of the early F_1 structures to produce late close to tight F_1 structures. No interference structures have been found between these early coaxial F_1 folds, which implies that the S_{0A} migmatitic fabric was cross-cut by an intrusive S_{0B} fabric during a single continuous fold episode. The progressive coaxial tightening and partitioning of strain developed around these F_1 folds combined with competence variations due to changes in thickness of the S_{0A} and S_{0B} fabrics caused a range of S_1 foliations to develop. A detailed interpretation of these structures has not been possible due to the scarcity of low-strain outcrop preserving migmatitic S_0 fabrics within the study area.

The dominant structures within the later D_2 and D_3 deformation episodes are related to the development of anastomosing shear zones (Section 3.2). The structural evolution during the D_2 and D_3 events determined for this study are therefore discussed relative to shear zone development.

Pre- to syn-shear zone structures and fabrics (early D_2) are described in Section 3.4, and syn- to post-shear zone structures and fabrics (late D_2) are described in Section 3.5. The D_2 structural evolution, was characterised by progressive

deformation and strain partitioning. As a result, a range of S_2 foliations were developed axial planar to early fold generations and folded in later fold generations and cross-cut by late S_2 foliations axial planar to the late F_2 structures. Early F_2 folds were coaxially refolded by late F_2 structures probably generated in association with the development of anastomosing shear zones. Mylonitic fabrics have been developed along shear zones and preserve evidence for the transition from the ductile, through the ductile-brittle and into the brittle regime.

Near the end of the late D_2 ductile-brittle event and into the brittle D_3 event (Section 3.5) a weak S_3 foliation was developed, more typically observed as jointing axial planar to F_3 folds. Folds of this generation are distinguished by their upright, open to close style with an approximate E-W axial trend. Kink bands were well-developed throughout the area and have been classified as F_4 folds. Most of the deformation during this structural episode occurred within the brittle regime, as illustrated by the development of incohesive fault gouge and late fractures.

The latest deformation event observed is extensive Neotectonic faulting which has disrupted the continuity of formations and structures throughout the area, and is responsible for the present topographic features.

PART II: Intrusions and their Relationship to Deformation

3.9 Pegmatites

Several formations in the Volvi area have been intruded by more than one generation of pegmatite sheets. The best examples crop out along the Rendina to Asprovalta road (Gun-emplacement Gneiss Formation, Section 2.2.2.1; Rendina Amphibolite Formation, Section 2.2.2.3), east of Stavros (Stavros Leucocratic Gneiss Formation, Section 2.2.2.2), east of Modhi (West Modhi Amphibolite Member, Section 2.2.3.1) and along the Arethousa to Vrasna road (Vrasna Feldspathic Gneiss Formation, Section 2.2.4.2). The state of deformation of the pegmatites appears to be dependent mainly upon the orientation of the pegmatite sheets relative to the shear zones at the time of emplacement, rather than simply to the relative age (Section 3.9.4). The intrusion sequence for the different generations of pegmatite within the area is based on:

i) Orientation and thickness of the intrusions
ii) Degree of deformation suffered by the intrusions
iii) Cross-cutting relationships
iv) Composition of the intrusions

These simple criteria although not mutually exclusive are necessary to differentiate between the successive generations of pegmatites.

3.9.1 Gun-emplacement Gneiss Formation (*see* Section 2.2.2.1)

The earliest (Pg_1) pegmatites (Plates 3.22a, b; Fig. 3.15) are generally preserved as discontinuous pods, veinlets and stringers (2-12 cm thick) with an homogeneous, medium- to fine-grained quartz-plagioclase-K-feldspar composition. This pegmatite generation is often aligned parallel to the main (S_2) foliation where it is usually boudinaged by layer-parallel extension along the (S_2) foliation planes. Alternatively the resulting stringers and veinlets are frequently folded by the early F_2 folds which are common within the gneissic host.

The second generation pegmatites (Pg_2) are composite, with a quartzofeldspathic outer zone 4-14 cm thick around a boudinaged central zone 4-10 cm thick containing randomly orientated, 1-4 cm long laths of biotite (Plate 3.22a; Fig. 3.15). These composite pegmatites occur as relatively continuous sheets, often cross-cutting the main (S_2) foliation.

The last recognised generation of pegmatite intrusions (Pg_3) is composed of large 1-3.5 m thick pegmatite/aplite sheets (Plate 3.22a; Fig. 3.15). These sheets are homogeneous, fine- to medium-grained and composed of quartz-plagioclase-K-feldspar and white-mica.

Plate 3.22

Fig. 3.15: Schematic view of the pegmatite generations at the gun-emplacement (Insert, Map G).

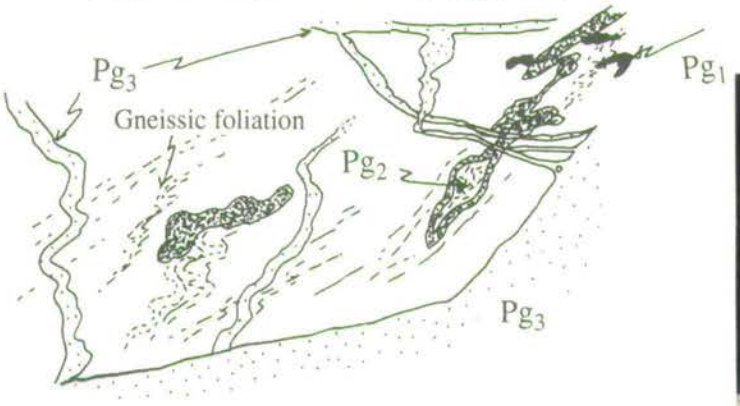

Plate 3.22a: Multiple generations of pegmatite intrusion at the WWII gun-emplacement, *see* Insert, Map G. View looking approximately E and about 4.5 m across. In the top right, three generations of cross-cutting pegmatites are shown. Folding of early pegmatite generations and gneissic host are shown in the bottom left.

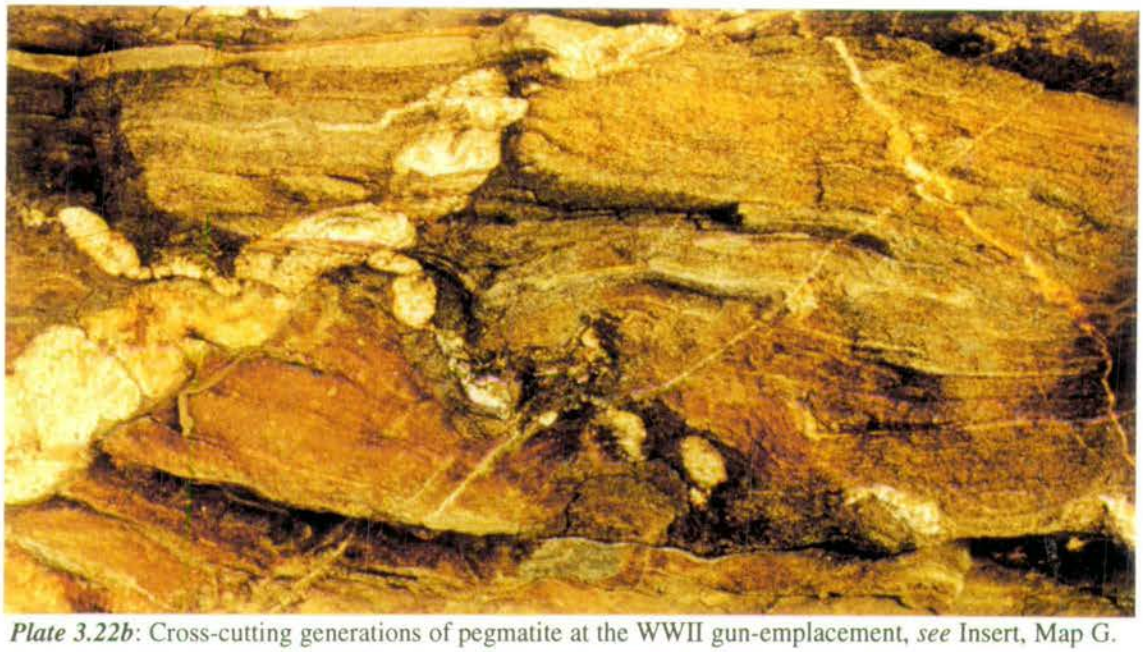

Plate 3.22b: Cross-cutting generations of pegmatite at the WWII gun-emplacement, *see* Insert, Map G. The strong foliation and F_2 folding of the biotite-rich matrix (possibly highly deformed migmatite) is well-displayed. The field of view is approximately 3 m across.

The Pg_3 pegmatites are usually sub-parallel to the main S_2 foliation, however, offshoots from these sheets cross-cut both of the earlier pegmatite generations.

3.9.2 Rendina Amphibolite Formation (*see* Section 2.2.2.3)

Four generations of pegmatite intrusions occur within this formation (Plates 3.23a to f). Two emplacement episodes are inferred, in each of which two closely related sets were intruded at different angles to a progressively deforming shear zone (Section 3.9.6).

The first generation of pegmatites (Pg_{1A}) are orientated parallel to sub-parallel with the main (S_2) foliation. These pegmatites have been boudinaged by layer parallel extension along the S_2 foliation plane (Plate 3.22a). In areas of particularly high-strain the pegmatites may only be preserved as isolated pods. A second pegmatite generation (Pg_{1B}) closely related in time consists of continuous quartzofeldspathic stringers (1-3 cm thick), which are folded into a series of asymmetric close to tight ptygmatic (F_2) folds. A well-developed (S_2) foliation is axial planar to these folds (Plate 3.23a). The strain state of these early pegmatites is variable. With increasing strain, the Pg_{1B} pegmatites are progressively tightened into tight to isoclinal folds and the Pg_{1A} pegmatites are further attenuated parallel to the S_2 foliation (Plate 3.23b). The strain is not evenly distributed throughout the rock, as folded Pg_{1B} pegmatites show thickened zones representing fold hinges separated by highly attenuated fold limbs (Plate 3.23b). A clearly later, third generation of pegmatites (Pg_{2A}) consisting of continuous, 2-4 cm thick sheets is orientated at a low-angle to, and cross-cuts the Pg_{1A} pegmatites and S_2 foliation (Plate 3.23c). Layer parallel extension has continued during intrusion of the third generation of pegmatites. However, there is a distinct change in the style and character of deformation from a ductile to brittle-ductile regime. This is shown particularly well where Pg_{1A} pegmatites are extremely boudinaged resulting in isolated pods wrapped by the S_2 foliation, to which they are now parallel; whereas the Pg_{2A} pegmatites (as in Plate 3.23c) are sub-parallel and only slightly boudinaged by continued extension along the S_2 foliation. In Plate 3.23d, the Pg_{2A} pegmatites have been attenuated by ductile-brittle extension.

The strain variations within this area are complex. Areas of relatively low-strain where relationships between pegmatites are fairly clear, grade into areas of very high-strain, where they are not. Plate 3.23e shows an area of high-strain, where the highly boudinaged (podded) pegmatite usually typical of Pg_{1A}, may actually be a highly deformed Pg_{2A} pegmatite, with the Pg_{1A} pegmatite extremely attenuated parallel to, and incorporated along the intense S_2 foliation. In areas of fairly intense

Plate 3.23

Four generations of pegmatite within variably strained outcrops of the Rendina Amphibolite Formation. All these plates are from along the Rendina to Asprovalta road looking approximately N. Scales and fields of view are: (A) pen, 14 cm long, (B) approximately 40 cm across, (C) approximately 1.5 to 2 m across, (D) approximately 1.5 to 2 m across, (E) coin, 28 cm in diameter, (F) approximately 3 m across.

Plate 3.23a: Two of the earliest generations of pegmatite are shown. Isolated pods and fine stringers (Pg_{1A}) are attenuated by and run parallel to the well-developed (S_2) foliation (bottom left to top right). Thin (1-2 cm wide) pegmatites (Pg_{1B}) are folded into a series of tight to isoclinal ptygmatic structures. Progressive attenuation of the fold limbs along the S_2 foliation starts to develop a blebby augen texture.

Plate 3.23b: With increased strain developed by shear parallel to and flattening perpendicular to the S_2 foliation, the pegmatitic (Pg_{1B}) folds are tightened into large clusters with highly attenuated limbs. Pg_{1A} pegmatites continued to be sheared along the S_2 foliation.

Plate 3.23c: The earliest pegmatite generation Pg_{1A} which is aligned parallel to the well-developed S_2 foliation is attenuated into a series of pods and stringers by layer parallel extension. A second generation of pegmatites Pg_{2A} are intruded which cross-cut the Pg_{1A} pegmatites and the S_2 foliation. Minor boudinage (pinch and swelling) of this (Pg_{2A}) pegmatite indicates layer parallel extension is still active.

Plate 3.23d: The Pg_{2A} pegmatite generation was intruded during a transition from a ductile to brittle deformation phase, as ductile-brittle extensional (pull-apart) structures are progressively developed.

Plate 3.23e: However, variations between low- to high-strain zones developed along the Rendina to Asprovalta road, often obscure the true pegmatite relationships. The main foliation (bottom left to top right) is an S_2 shear related fabric. The isolated pegmatite pod (centre) could be of either a Pg_1 or Pg_2 generation. The generation of the faint ghost folding (bottom right) of the amphibolite fabric is also uncertain due to the intense shearing along the S_2 foliation.

Plate 3.23f: Within areas of fairly low-strain the S_2 foliation is characterised by a more blocky development (bottom left to top right) while (Pg_{2B}) pegmatite (leucocratic/aplitic) sheets are close to tightly folded into F_2 structures.

Plate 3.23

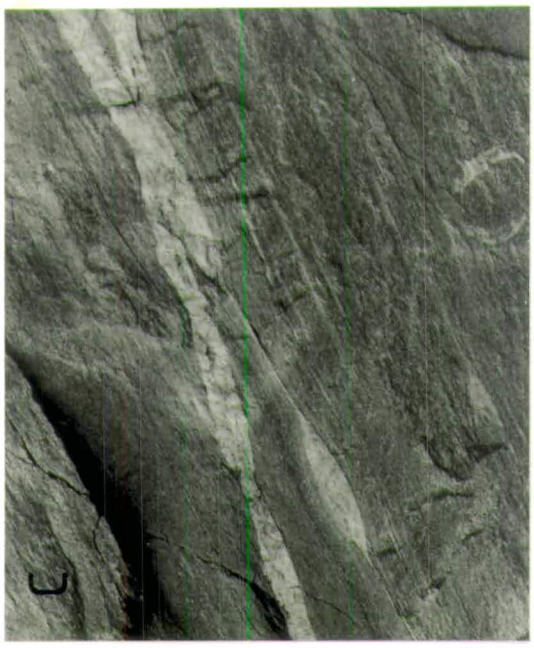

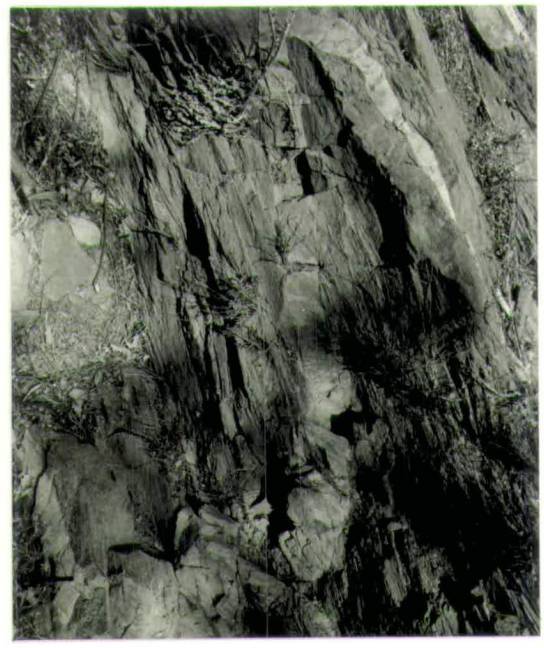

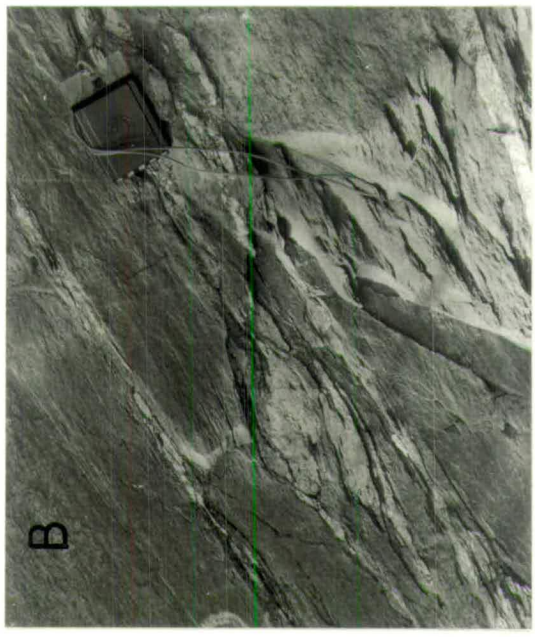

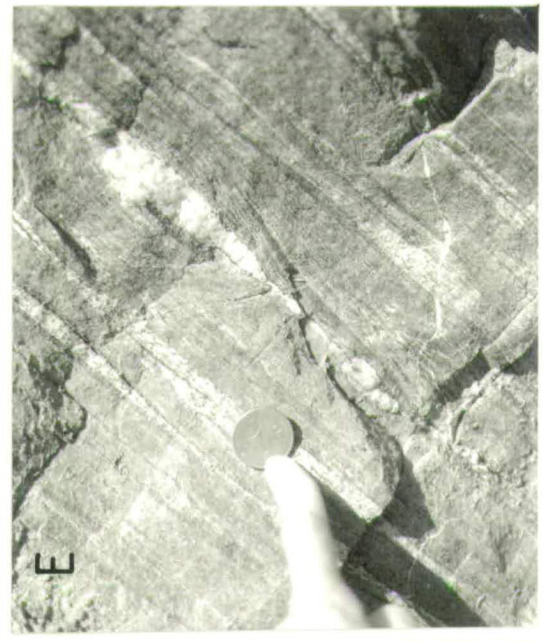

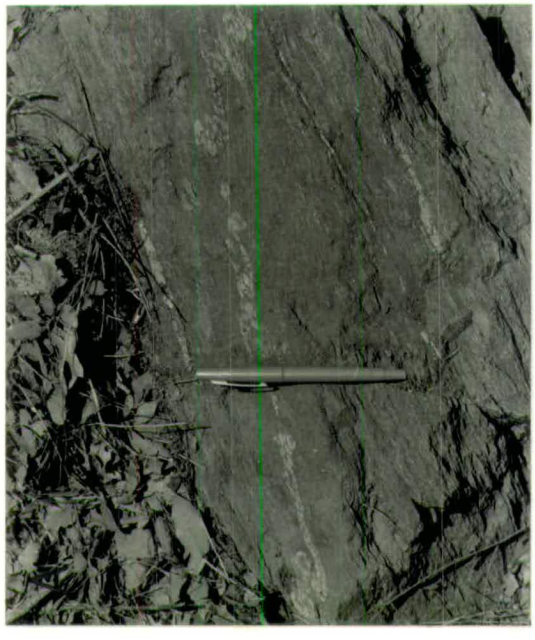

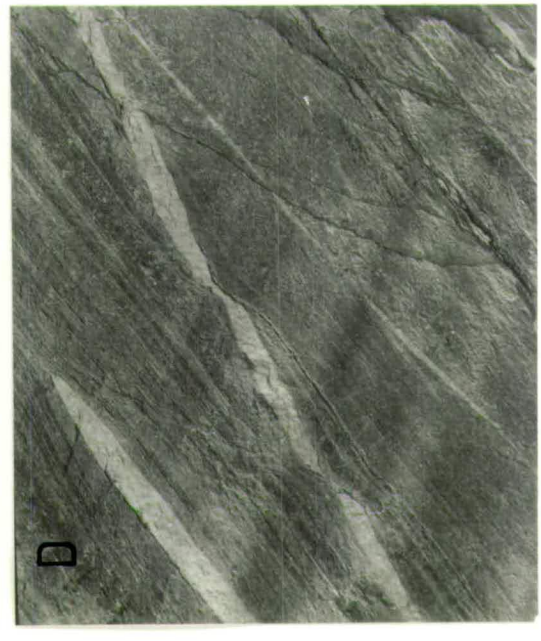

S_2 foliation, a fourth generation of pegmatite intrusions (Pg_{2B}) occurs. The Pg_{2B} pegmatites are continuous, 20 cm to 1 m thick, homogeneous, aplitic sheets which are close to tightly folded with the S_2 foliation as an axial planar cleavage (Plate 3.23f).

3.9.3 Stavros Leucocratic Gneiss Formation (*see* Section 2.2.2.2)

Four generations of pegmatitic/aplitic leucocratic sheets are intruded into this gneissic formation (Plate 3.24; Fig. 3.16). The earliest generation is preserved as thin (1-3 cm thick) pods and stringers intercalated along the main flat-lying (S_2) foliation. The second generation occurs as semi-continuous stringers, boudins, or pods (5-20 cm long), parallel or sub-parallel to the main (S_2) foliation. The third generation consists of 10 cm to 1.3 m thick sheets, which are folded into a series of semi-continuous, recumbent, asymmetric, tight to isoclinal (F_2) folds. It is proposed that this last generation of pegmatite was intruded then boudinaged during an early shear event which folded the second generation of leucocratic sheets. The already boudinaged sheets were then folded in a later shear regime. The exposure cannot be explained simply as an effect of the variable orientation of several sets of sheets within a progressively developed shear zone. Extension parallel to the S_2 foliation remained active after folding, causing attenuation of the already thinned fold limbs, parallel to the S_2 foliation. The S_2 foliation maintains a generally horizontal trend and is axial planar to the folded third generation of leucocratic sheets. The fourth generation consist of sheets orientated at varying angles to the S_2 foliation but always anticlockwise of it when looking down plunge of the intersection lineation between the S_2 foliation and leucocratic sheet . These leucocratic sheets are 5-30 cm thick and are relatively undeformed, cross-cutting the earlier generations of leucocratic sheets and the main (S_2) foliation.

3.9.4 West Modhi Amphibolite Member (*see* Section 2.2.3.1)

Contained within this amphibolite member is a large distinctive composite pegmatite (Plate 3.25; Fig. 3.17). The top and bottom marginal zones are composed of fine-grained, homogeneous, quartz-plagioclase-K-feldspar rock. The top marginal zone appears irregular in thickness (possibly boudinaged), whereas the lower margin is highly sheared and subsequently mylonitised. The central section is composed of columnar quartz growth, perpendicular to the margins. The mylonitic lower margin and the overall orientation of the sheet suggests that it is associated with the flat-lying shear zones. This supports the correlation of fluid mobility with shear zone development (Chapter 4), and possibly fluid related mechanisms for the geochemical variations within the mafic lithologies (Chapter 5).

Plate 3.24

Plate 3.24: Road cutting showing the Stavros Leucocratic Gneiss Formation approximately 1.5 km east of Stavros. Intrusive leucocratic sheets indicate a progressive and synchronous intrusive and deformation history. Field of view is approximately 8 m across.

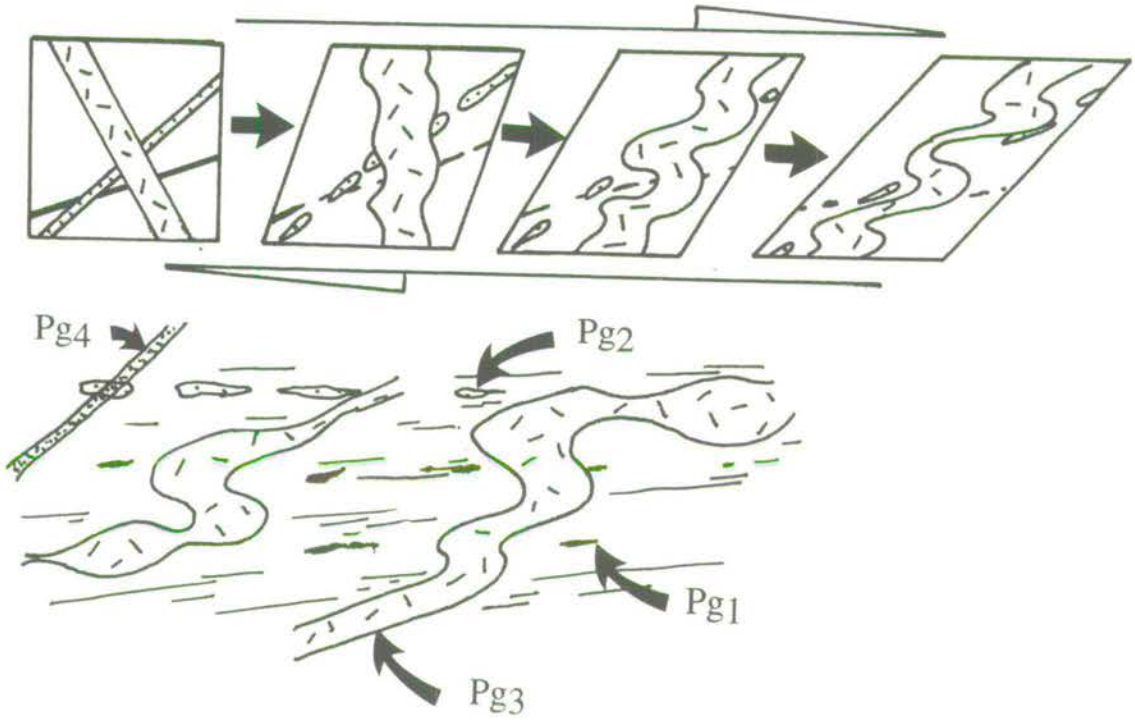

Fig. 3.16: Synoptic diagram for the deformation of leucocratic sheets outcropping to the east of Stavros depicted above in Plate 3.24.

Plate 3.25

Plate 3.25: Composite pegmatite sheet within amphibolite and Garnet Kyanite Schists approximately 2 km east of Modhi. View is of a road cutting approximately 5 m across looking N to NE.

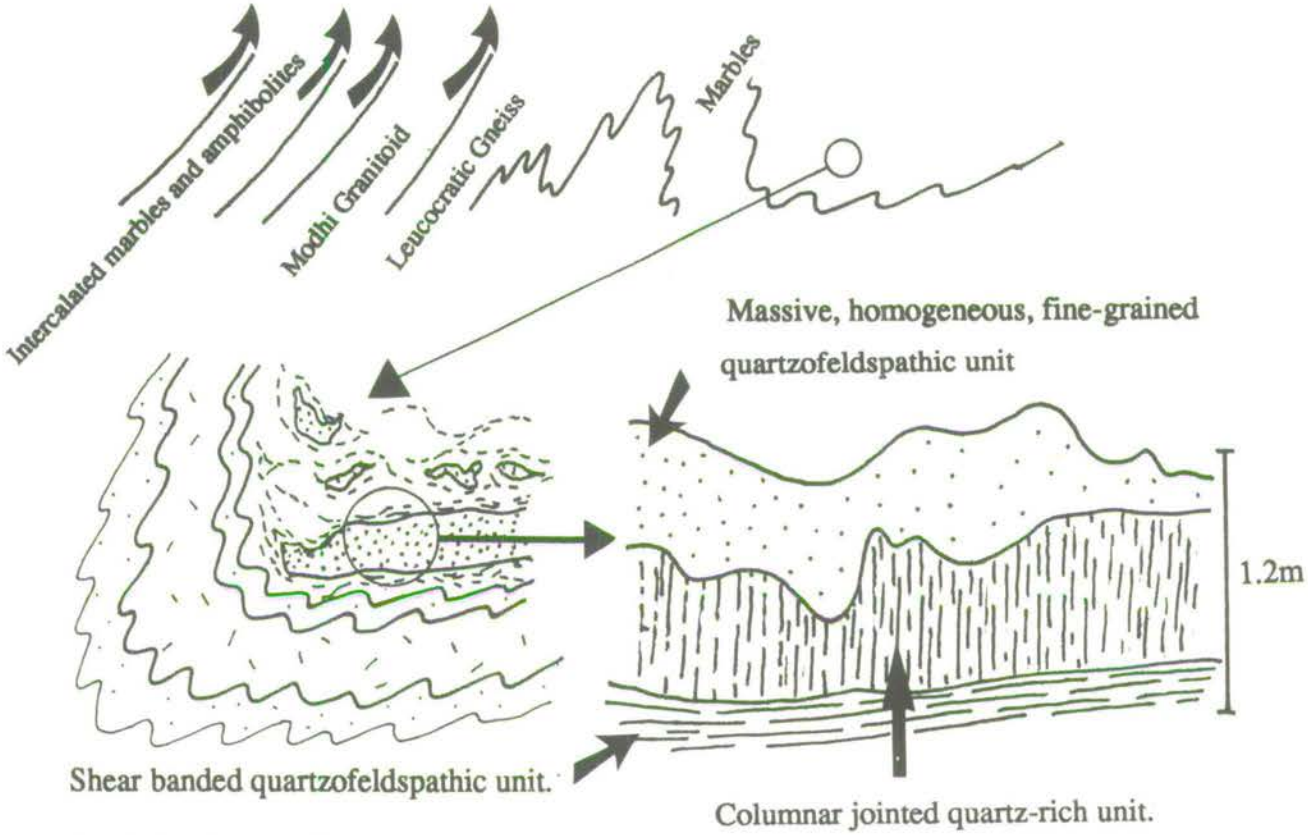

Fig. 3.17: Schematic diagrams of, (a) the composite pegmatite intrusion to the east of Modhi depicted above in Plate 3.25, and (b) the simplified structural context in which it is found.

3.9.5 Vrasna Feldspathic Gneiss Formation (*see* Section 2.2.4.2)

The pegmatite relationships within this formation are more complex than in the previous formations due predominantly to their spatial arrangement with respect to major (km-scale) shear zones. Three distinctive areas which display pegmatite intrusion have been noted. At the west contact of this formation a single highly sheared generation of pegmatites has been recorded. However, due to the intensity of the S_2 foliations, these pegmatites occur as highly disrupted discontinuous pods and stringers, and often lose their pegmatitic characteristics and appear as an integral coarse-grained, quartzofeldspathic component of the formation. Away from the west boundary (approximately 2 to 3 km), to the east along the Arethousa to Vrasna road, two generations of pegmatite are developed which cross-cut the gneissic banding and penetrative (S_2) foliations (Plate 3.26a). These cross-cutting pegmatite generations are preserved in low-strain pods wrapped by a more intense (S_2) foliation related to anastomosing shear zones. Hence, in a progression from low-strain core into the high-strain rim, the pegmatites become progressively folded into gentle to isoclinal F_2 folds (Plate 3.26b), and are finally completely obliterated by shearing, developing a distinctive quartzofeldspathic banding (0.2 to 3 cm thick) parallel to the main (S_2) foliation within the rest of the outcrop (Plate 3.26c). The progressive deformation of the pegmatites is interpreted as an effect of progressive shear zone development, which enveloped the low-strain pods, after intrusion of the two generations of pegmatite.

Further east (approximately 4 to 5 km) along the Arethousa to Vrasna road, single large (m-scale) pegmatites represent a third generation of intrusion. These pegmatites cross-cut the main foliation but there is some doubt as to whether it is S_2 in this area. This foliation could infact represent an S_1 foliation in a large low-strain pod. If this was the case, this pegmatite generation is older than the two cross-cutting pegmatites further to the west.

Therefore the different suites of pegmatite may actually reflect differences in the relative depth of intrusion, which are inferred to be progressively stratigraphically deeper and structurally lower to the east (shallow and deep depths of intrusion, W to E respectively). The present relationships may therefore represent displacement along large km-scale anastomosing shear zones. Evidence for the large-scale shear zones is shown by the varying degrees of deformation of the pegmatites. The most intense deformation and possibly one of the major regional shear zones is seen in outcrops along the Arethousa to Vrasna road, at the contact with the Vrasna Marble Formation (Section 2.2.4.3).

Plate 3.26

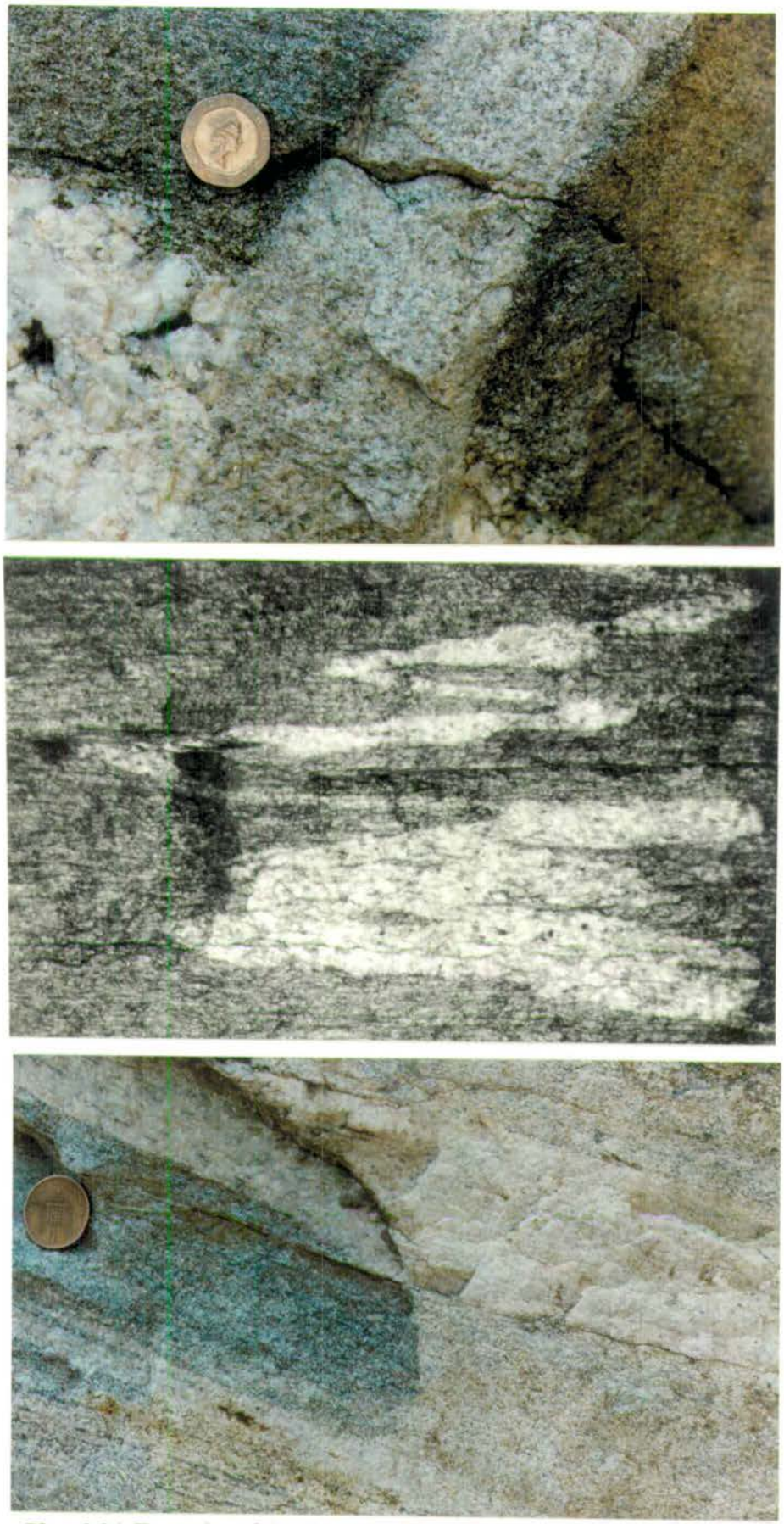

Plate 3.26: Examples of the Vrasna Feldspathic Gneiss Formation from halfway along the Arethousa to Vrasna road, views looking approximately S to SE. Field of view for A, B and C is approximately 12 cm across.

3.9.6 Summary

All the different pegmatite generations were emplaced into actively deforming (progressively sheared) gneisses. However, the lack of pegmatites in the more pelitic carbonate sequences common in the area suggests either that pegmatite intrusion ceased prior to the deposition of these sedimentary lithologies, or more probably that they were only emplaced at depth and not in the higher level sedimentary lithologies. Distribution of the pegmatite intrusions suggest that the area was actively deforming over a wide range of structural levels. The style of deformation, e.g. folding versus boudinage, is dependant on the original attitude of the pegmatite sheet relative to the main (S_2) foliation, at the time of intrusion (Fig. 3.18). Thus, early pegmatites, intruded sub-parallel to the maximum compressive stress direction in the shear zone, have been buckled and the folds then disrupted and their limbs attenuated, whereas pegmatites parallel to the extension direction have been boudinaged without buckling. Later pegmatites can be identified as sheets in a similar attitude to "early" highly deformed pegmatites, but showing much weaker internal shear-fabrics and less intense folding or boudinage.

3.10 Volvi Complex

Determination of the emplacement history for the Volvi Complex within the gneissic and metasedimentary envelope was the major objective of this work. The internal deformation and intrusive history of the Volvi Complex (*s.s.*) is considered a separate problem and an area for further study. Hence, studies have been concentrated in three main areas just within the margin of the complex (along the Vamvakia river, Section 3.10.1; around Lefkoudha, Section 3.10.2; east of Megali Volvi, Section 3.10.3). Evidence from the contact relationships between the Volvi Complex (*s.s.*) and envelope and the relationships between dykes (Section 3.11) within the envelope and the Volvi Complex have helped to resolve the emplacement history of the complex.

3.10.1 The Eastern Marginal Zone (*see* Section 2.3.2.5)

The exposed outcrop of the mafic formation includes evidence of a number of intrusive events. However, due to the pod-like character of the formations along the Vamvakia river, correlation between these intrusive events is not possible. Along Section A^{V}-A^{VI} (Insert, Map C), medium- to coarse-grained gabbro is intruded into a dark, fine-grained dolerite and folded into large amplitude (2 to 4 m), narrow wavelength (20 to 30 cm), recumbent, tight to isoclinal folds. In an adjacent boudin a similar intrusive-structural relationship is developed, although with the folds on a

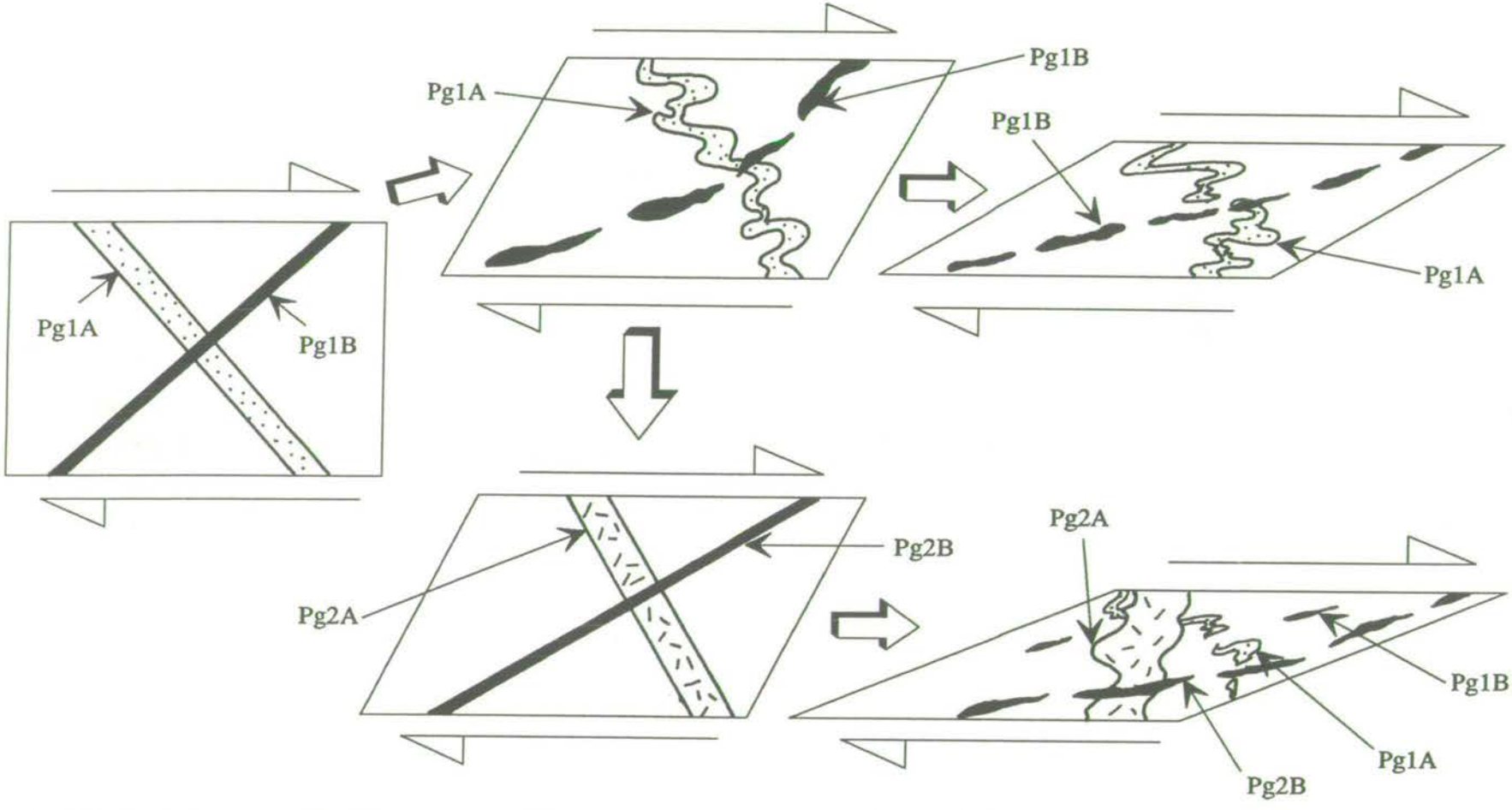

Fig. 3.18: Synoptic diagram for the progressive deformation of successive generations of pegmatite intrusions within a shear dominated environment.

smaller scale. Extensive veinlets of green epidote emanate from the gabbro into the dark mafic host along numerous fractures, and are interpreted as evidence for a late retrogressive or hydrothermal event (Plate 3.27a). The entire outcrop has subsequently been sheared and incorporated into the anastomosing shear zones.

At the beginning of Section A^{V}-A^{VI}, medium-grained gabbro with a strong sub-vertical fabric is juxtaposed and lies beneath a mylonitic-ultramylonitic (probably ex-migmatite) lithology with a sub-horizontal fabric (Plate 3.27b). The fabric within the gabbro is rotated at the contact from steep to flat-lying, with the change in direction indicating a top to north shear direction. This relationship implies juxtaposition prior to or early within the history of shear zone development.

Approximately halfway along Section A^{IV}-A^{V}, a fine-grained, homogeneous, grey, doleritic intrusion cross-cuts a strongly S_2 banded purple gneiss and preserves sharp angular contacts. The dolerite and gneiss are subsequently sheared (top to north), with folding and attenuation of the gneissic fabric parallel to the shear zone.

Apart from the obvious intrusions of the mafic formation and mafic members of the country rock, several exposures exhibit complex inter-relationships between the intrusive rocks. Approximately a third of the way along the transect from A^{IV}-A^{V}, medium-grained gabbros (which have weathered to a rust-red colour) are present within a homogeneous, fine-grained, dark-grey, doleritic host (Plate 3.28a). The gabbros are preserved as pods and stringers of varying sizes throughout the outcrop. No chilled or baked contacts are developed indicating that both lithologies were at similar temperatures. The similarity in temperatures between the two lithologies may account for the ductile folding and boudinage effects developed in some outcrops. The larger gabbroic xenoliths contain elongate, thin seams of a dark doleritic lithology. In an adjacent low-strain pod, separated by a narrow shear zone the main lithology is still a fine- to medium-grained, mottled dolerite. However, this dolerite host contains no gabbroic xenoliths but instead contains small pods (5 to 10 cm in diameter), of an homogeneous, fine-grained, dark-grey dolerite. These enclaves are similar to the lithology which was contained or possibly injected into the gabbro. hence, a complex intrusion and emplacement sequence is proposed with gabbro as the dominant early lithology, intruded/injected by a minor volume of a dark early dolerite, and finally both lithologies enveloped by the second generation of dolerite. The undetermined displacement along the shear zone disrupts the original intrusive relationships and inhibits any further interpretation of the successive intrusions.

Further evidence of multiple intrusive events is found at the end of Section A^{VI}, (Insert, Map C). Large angular blocks (20 cm to 1.5 m across) of fine-grained dolerite are incorporated (by stoping) into a more evolved leucocratic magmatic unit

Plate 3.27

Plate 3.27a: View of igneous relationships within the Vamvakia river (Section A^{V}-A^{VI}, Map C). Intrusion of gabbroic body into a hard, flinty, dark, fine-grained doleritic host. A sharp flat-lying contact is preserved above the hammer, while an irregular contact is preserved to the left. The characteristics of this doleritic host is attributed to baking by the gabbro. The gabbro is extensively retrogressed to a green-epidote matrix. The whole outcrop has been permeated by hydrothermal fluids from the numerous veinlets and fractures now filled by epidote. Hammer is 52 cm long.

Plate 3.27b: Deformation contact relationships along the Vamvakia river (Section A^{V}-A^{VI}, Map C), view looking approximately NW. A coarse-grained, well-banded upright amphibolite fabric has been overlain by a blastomylonitic lithology (mylonitised migmatite) with a flat-lying fabric. The amphibolite fabric is rotated into parallelism with the overlying fabric towards the contact, with the sense of shear top to the ENE. Head of hammer is 14 cm long.

Plate 3.28

Examples of magmatic relationships. Plates are from the northern section of the Vamvakia river, see Insert, Map C. Coin is 28 mm in diameter, hammer is 52 cm long and the field of view in Plate 3.28b is approximately 4 m across.

Plate 3.28a: Semi-rounded xenoliths of gabbro (2 to 10 cm across) are contained within a homogeneous dark, fine-grained doleritic host. No chilled or baked contacts are developed indicating that both lithologies were at similar temperatures. The large gabbroic xenolith contains elongate, thin (7 mm wide) seams of a similar (but slightly darker) doleritic lithology to the host. Hence, the gabbro is interpreted as being injected by an early doleritic magma prior to being enveloped by its present doleritic host.

Plate 3.28b: Angular blocks (20 cm-1.5 m across) of fine-grained dolerite are enveloped by an extensive network of a more evolved leucocratic magma. This feature is indicative of a developing multiply intrusive magmatic body.

Plate 3.28c: A homogeneous, fine-grained doleritic host (blue-grey) has intruded and almost completely assimilated a purple migmatite. These rocks have subsequently developed a small volume of melt along the main S_2 foliation. These have been intruded by a larger volume of locally derived melts (above hammer). Within the dolerite to the right of the hammer this S_2 foliation is possibly a remnant of the assimilated purple migmatite. The melt and fluids derived from the melt have been interpreted as the cause of the purple colouration of the host. The purple colouration (caused by garnet development) takes on several forms, to the right of the plate complete purple colouration of the dolerite has developed. To the left of the plate the purple colouration is less extensive and grades from a mottled character to individual clusters (snowflakes) and individual garnet porphyroblasts.

Plate 3.28

(Plate 3.28b). Away from the magmatic interface, doleritic blocks are progressively reduced in size and finally completely resorbed by the evolved component. Similar magmatic relationships are observed within the main body of the Volvi Complex (Dixon, pers. Comm.).

Intrusive gneissic host relationships are seen mainly along the margins of the Volvi Complex, although they are usually obscured by intense deformation (shearing). Most of the contacts are now mainly tectonic, with juxtaposition of the two rock-types along variably orientated shear zones. Consequently, the original igneous textures and fabrics are usually only preserved within low-strain cores. This phenomenon is well-displayed by a sheared gabbroic body (2 to 4 m wide) within a migmatitic host (Fig. 3.19). A range of gabbroic textures and successive S_2 shear-related fabrics are developed from the low-strain core to high-strain rim (Plates 3.29a to d). The changes in textures and mineralogy are described in Chapter 4. The original coarse-grained igneous gabbroic texture is shown in Plate 3.29a, whereas in the remaining Plates this fabric is seen to be progressively sheared.

Along the southern section of the Vamvakia river, contact relationships between well-banded amphibolites (a possible sheeted dyke complex) and a metasedimentary body (Siberian Tiger Formation) are exposed (Plate 3.30a). Interpretation of this particular contact relationship is hindered by poor exposure. However, on the basis of comparisons between the distinctive fabric of the metasedimentary formation (Plate 3.30b) and a similar lithology exposed near the western margin of the Volvi Complex (Section 3.10.3; Plate 3.31c), it is interpreted as sedimentary screens intruded by sheeted dykes. This implies that the Volvi Complex may have been intruded at a fairly shallow level within a sediment-filled basin, so that sheeted dykes are preserved cutting fairly undeformed layered meta-sediments.

A number of doleritic pods have developed a distinctive, blotchy, purple colouration (Plate 3.28c) caused by garnet in small, diffuse clusters (0.5 to 1.5 cm in diameter) resembling "snowflakes". They are abundant enough in some outcrops to give a complete purple colouration to the rock. These dolerites are inferred to have been modified by incorporating aluminous material derived locally from the migmatites (Chapter 4).

3.10.2 The Northern Marginal Zone (*see* Section 2.5.4.1)

Foliations developed within the amphibolites of the Volvi margin vary in intensity and become more penetrative as the percentage of biotite present in the outcrop increases. The main S_2 foliations generally maintain an approximate NW-SE trend, with variable values of dip although occasionally both the dip and strike of the

Fig. 3.19: Gabbroic pod within the Vamvakia Migmatite Formation (Insert, Map C). Variations in strain from core to rim are shown by the development of a range of fabrics shown in Plate 3.29.

Plate 3.29

Progressive strain associated with shear zone development is a prevalent theme throughout this work. This is shown by fabrics developed within areas of low-strain through a range of intermediate-strain fabrics and finally in to intense high-strain fabrics. These relationships are particularly well-developed in a number of pods and boudins. Fig. 3.19 and Plate 3.29 show a gabbroic pod which has been preserved within a migmatitic host (a possible original intrusive relationship) and finally sheared. Samples are from the northern section of the Vamvakia river (Samples, VAMR9 to 13), *see* Insert, Map C. Coins are approximately 28 mm in diameter.

Plates 3.29a to 3.29d: Show a progressive development from original igneous textures in the core of an isolated pod to the S_2 related shear fabrics at the rim. Variations of the mineralogy associated with this strain history are reviewed in Chapter 4.

Plate 3.29

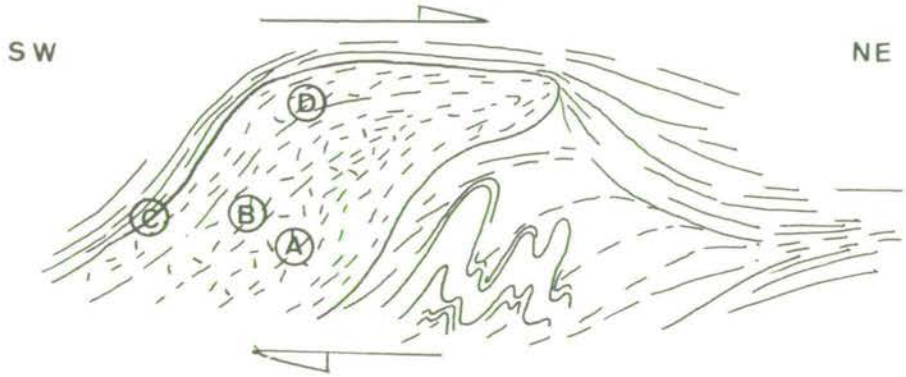

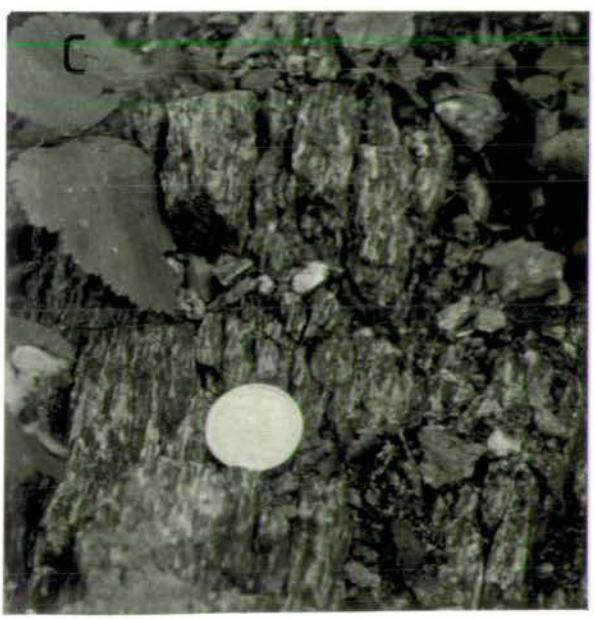

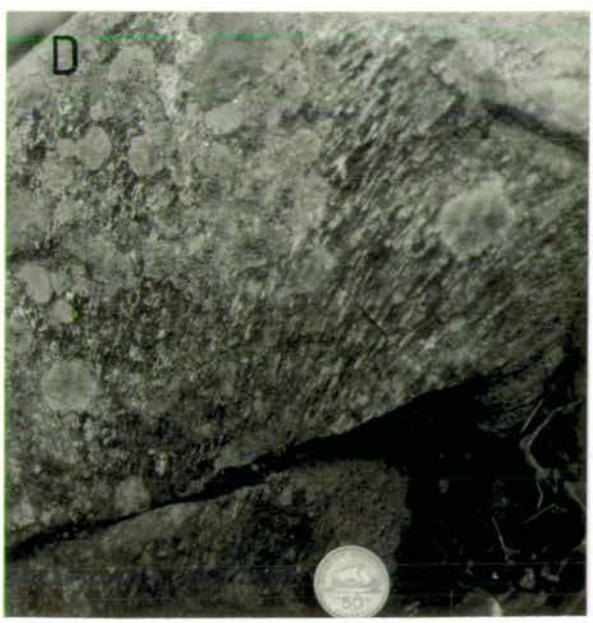

Plate 3.30

Plate 3.30a: This plate shows the contact relationships between the Siberian Tiger Formation and Vamvakia amphibolites, within the southern section of the Vamvakia river, *see* Insert, Map F. View is looking approximately SW with the field of view approximately 4-5 m across. The bottom left corner is composed of the Siberian Tiger Formation. Early fabrics are lost at the contact with the overlying amphibolites possibly caused by baking of the contact. The amphibolites are well-banded with the main fabric dipping between 45° and 50°W.

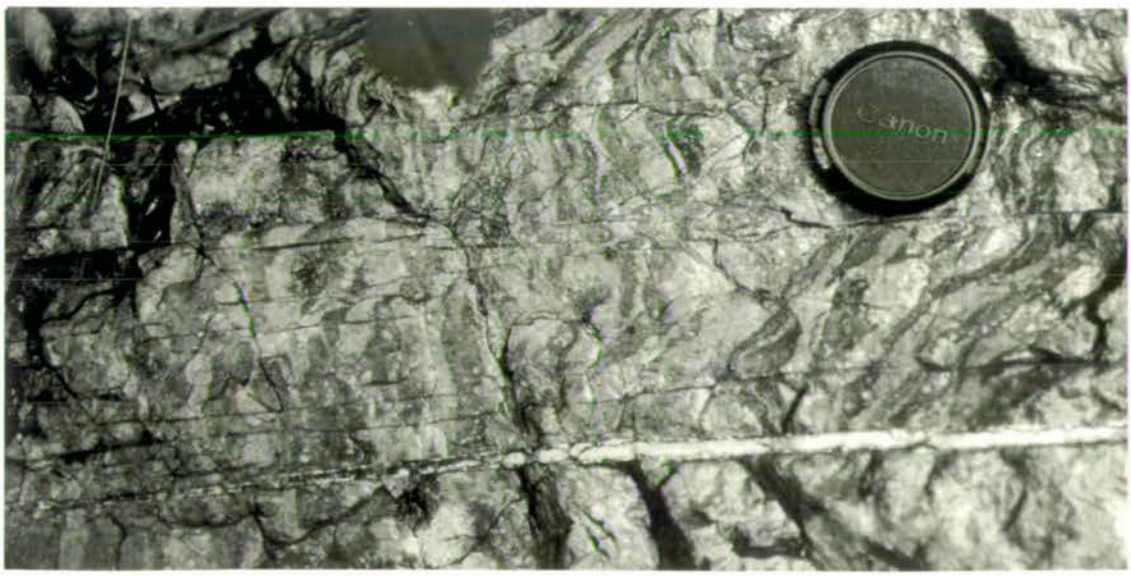

Plate 3.30b: Typical fabric of the Siberian Tiger Formation, consisting of dark, variably elongate, discontinuous pods, wrapped by a leucocratic matrix. Lens cap is 52mm in diameter.

foliations become far more varied due to local peculiarities. However, within the doleritic kernels, the S_2 foliation is not as intensely developed and evidence of an earlier S_1 foliation is preserved. Fig. 3.20 shows a schematic sketch of a 100-150 m long section from the main stream directly west of Lefkoudha. This section shows the effects of local granitic intrusions and the structures developed during emplacement. The earliest structures are preserved in low-strain dolerite kernels within the amphibolite. Zones of mylonitization and folds truncated by shear zones indicate ductile events, while brecciation and development of fault gouge provide evidence for brittle events. Variations in grain-size are attributed to original textural variations created during intrusion and cooling, and to the varying degree and style of deformation developed across the area (i.e. areas of high deformation are subjected to grain-size reduction). The gabbro ranges from undeformed to extremely sheared and foliated. In the least deformed gabbros, an original weak igneous foliation is defined by the alignment of plagioclase phenocrysts. However, more common foliations defined by wispy, elongate, subhedral crystals, suggest a relatively thorough metamorphic overprint. Occasionally the gabbros are highly deformed by shear zone development and progress gradually into a gneissose texture.

Along the NE margin of the gabbro, numerous doleritic intrusions are present within the gabbro. In this area the dolerites are clearly chilled against gabbro, with chill zones up to 0.5 m across. This suggests that the gabbro was completely solidified and cooled at the time of dyke emplacement. Contacts between minor dolerite intrusions and the gabbro often show the development of a localised foliation in the gabbro sub-parallel to the dyke orientation. Gabbro is locally sheared against the more competent dyke. The evidence that shearing is concentrated along dyke boundaries could explain the lack of visible cross-cutting phenomena in dykes in other more highly deformed lithologies (*see* the Vamvakia river, Section 2.3.2). However, evidence for late dolerite dyke intrusion post shearing is evident from fine-grained dykes which cross-cut the gabbro fabrics.

An overlapping intrusive and deformational history is supported by evidence of doleritic pods without chilled margins incorporated into the gabbro and wrapped by the metamorphic gabbroic foliation. This is interpreted as boudinage of the minor intrusions parallel to the metamorphic gabbroic foliation. However, originally sinuous dykes also cross-cut and hence post-date the metamorphic gabbroic foliation.

Along the stream section directly to the west of Lefkoudha, sequences of NW-SE trending doleritic dykes (0.5 to 1 m thick) are intruded into one another, creating a sheeted dyke sequence, ranging over a distance of at least 50 to 100 m. Chilled contacts are rarely exposed along this sequence. However, the few chilled contacts

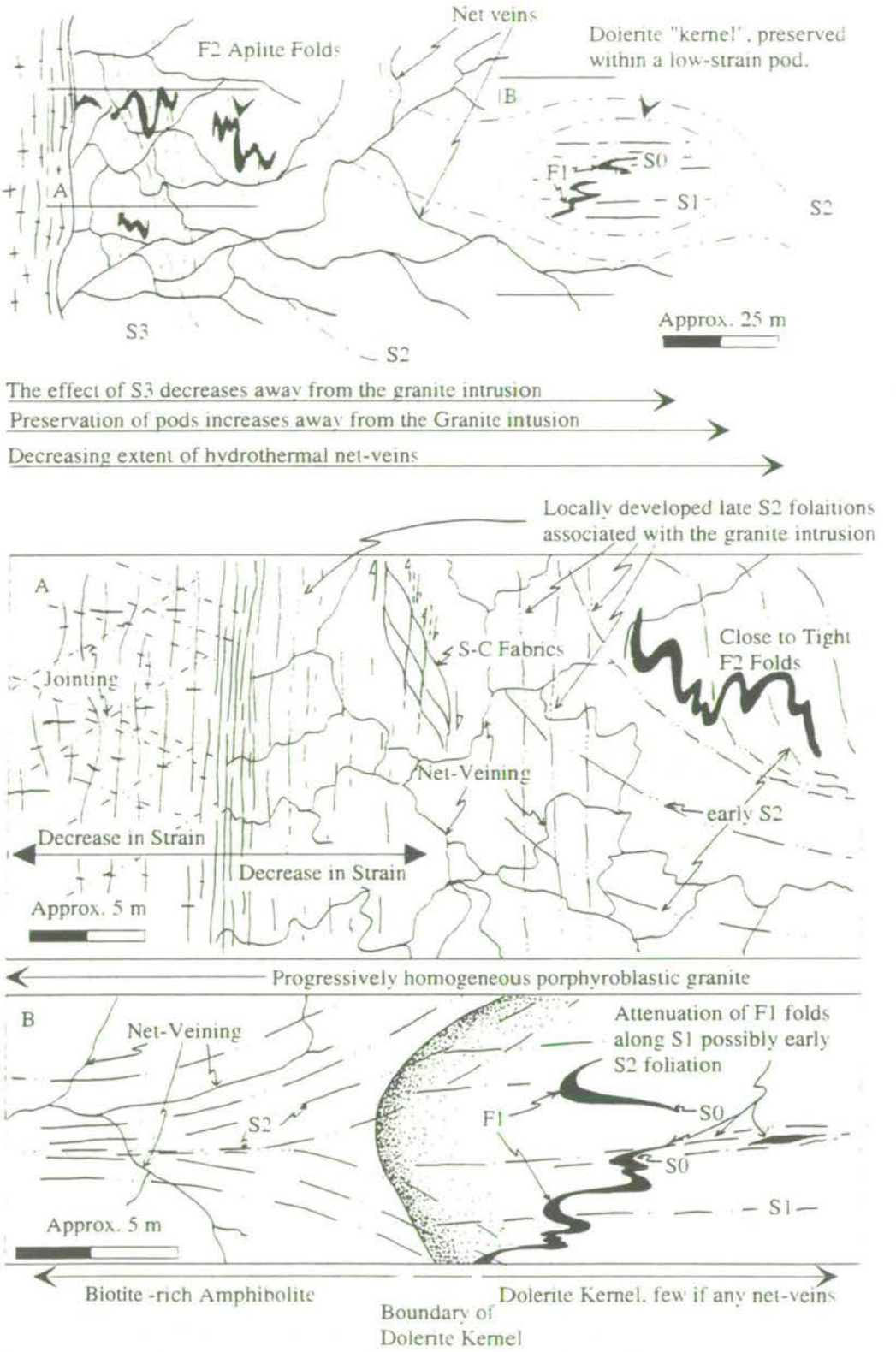

Fig. 3.20: Structures, fabrics and intrusive phenomena observed along the main stream section (100-150 m long) to the west of Lefkoudha, *see* Insert, Map H. (A) Fabrics and structures adjacent to a granitic intrusion, (B) transposition of foliations and tightening of structures from aweakly altered low-strain doleritic pod preserved within a high-strain biotite-rich amphibolite.

exposed appear to show a consistent polarity and indicate a younging direction for the minor intrusives from NE-SW, in this case towards the centre of the body. A series of later dykes cross-cut the sheeted dyke sequence to the west and the gabbro body to the north of Lefkoudha and are orientated with an approximate NW-SE trend

Original igneous textures are preserved in some of the dykes. Large, euhedral, plagioclase phenocrysts are aligned parallel to sub-parallel with the strike of the intrusions. A single weak foliation generally cross-cuts the sheeted dyke sequence, consistent with a relatively late time of emplacement in the overall intrusive and deformation sequence.

3.10.3 The Western Marginal Zone (*see* Section 2.5.3)

Large bodies of gabbro exposed within the Volvi Complex (*s.s.*) have a range of textures from completely undeformed to thoroughly sheared (Plate 3.31a). The amphibolite formation characteristic of the western boundary is composed of a series of variably deformed gabbros and dolerites. These mafic lithologies have been progressively sheared to produce striped amphibolites with leucocratic bands (0.1 to 10 cm thick). Within low-strain zones the leucocratic layers are tightly folded. These folds are progressively tightened and eventually obliterated by the shear zones which are represented by a series of well-defined leucocratic bands (Plate 3.31b).

A series of outcrops containing semi-continuous layers of dark-green/black hornblende-rich and white plagioclase-rich lithologies are exposed along some of the rivers in the Volvi Complex, approximately 500 m to 1 km east of the undisputed western boundary (Plate 3.31c). These "tiger-striped" lithologies are always bounded by sheeted dykes and appear in outcrop as screens. They have been interpreted as calcareous sediments which were undeformed and unmetamorphosed prior to intrusion of the dykes (*see* Sections 2.5.2 and 2.3.2.4). These outcrops are particularly important for the interpretation of the intrusive environment for the Volvi Complex (Section 2.3.2.4).

3.11 Dykes

One of the main objectives of this work was to determine whether dykes within the envelope to the Volvi Complex were truly related to it and its intrusive history, or whether they were related to a different source and intrusive evolution. The relationship between the Volvi Complex and dykes within its envelope, is crucial for any interpretation of the origin and tectonic setting of the complex. Numerous dykes are found throughout the Vertiskos Group to the west of the Volvi Complex, but they are less common to the east of the complex and rarely found to the south of

Plate 3.31

The western margin of the Volvi Complex is typified by a range of variably sheared gabbroic to amphibolitic lithologies. These mafic lithologies either grade progressively into gneisses and schists of the Vertiskos Group via broad shear zones or are abruptly juxtaposed via faults. These plates are from rocks which outcrop immediately within the western boundary of the Volvi Complex. (A) lens cap is 52 mm in diameter, (B) field of view is approximately 60 cm across.

Plate 3.31a: Coarse-grained, strongly sheared gabbro. Mafic component (olivine, hornblende) developing into augen, wrapped by the leucocratic matrix to produce a flaser-gabbro texture.

Plate 3.31b: Close to tightly folded amphibolitic fabrics (from bottom to top) are progressively tightened and sheared. The sequence consists of a feldspathic amphibolite possibly derived from a gabbro (Plate 3.31a is a potential precursor).

Plate 3.31c: Black and white "tiger-striped" formation from the first main stream within the western margin of the Volvi Complex, approximately 2-2.5 km east of Megali Volvi. Apart from the distinct separation into leucocratic and melanocratic segregations, a well-developed zonation can be seen within the dark selvedges. This lithology is interpreted as being a metasedimentary screen enveloped by extensive dyke intrusion. The fabric is the result of local metasomatism at the contacts of compositionally distinct original layers during metamorphism.

Plate 3.31

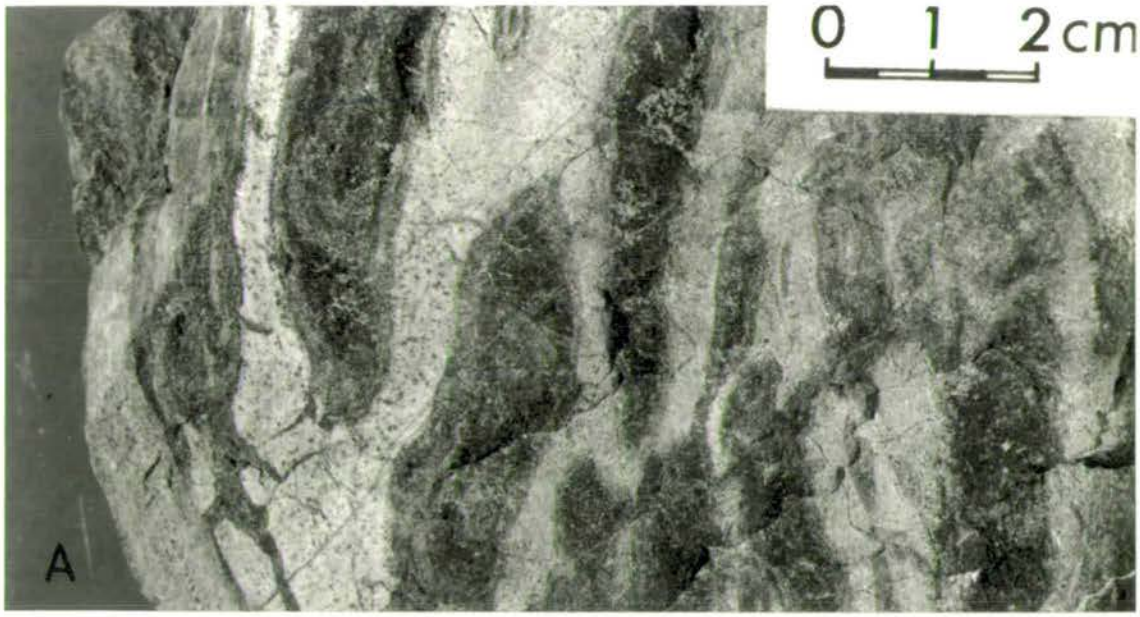

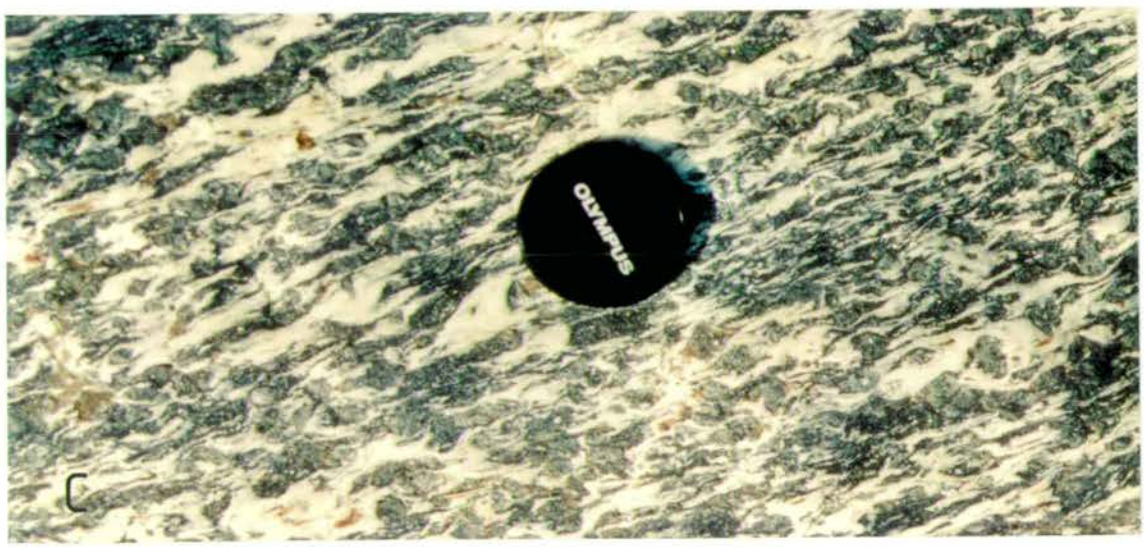

Lake Volvi. No dykes are found within the formations of the Volvi Metasedimentary (re: Svoula) Group (Section 2.4). A range of contact relationships between dykes and country rock have been developed which are dependent on the time of intrusion and the local deformation and strain history (see below).

A dyke has been defined for this study as: Any continuous or semi-continuous mafic body, which has a discernible width (usually 0.5-4 m wide) and can be traced laterally for a significant distance (>8 m), or across a stream section. It must also have sharp contacts with the country rock. When a mafic body is attenuated to the point where only small, isolated, elongate pods are preserved intercalated along a foliation, it can no longer be unequivocally classified as a dyke and is instead identified simply as a highly attenuated amphibolite.

Absolute timing of intrusion of the dykes is problematic. Due to the heterogeneous structural development across the area, it is not possible to uniformly categorise dykes as early or late entirely by their state of strain, as late dykes within a shear zone may be more deformed than early dykes within a low-strain core. However, some indication of the timing of dyke intrusion is given by the relative state of strain of the dyke compared to that of the enveloping rock.

Dykes vary from black to a light blue-green, with an homogeneous, fine- to medium-grained matrix, or a mottled (plagioclase-rich), fine-grained matrix. Contact relationships with the country rocks can be divided into the following categories; i) dykes cross-cut foliations and fold structures while remaining undeformed (Plate 3.32b), ii) dykes cross-cut foliations and fold structures and have then been themselves folded by tightening of the same structures and/or later-folds (Plate 3.32a), iii) dykes are parallel to the local foliation (Plate 3.33a), or occasionally sub-parallel with the main (S_2 shear) foliation in the country rock, while containing an earlier internal foliation parallel to their contacts. The third category of dyke intrusion is the most commonly found within the study area.

A number of distinctive phenomena occur along the boundaries between dykes and country rock. Plate 3.34a shows extensive retrogression of the dyke along the contact with the country rock and also along fractures into the dyke. Plate 3.33a shows a more complex outcrop where a 12 cm wide reaction rim is developed between the dyke and the quartzofeldspathic gneissic host. Plate 3.35a shows a mesh of needles of hornblende between the dyke and gneiss. Plate 3.33b shows the progressive development of a sheared margin between a feldspar-rich host and mafic dyke. The mottled blebs of plagioclase become flattened towards the contact with the gneiss. A 2-3 cm thick reaction rim is developed between the dyke and gneiss. Plate 3.34b is more problematic; this dyke appears to have been intruded into a fractured

Plate 3.32

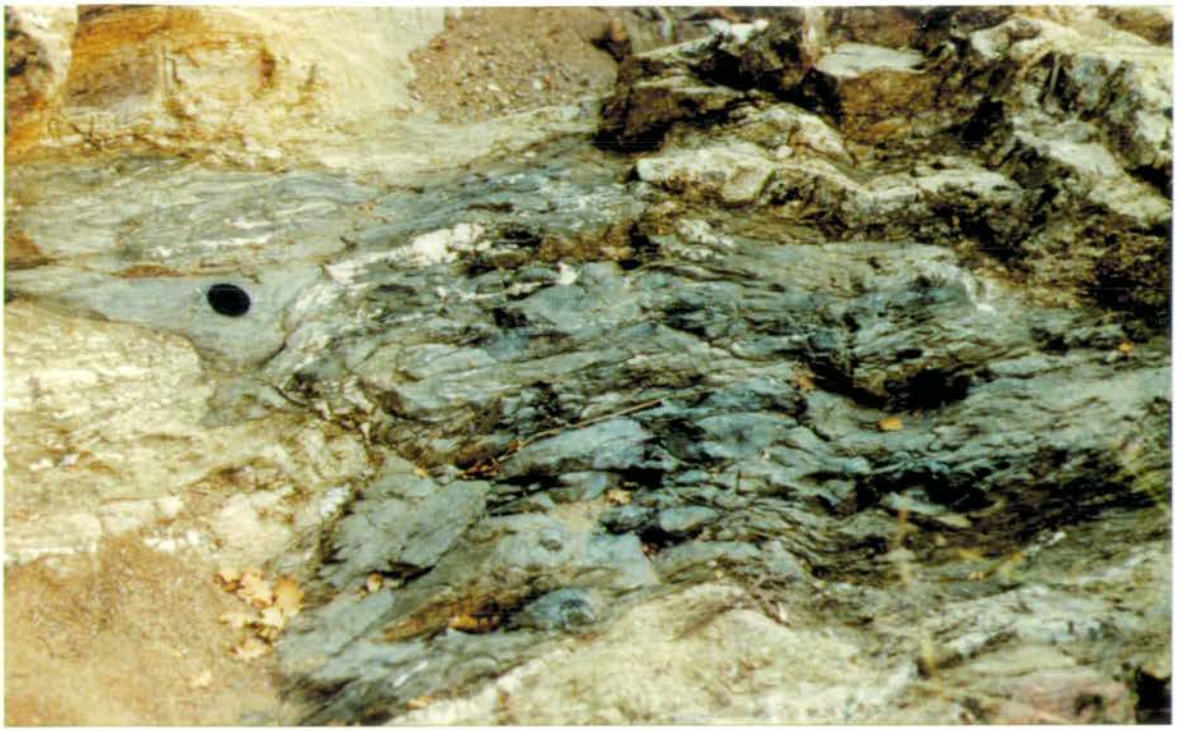

Plate 3.32a: The dyke cross-cuts early country rock fabrics within a quartzofeldspathic gneiss and is in turn folded into a close to tight (F_2) fold. The dyke has also been folded by late (F_3) kink bands. Lens cap is 52 mm in diameter.

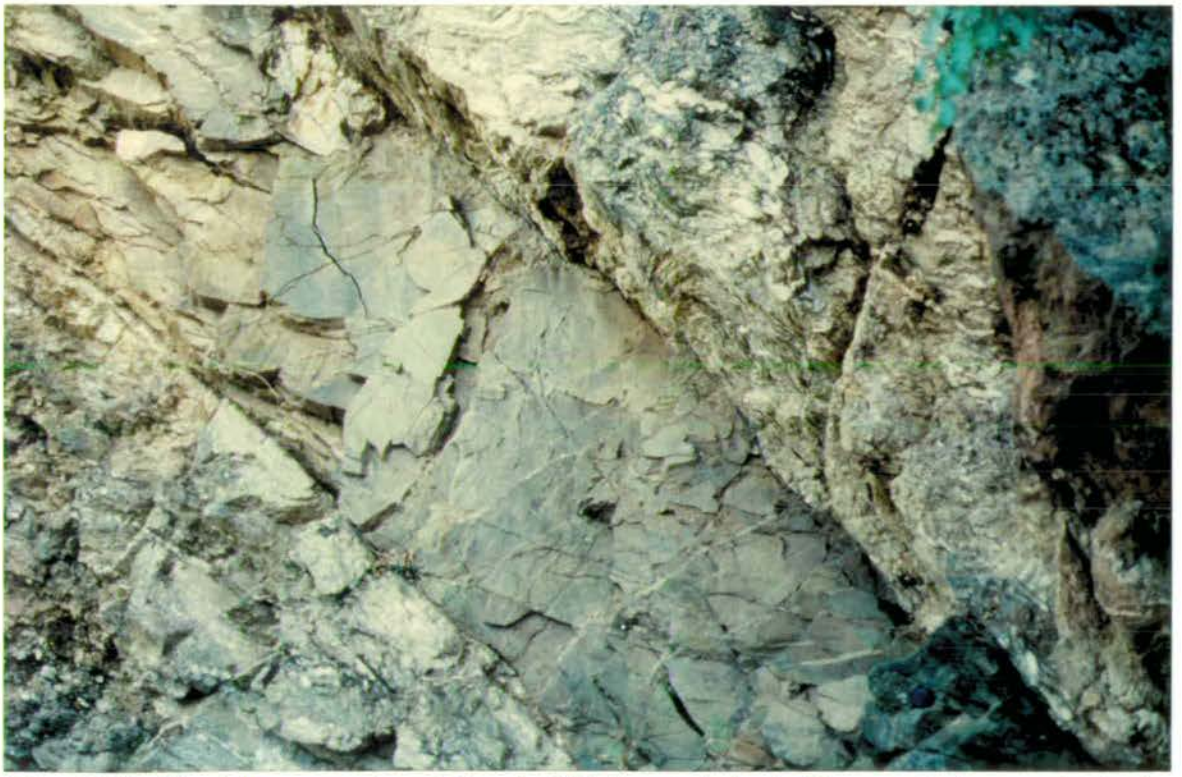

Plate 3.32b: The dyke cross-cuts an intensely folded gneissic host. Sharp contacts are maintained along the entire length of the dyke. There are no chilled contacts or baked margins. There is no attenuation (pinch and swelling) over the exposed outcrop of this dyke. Horizontal field of view is about 6 m across.

Plate 3.33

Plate 3.33a: A 12 cm reaction rim between the dyke and augen orthogneissic host highlighting a sheared contact. The shearing is likely to have been assisted by fluids migrating along the contact and weakening the initial contact zone. Lens cap is 52 mm in diameter.

Plate 3.33b: Highly sheared boundary between a mottled (feldspathic blebs) dyke and quartzofeldspathic host. A progressive shear fabric is developed from the bottom of the photograph to the contact and truncates the fabric within the host. A reaction rim (2-3 cm thick) is developed between the dyke and gneiss, probably due to fluids migrating along the contact. Lens cap 52 mm in diameter.

Plate 3.34

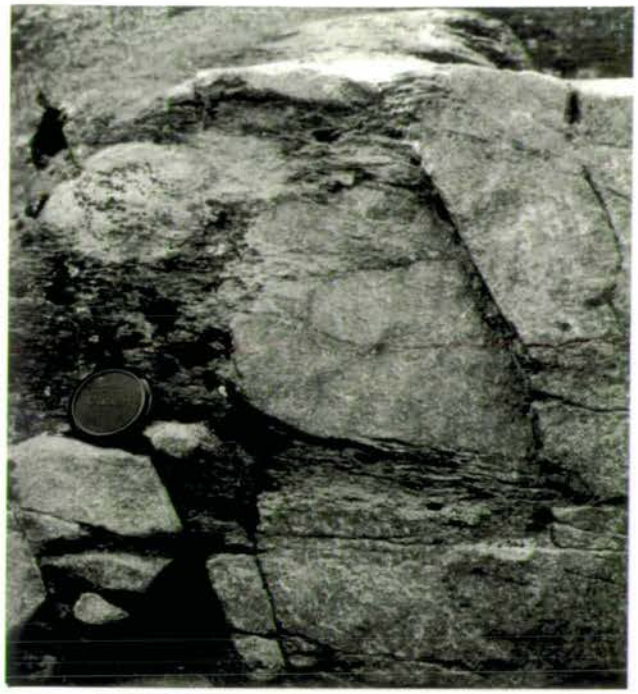

Plate 3.34a: Boundary of the dyke and fractures into the dyke are highly retrogressed. Lens cap is 52 mm in diameter.

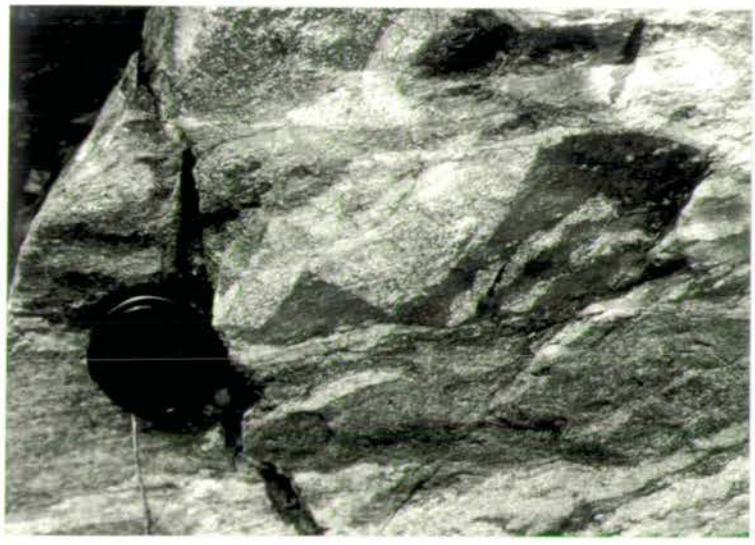

Plate 3.34b: Sharp angular contacts are developed between the dyke and quartzofeldspathic gneiss. The dyke is interpreted as a late intrusion, as brittle fractures which accommodate intrusion are a late event. There is no alteration or reaction rim along the conatcts. Lens cap is 52 mm in diameter.

Plate 3.34c: The dyke (bottom of plate) cross-cuts a highly foliated and folded quartzofeldspathic gneiss. The contact is sharp and undulating. The undulation is interpreted as an effect of post-intrusion compression, creating cuspate structures. Horizontal field of view is approximately 1 to 1.5 m across.

Plate 3.35

Plate 3.35a: Zones of large and small hornblende needles, which create a distinctive dense mesh-like fabric at the contact between the dyke and country rock, are separated by a leucocratic segregation. These zones are attributed to fluid reactions along the contact. Lens cap is 52 mm in diameter.

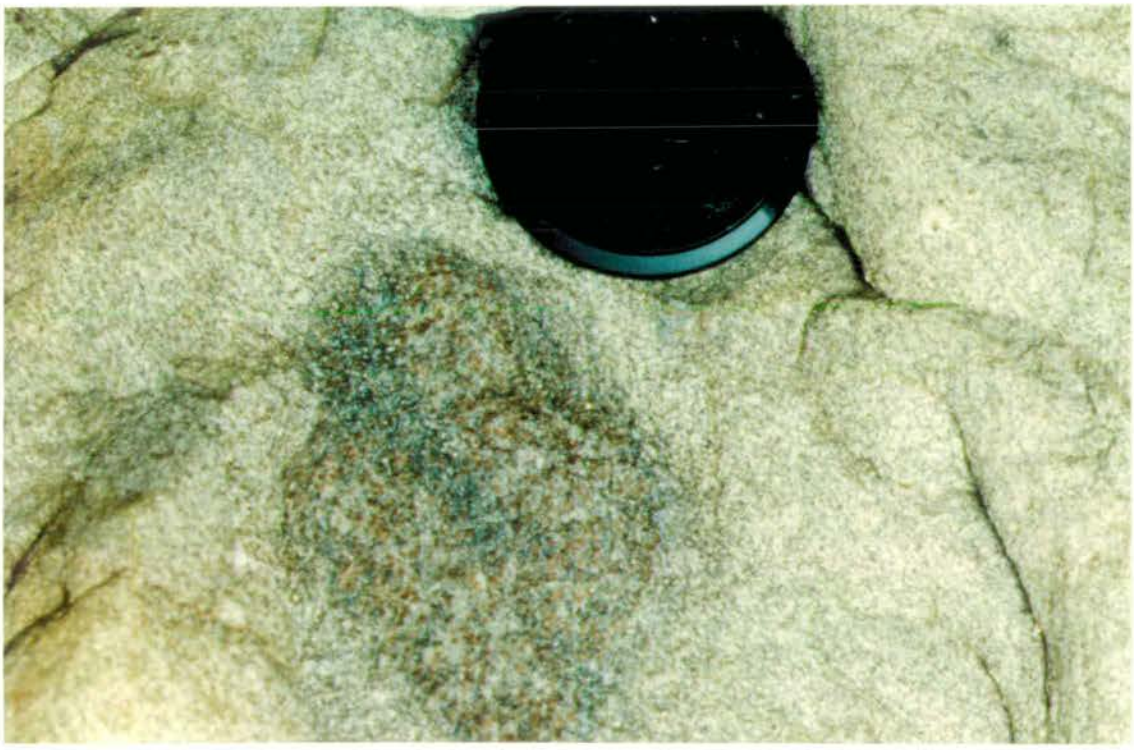

Plate 3.35b: This garnetiferous pod (xenolith) is preserved within a feldspar-rich dyke. The rounded shape and partial assimilation of this pod suggest a stoping mechanism for the intrusion of this dyke. Lens cap is 52 mm in diameter.

quartzofeldspathic gneissic host with sharp angular contacts preserved. Plate 3.35b shows a 5-8 cm diameter xenolithic inclusion within a mottled, quartzofeldspathic, basic dyke. The diffuse boundaries indicate that the xenolith has been partially assimilated into the dyke, however, the core preserves a garnet-mica schist. Although the field observations do not link the dykes with certainty to the Volvi Complex, the geochemistry of the dykes provides very strong support for a correlation (Chapter 5).

3.12 Granites

The main granitic outcrops within the area are the Arnaea granite (*s.s.*) and Askos Augen Orthogneiss Member, plus a range of related apophyses and veinlets (Section 2.6.3), the Modhi granitoid suite (Section 2.6.4) and Lefkoudha granites (Section 2.5.4.4). Further important rocks of granitic composition are locally derived melts within the Vamvakia Purple Gneiss Formation (Section 2.3.2.2) and Rendina Amphibolite Formation (Section 2.2.2.3). A relative time-scale can be developed for these different granitic intrusions based on their intrusion and subsequent deformation histories, and also from the affects they have had on their host lithology.

3.12.1 Arnaea Granite (*see* Section 2.6.3)

A sub-vertical foliation parallel to the regional S_2 foliation is developed within the Arnaea granite, and becomes progressively more intense towards the eastern margin of the granite and its contact with the Askos Marginal Amphibolite Formation (Section 2.3.3.1). This steep foliation is associated with the development of a set of anastomosing shear zones (SZ_{1W}) which maintain a NNW-SSE trend and dip between 45° to 80°W. These anastomosing shear zones become progressively more intense towards the contact with the amphibolite formation, and low-strain pods increasingly more flattened and reduced in size by the encroachment and progressive development of the bounding (S_2) foliations. A second locally developed set of broadly spaced (5-10 m apart) shear zones (SZ_{2W}) with a weak anastomosing character are typified by shear planes with a low-angle of dip (5° to 35°SW). Preserved between both sets of shear zones are relatively undeformed low-strain cores which contain rectangular (1-3 mm long), euhedral, plagioclase phenocrysts, showing poor alignment (Fig. 3.21).

Intensification of the (SZ_{1W}) shear zones and development of the S_2 foliations have generally obliterated the original granitic textures (Fig. 3.21). The progressively developed tectonic fabrics are manifest by grain-size reduction and crystallisation, intense foliation development and ultimately mylonitic banding (Fig. 3.21). Rotation and alignment of foliations into parallelism with shear zones as they are approached is a common occurrence. Due to the extreme flattening of the majority of the shear

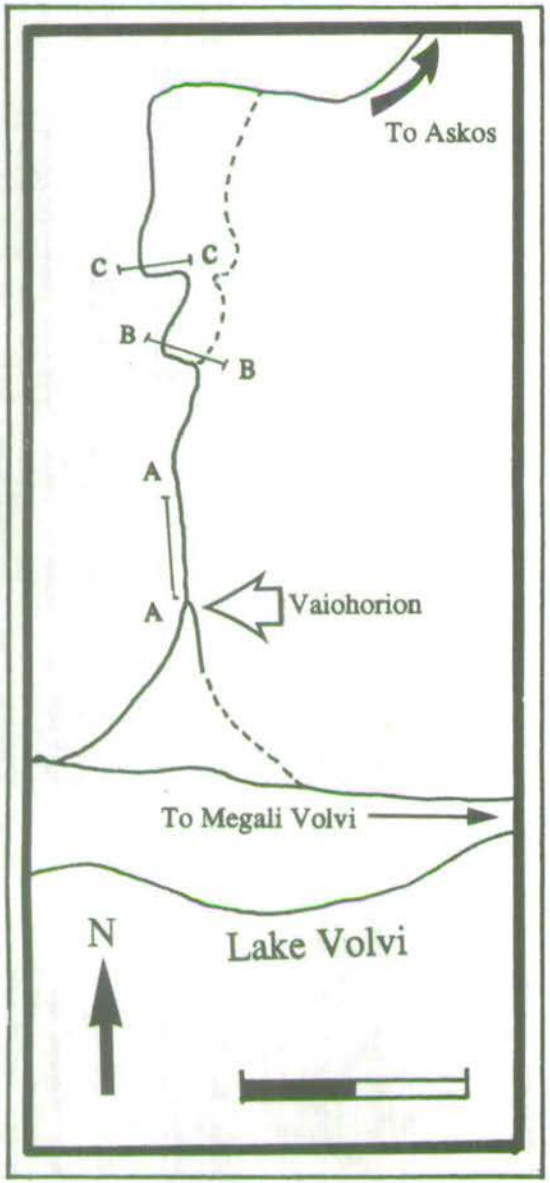

Fig. 3.2.1: Road cuttings along the road from Vaiohorion to Askos. Each section depicts a sequence of increasing low- to high-strain deformation, fabric and structural development related to the onset and progressive evolution of local shear zones.

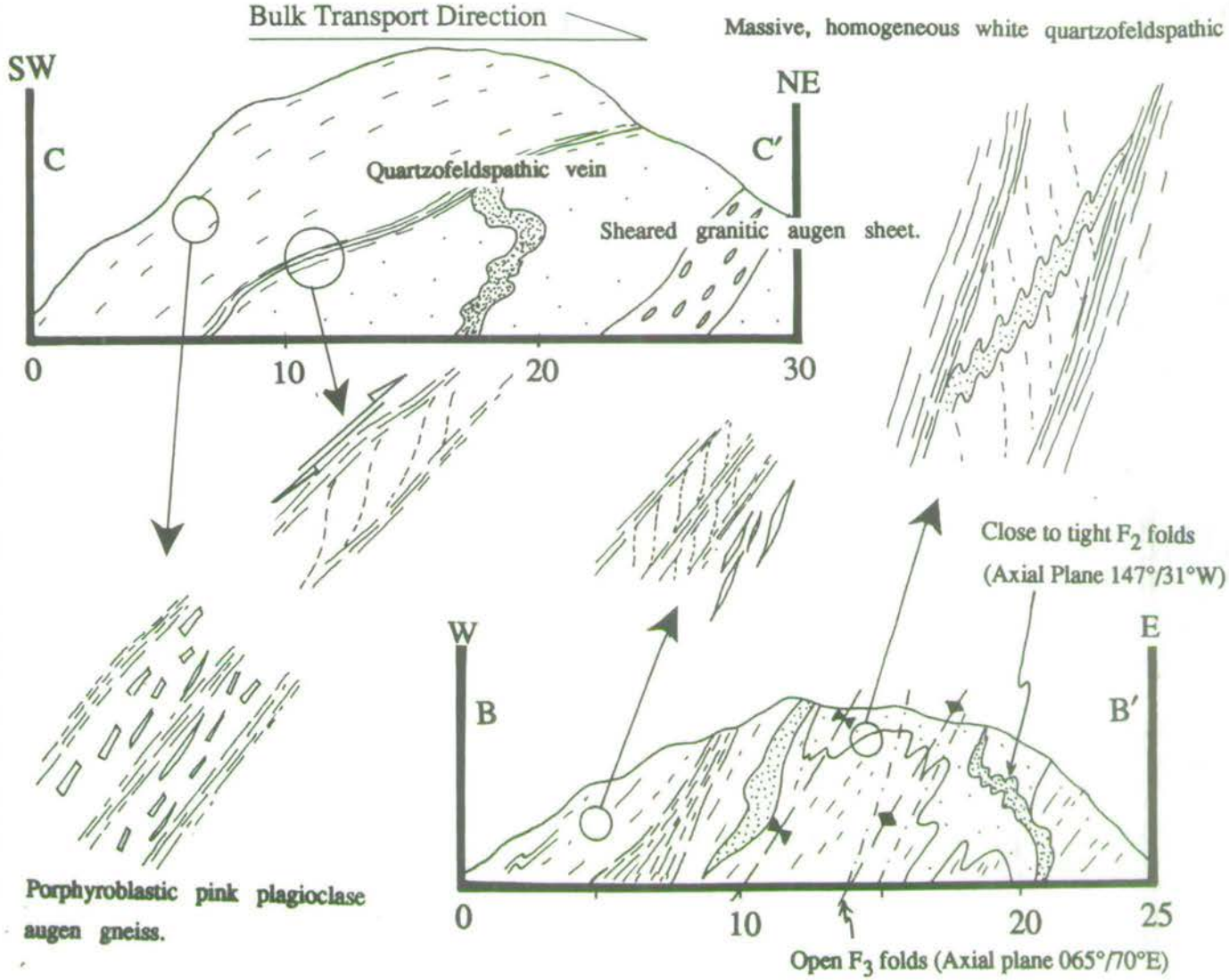

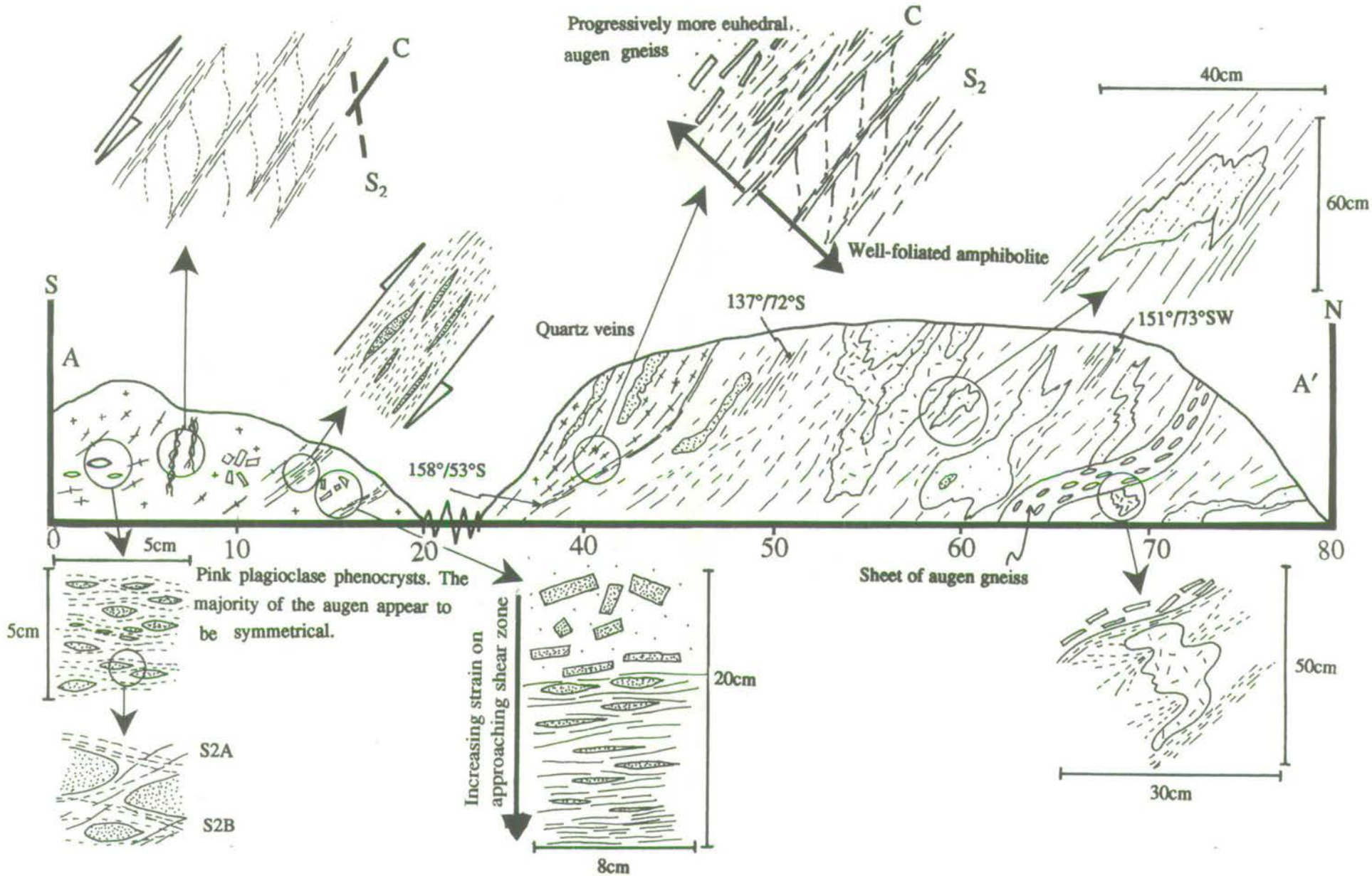
C
S_2
Progressively more euhedral, augen gneiss
C
S_2
40cm
60cm
Well-foliated amphibolite
S
A
Quartz veins
137°/72°S
151°/73°SW
N
A'
158°/53°S
0
10
20
40
50
60
70
80
5cm
Pink plagioclase phenocrysts. The majority of the augen appear to be symmetrical.
5cm
S2A
S2B
Increasing strain on approaching shear zone
20cm
8cm
Sheet of augen gneiss
50cm
30cm

zones, there are rarely any angular discordances between foliations within the low-strain cores and the foliations developed with the shear zones. Hence, the area in general appears to have a single, slightly varying foliation trend.

Evidence for a prolonged period of granitic intrusion during different stages of a progressive deformation is well-developed in the area. Along the Vaiohorion to Askos road, shear zones are developed on a m-scale and it is therefore relatively easy to constrain the sequence of events. The best granitic fabrics are preserved in a number of low-strain cores which are exposed in a series of road cuttings (Fig. 3.21). A series of small, fault-bounded outcrops approximately halfway along and west of the road also show a range of intrusive-deformation relationships (Fig 3.22).

Pre-deformation intrusions: Euhedral, plagioclase phenocrysts are preserved within the cores of low-strain pods. These phenocrysts are progressively flattened towards the shear zone, becoming elliptical augen then porphyroclasts in a mylonite. These fabrics provide evidence for the progressive encroachment of the shear zone as the low-strain cores are flattened and elongated. One of the characteristic features of these sheared augen is that they rarely provide useful kinematic indicators, as they are symmetrically flattened. When an asymmetric augen fabric is developed, it is usually ambiguous with rapidly alternating sense of shear over the space of a few centimetres. Within the outcrops along the road there are also a number of podded veinlets, stringers and sheets which are aligned parallel to and contain the regional foliation (Fig. 3.22). Folded granitic/aplitic sheets and veinlets also occur within low-strain cores. The folds vary from early isoclinal or tight, fold-closures with highly attenuated limbs preserved in low-strain pods. Large (1-2 m wide), late granitic sheets which are open to tightly folded cross-cut the early folds. Within the low-strain cores, the degree of tightness of the different granitic/aplitic sheets can be clearly attributed to their time of emplacement in a progressively deforming regime. However, as the margins of these low-strain cores are approached the ambiguity increases and the local effects of the shear zone obliterate the true time-deformation relationship, as there is also evidence for tightening of folds due to localised shear (Fig. 3.21, 3.22). Within the fault bounded outcrops along the road, locality 1 (Fig. 3.22) exhibits an irregular granitic intrusive contact which cross-cuts a foliated (S_2) fabric within the amphibolite. Several small (1-5 cm wide) irregular shaped amphibolite blocks are isolated within the granite matrix. This outcrop indicates stoping as a mechanism for at least a small part of the granite intrusions in the area.

Syn-Shear Zone Intrusions: This generation of granitic intrusion consists predominantly of veinlets which cross-cut the S_2 foliations and are subsequently stretched in shear zones which are parallel to the same foliation (Fig. 3.22). A

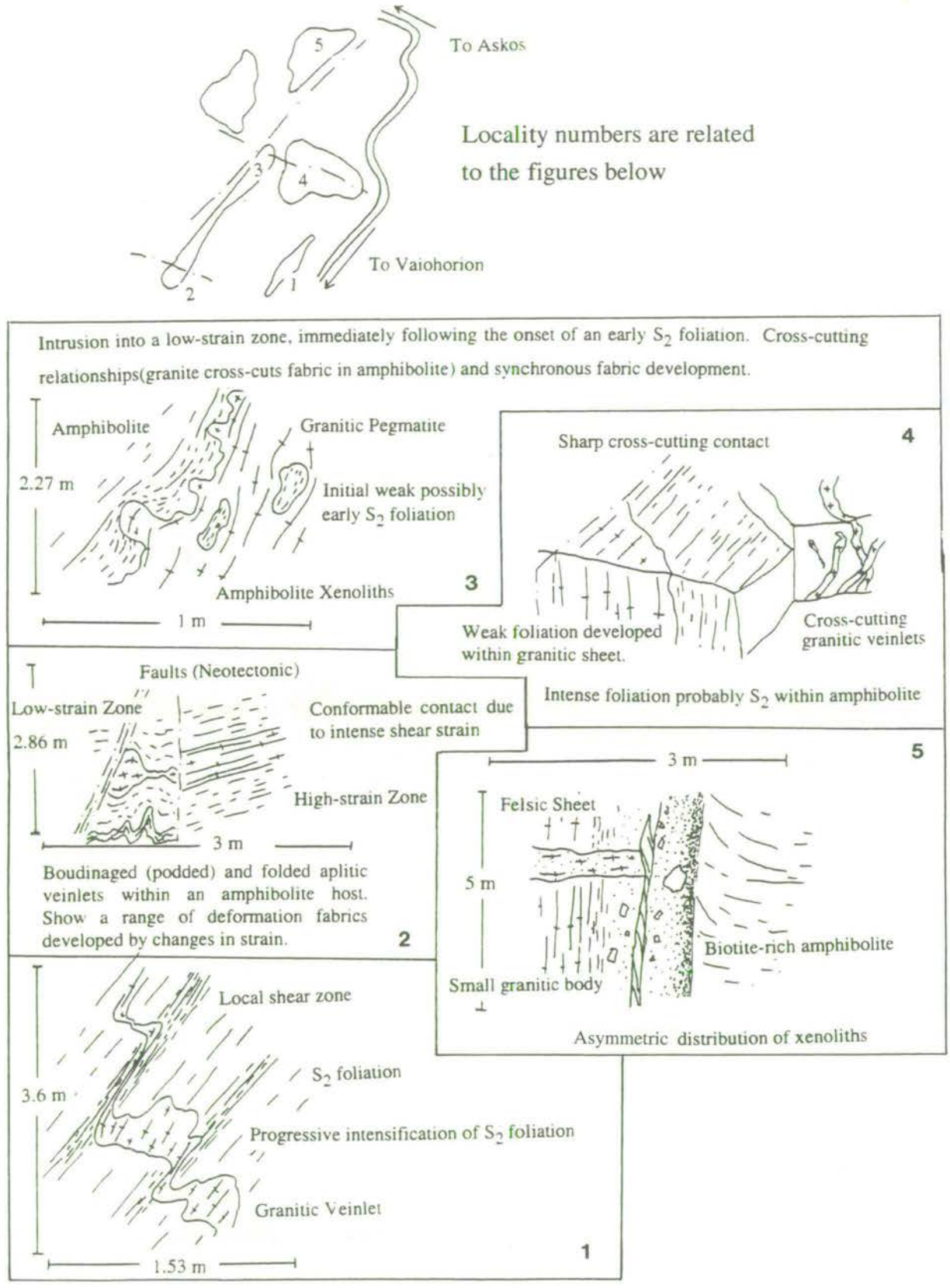

Fig. 3.22: Contact relationships between the Arnaea granite and its envelope lithologies. From the boundary zone between deformed granite and marginal amphibolite lithologies, cropping out to the east of the Askos to Vaiohorion road (Insert, Map B).

number of examples of these syn-shear zone intrusions crop out in the fault bounded outcrops along the road (Fig. 3.22).

Post-Shear Zone Intrusions: This generation of granitic veinlets cross-cuts the S_2 foliations which have been intensified by the shear zones, and the veins also cross-cut one another with only minor realignment. Hence these intrusions preserve a series of ramifying angular net-veining contacts (Fig. 3.22).

The latest generation of granitic intrusion is represented by fine-grained aplitic sheets which must have been intruded during the earliest stages of brittle deformation, as they cross-cut a coarse, angular amphibolite breccia, which is itself truncated and juxtaposed against a more intense zone of faulting within a fine-grained brecciated matrix (Fig. 3.22).

3.12.2 Modhi Granitoid Formation (*see* Section 2.6.4)

This formation acted as an ideal medium for channelling a major ductile shear zone. The formation contains a well-developed sub-vertical foliation with a N-S trend. Within the series of outcrops around Modhi there is a gradational sequence of augen to mylonitic gneisses, from W to E respectively. A number of samples from this sequence are similar to samples from the Arnaea granite. The augen consist of 0.5-1.5 mm long, anhedral to subhedral, plagioclase porphyroclasts wrapped by an anastomosing spaced cleavage consisting predominantly of white-mica.

3.12.3 Lefkoudha Granites (*see* Section 3.6.5)

These granitic outcrops are fairly limited in size, but have had a significant local effect on their host. The granites preserve intrusive contacts which cross-cut the strong (S_2) foliation within the amphibolite host (Plate 3.36), but more commonly have sheared or faulted margins. Fig. 3.20 shows a range of local phenomena which are caused by the granites. Immediately adjacent to the granitic intrusion there is a marked increase in strain, with strong fabrics (augen to mylonites) within the granite and S-C fabrics developed within the amphibolite. Within the amphibolites adjacent to the granite, a locally developed S_3 foliation overprints a progressively rotated S_2 fabric. Within this area, 2-8 m away from the contact, are a number of close to tight, upright folded aplitic veinlets. Further from the intrusion, the folds became more open once the S_2 foliation takes on a more horizontal attitude.

Also associated with the intrusion are a series of ramifying angular net-veins. These veins appear to be the cause of the biotitisation of the amphibolite. These net-veins also exhibit extensional pull-apart structures and are caught up in local shear zones (Plate 3.37).

Plate 3.36

Plate 3.36a: View of intrusive granitic contacts within banded amphibolites, cropping out along the main stream section 1 to 1.5 km west of Lefkoudha. The amphibolite foliation (S_2) is truncated along a sharp contact by a coarse-grained phenocrystic granitic matrix. There are no baked or chilled margins which suggests that the amphibolite was at an equivalent temperature to the granitic intrusion. Lens cap is 52 mm in diameter.

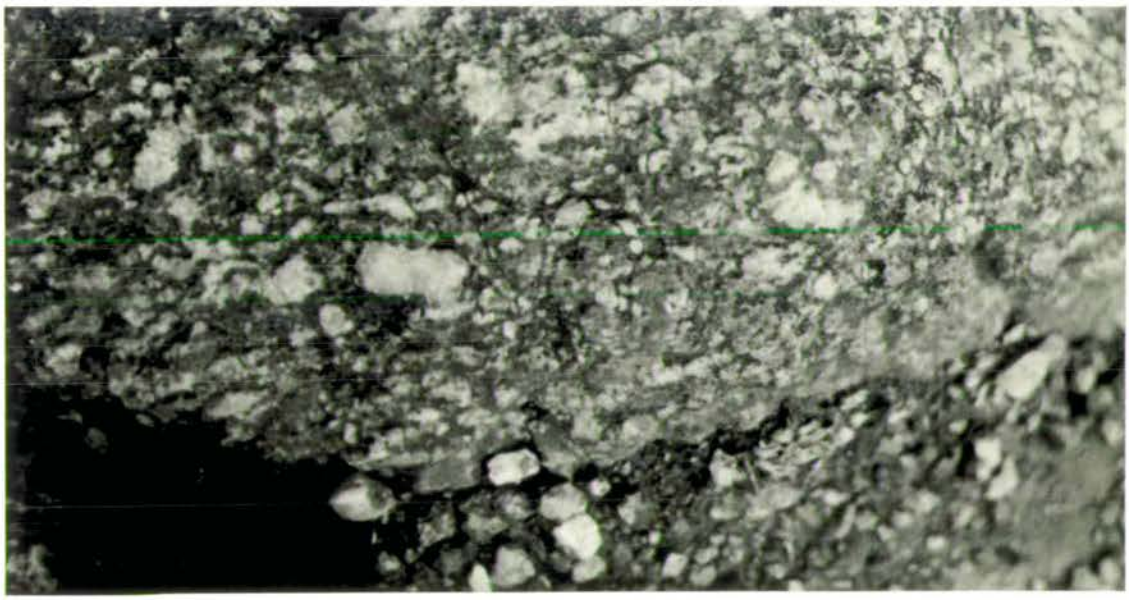

Plate 3.36b: The coarse-grained phenocrystic granite shows the development of a weak fabric. This fabric is defined by the alignment of rectangular euhedral to subhedral phenocrysts and more highly deformed wispy anhedral augen. From the range of fabrics developed, the intrusion is interpreted as being emplaced during the second deformation event.

Plate 3.37

Net-veining and inclusions (pods) within the doleritic to amphibolitic sequences exposed along the main stream sections west of Lefkoudha. The hammer is 57 cm long and the pen and head of the hammer are 14 cm long.

Plate 3.37a: Extensive chaotic net-veining has altered the original dolerite lithology which has subsequently been converted to biotite amphibolite close to the veins. Due to this alteration connected with net-veining large kernels of relatively unaltered dolerite are preserved.

Plate 3.37b: Occasionally angular net-veins are locally developed within the retrograded doleritic host. Note the sense of sinistral "pull-apart".

Plate 3.37c: A large (1-3 m diameter), rounded ultramafic pod is preserved within the doleritic-amphibolitic matrix wrapped by the strong S_2 foliation. A reaction rim (50-70 cm wide) comprised of a fine-grained matrix and a coarse pegmatitic sheet are also preserved.

Plate 3.37

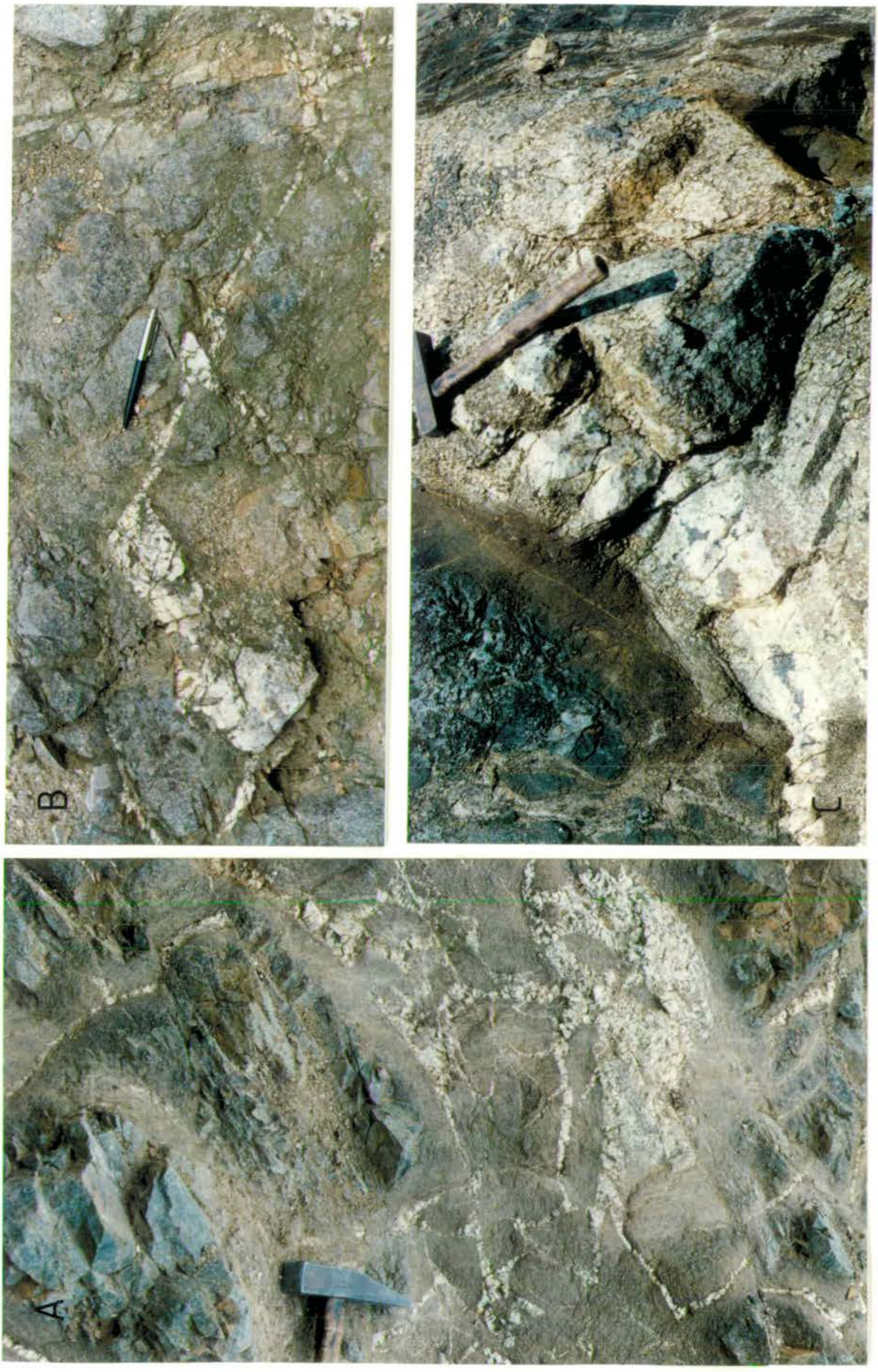

3.12.4 Melts

3.12.4.1 Rendina Amphibolite Formation (see Section 2.2.2.3)

The leucosomes cross-cut the strong banding and foliation (S_2) and are slightly flattened and attenuated sub-parallel to the (S_2) foliation. In several areas, highly attenuated quartzofeldspathic pods are intercalated along the S_2 foliation, and tight to isoclinal folds and ghost-folding are also observed (Plate 3.38a). The variety of structures is interpreted as an effect caused by variations in strain between different areas of the amphibolite sequence. Leucosome segregation is attributed to a melting event post-dating the banding and early foliation development, and pre-dating or synchronous with the late (S_2) foliation.

3.12.4.2 Vamvakia river (see Section 2.3.2)

The most extensive melts within the study area are found within the outcrops along the Vamvakia river (Insert, Map C). The melts are contained within and interpreted as being derived from the purple migmatites. The intrusive or in situ development of these melts have been extensively modified by the anastomosing shear zones. Therefore a wide range of fabrics and intrusive relationships have been developed showing a range of deformation-related fabrics. Good examples of original intrusive cross-cutting contacts are preserved, with angular purple gneiss blocks (5 cm to 1 m long) with a banded fabric surrounded by local melts with sharp cross-cutting contacts which crop out half-way along section A^{IV}-A^{V} (Insert, Map C). These outcrops of purple gneiss within a locally derived melt component are always found as the structurally lowest pods within the river (Plate 3.39). As strain increases towards the margin of the pods, blocks and melt are progressively flattened and realigned parallel to the local shear zone indicating relative motion between the pods. When contacts between pods containing the purple gneiss and melt assemblage are exposed, they are almost always juxtaposed with gabbros or dolerites via narrow (0.5-1.5 m wide) low-angle shear zones (Section 2.3.2.5). The melts can be attributed to pre- and possibly syn-shear zone development. As the gabbros and dolerites (Section 2.3.2.5) are derived from the Volvi Complex (Chapter 5), localised melting within the gneiss is inferred to coincide with emplacement or juxtaposition of the complex.

In pods preserving a medium- to fairly high-strain assemblage of purple gneiss and melts, a complex deformation history overprints the melt fabrics and contacts. In Plate 3.38b the main (S_2) foliation within the purple gneiss (migmatite) is highlighted by a flat-lying and semi-continuous fabric. This is cross-cut by thick 2-4 cm wide leucocratic sheets which are subsequently folded into flat-lying tight F_2 folds. This

Plate 3.38

A range of melt fabrics are developed throughout the area and are particularly well exposed along the Rendina to Asprovalta road (Plate 3.38a) and northern section of the Vamvakia river (Plates 3.38b, c). Coin is 28 mm in diameter and the pen is 14 cm long.

Plate 3.38a: Melts cross-cut the S_2 fabric which is highlighted by the feldspathic component within the amphibolite (the S_2 fabric is flat-lying and runs from left to right). The melts are also close to tightly folded with the S_2 foliation axial planar to fold closures.

Plate 3.38b: Vamvakia Purple Gneiss (migmatite) showing the well-developed main (S_2) foliation. The S_2 foliation is highlighted by a flat-lying and semi-continuous fabric. Rare isolated F_1 or possibly early F_2 folds are preserved along this fabric. Cross-cutting the S_2 fabric is a thick 2-4 cm wide leucocratic sheet coaxially folded into flat-lying tight late F_2 folds. This cross-cutting melt intrusion, post-dates the earliest (S_2) fabrics, but is deformed by the late (S_2) fabric development.

Plate 3.38c: Vamvakia Purple Gneiss (migmatite) with a highly sheared S_2 foliation (right). Within highly sheared purple gneisses (migmatites) the S_2 foliation is well-developed. Hinges of rootless isoclinal folds are preserved as large leucocratic blebs. The S_2 fabric has been cross-cut by an homogeneous medium-grained melt. This cross-cutting melt has an intermediate composition and contains a weak fabric immediately adjacent to the contact. The contact zone is possibly a reaction rim between the two components. This melt generation clearly post-dates the main (S_2) fabric forming event, but is truncated (not in view) by the late shear zones.

Plate 3.38

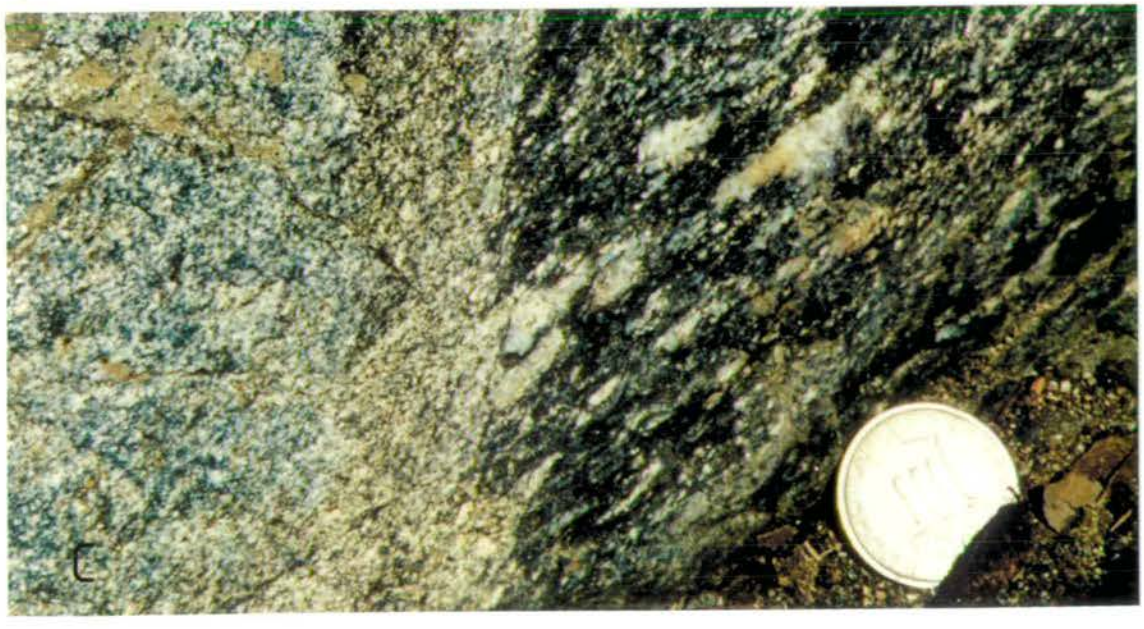

Plate 3.39

A range of melt fabrics intruding purple gneisses which comprise the structurally lowest units outcropping along the northern section of the Vamvakia river (Insert, Map C). Pen is 14 cm long, hammer is 57 cm long and the head of the hammer is 12 cm long.

Plate 3.39a: Angular partially disorientated blocks of banded purple gneiss within a matrix of course-grained mottled leucocratic hybrid melt.

Plate 3.39b: Network of small angular blocks of purple gneiss within a course network of leucocratic melt. Blocks of purple gneiss are partially aligned, sub-parallel with the hammer.

Plate 3.39c: Large attenuated blocks of purple gneiss, approaching a shear zone.

Plate 3.39d: Blocks of purple gneiss within a fine network of hybrid melt. At the top of the photograph adjacent blocks maintain a semblance of their original orientation. Towards the bottom of the photograph, the percentage of melt within the rock has increased and the gneissic blocks have been rotated.

Plate 3.39

melt intrusion therefore post-dates the earliest (S_2) fabrics, but is caught by the late (S_2) fabric development. In Plate 3.38c S_2 foliations within highly sheared purple gneisses (migmatites) are well-developed. The larger leucocratic blebs are actually hinges of rootless isoclinal folds. This (S_2) fabric is cross-cut by a homogeneous medium-grained melt which contains a weak fabric immediately adjacent to the contact. This contact zone is possibly a reaction rim between the two components. This melt generation clearly post-dates the main (S_2) fabric forming event, but is truncated by the late shear zones.

3.12.5 Summary

The main conclusion which can be derived from the intrusive events and structural history within the study area is that the intrusions occurred over a relatively short time span. This factor is one of the main components of the final regional model and interpretation (Chapter 6). The final models suggest the intrusions were probably initiated in the mid Jurassic and terminated in the Late Jurassic/Early Cretaceous.

Successive generations of pegmatites have been intruded into an actively deforming ductile structural regime, with the final deformation recorded within the brittle regime (Section 3.9). Deformation of these successive generations of pegmatites is variable, dependent on their position relative to the shear zones.

The intrusive history of the Volvi Complex (*s.s.*) has not been studied in detail. However, brief observations from the marginal zones (Section 3.10) show a complex multiple intrusive history. Dykes within the envelope of the Volvi Complex have been inferred to be related to the complex (also supported by the geochemistry, *see* Chapter 5). Therefore the Volvi Complex can be unequivocally interpreted as an in situ mafic body (Chapter 6). Only local timing of intrusion can be determined for the dykes into the country rock, based on local structural sequences. This is due to the development of the shear zones.

The Arnaea granite has been dated by de Wet (1989) to give an intrusion age of 155 Ma. As no Volvi dykes cross-cut the granite, dyke emplacement is interpreted to have stopped by the time Arnaea is emplaced. From the geochemistry (Chapter 5) the Arnaea granite and the various granitoid bodies and melts within the Volvi area are interpreted to be the result of crustal anatexis caused by the perturbed local crustal geotherm and the emplacement of the Volvi Complex.

The Volvi Complex contains the main elements of the D_2 deformation event, although not uniformly developed. This may be due to the combined efforts of strain-partitioning and progressive deformation resulting in high and low-strain zones related to shear zones or to successively later intrusions which have simply not been

subjected to the wide range of events. The minor melts are clearly related to the intrusion of the Volvi Complex and the local thermal perturbations which the complex caused. Hence, melts range from syn- to post-intrusion of the Volvi Complex. Products of the melting event are both deformed by, and cross-cut fabrics developed throughout, the D_2 event, which was related to the onset and progressive intensification of shear zones.

CHAPTER 4

PETROGRAPHY AND P-T-t HISTORY

CHAPTER 4

4.1 Introduction

This chapter presents petrographic descriptions of various lithologies (migmatites, gneisses, metasediments, basic and acidic intrusives) from around Lake Volvi, and uses the mineral assemblage and textural data to determine the metamorphic history of the area. Sample localities of the lithologies discussed are marked on the Maps B to H inserted at the back of this thesis. The different lithologies show assemblages and textures, reflecting various parts of a polyphase metamorphic (this chapter) and deformation history (Chapter 3). Early prograde metamorphic assemblages have been disrupted by intense deformation (Chapter 3) making it difficult if not impossible to reconstruct features such as thermal aureoles around igneous intrusions, or regional P-T gradients. Late retrograde assemblages are closely related to this intense progressive deformation, with the youngest, lowest grade assemblages distributed along zones of high strain, and the oldest, highest grade assemblages preserved in low-strain cores.

Three main regional metamorphic episodes (M_{1-3}) are proposed from the evidence derived from this study, in addition to a local thermal event (M_{2T}) associated with the intrusion of the Volvi Complex during the regional M_2 event. M_1 was a migmatite event which affected lithologies representing the original basement of the SMM. Timing of the M_1 event is uncertain but it is possibly Hercynian in age (Chapter 1). The main regional (M_2) metamorphic episode can be correlated with the early (D_2) structural history (Chapter 3) and was a prograde event with its peak in the upper amphibolite-facies. However, granulite-facies assemblages have been found locally developed in the study area, in close proximity to gabbroic bodies, and are interpreted to reflect the presence of a thermal aureole. Similar assemblages and textures of high-T rocks found outside the study area (e.g. Guevgeli; Thessaloniki-Serres road) could similarly be interpreted to reflect local increases in the thermal budget from igneous intrusions. However, evidence for local igneous intrusions is not always present (e.g. along the Thessaloniki-Serres road; Dixon and Dimitriadis, pers. comm.), suggesting that high-T rocks may preserve relics of a regional granulite-facies event. Therefore if granulite-facies assemblages in the study area are actually developed during a regional event, then the igneous intrusions would simply intrude already high-T rocks and so would not develope an aureole. However, from the spatial arrangement of lithologies (Insert, Map C) and the relationships between

locally derived melts and the structures and fabrics developed during the progressive deformation (Chapter 3), a locally developed thermal aureole model is proposed. The most widespread assemblages in the area belong to the last (M_3) metamorphic episode which produced a progressive sequence of retrograde assemblages associated with the development of the late D_2 shear zones (Chapter 3). A sequence of M_3 assemblages can be identified representing retrogression from early upper greenschist to late lower greenschist-facies conditions. To the west of the complex the M_3 metamorphic episode has largely overprinted all evidence for the early (M_{1-2}) metamorphic history, but to the east of the Volvi Complex, early (M_{1-2}) assemblages are preserved, as low-strain cores wrapped by anastomosing M_3 shear zones (Chapter 3). These low-strain cores also preserve evidence for local thermal overprints caused by the basic (Volvi Complex) and acidic (Arnaea granite) intrusions. The main points considered in this chapter are:

i) What are the mineral assemblages developed in different lithologies?
ii) Which minerals are stable or unstable within which fabric forming event?
iii) How do the different lithologies vary with increasing strain?
iv) Can local thermal events associated with intrusions be identified?
v) Which fabrics and assemblages can be correlated between the country rock and basic intrusions?

This chapter is divided into sections which discuss the mineral assemblages and textures, and their relationship to progressive fabric development, for each of the major rock types. The lithologies within the area can be divided into four broad categories, i) migmatites (*s.s.*) and migmatitic gneisses (Section 4.4), ii) ortho-gneisses, para-gneisses and semi-pelitic to pelitic schists (Section 4.5), iii) marbles and calc-silicates (Section 4.6), iv) amphibolites and basic intrusives (Section 4.7). Due to the correlation between progressive deformation and an increase in retrogression, the lithological categories are reviewed from their low-strain to high-strain examples and relevant metamorphic episodes. At the end of each section these relationships between mineral assemblages (Table 4.1) and textures are used to propose qualitative P-T-t models. Correlation of the assemblages, textures and fabrics developed during the successive metamorphic episodes and the individual qualitative P-T-t models are combined at the end of the chapter (Section 4.8) to produce a simple metamorphic framework which can be used to determine the tectonic setting of the Volvi Complex.

Table 4.1: Examples of the mineral assemblages or sub-assemblages diagnostic of the metamorphic facies present in the study area (after Yardley, 1989).

FACIES	METABASIC ROCKS	PELITIC ROCKS (with Quartz)
Albite Epidote Hornfels	albite + epidote + actinolite + chlorite. actinolite+oligoclase.	muscovite + biotite + chlorite
Hornblende Hornfels	hornblende + plagioclase ± cummingtonite	aluminosilicate + biotite + muscovite
Greenschist	actinolite epidote ± albite ± chlorite (*low temperature zone*). hornblende ± actinolite + albite + chlorite+ epidote ± garnet (*high temperature zone*).	chlorite + muscovite + albite (*low temp*). chlorite + muscovite + biotite + albite garnet + chlorite + muscovite + biotite + albite (*high temp*)
Amphibolite	hornblende + plagioclase ± epidote ± garnet	staurolite, kyanite + muscovite (*low temp*). aluminosilicate + K-feldspar ± muscovite + cordierite or garnet aluminosilicate + garnet + cordierite, *no* K-feldspar (*high temp*).
Granulite	orthopyroxene + clinopyroxene + plagioclase ± olivine ± hornblende (*low pressure*). garnet + clinopyroxene + orthopyroxene + plagioclase ± hornblende (*medium pressure*). garnet + clinopyroxene + quartz + plagioclase ± hornblende (*high pressure*).	cordierite + garnet + K-feldspar + aluminosilicate (*medium pressure*). kyanite+K-feldspar (*high pressure*).

4.2 Previous Work

Previous work in the area is limited (Chapter 1), with metamorphic studies restricted to four main sources (Dixon and Dimitriadis, 1984; Papadopoulos and Kilias, 1985; Sakellariou, 1990; Dixon, pers. comm.).

4.2.1 A Review: Dixon and Dimitriadis (1984, pers comm.)

Dixon and Dimitriadis (1984) concentrated predominantly on lithologies within the Volvi Complex with only minor discussion of the country rock. From observations made outside the Volvi Complex and along the Thessaloniki to Serres road, Dixon and Dimitriadis (1984) interpreted the central and eastern part of the SMM (basement and Triassic/Jurassic cover) to have been affected by an amphibolite-facies regional metamorphic and deformational event in the Upper Jurassic-Early Cretaceous. This interpretation provoked Dixon and Dimitriadis (1984) to present a new model for the tectonic history of the SMM as their results and interpretation disagree with the original interpretation of Kockel *et al.*, (1971, 1977; *see* Chapter 1).

Metasedimentary sequences with intercalated slivers of marble occur immediately adjacent to the western margin of the Volvi Complex (Volvi Metasedimentary Group; Insert, Map D), and according to Dixon and Dimitriadis (1984) show no internal structural or metamorphic discontinuities. They were interpreted as a complex sequence of interbedded marbles and dolomites, calcareous, pelitic and graphitic schists (Dixon and Dimitriadis, 1984).

Assemblages in the metasedimentary schists contain syn-tectonic staurolite and garnet. Minor dolomitic interbeds have undergone syn-metamorphic reactions with adjacent carbonate-free horizons, indicating that the various lithologies were juxtaposed prior to metamorphism (Dixon and Dimitriadis, 1984). Dixon and Dimitriadis (1984) interpreted the main fabric-forming event in this part of the massif to have occurred under *regional metamorphic* conditions of *at least staurolite grade*. They regarded this regional metamorphic event to be Jurassic in age (Chapter 1), indicating a more comprehensive overprinting event at this time than the interpretation of Kockel *et al.*, (1977).

Dixon and Dimitriadis (1984) interpreted the dominant fabric in the Volvi Complex to be syn-metamorphic and even in part a late magmatic fabric. Likewise, the Kerdilion migmatitic gneisses to the east show high-grade mineral assemblages, syn-metamorphic fabrics and generally little evidence of retrograde reaction (Dimitriadis, 1974). Dixon and Dimitriadis (1984) therefore concluded that one or more post-Palaeozoic regional metamorphic events affected the SMM and its cover.

Dixon and Dimitriadis (1984) attributed the mineral assemblage and appearance of the metamorphosed gabbros to two largely independent processes (saussuritization "a fluid-infiltration-driven post-metamorphic-peak metasomatic process" and metamorphism). In completely undeformed parts of the Volvi Complex, relict masses of "fresh" gabbro occur with distinctive purplish plagioclase feldspars and a characteristic extreme toughness. These gabbroic masses may be up to a few hundred metres across, but in more deformed areas are commonly reduced to metre-sized rounded "kernels" transected by planar alteration zones (Dixon and Dimitriadis, 1984). The feldspars in these alteration (saussuritization) zones are milky white and pyroxenes are rimmed by, or transformed to, fine-grained green amphibole. A thin white veinlet, 1-2 mm across, frequently lies along the centre of the amphibolite alteration zones representing the locus of fluid infiltration. The saussuritization zones within the highly deformed areas can be traced into less deformed parts of the body where they are less prominent, but clearly *post-tectonic* in that they cut the schistosity and are unrelated in their orientation to shear zones. The strongly deformed gabbros are also pervasively saussuritized in appearance being typically milk-white/deep-green in felsic and mafic areas respectively (Dixon and Dimitriadis, 1984).

Spectacular coronas are developed at the junctions between olivine and plagioclase in the completely undeformed and unsaussuritized gabbros. These coronas comprise, from olivine outwards, layers of orthopyroxene, garnet and hornblende. Within increasingly deformed gabbros, saussuritization reactions shown by the growth of randomly orientated zoisite porphyroblasts within the feldspar and complex hydration reactions in the coronas around clinopyroxenes and remaining olivine are developed. Extensively deformed gabbros, however, typically contain no olivine and consist of hornblende, garnet, plagioclase and an epidote group mineral, with well-annealed textures even in foliated rocks. Random growth of a Ca-Al-silicate in the plagioclase indicates subsequent saussuritization of these rocks (Dixon and Dimitriadis, 1984).

Dixon and Dimitriadis (1984) interpretated the coronitic and sheared gabbros as partial and more or less complete transitions respectively, to essentially the same high-grade amphibolite-facies assemblage. Although deformation clearly promoted recrystallisation of gabbro to gabbroic garnet amphibolite it was not necessarily synchronous with the growth of the new assemblage, which may have instead inherited an anisotropic fabric from a higher temperature stage when the igneous assemblage was still intact (Dixon and Dimitriadis, 1984). Saussuritization occurred still later and is most prominent as a secondary vein-controlled process in the

undeformed gabbros. The saussuritised gabbros had greater modal abundance of calcic plagioclase and no preferential schistosity-parallel paths for the entry of metasomatizing fluids.

Similar patterns of variable, late saussuritization were recognised in the fine-grained dyke rocks but the undeformed rocks show little or no evidence of saussuritization. Instead, rocks commonly have hornfels-like textures with assemblages of garnet-plagioclase-hornblende ± clinopyroxene-epidote (or zoisite), and even hornblende-hypersthene-plagioclase (Dixon and Dimitriadis, 1984). Schistose and striped amphibolites have a range of textures and mineral assemblages and although many are dominantly hornblende-garnet-plagioclase-epidote/zoisite rocks, some evidently equilibrated at lower temperatures as they contain an assemblage of hornblende-plagioclase-epidote-chlorite-sphene-quartz in apparent textural equilibrium (Dixon and Dimitriadis, 1984). The "tiger-striped" metasediments contain plagioclase + epidote in the leucocratic bands and hornblende-(green)diopside-garnet-epidote-plagioclase in the mafic layers. Dixon and Dimitriadis (1984) interpreted these observations as indicating a generally consistent peak metamorphic grade (amphibolite-facies) for assemblages in completely undeformed rocks as well as in foliated gabbros, amphibolites and metasediments.

These conclusions were supported to a surprising degree by some preliminary geothermometry. Dixon and Dimitriadis (1984) analysed hornblende-garnet pairs in a small number of representative rocks and applied a calibrated Mg/Fe^{II} exchange thermometer (Graham and Powell, 1984). The results from four different rocks are summarised below.

Sample		T°C	Mol% Pyr
ΛΛX2	Coronitic Metagabbro	720	37
(Grt+Hbl in contact in a corona around olivine)			
MB5	Fine-grained "porphyritic" amphibolite	753	19
(Plag-Grt-Hbl-Ilm)			
ZN3	Undeformed fine-grained dyke	772	9
(Plag-Grt-Cpx-Ep)			
ANMΠO4	"Tiger-striped" metasediment	768	7
(Grt-Hbl-Plag-Ep-Ilm)			

Dixon and Dimitriadis (1984) noted the remarkable consistency of the implied temperature of equilibration for the deformed and undeformed igneous rocks, and also metasediments sampled. Taken with the evidence of an overlap in time between magmatism and deformation, Dixon and Dimitriadis (1984) concluded that these assemblages were equilibrated during the initial cooling of an actively deforming, recently intruded, mafic complex.

The presence of a sheeted-dyke complex implies some form of active crustal extension. Dixon and Dimitriadis (1984) inferred that this complex was intruded at a significantly deeper level than a typical mid-ocean ridge ophiolite, since the garnet-orthopyroxene coronas and the pervasive high-grade garnet amphibolite assemblages with both clinopyroxene and orthopyroxene contrast with the typical sub-sea floor epidote-amphibolites of ophiolitic sheeted-dyke complexes (Gass and Smewing, 1974). Dixon and Dimitriadis (1984) proposed that the Volvi Complex initially equilibrated at temperatures some 200-250°C higher than the staurolite-bearing schists immediately adjacent to it, and that the envelope lithologies never reached the higher temperatures due to the absence of partial melting evidence.

4.2.2 A Review: Papadopoulos and Kilias (1985)

A complimentary study to that of Dixon and Dimitriadis (1984) was made by Papadopoulos and Kilias (1985) who worked predominantly on country rock lithologies to the west of the Volvi Complex. Papadopoulos and Kilias (1985) recognised three main metamorphic episodes within this area.

Their first metamorphic episode was a syn- to post-deformation, prograde event that reached the amphibolite-facies. Typical metasedimentary assemblages consist of garnet ± kyanite ± staurolite ± muscovite ± biotite + quartz + plagioclase + accessories with fabrics consisting of large porphyroblastic minerals (e.g. garnet, plagioclase) containing abundant fine-grained inclusions (e.g. muscovite, quartz) within a medium- to fine-grained matrix composed of varying modal proportions of all the minerals. This suggests a prograde metamorphic event as neither an earlier phase of mineral growth or change of mineral colouration was observed (Papadopoulos and Kilias, 1985).

Papadopoulos and Kilias (1985) proposed that evidence for the main metamorphic event was also preserved in the gabbro-amphibolite lithologies. They distinguished three different parageneses in these rocks of magmatic origin, which were categorised and grouped with respect to their spatial distribution in the field.

i) Margin Group:

green hornblende + plagioclase ± biotite ± garnet ± epidote/ clinozoisite/ zoisite + titanite/ rutile ± quartz ± chlorite + accessories

ii) Intermediate Group:

green and brown hornblende ± pyroxene + plagioclase ± garnet ± epidote/ clinozoisite/ zoisite ± chlorite ± biotite + titanite/ rutile + accessories

iii) Central Group:

olivine + pyroxene + brown hornblende ± garnet ± biotite ± epidote/ clinozoisite/ zoisite ± chlorite + titanite/ rutile + accessories

Olivine, pyroxene, brown hornblende and plagioclase are considered to be relics of the original magmatic assemblage, which is progressively lost in the intermediate and the marginal areas. Pyroxenes are changed partly to hornblende, while old brown hornblendes change to green hornblende and minerals of the epidote group are newly formed. The initial descriptions of the assemblages are similar to those of Dixon and Dimitriadis (1984). The basic interpretations of Papadopoulos and Kilias (1985) for these assemblages do not distinguish between the metamorphic and metasomatic assemblages of Dixon and Dimitriadis (1984).

The second metamorphic episode was a retrograde, syn-tectonic greenschist-facies metamorphic event. Papadopoulos and Kilias (1985) dated white-mica, biotite and hornblende from metasediments using K/Ar and Rb/Sr techniques and derived a Cretaceous age for this event. Further textures developed in this event include the formation of inclusion-free garnet rims around older dusty inclusion-rich garnet grains (Papadopoulos and Kilias, 1985). The M_2 recrystallisation episode in the gabbro-amphibolite group was represented by further growth of green hornblende and biotite.

The third metamorphic episode was a very low-grade greenschist-facies event regarded as the final stage of the M_2 episode or as a younger and distinct metamorphic episode (Papadopoulos and Kilias, 1985). Reactions and new mineral assemblages in the metasediments include marginal chloritisation of staurolite + kyanite, complete disintegration of garnet + biotite, pseudomorphs of chlorite after biotite and garnet, and decomposition of plagioclase and K-feldspar. In the gabbro-amphibolite group, partial chloritisation of biotite and hornblende is developed while further decomposition of plagioclase as well as a further crystallisation of epidote and zoisite occur (Papadopoulos and Kilias, 1985).

4.2.3 A Review: Sakellariou (1990)

The final source for comparable metamorphic studies within the Lake Volvi area is Sakellariou (1990). Five metamorphic episodes were recognised based on assemblages and textures from the country rock lithologies south of Lake Volvi.

The first metamorphic episode described by Sakellariou (1990) was an inferred regional eclogitic event of unknown age indicated by minor outcrops preserved within amphibolitic rocks of the SMM (see also Dimitriadis and Godeltsas, 1991). This event is probably part of the basement history and therefore of uncertain

age and character, but possibly related to the inferred migmatitic Hercynian event (Chapter 1).

The second metamorphic episode (the first metamorphic event observed to the S of Lake Volvi but inferred to be the second event of the Vertiskos Unit) was a prograde event reaching the middle amphibolite-facies (almandine/epidote-amphibolite-facies). Typical metasedimentary mineral assemblages are quartz + muscovite + garnet (I) + biotite + staurolite + kyanite + Mg-chlorite. Garnets are either syn-tectonic with typical rotational structures or post-tectonic. Muscovite, biotite and Mg-chlorite crystallise parallel to the S_1 foliation (Sakellariou, 1990). This event is equivalent to the regional amphibolite-facies event of Dixon and Dimitriadis (1984), also identified by Papadopoulos and Kilias (1985) and this study.

The third metamorphic episode (the first metamorphic event to affect the Arnaea granite) was a retrograde event in the almandine amphibolite-facies to upper greenschist-facies. Typical metasedimentary assemblages are quartz + muscovite ± garnet (II) + biotite (II) + staurolite (II) + Mg-rich chlorite. Biotite, muscovite and Mg-chlorite are developed parallel to the main S_2 foliation. Garnets are either pre- or syn-deformational. The minerals formed during the earlier prograde stage are either deformed or broken down (Sakellariou, 1990). This correlates with the retrograde events previously described and is comparable to the early M_3 event of this study.

The fourth metamorphic episode was a weak locally-developed retrogression to the lower greenschist-facies. Typical metasedimentary assemblages are:

(a) chloritoid + Fe-chlorite + muscovite + quartz

(b) biotite (III) + garnet (III) + Fe-chlorite + muscovite + quartz

Assemblage (a) is stable under *all* greenschist P-T conditions, whereas assemblage (b) is restricted to upper greenschist P-T conditions (almandine sub-facies). Fe-chlorite, muscovite and biotite are parallel to the S_3 foliation, while retrogression of early garnets to Fe-chlorite + staurolite assemblages and staurolite to muscovite + possibly sericite assemblages is developed. There is also extensive deformation of those minerals which do not recrystallise. Graphitic schists of the Nea Madhitos Group and quartz + muscovite + Fe-rich chlorite + chloritoid are indicative of metamorphic conditions of the upper greenschist-facies (Sakellariou, 1990). Similar assemblages and textures observed during this study are attributed to the late M_3 event in this thesis.

The fifth metamorphic episode occurred under low greenschist-facies conditions. This event is identified by partial recrystallisation of quartz and Fe-rich chlorite + white-mica (possibly phengite) growing parallel to the S_4 foliation.

Assemblages of quartz + Fe-chlorite + muscovite (possibly phengite) occur locally and are stable under lower greenschist-facies conditions (Sakellariou, 1990). Evidence for this metamorphic episode is poorly developed and usually attributed to the latest stages of the M_3 event (this study). Although descriptions of lithological assemblages by Sakellariou (1990) are fairly detailed, there is no indication of a metasomatic or thermal event, as identified in this study north of Lake Volvi.

4.3 P-T Paths and Reaction Grids

The metamorphic peak represents only one instant during the evolution of a rock, and much more information regarding metamorphic and tectonic processes can be obtained if evidence is preserved of other stages of the metamorphic history. Such information is commonly used to deduce a pressure-temperature path. Ideally these depict both the prograde and retrograde path, but high-grade rocks rarely preserve evidence of the prograde evolution.

A useful approach towards determining the P-T path is to use mineral reaction textures. If the position and orientation of a given reaction in P-T space is well known, then the texture preserving that reaction can be related to a vector in P-T space. If several reactions are identified, a series of P-T vectors can be determined and a pressure-temperature path defined. This approach is best suited to lithologies which commonly preserve reaction textures and have well-understood phase relationships. It is difficult to satisfy both of these conditions since reaction textures are most widespread in those lithologies with complex phase relationships, and consequently those lithologies for which the phase relationships are poorly understood.

Reactions in high-grade metabasites are relatively simple and well-studied (e.g. Green and Ringwood, 1967; Liou, 1971a; Perkins and Newton, 1981; Saxena and Eriksson, 1985), although they become more varied under low-grade conditions (e.g. Nitsch, 1970; Winkler, 1979). In contrast, metapelite lithologies have complex phase relationships involving characteristic index minerals, and commonly preserve reaction textures. The sensitivity of pelitic compositions to pressure and temperature change is reflected in the proportion of metamorphic studies based on metapelite compared to its volumetric abundance in metamorphic terranes. Since the pioneering work of Barrow (1893, 1912) in the Scottish Highlands, pelitic lithologies have been used as an indicator both of spatial metamorphic variation within a terrane, as in the Barrovian example, and of temporal metamorphic variation within individual specimens preserving mineral reaction textures or various generations of porphyroblasts or mineral inclusion.

Mineral reactions can be divided into "discontinuous" and "continuous" types. Discontinuous reactions occur at a fixed pressure for a given temperature, and are represented as lines in P-T space. A rock of fixed bulk composition is only stable at one point on a discontinuous reaction boundary in P-T space. Continuous reactions occur over a range of pressure at a given temperature, and are represented as bands in P-T space. A rock of fixed bulk composition is stable within the reaction band over a range of pressures and temperatures, but the compositions of at least two participating phases change as the reaction proceeds with changing pressure and temperature.

Discontinuous reactions, and assemblages comprising all the participating phases in a discontinuous reaction are referred to as "univariant". Evidence for discontinuous reactions in an individual rock sample is less common than evidence for continuous reactions. However, an understanding of the disposition of continuous reactions in P-T space is important because the fields where continuous reactions occur are bounded in P-T space by a fixed grid of discontinuous reactions. This is commonly called a petrogenetic grid, and many such grids have been published for particular rock compositions. This chapter uses appropriate P-T grids to propose qualitative P-T paths for the rocks of the Lake Volvi area using constraints from mineral assemblages and textures.

4.4 Migmatites (*s.s.*) and Migmatitic Gneisses

Several lithological members (with varying bulk compositions) representing a migmatitic basement, are interpreted to have been developed in a metamorphic event (M_1) of uncertain age (possibly Hercynian, *see* Chapter 1), are preserved within the area (Chapter 2). The earliest S_0 fabrics which have been preserved in the area were developed during this metamorphic event (Chapter 3). The migmatitic lithologies have subsequently been subjected to varying episodes of the complex polyphase deformation (Chapter 3) and metamorphic history (this Chapter). To the west of the Volvi Complex, unambiguous outcrops of migmatite are rare and when present have been extensively retrogressed to the greenschist-facies during the M_3 metamorphic episode and overprinted by late D_2 and D_3 structures. Migmatitic outcrops related to an early basement are rarely found to the south of Lake Volvi. This lack of migmatitic lithologies is attributed to intense D_2 and D_3 deformation and retrogression to the lowest greenschist-facies in the M_3 metamorphic event. To the east of the Volvi Complex, within the Kerdilion Group, migmatites are poorly exposed and only occasionally preserved in low-strain zones (Chapter 2). Relationships with adjacent lithologies have to be inferred and these examples are therefore of limited use in

assessing the progressive deformation and metamorphic history of the area. The best outcrops of migmatite are represented by two well-exposed suites, which are preserved in variable states of strain along the northern section of the Vamvakia river (Insert, Map C). These migmatites show progressively-developed fabrics which preserve evidence for deformation throughout early (D_1 and early D_2) structural events, culminating with the complete transposition of early fabrics within main D_2 shear structures (Chapter 3). Locally-derived melts (Chapter 3; Insert, Map C) and granulite-facies assemblages (this chapter) indicate that there was either a local thermal perturbation event from the amphibolite-facies conditions that typify most syn-M_2 assemblages, or that the regional metamorphism actually developed at the granulite-facies with only remnants now preserved in low-strain zones. However, this study suggests that the granulite-facies assemblages were probably related to the intrusion of the Volvi Complex and therefore are of local extent (Chapter 3). The two main migmatite suites are now described.

4.4.1 Black and White Migmatites

The least deformed members of this migmatite suite, and the type section for the earliest D_1 fabrics (Chapter 3) and mineral assemblages preserved in the study area, crop out at Migmatite Bluff (Section 2.3.2.1; Insert, Map C). Progressively deformed (sheared and mylonitised) members are associated with the increased strain towards and into shear zones (Chapter 3). The general mineral assemblage for these variably deformed migmatites consists of:

quartz + plagioclase + K-feldspar + garnet + biotite ± white-mica

Accessories also commonly present are sphene, epidote, zoisite, allanite, chlorite, apatite and ilmenite. The bulk compositions and modes of this migmatite suite remain remarkably constant throughout the different strain states. The main variations and changes in textural characteristics are progressive grain-size reduction with increase in strain related to the development of the anastomosing shear zones.

In the low-strain member, quartz, plagioclase and K-feldspar are closely associated and represent the main components of the leucocratic segregations (S_0, Chapter 3). Subgrain textures (e.g. undulose to polycrystalline extinction, mortar structures) are developed along with a host of mineral intergrowths (symplectites, myrmekites, perthites). Euhedral garnet porphyroblasts occur in all the migmatite samples and are associated with biotite in diffuse clusters and weakly developed bands. Distribution of these garnet-biotite associations is random throughout the low-strain migmatite members and they represent one of the main constituents of the melanosome.

Biotite is the most variable mineral within this migmatite suite. Changes in colour vary from the typical pleochroic dark to light-green which contributes towards the black and white aspect of this rock, to a dark reddish-brown colouration (Sample, 90VAMR75) more typical of biotite within the Purple Migmatitic Gneisses (Section 4.3.2). This alteration in the colour of biotite only occurs in close proximity (0.5 to 1.5 m) to lithologies with a distinctive purple aspect such as the Purple Migmatitic Gneisses (Section 4.4.2) or Purple Schists (Section 4.5.2). The alteration is attributed to reaction caused by a very local thermal overprint. In the low-strain members, long laths of biotite are rare and when preserved tend to be kinked or folded. Biotite laths are more commonly short and stubby with a well-developed cleavage.

White-mica is generally absent from the main assemblage, however, it may be found along D_3 fractures. Accessory minerals are present in varying quantities.

With an increase in strain the three main leucosome minerals are progressively deformed, and subgrain textures and mineral intergrowths are progressively simplified and obliterated due to recrystallisation and grain-size reduction. At the same time garnet porphyroblasts become progressively subhedral in shape and are progressively embayed and fractured, with the volume of inclusions (predominantly quartz) increased. Banding is progressively well-defined, with alignment of the garnet porphyroblasts and associated biotite laths parallel to the main (S_2) foliation.

Within high-strain samples, biotite is partially altered to chlorite and in sample 90VAMR78, is pseudomorphed by a fine-grained sericitic matrix.

With increasing strain there is a minor increase in the volume percentage of white-mica aligned along a strong S_2 shear fabric. However, when the rock is intensely sheared and mylonitised (Sample 90VAMR49) the large laths of white-mica are also sheared and reduced in size with no new white-mica formed.

Accessory minerals are present in varying quantities. Only the number of zoisite porphyroblasts increase in quantity with the most intense shear and mylonitisation, possibly reflecting the alteration of (M_2) plagioclase. Allanite porphyroblasts are fairly common and are most probably an indication of a primary magmatic origin, which has been largely obscured by the later shear fabrics.

In the most deformed high-strain members, rounded porphyroclasts of plagioclase-K-feldspar-zoisite are preserved in a fine-grained ultramylonitic quartz-plagioclase-K-feldspar-white-mica matrix.

This migmatitic suite is peculiar in that there is a general lack of change or alteration (or at least relatively minor) of the mineral assemblage with time and deformation. This probably reflects the unreactive nature of the mineral assemblage.

It will be argued that the initial migmatite event M_1 was superceded by a recrystallisation event (early M_2) promoted by basic intrusions at low P. However, the M_2 event reached its peak in the amphibolite-facies, when the migmatite assemblage was indeed metastable.

4.4.2 Purple Migmatitic Gneisses

Purple Migmatitic Gneisses crop out along the Vamvakia river (Section 2.3.2.2; Insert, Map C), west of Lefkoudha (Insert, Map H) and along the Arethousa to Vrasna road (Insert, Map F). The distinctive mineral assemblage and characteristic textures of these migmatites, makes it possible to correlate them with similar and related migmatitic suites elsewhere (i.e. from Guevgeli and the road which traverses the SMM from Thessaloniki to Serres; Dixon and Dimitriadis, 1989, pers. comm.; Sidiropoulos and Dimitriadis, 1989; Dixon, pers. comm.). The original assemblage and early prograde assemblages of the Purple Migmatitic Gneisses are extensively pseudomorphed or completely obliterated within the study area. However, correlation with less-deformed samples outside the area has enabled a fairly unambiguous insight into the earliest mineral assemblages preserved within the SMM.

The development of anastomosing shear zones has produced a range of fabrics, from early migmatitic segregations (S_0) preserved in low-strain cores to late (S_2) shear fabrics at the high-strain sheared rims (Chapter 3). The progressively developed structural fabrics within the Purple Migmatitic Gneisses are very similar to those of the Black and White Migmatites (Section 4.4.1) *see* Chapter 3. The purple and black and white migmatitic lithologies possibly represent minor lithological variations, with the Purple Migmatitic Gneisses containing a more varied and reactive precursor mineral assemblage than the Black and White Migmatites (Section 4.4.1). The purple aspect to this migmatite suite is caused by the present garnet-biotite-kyanite assemblage which records in its external development the complex polyphase metamorphic history. The general mineral assemblage for this migmatitic suite is:
quartz + plagioclase + K-feldspar + garnet (I) ± garnet (II) + kyanite + biotite ± white-mica
Accessories also commonly present are sphene, epidote, zoisite and ilmenite.

Two main low-strain members to the general high-strain Purple Migmatitic Gneiss have been identified (Sections 4.4.2.1, 4.4.2.2). These precursors share a similar mineral assemblage but differ in their metamorphic and fabric evolution. These differences are well-defined within the low-strain examples, and are progressively reduced with increasing strain (Table 4.2). Locally-derived melts have

been injected into these purple lithologies during the progressive deformational events complicating the migmatitic history and the identification of the different precursors.

4.4.2.1 Simple Low-strain Member

In the low-strain Purple Migmatitic Gneiss Member (Sample LEF21-1; Plate 4.1a), the leucocratic assemblage consists of quartz, plagioclase and K-feldspar, homogeneously distributed throughout the rock with a uniform grain-size. Plagioclase usually has multiple twin lamellae while K-feldspar is identified by simple or cross-hatch twinning. A range of subgrain textures and poorly-developed perthites are developed. Due to the distribution of the mineral assemblage and the simple textures developed a metasedimentary origin is proposed as a possible precursor for this simple low-strain lithological unit.

Initially only one phase of garnet porphyroblast growth is present. These garnet (I) porphyroblasts vary from subhedral to euhedral in shape but have a uniform size (1 mm diameter) and contain no inclusions. They are randomly distributed throughout the rock in small clusters associated with numerous, small (0.5 mm long), euhedral, randomly orientated laths of early kyanite (I) which swarm around the garnet porphyroblasts. Large, subhedral, randomly orientated laths of biotite are also associated with the garnet and kyanite in the melanocratic clusters. Further individual laths of biotite are distributed throughout the rock and highlight a weak early (S_2) foliation. Biotite is one of the most abundant minerals of this low-strain member and has a distinctive reddish-brown colour.

With increased strain a number of textural and compositional changes are developed, most noticeably the melanocratic minerals are progressively grouped together and form well developed bands separated by leucocratic layers parallel to the main (S_2) foliation (Plate 4.1b). Components of the leucocratic mineral assemblage are progressively reduced in size and finally develop a mylonitic fabric (Sample VAM23). Within low-strain samples plagioclase develops numerous inclusions of fine-grained kyanite, zoisite or laths of white-mica.

A second generation of garnet (II) porphyroblasts are developed within the melanocratic layers. The first generation garnet (I) porphyroblasts have apparently increased in size and now consist of single large (up to 2 mm diameter), subhedral porphyroblasts, however, this may simply reflect variations in the original composition. These porphyroblasts are fractured perpendicular to the main (S_2) foliation and contain only minor inclusions (up to 0.5 mm in diameter) of quartz, biotite and ilmenite. The second generation garnet (II) consists of numerous small (up to 0.5 mm diameter) euhedral porphyroblasts, which occur in chains and clusters and

General Mineral Assemblage: quartz + plagioclase + K-feldspar + garnet (I) ± garnet (II) + kyanite + biotite ± white-mica		
	Precursor 1: LEF21-1	*Precursor 2: LEF3-2*
Low-strain	Homogeneous distribution of leucocratic minerals. Only perthitic textures are developed (possibly had a metasedimentary precursor). Subhedral to euhedral porphyroblasts of garnet (I) + kyanite (I) + biotite, randomly orientated in clusters throughout the rock.	Distinctive leucocratic segregations. Melanocratic layers contain large individual, subhedral to euhedral porphyroblasts of garnet (I) enveloped by chains and coronas of garnet (II). Also a pseudomorphed mineral (cordierite), and a very minor modal proportion of biotite. Contains perthitic, myrmekitic and granophyric textures (possibly had a magmatic precursor).
	Locally derived melts have been injected during deformation, complicating the migmatitic history.	
Intermediate-strain	Melanocratic mineral clusters progressively grouped and a gneissic fabric developed. Garnet (II) + kyanite (II) developed within melanosomes.	Evidence for pseudomorphed mineral obliterated. Modal proportion of biotite vastly increased.
	Locally derived melts have been injected during deformation, complicating the migmatitic history.	
High-strain	Intensely banded fabric, characterised by dense swarms of small euhedral laths of kyanite interspersed with numerous small subhedral dusty (kyanite filled) garnet porphyroclasts. Kyanite and garnet (II) wrap large subhedral porphyroclasts of garnet (I).	

Table 4.2: Summary of some of the main characteristic textures of the Purple Migmatitic Gneiss evolution, from low- to high-strain.

Plate 4.1

Plate 4.1a: Simple precursor to the Purple Migmatitic Gneiss (Sample LEF21-1). Note the random distribution of the leucocratic and melanocratic assemblages. However, large clusters of garnet-kyanite-biotite are common. Field of view is approximately 3 mm across.

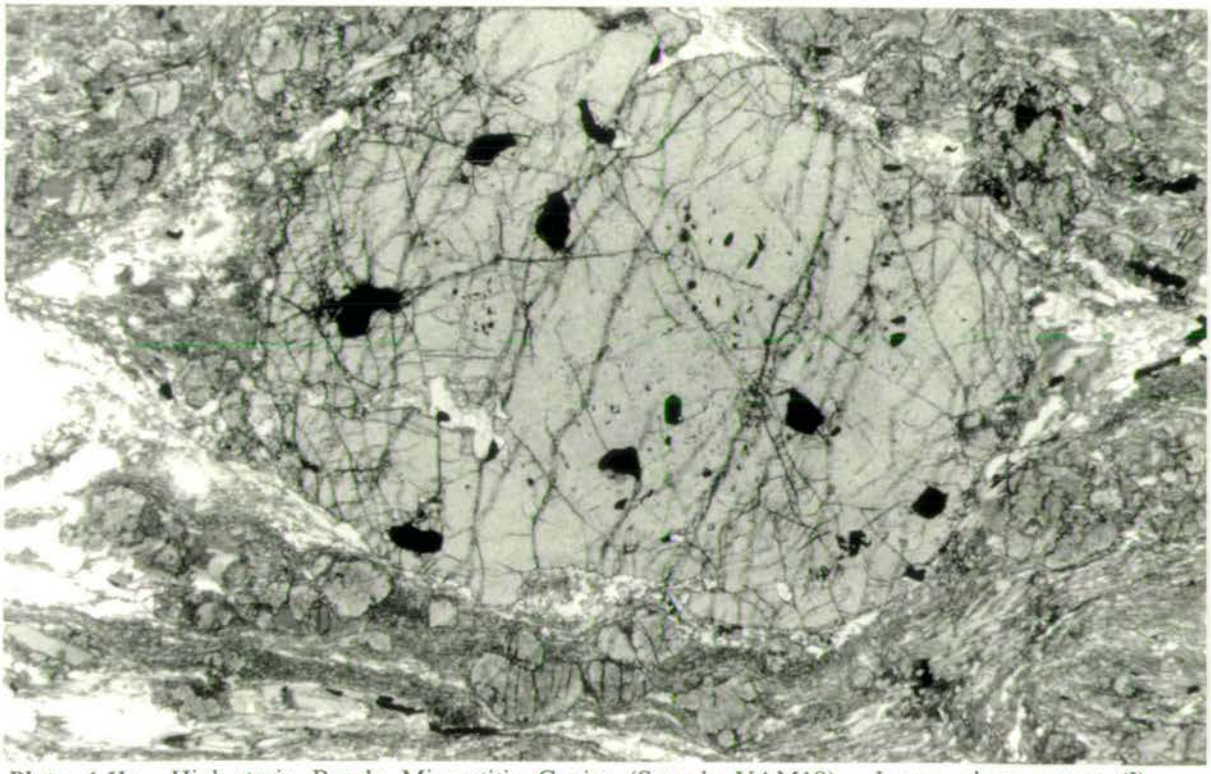

Plate 4.1b: High-strain Purple Migmatitic Gneiss (Sample VAM19). Large, clean garnet (I) porphyroclast fractured perpendicular to the main (S_2) foliation. Symmetric pressure shadows have been developed. The garnet (I) porphyroclast is wrapped by a dense melanocratic matrix of garnet (II)-kyanite (II)-biotite porphyroclasts. Field of view is approximately 6 mm across.

commonly appear to have been numerous individual porphyroblasts which have now grown together (and appear like snowflakes). The garnet (II) porphyroblasts also contain numerous randomly orientated inclusions of fine-grained kyanite (I) resulting in a dark dusty appearance. Garnet (I) porphyroblasts are contained within the melanocratic layers and have been surrounded by a melanocratic association of garnet (II) porphyroblasts, kyanite and biotite.

The melanocratic layers also contain numerous small (0.1-0.3 mm long) euhedral laths of kyanite (II). These are distributed predominantly at the margins of the melanosomes, however, they also occur along the main (S_2) foliation and wrap plagioclase and K-feldspar porphyroblasts within the leucosomes. Early euhedral laths of kyanite (I) are partially preserved within the cores of the melanosomes.

Biotite has been subjected to grain-size reduction (to biotite, II) and now consists of numerous small laths (0.1-0.4 mm long) highlighting the main (S_2) foliation along with kyanite (II). The overall abundance of biotite (i.e. biotite I) has been reduced, and is interpreted to have been converted to garnet (II) + kyanite (II) + biotite (II).

Laths of white-mica are distributed in densely packed semi-continuous layers along the main (S_2) foliation, and individual laths throughout the leucocratic assemblage. This suggests strain as the rock cooled and underwent a reaction consuming kyanite + K-feldspar + water to produce white-mica. With progressive increases in strain, laths of white-mica increase in size and are aligned parallel to the main (S_2) foliation. Epidote is often associated with the white-mica. Sphene and ilmenite are common and represented by accessory minerals within the melanocratic layers and are occasionally completely surrounded by chains of garnet (II) porphyroblasts.

With increasing strain (prior to mylonitisation) porphyroblasts of garnet (II) are disrupted and distributed in a random fashion throughout the melanosome. In this state of strain, the melanocratic assemblage, textures and fabrics cannot be distinguished from those derived from the more complex precursor (Section 4.4.2.2) to the high-strain Purple Migmatitic Gneisses.

4.4.2.2 Complex Low-strain Member

In the complex low-strain Purple Migmatitic Gneiss Member (Sample LEF3-2) quartz, plagioclase and K-feldspar are associated in well-developed leucosomes, and show numerous subgrain textures (Plates 4.2a, b). Within the leucosomes, amalgamations of fine-grained recrystallised quartz have pseudomorphed original

Plate 4.2

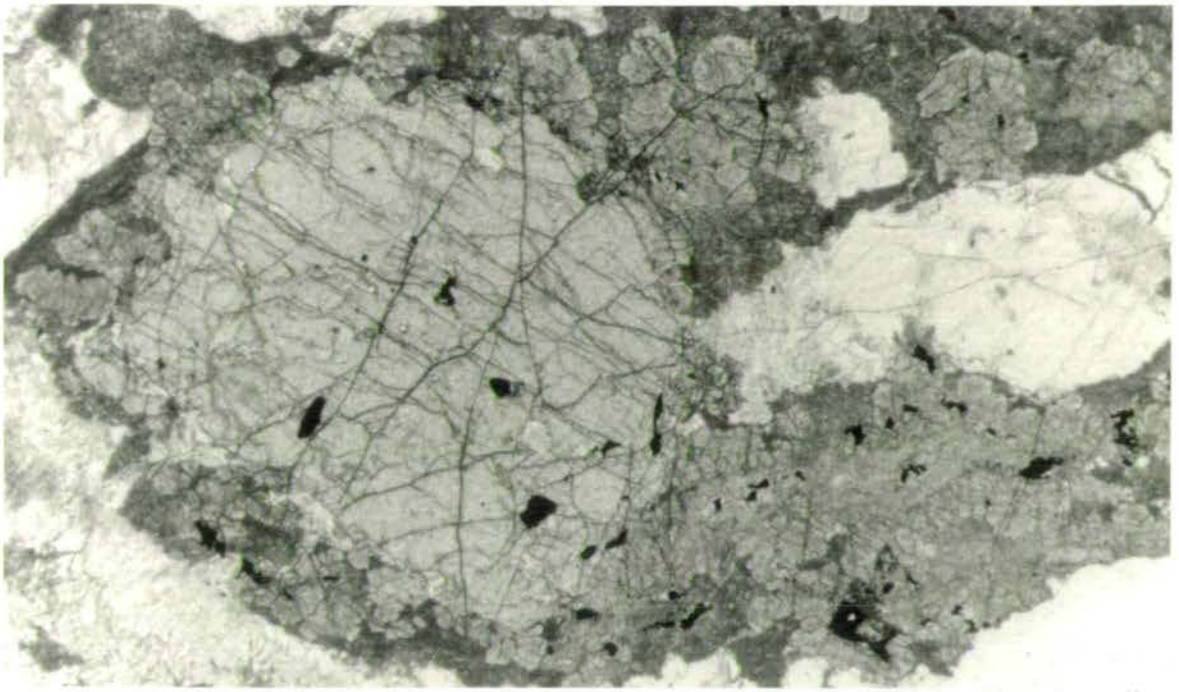

Plate 4.2a: Complex precursor to the Purple Migmatitic Gneiss (Sample LEF3-2). Note the well-developed and distinctive migmatitic banding even within a low-strain sample. Large garnet (I) porphyroblast enveloped in a randomly orientated fabric of garnet (II)-kyanite (I)-kyanite (II)-cordierite (fine-grained pseudomorph). Of particular interest is the abundance of the fine-grained pseudomorphed mineral (cordierite) which constitutes one of the dominant melanosome components. Field of view is approximately 4 mm across.

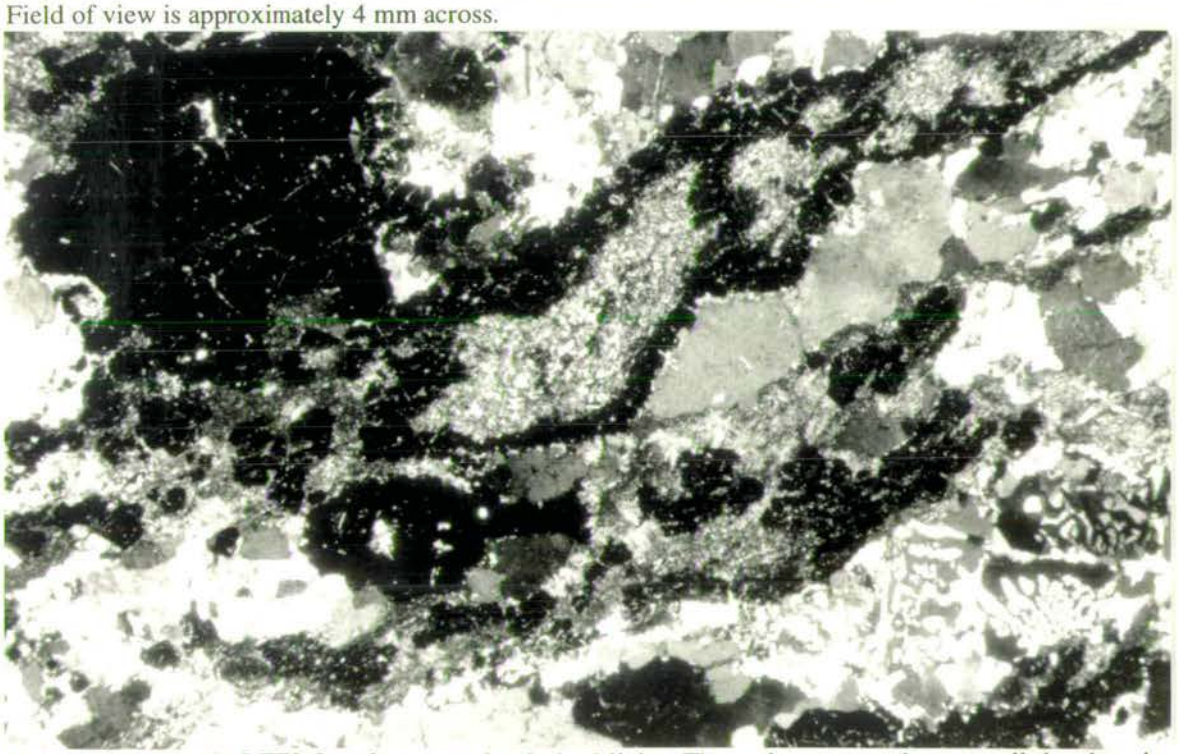

Plate 4.2b: Sample LEF3-2 under crossed polarised light. The melanosomes show a well-developed garnet corona, between the kyanite (I) core and leucosome assemblage. Well-developed granophyric textures are also developed (bottom right) which are indicative of a melt. Field of view is approximately 6 mm across.

large subhedral quartz porphyroblasts. Quartz, the dominant matrix mineral, is also distributed in small anhedral clusters, and also distributed along grain boundaries between large plagioclase and K-feldspar porphyroblasts. Plagioclase usually has multiple twin lamellae while K-feldspar is identified by simple or cross-hatch twinning. Numerous examples of perthitic, myrmekitic and granophyric textures are well-developed, and are interpreted as indicating a possible magmatic origin.

Two generations of garnet are already developed within the lowest strain rocks. The first generation garnet (I) is represented by single large (0.5-1.5 mm diameter) subhedral porphyroblasts with only minor inclusions (up to 0.5 mm in diameter, mainly quartz, sphene, epidote and ilmenite). Apart from these few distinctive inclusions the garnets are clean. Fractures are well-developed perpendicular to the main (S_2) foliation. The second generation garnets (II) are far more abundant and are small (0.1-0.5 mm diameter) euhedral porphyroblasts. These garnet (II) porphyroblasts contain numerous inclusions of randomly orientated kyanite (I) laths. The garnet (II) porphyroblasts are restricted to the melanocratic layers and are arranged in semi-continuous to continuous chains, rings and bands, usually arranged as a corona to the melanosome. From this distribution of the garnet (II) porphyroblasts, a reaction is implied between the core of the melanosome and the leucosome. However, the garnet (II) porphyroblasts are occasionally so abundant they are distributed throughout the melanosome and the banded reaction rim (corona) texture is obscured.

The second major mineral in the melanosome layer is kyanite. Two generations are evident, and are interpreted as the products of two different reactions. The first generation of kyanite (I) consists of amalgamations of small (>0.1 mm wide) randomly orientated subhedral to anhedral, stubby tabular crystals. These are distributed within the cores of the melanosomes, wrapped by garnet (II) coronas. The second generation of kyanite (II) is more typical of the kyanite generation observed in the other low-strain precursor (Section 4.4.2.1) in that it consists of small randomly orientated, elongate, euhedral laths. This kyanite (II) generation is distributed along the margin of the melanosomes in three distinctive positions; 1) as inclusions within the second generation garnet (II) which form the corona to the mesosome, 2) as randomly orientated inclusions within K-feldspar which rims the melanosome between the garnet (II) coronas and plagioclase within the core of the leucosome, 3) as fine-grained, densely packed, randomly orientated laths (along with minor biotite) completely pseudomorphing a euhedral precursor (Plate 4.3). Densely packed, short stringers of kyanite (II) are also found along grain boundaries within the leucosome.

Plate 4.3

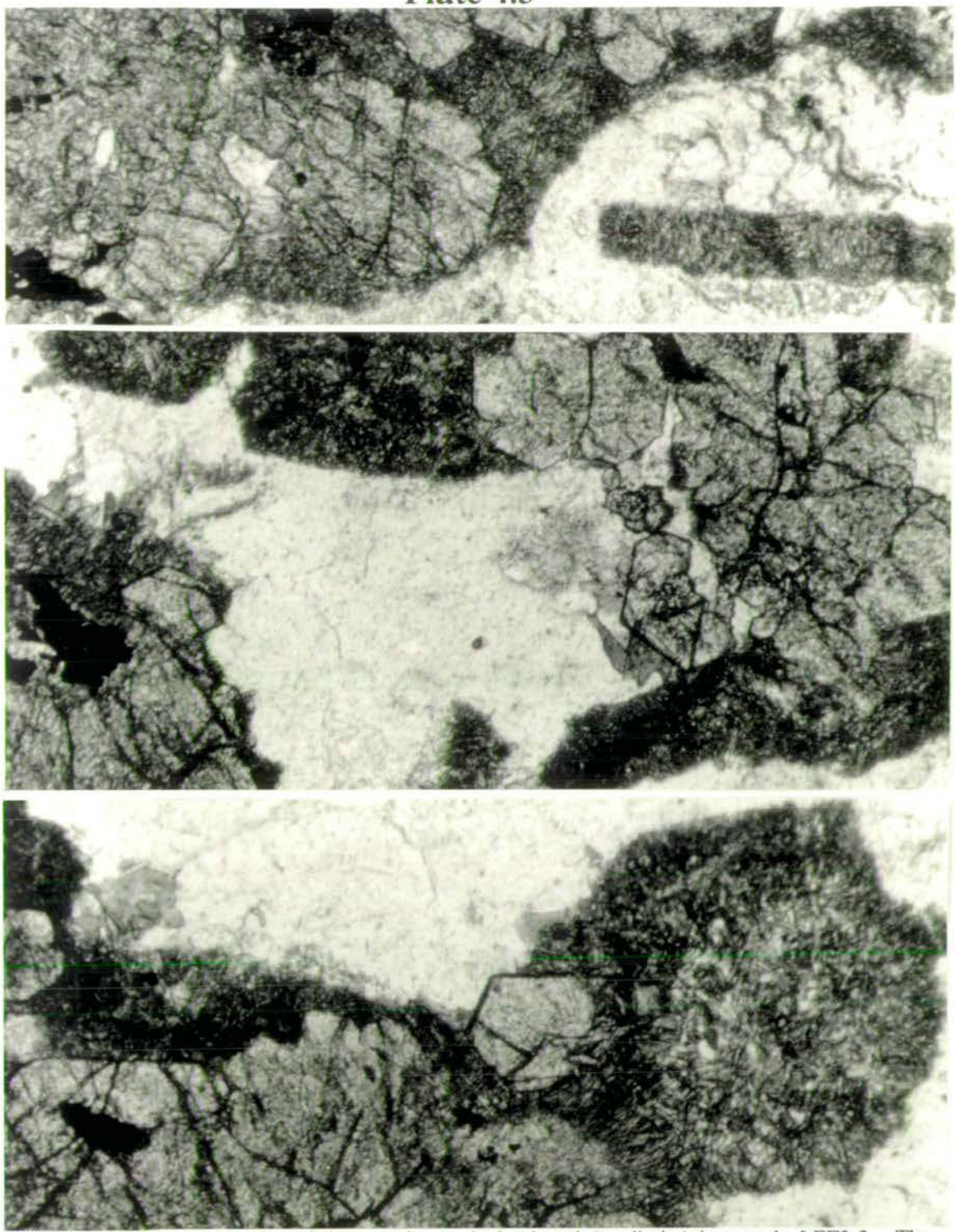

Plate 4.3: Various examples of the pseudomorphed mineral (cordierite) in sample LEF3-2. The distinctive euhedral shapes are indicative of a cordierite precursor. Similar mineral assemblages with comparable textures have been found around Guevgeli and along the Thessaloniki-Serres road by Dixon and Dimitriadis (1982, 1984, 1989); Sidiropoulos and Dimitriadis (1989); Dixon (pers. comm.), however, around Guevgeli cordierite is still preserved. Within sample LEF3-2 the pseudomorphed mineral is replaced by fine-grained laths of kyanite (II), euhedral porphyroblasts of garnet (II) and initially only minor proportions of biotite. Field of view is approximately 3 mm across.

Plate 4.3 shows a pseudomorphed mineral which is critical to the understanding of the early P-T history for the study area. It is distributed predominantly along the margins of the melanosome, although occasionally it is also found in the centre and when extremely abundant it forms the entire width of the melanosome. These dark fine-grained pseudomorphs consist of a sericitic type matrix (possibly pinite) which is subsequently replaced by amalgamations of fine-grained kyanite (II)-garnet (II)-minor biotite. An assortment of original crystal shapes have been preserved and consist of euhedral square, rectangular and hexagonal porphyroblasts. Although a complete euhedral crystal form is not commonly preserved, sharp boundaries are commonly preserved where the pseudomorphed mineral is in contact with leucosome minerals. The characteristic shapes and the assemblages replacing these pseudomorphed minerals, combined with a comparison of the similar purple migmatite samples from the new road and at Guevgeli near the Yugoslav-Macedonian border, where sheeted dykes have remelted sillimanite migmatites at low pressure (work in progress by Dimitriadis and students), suggest that the potential precursor for the pseudomorphed mineral in the study area is cordierite.

Biotite is initially rare and maintains the distinctive reddish-brown colour typical of the purple lithologies. Biotite only occurs in association with the fine-grained pseudomorph (cordierite), kyanite (II), garnet (II) and the leucocratic matrix. Therefore biotite is interpreted as a product of a reaction between the pseudomorphed mineral (cordierite) and K-feldspar.

$$\text{cordierite} + \text{K-feldspar} \rightarrow \text{kyanite (II)} + \text{biotite (II)} + \text{garnet (II)}$$

With increasing strain the mineral assemblage and textural characteristics are progressively altered. Most notably the well-banded reaction textures are obscured by intensification of the main (S_2) foliation. Components of the leucocratic mineral assemblage are progressively reduced in size and finally develop a mylonitic fabric. With increased strain and associated metamorphism the plagioclase develops numerous inclusions of fine-grained kyanite, zoisite or laths of white-mica. Both garnet generations are preserved, but garnet (II) is more abundant and randomly distributed in dense swarms along the main (S_2) foliation rather than as distinctive chains, rings and coronas. The first generation garnet (I) is simply wrapped by the main (S_2) fabric. The first generation kyanite (I) is mainly obliterated with only rare pods remaining within Purple Migmatitic Gneiss Members subjected to high levels of strain. However, the second generation kyanite (II) has progressively developed and now constitutes one of the main minerals of the medium- to high-strain Purple

Migmatitic Gneiss Member. Randomly orientated kyanite or possibly zoisite is found as inclusions within all of the plagioclase crystals within the leucocratic assemblage. However, small (0.1-0.3 mm long) euhedral kyanite (II) porphyroblasts now highlight the main (S_2) foliation along with biotite. The kyanite (II) porphyroblasts are strongly aligned and are densely packed within the melanocratic layers and are also strongly aligned in dense clusters and stringers along grain boundaries in the leucosome. Increased strain has completely obliterated evidence for the pseudomorphed mineral (cordierite) in association with alteration of cordierite with K-feldspar to develop kyanite (II), biotite and garnet (II).

Sphene, white-mica and ilmenite are developed and become increasingly abundant with an increase in strain and the associated intensification of the main S_2 foliation. White-mica tends to be concentrated in and distributed throughout the leucocratic section of this lithology. This suggests strain as the rock cooled and underwent a reaction consuming kyanite + K-feldspar + water to produce white-mica. With an increase in strain, laths of white-mica increase in size and are aligned parallel to the main (S_2) foliation. Epidote is often associated with the white-mica, whereas sphene and ilmenite occur with the garnet (II), kyanite (II) and biotite assemblage.

4.4.3 Reactions and P-T Settings

The suite of black and white migmatites (Section 4.4.1) are of little use in determining the P-T history due to their unreactive mineral assemblage. The purple migmatites (Section 4.4.2), however, are far more informative and preserve evidence for a complex P-T history and the development of melts (Fig. 4.1). Of particular interest is the complex Purple Migmatite Member (Section 4.4.2.2) which contains pseudomorphed cordierite. The purple migmatite assemblages are probably developed by continuous reactions such as:

biotite + Al-silicate + quartz → K-feldspar + cordierite + melt

biotite + Al-silicate + quartz → K-feldspar + garnet + melt

Under these conditions the migmatite assemblage was probably metastable. The nature of the aluminosilicate phase is not certain, but sillimanite is found in the equivalent migmatitic rocks which have been intruded by dykes around Guevgeli. Whether cordierite or garnet develops depends partly on pressure (cordierite is favoured by lower pressures, garnet by higher pressures) and partly on the Mg/Fe ratio of the rock (garnet will form in Fe-rich rocks, cordierite in Mg-rich ones).

The reactions above lead to melting in Mg-rich and Fe-rich compositions respectively due to dehydration breakdown of biotite, but melting only takes place in

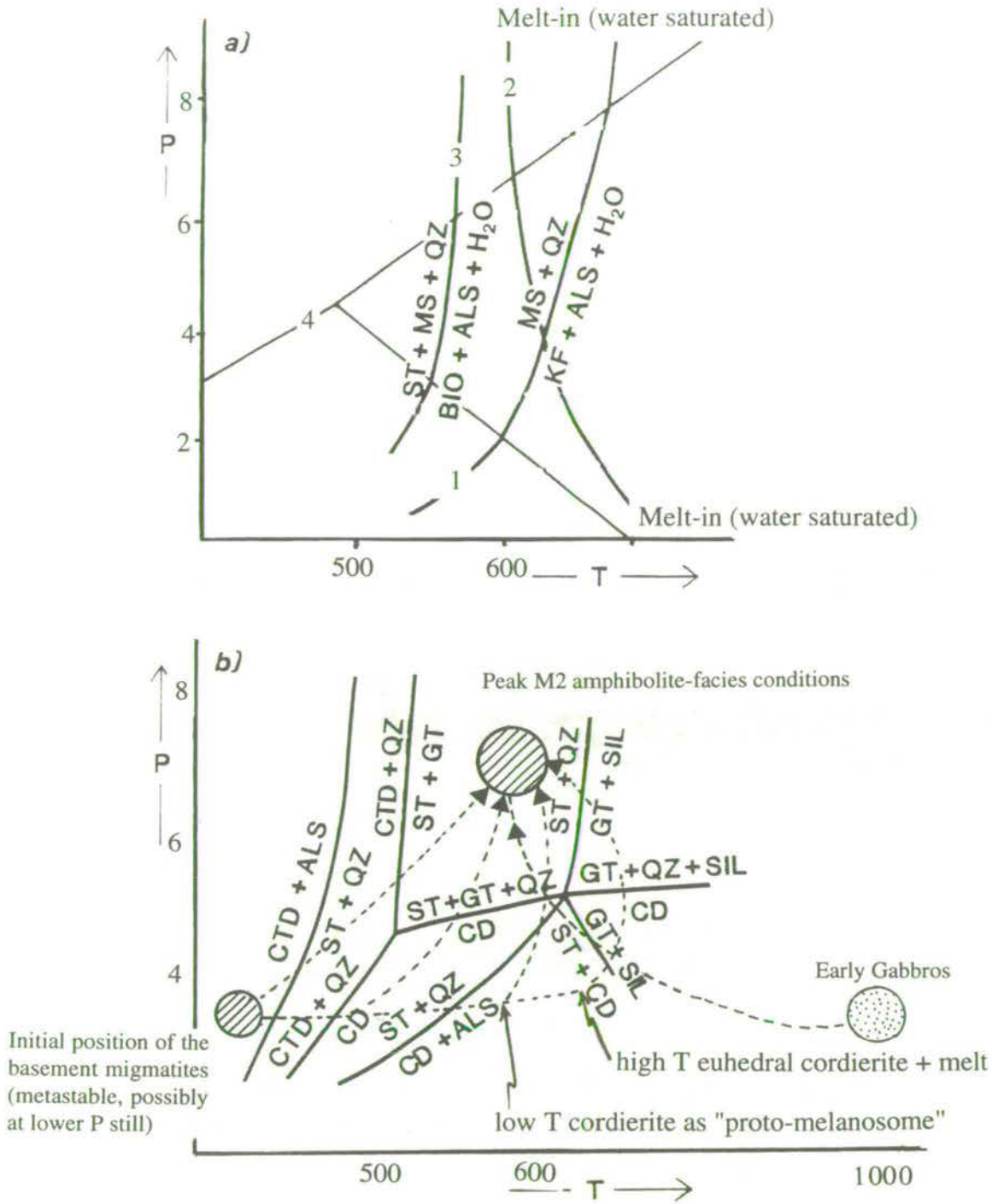

Fig. 4.1: Schematic P-T diagrams to illustrate the potential to develop cordierite from low pressure metapelites by isobaric processes. (a) The relationship between the Al-silicate stability field, first appearance of Al-silicate in normal pelites, muscovite breakdown and the onset of melting. Curves are based on; (1) Althaus *et al.*, (1970); (2) Tuttle and Bowen, (1958); Merrill *et al.*, (1970); (3) Richardson, (1968); (4) Holdaway, (1971) (b) Illustration of the relationships between assemblages involving chloritoid, staurolite, garnet, cordierite and Al-silicate as a function of pressure and temperature. Based on Richardson (1968).

the full range of biotite-aluminosilicate schists when the temperature for the discontinuous reaction is attained. Lower temperature reactions will have produced the continuous regions of cordierite from biotite-aluminosilicate which subsequently return to biotite (II)-garnet (II)-kyanite (II).

biotite + Al-silicate + quartz → cordierite + garnet + K-feldspar + melt

The garnet-cordierite-K-feldspar assemblage is typical of high grade pelitic migmatites and is often taken to mark the beginning of the granulite-facies (Yardley, 1989). The cordierite bearing migmatites are interpreted as being low pressure high temperature lithologies, which have subsequently been promoted up pressure resulting in the pseudomorphing of cordierite (Section 4.4.2.2) via the following reaction.

cordierite + K-feldspar → kyanite + biotite + garnet

The high temperature conditions necessary for cordierite development were probably caused by extensive intrusion of dykes and gabbros during the early emplacement of the Volvi Complex (Chapter 6). Alteration of cordierite is interpreted to coincide with an increase in pressure while still at high temperature. Later melting without cordierite growth at high pressures is interpreted to be caused by later small gabbroic intrusions (Section 4.7.2). The absence of cordierite is considered to be related to either the pressure being too high for cordierite development or the rock into which the gabbro was intruded being unsuitable in composition. A further point which should be considered is whether the rock was wet or dry at the time of thermal perturbation, as hydrous conditions would favour cordierite development.

4.5 Gneisses, Schists and Acidic Intrusives

Paragneisses and semi-pelitic to pelitic schists represent the majority of the country rock within the Lake Volvi area. A variety of orthogneisses are progressively developed with increasing strain in association with acidic intrusives (e.g. Arnaea granite) and are in turn intercalated with the country rock lithologies. Comparisons between samples of gneiss and schist from the Kerdilion, Vertiskos and Volvi Metasedimentary groups show a close similarity in their mineral assemblages and textural development.

Timing of intrusion for the parent rock of the orthogneiss, into the country rock can be determined approximately by comparison of the textures and retrogressive assemblages developed in the orthogneisses with those in the paragneisses and schists (Section 4.8). Most of the ortho- and paragneisses and especially the semi-pelitic to pelitic schists, are extremely susceptible to retrogression and equilibration in the early to late (M_3) greenschist-facies event. However, early P-T conditions are preserved in

low-strain cores which also provide a rare opportunity to investigate the local thermal gradients caused by the intrusion of the Volvi Complex.

4.5.1 Paragneisses

The paragneiss lithologies (Chapter 2; Inserts, Maps B to H) have a predominantly quartzofeldspathic assemblage. Variations in the bulk mineral assemblage are developed due to the variable states of strain caused by the anastomosing shear zones (Chapter 3). The general mineral assemblage for these variably deformed paragneisses consists of:

quartz + plagioclase ± biotite ± white-mica ± garnet

Accessories also commonly present are zoisite, chlorite, calcite, ilmenite and hematite.

These lithologies are of little use in determining the polyphase metamorphic history due to the unreactive mineral assemblage and the lack of characteristic index minerals. In particular they are not particularly per-aluminous and lack K-feldspar. If melting has occurred in the viscinity of basic intrusions through muscovite breakdown it is not very obvious. Some migmatites with minor kyanite (II) could have been paragneisses subjected to local heating However, they are useful in providing kinematic indicators and structural fabrics (Chapter 3).

In the low-strain samples, quartz and plagioclase are closely associated in a fine-grained matrix which represents a large volume percentage of the rock. Quartz also occurs in semi-continuous tight to isoclinally folded ribbons with their attenuated limbs parallel to the main (S_2) foliation. However, the folded quartz ribbons are rarely preserved as the fold closures are usually obscured by disruption of the fold limbs along the main (S_2) foliation (Fig. 4.2). Quartz and plagioclase are usually fine-grained, anhedral in shape, and show numerous sub-grain textures. Plagioclase usually has lamellar twins or a distinctive perthitic texture.

Unaltered "fresh" biotite is rare but occurs as small discrete folded and kinked laths which are distributed throughout the rock and arranged along S_1 or early S_2 foliations at an angle (5-20°) to the main (S_2) foliations. Original biotite distributed along the S_1 (or early S_2) foliation is attributed to the prograde amphibolite-facies (M_2) metamorphic episode.

White-mica is the dominant micaceous mineral within the paragneiss lithologies and is commonly present in two forms in the low-strain samples, and are interpreted to represent two generations of mineral growth.

The first generation of white-mica consists of small, subhedral to anhedral, fine-grained (0.1-0.3 mm long) laths, in loosely packed semi-continuous stringers.

The first generation of white-mica is aligned at an angle (5-20°) to the main (S_2) foliation, sub-parallel to the (M_2) biotite laths, and subsequently folded in the same or closely related structural D_2 event (Chapter 3). Due to the overprinting characteristic of the white-mica (I), it is attributed to the retrograde upper greenschist-facies (early M_3) metamorphic episode. The second generation of white-mica (II) consists of large (0.5 to 1.5 mm long) subhedral laths weakly aligned parallel to the main (S_2) foliation, and may represent a middle or low greenschist-facies (late M_3) metamorphic event.

Garnet porphyroblasts are randomly distributed throughout the paragneiss lithologies. The porphyroblasts are subhedral and highly fractured with the fractures subsequently infilled with epidote. This textural feature is attributed to a retrograde lower greenschist-facies (late M_3) metamorphic episode related to the (D_3) brittle deformation event (Chapter 3).

With increasing strain, grain-size reduction (especially in quartz) and recrystallisation are common. This is shown by regular, sharp grain boundaries and recrystallised quartz and plagioclase, elongate parallel to the main (S_2) foliation. Biotite is typically found as a retrogressed (chloritised) component occuring as small discrete folded and kinked laths which are distributed throughout the rock and progressively rotated and realigned sub-parallel to the main (S_2) foliation (Fig. 4.2). Initial retrogression of the biotite to chlorite associated with increasing strain is attributed to the retrograde upper greenschist-facies (early M_3) metamorphic episode. Complete retrogression of the biotite and realignment of the chlorite pseudomorphs is attributed to high-strain zones in the lower greenschist-facies (late M_3) metamorphic episode.

With increasing strain white-mica (I) is progressively aligned parallel to the main (S_2) foliation. At the same time white-mica (II) laths become progressively more abundant and are intensely aligned parallel to the main (S_2) foliation. This alignment of white-mica is attributed to the progressive (D_2) shear deformation (Chapter 3). The laths of white-mica (II) wrap garnet porphyroblasts and cross-cut the earlier generation of white-mica (I) and the early (S_1 or early S_2) fabric highlighted by the biotite laths (Fig. 4.2). Therefore, the second generation of white-mica is attributed to the retrograde middle to lower greenschist-facies (late M_3) metamorphic episode. With increasing strain accessory minerals are also increasingly abundant.

The micaceous component of these lithologies provides the best evidence for the metamorphic and deformation relationships. Within the paragneiss lithologies, the variation from total biotite with no white-mica to pseudomorphed chloritised biotite and predominantly second generation white-mica is interpreted as progressive

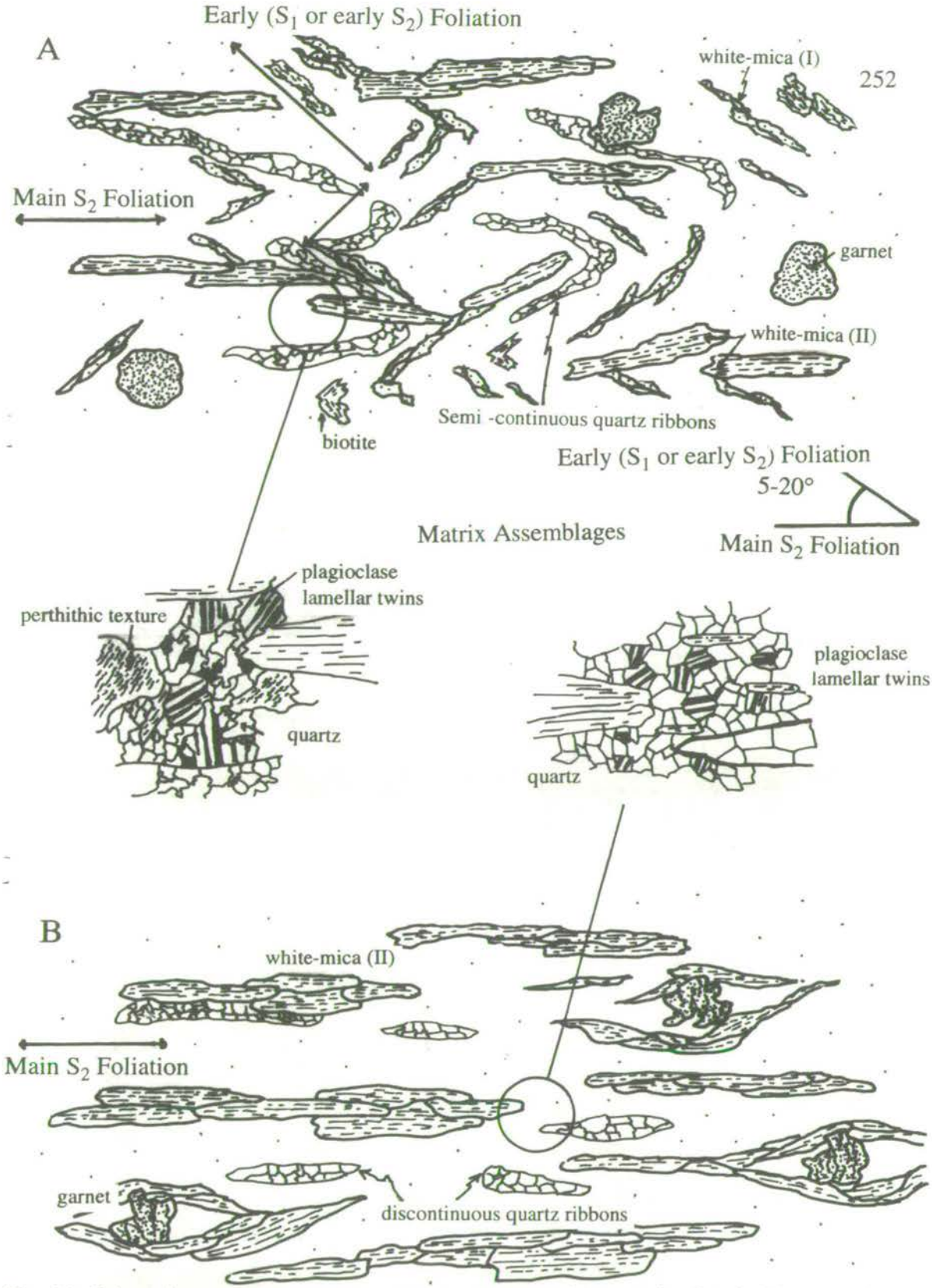

Fig. 4.2: Schematic representation of the mineral assemblage and textures developed with progressive strain for a standard paragneiss lithology. (A) Low-strain, two weak foliations developed, and semi-continuous quartz ribbons are preserved possibly indicating an early fold episode. (B) High-strain, only one dominant foliation which is highlighted by white-mica (II). Garnet porphyroclasts are fractured and extensively embayed and wrapped by the white-mica (II) laths. Extensive grain-size reduction and recrystallisation of the matrix has occurred.

retrogression from the prograde amphibolite-facies (M_2) metamorphic event to the M_3 metamorphic event, representing upper greenschist-facies (early M_3) to lower greenschist-facies (late M_3) metamorphism.

4.5.2 Semi-pelitic to Pelitic Schists

The schistose lithologies (Chapter 2; Inserts, Maps B to H) have a broad range of assemblages reflecting their original composition. Further variations are developed due to the variable states of strain caused by the anastomosing shear zones, which are intensely developed within these lithologies (Chapter 3). The general mineral assemblage for the majority of schists within the Lake Volvi area consists of:

quartz + plagioclase + biotite + garnet ± staurolite ± white-mica

Accessories also commonly present are sphene, epidote, zoisite, chlorite, calcite hematite, ilmenite and graphite.

However, immediately to the east of the Volvi Complex, around Lefkoudha (Insert, Map H) and along the Vamvakia river (Insert, Map C), semi-pelitic to pelitic schists have a distinctive purple aspect and an assemblage which consists of:

quartz + plagioclase + K-feldspar + biotite + garnet ± kyanite ± white-mica

Accessories also commonly present are epidote, rutile, sphene, chlorite, ilmenite and hematite. Zoisite is also present as a porphyroblastic accessory when these purple schists are extensively sheared.

4.5.2.1 Standard Schist Member

In the vast majority of semi-pelitic to pelitic schists throughout the area, quartz, plagioclase, biotite and white-mica have a similar metamorphic and textural evolution to the paragneisses (Section 4.5.1). The classification of schists is based on the modal percentage of micas which is greater for the more pelitic lithologies.

In low-strain samples, euhedral unfractured garnet porphyroblasts are randomly distributed throughout the rock. The majority of the garnet porphyroblasts have no inclusions, but distinctive inclusion trails highlighted by graphite are preserved within the Megali Volvi Garnet Graphite Schist Formation (Section 2.4.3; Chapter 3).

Staurolite is a rare component, which provides a useful index mineral for constraining the P-T history. The staurolite porphyroblasts are only preserved within low-strain zones to the west of the Volvi Complex and have an anhedral shape with numerous rounded quartz inclusions. The porphyroblasts appear to overgrow the earliest generation of white-mica, but are wrapped along with the garnets by second generation white-mica. Rounded staurolite porphyroblasts have also been found as

inclusions within garnet. The rarity of staurolite poses the question of whether it represents a regional (M_2) metamorphic episode which has been largely overprinted or a local thermal event related to the progressive emplacement of the Volvi Complex. Lithologies with a similar mineral assemblage, textural and fabric development, but which do not contain staurolite, are common throughout the area.

With increasing strain, quartz, plagioclase and biotite are developed in a similar manner to the paragneisses (Section 4.5.1). However, garnet porphyroclasts become progressively subhedral and fractured with increasing strain and the fractures infilled with epidote (Section 4.5.1).

The absence of staurolite and the general lack of any high-grade index minerals such as kyanite (which is found in abundance to the east of the Volvi Complex, but rarely and in only minor quantities west of the complex) is attributed to a thorough regional greenschist-facies (M_3) retrogression. The distribution of the high-grade minerals may be directly related to the regional structure and present-day levels of exposure (Chapter 3), with widespread, intense deformation to the west of the Volvi Complex, but more localised shear zone deformation to the east of the complex (Chapter 3).

4.5.2.2 Purple Schist Member

In low-strain samples quartz, plagioclase and K-feldspar are abundant and are randomly distributed throughout the rock. Quartz varies in its appearance from rare, large grains to more typical fine-grained, recrystallised mosaics of anhedral crystals showing a variety of subgrain textures; (a) When scattered mosaics composed of recrystallised medium- to fine-grained quartz are developed, with sharp, subhedral, subgrain boundaries and triple junctions at 120°, static re-equilibration under low-strain conditions is inferred. (b) When partial recrystallisation and grain-size reduction around large quartz porphyroblasts with polycrystalline extinction is evident, recrystallisation of quartz is inferred to be caused by deformation. Porphyroblasts of plagioclase usually show lamellar twinning, while K-feldpar has a distinctive perthitic texture.

Minor laths of white-mica and possibly kyanite occur as randomly orientated inclusions within individual plagioclase porphyroblasts, although these fine-grained mineral growths are usually concentrated and weakly aligned along grain boundaries.

Biotite is generally abundant, especially in low-strain samples which do not contain kyanite or white-mica. Biotite often occurs as pleochroic reddish-brown, subhedral laths (similar to the Purple Migmatitic Gneisses, Section 4.4.2), and is randomly distributed throughout the rock.

Garnet is a common constituent and usually developed as medium-grained, subhedral to euhedral porphyroblasts (up to 1.5 cm in diameter). The spatial arrangement of these porhyroblasts is variable, although they are usually distributed randomly throughout the rock or in diffuse clusters often associated with biotite.

Kyanite is common, but not always present. The first form of kyanite (I) is as large subhedral porphyroblasts, scattered throughout the rock. These porphyroblasts are often folded or kinked and orientated at a high angle to the main (S_2) foliation. This generation of kyanite, although broken, fractured and containing inclusions of quartz, is usually stable in the presence of large laths of white-mica. The second and more common form of kyanite (II) occurs as fine-grained laths, randomly orientated throughout the rock and as inclusions in plagioclase. This is an important observation, implying that the original migmatitic rocks (Hercynian?) were probably interstratified with kyanite-garnet schists.

White-mica is variably developed and occurs as short subhedral laths which are orientated at varying angles to the main (early S_2) foliation and are invariably kinked and folded.

With increasing strain quartz, plagioclase and K-feldspar progressively occur in continuous bands, attenuated stringers and isolated pods. This main banding fabric is parallel to the main (S_2) foliation, and related to the anastomosing shear zones (Chapter 3). With increasing strain deformation of quartz is extensive and a mylonitic fabric is developed. Due to strain partitioning and the preferential deformation of some minerals compared to others, the mylonites are banded into mylonitic, ultramylonitic and blastomylonitic layers. Plagioclase and K-feldspar are often preserved as subhedral fractured porphyroclasts within a much finer quartz-plagioclase-K-feldspar matrix.

With increasing strain the modal percentage of biotite decreases and is increasingly retrogressed, pseudomorphed by fine-grained sericitic white-mica. Fine-grained laths of kyanite (II) also occur as inclusions within plagioclase in those samples with retrogressed biotite. In samples which already contain large kyanite (I) porphyroblasts, the biotite laths are usually poorly preserved and often simply retrograded to chlorite. With the instigation of ductile deformation shown by recrystallisation of quartz and plagioclase, the large kyanite porphyroblasts start to breakdown into small subhedral laths.

An increase in the modal percent of white-mica is developed related to deformation and/or retrogression. Fine-grained bundles of sericite pseudomorph biotite laths, while larger anhedral laths of white-mica are arranged along

recrystallised quartz-plagioclase grain boundaries and highlight the main (late S_2) foliation. Therefore the development of an early generation of white-mica is proposed which has subsequently been overprinted by a later generation associated with the development of the main (S_2) foliation (Section 4.5.1).

4.5.3 Acidic Intrusives and Orthogneisses

The most important acidic intrusions within the area are the Arnaea granite and its sheared margin, represented by the Askos Augen Orthogneiss Member (Section 2.6.3; Insert, Map B) and the Modhi Granitoid Formation (Section 2.6.4; Insert, Map G). As noted by De Wet *et al.*, (1989), the Arnaea granite is a very siliceous body (ca. 76.3wt.% SiO_2, Appendix I; for the structural implications *see* Chapter 3), with an assemblage of:

quartz + K-feldspar + plagioclase + white-mica + biotite

Accessories also commonly present are allanite (occasionally zoned), epidote, sphene, ilmenite and hematite. Numerous different granitic and orthogneiss lithologies are developed, both within the main body of the Arnaea granite and the numerous apophyses and veinlets derived from it, due to variations in the modal percent of the minerals present and the degree of strain incurred by the rock (Chapter 3). Changes in the composition of these acidic intrusive and orthogneiss lithologies reflect variations in the modal percentage of the components, quartz (40-60%), total feldspar (20-40%) and total mica (5-20%).

In low-strain cores within the main body of the Arnaea granite (Chapter 3) relics of an original igneous texture are preserved. This original granitic texture consists of clusters of large, subhedral phenocrysts of quartz, plagioclase and microcline. Quartz occurs as large, subhedral phenocrysts. Microcline is abundant and shows well-developed cross-hatch twinning. K-feldspar also occurs as large (up to 5 mm diameter) perthitic, subhedral to euhedral phenocrysts within a finer-grained matrix of quartz and plagioclase. The perthitic feldspar textures are often overprinted and cross-cut by later broad, widely spaced, exsolution lamellae. Some of the large K-feldspars contain inclusions of plagioclase with undeformed twin lamellae, along with zoisite, epidote and quartz. Occasionally K-feldspars occur with an abundance of fine-grained inclusions resulting in a sieve texture. Plagioclase shows a range of multiple-twin lamellae ranging from undeformed to highly deformed. There is no clear evidence of pre-solidification fabrics, e.g. original alignment of the plagioclase crystals, as a strong solid-state tectonic overprint is now fully developed (Chapter 3).

Biotite occurs as minor, subhedral laths (0.1 to 0.3 mm long), randomly distributed throughout the rock. The biotite laths vary in colour from brown to olive-

green. This colour variation is interpreted as a retrogressive effect from an amphibolite-facies (M_2) metamorphic event to a greenschist-facies (M_3) metamorphic event respectively.

Subhedral laths of muscovite (0.2-1 mm long) usually occur in strongly aligned bundles or less well-aligned clusters, which invariably define the main local foliation in a high-strain or low-strain condition respectively.

However, with increasing strain these relics are rarely preserved even within low-strain zones up to 800 m west of the proposed boundary between the Arnaea granite and Askos Marginal Amphibolite Formation (Section 2.3.3.1; Insert, Map B). The igneous textures are generally weakly deformed and rapidly pass into the dominant recrystallised quartzofeldspathic tectonite fabric. Quartz occurs more commonly as fine-grained, anhedral grains in the groundmass with quartz ribbons arranged parallel to the main (S_2) foliation. Feldspathic phenocrysts are frequently fractured perpendicular to the main (S_2) foliation, and infilled with recrystallised quartz in the more strongly deformed granites and orthogneisses. Subgrain textures are common and grain-size reduction and recrystallisation occur along with muscovite development in association with increasing strain.

Biotite is frequently partially or completely altered to chlorite and epidote, and orientated parallel or sub-parallel with the main (S_2) foliation. This final retrogression during the lower greenschist-facies (late M_3) metamorphic event is possibly a result of continued deformation and fluid channelling along the main (S_2) foliation.

Muscovite is especially abundant within discrete anastomosing shear zones characterised by grain-size reduction and recrystallisation of fine-grained quartz, plagioclase and K-feldspar. Hence, muscovite is interpreted as an early M_3 upper greenschist-facies mineral, with chlorite and epidote representing late M_3 lower greenschist-facies metamorphic minerals.

Hematite, ilmenite and increased amounts of retrogressive (late M_3) lower greenschist-facies epidote and white-mica are progressively more abundant. These mineral growths are interpreted as possible localised fluid channels following minor shear zones. A discussion of element mobility within the Arnaea granite and its associated lithologies, with reference to shear zones, is presented in Chapter 5.

Late second generation (M_3) metamorphic epidotes are found at the triple junctions between recrystallised quartz and also aligned along and parallel to the developing regional shear induced foliation (S_2), where they occur with bundles of white-mica laths and composite bands of recrystallised quartz, plagioclase and K-feldspar.

The Modhi Granitoid Formation (Section 2.6.4; Insert, Map G) has a similar composition and fabric development history to the Arnaea granite, with mineral assemblages varying in accordance with deformation. Within the granitic lithologies, muscovite laths occur in bundles and fairly continuous layers which wrap quartzofeldspathic augen. These micaceous laths are typically kinked and folded. Hence, a late brittle (D_3) deformation event is proposed synchronous with or post-dating muscovite development during the retrogressive (early to late M_3) metamorphic event.

4.5.4 Reactions and P-T Settings

In general, the country rock lithologies in the Lake Volvi area only preserve extremely retrogressed greenschist-facies assemblages. However, a sequence from a peak at the amphibolite-facies to the low greenschist-facies can be reassembled. Locally derived melts and purple migmatites to the east of the Volvi Complex and the abundance of garnet-rich amphibolites throughout the area are indicative of high grade assemblages. The remaining lithologies are fairly restricted in their mineral assemblages and are therefore relatively unreactive. The country rock pelites however, show a broad spectrum of mineral assemblages and reactions. Remnants of staurolite are preserved within a few samples however, partly replaced with garnet and kyanite, a reaction which restricts the country rock to a well-defined P-T field with temperatures between 600-700°C and pressures above 5 kb (Fig. 4.3). With the onset of retrogression, kyanite is replaced by assemblages representative of the early M_3 upper greenschist-facies event (Fig. 4.3). With further retrogression, assemblages of the late M_3 lower greenschist-facies are developed (Fig. 4.3).

4.6 Marbles and Calc-silicates

An assortment of crystalline marbles and calc-silicates crop out throughout the area (Volvi Metasedimentary Group, Section 2.2.3.3; Vrasna Marble Formation, Section 2.2.4.3; Stefanina Marble Formation, Section 2.2.5.2; Inserts, Maps B, E, F and G). The marbles and calc-silicates are generally monotonous with a limited mineral assemblage:

$$\text{calcite} + \text{dolomite} \pm \text{white-mica} \pm \text{quartz}$$

Few if any distinctive reactions have been developed within these lithologies and consequently they have only been briefly studied. The contact between the two rock types is in general gradational. Precursors for the marble/calc-silicate sequences are uncertain as many calc-silicates result from metamorphism of impure calcareous

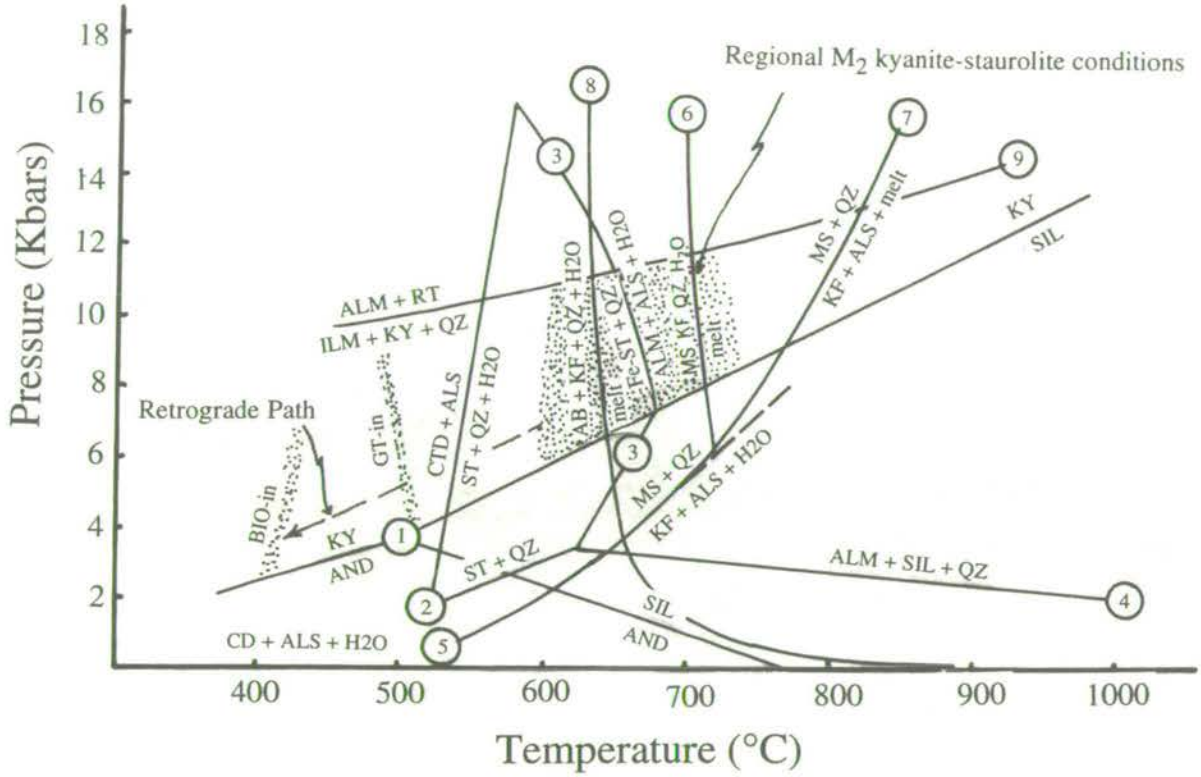

Fig. 4.3: Petrogenetic grid for pelitic metasediments with P = P_{H2O} (except curve 7), modified after Yardley (1989). Abbreviations used are: AB = albite; ALM = almandine; ALS = l-silicate; AND = andalusite; BIO = biotite; CD = cordierite; CTD = chloritoid; GT = garnet; ILM = ilmenite; KF = K-feldspar; KY = kyanite; MS = muscovite; QZ = quartz; RT = rutile; SIL = sillimanite; ST = staurolite. Data sources for the curves are as follows: (1) Holdaway (1971); (2) lower P-T limits of Fe-staurolite + quartz fitted to data of Richardson (1968) and Rao & Johannes (1979); (3) Yardley (1981b), compiled from Richardson (1968), Ganguly (1972) & Rao & Johannes (1979); (4) Holdaway & Lee (1977); (5) Chatterjee & Johannes (1974); (6) & (7) Thompson (1982) (calculated), note that curve (7) is for H_2O-absent conditions; (8) Luth, Jahns & Tuttle (1964); (9) Bohlen, Wall & Boettcher (1983a). Stippled bands are approximate conditions of the biotite and garnet isograds. N.B. Experimental uncertainties are invariably much greater than the thicknesses of the lines drawn.

sediments such as marls, whereas others are probably of metasomatic origin, formed by interactions between original thin limestone layers and adjacent pelite.

The general lack of reactions in these lithologies is attributed to quartz sand being the only major impurity in the original calcite limestones producing a calcite-quartz assemblage which is only reactive under extreme conditions of pressure (calcite would be replaced by aragonite) or temperature (wollastonite may form if the pressure was low). However, extensive textural changes took place during metamorphism of the marbles even where no mineralogical reaction has occurred. The textural changes consist mainly of grain-size variations with recrystallisation during ductile deformation and brittle fracturing, and mylonitisation during the later deformational events. There are also numerous episodes of cross-cutting veins, which can be observed as composite growth structures using cathodoluminesence techniques (Chapter 3). Dolomite-rich limestones, however, were much more reactive during metamorphism in the presence of silica. A good example is the "tiger-striped" lithology (Section 2.3.2.4 and 2.5.2). In general at low grades, talc would be expected to appear in dolomitic marbles, progressively succeeded by tremolite, diopside and diopside + forsterite. The conditions at which such reactions take place are however strongly dependent on the composition of the fluid phase present (Yardley *et al.*, 1990).

Calc-silicates are very much more variable in their mineralogy. Samples within the area commonly contain phases which include actinolite, hornblende, biotite, plagioclase, diopside, microcline, epidote/clinozoisite, zoisite, garnet and sphene. There is usually a progressive gradation in composition between the intercalated bodies of the Volvi Metasedimentary Group and the Vertiskos Group. Precise P-T constraints however cannot be readily applied as fluid composition plays a very important role in determining which minerals are developed, in addition to temperature and pressure (Yardley *et al.*, 1990).

4.7 Amphibolites and Basic Intrusives

Mafic lithologies studied within the Lake Volvi area (Inserts, Maps B to H) are represented by two main groups, (a) a series of variably sized amphibolite bodies intercalated with the country rock gneisses and schists (the amphibolite formations of Rendina, Section 2.2.2.3; Modhi, Section 2.2.3.1; Vrasna, Section 2.2.4.1; Stefanina, Section 2.2.5.1; Askos, Section 2.3.3.1 and Nea Madhitos, Section 2.3.4.1) and dykes (Section 3.11), and (b) a range of doleritic to gabbroic intrusions predominantly from the margin of the Volvi Complex (Sections 2.5 and 3.10).

The mineral assemblages, textures and fabrics of the mafic lithologies are extremely variable due to:

(a) A polyphase metamorphic history.

(b) Original variations in the composition of the mafic lithologies from Mg-rich to Fe-rich end members.

(c) A wide range of strain-states related to the progressive and variable regional deformation (Chapter 3).

The following sections describe mineral assemblages and textures developed during a progressive increase in strain in (1) early intrusive lithologies at low-P high-T conditions and, (2) in later intrusive lithologies at constant high P-T conditions, and (3) in lithologies which have been subjected to progressive increases in strain during retrogression to lower P-T conditions.

4.7.1 Amphibolites

Determination of the origin and time of intrusion of the amphibolites within the study area is difficult due to the wide variation in composition and states of strain. However, it is highly improbable that these wide variations are simply the result of a single intrusive event with the amphibolites derived by deformation of early mafic lithologies (gabbros or dolerites) at peak amphibolite-facies P-T conditions during progressive, strain-partitioned deformation. This study therefore proposes that the amphibolites and mafic lithologies within the study area represent a spectrum of early to late intrusions. This is supported by the distribution of large expanses of amphibolite (interpreted as early intrusives at low-P, high-T), intruded by relatively small, "fresh", medium- to coarse-grained gabbroic bodies (interpreted as late intrusives at high-P, high-T). The amphibolites within the study area can be divided into three main groups based on different modal assemblages within the low-strain members. Each of the three groups show a range of low- to high-strain mineral assemblages and textures due to progressive increase in strain at peak P-T conditions and also during retrogression to progressively lower P-T conditions.

4.7.1.1 The First Amphibolite Group

This group (e.g. Samples EMV2, L87-B, L119-3) contains the most complex low-strain amphibolite assemblage within the study area (Plate 4.4a). The assemblage is in disequilibrium and consists of:

quartz + plagioclase + K-feldspar + hornblende (I) + hornblende (II) + epidote + zoisite

Plate 4.4

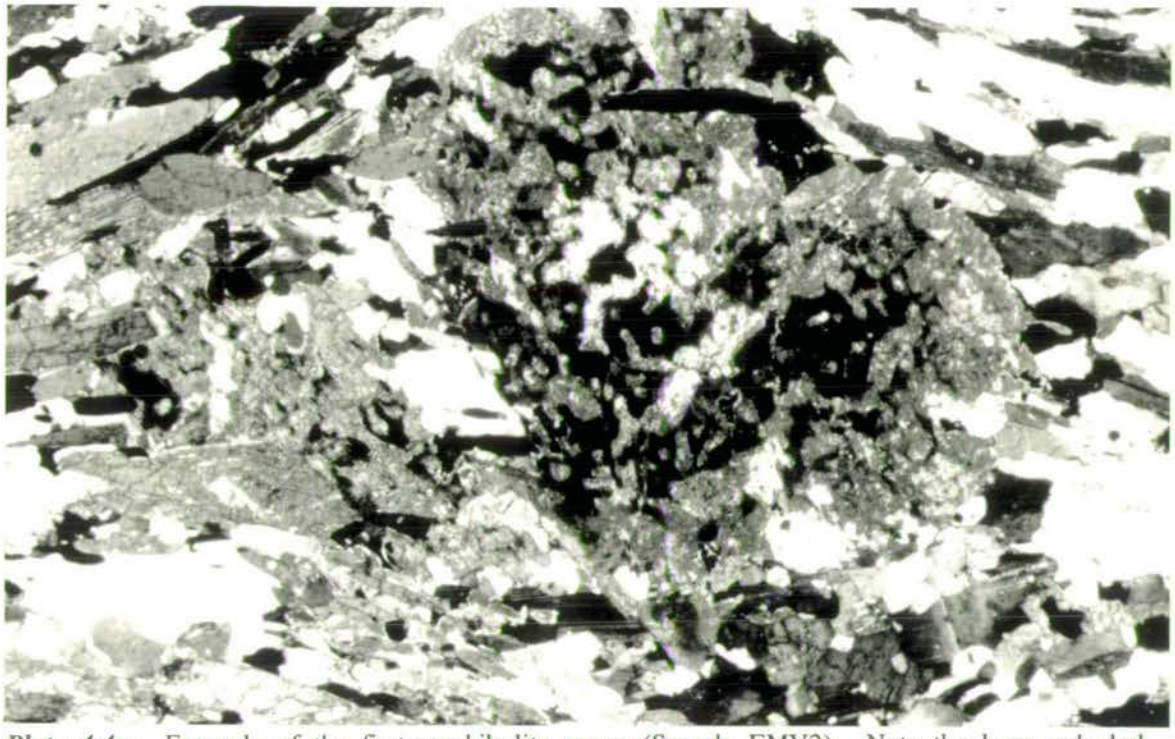

Plate 4.4a: Example of the first amphibolite group (Sample EMV2). Note the large anhedral extensively embayed amphibole (I) porphyroclast. This porphyroclast is interpreted to represent a relict early amphibolite equilibration fabric. The amphibole (I) porphyroclast is wrapped by well-aligned subhedral laths of later amphibole (II) porphyroblasts. Field of view is approximately 6 mm across.

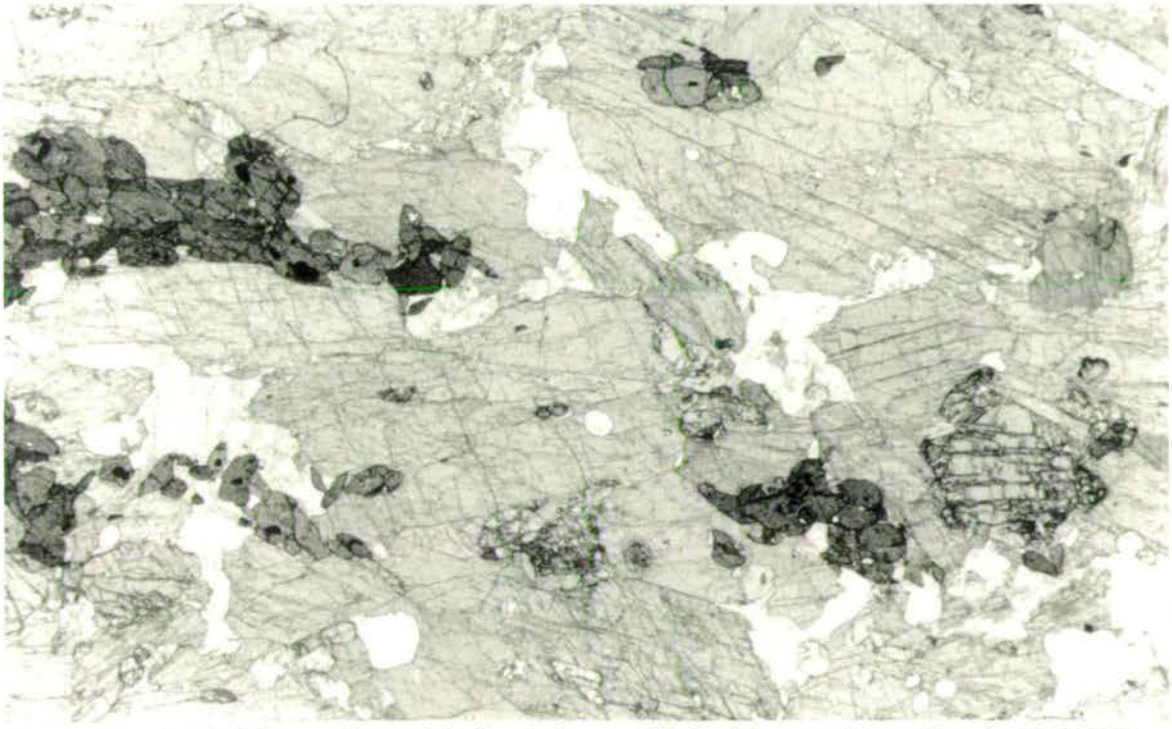

Plate 4.4b: Typical low-strain amphibolite-facies amphibole-rich assemblage (Sample VAM19B). The amphibolite contains abundant subhedral garnet porphyroblasts and clusters of sphene and rutile. Field of view is approximately 6 mm across.

Accessories also commonly present are sphene, rutile and ilmenite.

Within the low-strain samples quartz, plagioclase and K-feldspar are distributed randomly throughout the rock and show an assortment of subgrain textures which are developed. The majority of the grain boundaries are sharp and straight with 120° angles between the quartzofeldspathic components and 90° angles with elongate laths of hornblende (II) representing a recrystallised and re-equilibrated metamorphic assemblage. Feldspars are distinguished by multiple twinning in plagioclase and cross-hatch or simple twins in K-feldspar.

Two generations of amphibole are developed. Hornblende (I) consists of 4 to 6 mm diameter, subhedral porphyroblasts, randomly distributed throughout the rock (Plate 4.4a). These porphyroblasts are extensively embayed by intergrowths of quartz, plagioclase and hornblende (II) and are overgrown by ilmenite, epidote and hornblende (II). The hornblende (I) amphibole generation was part of an early metamorphic assemblage pseudomorphing original magmatic pyroxenes. The second generation of amphiboles (Plate 4.4a) is typical of the amphibolites throughout the area and occurs as elongate subhedral to euhedral laths (0.5-3 mm long) which are pleochroic from dark-green to light-brown.

Accessory minerals are selectively distributed, with ilmenite restricted to the cores of the hornblende (I) porphyroclasts, while sphene is randomly distributed throughout the rock, and rutile is associated with the sphene and commonly found within the core of larger euhedral lozenge shaped sphenes.

With increasing strain quartz, plagioclase and K-feldspar are progressively developed into well-defined, bands and stringers. At high P-T conditions, plagioclase and K-feldspar are lost and quartz develops a wide range of subgrain textures. Further strain causes recystallisation and grain-size reduction. The same characteristics and textures are developed during increasing strain and retrogression to low P-T conditions. Hornblende (I) porphyroclasts are broken down and distributed throughout the rock while the second generation of amphibole is simply reduced in size (0.3-1.7 mm long) and remains as subhedral elongate laths. The hornblende (II) grains are aligned parallel to the main (S_2) foliation and wrap the hornblende (I) porphyroclasts.

During increased strain at high P-T conditions and during retrogression, sphene and rutile are lost and ilmenite appears as a matrix phase randomly distributed throughout the rock.

During retrogression to low P-T conditions, the hornblende (II) porphyroblasts are progressively pseudomorphed by a third amphibole (III), possibly tremolite. This

third generation of amphibole is extremely fibrous and replaces the hornblende (II) in a mottled, patchy, corona-type manner.

4.7.1.2 The Second Amphibolite Group

Within this amphibolite group (e.g. Samples VAM19B, LEF21E, L78-2, VAM42-1) the low-strain assemblage consists of:

quartz + plagioclase + hornblende (I) + hornblende (II) + garnet + epidote

Accessories commonly present are sphene and rutile.

In the low-strain member (Plate 4.4b) large (up to 1.5 mm in diameter), subhedral quartz and plagioclase porphyroblasts are randomly distributed throughout the rock and showing numerous subgrain textures. Plagioclase has well-developed lamellar twins and often contains abundant inclusions of a fine-grained high-relief mineral creating a dusty appearance.

Hornblende (I) porphyroblasts occur as large (1.5 to 3 mm long) subhedral to anhedral laths, randomly orientated throughout the rock. Garnet porphyroblasts are present as an original constituent of the mineral assemblage and probably reflects a more Fe-rich precursor than group 1 (Section 4.7.1.1). Garnet porphyroblasts are large (up to 4 mm in diameter), subhedral, highly fractured, and randomly distributed throughout the rock (Plate 4.4b). In the low-strain high P-T member, sphene is abundant as euhedral lozenge-shaped grains, occasionally overgrown with minor rutile grains.

Increasing strain at high P-T conditions caused re-equilibration and the quartz-plagioclase matrix is recrystallised and reduced to a uniform grain-size (0.2 mm diameter) with sharp grain boundaries at approximately 120° angles. However, lamellar twins in the plagioclase are not deformed and all the quartz and plagioclase grains have a clean appearance. Hornblende (I) porphyroclasts are subjected to equilibration and grain-size reduction resulting in subhedral (0.2 mm diameter) grains, whereas, garnet porphyroclasts are reduced in size along with quartz-plagioclase-hornblende. However, the numerous small (0.2-0.3 mm diameter) garnet porphyroblasts are amalgamated in diffuse clusters and appear similar to "snowflakes".

With increasing strain during retrogression to lower P-T conditions, the quartz and feldspars are deformed, with quartz subjected to more advanced grain-size reduction. Recrystallisation also results in the development of elongate quartz grains parallel to the main (S_2) foliation, creating well-defined banding and stringers. Hornblende (I) porphyroblasts are broken down and deformed into elongate laths and

intergrown with porphyroblasts of hornblende (II). Further retrogression results in hornblende (II) being pseudomorphed by fibrous amphibole (III) which is possibly tremolite. The elongate amphibole (II) and (III) laths are orientated parallel to the main (S_2) foliation.

Garnet porphyroclasts are broken-down, fractured and wrapped with the matrix minerals. With increasing strain and retrogression, biotite, zoisite and chlorite become the dominant accessory minerals, and are distributed throughout the rock.

4.7.1.3 The Third Amphibolite Group

This amphibolite group (e.g. Samples STAV5, STAV7) has the simplest low-strain assemblage of all the amphibolites within the study area (Plates 4.5a, b, c). This equilibrated assemblage consists of:

quartz + plagioclase + hornblende (II) + epidote

Accessories commonly present are sphene and ilmenite.

Within low-strain samples quartz and plagioclase consist of large (up to 0.4 mm wide), subhedral grains which show a variety of subgrain textures. Plagioclase grains are typified by lamellar twins. Hornblende is of a second generation type, consisting of long (0.2 to 0.4 mm long) euhedral, elongate laths randomly orientated throughout the rock. Ilmenite is randomly distributed throughout the rock and aligned parallel to the main (S_2) foliation (Plates 4.5a, b).

With increasing strain, the quartz and plagioclase are recrystallised and reduced in size (0.1 mm diameter) with re-equilibration developing sharp boundaries at 120° between quartz and plagioclase and 90° with elongate hornblende (Plate 4.5b). Hornblende (II) porphyroblasts are aligned parallel to the main (S_2) foliation and appears to wrap leucocratic cores. At this stage the hornblende (II) consists of laths (0.2-0.4 mm long) and subhedral to euhedral in shape. Ilmenite fabrics are generally preserved. However, of particular note is that anhedral porphyroblasts of garnet have been developed (0.2 mm diameter) and some hornblende or biotite has altered to chlorite (Plate 4.5c).

4.7.2 Gabbroic and Doleritic Lithologies

The low-strain varieties of gabbro and dolerite preserve an assortment of original magmatic mineral assemblages and textures between plagioclase and pseudomorphed pyroxene and/or olivine porphyroblasts. However, the magmatic mineral assemblages are extensively modified during cooling to the ambient P-T conditions resulting in the development of distinctive corona structures. Similar

Plate 4.5

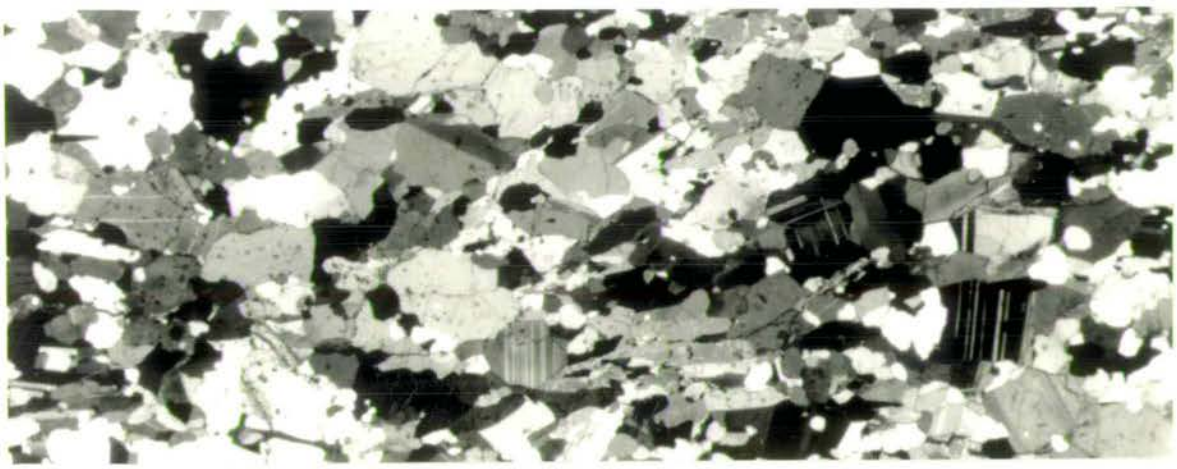

Plate 4.5a: Low-strain partially equilibrated amphibolite assemblage (Sample STAV5), typified by a weak fabric and variable grain-size. Field of view is approximately 6 mm across.

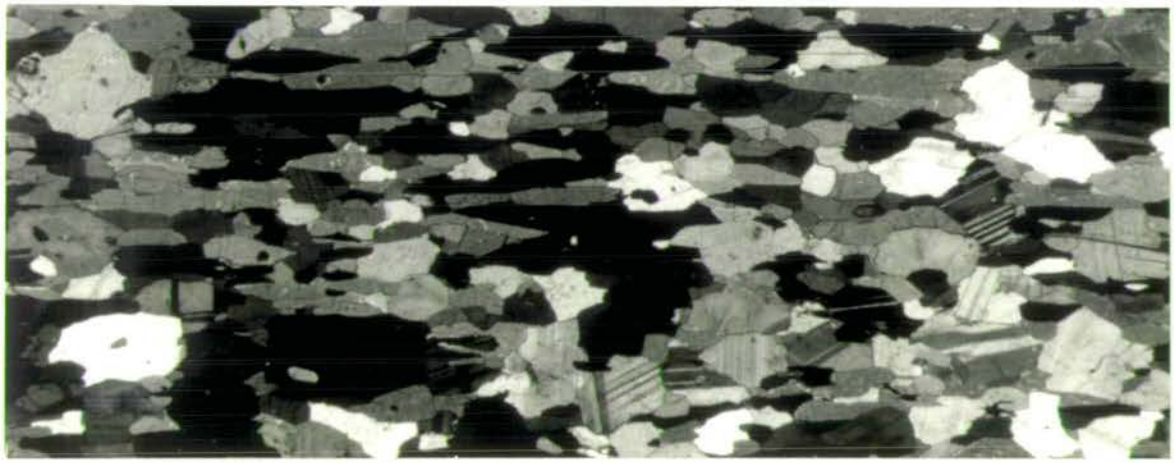

Plate 4.5b: Re-equilibrated amphibolite assemblage (Sample STAV7) showing a well-developed (S_2) fabric. The re-equilibrated assemblage is typified by a uniform grain-size and sharp angular boundaries. Field of view is approximately 6 mm across.

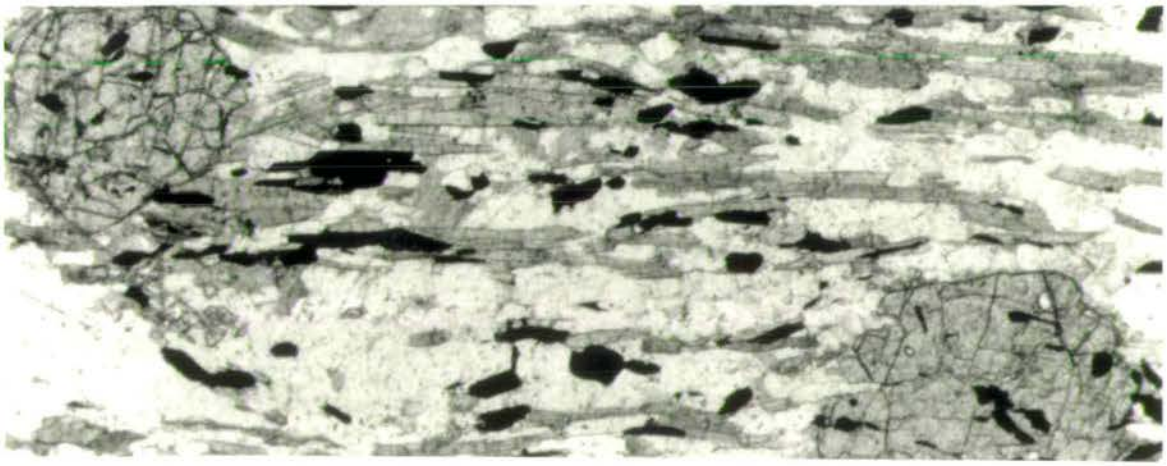

Plate 4.5c: Retrogressed greenschist-facies amphibolite assemblage (Sample ASK34). Subhedral garnet porphyroblasts appear to overprint a well-banded retrogressed amphibolite fabric. Amphibolite altered predominantly to tremolite and chlorite. Field of view is approximately 6 mm across.

textures and mineral assemblages have been identified within the Volvi Complex by Dixon and Dimitriadis (1984; *see* Section 4.2.1). Further reaction textures are developed which are dependent on the bulk composition, the input of fluid which is usually synchronous with deformation, and on the P-T conditions prevalent during deformation. The range of textures result both from deformation and re-equilibration at constant high P-T conditions, and progressive retrogression in association with increasing strain and lower P-T conditions.

The wide variation of mineral assemblages in the mafic lithologies is partly due to the original bulk composition of the rock. In Mg-rich dolerites little or no garnet will be produced under any conditions, whereas in the more evolved Mg-rich dolerites and diorites a range of reactions and subsequent assemblages are developed with the input of fluid.

4.7.2.1 Gabbroic Lithologies

Two broad groups of gabbro and a suite of dioritic lithologies are found within the study area. Mineral assemblages within the first group of gabbros are interpreted as the result of equilibration of the original magmatic assemblages to the regional ambient conditions under relatively anhydrous conditions (Section 4.7.3). The low-strain anhydrous assemblage consists of (Plate 4.6a):

plagioclase ± quartz ± olivine + orthopyroxene + clinopyroxene + amphibole ± garnet + ilmenite

Accessories commonly present are sphene, rutile, biotite, spinel and zoisite.

The mineral assemblage within the second gabbroic group is interpreted as the result of retrogression under hydrous conditions (Section 4.7.3). The textures are similar to the gabbros of the first group, but are pseudomorphed by hydrous retrogressive mineral assemblages. The low-strain hydrous assemblage consists of (Plate 4.6b):

plagioclase ± quartz + amphibole ± garnet + ilmenite

Relics of ortho- and clinopyroxene are found in samples along the progression from anhydrous to hydrous alteration (saussuritisation). Accessories commonly present are sphene, rutile, zoisite and spinel.

Low-strain samples of both anhydrous and hydrous groups preserve original igneous textures (e.g. ophitic to sub-ophitic, intersertal and intergranular; Plates 4.6a, b) and metamorphic effects are largely confined to the formation of corona structures around primary igneous olivine, clinopyroxene, orthopyroxene and ilmenite (Plates 4.7, 4.8. 4.9; Fig. 4.4).

Plate 4.6

Plate 4.6a: Low-strain anhydrous gabbro assemblage (Sample 90VAMR88) with well-developed coronitic structures developed by the reactions between olivine, clinopyroxene and ilmenite cores and plagioclase. Field of view is approximately 3 mm across.

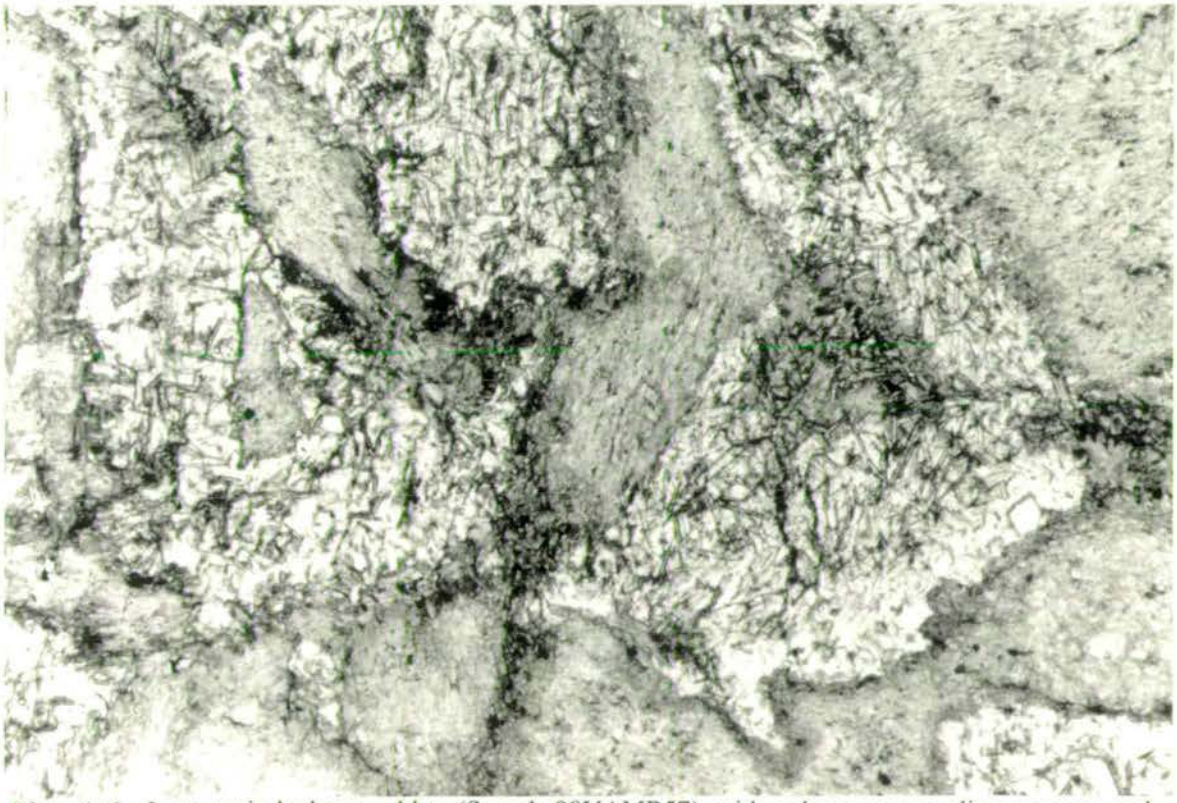

Plate 4.6b: Low-strain hydrous gabbro (Sample 90VAMR57), with orthopyroxene, clinopyroxene and olivine extensively pseudomorphed by amphiboles. Plagioclase phenocrysts are filled with zoisite laths due to saussuritization. Field of view is approximately 6 mm across.

Plate 4.7

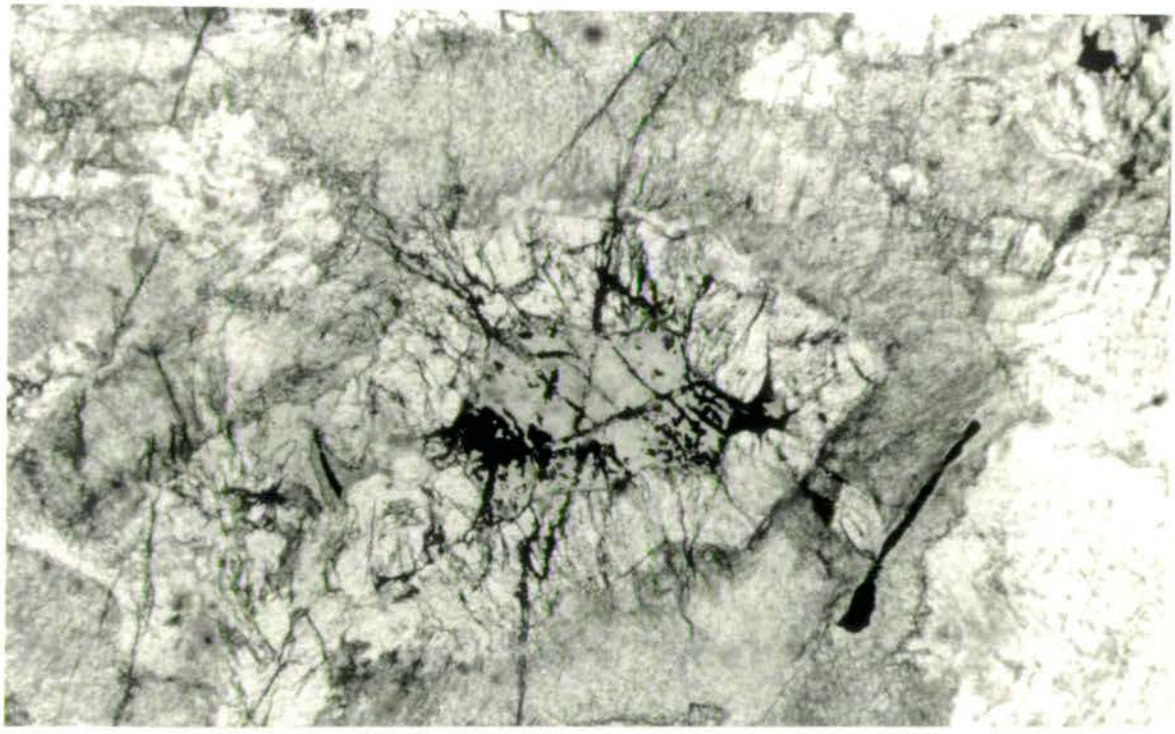

Plate 4.7a: Coronitic sequence of pseudomorphed olivine within the core (now pseudomorphed by tremolite-ilmenite), enveloped by subhedral orthopyroxene, followed by amphibole. Field of view is approximately 1.5 mm across.

Plate 4.7b: Mosaic of orthopyroxene which has completely pseudomorphed an original olivine core. The original core was probably wrapped by orthopyroxene, garnet (note the extensive inclusions) followed by a thin partial rim of granular amphibole. Also note the dense fine-grained dusting (probably zoisite) within the leucocratic minerals. Field of view is approximately 1.5 mm across.

Plate 4.8

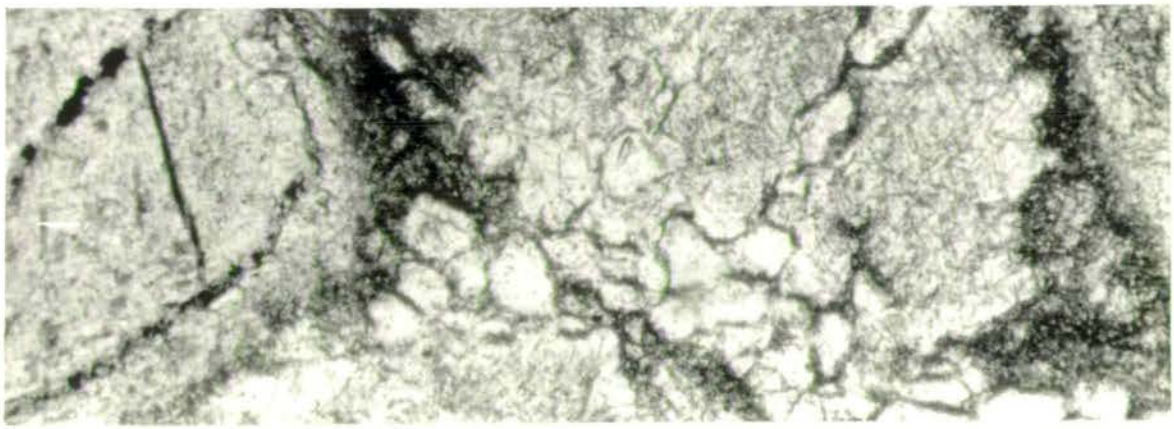

Plate 4.8a: Clinopyroxene core successively wrapped by granular amphibole followed by fibrous amphibole. Plagioclase is extensively filled with randomly orientated zoisite laths. Concentrations of fine-grained laths are distributed along the boundaries between quartz and plagioclase. Field of view is approximately 2 mm across.

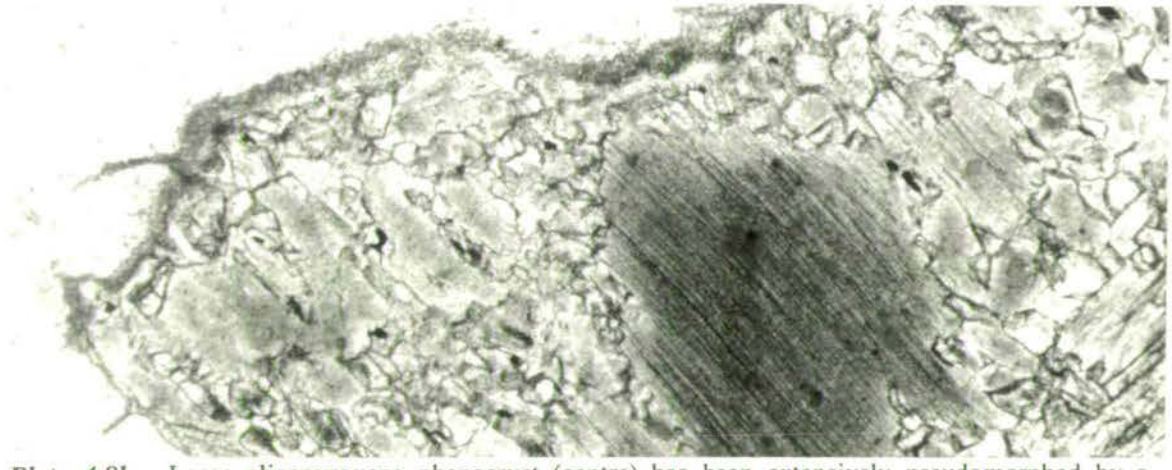

Plate 4.8b: Large clinopyroxene phenocryst (centre) has been extensively pseudomorphed by a mosaic of orthopyroxene-clinopyroxene intergrowths. The original clinopyroxene phenocryst rimmed by successive coronas of granular followed by fibrous amphibole. Field of view is approximately 1.5 mm across.

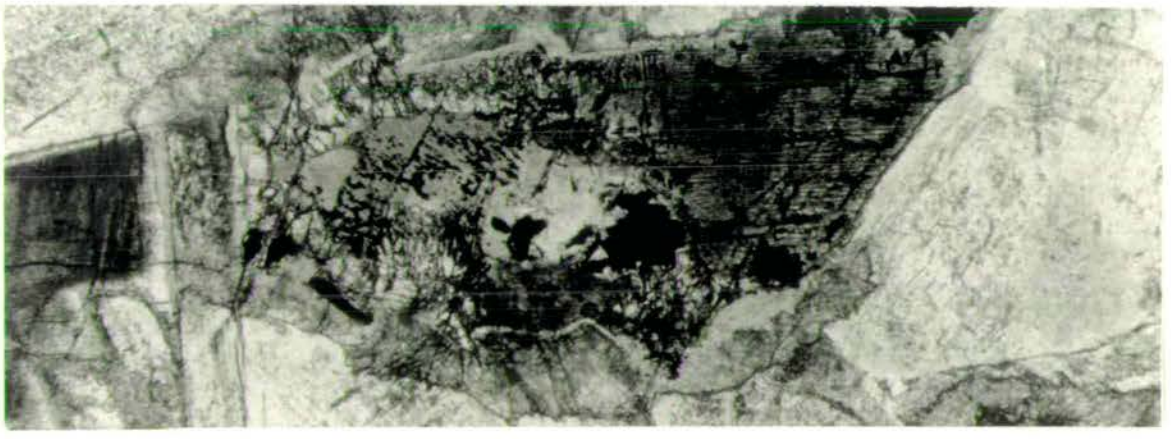

Plate 4.8c: Large clinopyroxene and pseudomorphed olivine (now tremolite-ilmenite) phenocrysts, both rimmed by successive granular and fibrous amphibole layers. However, the pseudomorphed olivine has been wrapped initially by orthopyroxene. Large ilmenite grains also have a similar multiple amphibole corona Field of view is approximately 2 mm across.

Plate 4.9

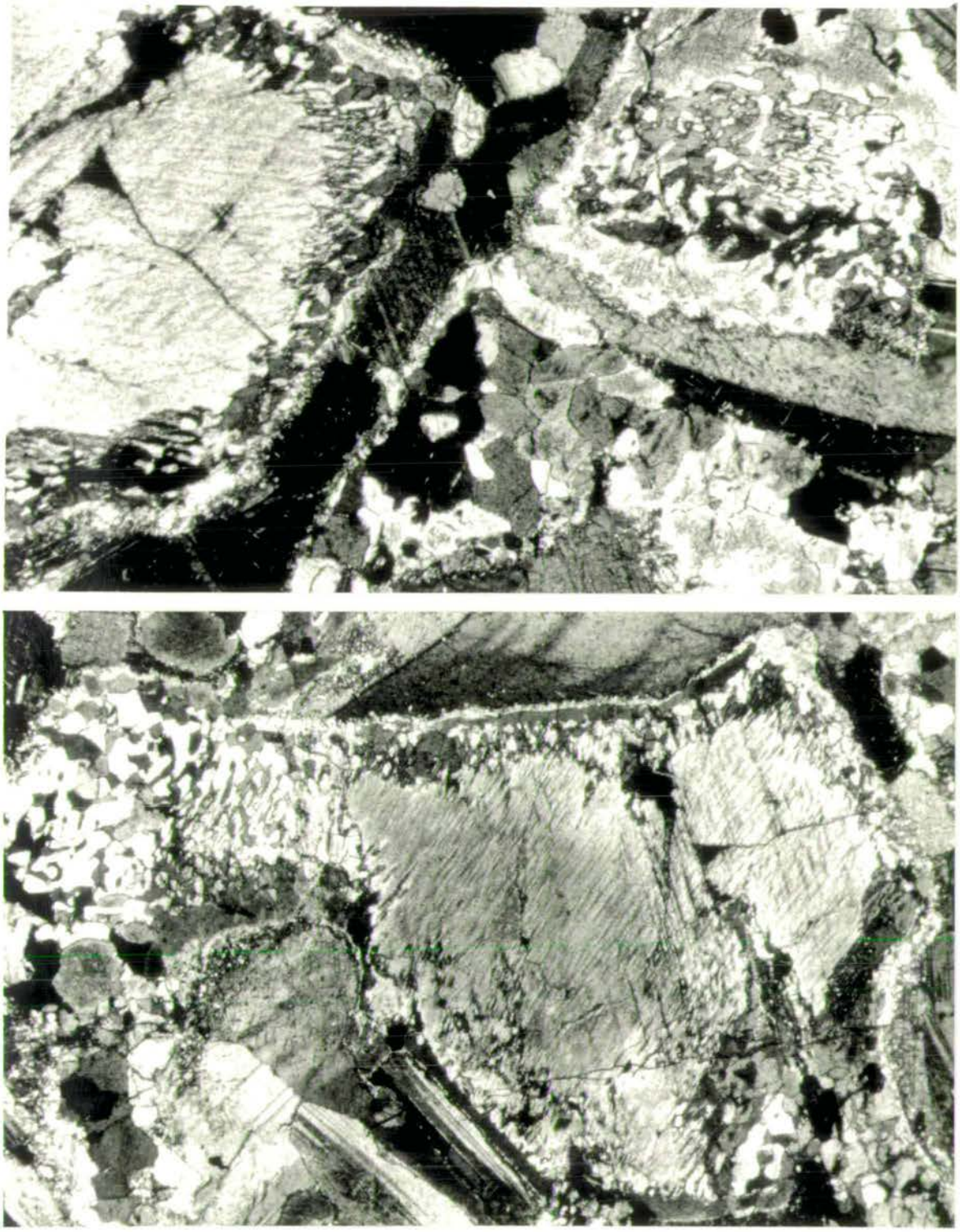

Plate 4.9: Large clinopyroxene phenocrysts show complex corona textures. The clinopyroxene core is initially rimmed by well-developed symplectic intergrowths with orthopyroxene. This coronitic layer is in turn enveloped by granular and fibrous amphibole layers respectively. Large mosaics of orthopyroxenes peudomorph a subhedral precursor, possibly with an olivine core. The orthopyroxenes are also wrapped by successive granular followed by fibrous coronitic textures. A fine-grained dense dusting of zoisite is developed within the plagioclase. Field of view is approximately 3 mm across.

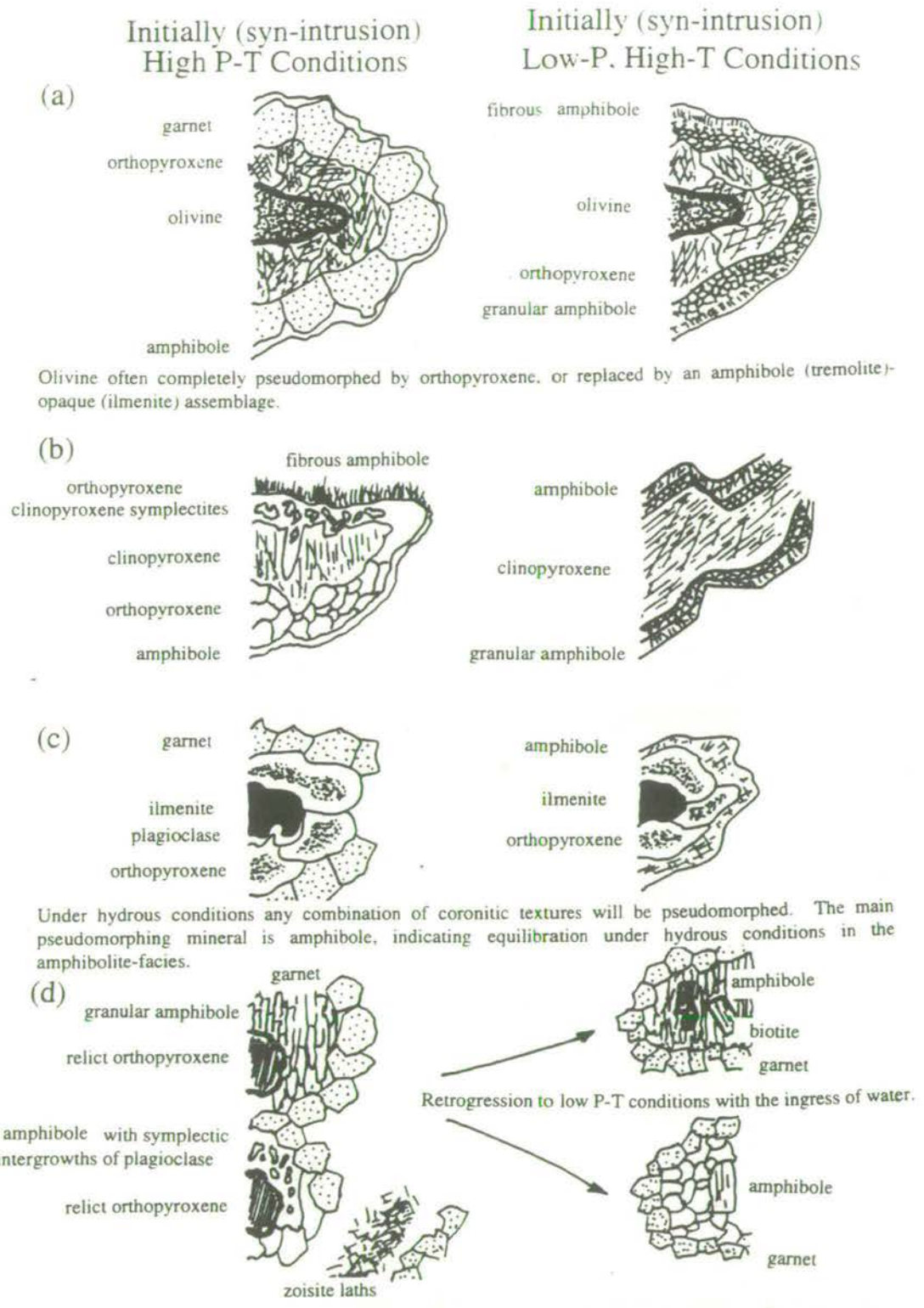

Fig. 4.4: Schematic interpretation of corona structures developed within gabbros. Examples of the main corona textures developed by reactions in anhydrous conditions between (a) olivine-plagioclase, (b) clinopyroxene-plagioclase and (c) ilmenite-plagioclase, and pseudomorphing textures developed in hydrous conditions (d).

Large euhedral plagioclase phenocrysts with well-defined lamellar twins are randomly orientated throughout the gabbros. These plagioclase laths are variably filled by a mesh-work of randomly orientated and variably sized laths of euhedral zoisite. Zoisite growth is attributed to the action of fluids and hydration of the plagioclase. Usually the plagioclase cores are filled with inclusions, whereas the rims in contact with other mineral phases are clean (Section 4.7.3).

Olivine is rarely preserved, but when present is found within cores of a multi-shelled corona structure (Plate 4.7a; Fig. 4.4). However, olivine is usually exhausted and completely pseudomorphed during ambient cooling reactions with plagioclase (Plate 4.7b; *see* Section 4.7.3, for a discussion on the reaction sequence between olivine and plagioclase).

The remnant olivine is highly fractured and anhedral in shape. Typical pseudomorphs consist of large subhedral orthopyroxene porphyroblasts or a mixture of fine-grained clino- and orthopyroxenes. The olivine (or ex-olivine) core is encapsulated within a shell of large, subhedral orthopyroxene, which is in turn surrounded by an amphibole shell. Occasionally a garnet shell is developed between the coronas of orthopyroxene and amphibole.

Orthopyroxene is present in several forms; as an original magmatic mineral, as coronas (to olivine, oxides and clinopyroxene), and as symplectic intergrowths with magmatic clinopyroxene. Magmatic orthopyroxene occurs as single large subhedral to anhedral phenocrysts. With increasing strain and ingress of fluid it is pseudomorphed by granular and fibrous amphibole. The large orthopyroxene crystals have a well-developed cleavage and weak exsolution lamellae developed parallel to the cleavage. These magmatic orthopyroxenes are usually rimmed by a single corona of fine-grained amphibole aggregates. However, occasionally a second corona of dark fibrous minerals (possibly amphibole, zoisite, spinel) are also developed. Withinthese fibrous shells, small laths of reddish-brown biotite are also present.

Orthopyroxene is far more common as subhedral aggregates at the core of multiple shelled coronas. When in this configuration they are interpreted to have completely pseudomorphed original olivine, since the coronas around the orthopyroxene aggregates are the same as those surrounding relict olivine.

Coronas of orthopyroxene also occur as large subhedral to anhedral laths around ilmenite. In this association the orthopyroxene has a zoned, pleochroic, reddish-brown colouration. The zoning is produced by a dense dusting of fine-grained particles (possibly spinel) within the core whereas rims with adjacent minerals are clean. In samples which have remained dry and at high P-T conditions,

orthopyroxene is found as symplectic intergrowths with clinopyroxene. These symplectic intergrowths are commonly observed in broad coronas around clinopyroxene cores. Orthopyroxene is also found along exsolution lamellae within the large clinopyroxenes.

Clinopyroxene is found predominantly as large subhedral to anhedral magmatic crystals with well-defined exsolution lamellae parallel to the cleavage. The clinopyroxene crystals are enveloped in successive shells of subhedral, granular orthopyroxene, followed by fine-grained granular aggregates of amphibole. Brown inclusions of an unknown mineral are occasionally found along the clinopyroxene exsolution lamellae. Clinopyroxene may also be developed in coronas around olivine (Section 4.7.3), but, this is difficult to assess in the available samples.

Amphibole is present within both groups of gabbros. In the first group, amphibole is only present as the outermost shell to the original magmatic minerals. This distribution of amphiboles is probably due to the composition of the rock studied, however, the amphibole coronas may be due to late minor ingress of water.

Hydration and the development of amphibole is well displayed in the gabbros of the second group. Within these gabbros, several generations of amphibole occur, which pseudomorph the magmatic olivine, ortho- and clinopyroxene and also the corona textures developed around these minerals. Saussuritisation is therefore interpreted to have taken place after cooling of the gabbro to the regional ambient temperature. The extent of saussuritisation within the area appears to have been controlled on a local scale given the wide variety of fresh (anhydrous) and saussuritised (hydrous) gabbros which occur. The saussuritised gabbros appear to be associated with deformation, since they preserve textures and progressively intensified fabrics which are related to shear zone development. Therefore equilibration of the original magmatic assemblages at the ambient P-T conditions is inferred to have occurred prior to the development of shear zones and synchronous saussuritisation.

Several different coronas are developed around the oxide minerals (usually ilmenite, although occasionally magnetite or brownish-green spinel are also present) within the low-strain anhydrous, high P-T gabbros (Plates 4.8). These consist of an anhedral oxide core usually surrounded by subhedral granular brown amphibole. This amphibole shell is occasionally surrounded by a corona of subhedral to euhedral garnet porphyroblasts. More rarely the oxide is surrounded by zoned orthopyroxene with a distinctive orange-brown colour.

Garnets are variably developed and occur as a range of different coronas. Depending on the composition of the rock and the specific reactions which have taken

place, garnet occasionally occurs as clear porphyroblasts but more frequently is crowded with inclusions. The inclusions occur as either vermicular intergrowths or small equidimensional grains. The inclusions may be clinopyroxene, hornblende, spinel or plagioclase.

Continued deformation and saussuritisation of the gabbros has produced a broad range of amphibolite assemblages. Equilibration of these saussuritised and deformed ex-gabbros at peak amphibolite-facies conditions will result in a range of well-equilibrated amphibolites. Retrogression and deformation of these equilibrated amphibolites has then resulted in the range of amphibolites found within the study area (Section 4.7.3).

4.7.2.2 Dioritic Lithologies

The dioritic lithologies (Samples LEF1, 90VAMR33, 90VAMR26) show a similar evolution to the gabbroic lithologies, with high P-T conditions during initial intrusion and subsequent deformation and hydration to varying degrees. The original magmatic and subsequent cooling assemblage consists of (Plate 4.10):

plagioclase + quartz + hypersthene + garnet + biotite + ilmenite + amphibole

Accessories commonly present are zoisite and sphene.

In low-strain samples plagioclase and quartz are the dominant minerals distributed homogeneously throughout the rock, and show various subgrain textures. Large phenocrysts are preserved with well-defined multiple lamellar twins developed in the plagioclase. Grain-size reduction and recrystallisation occurs with increased strain, particularly in quartz.

The other minerals are distributed in discrete clusters and semi-continuous stringers throughout the rock (Plates 4.10, 4.11). Hypersthene occurs as large (0.5 to 1.5 mm wide) stubby anhedral laths, with a pleochroic pink and green colouration. All hypersthene grains have either a fine-grained, narrow (0.01 to 0.03 mm wide) corona of subhedral granular amphibole or a partial or complete corona of large (0.1 to 0.3 mm diameter) euhedral to subhedral garnet porphyroblasts. A narrow (0.01 mm wide) corona of quartz or plagioclase is usually developed between the hypersthene and garnet. Garnet coronas also occur around ilmenite and biotite. The different types of corona around hypersthene are attributed to variations in the modal proportion and composition of adjacent feldspar (Fig. 4.5).

Biotite has a reddish-brown colouration and varies from anhedral masses to subhedral laths with increased deformation and the development of a well-defined cleavage.

Plate 4.10

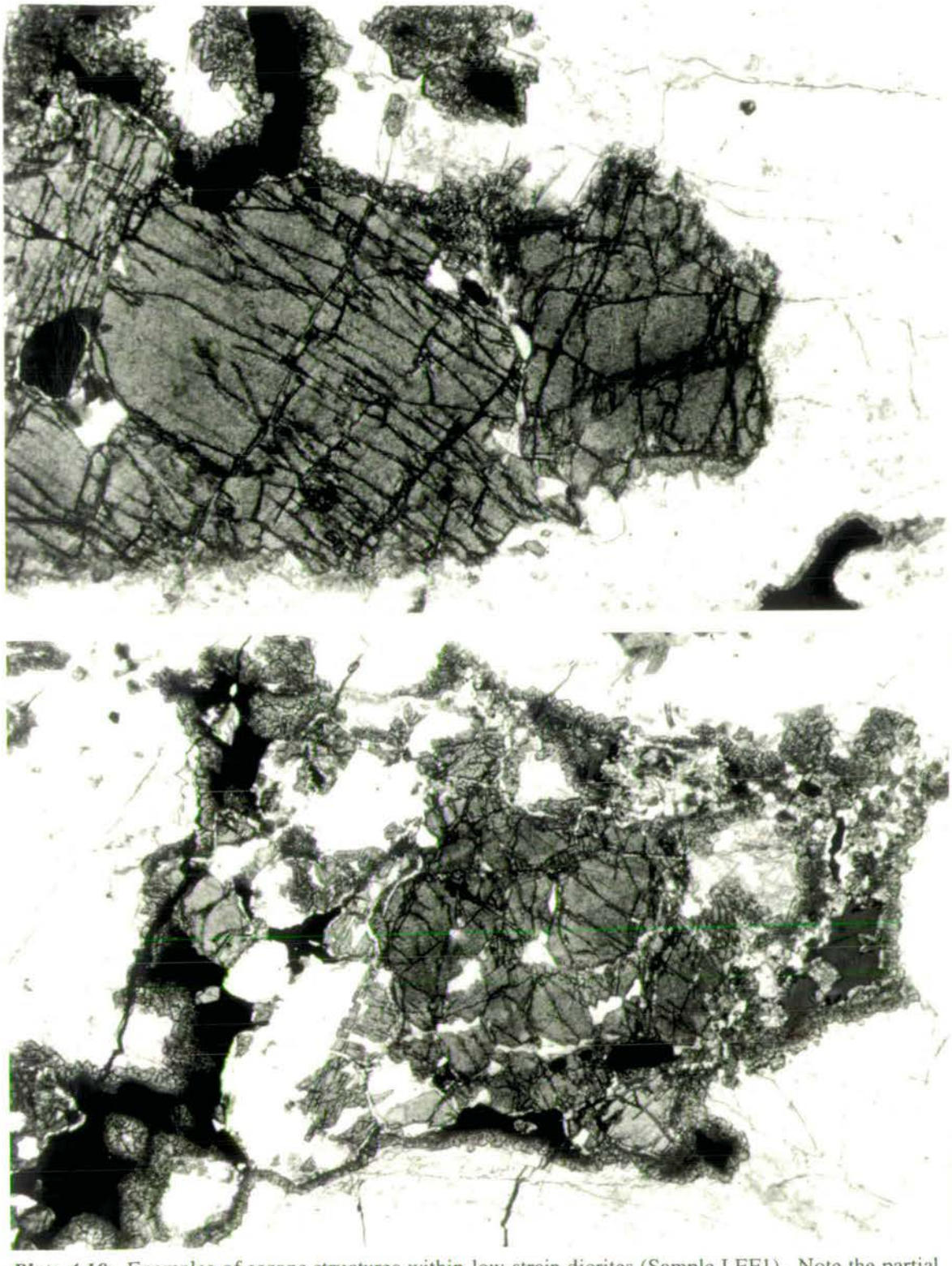

Plate 4.10: Examples of corona structures within low-strain diorites (Sample LEF1). Note the partial coronas of garnet and amphibole within close proximity around the same or adjacent hypersthene porphyroblasts. This is attributed to reactions preferentially developed resulting from the distribution of plagioclase and K-feldspar in the leucocratic matrix. Filled of view is approximately 2 mm across.

Plate 4.11

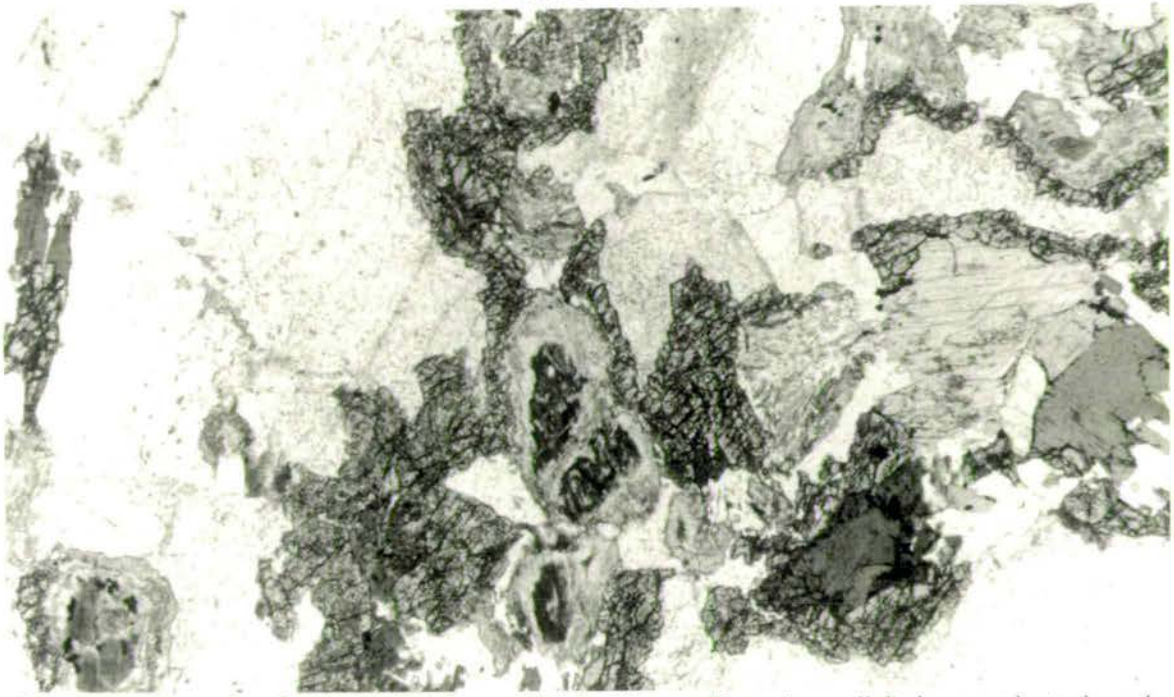

Plate 4.11: Example of a dioritic lithology which has been subjected to a slight increase in strain and retrogression (Sample 90VAMR33). Note the weak layering of the melanocratic assemblages. Hypersthene has been at least partially retrogressed to amphibole (tremolite-cummingtonite) with relicts only preserved within the cores. Biotite has increased in its total modal proportion within the rock, with laths having increased in size. Laths of randomly orientated, subhedral zoisite are abundant within the palgioclase. Field of view is approximately 3 mm across.

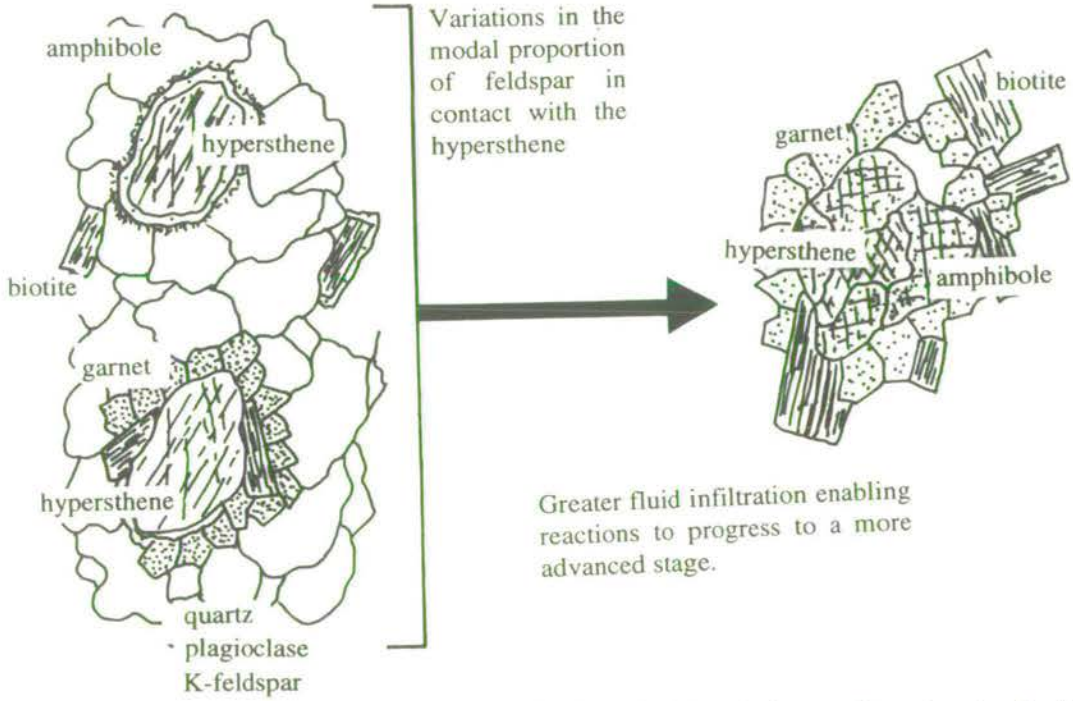

Fig. 4.5: Typical variations of corona textures developed within diorites, attributed to the distribution and modal proportion of K-feldspar and the subsequent reactions with hypersthene-biotite and ilmenite.

The modal proportion of the mineral assemblage is altered with increasing strain and ingress of water. Hypersthene is predominantly altered to subhedral elongate laths of amphibole (possibly cummingtonitic hornblende) and eventually to fibrous laths of amphibole (tremolite). Amphibole coronas around all the mineral phases are enlarged (now 0.2 to 0.3 mm wide) and consist of euhedral to subhedral grains.

The increase in the modal proportion of biotite is reflected by an enlargement of the laths, which now typically range up to 1.5 mm in length. Garnet is preserved as euhedral to subhedral porphyroblasts in semi-continuous to continous coronas around several mineral phases. However the increased strain has started to redistribute and realign the assemblage into a weak foliation (Plate 4.11).

4.7.3 Reactions and P-T Settings

The P-T conditions of formation of metabasic rock types in the greenschist-facies and amphibolite-facies are difficult to constrain. Although the lower temperature limit of the greenschist-facies is quite well defined by the breakdown of pumpellyite (Schiffmann and Liou, 1980, 1983), changes in metabasites within the greenschist and amphibolite-facies are largely the result of continuous reactions and no simple experimental system is of direct relevance. Even the changes found at lower pressures, in the hornblende- and pyroxene-hornfels-facies, are not clearly defined. The absence of simple discontinuous reactions makes it difficult to estimate P-T conditions using mineral assemblages and reaction grids. P-T estimates can be made using thermobarometric techniques based on compositional variation in phases like hornblende, garnet and plagioclase (e.g. Spear, 1980; Laird and Albee, 1981; Graham and Powell, 1984), but this is outside the scope of this thesis

Although the P-T conditions for metabasites are difficult to constrain, a progressive transition from magmatic mineral assemblages through a series of cooling reactions to ambient regional temperatures and subsequent retrogression can clearly be seen in the mineral assemblages and textures developed within the basic lithologies of the study area. Some of the most useful textures are in the coronitic gabbros. Coronas between olivine and plagioclase are well known and have frequently been described (e.g. Griffin, 1971a; Griffin and Heier, 1973; Whitney and McLelland, 1973; Grieve and Gittins, 1975; van Lamoen, 1979; McLelland and Whitney. 1980; Grant, 1988; Johnson and Carlson, 1990; Ashworth *et al.*, 1992; Turner and Stuwe, 1992). The corona structures within the Lake Volvi area are comparable to textures which are often found in metamorphosed gabbros from amphibolite and granulite-facies terranes (Gardner and Robins, 1974).

The development of many corona textures implies a direct transition from an unaltered igneous assemblage to an assemblage typical of high temperature, and usually high pressure, metamorphism, with no intervening stage of lower grade conditions. There are two ways in which this might be achieved. The effect of increased temperature would stabilise the low pressure granulite mineralogy (also typical of basic igneous rocks) during the transition to higher pressures (Fig. 4.6). Thus a magma crystallising at moderate depth in the crust might develop olivine + plagioclase initially, but as it cooled below the solidus would enter the medium pressure granulite field so that garnet is produced during the original cooling of the igneous rock (path A, Fig. 4.6). The second way of developing coronas would be for large basic igneous bodies to cool initially near the surface without metamorphism and then to undergo regional burial and reheating without metamorphism taking place until very high temperatures were attained (path B, Fig. 4.6). This might occur if the intrusion were emplaced into dry country rocks, such as acid gneisses, and was buried without being deformed. Both these circumstances would inhibit fluid entering the intrusion to produce the hydrous minerals typical of lower grades of metamorphism (Yardley, 1989). Griffin and Heier (1973) favoured the first type of model for the development of the Norwegian corona textures, but subsequent work on the geological evolution of this region has made the second model look more realistic (Mork, 1986). From the experimentally derived fields of Fig. 4.6, general estimates of the pressure and temperature conditons of corona formation can be derived (Whitney and McLelland, 1973). Whitney and McLelland (1973) made a similar interpretation for the gabbro coronas as Yardley (1989), which is depicted in Fig. 4.6, where the broken lines (A) and (B) represent two possible metamorphic histories for the coronites. One constraint is that in garnet-bearing rocks, pyroxene must be developed prior to garnet. Hence, the paths must pass through the pyroxene-spinel field before entering the garnet field. Path (B) represents slight cooling with rapid burial without any further heating probably resulting from shallow intrusion of the basic magma, followed by burial while still at high-T to maximum P-T conditions. Path (A) illustrates a "retrograde" origin for the coronas with intrusion at depth followed by cooling at constant or increasing pressure through the pyroxene-spinel and garnet fields.

A definitive answer for the development of the gabbros within the study area, however, is more problematic and a single model is probably insufficient to interpret the textures developed. The coronas within the gabbros are particularly helpful towards defining the P-T history for the basic rocks. Two main reactions occur:

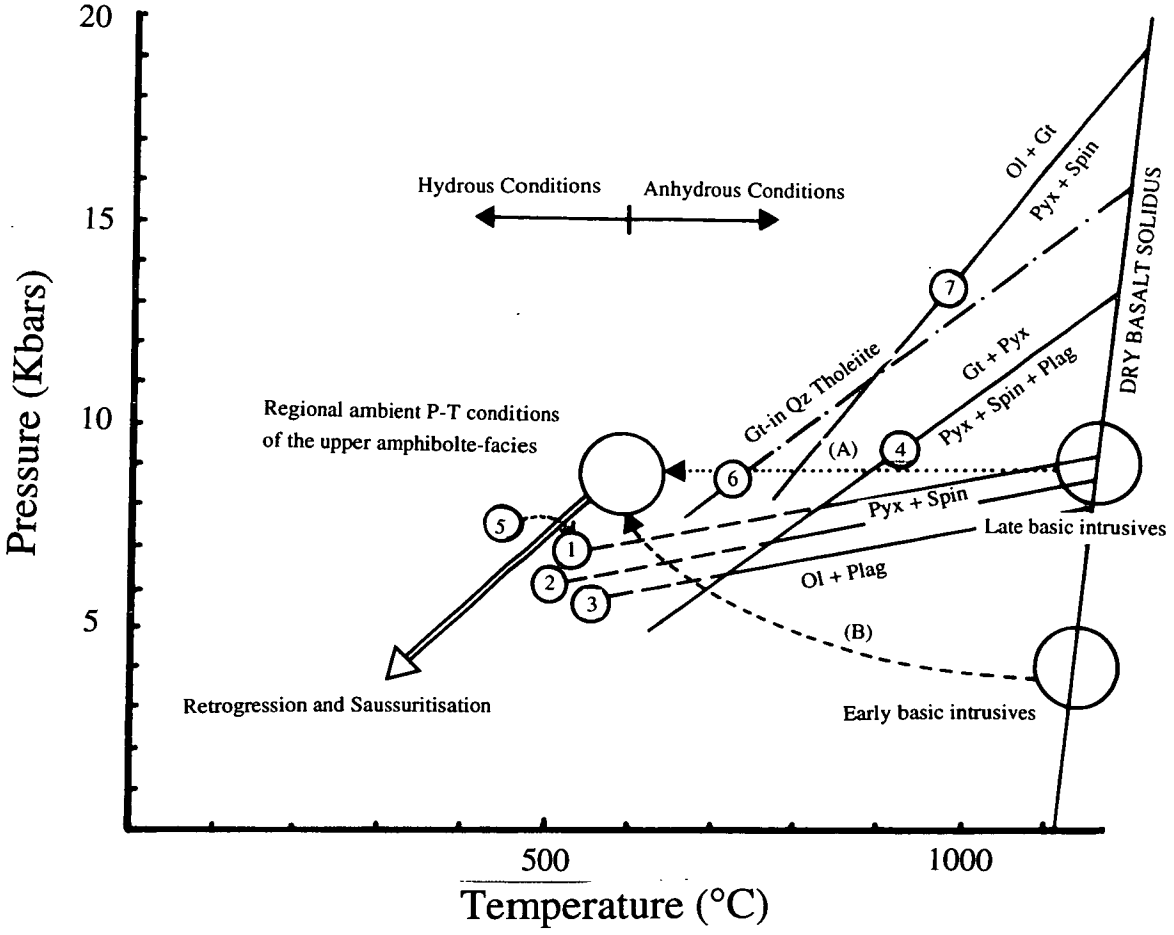

Fig. 4.6: Experimentally determined metabasite equilibria, after Griffin and Heier (1973); most are extrapolated to lower T for clarity.
(1) Disappearance of olivine; Green & Ringwood (1967)
(2) Disappearance of olivine; Irving & Green (1970)
(3) Disappearance of olivine; Fo-An system; Kushiro & Yoder (1966)
(4) Appearance of garnet and pyroxene; Fo-An system; Kushiro & Yoder (1966)
(5) Suggested approximate position for the disappearance of olivine, after Green & Hibberson (1970)
(6) Appearance of garnet; Green & Ringwood (1967)
(7) CaO-MgO-Al_2O_3-$SiO2$ system; MacGregor (1970). This curve will lie at higher P in systems containing Cr_2O_3 and Fe_2O_3.

Paths A and B illustrate different possible origins for corona textures between plagioclase and olivine. Path A denotes cooling of basaltic magma under deeper crustal conditions to produce coronas in a single stage of cooling (at slightly higher pressures, corona formation could commence above the solidus). Path B illustrates initial high level cooling to produce gabbro followed by regional burial and heating to high pressure conditions. These early low-pressure basic intrusives are the source of local heat for the cordierite + melt textures described in section 4.4.

olivine + plagioclase → orthopyroxene + clinopyroxene + spinel

plagioclase + orthopyroxene + spinel → garnet

Further reactions include the development of; (a) needle-like and dust-like spinel inclusions in primary plagioclase, which formed by replacement of the anorthite component of the plagioclase during the corona-forming reactions, and (b) amphibole coronas around opaque oxides formed by reaction between the oxides and plagioclase, with the addition of magnesium derived from coexisting olivine.

McLelland and Whitney (1980) noted that garnet occurs primarily as the outer rim of coronas surrounding olivine and pyroxene, and less commonly as lamellae or isolated grains within plagioclase. The formation of garnet and metamorphic spinel was interpreted to be dependent upon the anorthite content of the plagioclase. Plagioclase more sodic than $An_{38\pm2}$ does not exhibit spinel clouding and garnet rarely occurs in contact with plagioclase more albitic than $An_{36\pm4}$. As a result of these compositional controls, the distribution of spinel and garnet mimics and visually enhances original igneous zoning in plagioclase (McLelland and Whitney, 1980). Similar textures are found in the Volvi gabbros, but, more detailed petrographic and analytical studies are required in order to confirm the relevance of composition on specific corona assemblages.

Grieve and Gittins (1975) determined the P-T conditions for corona development in olivine-plagioclase systems to an average equilibrium temperature of approximately 850°C, which indicates sub-solidus temperatures for the corona reaction. However, Whitney and McLelland (1973), used published experimental data to propose P-T conditions of corona formation to be in the order of 8 kb and 800° C for the garnet-bearing coronas, with somewhat lower pressures indicated for the clinopyroxenes-spinel coronas.

In conclusion, the gabbroic coronites can be interpreted as showing a series of early and late textures. The early coronites show;

1) Crystallisation, probably from an undersaturated basic magma, at pressures possibly less than about 4 kb with the precipitation of olivine + plagioclase ± clinopyroxene.
2) Slow cooling initially at a constant pressure of approximately 4 kb, followed by a progressive increase in pressure to approximately 8 kb. This resulted in reaction between olivine and plagioclase to produce orthopyroxene.
3) With continued cooling amphibole was developed in most coronas in place of garnet.

The late gabbroic coronites can be interpreted as showing;

1) Crystallisation, probably from an undersaturated basic magma, at pressures less than about 9 kb with the precipitation of olivine + plagioclase + spinel ± clinopyroxene.
2) Slow cooling at constantly high pressures of approximately 8-10 kb. This resulted in reaction between olivine and plagioclase to produce orthopyroxene-clinopyroxene-spinel coronas, followed by the reaction between the olivine, pyroxenes, spinel and plagioclase to form garnet and at the expense of pyroxene.
3) With continued cooling, amphibole was developed in most coronas in place of garnet and clinopyroxene.

In most cases the presence of amphibolite-facies rocks with those of the granulite-facies, is a result of later reworking and infiltration of fluids (Yardley, 1989). This also appears to be true for the study area as the textures developed by slow cooling of magmatic assemblages are pseudomorphed or "saussuritised" by hydrous mineral phases, following the generalised reaction.

orthopyroxene + clinopyroxene → amphibole

The composition of the initial gabbroic lithology prior to saussuritisation and deformation may have determined whether the amphibolite contains garnet and zoisite. Re-equilibration of the deformed gabbros results in typical amphibolites. This interpretation is verified as a small pod (2-3 m wide) with a gabbroic core and sheared amphibole margin was found along the Vamvakia river (Insert, Map C).

4.8 Conclusions

Correlation of the P-T conditions estimated from distinctive mineral assemblages and textures developed within the various lithologies of the Lake Volvi area have enabled a composite qualitative P-T history to be produced (Fig. 4.7). The earliest component of the P-T history is the migmatitic basement which preserves evidence of an early (M_1) migmatite forming event, possibly of Hercynian age (Chapter 1). These early migmatites are inferred to have been in a metastable condition due to the preservation of their textures and fabrics. Therefore P-T conditions have been inferred to be approximately 200-400°C and 2-4 kb in order to have maintained the metastable conditions, and to enable a convenient starting point for the P-T path with early intrusions at low-P (Fig. 4.7). This is a necessary condition for the preservation of undeformed sedimentary screens between the dykes. During initial transtension of these basement lithologies, basic igneous intrusions (sheeted dykes and gabbroic bodies) of the Volvi Complex increased the local temperature gradient while remaining at low pressures (Fig. 4.7). The P-T conditions

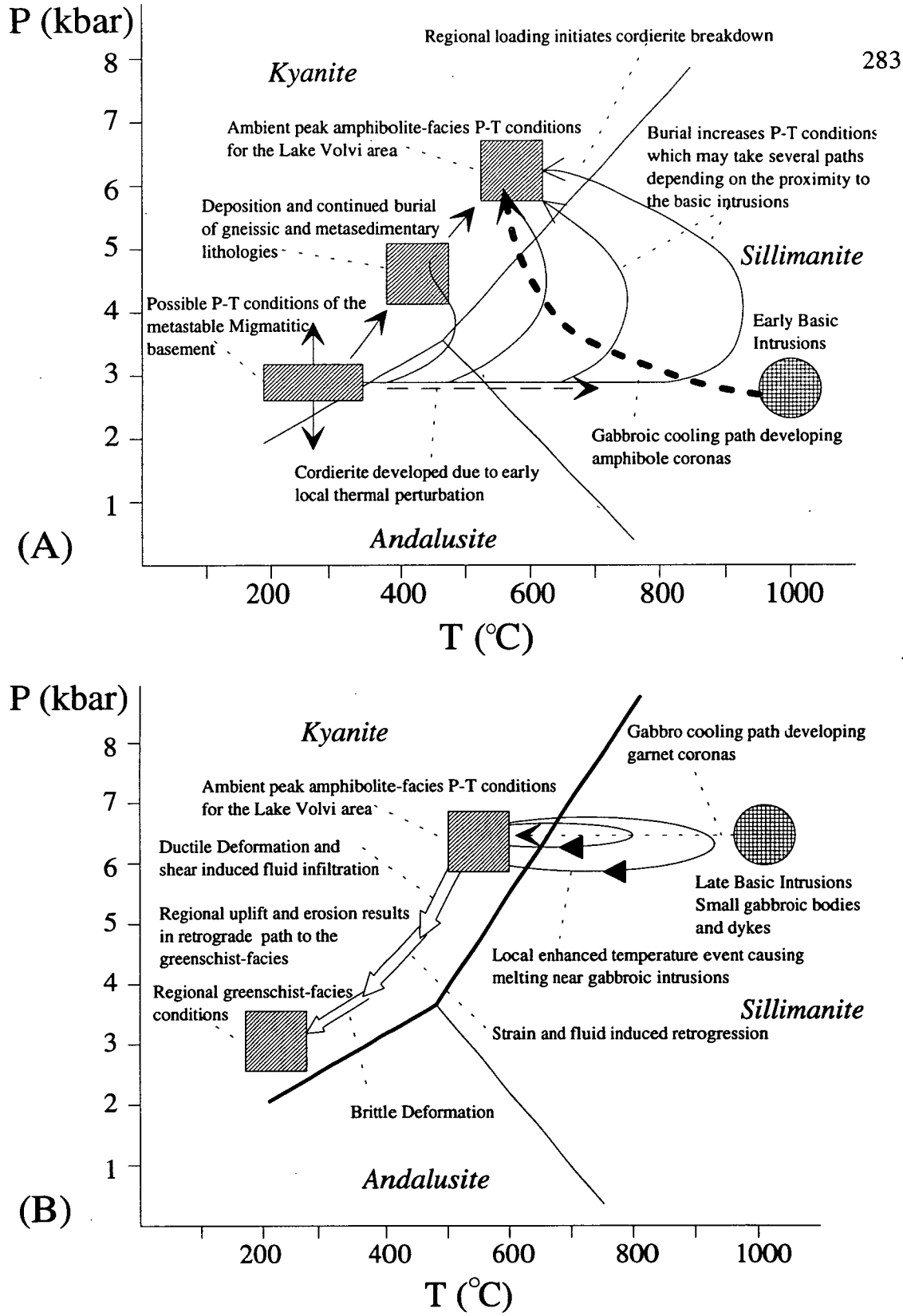

Fig. 4.7: Schematic qualitative P-T paths for the study area, determined from mineral assemblages and textures. (A) The initial prograde history, from the initial intrusion phase at low P up to the peak pressure caused by transpressional loading, (B) "Syn-loading" and subsequent unroofing history, showing highest P intrusions of gabbro and their effects, followed by tectonically assisted retrogression.

of these early intrusions are considered to be initial magmatic temperatures of 1000-1100°C intruded at relatively shallow depths at pressures of 2-4 kb (Section 4.7.3). Evidence for this early thermal event is shown by a distinctive cordierite bearing mineral assemblage within some of the Purple Migmatite lithologies which are in close proximity to the mafic intrusions (Section 4.4.2; Insert, Map C). The P-T conditions for the development of cordierite-bearing migmatites are proposed to be low pressures of approximately 2-4 kb and medium to high temperatures of approximately 600-800°C (Section 4.4.3). An isobaric P-T path for the migmatitic basement from low- to high-temperatures is therefore proposed (Fig. 4.7).

Continued development of the strike-slip basin, was associated with further magmatic input and thickening of the crust by tectonic processes and deposition of more recent material (Chapter 6). These processes slowly and progressively buried the migmatite basement lithologies which were not subjected to local thermal perturbation and early metasedimentary deposits within the deeper levels of the pull-apart basin to higher regional P-T conditions (Fig. 4.7). However, the onset of transpressional conditions caused a more rapid regional increase in pressure. From the inferred mechanism and degree of loading (Chapter 6), pressure conditions will be quickly promoted from 2-4 kb to approximately 5-6 kb. Increase in the crustal thickness, along with continued magmatic intrusion caused regional temperatures to increase to 550-650°C (Fig. 4.7). However, early cordierite-bearing lithologies (granulite-facies) reflecting local thermal perturbations will be rapidly promoted up-pressure while still thermally perturbed. This pressure increase resulted in the breakdown of the cordierite assemblage to the more common and distinctive garnet-kyanite-biotite bearing assemblage, characteristic of the upper amphibolite-facies to low granulite-facies (Section 4.4.3). At the same time, the early high-temperature, low-pressure basic assemblages were re-equilibrated resulting in various suites of basic amphibolite-facies assemblages being developed. Further support for the crustal loaded regional P-T conditions and evidence for late mafic intrusives are provided by small gabbroic bodies and late melts. These small gabbroic intrusions (Section 4.7) which are intruded at high pressures of approximately 5-7 kb and magmatic temperatures of 1000-1100°C caused local thermal perturbation of already high-P, medium-T rocks (approximately 550-650°C, 5-7 kb) resulting in local melting of the country rock (Fig. 4.7; Section 4.7.3). These "late" melts are cordierite absent and are interpreted as locally developed high-P, high-T assemblages (Sections 4.4.3). The late gabbros though are small in dimension, are medium- to coarse-grained and often intruded into fine-grained mafics and sheeted dykes suggesting intrusion at high-P,

into originally low-P rocks. Coronitic structures within the gabbro support the high-P, high-T conditions (1000-1100°C, 6-8 kb), equilibrating isobarically to regional amphibolite-facies conditions (Fig. 4.7: Section 4.7.3)

After a prolonged period of amphibolite-facies conditions caused initially by basic intrusions (Volvi Complex) and prolonged by burial and continued intrusion (Chapter 6), the area began to cool. Cooling is interpreted to have been relatively slow as various greenschist-facies assemblages were developed commonly in association with the development of shear zones and localised hydration causing saussuritisation of the basic lithologies. However, cooling may have been at least partially enhanced by tectonic unroofing and unloading (Chapter 6).

CHAPTER 5

GEOCHEMISTRY OF IGNEOUS LITHOLOGIES

CHAPTER 5

Part I: Mafic (Basaltic) Geochemistry

5.1 Introduction

The main aim of this thesis has been to constrain the origin and tectonic setting of the Volvi Complex (Sections 1.3 and 2.5). Therefore, with reference to previous work (Sections 1.2, 2.5 and 5.1.1), this study has concentrated on geochemical analyses from the margins of the Volvi Complex, and from mafic dyke and amphibolite outcrops within the surrounding country rock gneisses. Field observations from the mafic suites analysed during the course of this work are presented in Chapters 2 and 3. The locations of the analysed mafic samples are displayed on the Inserts, Maps B to H. Several important questions concerning the mafic lithologies are:

i) From geochemical analyses, can the various mafic bodies (amphibolites and dykes) be related to one another, and to the Volvi Complex proper?

ii) Do the amphibolites have an ortho- or para- origin (see also Section 3.11)? Furthermore, are the amphibolites within the Lake Volvi area of the same or similar age, or can they be divided into, (a) an "older" basement amphibolite suite, and (b) a "younger" intrusive suite, related to the Volvi Complex?

iii) Can the dykes be separated into groups representing magmatic or structural time markers within the realms of the regional tectonic evolution (see also Section 3.11)? Therefore, can a progressively evolving geochemical character be correlated with the varying states of strain?

Further questions which may be resolved with future work, and which are presently being studied by Dixon and Dimitriadis (pers. comm.) are:

iv) From the geochemical signature of the mafic lithologies, what is/are the potential origin(s) of the Volvi Complex?

v) From the geochemical signature of the mafic lithologies, what is the potential petrogenetic history of the entire Volvi Complex?

In an attempt to resolve these questions whole rock geochemical analyses were made using XRF techniques (Appendix I). A number (N=261) of mafic lithologies comprise the Lake Volvi data set (Appendix I). However, the area has been subjected to a complex polyphase deformational and metamorphic history (Chapters 3 and 4 respectively). It has therefore been necessary to screen the available data set (Section

5.1.3) to remove any analyses which have been subjected to extreme magmatic or alteration processes (Section 5.1.2). Due to the criteria used for screening the bulk data set, the screened analyses which satisfied the criteria (N=144) approach a general basaltic geochemistry. The screened data set has subsequently been used to determine the origin, tectonic setting and petrogenetic history of the Lake Volvi mafic lithologies and similar conclusions have been inferred for the Volvi Complex (*s.s.*). From the spatial arrangement of the sampled mafic lithologies around the Volvi Complex (*s.s.*), the data set has been divided initially into six main subgroups which have in turn been further subdivided in order to resolve the objectives above. The six main subgroups are:

i) *The Lefkoudha Mafic Lithologies* (LEF, N=24). Samples were taken from around and to the north of Lefkoudha (Sections 2.5.4, 3.10.2; Insert, Map H). Extensive sequences of amphibolitised dykes and a large gabbroic intrusion comprise the majority of the area. Extensive retrogression (biotitisation) of the amphibolites has taken place. Minor locally developed granitic bodies and extensive net veining is also common in the area. This sequence of lithologies has been interpreted to represent the northern margin of the Volvi Complex (*s.s.*).

ii) *The Western Boundary of the Volvi Complex* (EMV, N=8). Samples were taken from a series of streams across the diffuse (100-400 m wide) boundary between the Volvi Complex and the adjacent country rock gneisses. A number of stream sections within this area provide evidence of extensive sheeted dykes. The dykes appear to envelope screens of metasediments (Sections 2.5 and 2.3.2.4), indicating high-level intrusion into a sedimentary sequence.

iii) *The Eastern Boundary of the Volvi Complex* (VAM + VAMR, N=43). Samples were taken from along the entire length of the Vamvakia river and from the roads between Vamvakia, Arethousa and Vrasna (Inserts, Maps C and F). Along the river section the samples consisted of massive gabbros and amphibolites and a range of variably sheared mafic pods. These sheared pods were emplaced over and between bodies of high grade, partially melted country rock gneisses and migmatites by anastomosing shear zones (Section 2.3.2).

iv) *West of the Volvi Complex*: Country rock amphibolites and dykes (ASK + EAF + L, N=52). Samples were taken from numerous mafic outcrops (dykes and amphibolite bodies) intercalated with and intruded into the country rock gneisses of the Vertiskos Group (Section 2.3.3; Inserts, Maps B and D).

v) *East of the Volvi Complex*: Country rock amphibolites and dykes (STAV + MOD + NMAD, N=11). Samples were taken from the Rendina to Asprovalta road

(Section 2.3.2; Inserts, Maps C and F), from the track east of Modhi (Section 2.3.4; Insert, Map G) and from south of Nea Madhitos (Section 2.3.4; Insert, Map G). This suite of lithologies represents amphibolites which are traditionally considered to be part of the Kerdilion Group.

vi) *The Limni Mafic Lithologies* (LIMN, N=6). Samples were taken from along a stream section and hillside directly to the east of Limni. This data set is of particular interest as its geochemical characteristics appear to be anomalous when compared to the Lake Volvi mafic data set. The geochemical signature of the Limni suite appears to represent a relatively unaltered mid ocean ridge basalt.

5.1.1 Previous Work

In general, previous work within the Lake Volvi area is limited (Section 1.2). However, of particular importance to this thesis are the geochemical studies on the Volvi Complex undertaken by Dixon and Dimitriadis (1982, 1984, 1989, in progress). From provisional analyses Dixon and Dimitradis (1984) identified rocks with similar hybrid patterns to Pearce *et al.*, (1984). Pearce *et al.*, (1984) interpreted these hybrid patterns as representing superimposition of above subduction zone character on a mid ocean ridge basalt (MORB) "base". The island of Grenada is quoted by Pearce *et al.*, (1984) as an example of a hybrid tectonic setting (close to the southern transform terminating the lesser Antilles arc) accompanied by a matching hybrid trace element signature, similar to that of the Volvi Complex. However, the Volvi Complex (*s.s.*) and associated mafic bodies are represented by a suite of dykes (locally 100%) and gabbros intruded into continental crust. From field evidence (Chapters 2 and 3) the Volvi Complex can be shown to be a within plate intrusive phenomena and not a slice of ocean floor. However, MORB-normalised plots are still a useful way of comparing basalts to a "standard" product of a large degree of melting from a depleted source, i.e. MORB.

Consequently, the question "what is the tectonic setting as deduced from the geochemistry?" is restated more accurately as "what is the degree of source enrichment, or how small a degree of melting is implied (these two are really unresolvable from trace elements alone), and is there any arc-character and if there is, does it have to be from contemporaneous subduction?".

It is now increasingly recognised that basalts in continental rift settings can be derived in part from the lithosphere and that they may well show geochemical characteristics inherited from previous lithospheric enrichment events. The Basin and Range lavas studied by, e.g. Fitton *et al.*, (1988, 1991), show a clear "subduction

signature" (relative depletion in Nb c.f. LREE's of comparable incompatibility) in the early phase of extension, whereas, later lavas, including Quaternary eruptions have a "pure" asthenospheric character (Fitton *et al.,* 1991). There has been no active subduction beneath the Basin and Range since the Miocene. This signature is partially correlated with low Nd^{143}/Nd^{144} ratios implying association with an older, lithospheric component. Dixon and Dimitradis (1984) proposed an intra-continental rift setting above lithosphere affected by subduction, of unknown age, as one possible origin for the Volvi Complex as a result of their regional observations and the variable arc-signature in Volvi dyke rocks (Section 1.3). Dixon and Dimitriadis (1991) have further shown that the Volvi Complex rocks show marked enrichment in Fe and Ti, with fractionation, in a manner closely comparable to the suite of basalts, ferro-basalts and andesites from the Galapagos-Inca Transform region described by Perfit *et al.,* (1980). The Volvi Complex gabbros show a range of compositions consistent with there being cumulates related to this fractionation process. The inferred parental magmas are all olivine tholeiites and show generally low incompatible element enrichment with a moderate range, as well as a range of degrees of relative "depletion" in Nb relative to LREE's, considered to be a signature of slab involvement in the source region.

Geochemical analyses of a more general nature on the amphibolites of the SMM have been undertaken by Kassoli-Fournaraki (1981) and Sapountzis *et al.,* (1990). Sapountzis *et al.,* (1990) proposed a basic igneous origin and subsequent metamorphism to the amphibolite-facies in the case of the amphibolites of the SSM based on data derived from geochemistry and mineral paragenesis. A general tholeiitic composition for the parental magma, was deduced from normative compositions and chemical variation trends (Sapountzis *et al.,* 1990). Sapountzis *et al.,* (1990) further pointed out that discrimination diagrams based on major and trace elements indicate a possible ocean-floor tectonic affinity. However, as mentioned above the Volvi mafic lithologies have been intruded into continental basement metamorphics, and therefore the discrimination diagrams should be treated appropriately in terms of what they show of the geochemistry rather than as rigorous guides to tectonic setting.

5.1.2 Effects of Alteration

Basic lithologies can be affected by a number of alteration processes (e.g. weathering, metamorphism, spilitization, submarine alteration and albitisation) which will affect the more mobile elements. However, during these alteration processes a

number of elements are considered to remain stable (immobile), e.g. Sc, Ti, V, Cr, Fe, Y, Zr, Nb, and Ce (Frey *et al.*, 1968; Cann, 1970; Kay *et al.*, 1970; Elliot, 1973; Pearce and Cann, 1973; Field and Elliot, 1974; Herrmann *et al.*, 1974; Pearce, 1975; Ferrara *et al.*, 1976).

Around Lake Volvi the basic lithologies have been metamorphosed to the upper amphibolite-facies, followed by retrogression to the greenschist-facies (Chapter 4) and subjected to variable degrees of weathering. Therefore the use of some more mobile major and trace elements from the metabasic lithologies analysed during this study are questionable.

Igneous petrological evidence (Winchester and Floyd, 1976; Pearce, 1988) suggests that metamorphism in the amphibolite-facies does not affect the key immobile elements (e.g. Ti, Zr, Cr, Y, Nb) over the lower part of its temperature/pressure range. Therefore a direct comparison with fresh unaltered basic lithologies can be made. The effects of upper amphibolite-facies metamorphism however, are not well understood, and it is possible that the key immobile elements may not be informative when plotted on discrimination diagrams, especially if signs of partial melting are visible in the field or hand specimen (Pearce, 1988). In order to determine the reliability of the immobile elements the behaviour of the oxides, elements and the ratio between various combinations of oxides and elements must be monitored to see which of the so called immobile elements remain immobile, and which have become scattered and thus rendered unusable, or at least suspect (Cann, 1970).

The behaviour of MgO, Fe_2O_3[1], Al_2O_3 wt% during alteration is subject to a number of variables which are difficult to determine, e.g. submarine weathering, temperature of alteration, degree of crystallinity and extent of alteration as reflected in the H_2O content of the rocks. It is likely that Fe_2O_3 and Al_2O_3 are relatively immobile during the initial stages of submarine alteration, whereas MgO has been reported as variable (Thompson, 1973; Hart *et al.*, 1974).

Chemical studies on the derivation of amphibolite from gabbro have indicated that Y, Nb and TiO_2 are immobile, while P_2O_5 and Zr show a very slight increase during amphibolitization. However, the Zr/P_2O_5 ratio is known to show only very slight changes. By contrast several major elements frequently used in basalt magma type

---

[1]Fe_2O_3 is calculated as total Fe and is presented as Fe_2O_3 throughout this thesis.

discrimination, notably SiO_2, Na_2O and K_2O may undergo marked changes in concentration (Elliot, 1973; Field and Elliot, 1974). During progressive metamorphism from low amphibolite to low granulite-facies, TiO_2 values and Zr/P_2O_5 ratios show only a small proportional decrease (Engel and Engel, 1962). P_2O_5 is generally more mobile than Y, Nb, TiO_2 and Zr, as exemplified by its behaviour in a weathering regime (Vogel, 1975).

Cr and to a lesser extent Ni are fairly stable during alteration processes (Bloxam and Lewis, 1972). However, large variations in the abundance of Cr and Ni are possible as they are very sensitive to original magmatic characteristics, e.g. to olivine and pyroxene fractionation (Gunn, 1971).

Ba shows perhaps the greatest variation in original tectonic setting, e.g. being lower in ocean-floor than in volcanic arc basalts. It does however have many disadvantages as a tectonic discriminant being particularly mobile during weathering and metamorphism (Philpotts *et al.,* 1969). Sr can also be mobile during albitisation and extreme weathering and consequently must be used with caution (Cann, 1970; Pearce and Cann, 1973; Pearce, 1975). Rb and K are highly affected by alteration, being depleted during spilitization and enriched during weathering (Cann, 1970; Pearce, 1975). A summary of oxide and element mobility is presented in Table 5.1

Table 5.1. Summary of oxide and element mobility during secondary alteration processes.

Weathering	
Very Mobile	$+K_2O$, -CaO, -MgO, +Rb, +Ba
Mobile	$-Na_2O$, $-SiO_2$, -Sr, -Ni
Slightly Mobile	$+Fe_2O_3$, $+TiO_2$, -Cr
Immobile	Al_2O_3, Y, Zr, Nb
Greenschist-facies Metamorphism	
Very Mobile	-CaO, $-Al_2O_3$
Mobile	$+Na_2O$, $+SiO_2$, +MgO, $+Fe_2O_3$, $-K_2O$, -Rb, -Sr, -Ni
Slightly Mobile	$+P_2O_5$, -Cr
Immobile	TiO_2, Y, Nb, Zr
Amphibolite-facies Metamorphism	
Very Mobile	$\pm SiO_2$, $\pm Na_2O$, +Ba, +Sr, -Ni
Mobile	-Cr
Slightly Mobile	$+P_2O_5$, +Zr, -Rb, $-K_2O$
Immobile	TiO_2, Y, Nb

after, Engel and Engel (1962); Melson and Van Andel (1966); Cann (1969); Philpotts *et al.,* (1969); Hart (1970); Cann (1970); Gunn (1971); Elliot (1973); Thompson (1973); Pearce and Cann (1973); Field and Elliot (1974); Hart *et al.,* (1974); Pearce (1975); Vogel (1975).

5.1.3 Screening Criteria

The mafic lithologies analysed during this study have been screened to remove rocks which show either extremely evolved compositions as a result of fractionation processes, or more commonly consist of rocks which have been subjected to alteration processes (e.g. weathering, metamorphism). As a consequence of the screening criteria, the rocks approximate to a general "basalt" composition. The screening crtiteria used in this study consists of:

i) The range of SiO_2 used is above 43 wt % and up to a maximum of 60 wt %. If SiO_2 is less than 43% a sample is removed unless there is an associated enrichment in incompatible elements or if loss on ignition (LOI) >4%. In many diagrams a more restricted subset <57% SiO_2 is used.

ii) The range of CaO used is between 5 and 15 wt %. Anything outside this range may mean it has been subjected to radical alteration.

iii) The range of MgO used is between, 4 and 12 wt %. MgO and as other compatible elements such as Ni and Cr should correlate, any sample that has very high Ni but low MgO or vice-versa is removed.

iv) The range of Al_2O_3 used is below 18 wt %.

v) Caution must be applied to those elements which may commonly be found in abundance near, or below the detection limit of the analytical equipment used (Appendix I). This particularly affects the light rare earth elements (LREE) and Nb. Where this is a limiting factor, the elements have been omitted from multi-element plots.

5.2 Dyke versus Amphibolite Discrimination

The wide range of variably deformed mafic components found within the country rock gneisses of the Lake Volvi area have been divided by inspection into two approximate suites of, (i) dykes, and (ii) amphibolites (Section 3.11). These mafic suites have been separated on their general appearance in the field.

i) *Dykes:* These are recognised as parallel to sub-parallel sided mafic bodies which range between 0.5-6 m in width. Dykes tend to be laterally continuous across the outcrop within individual streams (unless truncated by a fault), however, they are rarely observed continuing in to adjacent stream sections. Contact relationships between dykes and country rock in zones of high-strain are invariably parallel, to sub-parallel with the main S_2 foliation and it is the continuity and consistent width which is used to distinguish these dykes from amphibolites. However, within areas of very high-strain, these "dykes" become

attenuated, initially boudined and finally podded and can no longer be unequivocally distinguished as a dyke. In areas of low-strain mafic sheets "dykes" are found cross-cutting the dominant local foliation and structures within the country rock gneisses (Section 3.11).

ii) *Amphibolites:* These are recognised as all the mafic bodies which cannot obviously be classed as dykes. Within the area amphibolites occur in two major forms, (a) massive laterally extensive bodies, containing numerous acidic sheets, veinlets and pods, e.g. the Askos Marginal Amphibolite Formation (Section 2.3.3.1), and (b) discrete laterally discontinuous bodies which are highly sheared and lie parallel to sub-parallel with the main S_2 foliation. The smaller amphibolite bodies do not always contain a banded feldspathic component, and from field evidence cannot be distinguished from highly deformed dykes.

Further problems with the amphibolites relate to whether they are igneous or sedimentary in origin (Section 5.2.1), and whether a distinction can be made between an "older" basement suite and a "younger" intrusive suite, related to the Volvi Complex. As field observations are not always reliable in distinguishing between dykes and amphibolites, let alone "older" or "younger" amphibolites, it is necessary to determine whether there are any geochemical variations which can be used to differentiate between the two groups, and hence determine whether any characteristics can be used to categorise samples which have been subjected to high strain.

5.2.1 Amphibolite Geochemistry

A large number of amphibolitic rocks (N=103) from numerous localities in the Lake Volvi area have been analysed in order to try and determine the nature of their protoliths. Previous work has shown that analyses of the amphibolites are relatively uniform throughout the whole region (Sapountzis *et al.,* 1990), despite the variable mineralogical contents and degree of alteration processes (e.g. metamorphism, weathering) to which the rock has been subjected. The same conclusion has been derived from the geochemical analyses carried out during this study (Appendix I).

From field observations the larger amphibolite bodies while highly deformed, tend to be extremely uniform in composition which suggests an ortho- origin, whereas a para- origin would be expected to result in a more heterogeneous composition, due to original banding or layering. The main problem in determining an ortho- or para-origin concerns the smaller (0.5-10 m long), highly sheared or boudinaged amphibolites. Due to their small size, and inter-relationship with the fabrics of the gneissic lithologies it is possible that these units represent para-amphibolite enclaves.

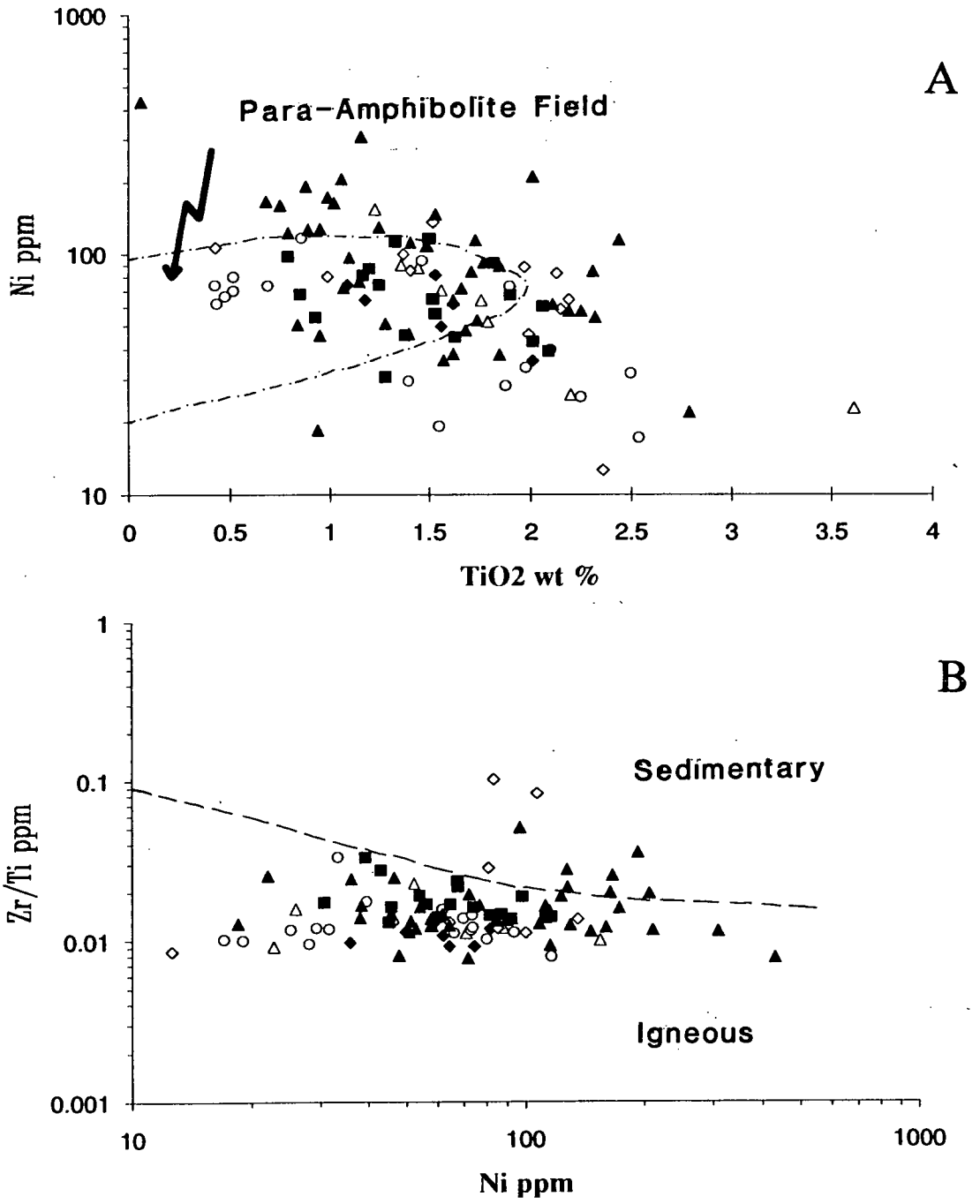

Fig. 5.1: Discrimination diagrams to distinguish between para- and ortho-amphibolites. (A) Ni *vs* TiO_2 discrimination diagram, after Van de Kamp (1969). The Volvi amphibolites do not show any apparent preference between an ortho- or para- origin, with half the mafic suite plotting in either field, (B) Zr/Ti *vs* Ni discrimination diagram, after Leake (1964). This diagram makes a fairly good distinction between an ortho- and para- origin, with the majority of the Volvi data set plotting in the igneous (ortho-) field, however analyses within the para- field can be observed from field evidence to be ortho-amphibolites. The symbols used for the amphibolites represent: filled squares = ASK + EAF + L; open triangles = EMV; filled diamonds = LIMN; open circles = LEF; open diamonds = STAV + MOD; filled triangles = VAM + VAMR. These symbols remain constant for the remaining graphs.

However, it is more probable that these amphibolites represent highly sheared dykes or small early intrusive ortho-amphibolite bodies.

Major and trace element geochemistry has been employed in an attempt to determine their origin. Screening of the amphibolite data (Section 5.1.3) should have removed samples subjected to extreme alteration processes, however, any sedimentary rocks should also have been removed at this stage. Therefore if the discrimination diagrams used to differentiate between ortho- and para-amphibolites are effective for upper amphibolite-facies rocks, then the screened (unequivocal) dyke and amphibolite data sets should all plot in the ortho-amphibolite field. In order to prove this has been successful the amphibolites have been plotted on Ni *vs* TiO_2 (after Van de Kamp, 1969; Fig. 5.1a) and Zr/Ti *vs* Ni (after Leake, 1964; Fig. 5.1b) discrimination diagrams. These diagrams are intended to discriminate between amphibolites of ortho- or para- origins. The Ni *vs* TiO_2 diagram (Fig. 5.1a) is inconclusive for the amphibolites around Lake Volvi as the screened data plots between the two fields. The samples plotting in the para-amphibolite field (open circles - from Lefkoudha) can be distinguished clearly on the basis of field observations, as ortho-amphibolites. The Ni *vs* TiO_2 diagram (Fig. 5.1a) is therefore of little use in distinguishing between ortho- and para-amphibolites which have been subjected to a high strain within the study area.

The Zr/Ti *vs* Ni discrimination diagram (Fig. 5.1b) however, makes a fairly marked separation between ortho- and para-amphibolites, with most of the screened Volvi amphibolite data set plotting as expected within the igneous field. However, the few samples plotting with an apparently para-amphibolite signature can be determined from field observations to have an igneous precursor. Therefore, the discrimination diagrams to distinguish between ortho- and para-amphibolites are not effective near their boundaries and so the use of geochemical signatures to distinguish between the two are at best questionable.

However, a clear ortho-amphibolite signature has been confirmed. Furthermore, the lack of mobility of key immobile elements at upper amphibolite-facies conditions for the Volvi amphibolites have enabled a close comparison with lithologies from the Volvi Complex (*s.s.*) to be made. These comparisons can be well displayed on a number of element-element and MORB-normalised discrimination diagrams.

5.3 Petrogenetic History

Major elements are considered to be mobile during a number of alteration processes, which often makes interpretation based on their trends and signatures

questionable (Section 5.1.2). Therefore, discrimination and multi-element diagrams using immobile trace-elements are preferred (Pearce and Cann, 1973; Section 5.1.2). A number of trace element diagrams have been used to show the chemical variations present within the Lake Volvi area (Figs. 5.1 to 5.7). Due to the immobility of some of the trace elements, samples can be identified which are considered representative of original magma liquid compositions, and thus an attempt can be made to discriminate between suites of primitive and evolved "basalts". The screened Volvi data set has been plotted on diagrams of Ce/Y *vs* Zr/Nb, Zr/Y *vs* Zr, Cr *vs* Y, Ti *vs* Zr, MgO *vs* Nb, and a number of MORB-normalised multi-element discrimination diagrams. A summary of trace element parameters useful in evaluating petrogenetic models is presented in Table 5.3.

Table 5.2: Summary of key trace element parameters useful in evaluating petrogenetic models (after Green 1980)

Elements	
Ni, Co, Cr	High values (e.g. Ni=250-300 ppm, Cr=500-600 ppm) for these elements are good indicators of derivation of parental magmas from a peridotite mantle source. Decrease of Ni (and to a lesser extent Co) through a rock series suggests olivine fractionation. Decrease in Cr suggests spinel or clinopyroxene fractionation.
V, Ti	These elements show parallel behaviour in melting and crystallisation processes. They are useful pointers to the fractionation of Fe-Ti oxides (ilmenite or titanomagnetite). When V and Ti show divergent behaviour, Ti substitution into some accessory phase such as sphene or rutile may be indicated.
Zr, Hf	These are classic incompatible elements, not readily substituting in major mantle phases. However, they may substitute for Ti in accessory phases such as sphene and rutile.
Ba	Substitutes for K in K-feldspar, hornblende and biotite. Change in Ba content or K/Rb ratio may indicate the role of one of these phases
Rb	Substitutes for K in K-feldspar, hornblende and biotite. K/Rb ratios provide possible indicators of the role of these phases in petrogenesis.
Sr	Substitutes readily for Ca in plagioclase and for K in K-feldspar. Sr or Ca/Sr ratio is a useful indicator of plagioclase involvement at shallow levels. Sr behaves more as an incompatible element under mantle conditions.
REE	Garnet and possibly hornblende readily accommodate heavy REE and so strongly fractionate light REE. Sphene has the opposite effect accommodating the light REE. Clinopyroxene fractionates the REE but only slightly. Eu is strongly fractionated into feldspars and Eu anomalies may reflect feldspar involvement
Y	Generally behaves as an incompatible element resembling the heavy REE. It is readily accommodated in garnet and amphibole, less so in pyroxene. The presence of accessory phases such as sphene and apatite could have a major effect on the abundance of Y, since these phases readily concentrate it.
Nb	Strongly incompatible and immobile element. Retained in rutile. Residual amphibole in mantle may account for Nb depletion relative to LREE's in arc basaltic rocks.

The Ce/Y *vs* Zr/Nb diagram (Fig. 5.2) can be used to determine the degree of partial melting and possible melt sources for each sample (Fig. 5.2a; for a discussion see Latin *et al.*, 1989). Since Ce is relatively more immobile than Y, low degrees of

partial melting will be characterised by high Ce/Y values. With increasing partial melting values the Ce/Y value will fall to asymptotically approach the value in the mantle with increasing values of Zr/Nb. Zr and Nb are also both immobile. Nb is the most incompatible and is thus most ready to enter a small melt fraction, thus Zr/Nb will start at low values and increase with increasing degrees of partial melting. Importantly these ratios are considered to be useful for discrimination as they are not affected by all but the most severe alteration or by moderate degrees of fractional crystallisation (MgO >4%). Instead they reflect the nature of the magma source (which will have variable original concentrations of Ce, Y, Zr and Nb) and the degree of partial melting involved to obtain the original liquids. Evolved rocks and picrites are not displayed on Fig. 5.2b. This diagram clearly shows a continuous spread over the small overall range of implied melt fractions from moderate Ce/Y to high Zr/Nb values with no distinction between the mafic suites. The spread of data sub-parallel to the Zr/Nb axis is consistent with moderate, rising to high degrees of partial melting (bulk of the data have values between approximately 2 to 15%; Fig. 5.2a) of a depleted (i.e. MORB-type) source, plus some variability in the depletion of Nb relative to other incompatibles which disperses Nb sideways and Ce to a lesser extent vertically.

Due to the continuous spread of data the Volvi dykes and Volvi Complex (*s.s.*) are considered to be derived from a range of closely associated but heterogeneous magmatic sources. These mafic intrusions in turn reflect progressive partial melting of the variable primitive sources followed by fractionation. The data fall in the region of moderate high degrees of melting for realistic mantle sources (approximately 10%). They are strikingly more depleted than, for example, alkali basalts from the Mesozoic North Sea rift. There is no evidence from the original gabbro mineralogy that the magmas had high water content, though minor interstitial biotite occurs in gabbro pegmatites. Thus, if the dry solidus controls melting some very large stretching factors approaching ∞ are implied by the analysis of McKenzie and Bickle (1988).

The Zr/Y *vs* Zr diagram (Fig. 5.3) of Pearce and Norry (1979), is useful in distinguishing between primitive and evolved magmas, and determining the extent of original source heterogeneiities and progressive partial melting. A strong positive linear trend is observed in Fig. 5.3 with the lowest Zr and Zr/Y values (within the IAB field), represented by a group of amphibolites from around Lefkoudha (open circles). These analyses with high Cr and very low incompatibles are representative of simultaneously, the most primitive, as well as the most depleted melt samples in the screened data set. They are consistent with very high degrees of partial melting of an

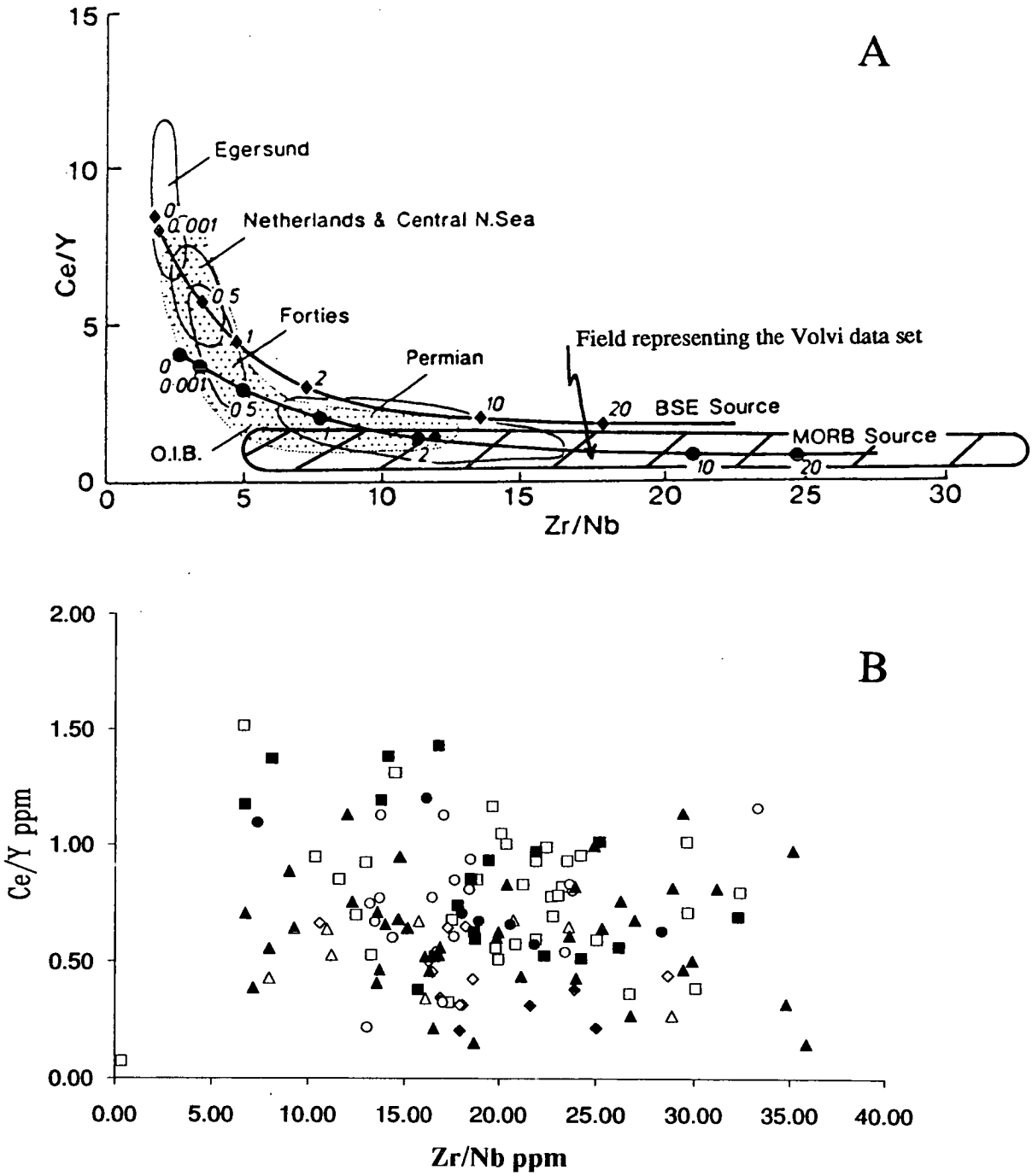

Fig. 5.2: Ce/Y vs Zr/Nb diagrams (MgO >4 wt%). (A) Equilibrium partial melting lines for melting of a MORB source (Fitton and Dunlop, 1985) and a BSE source (James, 1987, Kostopoulos, 1988). The melting lines area marked for per cent melting and were calculated assuming simple, single-stage, modal melting using the bulk distribution coefficients calculated by Fitton and Dunlop (1985), after Latin *et al.*, (1989). Fields for mafic igneous rocks from the North Sea and OIB's (unpublished data of J.G. Fitton and D. James) are also outlined, from Latin *et al.*, (1989). (B) Data from the Volvi mafic suite with no obvious distinction between the different subgroups. This suggests that the subsets are derived from a range of similar contemporaneous primitive sources.

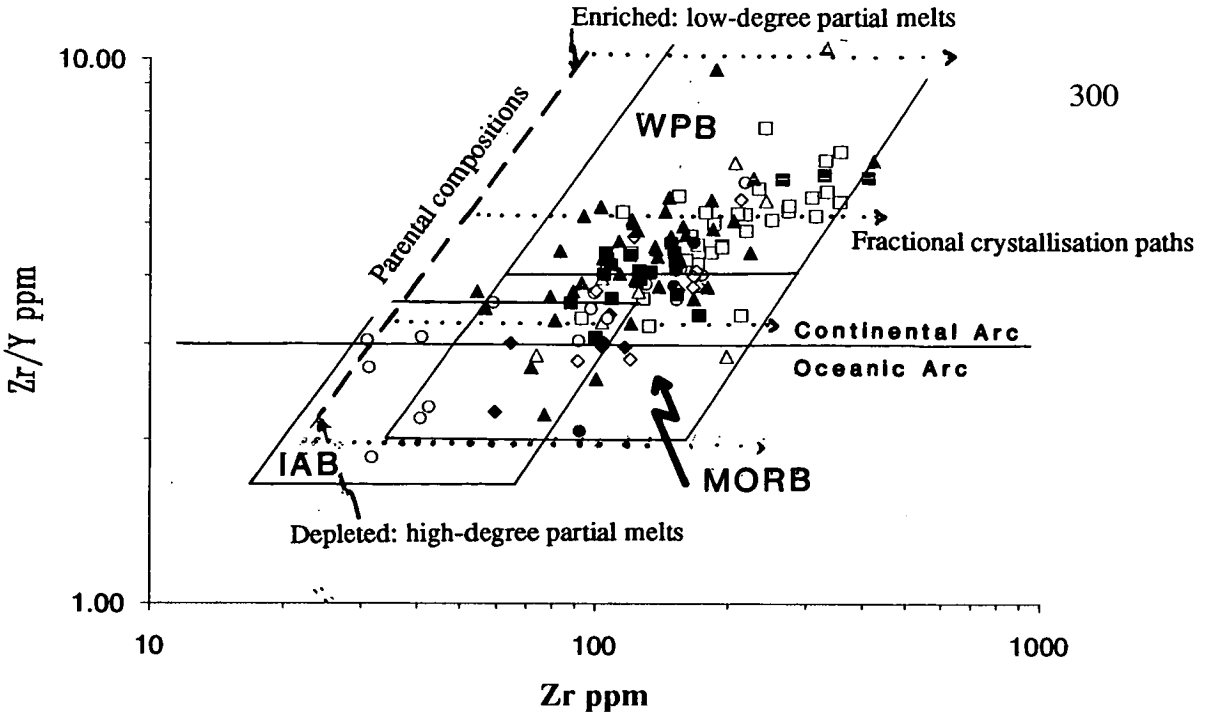

Fig. 5.3: Zr/Y *vs* Zr discrimination diagram, after Pearce and Cann (1973). A range of primitive parental magmas trend from depleted high degree melts (Lefkoudha amphibolites in the IAB field) to enriched low degree melts (Volvi dykes in the WPB field). A well-defined fractionation trend is shown parallel to the Zr axis. No clear tectonic classification can be made as the Volvi data overlaps all three fields; Within-Plate Basalts (WPB); Mid Ocean Ridge Basalts (MORB); Island Arc Basalts (IAB).

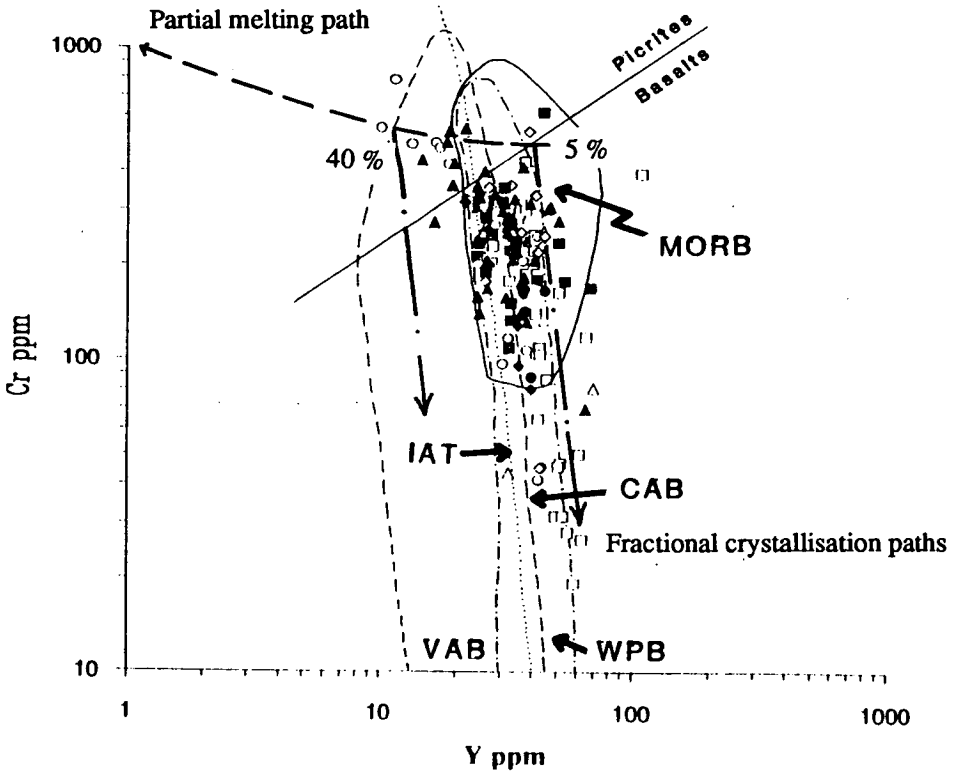

Fig. 5.4: Cr *vs* Y discrimination diagram, after Pearce (1982). A partial melting phase (sub-parallel to the Y axis) shows a range of partial melts from 5 to possibly 40%. A major fractionation phase (parallel to Cr axis) to values of 20-30 ppm Cr is developed. Primitive depleted analyses are represented by Lefkoudha amphibolites (open circles), whereas primitive enriched analyses are represented by the bulk of the data. Volvi dykes (open squares) represent the most enriched partial melts which have been fractionated within the area.

already depleted MORB source possibly undiluted by smaller degree melts from lower in the melt column. The highest Zr and Zr/Y values (within the WPB field) are represented predominantly by dykes from west of the Volvi Complex (open squares). These analyses are representative of the most, enriched (low-degree) melt samples in the screened data set. The spread of analyses parallel to the Zr/Y axis from the primitive to evolved samples can be explained by fractional crystallisation to at least values of 4% MgO. Excess scatter about the partial melting and fractionation paths can be attributed to alteration processes (Section 5.1.2).

On the Cr *vs* Y discrimination diagram (after Pearce 1982, see Fig. 5.4), dispersion of the data by partial melting and by fractionation can be differentiated. As Cr is strongly partitioned into mafic phases, Cr concentration in the melt should vary little during partial melting but decrease rapidly during fractional crystallisation (Pearce, 1982). On Fig. 5.4, the relatively narrow spread of data parallel to the Y axis (10-50 ppm Y) shows the most depleted and primitive melts (amphibolites from Lefkoudha - open circles), indicative of potentially 40% partial melting ranging down to the most enriched primitive low degree partial melts (approximately 5%) representative of the main bulk of the screened data set. The Lefkoudha amphibolites are candidates for wet melting of a depleted source to account for the almost island-arc-tholeiite level's of incompatible elements. The range of analyses parallel to the Cr axis is extremely large (20-900 ppm) and is indicative of a major episode of fractional crystallisation. The most evolved, fractionated suite with low values of Cr (20-30 ppm) are represented by the Volvi dykes (open squares).

The Ti *vs* Zr diagram (after Pearce *et al.*, 1980; Fig. 5.5) discriminates between basic and evolved lavas as olivine, pyroxene and feldspar, the predominant crystallising phases in basic magma, do not have a significant effect on the Ti/Zr ratio of their melt. However, once a Ti-bearing oxide becomes a crystallising phase, Ti becomes depleted in the magma while Zr continues to be enriched. Since crystallisation of this oxide phase correlates with and possibly causes a rapid increase in the SiO_2 content of the magma, the change from basic to acid composition is accompanied by a decrease in the Ti/Zr ratio. Again the Lefkoudha amphibolites are consistent with being primitive, depleted (high-degree) melts with low Ti:Zr values and the Volvi dykes enriched (low-degree) partial melts with high Ti:Zr values. The bulk of the data set plots with an average MORB-type composition, however, the spread of data parallel to the parental partial melt path, may reflect a wide range of original primitive partial melts. Further scatter parallel to this trend and to a small

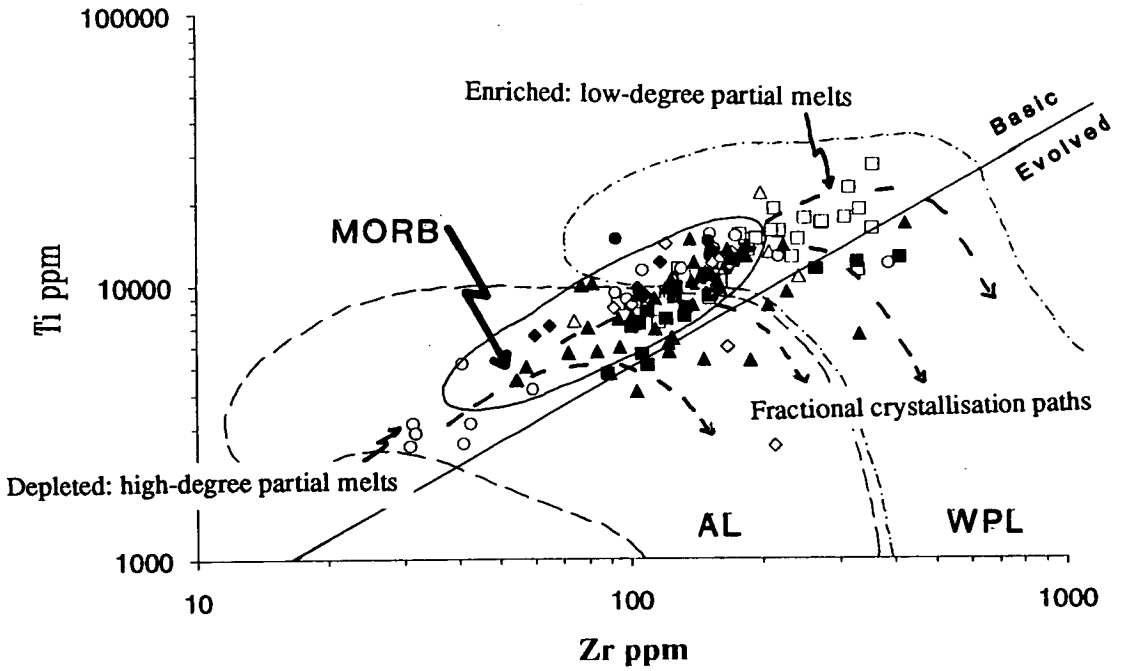

Fig. 5.5: Ti *vs* Zr discrimination diagram, after Pearce *et al.*, (1980). Depleted primitive magmas plot with low values of Ti:Zr (Lefkoudha - open circles) whereas enriched primitive magmas plot with high values of Ti:Zr (Volvi dykes - open squares). This diagram is useful for distinguishing between basic and more evolved lavas, and for carrying out a partial tectonic classification. The Volvi data set plots predominantly in the MORB field, but with overlaps into adjacent fields due to the range of initial magmatic sources.

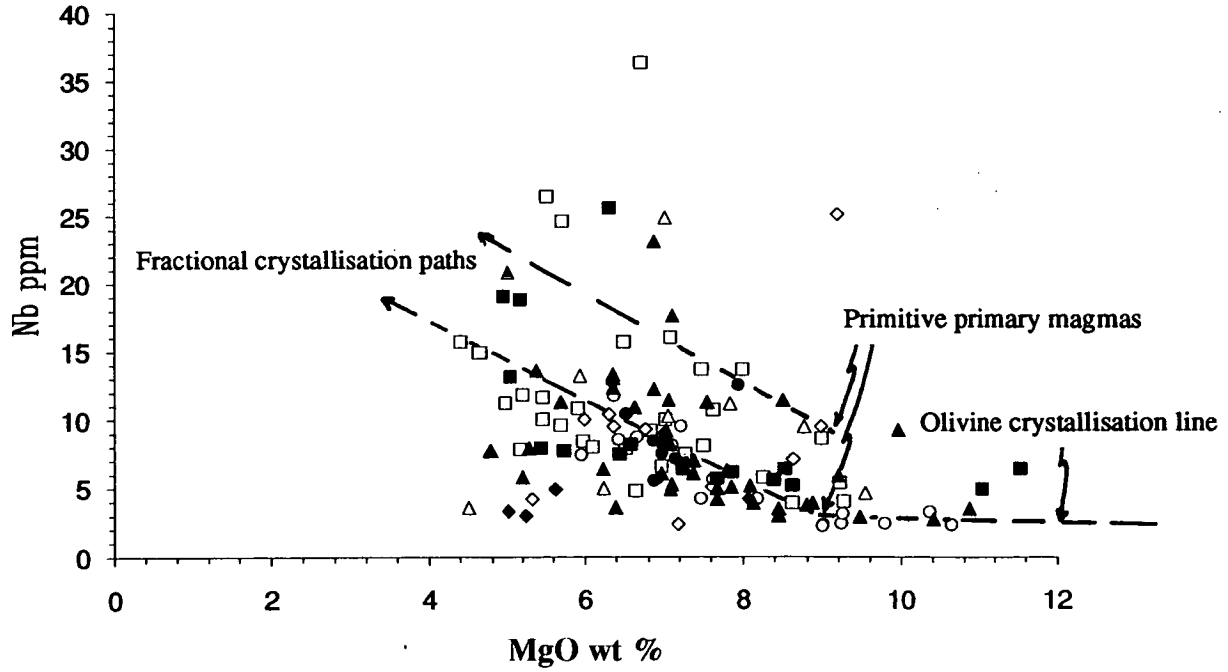

Fig. 5.6: Nb *vs* MgO discrimination diagram. No obvious distinction can be made between the different subsets of the Volvi mafic suite and correlatable MgO-Nb values. This provides a strong suggestion that the Volvi mafic suite is derived from a range of contemporaneous sources.

degree, perpendicular to it, will be caused by the combined effects of partial melting and fractionation.

The MgO *vs* Nb discrimination diagram (Fig. 5.6) can be used to identify different parental magmas and subsequent fractional crystallisation paths as values of MgO will fall rapidly as olivine is precipitated (Section 5.1.3). The concentration of a very incompatible element such as Nb, will reflect the original degree of partial melting of the magma and the extent the fractional crystallisation. Fig. 5.6 shows a scatter of data following an approximate asymptotic trend, with a few samples which have high Nb, low MgO values, through the bulk of the data set which covers a large area with low Nb, low MgO values, to a few samples with similar low Nb values and high MgO values. No clear distinction of magmatic groups can be determined from the spatial arrangement of the Volvi mafic set subgroups. The spread of data parallel to the Nb axis at, high (approximately 9%) MgO values is indicative of more than one primary source. This is reflected in the range of Zr/Nb ratios discussed earlier. The trend to higher Nb and lower MgO values are indicative of fractional crystallisation. As the analyses for Volvi dykes overlap with amphibolites from the Volvi Complex, the dykes are interpreted to be related to the Volvi Complex (*s.s*). Furthermore the dykes and amphibolites have undergone similar petrogenetic histories. Further scatter may be attributed to alteration processes (Section 5.1.2) as MgO is not necessarily immobile. The small spread of data with MgO values >9 wt% may be attributed to emplacement of olivine-rich primative magma, or a cumulate body which has continued to fractionate once in situ, and subsequently lost its evolved fraction before being amphibolitised, or a rare occurence of high-MgO unevolved melts.

5.3.1 Multi-element Diagrams

Multi-element discrimination diagrams provide an ideal way to observe the variation of the Volvi mafic lithologies relative to a recognised standard of normal-MORB (see Appendix I for normalising values). The trace elements are plotted with mobile elements on the left of the diagram (Sr-Ba) and immobile elements on the right (Nb-Cr), with the degree of incompatibility decreasing away from the division. These diagrams are particularly useful in conveying the relative degree of enrichment or depletion of elements resulting from magmatic processes (fractionation, partial melting) and during weathering and metamorphism when referred to an unaltered standard. The elements Ta, Hf, Sm and Yb cannot be analysed using XRF techniques and consequently have not been determined for the Volvi mafic data set, however, Nb, Zr and Y encompass the same range of incompatibility. Therefore the lack of Ta, Hf,

Sm and Yb does not detract from the use of these diagrams for determining tectonic or petrogenetic classification or evolution.

By plotting the screened data set on a series of multi-element diagrams seven distinctive groups (A-G) can be observed which depict progressive degrees of primary enrichment, and within each set, a range of variation attributable to fractionation. Sets which show relative depletion in Nb to LREE's (arc character) are distinguished from uniformly enriched suites (Figs. 5.7a-g). The distribution of the screened data set with respect to these groups are summarised in Table 5.3.

Table 5.3: Distribution of the mafic data set for the Lake Volvi area with respect to the MORB-normalised multi-element groups a to h (see Figs. 5.7a to g).

Figs. 5.7	ASK+EAF+L *Amphibolites*	ASK+EAF+L *Dykes*	EMV *Amphibolites*	LIMN *Amphibolites*	LEF *Amphibolites*	LEF *Dykes*	STAV+MOD *Amphibolites*	VAM+VAMR *Amphibolites*
A	-	-	-	-	7	-	-	1
B	-	-	-	6	-	-	-	-
C	4	4	2	-	-	-	1	12
D	4	5	-	-	1	-	-	2
E	3	4	4	-	4	4	2	9
F	3	10	2	-	2	1	8	3
G	2	3	-	-	3	1	-	12

Fig. 5.7a shows a set with enrichment in the mobile large ion lithophile elements (LILE's, e.g. Sr to Ba), and high Cr, but with elements from Nb to Y most noticeably depleted. The trend of the depleted elements is sub-parallel to the line of Rock/MORB=1.0, indicative of a depleted MORB (P-MORB) source which has been subjected to extensive partial melting. Analyses which show this primitive signature are restricted to the area around Lefkoudha which is in agreement with trace element discrimination diagrams from the same area (Section 5.5).

In Fig. 5.7b the elements plot approximately along a line equivalent to the Rock/MORB ratio=1.0. The analyses of Group B therefore have a MORB-normalised signature comparable to an ideal average MORB composition. However, this data set is anomalous in that it has apparently been subject to little if any element mobility, especially in the generally mobile elements (Sr to Ba). This data set consists solely of analyses sampled from the area east of Limni (Section 2.2.5.3) which is tectonically separated from the extreme NE margin of the Volvi Complex. It is therefore possible that this suite of MORB-like lithologies may actually belong to a separate magmatic unit, e.g. the Therma magmatic body, further to the north.

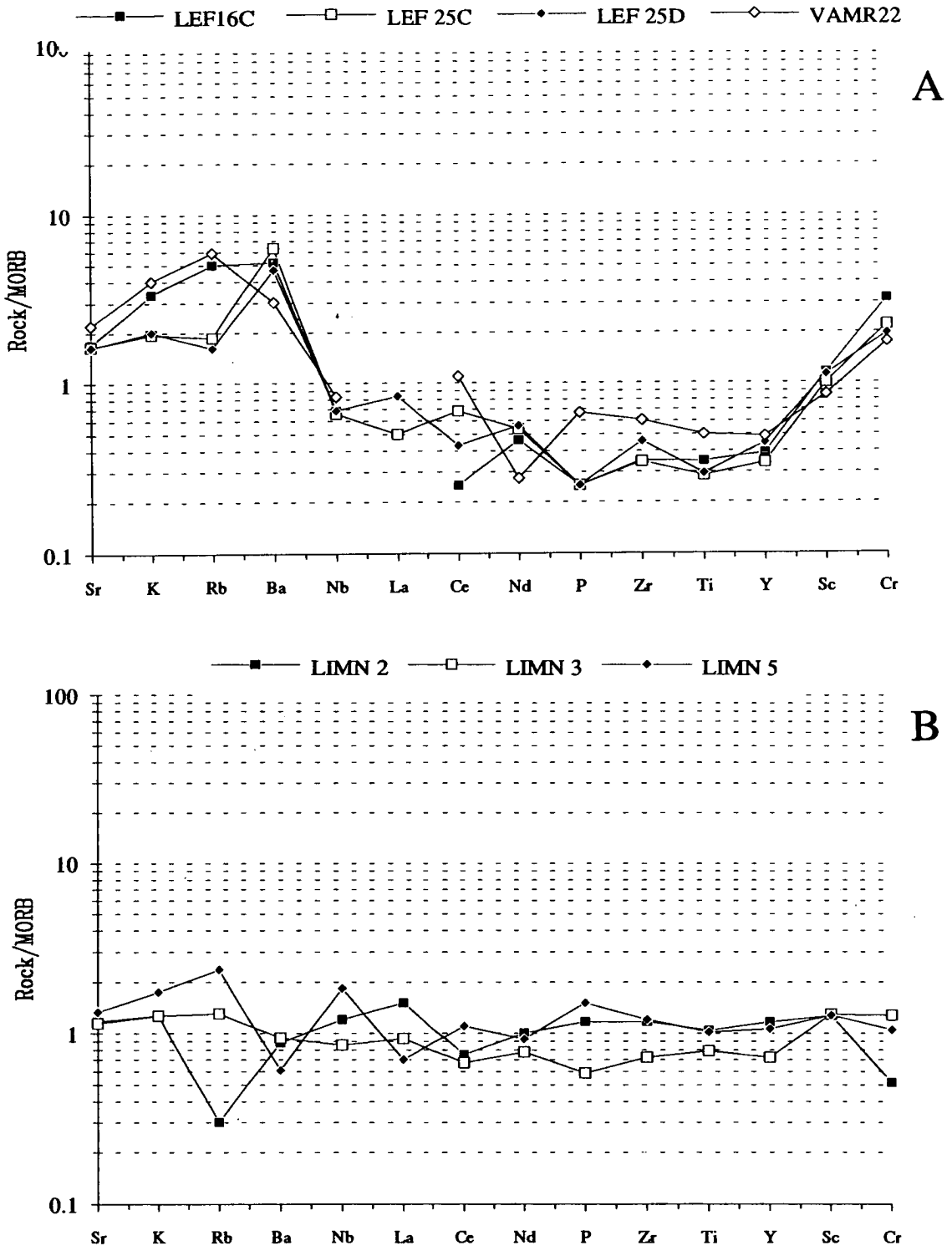

Fig. 5.7: Multi-element discrimination diagrams for the Volvi mafic data set, normalised to N-MORB (see Appendix I for normalising values). a) A P-MORB signature, with enrichment in mobile elements (Sr-Ba) and Cr. Depletion in immobile elements (Nb-Y). Values of Sc remain around 1.0. b) This set are close to N-MORB. Analyses are of a series of exposures from east of Limni.

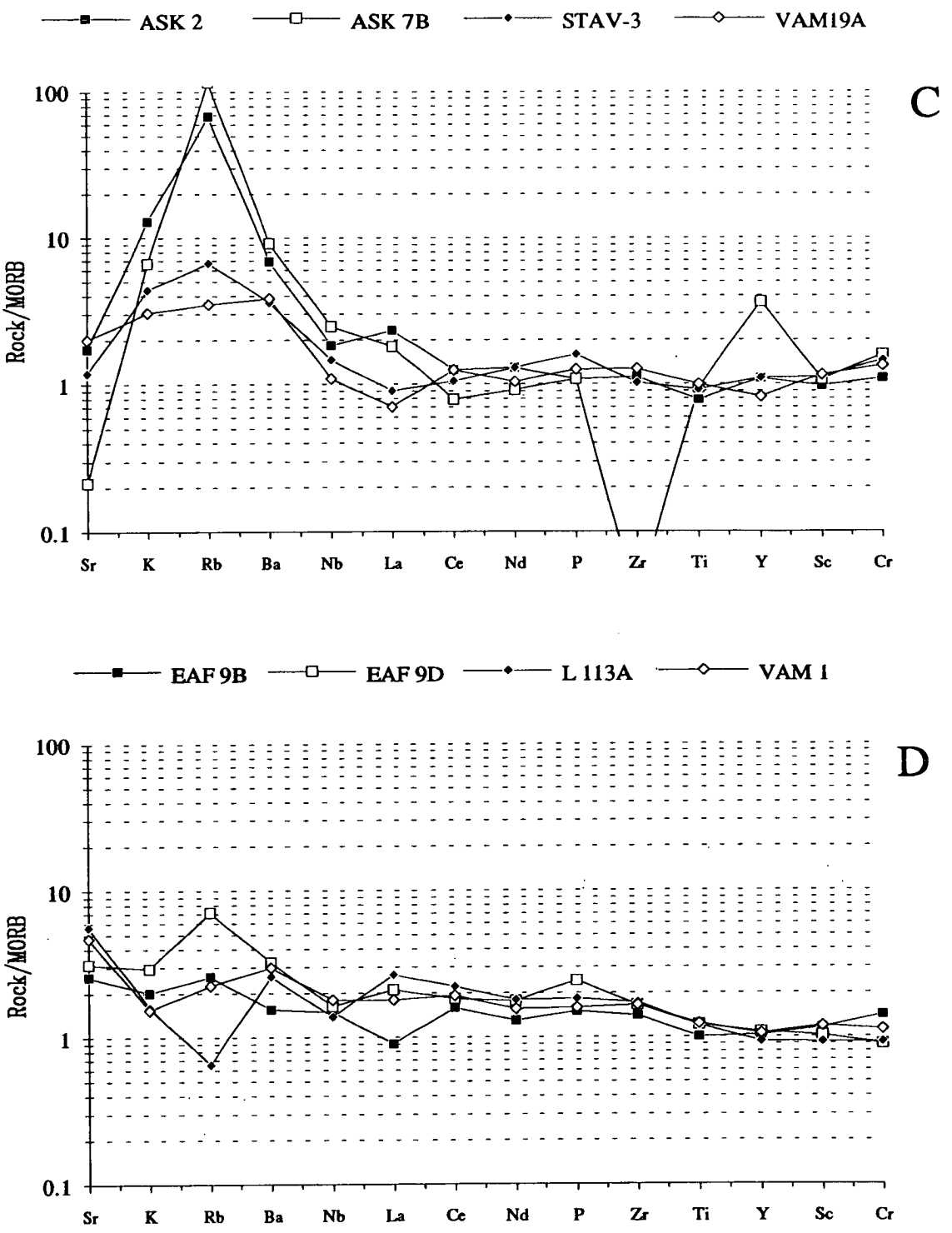

Fig. 5.7 cont., c) An N-MORB signature, with enrichment in mobile elements (Sr-Ba) probably due to hydrothermal alteration. d) A transitional signature, mildly enriched MORB. Enrichment in all the elements, with a slight negative slope from Sr to Y. Cr at MORB level suggesting that enrichment is primary.

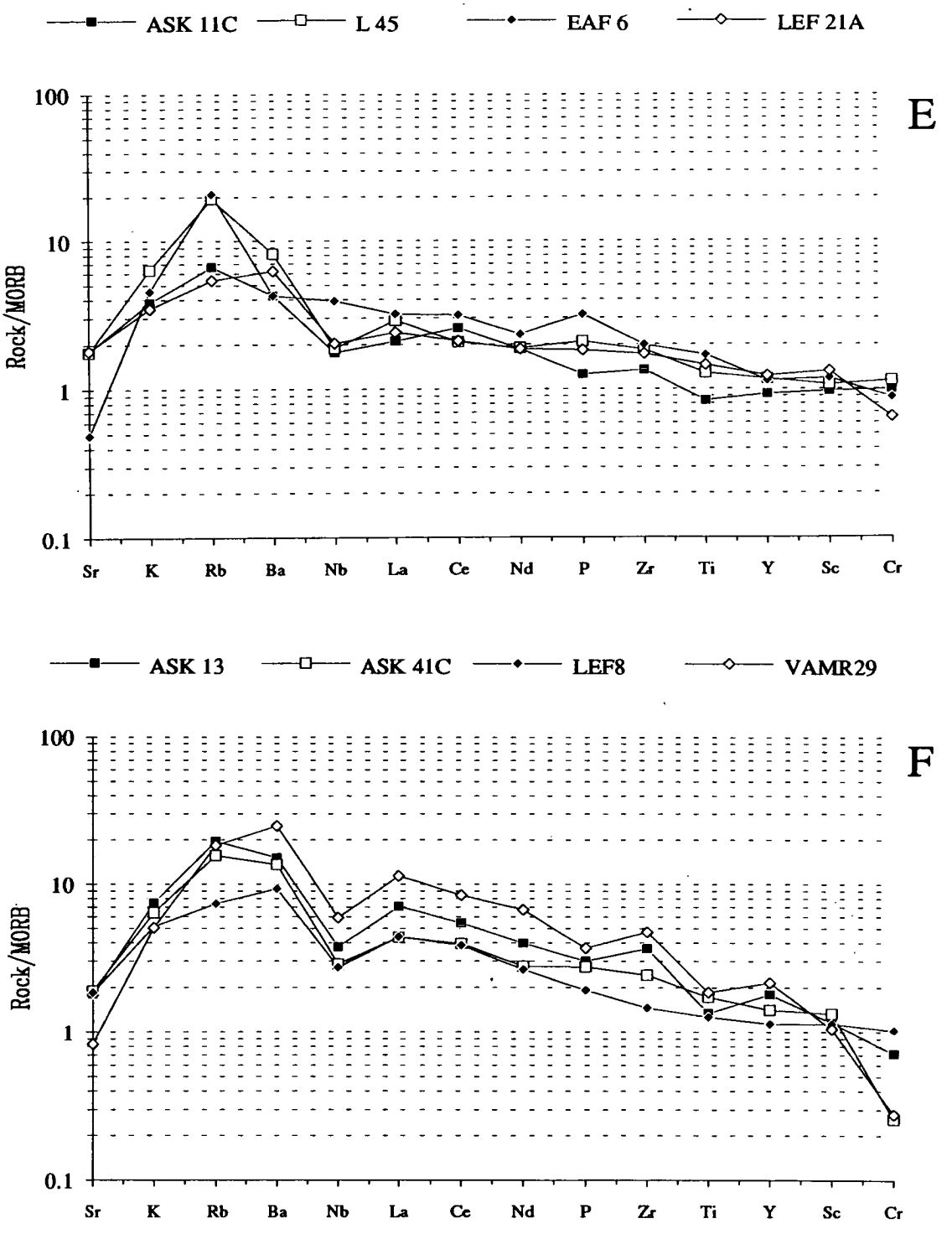

Fig. 5.7 cont., e) An E-MORB type signature with enhanced enrichment in mobile elements (Sr-Ba) and in three samples, some evidence of relative Nb depletion. Cr is slightly depleted in LEF21A due to fractionation. f) A combination signature showing within-plate-type enrichment combined with clear evidence of arc-type Nb depletion. Ti depletion is also evident. VAMR29 could be related to ASK13 by crystal fractionation. ASK41C may be evolved from a slightly less enriched parent.

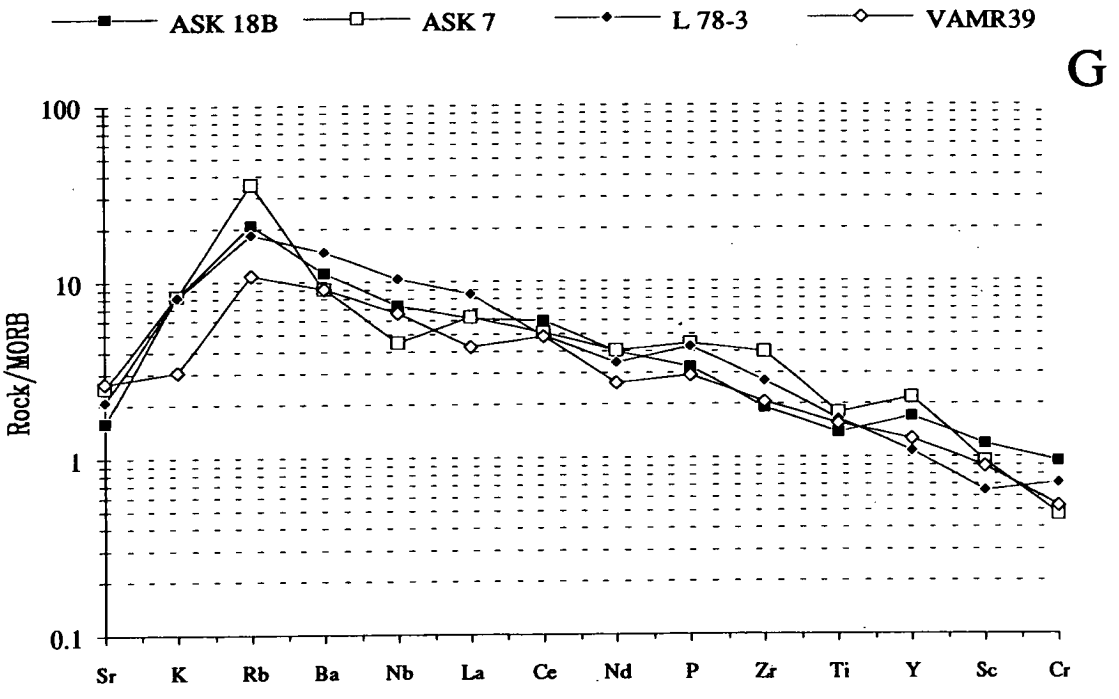

Fig. 5.7 cont., g) A WPB signature: low degree melt without the Nb depletion signature. Enrichment in all the elements from K to Y.

Fig. 5.7c, shows a similar MORB pattern to the Limni suite (Fig. 5.7b), with elements from Nb to Cr maintaining Rock/MORB values equal or close to 1.0. However, there is a marked increase in the mobile elements (Sr to Ba) which show a wide range in the values of their enrichment (e.g. from 1 to a 100 times MORB). This enrichment of the mobile LILE's is interpreted to reflect secondary alteration processes (Section 5.1.2) because it is not correlated with an arc-like relative depletion in Nb. Saussuritisation is known to be accompanied by K and Rb enrichment (Dixon, work in progress) and the visible metasomatic effects adjacent to granitic net-veins involving biotite growth are consistent with similar enrichments at the late magmatic/hydrothermal stage.

Fig. 5.7d shows a slight enrichment in both LILE's and incompatible elements with progressively increasing abundance from Y to Sr. The elements from Nb to Y remain sub-parallel with the line of Rock/MORB=1.0, and relative to N-MORB these melts are slightly enriched, probably because of a slightly lower than average degree of melting of the same source.

Fig. 5.7e shows an enriched E-MORB type signature with enhanced enrichment in mobile elements (Sr to Ba). In three samples some evidence of relative Nb depletion is developed possibly reflecting a remnant subduction signature. Evidence for fractionation is shown in one sample by the depletion of Cr.

Fig. 5.7f shows a combined signature of within-plate-type enrichment (well-developed characteristic hump from Sr to Cr) combined with clear evidence of arc-type Nb depletion. There is also a slight depletion in Ti. This signature is not generally distinctive by itself of a petrogenetic indicator (i.e. partial melting, fractionation) and is more probably an artefact of the original primitive magmatic source (possibly with a remnant VAB signature). Alternatively the Nb depletion may represent a degree of crustal contamination but only if other elements, including SiO_2 are enriched at the same time as a "depletion" cannot be added.

Fig. 5.7g shows a within-plate-type enrichment signature (enrichment in all the elements from K to Y) indicative of low-degree melt, without the Nb depletion signature.

5.4 Summary

The element-element and element ratio diagrams indicate that the dykes and amphibolite bodies found within the country rock gneisses and mafic lithologies from the margins of the Volvi Complex (*s.l.*) are all related to the Volvi Complex (*s.s.*).

A range of potential magmas have been identified with the bulk of the data set consistent with 5 to 10 % partial melting of an average MORB source. However, the range of basic rocks sampled includes more enriched primitive magmas (Volvi dykes) indicative of 2 to 5% partial melting and very depleted and unevolved magmas (Lefkoudha amphibolites) indicative of 15 to 20% (or possibly greater) partial melting. This variation in parental magmas and the implied range of partial melting values may be tentatively interpreted in terms of the pull-apart model for the Lake Volvi area (Chapter 6). There is an implied wide range of degrees of melting in basic rocks lacking any arc signature. No appeal to wet melting can be made for these. Taking McKenzie and Bickle's analysis at face value the MORB-like magmas imply large β-factors approaching ∞. The most enriched melts at 2 to 5% melting imply β factors of approximately 3, or crust thinned to approximately 10 km. Dykes could have been intruded into relatively thin crust during transtension while Lefkoudha amphibolites represent melts intruded directly into the core of the pull-apart basin. From the trends on some of the discrimination and multi-element diagrams an inherent arc-signature is inferred to be present in some of the primitive magmas. The simplest inference is that the signature resided in the lithosphere. The broad spectrum of primitive magmas have in turn been affected by fractional crystallisation. This has resulted in a wide spread of analyses and only weak trends being preserved. Further scatter on the discrimination diagrams is attributed to alteration processes (Section 5.1.2).

5.5 Tectonic Discrimination Diagrams

Discrimination diagrams have been widely used to indicate the tectonic environments in which basic igneous rocks have been produced; either (a) based on empirical comparison of data from modern day settings, e.g. Pearce and Cann (1973), or (b) from knowledge of the chemical and physical state of the magma source regions (asthenosphere and lithosphere) in an attempt to understand why lavas of one type should be expected in one setting rather than another, e.g. Pearce (1982, 1983).

The diagrams used to determine tectonic environments are usually divided into fields consisting of; within plate basalts/lavas (WPB/WPL), characteristic of ocean islands and areas of continental rifting; mid-ocean ridge basalts (N-, P-, E-MORB; normal, primitive and enriched MORB respectively), typical of mid-Atlantic type constructive plate boundaries and also some back-arc basins; Island arc tholeiites (IAT) and volcanic arc basalts/lavas (VAB/VAL), typical of oceanic arcs formed

above destructive plate boundaries and certain back arc basins; calc-alkaline basalts (CAB), produced at converging plate margins.

Ti, Zr, Y and Nb contents of basalts vary systematically with tectonic setting and are commonly used in tectonic discrimination diagrams (Pearce and Norry, 1977).

i) Most basalts erupted in within-plate settings can be identified by their high Ti/Y and Zr/Y ratios (Pearce and Cann, 1973: Floyd and Winchester, 1975; Pearce and Gale, 1977). This reflects the presence of enriched mantle sources as in plume settings or low degrees of partial melting of more depleted sources as in continental rifts.

ii) Most basalts erupted in island arc settings can be distinguished from mid-ocean ridge basalts (MORB) by their lower absolute abundance of Ti, Zr or Nb at any given Cr concentration (Pearce, 1975). The relative depletion of Nb was due to to a phase retaining it in the mantle residue, possibly amphibole (McKenzie and O'Nions, 1991). In addition, island arc tholeiites tend to be strongly depleted in immobile incompatible elements, presumably because of volatile-assisted melting.

These various basic distinctions of source composition, enrichment and melting process which vary from setting to setting account for the general success of the discrimination diagrams. There was never any *a priori* expectation that tectonic settings would yield absolute geochemical criteria for discrimination. The possibility of the lithosphere holding an enrichment signature and later releasing it will increase the possibility of blurred boundaries. However, the mafic lithologies within the study area consist of amphibolites and dykes intruded into what is inferred to be the crustal basement of a pull-apart basin subjected to a transtensional-transpressional tectonic regime (Chapters 3 and 6). Therefore the geochemical signatures might be expected to range from WPB to MORB. A lithospheric-hosted CAB/IAT signature could be signified if a prior subduction event had occurred but very high β-factors led to asthenosphere-dominated melts taking over from lithosphere-dominated melts. This is essentially what the normal discrimination diagrams show, i.e. general overlap in the region where WPB, MORB and CAB fields meet. Before these are described, a brief summary is given of other plots conventionally used to confirm magmatic character in altered rocks. Variations from the expected interpretation from tectonic discrimination and multi-element diagrams must therefore represent some combination of the variable elements of original source material, partial melting and fractionation. These have already been shown to be extremely variable in the Lake Volvi area (Section 5.3).

5.5.1 Major Elements

The use of major element analyses in petrographic studies, is severely restricted by the action of hydrothermal metamorphism and weathering on mobile elements. However, a number of major elements may remain fairly immobile and so can be used in discrimination diagrams. Major element plots of $Na_2O + K_2O$ *vs* SiO_2, Al_2O_3 *vs* TiO_2, and AFM ($Na_2O + K_2O$ *vs* Fe_2O_3 *vs* MgO), have been used.

The screened Volvi data set (Appendix I) when plotted on a alkali *vs* silica diagram (Cox *et al.*, 1979; Fig. 5.8) shows a wide spread of compositions, from picritic basalts to andesites. However, the screening has caused the vast majority of the data points to plot within the basaltic field. While showing that the dykes and amphibolites of the screened data set are now mostly of basaltic composition no indication of original composition prior to metamorphism can be determined. Therefore the alkali-silica diagram may be useless in classifying the original pre-metamorphic assemblage. However, despite the high grade metamorphism the samples of the screened data set still have basaltic total alkali levels. Therefore, it is proposed that the amphibolite and dyke samples within the Lake Volvi area may not have been much modified.

Plotting the edited data set on an Al_2O_3 *vs* TiO_2 wt % discrimination diagram (after Pearce, 1984; Fig. 5.9) shows the majority of data points plotting within the basalt field. The exact field of basalts (boxed area) will vary according to tectonic setting. The data points outside the boxed area may represent transitions from basalts representative of one tectonic setting into another. The diagram is used essentially to screen cumulate rocks and picrites from true basalts. The screening criteria (Section 5.1.3) has effectively restricted the data set along the Al_2O_3 axis to the basalt field. The spread of data along the TiO_2 wt % axis, is interpreted as a combined result of crystal fractionation and partial melting of an original magmatic source. The high TiO_2 values are consistent with the Fe and Ti enrichment trend in the basaltic andesites and andesites from within the Volvi Complex found by Dixon and Dimitriadis (1989 and unpublished work).

On an AFM diagram for the edited data set (Fig. 5.10) only a poor discrimination between tholeiitic and calc-alkaline compositions can be made, as the data points straddle the boundary of Irvine and Baragar (1971). However, the data points do have an elongated trend parallel to the FM axis, which is indicative of a tholeiitic trend and is supported by observations of Dixon and Dimitriadis (pers. comm.) from within the Volvi Complex. Lefkoudha amphibolites (open circles) are magnesian-rich while the most evolved basic rocks distributed towards the F apex are

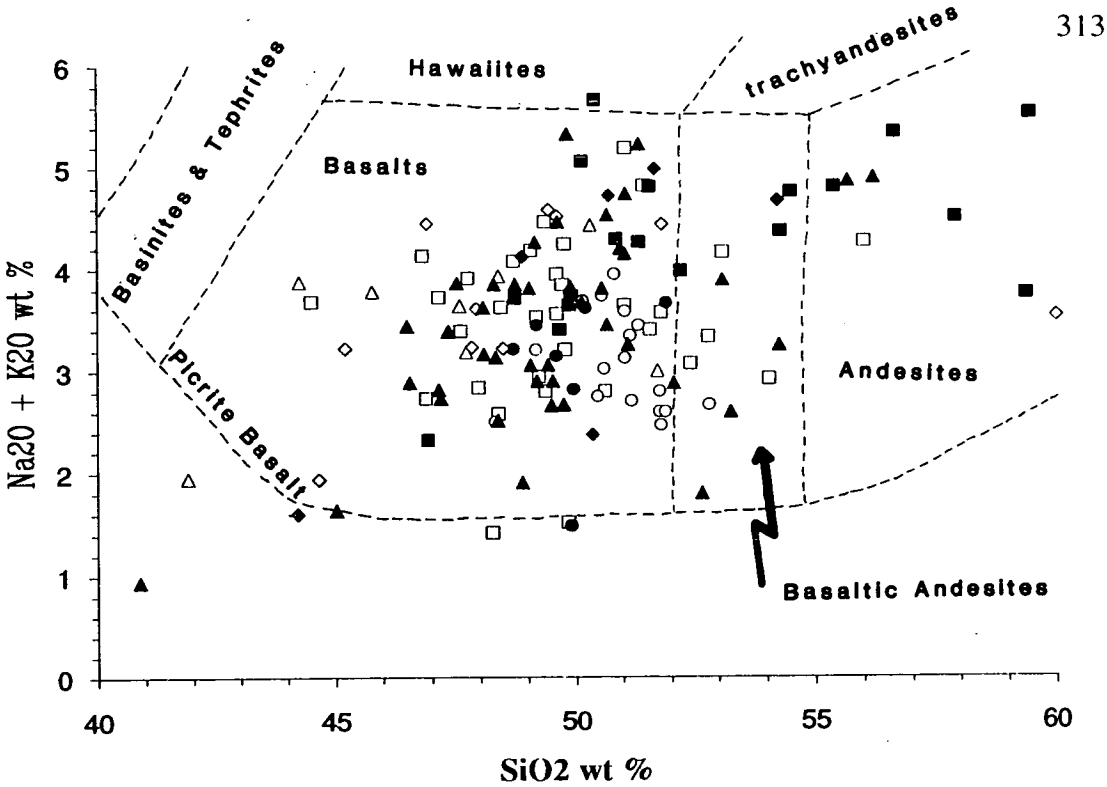

Fig. 5.8: $Na_2O + K_2O$ *vs* SiO_2 wt% discrimination diagram, after Cox *et al.*, (1979). This diagram shows the compositional range of the Volvi mafic data set. The majority of the analyses are observed plotting within the basaltic field.

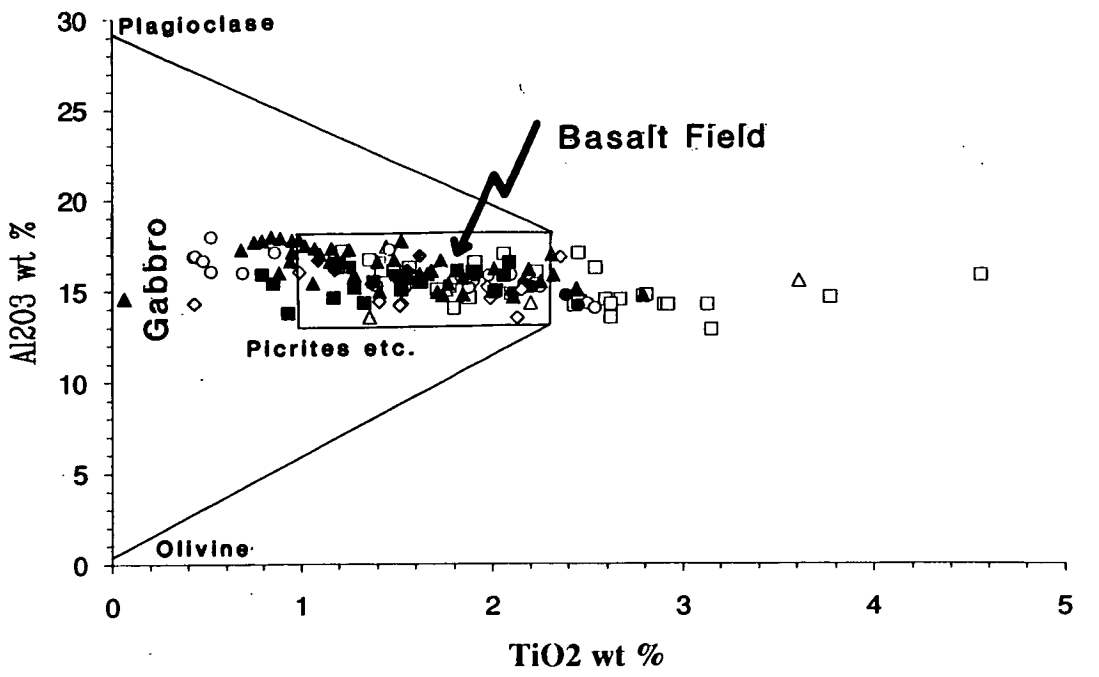

Fig. 5.9: Al_2O_3 *vs* TiO_2 wt% discrimination diagram, after Pearce (1984). Used for screening true basalts. The exact field of basalts (boxed area) will vary according to tectonic setting.

Volvi dykes (Section 5.4). The spread of data towards the A apex may reflect variable parental magmas showing varying degrees of iron enrichment.

5.5.2 Trace Elements

Tectonic discrimination diagrams are commonly used to determine ancient magmatic settings. However, the usefulness of these diagrams in areas which have a complex tectonic history are questionable. This study has determined from field criteria that the Volvi Complex is an in situ phenomena related to a pull apart basin (Chapters 2, 3 and 6). Therefore, the Volvi Complex should in theory plot with a WPB to MORB-type signature (Section 5.5).

On diagrams of, e.g. Zr/Y *vs* Zr (Fig. 5.3) and Ti *vs* Zr (Fig. 5.5), the Volvi data set plots across a range of tectonic settings. This distribution is best explained in terms of the petrogenetic history of the magmatic sources which comprise the Volvi Complex (Section 5.3). The spread of data is a consequence of the way tectonic discrimination fields are constructed, i.e. based on the abundance or depletion of characteristic trace elements within different tectonic settings (Section 5.5). Therefore, depleted magmas from high degree melts typically plot in the IAB/VAB/CAB fields. Conversely enriched magmas from low degree melts typically plot in the WPB field.

In order to keep the ambiguity of the tectonic discrimination diagrams to a minimum classification of samples into different tectonic settings are best carried out on diagrams which do not have overlapping fields. Furthermore, by increasing the number of elements involved, it should be possible to reduce the effects of element mobility and subsequently decrease the ambiguity when attempting to identify potential tectonic signatures. Therefore, diagrams of Ti/100 *vs* Zr *vs* Yx3 and 2Nb *vs* Zr/4 *vs* Y have been used.

The Ti/100 *vs* Zr *vs* Yx3 discrimination diagram (after Pearce and Cann, 1973; Fig. 5.11), shows a wide distribution of analyses, plotting in all the tectonic fields. The main concentration of analyses plot along the left hand boundary between the MORB + IAT and WPB fields, with an elongation trend through the bottom of the CAB field towards the Zr apex. The distribution of the Volvi data set across these fields for tectonic discrimination can be attributed to the range of primitive magmas resulting from different degrees of partial melting and remnant arc-type signature (Section 5.3).

The 2Nb *vs* Zr/4 *vs* Y discrimination diagram (after Meschede, 1986; Fig. 5.12), also shows a wide distribution of analyses. However, within this diagram the

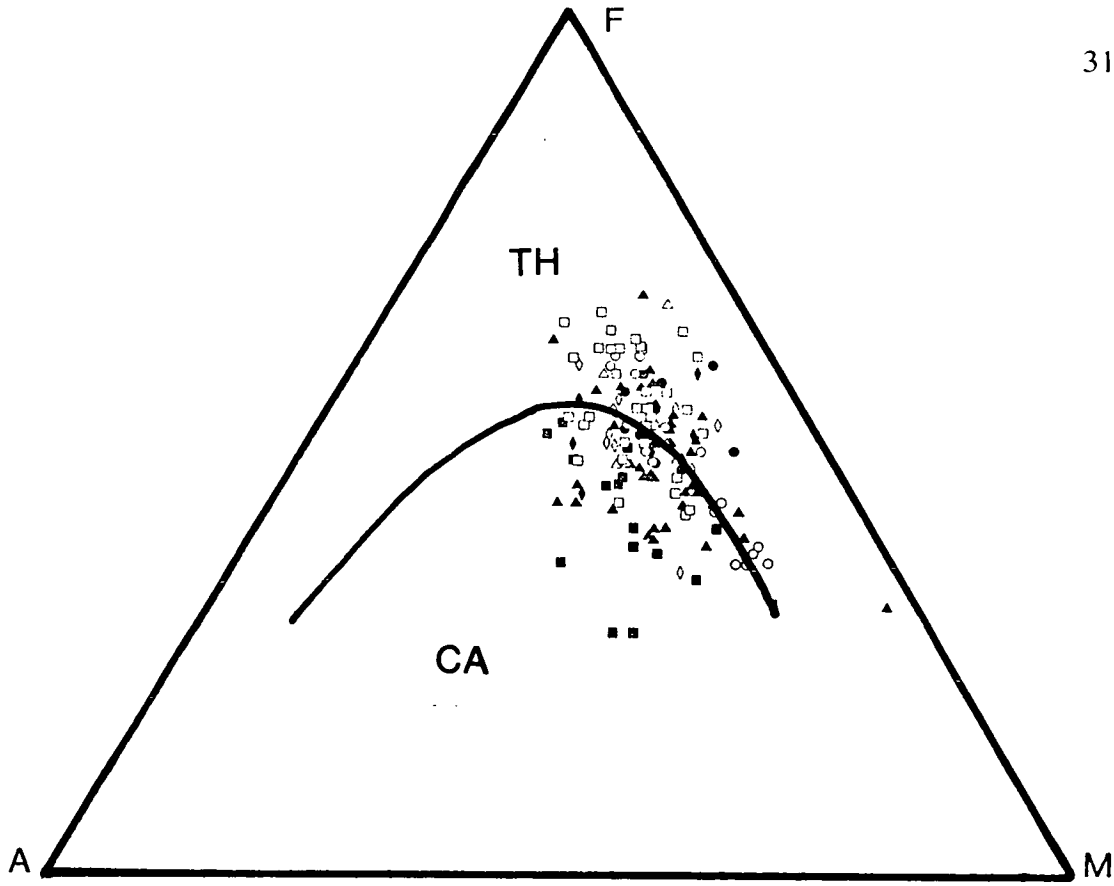

Fig. 5.10: AFM ($Na_2O + K_2O$ *vs* Fe_2O_3 *vs* MgO) discrimination diagram, showing the basaltic part of a tholeiitic magmatic trend. Tholeiitic (TH), Calc-alkaline (CA) boundary, after Irvine and Barager (1971).

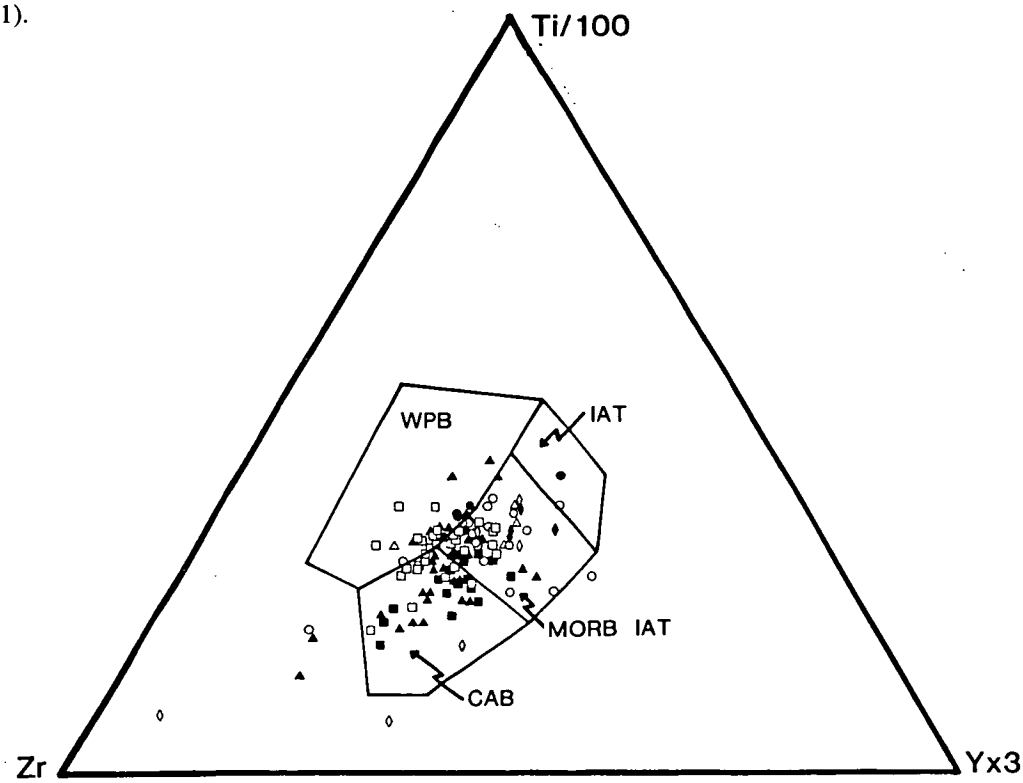

Fig. 5.11: Ti/100 *vs* Zr *vs* Yx3 discrimination diagram, after Pearce and Cann, (1973). A wide spread of analyses causes problems in tectonic classification. Within-Plate basalts (WPB); Island Arc Tholeiites (IAT); Mid-Ocean Ridge Basalts (MORB); Calc-alkaline Basalts (CAB).

bulk of the data set plot along the boundary between the fields of VAB and N-MORB or VAB, and are equally distributed between them. This diagram therefore reflects the remnant arc-type signature identified in section 5.3.

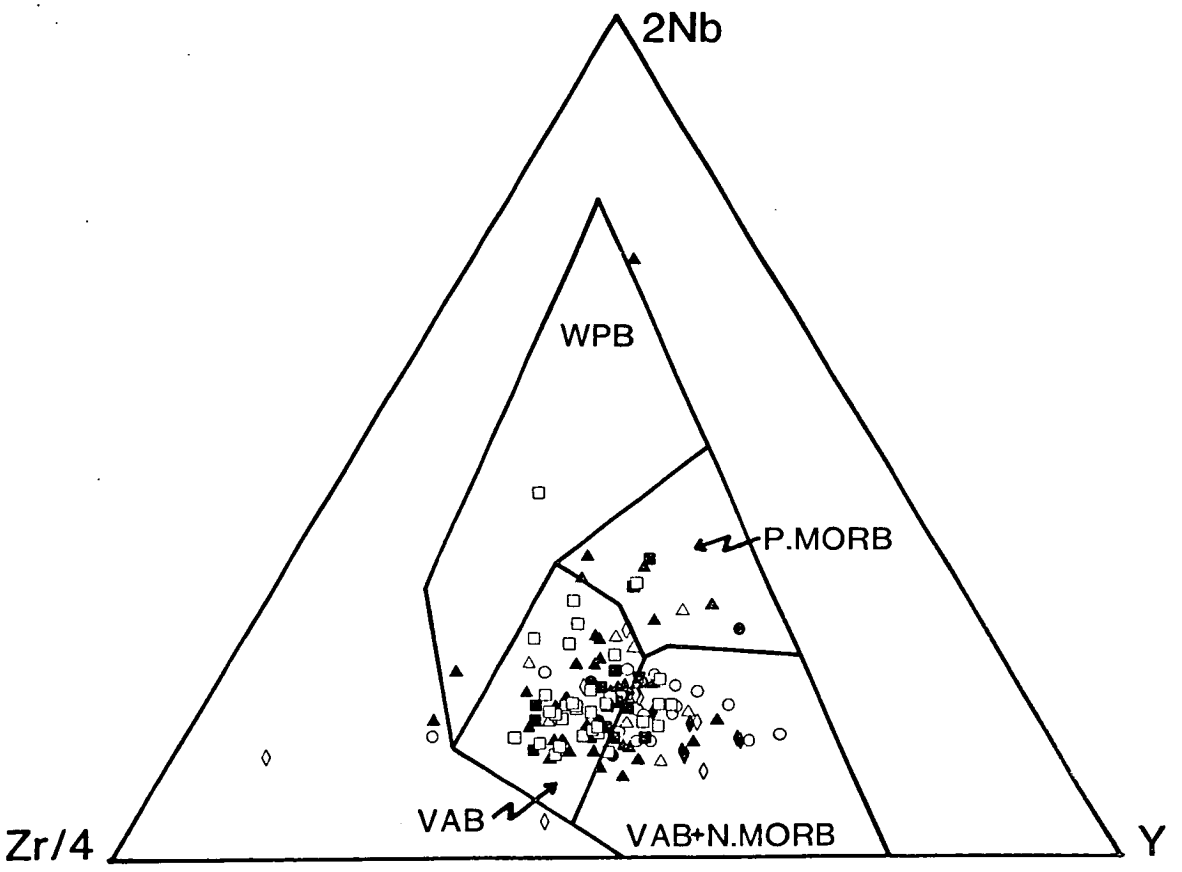

Fig. 5.12: 2Nb *vs* Zr/4 *vs* Y discrimination diagram, after Meschede (1986). A transitional tectonic setting between volcanic arc basalts and mid-ocean ridge basalts is suggested from the overlap of the Volvi data set into two main fields. Within-Plate Basalt (WPB); Volcanic Arc Basalt (VAB); Mid-Ocean Ridge Basalt (MORB); Plume-MORB (P-MORB).

Part II: Granitoid Geochemistry

5.6 Introduction

Around Lake Volvi numerous granitoid lithologies of variable extent crop out in a range of structural and lithostratigraphic settings (Section 2.6). The most extensive granitoid within the area is the Arnaea granite (Section 2.6.3). The remaining granitoids consist of localised melts, and minor outcrops represented by podded, banded and veined granitoid sheets (Sections 2.2 and 2.3). Within this section an attempt is made to categorise and correlate the granitoids of the Lake Volvi area by using whole rock geochemical analyses. Several important questions arise concerning the granitoid lithologies:

i) Can the various granitic bodies and minor intrusive granitoid suites be related to one another and to the Arnaea granite proper?

ii) From the geochemical signature, what is/are the potential origin(s) of the Lake Volvi granitoids?

iii) Given that in situ partial melting occurs close to the mafic Volvi body (Vamvakia river; Section 2.3.2), can the major granitic bodies as well as the minor intrusions be attributed to crustal melting?

iv) Do the Vamvakia melts (Section 2.3.2) represent a valid microcosm for the production of granitoid material in the Lake Volvi Area?

In an attempt to resolve these questions whole rock geochemical analyses were made using XRF techniques (Appendix I). A number (N=84) of silica rich lithologies (SiO_2 wt % > 60) comprise the Lake Volvi granitoid data set (Appendix I). The granitoids are divided into seven distinctive suites based on their field relationships, and spatial arrangement:

i) *The Arnaea Granite* (N=8). Samples were taken from within the sheared extension of the granite body north of Lake Volvi (Section 2.6.3; Insert, Map B). Comparisons with the Arnaea granite suite analysed by De Wet (1989) from south of Lake Volvi are made throughout this section and section 2.6.

ii) *The Askos Augen Orthogneiss Member* (N=24). Samples were taken from the sheared orthogneiss margin to the Arnaea granite and from augen orthogneiss bodies and granitoid sheets within the adjacent country rock (Section 2.6.3; Insert, Map B).

iii) *The Modhi Granitoid Suite* (N=12). Samples were taken from a highly sheared (mylonitic) sequence of granitoid lithologies from along the track to the east of Modhi (Section 2.6.4; Insert, Map G).

iv) *The Kerdilion Granitoid Suite* (N=6). Samples were taken from leucocratic sheets and felsic rich bands from along the Rendina to Asprovalta road (Section 2.2.2; Insert, Maps F and G), and from the main quartzofeldspathic lithology from the Arethousa to Vrasna road (Section 2.2.4; Insert, Map F).

v) *The Lefkoudha Granitoid Suite* (N=4). Samples were taken from small, locally developed (melt?) bodies and veinlets from around Lefkoudha (Section 2.5.4; Insert, Map H).

vi) *The Vamvakia River Granitoid Suite* (N=17). Samples were taken from along the Vamvakia river and consist of an extensive series of locally derived melts enveloping a restitic component (Section 2.3.2; Insert, Map C).

vii) *The JED Data Set* (N=13). Samples consist of leucocratic diorites and granites. These samples were collected by John Dixon, from within the Volvi Complex. These contain two distinct suites, one related to extreme fractionation of Volvi basic magmas, and occuring as minor dykes and net-vein matrices within the Volvi Complex, the other at the periphery is interpreted as a selection of country rock melts.

5.6.1 Previous Work

The Arnaea granite has been studied along with several other major granitic bodies in the Serbo-Macedonian Massif by De Wet (1989). The work concentrated mainly on the geothermometry/barometry, geochemistry and geochronology of the Halkidiki granites. De Wet (1989) proposed two possible scenarios for the Arnaea granite depending on the exact timing of intrusion:

i) Crustal melting in response to crustal thickening and temperature increase perhaps associated with the closure of the Innermost Hellenic Ophiolite Belt (IMHOB) during the Upper Jurassic.

ii) Crustal melting in response to extension and decompression, as proposed by Wickham and Oxburgh (1985) for Pyrenean granites, perhaps associated with the initiation of ocean basins in the IMHOB during the Upper Triassic.

De Wet (1989) excluded the possibility of the tectonic emplacement of ophiolitic complexes causing granite development, because the accepted models for the Halkidiki ophiolites (Dixon and Dimitriadis, 1984; Bébien *et al.*, 1986) propose largely autochthonous settings. Therefore crustal melting due to ophiolite emplacement is not considered as a possibility. De Wet (1989) drew the following conclusions about the Arnaea granite:

i) The Arnaea granite is a large, highly evolved granitic intrusion with a fairly restricted major element chemistry.

ii) The intrusion is parautochthonous as it has strongly sheared boundaries.

iii) The granite is probably an "S-type" granite resulting from crustal anatexis, as suggested by its petrology, chemistry and intrusion into the continental basement of the SMM.

iv) It is probably Upper Jurassic in age from its consistent Rb/Sr isochron age, but has been affected by Upper Jurassic or Lower Cretaceous greenschist metamorphism.

v) The Arnaea granite's spatial and temporal association with the Halkidiki ophiolites strongly suggests an inter-relationship between the two.

The work by De Wet (1989) on the Arnaea granite concentrated predominantly on the outcrop to the south of Lake Volvi. De Wet (1989) made only a brief study of the highly sheared extension of the Arnaea granite to the north of the lake, i.e. the main granite studied in this thesis. Comparison of the two main data sets, north (this study) and south (De Wet, 1989) of Lake Volvi, and data from other granitic bodies in the northern area around the Volvi Complex is a major aim of this section. A review of the isotope data analysed by De Wet (1989) is made in section 2.6.1.

5.7 Interpretation of Major and Trace Elements of the Volvi Granitoids

Rocks of granitic composition may be derived from a number of sources and via several mechanisms. The resulting granitic melts may have been modified by differentiation, mixing with other melts, or reaction with rocks of different composition. Therefore, from interpretation of the major and trace element geochemistry, the source and mechanisms involved in the emplacement and evolution of the Volvi granitoids may be constrained.

From the available data it is also possible to say that the granitoids have an "S-type" affinity, and were probably developed via crustal anatexis. This section presents the discrimination diagrams that support these statements. The discrimination diagrams also allow recognition of mineral reactions and alteration phenomena which affect the Volvi granitoids. This helps explain the overlap in the tectonic settings in the diagrams by Pearce *et al.*, (1984). In contrast to the basalt situation the tectonic setting for the granitoids is really an open question. Although they are "within plate" in position their parent magmas could have been the near-MORB type Volvi basalt magma which would give them ORG characteristics. They could be 100% crustal melts generated either by basaltic intrusion or self-heating in a collision, given them a

syn-collision character, or they could be variously augmented by calc-alkalic magmas of arc origin giving them VAG character. Finally, they could be differentiates of alkalic parents related to smaller degrees of extension than the Volvi mafic body, but never erupted and thus could be classic WPG. Combinations of these primary sources with crustal melts are possibilities. The first objective is thus to establish their character.

5.7.1 The Effects of Alteration on Granitoid Classification

Ideally for geochemical classification, granitic rocks should be fresh, non-porphyritic, non-cumulate, non-aplitic intrusive rocks. However, this is often not the case. Understanding the type and extent of alteration and its effect on element mobility is particularly important in classifying granitic settings. This is particularly relevant in the Lake Volvi area due to the high degree of tectonic and metamorphic activity to which this area has been subjected (Chapters 3 and 4).

Common types of alteration affecting minor elements used in discrimination observed within granites (Alderton *et al.*, 1980; Harris and Mariner, 1980; Harris, 1981; Baldwin and Pearce, 1982; Pearce *et al.*, 1984*b*) are:

i) Rb-enrichment, which occurs from alteration of K-silicate and sericite, due to the growth of secondary biotite and muscovite respectively.

ii) Rb-depletion, which occurs from chloritisation and argillic alteration, due to breakdown of feldspar and mica.

iii) Y and Nb depletion, which occurs during K-silicate alteration owing to "dilution" by added quartz.

iv) Y-enrichment, which occurs during chloritisation as it can be accommodated in the chlorite structure.

Volatile fluxing associated with the loss of volatile-rich aqueous fluids from the parent magma may result in depletion with respect to trace elements and they may promote subsolidus growth of crystal phases, e.g. K-feldspar megacrysts (Taylor, 1966; Buma *et al.*, 1971; Hanson, 1978; Hildreth, 1981; Baldwin and Pearce, 1982; Hudson and Arth, 1983). However, in general, granites suffer a much lower degree of secondary alteration such as weathering and metamorphism than basalts, so that the mobile, as well as immobile elements can often be used in their discrimination (Cann, 1970). However, granites can change markedly in trace element content in the last stages of fractionation. Granites are also susceptible to deformation-induced compositional change and hydrothermal alteration which is particularly relevant to this study. The interaction between deformation and melting processes resulting in

metasomatic effects in many shear zones has been studied by a number of workers (e.g. Beach, 1976, 1980; Robin, 1979; Winchester and Max, 1984; Knipe and Wintsch, 1985; O'Hara, 1988; Simpson and Wintsch, 1989; Dipple *et al.*, 1990; Jamtveit *et al.*, 1990). Shear zones provide ideal settings to study the relationships between chemical changes and mechanical behaviour of the rocks by allowing direct comparison of chemically altered mylonite with its undeformed and unaltered protolith over a scale of centimetres to metres. Furthermore, because many shear zones show evidence for fluid infiltration during shearing, these zones permit detailed studies of the effects of varying fluid-to-rock ratios on the chemical and rheological properties of the rocks.

However, studies of shear zones have indicated a bewildering array of chemical responses to shearing of various protoliths. For example, shear zones cutting granitic rocks in various localities show SiO_2 increasing (e.g. Winchester and Max, 1984), or constant (e.g. Beach, 1976; Vocke *et al.*, 1987), or decreasing (e.g. O'Hara, 1988) with increasing deformation. All other elements show similarly variable behaviour from one shear zone to another, including elements such as Al, Zr, Ti, Nb and Y, which are often assumed to be immobile during metamorphism. Obviously, the chemical changes recorded in a particular shear zone result from interactions between the initial rock composition, the composition of the infiltrating or evolved fluid, and the P-T conditions at which shearing occurred (Selverstone *et al.*, 1991).

5.8 Discrimination Diagrams

In order to classify the Arnaea granite geochemically, and identify natural groups major and trace element compositions have been plotted on various discrimination diagrams. Harker diagrams and element-ratio/element diagrams have been used to constrain the origin, and style of magmatic evolution of the Volvi Granitoids.

According to the Al/(K + Na + Ca) [A/CNK] *vs* SiO_2 diagram, the granitoids of the Volvi area are metaluminous and peraluminous. The bulk of the data set range in A/CNK values from 0.8 to 1.4 (Fig. 5.13) with several samples even higher. The northern extension of the Arnaea granite has A/CNK values between 0.9 and 1.2, which is similar to the value found by De Wet (1989) for the Arnaea granite south of Lake Volvi which has A/CNK values ranging from 0.95 to 1.2. The variation of A/CNK values for the remaining Volvi granitoid outcrops may be due to alteration

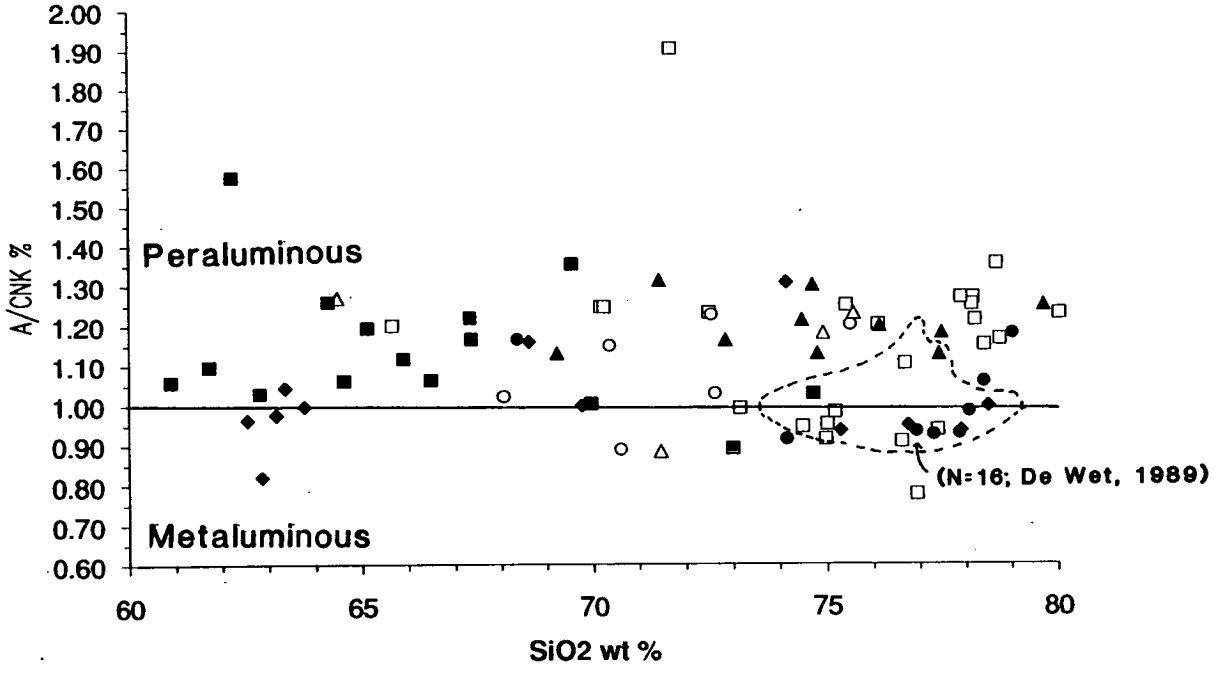

Fig. 5.13: Diagram of molecular Al/(K + Na + Ca) *vs* SiO_2 for the Lake Volvi granitoids. Values above 1.0 are peraluminous and below 1.0 are metaluminous. The symbols used remain constant throughout the remaining graphs, these are: filled squares = Vamvakia melts; open squares = Askos Gneisses; filled circles = Arnaea Granite; open circles = Stavros (Kerdilion) Gneisses; filled triangles = Modhi Granitoid; open triangles = Lefkoudha melts; filled diamonds = JED data set.

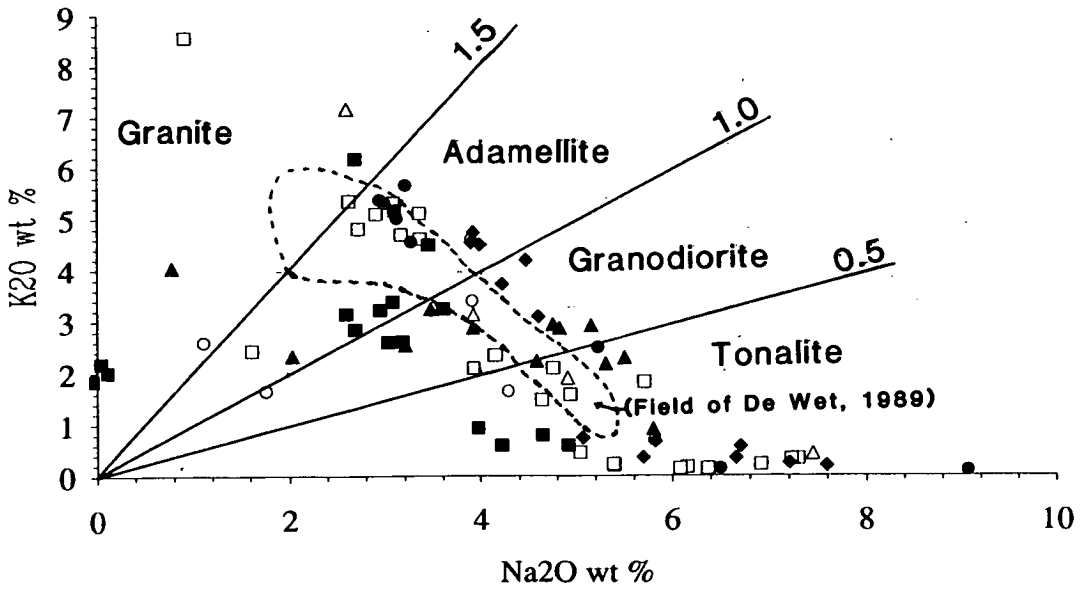

Fig. 5.14: Diagram of wt% K_2O *vs* wt% Na_2O, superimposed with the classification of rocks, after Harpum (1963). The granodiorite-tonalite boundary was changed from K_2O/Na_2O ratio of 0.6 to 0.5 after De Wet (1989).

caused by the extensive shearing evident to the north of the lake, and greenschist-facies metamorphism.

On the K_2O *vs* Na_2O diagram (Fig. 5.14) of Harpum (1963), the Volvi granitoids fall predominantly within the adamellite, granodiorite and tonalite fields, only a minor number (N=8) actually fall within the granite field. The Arnaea granite north of Lake Volvi falls predominantly within the adamellite field, one sample lies on the granodiorite-tonalite boundary and two samples appear along the Na_2O wt % axis, with virtually no K_2O wt % present. The Arnaea granite south of Lake Volvi (De Wet, 1989), falls predominantly in the granite-adamellite field, but some samples also plot in the tonalite and granodiorite fields (Fig. 5.14). The major drawback with the Harpum diagram is that only two parameters are used.

The $Na_2O + K_2O$ *vs* SiO_2 diagram (Fig. 5.15) of Cox *et al.*, (1979) is of limited use with classification restricted to diorites, granodiorites and granites. Due to the high wt % SiO_2 approximately half the data set is too evolved to plot within the granite fields.

The R1 *vs* R2 diagram (Fig. 5.16) of de la Roche (1980) is considered to be more useful in the classification of granitoid rocks as it incorporates the majority of the major elements. The R1 *vs* R2 diagram (Fig. 5.17) can also be used to indicate the probability of compositional trends involving fractional crystallisation, partial melting or magma mixing (Batchelor and Bowden, 1985). Tectonic settings can also be inferred and are based on the fields of Pitcher (1979, 1983) and Chappell and White (1977). From Fig. 5.16 the Volvi granitoids fall predominantly within the alkali granite, syenogranite, granodiorite and tonalite fields, with a number of other compositions also recognised. However, it must be noted that the cluster of data within the anatectic field (Fig 5.16) is inevitable, since all granitoids evolve toward minimum melting compositions (Tuttle and Bowen, 1958).

The Lake Volvi granitoids fall close to the anatectic field which corresponds to the "S-type" granite classification of Chappell and White (1974). However, the Vamvakia melts and JED data sets deviate from this dominant trend (Fig. 5.17). The Vamvakia melts plot in the field of destructive plate margins (pre-plate collision), whereas the JED data set plot in the field of Caledonian "Permitted" plutons (post-collision uplift). As both suites are spatially associated with obvious heat sources (basic intrusions) and derived visibly from (re-melted) migmatites, this chemical "signature" probably relates more to the original migmatite character than to the granite's origin. It illustrates the dangers of literal adherence to the "results" of discrimination diagrams. Most of the Arnaea granite to the south of Lake Volvi (De

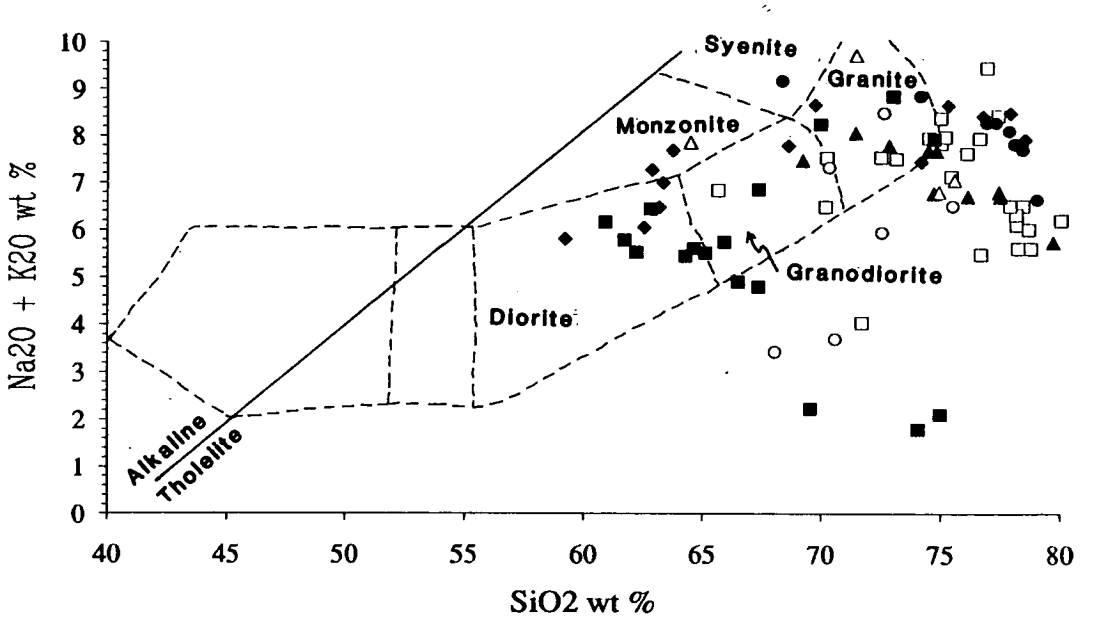

Fig. 5.15: Diagram of wt% ($Na_2O + K_2O$) *vs* wt% of SiO_2, superimposed with the classification of rocks, after Cox *et al.*, (1979). The oblique line divides alkaline (above) from tholeiitic (below) affinities, Hawaii (after Macdonald and Katsura, 1964)

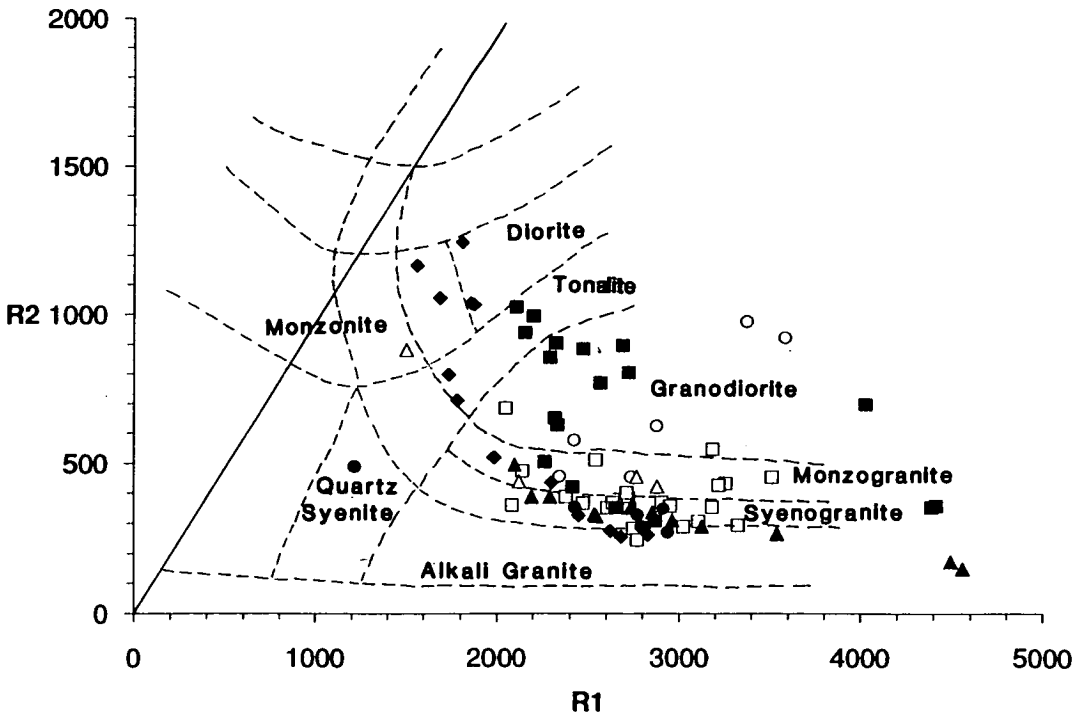

Fig. 5.16: R1 *vs* R2, multicationic diagram, after de la Roche *et al.*, (1980), superimposed with the classification of rocks.

R1 = 4Si - 11(Na + K) - 2(Fe + Ti)

R2 = 6Ca + 2Mg + Al

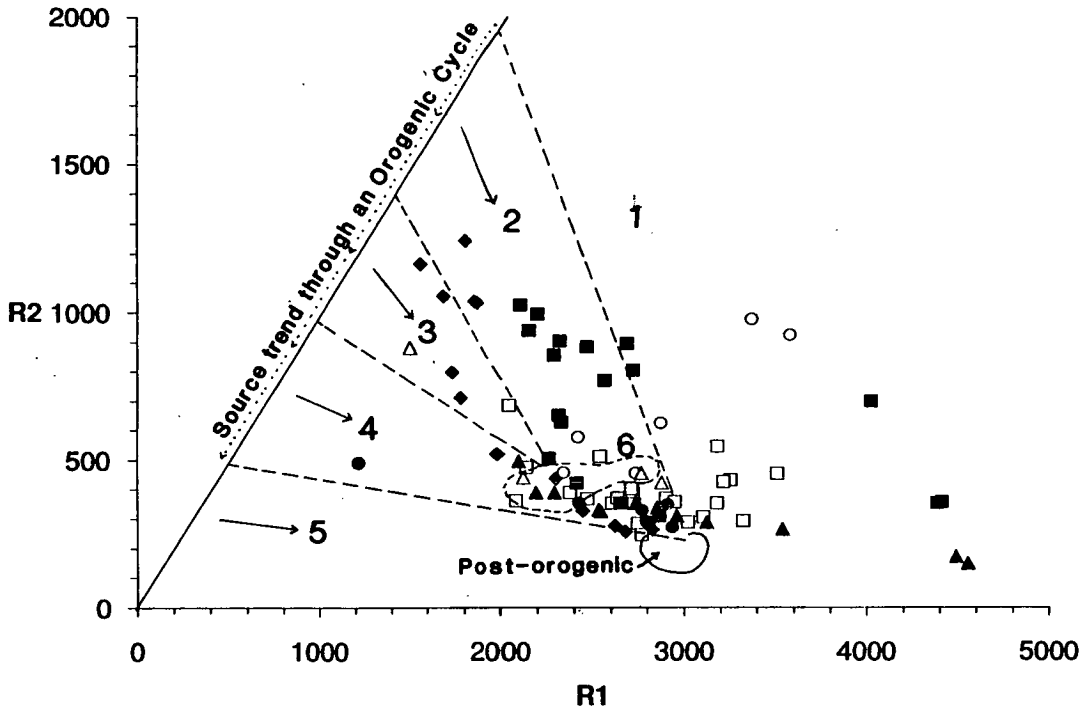

Fig. 5.17: R1 *vs* R2 multicationic diagram, superimposed with the tectonic interpretation after Batchelor and Bowden (1985). Tectonic fields are based on divisions postulated by Pitcher (1979, 1982), Harris *et al.*, (1983), Chappell and White (1977) and petrological equivalents after Lameyre and Bowden (1982). Group 1 = tholeiitic (mantle fractionation); Group 2 = Calc-alkaline and trondhjemitic (Pre-plate collision); Group 3 = High-potassic calc-alkaline (post-collision uplift); Group 4 = Sub-alkaline monzonite (late orogenic); Group 5 = Alkaline and peralkaline (anorogenic); Group 6 = Anatectic two mica leucogranites.

Wet, 1989) falls in the field of alkaline-peralkaline post orogenic or anorogenic (A-type) granites such as the Sabaloka Igneous Complex, Sudan (Harris *et al.*, 1983). Other criteria, however, exclude the classification of the Arnaea granite as being "A-type". This "incorrect" classification is probably caused by alteration of the granite by greenschist-facies metamorphism and/or the highly evolved composition which makes chemical classification more difficult.

Probably the most informative diagrams for interpreting the Lake Volvi granitoids are Harker diagrams of wt % oxides and elements *vs* SiO_2 wt % (range 60-80 wt %). These diagrams provide an indication of potential partial melting, fractionation and the degree of alteration to which the rock has been subjected (Figs. 5.18a, b). The scatter on a number of the diagrams is attributed to alteration, e.g. shearing and greenschist-facies metamorphism. The alkali metals and Ca show this well and should therefore be considered suspect if used on further diagrams. The remaining graphs show either linear or curved trends. These linear or curved trends are critical to the interpretation of the granitoid evolution. Furthermore, the distribution of analyses along these trends are represented by in situ local melts, i.e. Vamvakia melts (range from 60 to approximately 74 wt % SiO_2) and large "S-type" granitic bodies, i.e. Arnaea granite (range from approximately 74 to 80 wt % SiO_2). By assuming that the appropriate 74 wt % SiO_2 value represents a "parental (minimum) crustal melt" and the "least fractionated" Arnaea granite, a simple partial melting-fractionation history can be deduced.

If the initial rocks which are subjected to crustal anatexis are migmatites or quartzofeldspathic gneisses (the typical country rock within the area; *see* Chapter 2) the first melts will be close to the granite minimum. However, if the source rock is quartzofeldspathic, the micas will be quickly melted out and the composition will rapidly have quartz (initially ± feldspars) as a residue, and the composition will move towards quartz (≥ 80 wt % SiO_2) diluting all the incompatible elements. This could potentially produce a rock with a composition equivalent to the Arnaea granite. However, the trends shown by the Harker diagrams from 74 wt % SiO_2 do not point towards quartz.

Alternatively, if the initial rock was a much more biotite ± opaque ± garnet rich migmatite (peraluminous), typical of the Vamvakia Purple Gneiss (Chapters 2 and 4) the first melts will again have a composition with approximately 74 wt % SiO_2, but the residue will be peraluminous. Therefore, increased melting will progressively drive the composition towards lower values of SiO_2 (60 wt %) and higher values of Nb, Y etc. The abundance of Rb will increase as long as biotite lasts.

Fractional crystallisation of these high degree melts (approximately 60 wt % SiO_2) would result in the crystallising of (quartz)-feldspars-mafics resulting in melts with 74 wt % SiO_2 generating assemblages with 80 wt % SiO_2. The reliability of this argument is partially supported as an assemblage derived by compiling the values of the oxides given by the intersection of the straight line through 80 and 74 wt % SiO_2 with the axis for an extract at 60 wt % SiO_2 provides totals of approximately 100 wt %. However, this is only a crude guideline and ideally isotope investigations are requires to confirm this crustal anatectic model.

In conclusion the simplest model is that the range of Vamvakia melts represent melts under very high T conditions from 74 wt % SiO_2 back to 60 wt % SiO_2, as progressively more restitic material is incorporated. It should be noted that even the 74 wt % SiO_2 may actually contain unmelted residue. These high degree melts are subsequently fractionated resulting in an increase in SiO_2 wt %. Therefore, the Harker diagrams show that you can take the 74 wt % SiO_2 Vamvakia melt and fractionate the 60 wt % SiO_2 extract mixture of feldspar + mafics and go to a composition with 80 wt % SiO_2. Equilibrium melting probably goes from 74 to 60 wt % SiO_2. whereas, fractional crystallisation goes from 60 to 80 wt % SiO_2.

On the AFM diagram (Fig. 5.19) the Volvi granitoid suite straddles the tholeiite-calc alkaline trend. However, the Arnaea granite samples north of Lake Volvi are similar to those south of the lake (De Wet, 1989) and all plot very close to the A apex. Consequently the Arnaea granite cannot be distinguished from having a calc-alkaline or tholeiitic trend.

When plotted on the ternary Rb *vs* Ba *vs* Sr diagram (Fig. 5.20) of El Bouseily and El Sokkary (1975) the Volvi granitoids (and Arnaea granite) plot along the entire path of the proposed differentiation trend. The Arnaea granite south of Lake Volvi (De Wet, 1989) plots predominantly in the strongly differentiated granite field.

5.9 Tectonic Setting

The Harker diagrams (Section 5.8) when applied to in situ melts and the Arnaea granite show that the larger granite bodies have chemistry consistent with derivation from the same source as the Vamvakia melts, i.e. the migmatite "basement". The geochemistry of the granites will therefore reflect the geochemistry of these migmatites when "filtered" through a melting process. There is no clear evidence of mantle involvement from the trace elements, therefore, the in situ model of generation needs to be tested isotopically.

The basic rock chemistry could be accounted for by simple petrogenetic

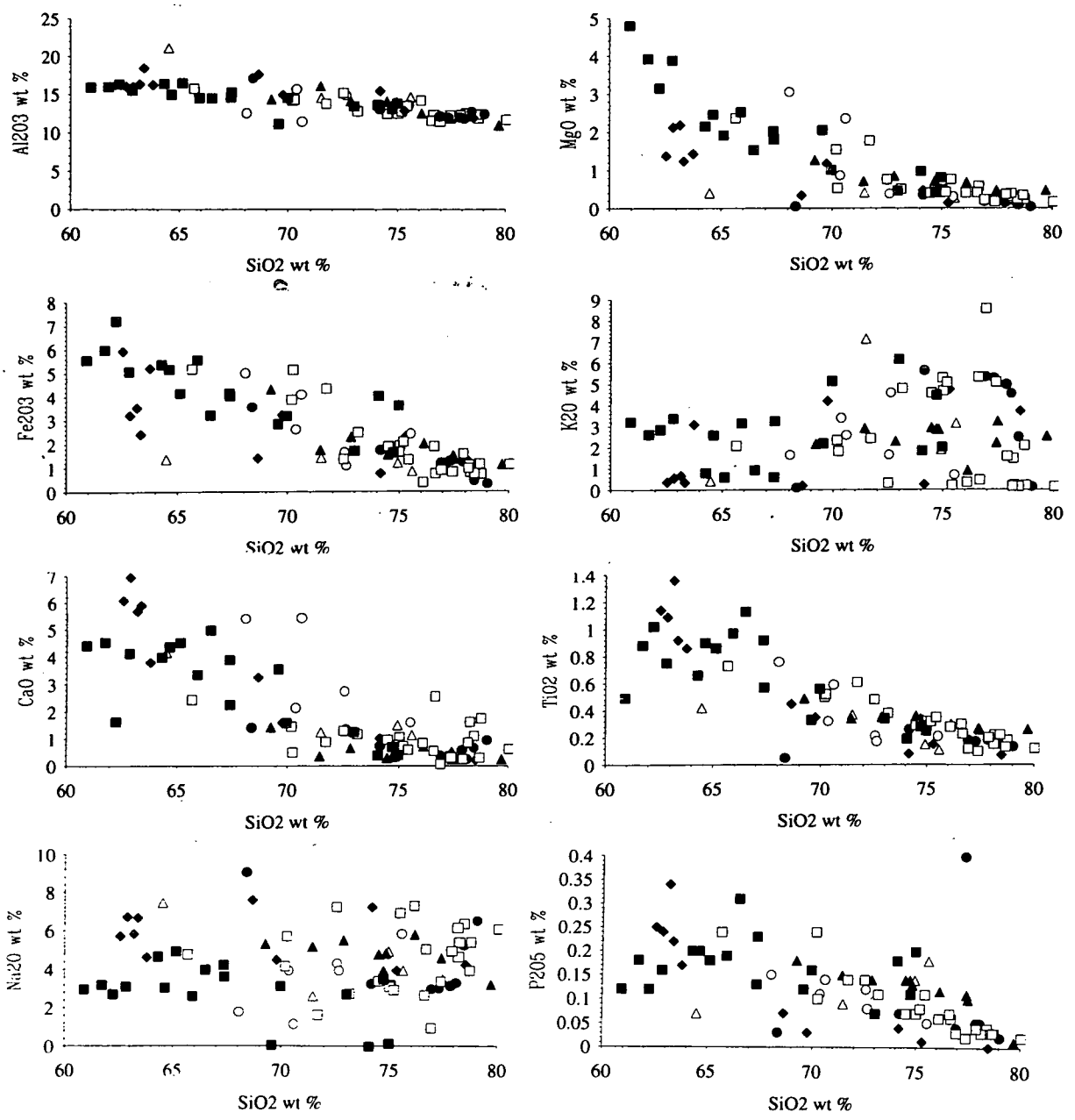

Fig. 5.18a, b: Harker diagrams of wt% oxides and elements ppm *vs* SiO_2 wt%.

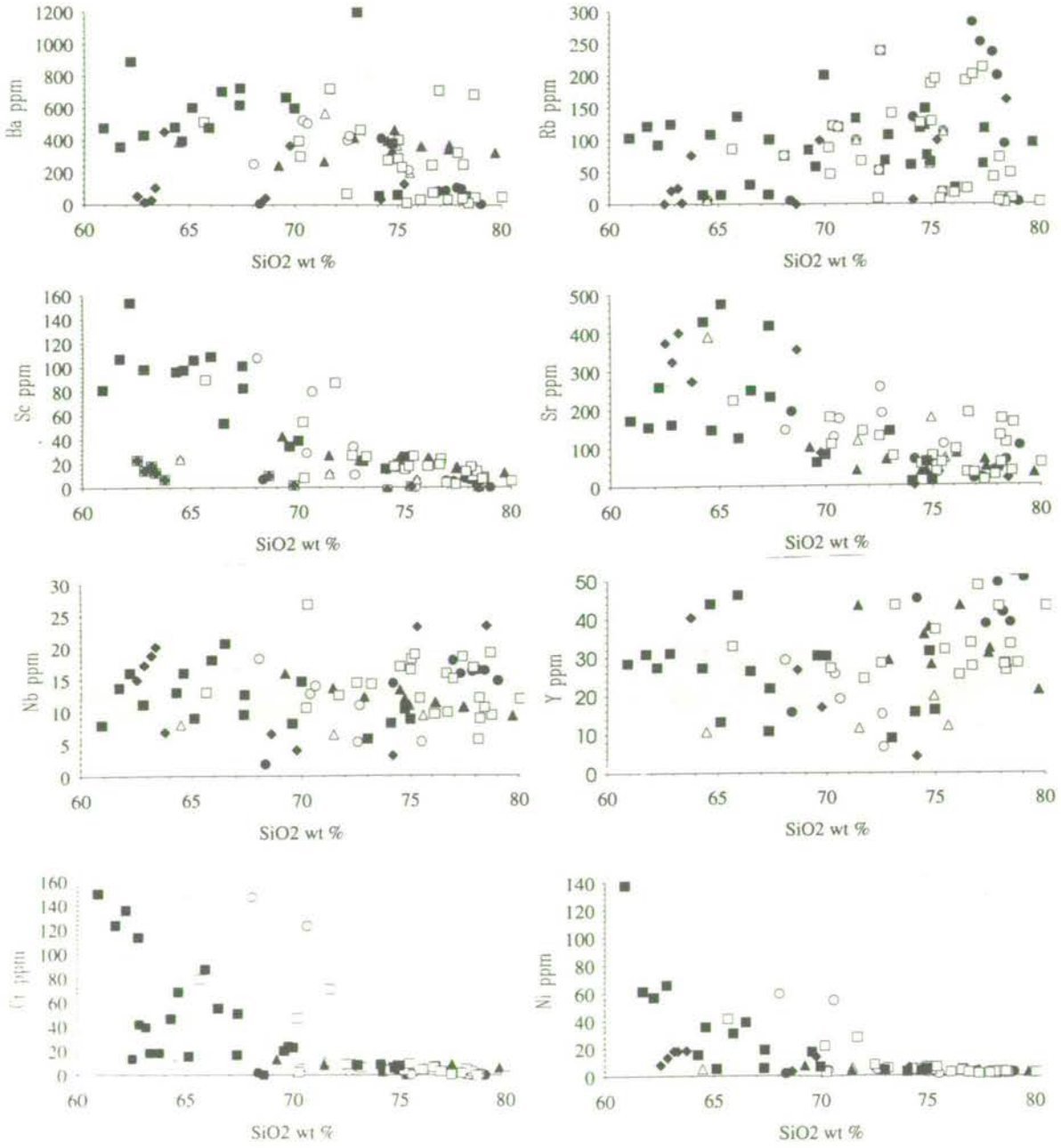

Fig. 5.18a, b: Harker diagrams of wt% oxides and elements ppm *vs* SiO_2 wt%.

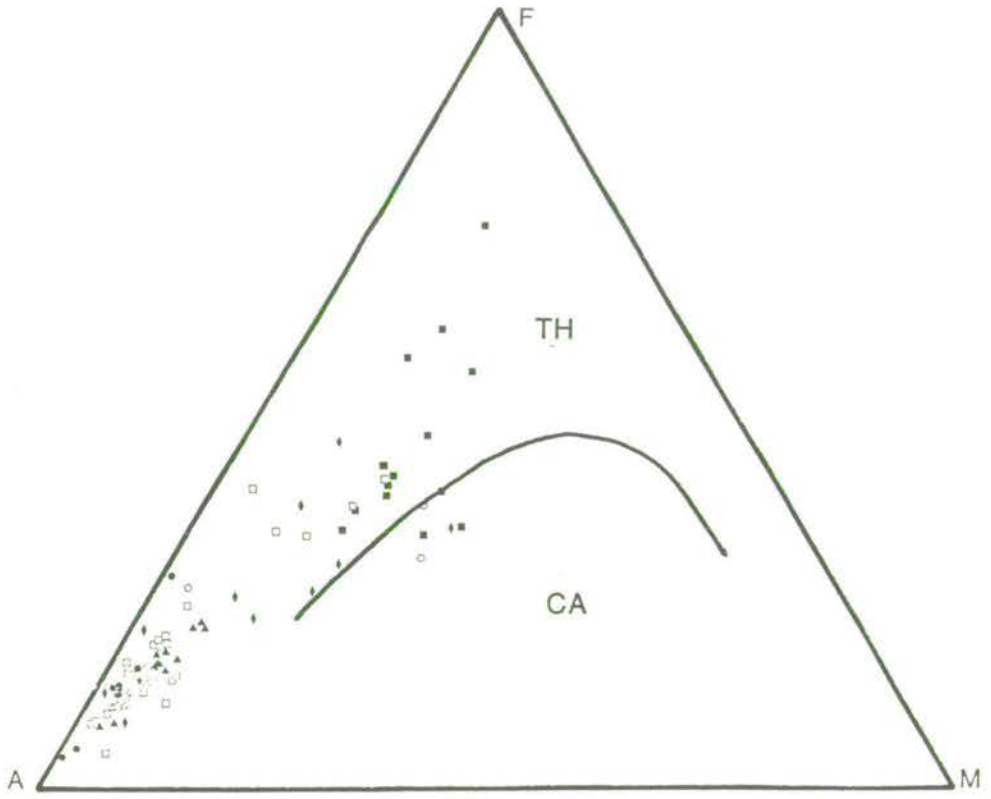

Fig. 5.19: AFM diagram of the Lale Volvi granitoids. The most silica-rich (Arnaea granite) samples, plot close to the A apex.

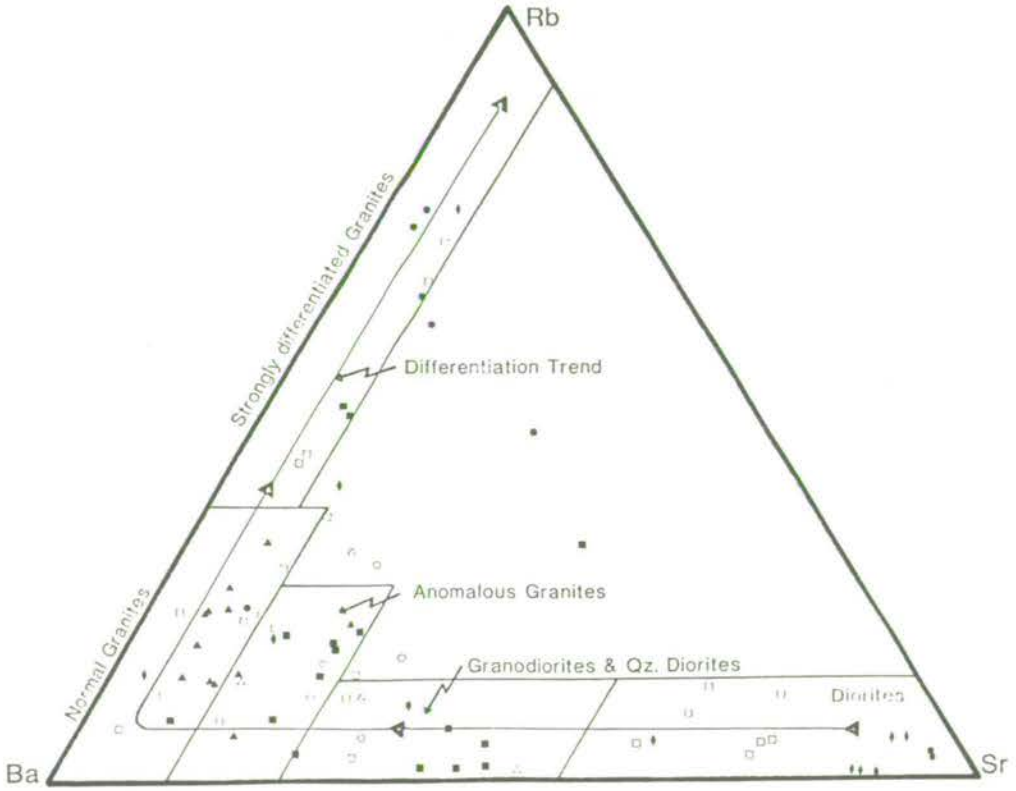

Fig. 5.20: Diagram of Rb vs Ba vs Sr superimposed with the granite fields of El Bouseily and El Sokkary (1975). The Arnaea granite plots predominantly within the well differentiated granite field.

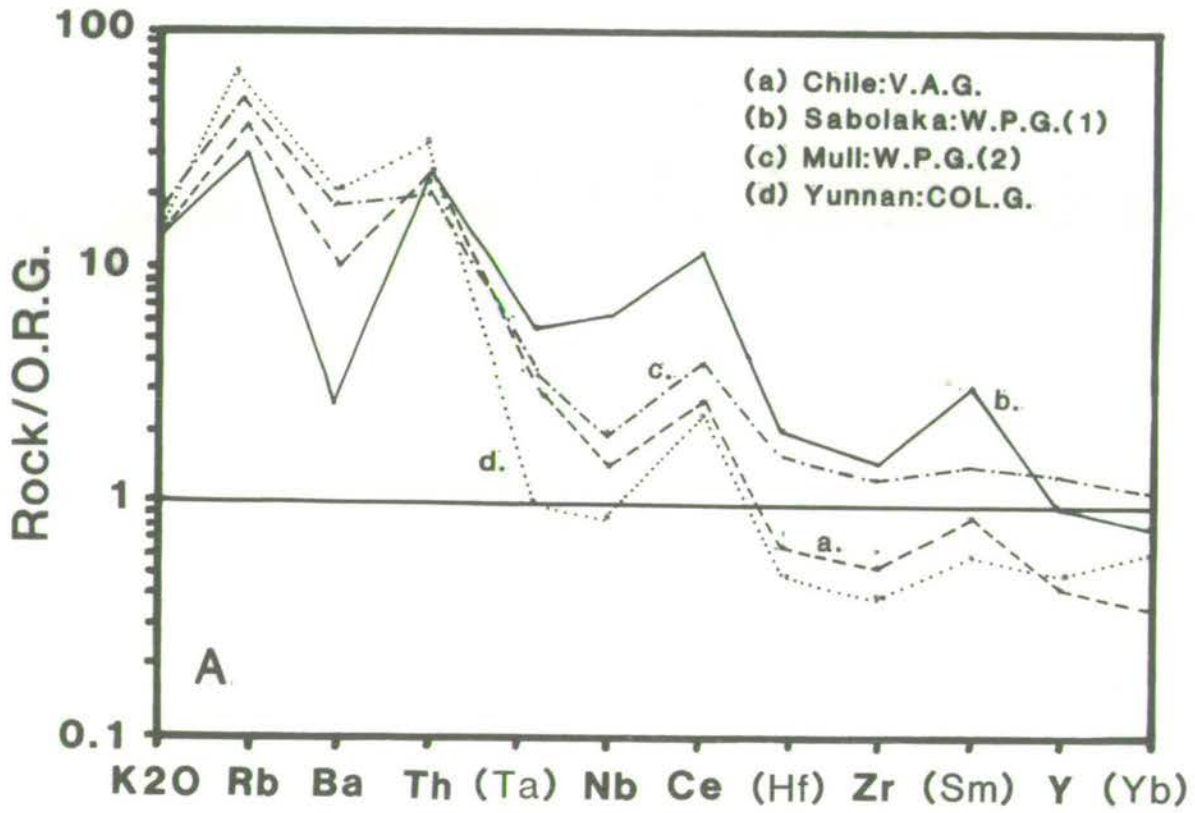

Fig. 5.21: Multi-element diagrams normalised to a hyperthetical ocean ridge granite (ORG), after Pearce *et al.*, (1984).

arguments so that tectonic discrimination diagrams were of limited use. The same is true of the granitic rocks. as might be expected they are generally closest to collisional granites on the ocean-ridge granite mormalised plots of Pearce *et al.*, (1984; Fig. 5.21) as they are most probably derived by crustal melting, from the evidence presented in the preceding section. In this case the problem is made more complex as the "source" is a migmatite complex which has already been partially melted.

5.10 Conclusions

The compositions of the Volvi granitoids have been modified by a number of alteration processes, i.e. shearing and greenschist-facies metamorphism. However, the Volvi granitoids can be seen to follow a related partial melting and fractionation trend which links the Volvi granitoids to the Arnaea granite proper. The Volvi granitoids maintain a predominantly "S-type" signature. The granite was probably derived as a WPG via crustal anatexis. The mafic Volvi Complex and its possible extension at depth is proposed as a potential source of heat to create partial melting of the crust. Subsequent fractionation and partial melting of the granitoids are likely to be associated in some way with the extensive shearing observed within the Lake Volvi area. It is proposed that melts found along the Vamvakia river are representative of an early stage of granitoid production here sampled at high-level which was active throughout the Lake Volvi area at deeper levels.

CHAPTER 6

DISCUSSION AND CONCLUSIONS

Chapter 6

6.1 Introduction

Until recently, many models treated collisional zones as orthogonal and two dimensional. However, with the recognition of apparently far-travelled suspect terranes and lateral-escape blocks transported by transcurrent faulting, as well as the preponderance of modern-day oblique-slip plate boundaries, strike-slip movements are now believed to be of major importance in the evolution of orogenic zones (Jones *et al.*, 1977; Tapponier *et al.*, 1982; Woodcock, 1986). Many of these lateral displacements are invoked on the basis of inferred geologic or geophysical evidence, rather than field-derived structural data.

Ellis and Watkinson (1987) proposed a two stage model for oblique convergence zones. They suggested that, in general, an early phase of orogen-parallel displacement will accommodate the strike-slip component of oblique collision, and that this is overprinted by a later phase of orogen-normal compressional thrusting. Alternatively the vectors of oblique convergence are combined in a single stage, resulting in transpression.

Transpression zones or convergent strike-slip structures have been recognised and described from upper crustal, mostly brittle deformation regimes for several years, e.g. in Svalbard (Harland, 1971; Lowell, 1972) and the western United States (Wilcox *et al.*, 1973; Sylvester and Smith, 1976; *see* Section 6.2). However, there is scarce information on what happens at deeper crustal levels within transcurrent zones. An increasing volume of indirect (e.g. seismic) structural data suggests that major lateral displacements have occurred in deeply eroded ancient orogens. Hence, there is a fundamental need to determine what structural patterns are produced at depth by oblique convergence. In this respect the Serbo-Macedonian Massif provides a useful insight into small-scale locally-developed (m- to km-scale), deep-level structures which help to bridge this current gap in our understanding of deep-level processes. If the structures are scale-invariant as field observations suggest then information at a scale of 10's of km is also available.

Holdsworth and Strachan (1991) proposed a major partitioned system of ductile strike-slip and thrust shear zones for the Caledonian structure of Dronning Louise Land, NE Greenland. The structures within this area have been interpreted as being formed at mid-crustal depths (10 km or more; amphibolite-facies) resulting from a regional phase of sinistral transpression. They also proposed that spatial

partitioning of deformation is prevalent in NE Greenland. Their model is comparable to modern, trench-linked strike-slip fault systems in that kinematic partitioning may be a general response to transpressional deformation at all levels in the continental crust. The basis of this model and the mechanism of deformation are considered to be applicable to the Lake Volvi area. The study area also contains evidence for a further component of extension represented by locally developed 100% sheeted dykes. It should be noted that all transcurrent regimes have zones typified by local extension and local compression. Therefore the overall (regional) sense of transtension and transpression is inherently difficult to determine from a study of a single segment.

Several models of deep-level crustal structures in extensional systems based on information from deep seismic profiling have been produced (Fig. 6.1), a) symmetrical rift graben, b) sub-horizontal, mid-crustal decoupling horizon, (Eaton, 1979; Miller *et al.*, 1983; Smith and Bruhn, 1984), c) lens or anastomosing shear zones (Hamilton, 1982, 1987; Kligfield *et al.*, 1984), d) crustal-penetrating shear zone (Wernicke, 1981). The model of Hamilton (1982, 1987) and Kligfield *et al.*, (1984) for crustal-scale intracontinental extension (Fig. 6.1c) is in some ways a modification of the crustal boudinage model of Davis and Coney (1979) and is of particular relevance to the models which are proposed in this study. In their interpretation, mid-crustal structures consist of a series of detachment faults which define the tops of great lenses that are separated by gently dipping, anastomosing ductile faults (Fig. 6.2). Within the low-strain cores of these lenses pre-faulting fabrics are preserved. Brittle to brittle-ductile extension is accommodated along the detachment faults and the middle crust is extended by discontinuous ductile flow (Fig. 6.2).

The top 10 km of the schematic seismic profile (Fig. 6.2), displays anastomosing zones of reflectors (Hamilton, 1987). Hamilton (1987) interpreted these reflectors to be shear zones, partly representing pre-existing lithologies transposed in the shear direction and partly velocity anisotropy in variably mylonitised rocks (c.f. Fountain *et al.*, 1984; Jones and Nur, 1984). Hamilton (1987) concluded that the accoustically transparent rock between reflective zones consists of large lenses that retain pre-shearing massive or heterogeneous fabric. Similar deformation patterns have been inferred on theoretical grounds by Sibson (1983). The middle continental crust may deform in the same general lenticular mode under compressive overthrusting as under extension (Hamilton, 1987). A specific example of this structural regime has been shown by reflection profiling, where the upper-crust basement Paleogene thrust that bounds the Wind River Mountains of Wyoming flattens downward into a series of lens-defining splays at depths of 17-26 km (Sharry

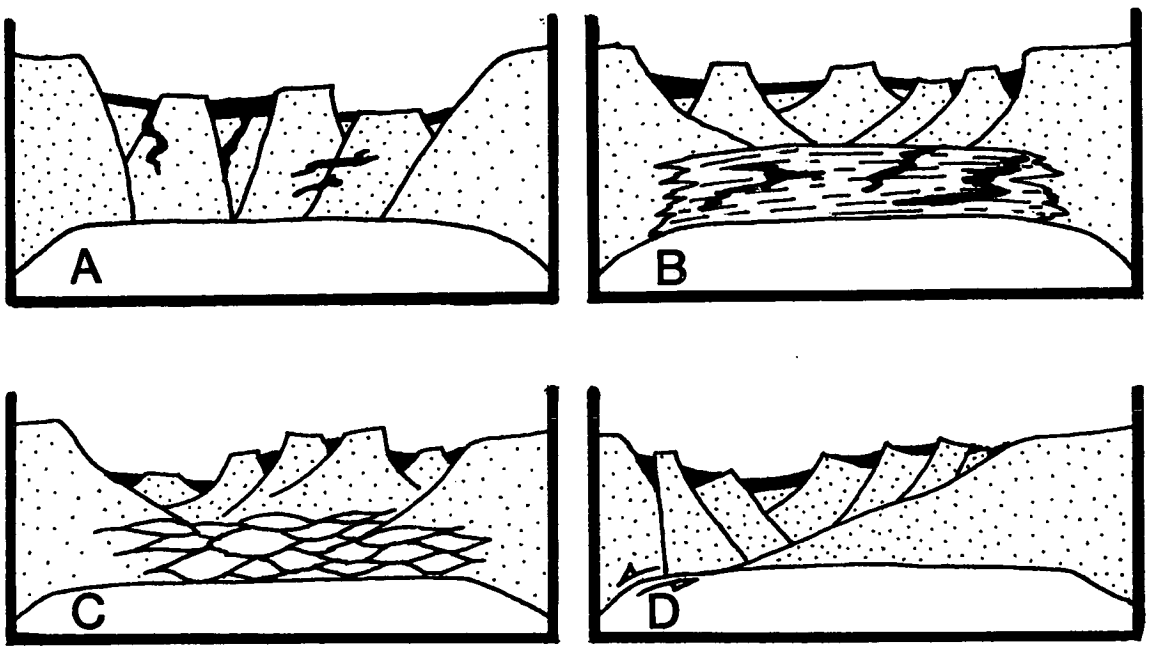

Fig. 6.1: Models for intracontinental extension; (a) symmetrical rift graben, (b) sub-horizontal, mid-crustal decoupling horizon (Eaton, 1979; Miller *et al.*, 1983; Smith and Bruhn, 1984), (c) lens or anastomosing shear zones (Hamilton, 1982; Kligfield *et al.*, 1984), (d) crustal-penetrating shear zone (Wernicke, 1981).

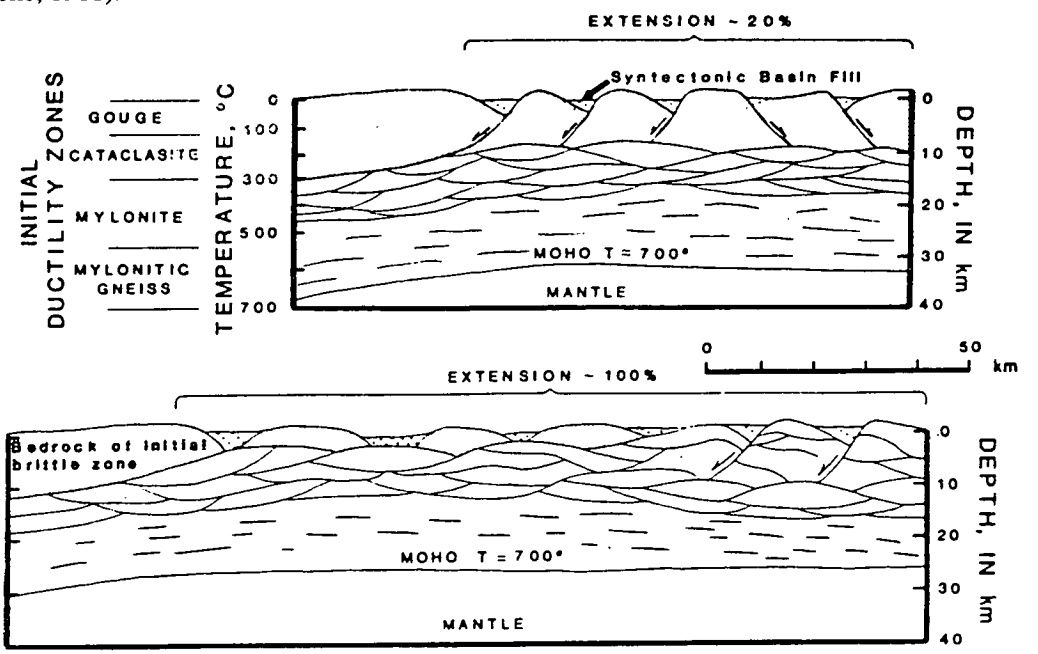

Fig. 6.2: Cross-sections of extending crust. Brittle upper-crust blocks rotate and separate. Middle-crust lenses slide apart along ductile shear zones; composite upper surface of lenses forms detachment faults that increase in total area with time. Lower crust flattens pervasively. Structural styles are superimposed as components rise to the surface with continuing attenuation. Attenuating crust is partly rebuilt by magmatism, and possibly also by phase change, so crust is thinned by a factor less than extension ratio, after Hamilton (1987). Ductility zones after Sibson (1983).

et al., 1986) acoustically appropriate for mylonitic zones (Jones and Nur, 1984). Examples of such thrust lenses bounded by ductile shear zones are exposed in the Proterozoic Grenville crustal-thrust terrane of Ontario, where pervasive deformation increases with depth of exposure within the lower crust (Davidson, 1984).

Obviously the models derived in this study for the Lake Volvi area (Section 6.6) are not an interpretation on a full crustal scale, but simply a microcosm of this deformation regime applied to a small area. The interpretation of a transpressive regime at mid-crustal depths (10-15 km; amphibolite-facies), and the development of low-strain pods wrapped by high-strain shear zones are combined to represent the main structural features prevalent within the study area. By considering this particular structural regime to be scale-invariant, I propose that the interpretation and models for the Lake Volvi area discussed above could successfully depict larger-scale deep-level structures in a generally transcurrent regime in which transpression and transtension were both prevalent..

6.2 Transpression-transtension

The terms transpression and transtension were introduced by Harland (1971) to describe oblique tectonic regimes: *transtensional regimes* operate in zones of oblique extension, while *transpressive regimes* operate in zones with oblique compression. These tectonic regimes have been mainly characterised by observations of the deformation of sedimentary and basement rocks at high crustal levels within major strike-slip fault systems. These tectonic regimes result in complex structural patterns which are also controlled in part by heterogeneities in local basement structures (Harland, 1971; Crowell 1974). Transpression may create en-échelon folds, thrusts and other features (e.g. uplift), whilst transtension can give rise to subsidence (e.g. graben and extensional magmatism; Harland, 1971).

Deformation within zones of transpression-transtension is generally complex as it tends to alternate both along strike and in time (Wilcox *et al.*, 1973; Reading, 1980; Sanderson and Marchini, 1984; Aydin and Nur, 1984; Christie-Blick and Biddle, 1985; Woodcock and Fischer, 1986; Sylvester, 1988). This is especially the case where regional strike-slip displacement is modified by strong convergent components of motion, causing offset and rotation of pre-existing strike-slip fault segments (Sylvester and Smith, 1976; Hancock and Atiya, 1979; Aydin and Page, 1984; Harding, 1985; Namson and Davis, 1988; Ron *et al.*, 1990). However, this study interprets the area around Lake Volvi to have been initiated at high structural levels in the form of a deep pull-apart basin (possibly oblique rift-basin), which was

subsequently buried to a mid-crustal level (20-25 km), where it continued to be deformed in a transpressional-transtensional regime (Section 6.6). This is reflected in the thermal model produced for the area (Section 6.5.2). In this model the contrast between compressional and extensional regimes shows that depth and temperature of mid-crust components increase with time in the former, but decrease in the latter (Hamilton, 1987).

6.3 Development of Pull-apart Basins

Since the introduction of the term in 1966, a pull-apart origin has been proposed for about sixty Quaternary basins along active strike-slip faults (Aydin and Nur, 1982; their Table 1) as well as several ancient basins in Alaska (Fisher *et al.*, 1979), California (Hall, 1981), Atlantic Canada (Bradley, 1982) and eastern Europe (Royden *et al.*, 1982). The actual geometry and development of pull-apart basins has been reviewed and the models refined by a number of workers (e.g. Freund, 1971; Crowell, 1974; Koide and Bhattacharji, 1977; Dewey, 1978; Rodgers, 1980; Aydin and Nur, 1982), *see* Fig 6.3. Progressive displacement on discontinuous faults causes extension between the faults where their ends overlap and results in a depression or pull-apart basin (Aydin and Nur, 1982; Mann *et al.*, 1983; Aydin and Page, 1984). The surface expression and basin-fill of even a simple pull-apart is complex (Fig. 6.4). Therefore reconstruction of a basin which has been highly deformed (such as around Lake Volvi) is not feasible, but may partly explain the variation and complexity of metasediments within the area.

Active strike-slip systems show that subsiding pull-aparts form at releasing bends and uplifting push-ups form at restraining bends (e.g. Crowell, 1973; Mann *et al.*, 1983). The inward-dipping geometry of faults under both pull-apart and push-up duplexes suggests that the faults may converge at depth into a single shear zone. In vertical section the faults define a flower structure (Sylvester and Smith, 1976; Figs. 6.5a, b, 6.6). This model is compatible with the duplex geometry observed in some seismic profiles across strike-slip flower structures (e.g. Harding, 1983, 1985). Pull-aparts may commonly be underlain by negative (normal faulted) flower structures and push-ups by positive (reverse faulted) flower structures.

A link between flower structures in section and "Riedel shear lenses" (either duplexes or isolated horses) in plan view is seen in sandbox experiments (Naylor *et al.*, 1986). Each Riedel shear has a helicoidal form so that at depth they unite into a single steep fault zone. Transtension suppresses the en-échelon nature of the Riedel shears whereas transpression increases the angle between the Riedels and the

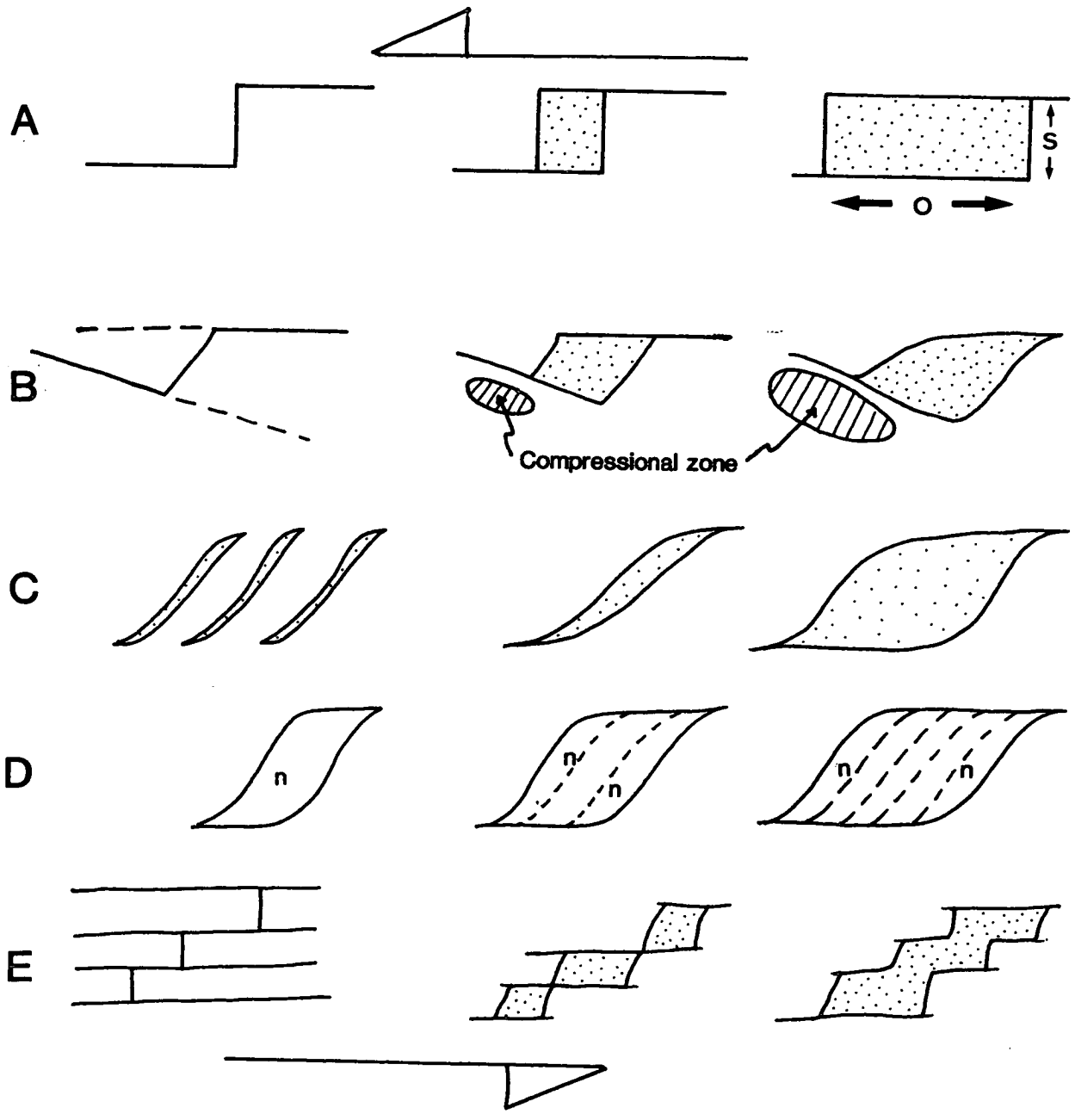

Fig. 6.3: Models of pull-apart basin development, as reviewed by Mann *et al.*, (1983). (A) Simple model of pull-apart opening between left stepping and sinistral "master" strike-slip faults; master fault separation (s) or basin width remains constant; master fault overlap (o) or basin length increases with strike-slip offset. (B) Modification of simple model based on detailed mapping of active pull-aparts by Freund (1971); opening across an oblique median fault and along non-parallel master faults results in an extensional gap on one side of the basin and a compressional overlap or bulge (shown in cross hatching) on the other. (C) Deformational pattern produced in shear box experiments suggested pull-aparts nucleate on en-échelon fractures (Koide and Bhattacharji, 1977). (D) Theoretical model of deformation in pull-aparts based on the elastic dislocation theory (Rodgers, 1980); "n" designates areas of predicted normal faulting. (E) Coalescing of adjacent pull-aparts was suggested by Aydin and Nur (1982), as one explanation for widening of pull-aparts with increased off-set.

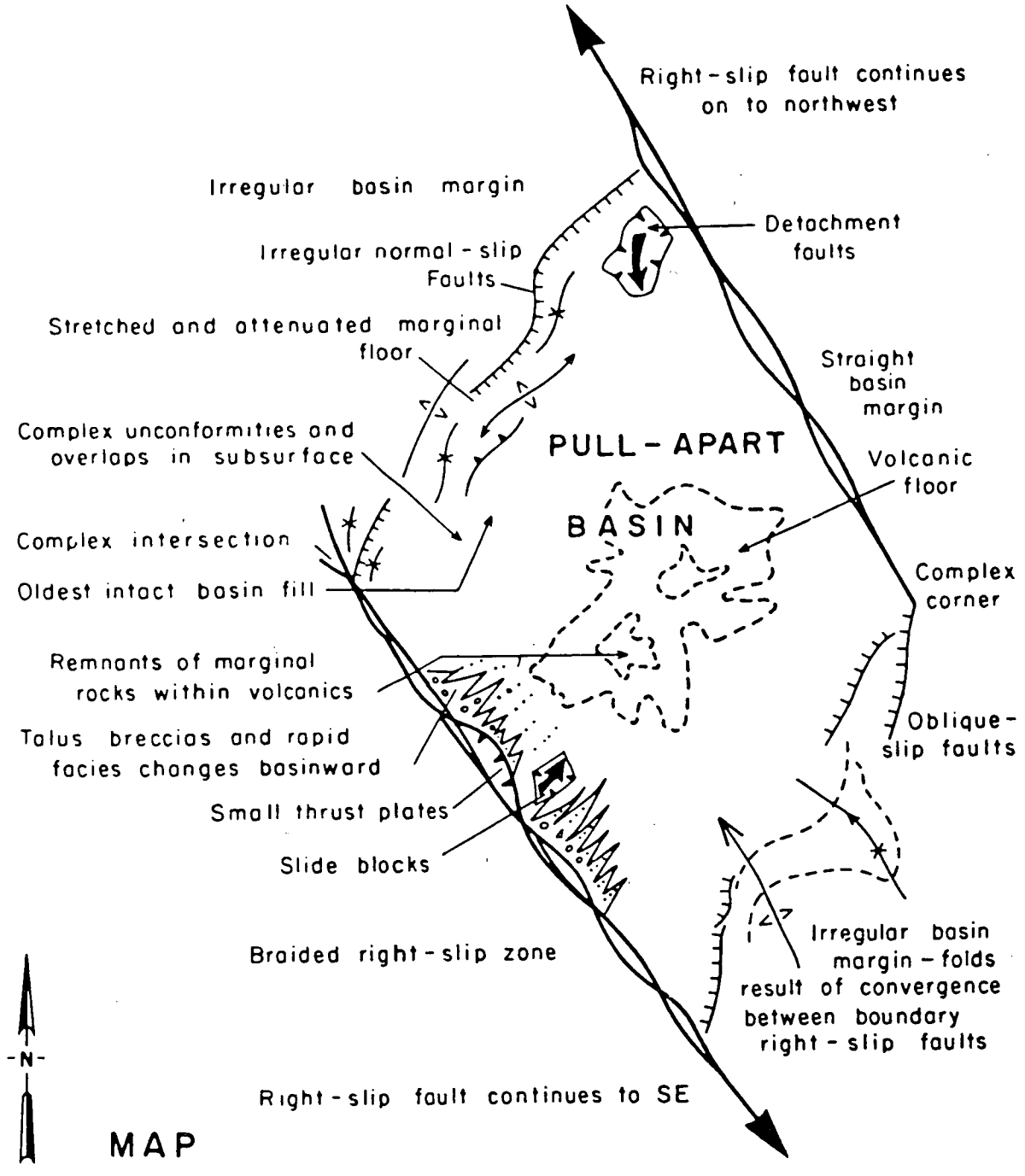

Fig. 6.4: Schematic sketch of an idealised pull-apart basin, from Crowell (1974). Note the expected complexity and distribution of the basin deposits. The abundance and nature of these deposits will be strongly dependent on the specific geometry of the basin and on the environment in which the pull-apart is developed.

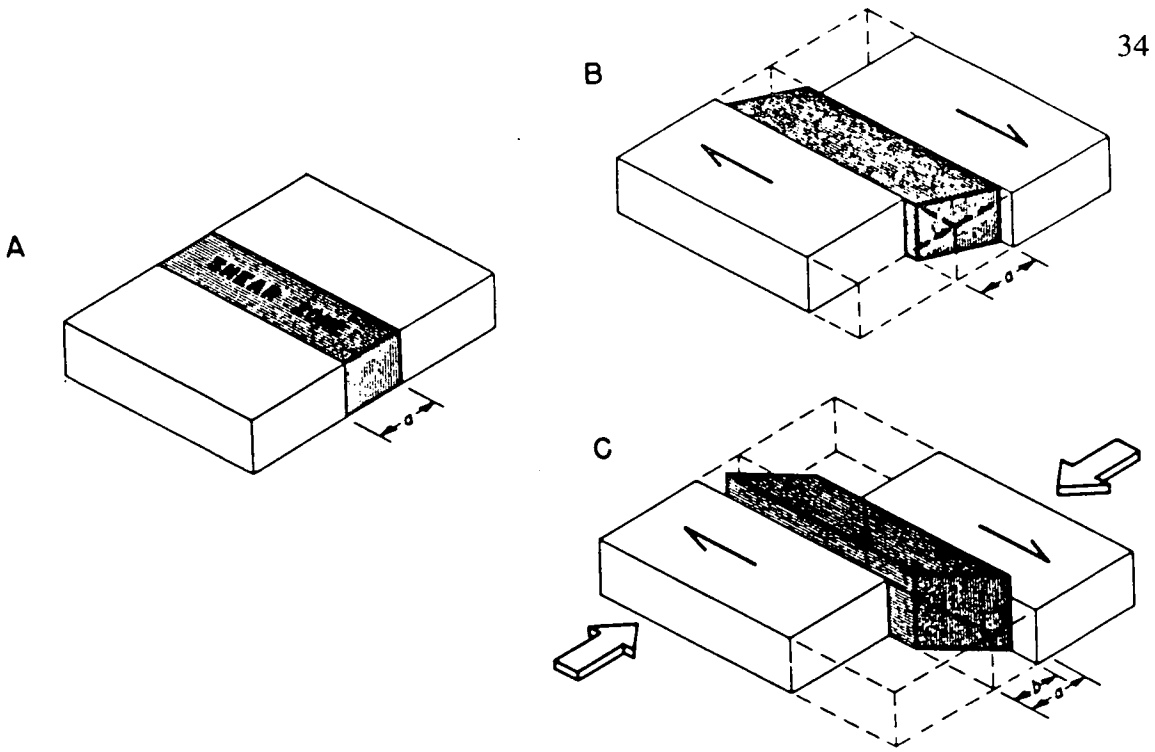

Fig. 6.5a: A simple conceptual model for deformation of basement lithologies in a transpressive regime, after Sylvester and Smith (1976). The shaded area may be considered representative of a consolidated mafic body (Volvi Complex) intruded during an earlier phase of extension.

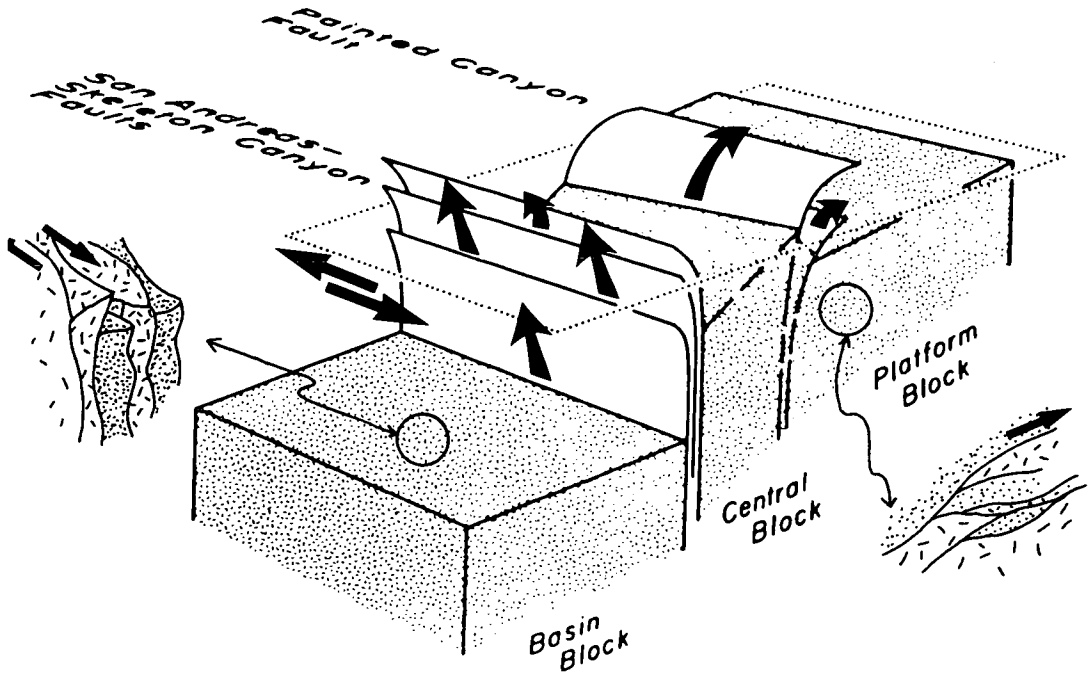

Fig. 6.5b: Idealised block diagram of basement and principal faults in Mecca Hills, after Sylvester and Smith (1976). Dotted parallelogram represents the present-day surface. Note the irregular displacement of blocks and the change in attitude (from steep to flat-lying) of the fault (shear) zones.

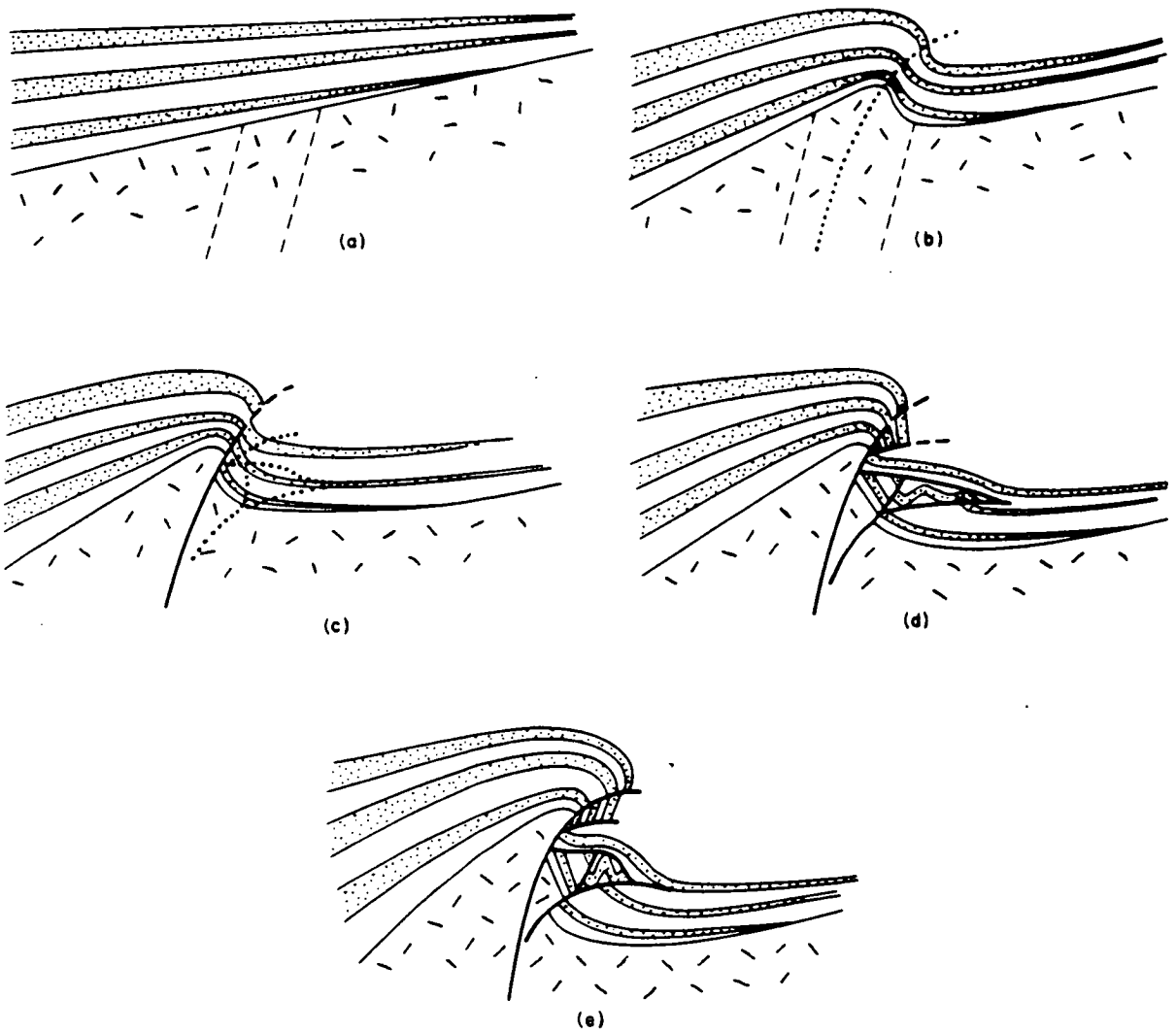

Fig. 6.6: Postulated structural evolution of Painted Canyon fault, after Sylvester and Smith (1976). (a) Initial geometry of basement and overlying sedimentary strata. (b) Flexure of basement by movement along closely spaced fractures and shear planes within zone indicated by dashed lines. (c) Rupture of basement along Painted Canyon fault. (d) Secondary faulting in syncline, incipient buckling of beds in "bookcover structure". (e) Continued vertical displacement on Painted Canyon fault, rotation of secondary faults, and continued buckling of strata on "bookcover structure". Note the change in attitude (from steep to flat-lying) and the development and arrangement of individual fault bounded blocks.

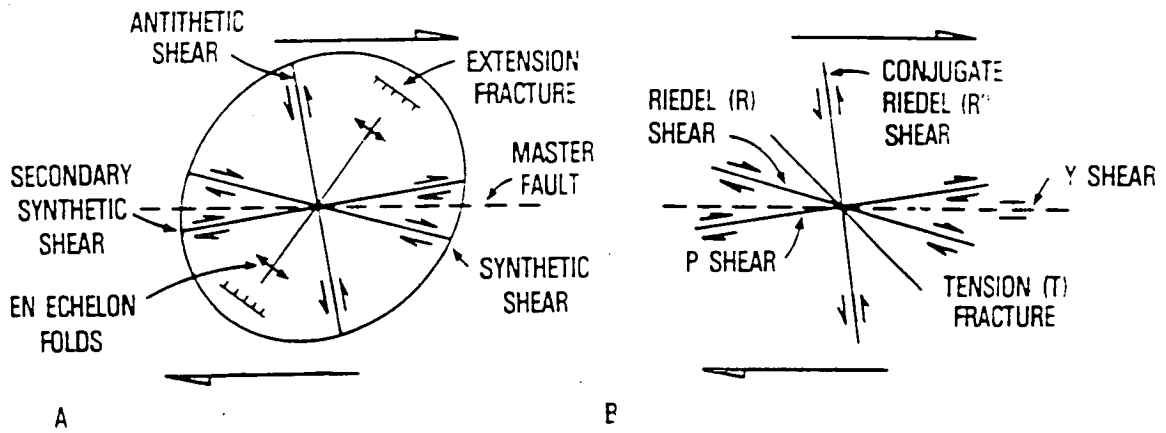

Fig. 6.7a: The angular relations between structures that tend to form in right-lateral simple shear under ideal conditions, compiled from clay-cake models and from geological examples. Arrangements of structures along left-slip faults may be determined by viewing the figure in reverse image. (A) Terminology largely from Wilcox *et al.*, (1973), superimposed on a strain ellipse for the overall deformation. (B) Riedel shear terminology, modified from Tchalenko and Ambraseys (1970) and Bartlett *et al.*, (1981). Extension fractures from when effective stresses are tensile (i.e. when pore-fluid pressure exceeds lithostatic pressure); tension fractures form when lithostatic loads become negative (Christie-Blick and Biddle, 1985). In geological examples, faults with normal separation tend to develop parallel to the orientation of the extension and tension fractures in (A) and (B); faults with reverse separation tend to develop parallel to the orientation of the fold in (A).

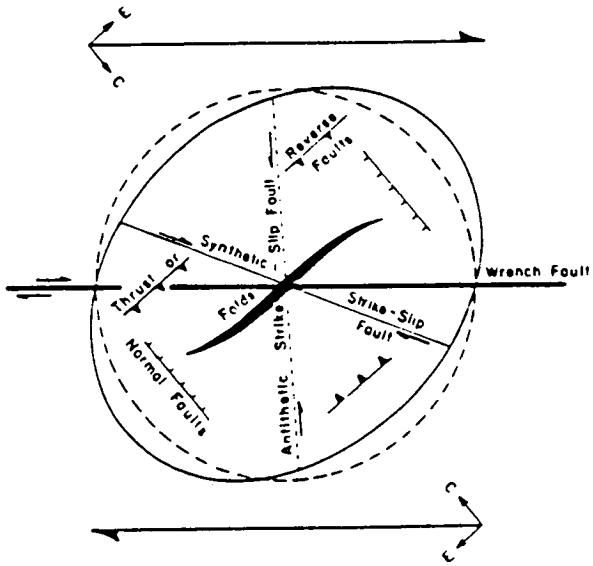

Fig. 6.7b: Conceptual diagram showing the geometric relations between folds and faults to a right-slip wrench fault. These features are combined schematically with a strain ellipse and principal strain directions, contraction (C), and extension (E). Axial traces of folds have flattened S-shapes, correseponding to field and laboratory observations. The geometry for a left-slip wrench fault is a mirror image of this diagram, after Sylvester and Smith (1976). Adapted from Harding (1974).

basement fault trend (Naylor *et al.,* 1986). This relationship is also predicted from theoretical modelling (Sanderson and Marchini, 1984; Figs. 6.7a, b).

An alternative geometry to, or a component of, flower structures for maintaining three-dimensional strain compatibility in the upper levels of the crust, is for steep strike-slip faults to be associated with or root into low-dip faults or shear zones. These faults allow various levels in the strike-slip system to move over one another and to rotate (strike-slip *flaking* of Dewey, 1982). These flat-lying structures are a kinematic requirement and are analogous to lateral ramps or transfer faults in dip-slip systems (Fig. 6.6). Flat detachment zones must necessarily delimit strike-slip systems at depth as they do dip-slip systems. Two possible sites are a mid-crustal discontinuity (e.g. Sibson, 1983) or a sub-lithospheric zone related to a transform fault zone (Woodcock and Fischer, 1986).

The importance of continental strike-slip regimes was highlighted in an influential paper by Reading (1980). He pointed out that a strike-slip tectonic regime created a special type of orogenic belt characterised by intense seismic activity and deformation, by important differential vertical movements, by rapid and varied sedimentation, but by comparatively feeble magmatic and metamorphic activity at high crustal levels. From the observations made during this study, I propose a model for the Lake Volvi area which involves the development of a pull-apart basin in a strike-slip system (Fig. 6.8).

6.3.1 Movement Along Strike-slip Duplexes

The development of low-strain lensoid bodies bounded by faults (or shear zones) can be developed by duplexing in strike-slip systems, whether at bends, offsets or along straights (review in Woodcock and Fischer, 1986). Differential movement of these fault bounded lensoid bodies creates a range of contact relationships. The lensoid bodies may be; *autochthonous,* preserved in their original stratigraphic and structural context; *cognate,* retaining a match with rocks on one fault-bounded surface; or *exotic,* with the fault-bounded bodies totally isolated from any of their parent rocks and from their original structural context (Woodcock and Fischer, 1986; Fig. 6.9). Exotic duplexes and horses are analogous to "far-travelled horses" in thrust systems (c.f. Elliott and Johnson, 1980).

The process of differential shunting along a strike-slip fault may be responsible for many of the small isolated lozenges of mismatching rocks in strike-slip systems (e.g. Crowell, 1975). The shunting processes is similar to one envisaged

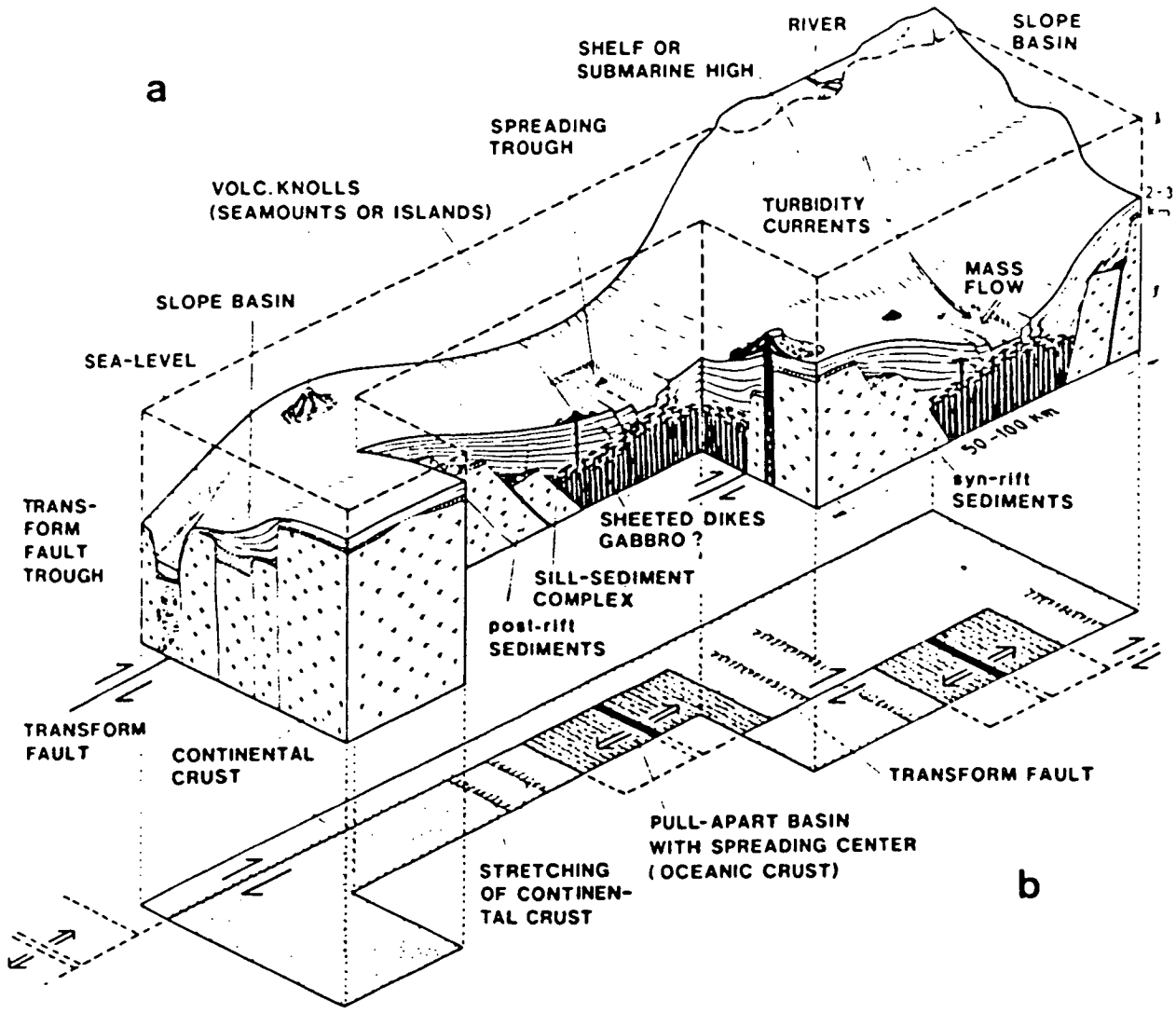

Fig. 6.8: A schematic three-dimensional interpretation of pull-apart basin development, after Einsele (1985, 1986). (A) Simplified block diagram and (B) plan view of gulf-type pull-apart basins in a stage of early rifting. Formation of sill-sediment complexes in spreading troughs.

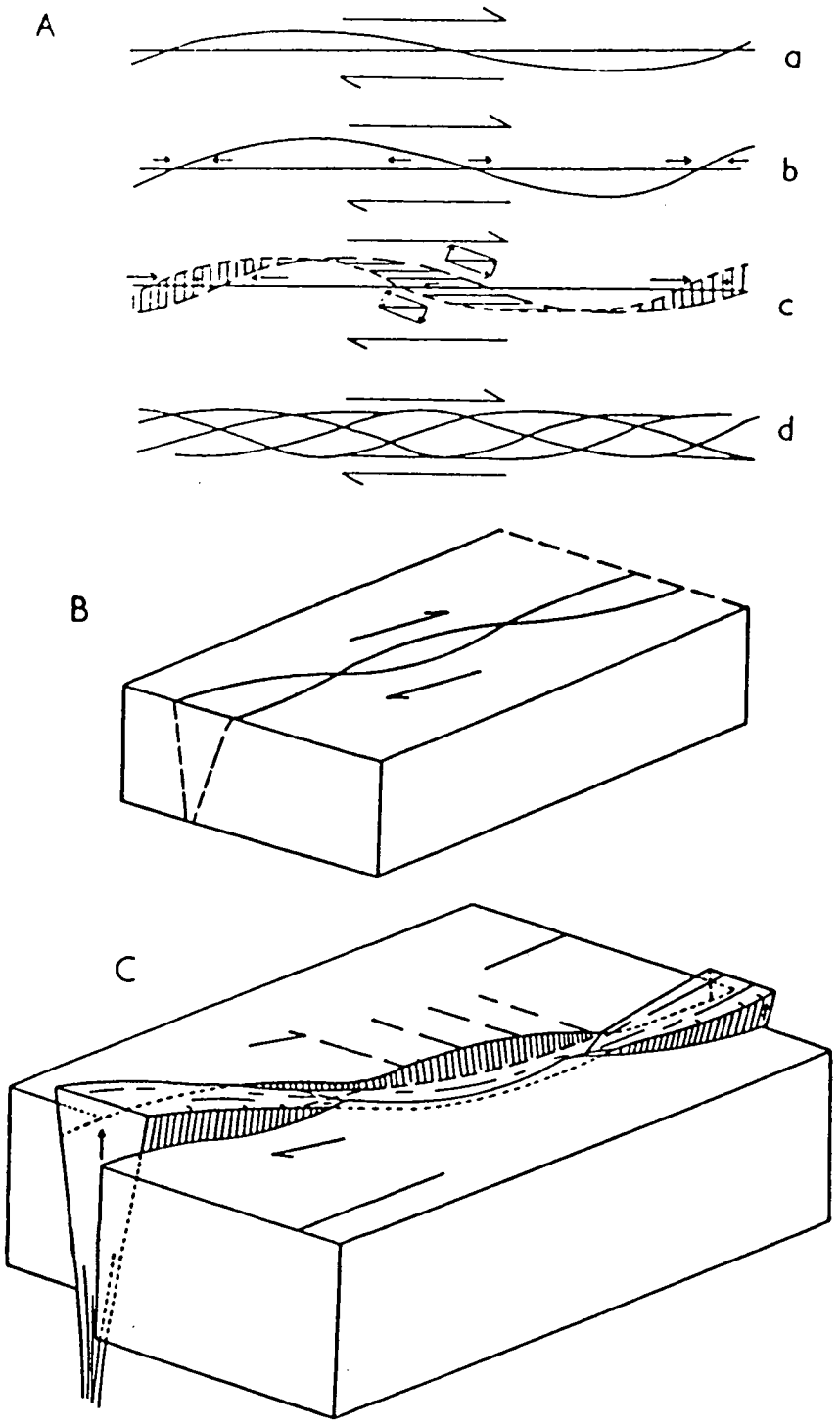

Fig. 6.9: Schematic interpretation for movement along strike-slip margins. (A) Stages in deformation and in change of direction along part of a dextral transcurrent fault; --- denotes tensional and sinking areas; +++ denotes compressional and rising areas. (B) Dextral transcurrent fault-zone before movement. (C) Same fault-zone after movement has taken place; development of horsts and grabens, after Kingma (1958). Movement along fault planes results in variable vertical displacements. with the onset of further anastomosing blocks, lateral translation is also undertaken. The three-dimensional model developed in this thesis invokes the possibility of movement in any direction.

on a larger scale for transporting allochthonous terranes in orogenic belts (review by Schermer *et al.,* 1984) and termed *sidling* by Dewey (1982).

The results of this study suggest that transportation models are applicable to the anastomosing shear-bounded pods (halibuts) within the Lake Volvi area. However, within the study area there is an important variation, as the fault bounded "halibuts" are in fact developed in three-dimensions. Hence, movement and displacement can be in any direction, provided the bulk movement vector for the strike-slip displacement is satisfied.

This tendency of duplexes and of isolated fault lozenges to be uplifted and to subside alternately, or to move in a more complex three-dimensional configuration as they move along a strike-slip system has been called *porpoising* (Crowell and Sylvester, 1979). This pattern of complex three-dimensional movement is considered to be one of the main components in developing the heterogeneous arrangement of lithological formations and structures which outcrop within the study area.

An inevitable consequence of this complexity is that zones of thickening and thinning will alternate in time and space. Thickening will be limited by the work to be done against gravity and thinning by resistance of the lithosphere to extension. In the simple case of a restraining bend involved in a continuously moving strike-slip system is for the restraining bend to progressively override the pull-apart basin. This would result in the rapid burial and metamorphism of the underlying units, equivalent to thrust emplacement. With continued strike-slip along this system the restraining bend would completely pass over the pull-apart basin, resulting in tectonic unroofing of the lower units. This would be a crustal scale manifestation of the transient "piggy-backing" of porpoises(!) in a smaller-scale zone. The thermal implications of this will be considered later (Section 6.5).

6.4 Model for the Distribution of Mafic Bodies

A basic consideration in any extensional or compressional region within a transcurrent zone is asymmetry, whereupon, a pull-apart or duplex will have monoclinic symmetry related to the overall shear sense. This will introduce fundamental asymmetries into the local stress distribution around the transcurrent feature. The Volvi basic intrusions may reflect this on a 10's of km scale. One of the curious anomalies of the area is the spatial arrangement of dykes and discrete amphibolite bodies within the envelope of the Volvi Complex. These mafic components are abundant and randomly distributed within the envelope to the west of the Volvi Complex, whereas they rarely crop out to the east. This difference echoes

the contrast in the regional structural trends which consist of steeply inclined to moderately inclined foliations west of the Volvi Complex and flat-lying to gently inclined foliations east of the complex (Chapter 3). The mafic bodies and dykes also appear to have been intruded throughout the main D_2 deformation event as the style of the intrusive contacts is always extensively modified by the shear zones unless preserved in low-strain pods. No dykes or mafic bodies have been found that cross-cut a D_2 shear zone.

Similar examples of this sort of behaviour occur around the Great Slave Lake shear zone (Hoffmann, 1987; Hanmer, 1988a; Hanmer *et al.*, 1992). Within this area swarms of stubby "mafic-filled" pull-aparts, flattened isolated lenses or long, parallel-sided bands of a mafic component are aligned parallel to the mylonitic foliation of the host rock. The first two types of mafic body are considered to represent originally discontinuous mafic bodies filling in pull-apart spaces, whereas, the last type of mafic body may be intact or pervasively fractured, dilated and sealed with pegmatitic fill. This last type of mafic component is probably a set of continuous mafic dykes (Hanmer and Lucas, 1985). Hanmer *et al.*, (1992) consider the absence of post-tectonic dykes within the Great Slave Lake area to be evidence of a causal relationship between active shearing and the locus and mechanism of dyke emplacement. In the case of the Lake Volvi area, a similar range of mafic outcrops occurs, however, with dykes clearly observed. Due to the extensive progressive deformation during continued intrusion within the area, it is often difficult to determine from field relationships, whether the Volvi mafic bodies are highly deformed dykes or originally discontinuous intrusive mafic-filled pull-aparts. However, on a regional scale, discontinuous injection into a mafic-filled pull-apart structure (Volvi Complex) is evident. Therefore, in order to maintain scale-invariance, discontinuous injection into small pull-aparts would have to be inferred to actively develop on an outcrop scale.

According to the deformed dyke model of Sibson *et al.*, (1988), vertical fluid flow is enhanced in a strike-slip environment, but impeded in a dip-slip regime (Fig. 6.10). Applying this reasoning to dyke emplacement, one can effectively account for the distribution of syntectonic mafic dykes in the area of the Great Slave Lake shear zone and equally so around Lake Volvi. However, this would require the presence of both a steep and a flat-lying fabric either prior to intrusion or at least early in its course. It must also be noted that due to strain partitioning and the heterogeneiity of the envelope, input of dykes and mafic injections would alter the initial strain field which had permitted or inhibited early dyke intrusion. Hence, subsequent intrusions would be orientated in the appropriate local strain-field. The final arrangement of

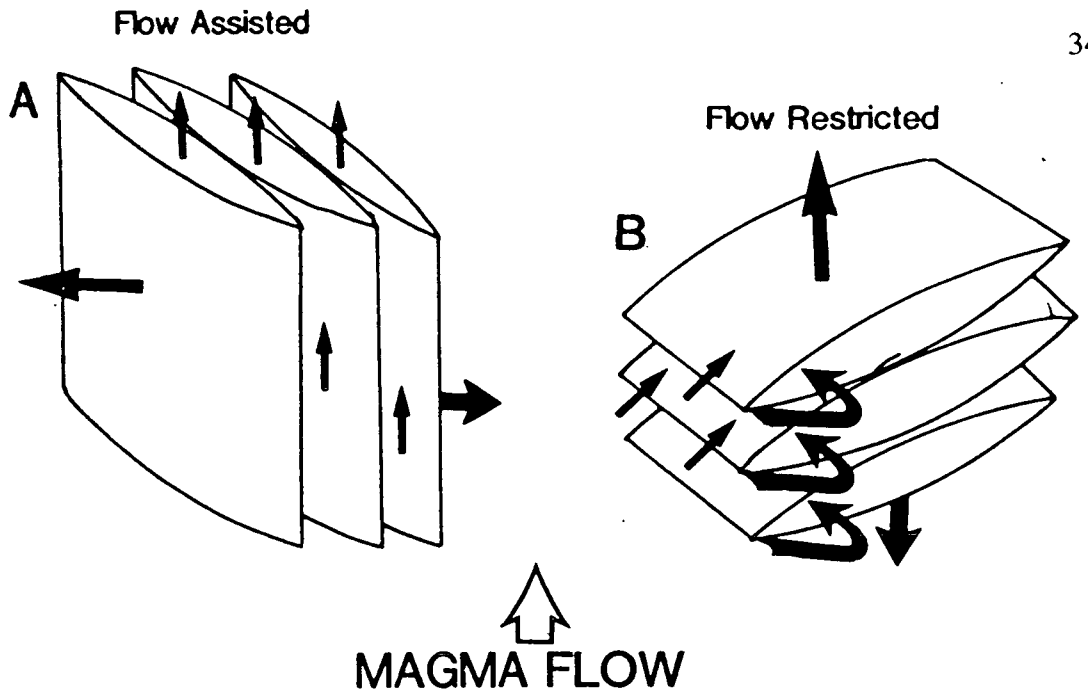

Fig. 6.10: Schematic illustration of the effect of the orientation of arrays of en-échelon initial Riedel fractures (e.g. Logan, 1979) associated with vertical magma flow. (A) The long dimensions of the initial en-échelon components in a strike-slip array are aligned so as to favour the emplacement of magma, especially if such arrays are vertically interconnected. (B) The en-échelon components in a dip-slip fracture array act as baffles to the emplacement of a vertically rising magma and do not enhance magma access. Modified after Sibson *et al.*, (1988).

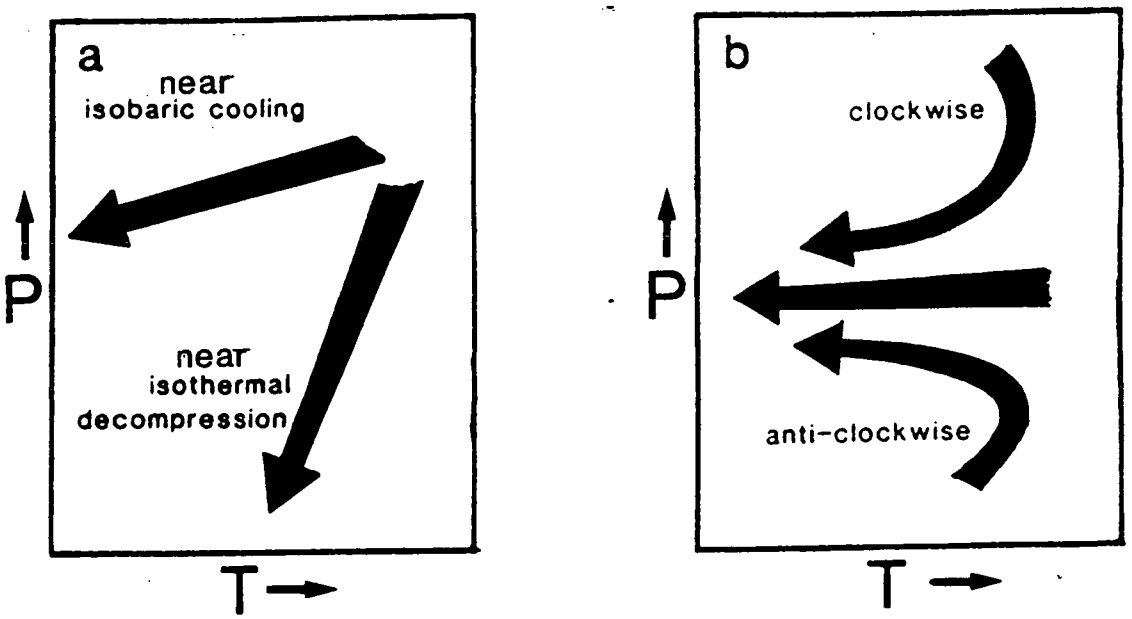

Fig. 6.11: A classification of pressure-temperature paths. (a) Illustrates a two-fold division of retrograde paths into isobaric cooling and isothermal decompression (Harley, 1989). (b) Illustrates a three-fold division of isobaric-cooling paths into clockwise and anti-clockwise paths preserving some evidence of pre-cooling decompressional and compressional history respectively, and simple cooling paths which preserve no evidence of an earlier history (Bohlen, 1991), after Fitzsimons (1991).

dykes and mafic intrusions may therefore not reflect the pattern in a simple extensional regime. This point should be considered when dykes are used to determine extension directions and strain parameters in other complex terranes.

6.5 Tectonic Processes

Much of the study of metamorphic rocks is based upon the basic assumption that the mineral assemblage of a rock will reflect at least part of its pressure-temperature evolution. Hence, the spatial variation in mineral assemblage developed in a metamorphic terrain, or the "metamorphic field gradient" (Schumacher *et al.*, 1990), is some function of the thermal gradients developed in the crust during the metamorphic event. Miyashiro (1961) suggested that the field gradients preserved in most metamorphic belts could be classified into one of three "facies series", which reflect three different types of thermal regime characteristic of the crust. The high-pressure facies series is characterised by blueschist- and greenschist-facies assemblages. The intermediate- and low-pressure series are distinguished by the aluminosilicate polymorphs developed in metapelitic lithologies. The former is characterised by a prograde transition of kyanite to sillimanite, and the latter by a prograde transition of andalusite to sillimanite, which are typical of the Barrovian and Buchan terranes in the Scottish Highlands respectively (Harte and Hudson, 1979).

Development of simple thermal models for various tectonic processes led to a number of preliminary correlations between metamorphic facies series and tectonic settings (e.g. Oxburgh and Turcotte, 1971, 1974; Bickle *et al.*, 1975; Richardson and Powell, 1976) and subsequently to more rigorous numerical modelling (e.g. England and Richardson, 1977; Wells, 1980; England and Thompson, 1984, 1986; Sandiford and Powell, 1986a; England, 1987; Loosveld and Etheridge, 1990). England and Richardson (1977) emphasised the distinction between the pressure-temperature conditions indicated by the metamorphic field gradient, and the actual pressure-temperature paths followed by the rocks. Each rock preserves a mineral assemblage developed at some point on the pressure-temperature path it followed during the metamorphic event, unless kinetic effects produce an apparent path unrelated to the actual evolution. This point is most probably the point of maximum entropy experienced by the rock, and is generally thought to be at, or close to, the thermal maximum of the pressure-temperature conditions. The metamorphic field gradient defined by these rocks bears no relation to any one geotherm that existed during the metamorphic event, and in fact must represent a diachronous array of single points from a number of geothermal gradients. Direct evidence of the pressure-temperature

path followed by a rock can be derived from evidence of mineral reaction, either in terms of textural relationships between reactant and product phases (e.g. Ellis *et al.*, 1980), or mineral zonation profiles (e.g. Spear and Selverstone, 1983). However, the possibility that such features reflect an overprint by an unrelated event, rather than a continuous evolution during a single metamorphic event, must be carefully considered.

Pressure-temperature paths should be independent of variables such as the age, lithological constitution and present tectonic setting of a metamorphic rock, and merely reflect the tectonic processes operating during and immediately after metamorphism. The tectonic setting of metamorphism is commonly assessed by comparison of the actual pressure-temperature path with paths developed from theoretical models for particular tectonic settings. This section summarises some examples of the various pressure-temperature paths identified in high-grade metamorphic terranes, and the tectonic models which have been proposed to explain them. The regional pressure-temperature paths identified in the Volvi area and the local thermal excursions attributed to the emplacement of the Volvi Complex are assessed and the relevance of the various tectonic processes are considered.

6.5.1 Pressure-temperature Paths

Preservation of the prograde pressure-temperature path within the Lake Volvi area is poor and usually obscured by an intense overprinting by the retrograde (greenschist-facies) history (Chapter 4; Section 6.5.2). However, the ex-cordierite bearing granoblastic purple migmatites from the Vamvakia river, record a local thermal temperature excursion to the granulite-facies and its subsequent retrograde path. Retrograde pressure-temperature paths are generally grouped into a small number of broad categories on the basis of path shape. Ellis (1987) and Harley (1989) have distinguished between paths dominated by near-isothermal decompression and those dominated by near-isobaric cooling (Fig. 6.11a), but this simple division is complicated by the existence of three types of isobaric-cooling path (Harley, 1989; Bohlen, 1991; Fig. 6.11b):

a) *"Clockwise"* paths with an initial stage of decompression preceding the cooling (i.e. a path involving near-isothermal decompression and near-isobaric cooling).

b) *"Anti-clockwise"* paths in which the attainment of peak temperatures is accompanied by compression, with a small compressional component continuing during the initial retrograde cooling.

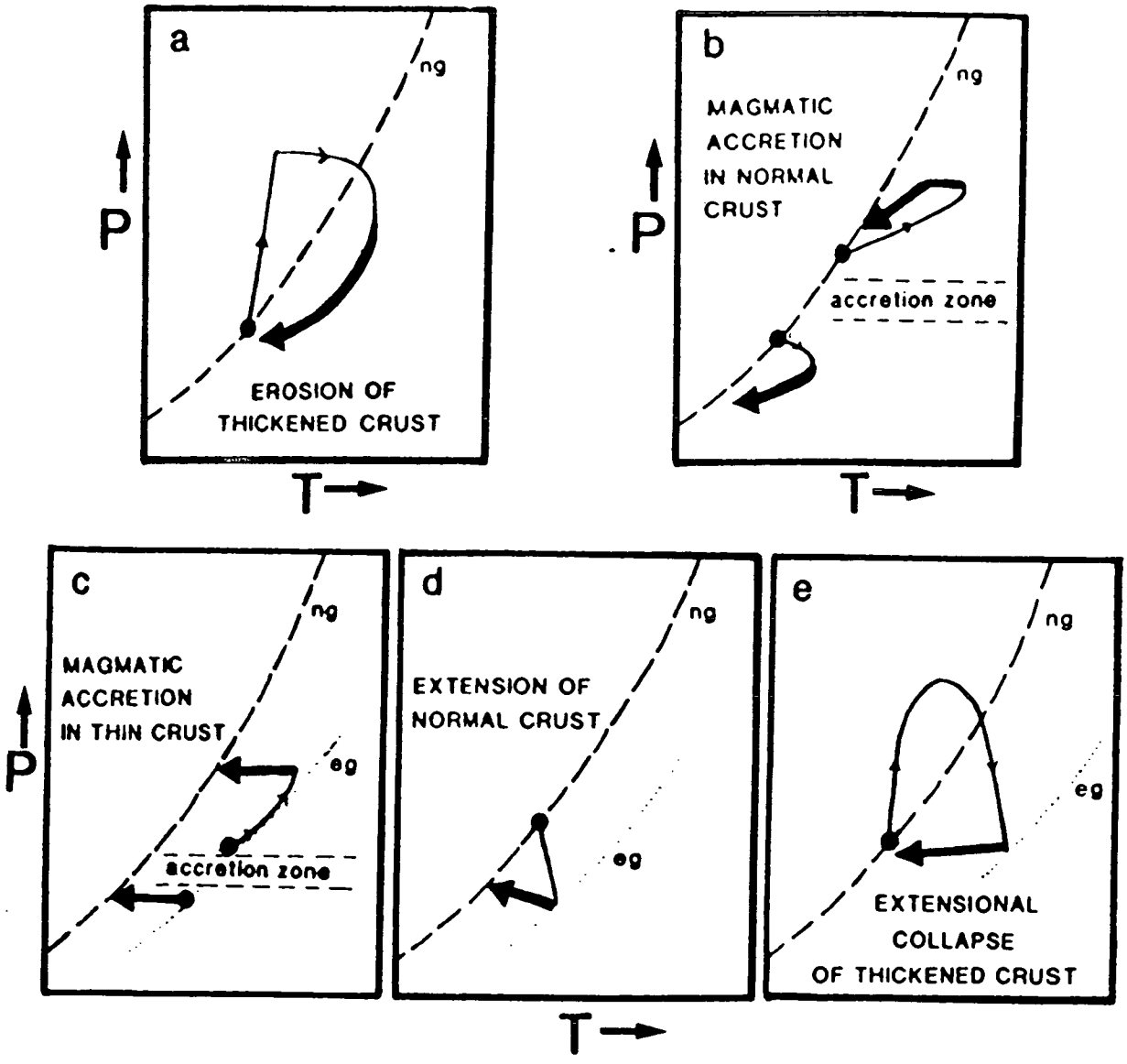

Fig.6.12: Schematic pressure-temperature paths for a variety of tectonic settings (adapted from Harley, 1989). In all the figures, the heavy lines represent those parts of a retrograde path that are likely to be preserved, and "ng" represents the stable geotherm for normal-thickness crust. (a) Is a decompression-dominated clockwise path for erosion of crust thickened during continental collision (England and Richardson, 1977; England and Thompson, 1986). (b) Depicts two paths resulting from magmatic accretion into crust of normal thickness (Wells, 1980). Rocks above the accretion zone follow a clockwise path, whereas rocks below it follow an anti-clockwise path. Both paths are dominated by cooling, with some decompressional component reflecting the isostatic response of magmatically-thickened crust. (c) Depicts two paths for magmatic accretion into thin crust with an "extended" geotherm (eg), one for rocks above and one for rocks below the accretion zone. Both paths are dominated by isobaric cooling. (d) Is a clockwise path followed by rocks during extension of normal-thickness crust, reflecting relatively-rapid syn-extensional decompression and heating to a transient extended geotherm (eg), followed by thermal relaxation. (e) Is a clockwise path for extensional collapse of thickened crust, comprising rapid syn-extensional decompression to the extended geotherm (eg), followed by thermal relaxation to the stable geotherm (England, 1987). The pressure-temperature paths preserved by rocks in models (b) to (e) are likely to be dominated by near-isobaric cooling.

c) *"Simple cooling"* paths which preserve no evidence of a precursor path, and could be a partly-preserved clockwise or anti-clockwise path, or unrelated to either.

Paths involving significant retrograde decompression are generally thought to reflect isostatic disequilibrium, and are traditionally attributed to the evolution of thickened crust in collisional zones, whereas isobaric-cooling paths have been conventionally ascribed to magmatic accretion (England and Richardson, 1977).

Tectonic thickening during continental collision is often cited as a likely cause of high-grade metamorphism, even up to granulite-facies. Evidence for crustal thickening in some granulite terranes includes the presence of high-pressure relics, such as eclogite bodies, and the presence of syn-collisional magmatic lithologies consistent with crustal melting at depth, such as orthogneiss with depleted heavy rare-earth element contents (e.g. Ellis, 1987). The clockwise nature of pressure-temperature paths expected to be produced by continental collision and subsequent erosion of the overthickened crust (Fig. 6.12a) has been demonstrated by several modelling studies (e.g. England and Richardson, 1977; England and Thompson, 1984, 1986). These models can only account for the attainment of granulite-facies conditions if temperatures are enhanced using some combination of unrealistically high rates of internal heat production and/or basal heat flux, and unrealistically low values for the crustal thermal conductivity (Thompson and England, 1984; Bohlen, 1991), without these an external heat source is needed to achieve granulite conditions, such as substantial syn-to post-collisional addition to the thermal budget of the crust from mantle-derived magmas (e.g. England and Thompson, 1986; de Yoreo *et al.*, 1989). The localised cordierite-bearing granulite fabrics overprinted by garnet-kyanite assemblages observed along the Vamvakia river (Chapter 4) are interpreted to be the product of thermal perturbation followed by rapid crustal thickening. The strike-slip model invoked for the development of these conditions consist of a restraining bend quickly overriding a pull-apart basin (Section 6.6). The timing of the overriding (loading) event is crucial and must be "quick" as the pull-apart basin must remain thermally perturbed (i.e. hot at shallow depth) at the time of thickening (Section 6.5.2).

An enhanced basal heat flux is likely to have been present due to crustal thinning during the development of the pull-apart basin. This will warm up the cold top of the lower plate back on to the geotherm (Section 6.5.2). The hottest part, now shallow after thinning is then promoted locally further up temperature by intrusion and then up-pressure by overriding of the strike-slip restraining bend and can pass into

granulite-facies to upper amphibolite-facies conditions followed by progressively cooling back on to the normal crustal geotherm to amphibolite-facies and upper greenschist-facies conditions (Section 6.5.2).

From the visible evidence of mafic magma throughout the study area, no problems are envisaged for developing conditions of high temperature at moderate depth. However, it is necessary for a sufficient pressure load to be present after the initial development of cordierite and while the area is still subjected to thermal perturbation. It is therefore useful to review the results of more detailed modelling of settings involving active magmatic intrusion as well as crustal thickening and loading (this section).

Magmatic accretion produces a transient thermal perturbation and thickening of the crust, and models of magma accretion can produce a number of theoretical pressure-temperature paths depending principally on the thickness of the original crust and the amount and position of accretion (Wells, 1980). The addition of magma to crust of normal, or near-normal, thickness causes overthickening of the crust, and the retrograde evolution includes a period of decompression reflecting isostatic response of the thickened crust. The amount of decompression is directly dependent on the volume of magmatic accretion. Rocks beneath or within a zone of accretion experience an initial increase in pressure and heating, followed by cooling and decompression, whereas rocks above the accretion zone are heated isobarically, and then experience a similar cooling and decompressional retrograde history to that of the deeper rocks. Hence, rocks below the accretion zone preserve an anti-clockwise pressure-temperature path, and rocks above it preserve a clockwise path (Fig. 6.12b). However, substantial magmatic additions to the crust could be associated with pre- or syn-magmatic extension. If magma is added to thin crust, less unroofing is required to achieve isostatic equilibrium. No unroofing would occur if the crust was thinned sufficiently, and rocks below and within the accretion zone would follow an anticlockwise compression and cooling path. In contrast rocks above the accretion zone would follow an isobaric heating and cooling path (Fig. 6.12c).

It has been suggested that the occurrence of peak temperatures over a range of depths is a reflection of the buffering effect of magma crystallisation (Waters, 1986; Bohlen, 1987), and hence indicative of magmatic accretion. However, extensive crustal melting, which is believed to be common at high-grade conditions whatever the tectonic setting (Thompson and England, 1984), would have a similar effect (Hodges *et al.*, 1988; Vielzeuf *et al.*, 1990). In addition to citing a similarity in peak temperatures as evidence for magmatic accretion, Bohlen (1987, 1991) also

paradoxically claimed that an isobaric transition from amphibolite to granulite-facies reflects differences in the amount of magmatic heating at similar depths and is hence indicative of magmatic accretion.

Extension of normal-thickness crust is another proposed mechanism for high-grade metamorphism, particularly at low pressures (Wickham and Oxburgh, 1985; Sandiford and Powell, 1986a). Crustal extension compresses the vertical thermal structure of the lithosphere, resulting in an increased heat flow which is likely to be enhanced by mantle-derived magmas. The resultant thermal perturbation subsequently decays as temperatures adjust to a stable geotherm. Extensional pressure-temperature paths comprise some combination of prograde decompression and heating, followed by cooling (Fig. 6.12d) which may be accompanied by some pressure-rise if the thermal relaxation is associated with thermal subsidence and the development of substantial sedimentary basins (McKenzie, 1978). The relationship between the extent of decompression and the maximum temperature depends on the model of extension. If extension is symmetrical, maximum temperatures are attained in the area of maximum extension and therefore maximum decompression. Heterogeneous extension models, for example extension involving crustal-scale detachments (Wernicke, 1985; Lister *et al.,* 1986), produce a maximum thermal perturbation, reflecting maximum thinning of the mantle lithosphere, which does not coincide with the area of maximum crustal extension and decompression. In the former model, pressure-temperature paths for high-grade metamorphic rocks are clockwise with prograde decompression and retrograde cooling, whereas in the latter model, the high-grade crustal rocks occur in areas of little deformation, and follow a near-isobaric heating and cooling path (Sandiford and Powell, 1986a). In general, rocks in all of these extensional modes are likely to record near isobaric-cooling paths since any decompression precedes the metamorphic peak. However, indirect evidence of an extensional origin can be provided by syn-metamorphic flat-lying structures and syn- to post-metamorphic basic magmatism.

It has been recognised that extension can play a major role in evolution of collisional metamorphic terranes as well as being a potential cause of high-grade metamorphism by itself. Classical models of continental collision assume that thermal relaxation towards the enhanced geotherm applicable to thickened crust is terminated by erosion and uplift. Tectonic thinning in some collisional orogenic belts will modify this substantially (e.g. Molnar and Tapponnier, 1975, 1978; Tapponnier *et al.,* 1981). This thinning occurs principally by lateral extension, driven by a potential energy contrast between the overthickened crust and its surroundings, and is more

rapid than simple erosion. Extension occurs when the gravitational forces exerted by overthickened crust exceed any compressional forces by some critical amount dependent on the strength of the lithosphere (England, 1987; Sonder *et al.*, 1987), and the resultant pressure-temperature paths have been modelled by England and Thompson (1986), England (1987) and Sonder *et al.*, (1987). These paths have a higher dP/dT than theoretical curves derived from an erosion model (Harley, 1989), and commonly match the shape of observed decompressional paths more closely than erosional models. Extensional collapse (Platt, 1989) is thought to be particularly rapid, such that the bulk of decompression can occur before peak metamorphic temperatures are attained (Fig. 6.12e) and the rocks only preserve the post-decompressional cooling part of the path (e.g. Sandiford, 1989a; Anovitz and Chase, 1990). Hence, collisional tectonics can produce isobaric-cooling paths in addition to the clockwise paths characteristic of erosion; in fact a spectrum of paths between isothermal decompression and isobaric cooling can be recorded by rocks in collisional zones (Harley, 1989) depending on the amount and rate of post-collisional extension. The possibility of extension is enhanced for particularly wide and thick collisional zones, such as the Himalayan belt and can be initiated by removal of the compressional stresses at the cessation of convergence, or weakening of the lithosphere surrounding the elevated region. Evidence for extensional collapse of thickened crust includes the development of horizontal structures during peak and retrograde metamorphism, with associated basic magmatism as the mantle decompresses and the crust approaches normal thickness. Overthickened terranes dominated by erosion should achieve their metamorphic peaks after the pervasive deformation. Rapid uplift by extensional collapse can also produce higher temperatures at low pressure than erosional models. These conditions can also be met in transpressional zones, where it is possible for the initial crustal thickening to be transient. Thus, tectonic unroofing would be driven by continued strike-slip rather than gravity.

The metamorphic peak in extensional terranes should coincide with, or just post-date, the end of extension (Loosveld and Etheridge, 1990). This means that the syn-metamorphic compression indicated by many high-grade terranes would have to immediately follow lithospheric extension. An alternative means of combining crustal thickening with thinning of the mantle lithosphere is "convective thinning" at the base of thickened lithosphere in a collisional orogenic zone, causing detachment of the "thermal boundary layer". The thermal boundary layer comprises the lowermost part of the mantle lithosphere, and separates the asthenosphere, which is

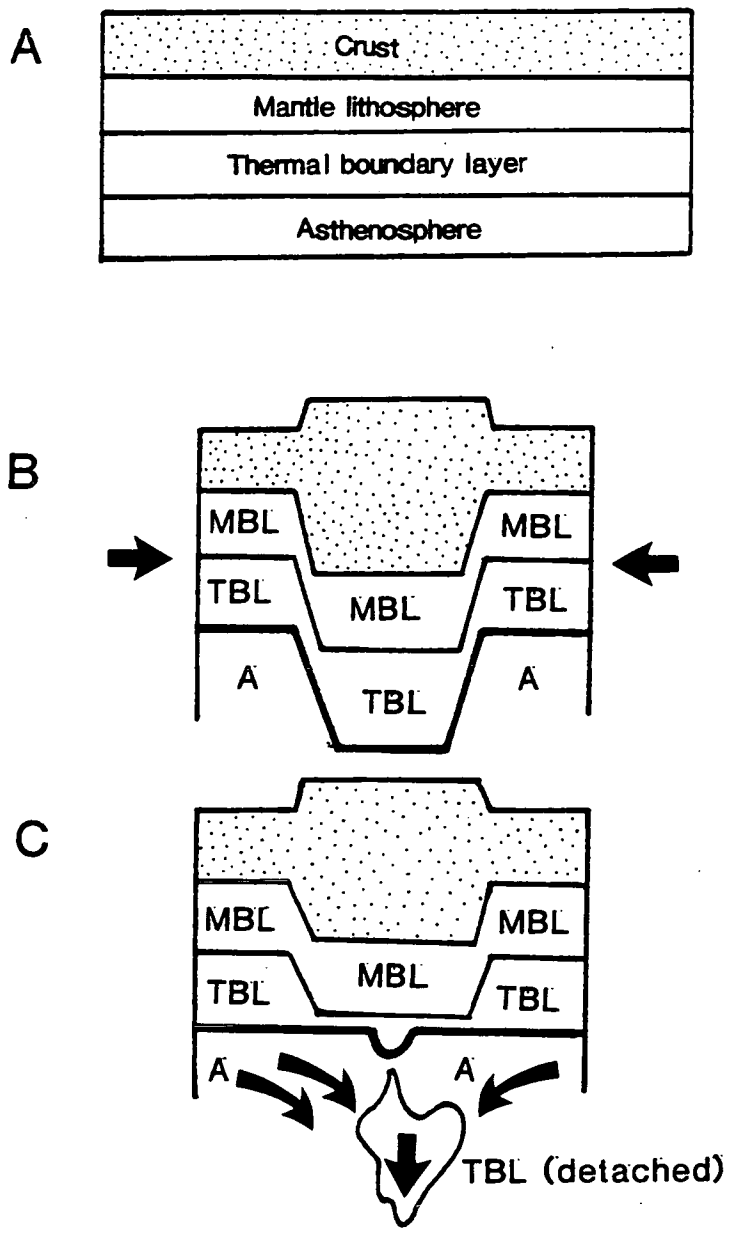

Fig. 6.13: A schematic illustration of the structure of normal-thickness and thickened continental lithosphere, adapted from Sandiford (1989b). (a) Depicts thermally-stable continental lithosphere of normal thickness, with a thermal boundary layer separating the mechanical boundary layer, comprising crust and mantle lithosphere, from the asthenosphere. (b) Depicts a homogenous thickening of the mechanical and thermal boundary layers, and (c) Shows how the thermal boundary layer, which forms a dense root, can be detached and replaced by hot asthenospheric mantle. The relative thicknesses of the layers are not to scale.

dominated by convective heat transfer, from a mechanical boundary layer which is dominated by conductive heat transfer and comprises the crust and uppermost part of the mantle lithosphere (Parsons and McKenzie, 1978). Houseman *et al.*, (1981) have shown that a thermal boundary layer thickened by continental collision is colder and denser than its surroundings and that convective instabilities can cause the detachment of this layer from the base of the lithosphere (Fig. 6.13). Detachment of the thermal boundary layer by convective thinning has profound implications for both the thermal and tectonic evolution of the belt: hot asthenospheric mantle replaces dense lithospheric mantle, which increases the heat flow and causes a rapid increase in surface elevation, in turn promoting extensional collapse of the "top-heavy" lithosphere (Houseman *et al.*, 1981; Sonder *et al.*, 1987; England and Houseman, 1988, 1989). Hence, convective thinning can cause high temperatures of metamorphism, perhaps followed by rapid decompression.

Several recent thermal models for high-temperature low-pressure metamorphism have been based on detachment or convective thinning of the lower lithosphere (Sandiford, 1989a, b; Loosveld and Etheridge, 1990; Oxburgh, 1990; Sandiford and Powell, 1991). These models can produce anti-clockwise, clockwise and isobaric-cooling paths, depending on the relative timing and rates of overall lithospheric shortening, mantle-lithosphere thinning, thermal relaxation of the upwelled asthenosphere and extensional collapse. An elegant means of depicting the relationships between these various parameters has recently been described by Sandiford and Powell (1990), who represented the evolution of collisional belts in terms of the vertical strain developed in the crust and in the lithosphere as a whole.

6.5.2 A Schematic Model for the P-T-t History

A geotherm represents temperature as a function of depth at a fixed time. Plate tectonic processes, such as extension, burial and uplift, perturb the geotherm. During a crustal thickening event, a metamorphic rock will generally follow a counter-clockwise loop in pressure-temperature space (with pressure increasing downward). The mineral assemblage generally reflects the maximum temperature (T_{max}) and the concomitant pressure (P_{Tmax}) achieved by the rock. The locus of T_{max}-P_{Tmax} points preserved in a metamorphic terrane is called the metamorphic P-T array (Peacock, 1989); metamorphic geotherm, (England and Richardson, 1977); metamorphic field gradient, (Spear *et al.*, 1984). Different rocks will reach T_{max} at different times, thus, the metamorphic P-T array does not reflect a geotherm that existed at any single time.

In order to construct a P-T model for the top 10-20 km which represents the initial position of the study area, it is necessary to consider the entire crustal geotherm and relevant melting curves (Figs. 6.14a, b). In a steady-state equilibrated regime, temperature will simply increase with depth and melting would not be initiated until temperatures of at least 600°C and depths of 37 km were reached. As the interpretation and tectonic model for the Lake Volvi area suggests initial conditions of 10-20 km depth, melt is not predicted to be produced. However, with extension of the crust the "normal" geotherm will be perturbed and an increase in temperature with respect to depth will arise (Fig. 6.15b). It is proposed that this perturbation occurred during the evolution of a transtensional pull-apart basin. Extension of the crust in the Lake Volvi area would increase the regional thermal effects, melting the mantle and initiating the intrusion of basic magmas into the crust, but would still not initiate melting within the vicinity of Lake Volvi. However, at depths of 20-25 km the melting curves (both wet and dry) would easily be surpassed and melting initiated. Subsequent migration of deep level melts, the proto-Volvi Complex basic magmas, and their emplacement in the higher-level crust would raise the regional temperature and so cause the pelite and granitic (i.e. old migmatite) melting curves to be crossed. Hence, anatectic melts of crustal origin (Arnaea granite and Volvi granitoids) could be formed (Fig. 6.15a).

The resultant P-T vector for extension and magmatic emplacement is probably an enhanced composite effect of the two events (Fig. 6.15a). However, rocks nearer the surface which had not been intruded would have remained cool, while deeper-level lithologies which were adjacent to large intrusions were heated to a greater degree (Fig. 6.15a).

The structural regime within the Lake Volvi area is essentially one of oblique extensional and compressional strike-slip (Section 6.6). During the early transtensional phase, the development of a pull-apart basin and the intrusion of basic magma are the dominant tectonic features. Both of these phenomena result in the thermal perturbation of the crust (Section 6.5.1). The change in the dominant structural regime from predominantly transtensional to transpressional leads local thickening of the crust. However, from the structural geometry developed within a strike-slip regime, it is possible and indeed probable that a restraining bend may decouple at depth (e.g. the ductile-brittle transition zone at approximately 15-20 km depth) and be progressively transported over the pull-apart basin during continued transpression. This interpretation provides a mechanism for overthrusting a 15-20 km slab, with "normal" geothermal gradient over the still thermally perturbed basin. A

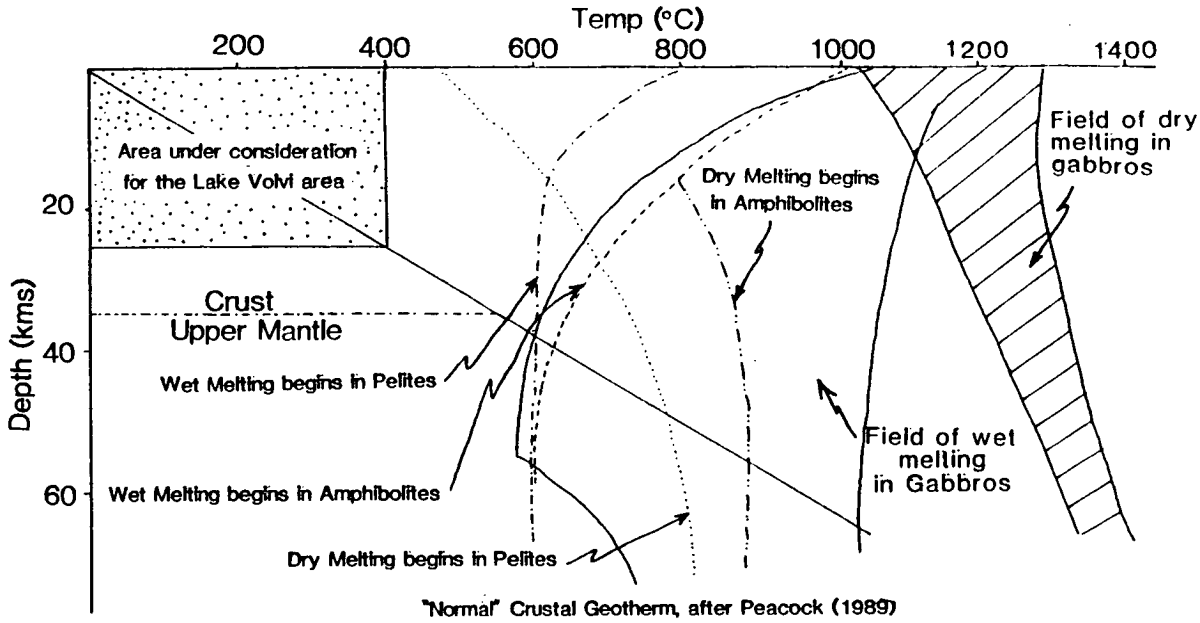

Fig. 6.14a: "Normal" thickness crustal geotherm and crustal melting curves. Initial melting of pelite (wet and dry) is taken from Thompson and Tracy (1979). Initial melting of amphibolite (wet and dry) is modelled on the results of Yoder and Tilley (1962).

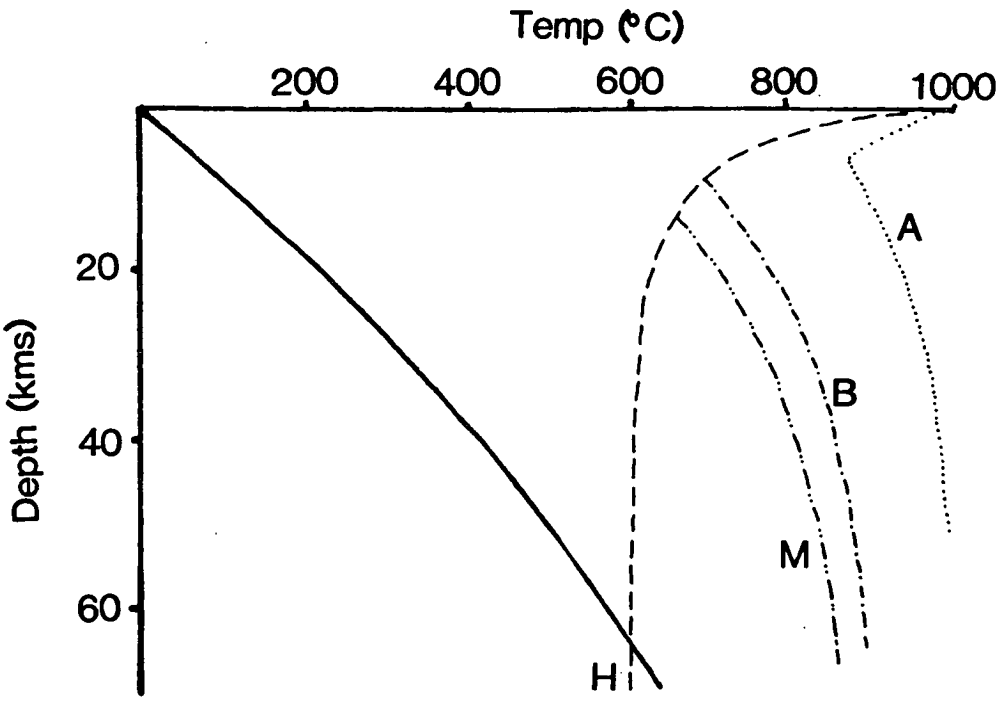

Fig. 6.14b: Approximate curves for the melting of crustal rocks in the presence of excess water (H) and for the onset of melting in the fluid-absent system accompanying the breakdown of muscovite and biotite in metapelites (M), biotite and hornblende in granodiorites and tonalites (B) and hornblende in amphibolites (A).

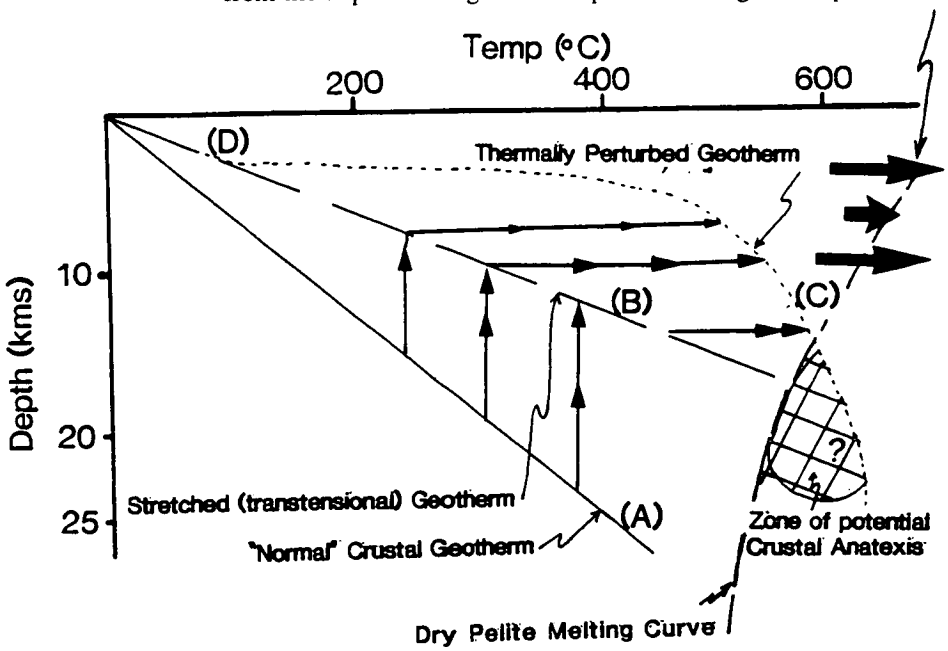

Fig. 6.15a: Extension raises the crustal geotherm from (A) to (B). However, with injection of basalts, which have been melted at depth due to extension, a perturbed geotherm is developed (C). The thermal perturbation only affects rocks which have been subjected to magmatic emplacement, resulting in a curved geotherm near the surface (D).

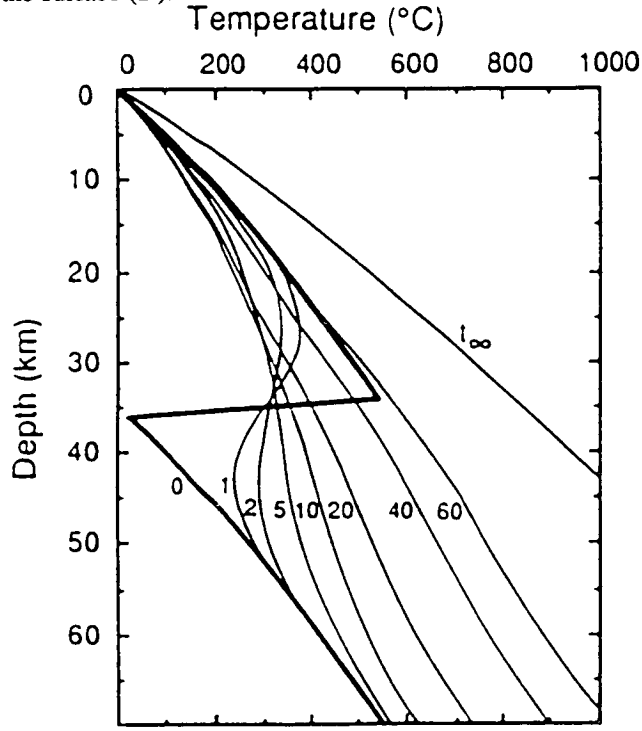

Fig. 6.15b: Thermal evolution of the sawtooth model, developed by overthrusting of crustal material. Curves labelled with time in millions of years after instantaneous thickening. During the first several million years, heat is conducted rapidly from the upper plate downward into the lower plate. Subsequently, temperatures increase slowly as a result of the decay of radioactive elements and the conduction of heat into the base of the thickened crust from the mantle. Curve labeled t_∞ represents steady-state solution, after Graham & England (1976).

good modern-day, or rather future, scenario would be the Salton Trough being overridden by the Transverse Ranges. This model is discussed in more detail in section 6.7 below. Furthermore, at the present rate of strike-slip translation (approximately 5 cm/yr) the Transverse Ranges could possibly be thrust over the Salton Trough (present distance between the two is approximately 200 km) within approximately 4 Ma (i.e. geologically very quick). 4 Ma is far shorter than the thermal relaxation time for the lithosphere even if stretching and magmatism had ceased. Hence, the emplacement of this 15-20 km slab (restraining bend) over an already thermally perturbed basin would create a range of P-T phenomena.

1) Unmetamorphosed sediments at the top of the succession (basin-fill) would be metamorphosed for the first time to the greenschist-facies along a typical counter-clockwise P-T path predicted for crustal thickening. This would be caused by the sediments re-equilibrating on to the "normal" crustal geotherm. A similar prograde P-T path would be developed for crustal sequences which were not subjected to the extensional and magmatic heating caused by the emplacement of the Volvi Complex and dykes. Fig. 6.15b, shows the thermal evolution of the sawtooth model, depicting the perturbation of the geotherm caused by overthrusting. During the first several million years, heat is conducted rapidly from the upper plate downward into the lower plate. Subsequently, temperatures increase slowly as a result of the decay of radioactive elements and the conduction of heat into the base of the thickened crust from the mantle.
2) Previously very low-grade metasedimentary rocks which had been buried more deeply (e.g. Tiger-striped lithology, *see* Chapter 2) are thermally perturbed by crustal stretching during the formation of the pull-apart basin and the injection of basic magmas and locally hornfelsed by dykes. They are then raised to high-pressures by the arrival of the crustal slab of the restraining bend over the pull-apart basin. These lithologies may therefore be in a position close to the "normal" geotherm (i.e. they are hot for their depth after stretching but not after crustal loading) and are likely to show only minor metamorphic reactions in order to re-equilibrate from, e.g. low to moderate pressure hornblende hornfels-facies to amphibolite-facies (Fig. 6.16).
3) The high-grade metamorphic rocks (e.g. migmatites and purple gneisses, *see* Chapter 2) which have been subjected to thermal anomalies from extension and magmatic influx, show a clockwise P-T path contrary to crustal thickening models (Fig. 6. 16). This P-T path occurs due to loading of the 15-20 km's of crust being insufficient to place the high-grade lithologies below the "normal"

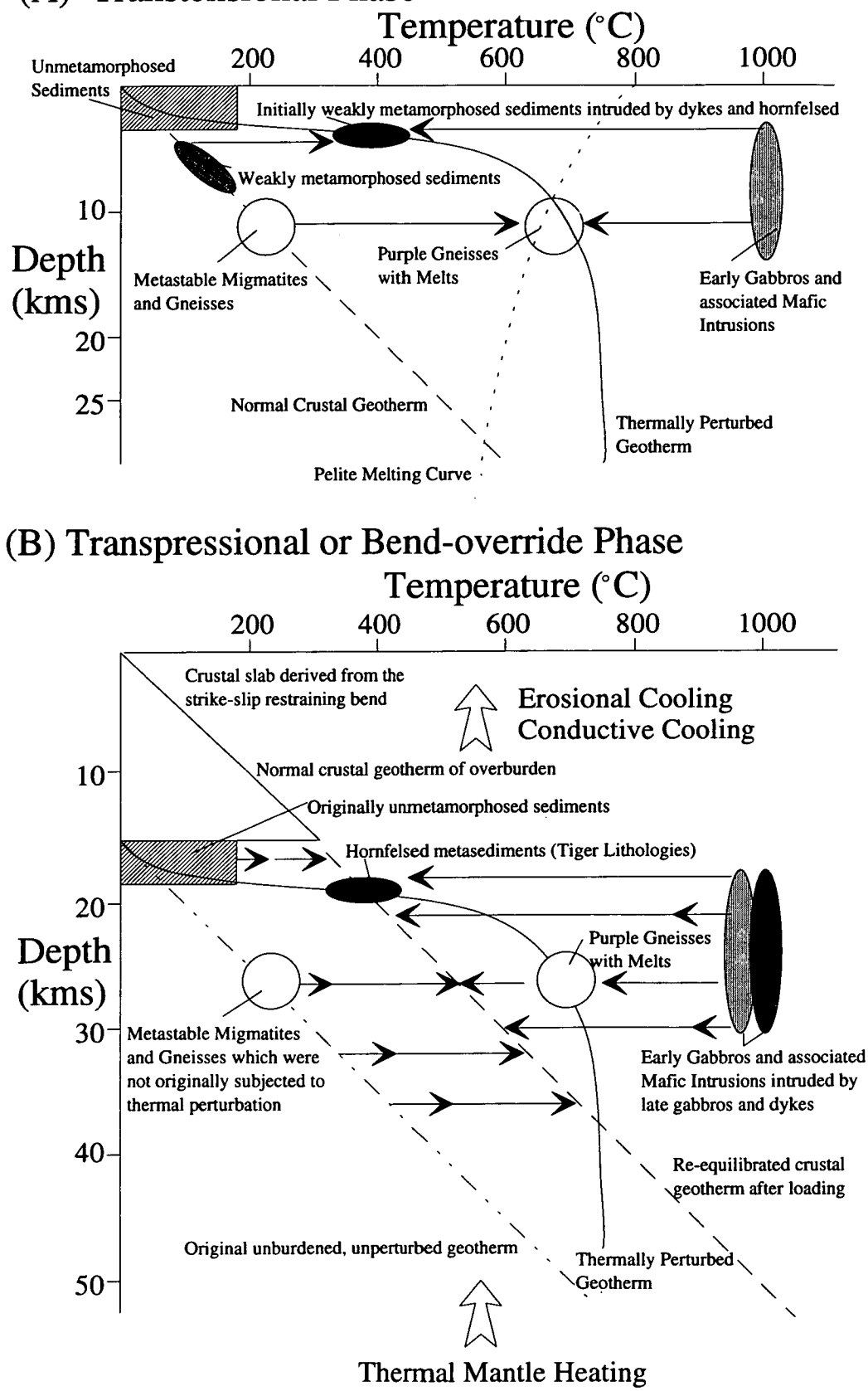

Fig. 6.16: Scematic P-T evolution for the Lake Volvi area. (A) Represents an originally unburdened but thermally perturbed geotherm as a result of crustal extension and magmatic intrusion. (B) Represents the evolution of the sawtooth P-T model as a result of subsequent crustal thickening by the strike-slip restraining bend overriding the thermally perturbed basin.

crustal geotherm. The original basement migmatites have an initial metastable amphibolite-facies assemblage which is returned to active amphibolite-facies conditions with the advent of crustal loading. The purple gneisses however, are initially equilibrated locally at low P and high T conditions to produce assemblages containing cordierite and melt. With the advent of crustal loading these lithologies are taken to amphibolite-facies or high P granulite-facies conditions. During this episode of increasing P, while still anomalously hot, cordierite is replaced by garnet and kyanite (Chapter 4). Re-equilibration of these lithologies follows a retrograde path to the greenschist-facies during continuing deformation (Fig. 6.16). This phenomenon could account for the transition in structural regime from ductile to brittle deformation with a greenschist-facies metamorphic assemblage.

4) Finally, conduction and cooling at the surface combined with erosion contribute a greater total heat loss than thermal input by conduction from the mantle. The area therefore exhibits a uniform retrograde path to the low greenschist-facies, while deformation continued, with possible tectonic unroofing as the restraining bend passed (Fig. 6.16).

6.6 Summary and Interpretative Model

Field observations (Chapters 2 and 3), petrographic studies (Chapter 4) and geochemical analyses (Chapter 5) are summarised in Fig. 6.17. These events are placed in a deformation-time sequence and show a progressive development from a ductile to brittle regime of gneisses and metasediments which overlay and are intercalated with an older migmatitic basement. The Volvi Complex is interpreted to have been emplaced in a small, relatively short-lived pull-apart basin, developed in a transpressional-transtensional regime (Fig. 6.18). The Volvi Complex (*s.s.*) is considered to have been intruded beneath and fairly close to a thick, relatively unconsolidated, undeformed sedimentary sequence, as screens of undeformed metasedimentary lithologies (Tiger-striped lithology and Siberian Tiger Formation; *see* Chapter 2) have been preserved within sheeted dyke complexes (Section 6.7). In addition, suggestions of an initially high-level pull-apart basin scenario are supported by the occurrence of serpentinite bodies (the anomalously positioned Volvi Ultramafic Formation) or even gabbros which could have been wedged up along fault traces associated with the pull-apart (e.g. Dietrich and Oberhänsli, 1976).

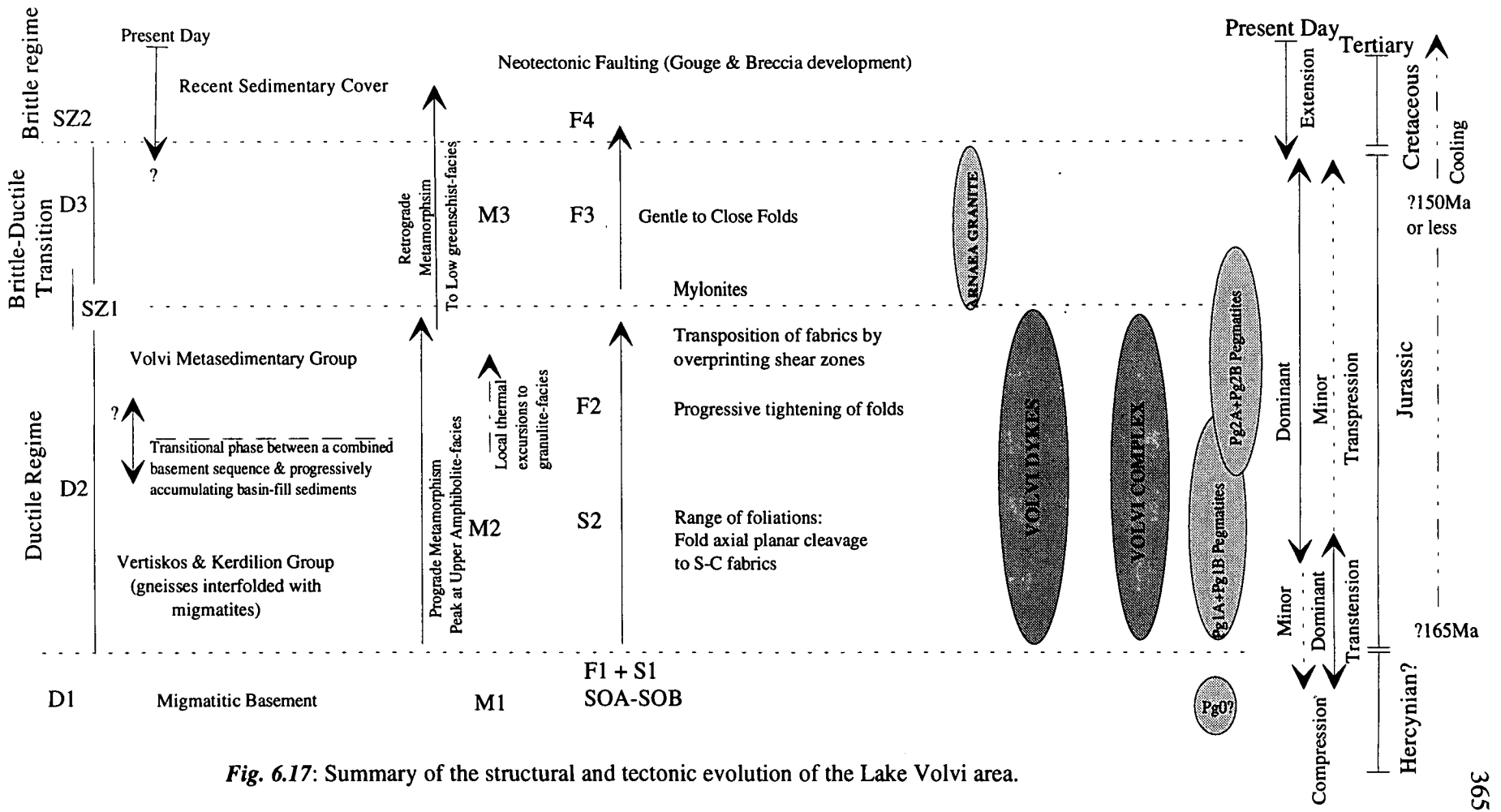

Fig. 6.17: Summary of the structural and tectonic evolution of the Lake Volvi area.

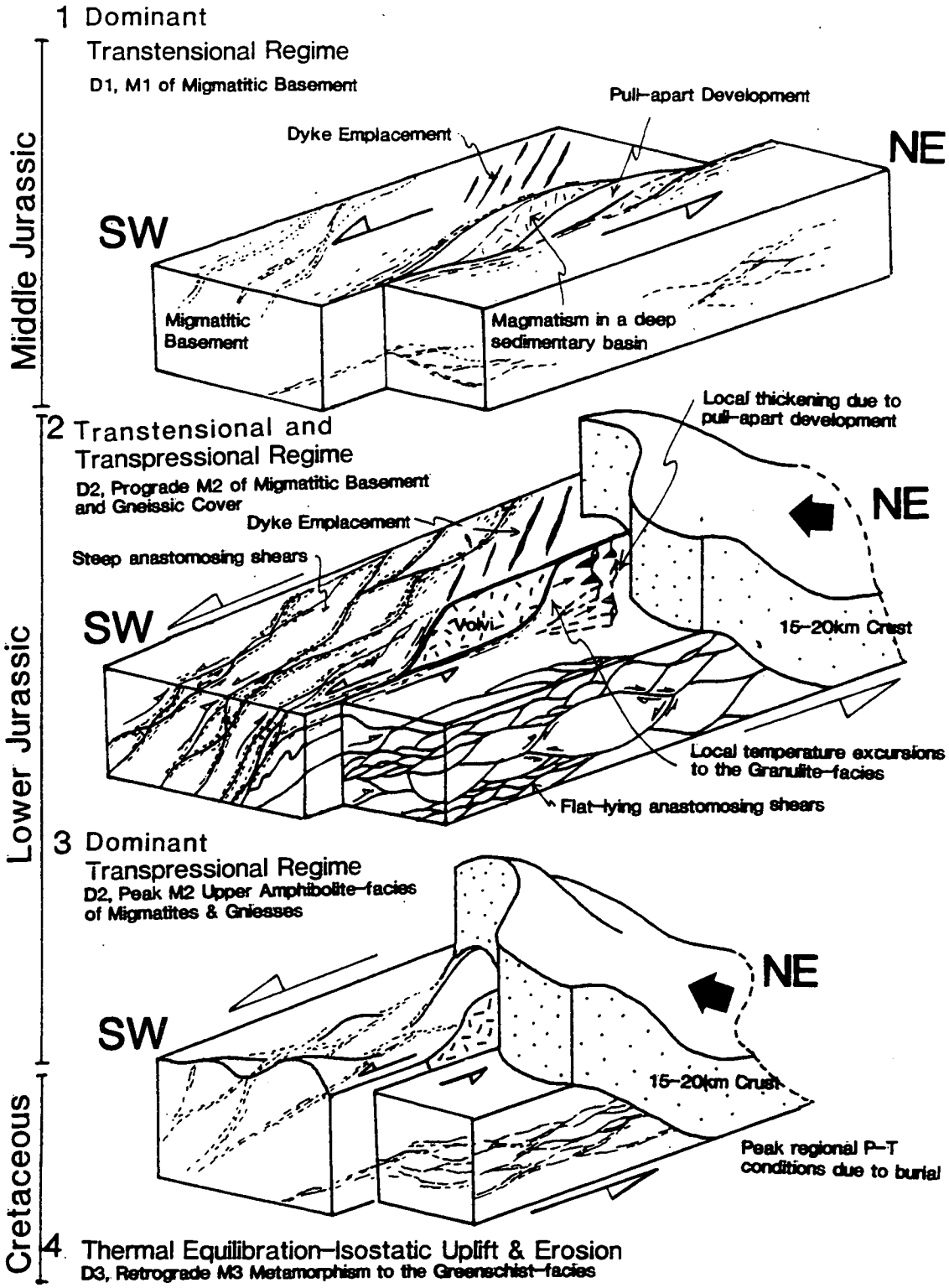

Fig. 6.18: Schematic interpretation and models for the evolution of the Lake Volvi area, with respect to the changing tectonic regimes and time.

Formation of a strike-slip basin in a transtensional regime permitted the initial intrusion of the Volvi Complex (*s.s.*), and discrete mafic bodies and dykes related to the Volvi Complex into the envelope. Local thickening of crust created unfavourable areas for dyke emplacement, while the overall extension allowed magmatic input and a regional isobaric temperature rise (Section 6.5.2). The intrusion of the Volvi Complex further raised the temperature within the area. During the initial dominant transtensional regime associated with the intrusion of the Volvi Complex the present geometries and transport directions of the anastomosing shear zones were probably initiated. Local changes in the transtensional and transpressional regimes were probably developed throughout the area depending on the local geometry of the strike-slip system. Locking of the regional strike-slip system along the SMM-Rhodope shear boundary probably caused the Volvi pull-apart basin to be overthrust by a thick slice of continental crust (note the analogy with the Transverse Ranges of the U.S.A., Section 6.7). Overprinting of the pull-apart basin by th restraining bend along the same strike-slip fault system put the area down by an extra 15-20 km to approximately 25-30 km and raised the regional equilibrium P-T conditions to the upper amphibolite-facies. However, during loading within a predominantly transpressional regime (regional) the Volvi Complex is inferred to have still been actively intruding in a transtensional regime (probably more localised) at depth. With the increased heating and loading, anatexis of the crust developed a granitoid melt which led to Arnaea and other Volvi granitoids being developed and emplaced and locally granulite-facies assemblages being developed. Continued deformation during the crustal thickening event and during the subsequent cooling down to the "normal" geotherm has developed the structural variations characteristic of the ductile to brittle regimes. Finally the lowest greenschist-facies assemblages were developed with the unroofing and subsequent uplift of the area. It follows from this that the timing of the intrusion of basic and acid magmas must be close and that if Arnaea is 155 Ma then Volvi must be no more than 10 Ma older.

Explanations of the distribution of the Volvi Metasedimentary sequence and correlations with similar units within the SMM are at best tentative. However, whatever model is proposed it must satisfy the P-T history above, with the metamorphic grade and extent of deformation greatest in the east, decreasing progressively westward. The main problem concerns the historical correlation with the Svoula Group to the west (Kockel *et al.*, 1971, 1977; Kauffmann, 1976). No clear evidence has been found for or against this correlation during this study and the proposed models are based predominantly on the configuration of the migmatitic

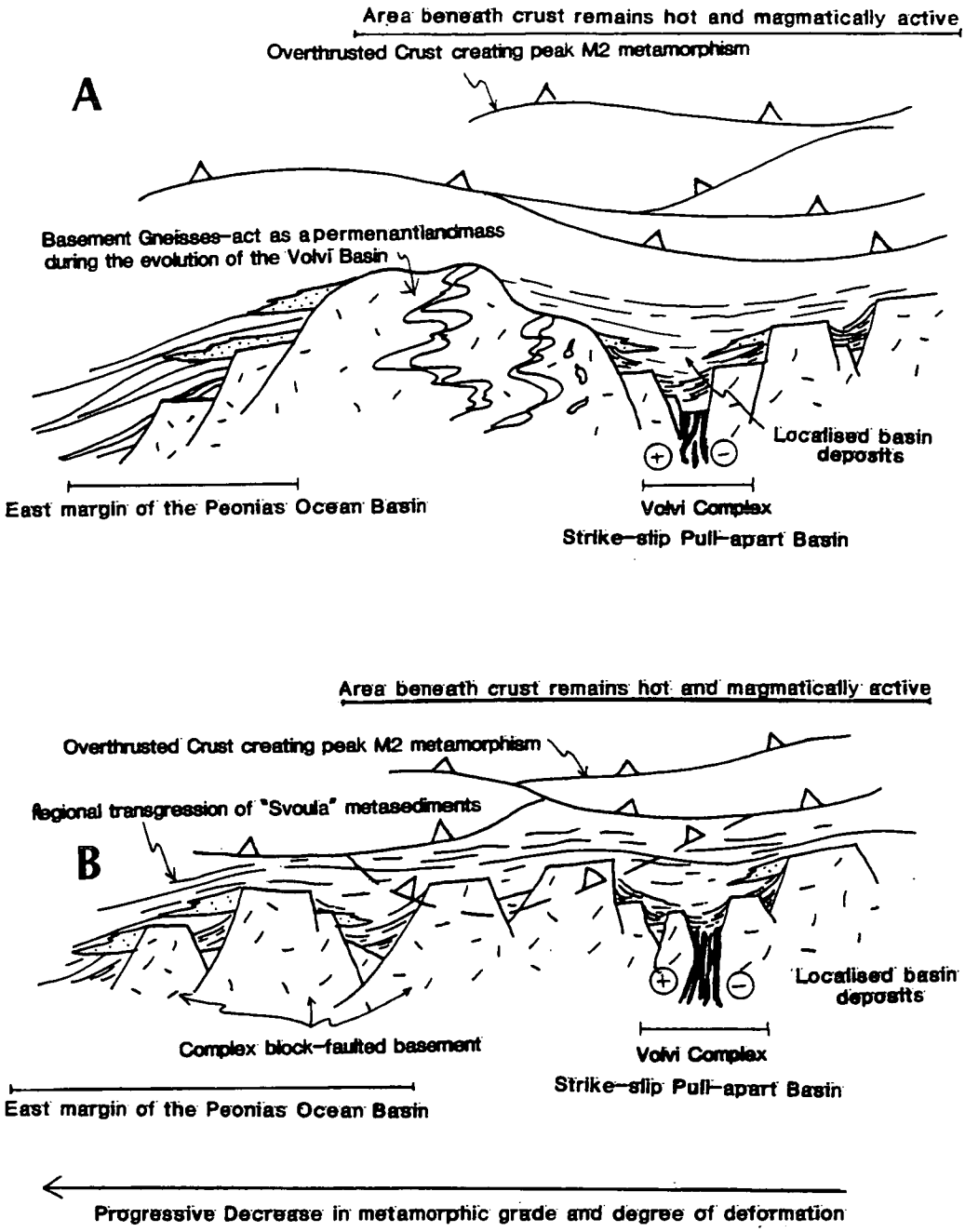

Fig. 6.19: Possible interpretations and models for the land mass separating the Volvi extensional pull-apart basin and the Peonias ocean basin.

gneissic basement (Fig. 6.19). Two simple scenarios can be proposed (Fig. 6.19), a) a basement high was present between the Volvi Metasedimentary Group basin and the Svoula Group basin and the two sedimentary sequences developed separately, although possibly at similar times, b) the two groups were linked via numerous small, shallow, interconnected basins with greatest deposition around the Volvi pull-apart basin and the Peonias ocean to the west.

6.7 Present-day Analogues

A suitable modern analogue for the study area requires a young narrow ocean basin or a pull-apart basin with a high rate of sedimentation, which has a strong possibility of being overridden by a landmass several kms thick (e.g. restraining bend; subduction zone). The Red Sea, for example, has a comparatively low-sedimentation rate and is difficult to investigate because of thick but mobile Miocene salt deposits and it has no immediate prospect of being buried. Similarly, the Gulf of Aden and some other basins with deep spreading centres are two wide for a sufficiently high sedimentation rate, although they provide a good analogy for the Neotethyan continental configuration of a collage of small strike-slip bounded plates. However, the Gulf of California presents a suitable (although rare) modern day analogue for interactions between basaltic magma and rapidly accumulating sediments in a young spreading centre (Einsele, 1986). This area also has the potential to be overridden by the Transverse Ranges (the major restraining bend on the same San Andreas system) within a relatively short time-span, unless the master strike-slip fault jumps E to isolate it.

However, it must be noted that it is the tectonic setting and rates of sedimentation which are considered analogous to the Lake Volvi area and that the sedimentary basin infill in the study area is regarded as being typical of Neotethyan deposits.

6.7.1 The Salton Sea, Gulf of California

The Salton Sea is located at the northern end of the Gulf of California and represents a pull-apart basin created by strike-slip movement along the San Andreas Fault. Kelts (1981) proposed a comparison of deep pull-apart filled basins in Greece and the Gulf of California (Fig. 6.20). The Imperial Valley and Salton Trough are being continuously filled by river sediments which fill the spreading basins to about sea-level. This results in the development of rift-stage crust as well as newly formed oceanic crust subsiding isostatically (c.f. Moore, 1973; Fuis *et al.*, 1982). In this case,

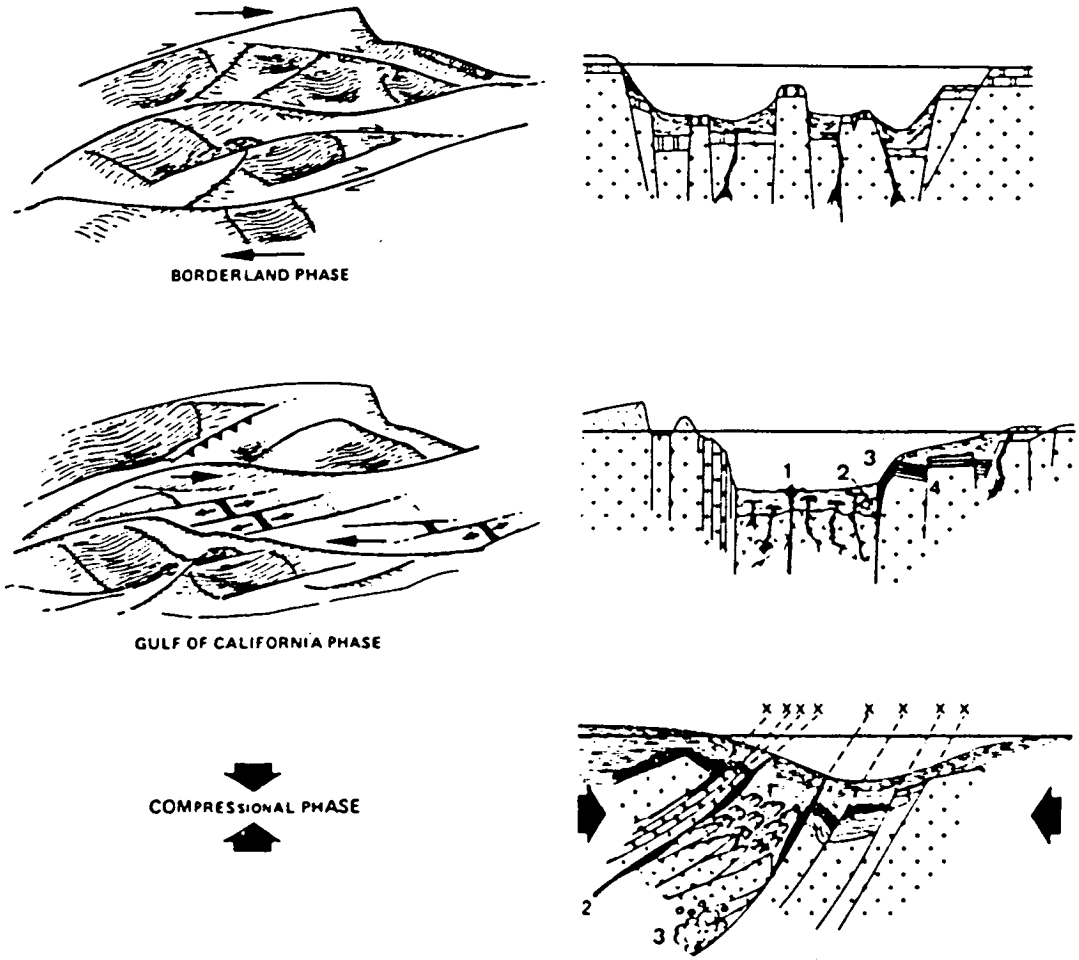

Fig. 6.20: A proposed process-model for a translational margin, as a guide to the paleogeography of the Mesozoic Northern Penninic (Tethys) Ocean, after Kelts (1981).

Borderland Phase: based on the modern California Borderland region: Junger (1976); Crowell (1974); Crouch (1981). Translational stress applied over a large region leads to lozenge-shaped basin and ridge features with differential sedimentation. Some are isolated from terrigenous input. Facies include a large variety of pelagic, hemipelagic, and mass flows deposited on subsided continental crust, segmented by deep vertical faults. Volcanics in various positions.

Gulf of California Phase: Characterised by oblique rifting of continental blocks with spreading centres forming ocean crust, which may isolate some continental slivers. Marginal basins become quiescent as lateral motion is accommodated along a restricted medial section. A narrow belt of irregular ocean crust forms in basinal areas with (1) Sills injected into rapidly deposited soft hemipelagic oozes. (2) In some cases with concomitant hydrothermal alteration. (3) Ultramafic bodies may be tectonically emplaced along transform traces whilst, (4) Unconformities and changes in the hemipelagic slope facies area caused by differential dilational and compressional movements and tilting which affects continental blocks in the translational setting.

Compressional Phase: During initial compression, particularly if lateral motion continues, deep-seated transform or transcurrent faults may play a role in determining the zones of reverse and thrust fault shearing. Some possible concurrent events include: (1) Deformation of interlayered sills and basinal sediment, (2) Mobilization of ultramafic pods, (3) Imbrication and shallow subduction of some oceanic crust, (4) Metamorphism at fairly shallow depths whereas normal hemipelagic sedimentation continues above.

the sedimentation rate equals or surpasses the spreading and subsidence rate of the pull-apart basins. Magmatic intrusions into sediments are therefore hampered by lithostatic pressure resulting from relatively high bulk densities and compaction as well as by lithification of the fluvial and deltaic sediments overlying the young oceanic crust.

Sill-sediment complexes or some relicts of them can be expected in orogenic belts where pull-apart basins or narrow ocean basins with high sedimentation rates have later been deformed along convergent plate boundaries (Kelts, 1981). However, in this case it would be difficult to recognise them and to reconstruct their original basin configuration (Einsele, 1985).

Within deep sediment filled basins, magma can only rarely extrude and form small volcanic cones in the middle of a fluvial-deltaic plain (e.g. Robinson *et al.*, 1976; Einsele, 1986; *see* Fig. 6.21). A sill-sediment complex is probably not developed. If a relatively short phase of basinal growth between divergent plates is succeeded by the development of a subduction zone (particularly prevalent in a strike-slip regime) the basinal complex may come to be buried (c.f. Karig, 1982; Leggett, 1982). A model involving a strike-slip system could also result in a similar structural configuration. This would arise if a restraining bend were to override the pull-apart basin along the same strike-slip system. However, a distinct difference between these two models arises, as although the basin would be buried there is no requirement for intrusion to cease if the underlying extensional regime continued to extend down to the base of the lithosphere and would therefore probably continue to be active. Therefore, sill-sediment complexes can be expected to develop in orogenic belts where pull-apart basins or narrow ocean basins with high sedimentation rates have been deformed along convergent plate boundaries (Einsele, 1986). Possible examples of a buried, yet contemporaneous active pull-apart basin include the Mesozoic Bündnerschiefer and its tholeiitic intrusions, deposited in the Penninic Trough of the Alps (Kelts, 1981); and some Proterozoic embryonic ocean basins containing tholeiitic dyke swarms in flysch-like sediments from the Canadian Shield (Easton, 1983).

6.8 Role of the Serbo-Macedonian Massif within the Internal Hellenides

An abundance of detailed geological and palaeomagnetic data indicates a complex evolution for the eastern Mediterranean. Interpretations of the region have included the formation and destruction of a number of oceanic basins of various ages, together with accompanying sedimentation, plutonism, volcanism, deformation and

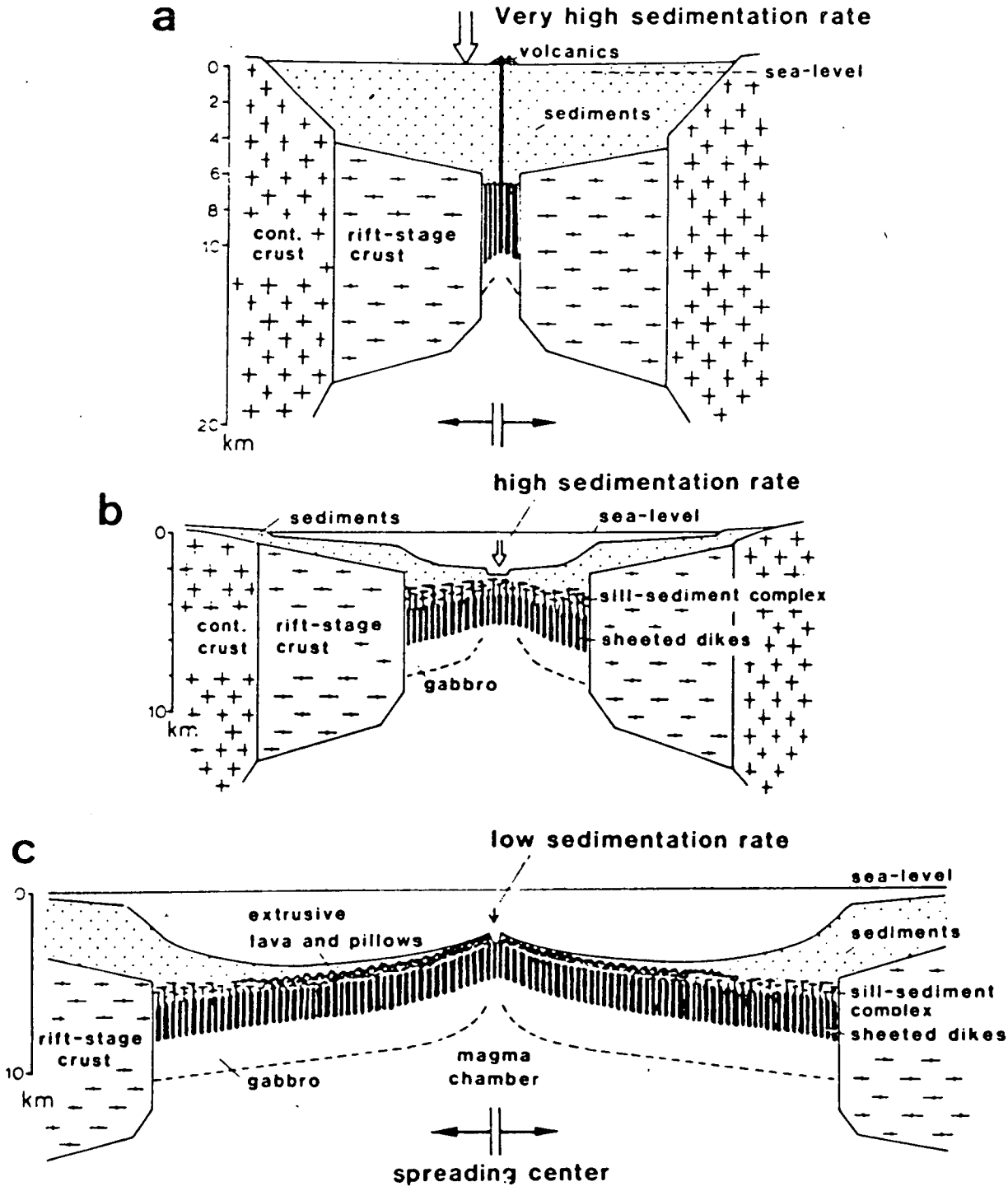

Fig. 6.21: Different stages of development of pull-apart or ocean basins with or without sill-sediment complexes on top of a sheeted dyke zone. (a) Transition from rifting to drifting with very high sedimentation rate on top of a spreading centre (about equal to spreading rate). Rift-stage crust is depressed under thick sediment load. (b) Gulf-type spreading centre in stage of early drifting with high sedimentation rate at spreading trough and formation of sill-sediment complex. (c) More advanced stage of "classic" ocean basin with elevated mid-ocean ridge, low-sedimentation, and extruded lava in central part of basin. However, stage (b) may be found along margins buried under thick slope deposits.

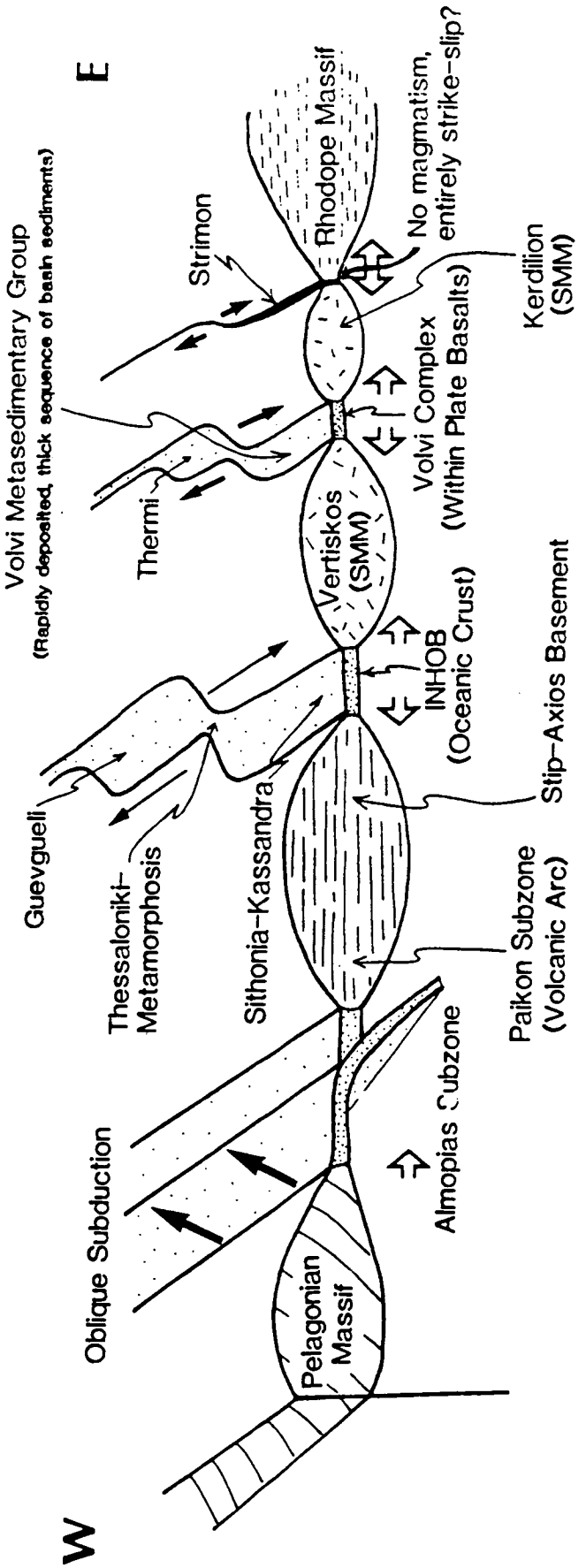

Fig. 6.22: Synoptic diagram showing a possible strike-slip scenario for the origin of the Vardar-Axios ophiolites (Almopias Subzone and IMHOB) and Volvi Complex (Thermi-Gomati Complexes), interpreted from Bebien *et al.*, (1986); Baroz *et al.*, (1987); De Wet (1989) and this study.

metamorphism (e.g. Dixon and Robertson, 1984; Robertson and Dixon, 1984; Robertson *et al.,* 1991; Kolocotroni, 1993). However, a unified model for the evolution of this region has remained contentious (Chapter 1). A review of the arguments and points of contention within the eastern Mediterranean was made by De Wet (1989), and has been modified accordingly to satisfy the findings of this study (Fig. 6.23). Points of agreement in all models (*see review in:* Smith and Woodcock, 1982; De Wet, 1989) consist of:

1) The Tethys (Palaeotethys) came into existence at the time of the assembly of Pangea in the Paleozoic.
2) Some Neotethyan oceans have been destroyed (shown by deformed continental margins and ophiolites), while others have survived (i.e. the Black Sea and eastern Mediterranean Basins).
3) Relative movement of Gondwana and Eurasia probably played a large part in the tectonics of the eastern Mediterranean from the Mid-Jurassic to Tertiary.
4) Some continental fragments have moved independently of Gondwana and Eurasia for at least some of the time.
5) Tethyan evolution spans Late Palaeozoic to Cenozoic time (Sengor, 1984; Robertson and Dixon, 1984).
6) According to plate reconstructions, even taking into account continental shortening, there is insufficient continental crust to bridge the gap between Eurasia and Gondwana until Mid-Tertiary time. Thus Palaeotethyan and/or Neotethyan oceans must have persisted until the Tertiary (Robertson and Dixon, 1984).
7) All authors concur that it is difficult to ascertain whether a microcontinent has a Gondwanan or Eurasian origin. This is particularly applicable for the Serbo-Macedonian Massif, which has been interpreted by Robertson and Dixon (1984) as probably Gondwanan, maybe Eurasian; by Sengor *et al.,* (1980), and Mountrakis (1986), as Eurasian; by Sengor *et al.,* (1984) as Gondwanan; and by Smith and Woodcock (1984) as a continuation of the Pelagonian Zone and therefore Gondwanan.
8) The extent and role of transcurrent or strike-slip tectonics is controversial in the evolution of the Tethys in the eastern Mediterranean. Strike-slip fault systems are important in present day plate boundaries. Over half of present day plate boundaries have relative velocity vectors that are markedly oblique (>22°) to the boundary normal (Woodcock, 1986). There is no reason to believe this was not the case in the eastern Mediterranean during the Late Paleozoic, Mesozoic and

Tertiary. Strike-slip faults in the eastern Mediterranean have been identified by numerous authors including Smith and Woodcock, (1982) and Robertson and Dixon (1984). Evidence presented in this work and elsewhere (e.g. Bebien *et al.*, 1986; De Wet, 1989) strongly support a major role for strike-slip tectonics in the evolution of the Serbo-Macedonian Massif and the eastern Mediterranean in general.

6.8.1 Suture Zones in the Hellenides

In the Hellenides there is still some controversy over the position of the suture zones which are indicated by the presence of Palaeozoic or younger oceanic ophiolites. The problem arises because of the complex deformation which has affected the Hellenides since oceanic spreading occurred. In summary of a review by De Wet (1989), the following scenarios could account for the evolution of the Hellenides:

One root zone: The root zone was located in the Vardar-Axios zone and consequently the western ophiolites (Pindos) were emplaced from this zone (Bernoulli and Laubscher, 1972; Dewey *et al.*, 1973; Mercier *et al.*, 1975; Celet *et al.*, 1976; Vergeley, 1976), alternatively the root zone was located in the western belt and the Vardar-Axios ophiolites were emplaced from the west. This single root zone was in turn duplicated by strike-slip tectonics (Smith and Spray, 1984).

Two root zones: These were located in the Vardar-Axios (eastern) and Subpelagonian (western) zones (Hynes *et al.*, 1972; Barton, 1975; Smith *et al.*, 1975; Smith *et al.*, 1979; Robertson and Dixon, 1984; Mountrakis, 1986).

More than two root zones: In addition to the well recognised Subpelagonian and Vardar-Axios root zones, the IMHOB and the Volvi and possibly the entire TVG complexes also represent root (suture) zones (Bebien *et al.*, 1986; Baroz *et al.*, 1987; De Wet, 1989).

The existence of a Vardar-Axios ocean is not disputed. There is, however, evidence that the Vardar-Axios Zone contains two ophiolite belts which originated in two separate ocean basins (Robertson and Dixon, 1984; Vergeley, 1984; Bebien *et al.*, 1986, 1987; Mussallam and Jung, 1986; De Wet, 1989). The western belt or Almopias Subzone represents an oceanic basin in which ocean-floor spreading occurred during the Early and Middle Jurassic. Initiation of an east-dipping oblique subduction zone may have occurred during Middle Jurassic time (Baroz *et al.*, 1987). In any case it is possible to draw the following conclusions about suture zones within the Hellenides.

1) There are at least four main potential root zones in the Hellenides: a) the Othris-Maliac Zone, b) the western Vardar-Axios Zone (Almopias Subzone), c) the eastern Vardar-Axios Zone (IMHOB), and d) the Volvi (Therma-Gomati) Complex. There is also a possible failed root zone related to the boundary between the SMM and Rhodope Massif, along the Strimon Valley (Fig. 6.23).
2) The IMHOB and Volvi (Thermi-Gomati) Complex are separate from each other and the main Vardar-Axios ophiolites (Almopias Subzone), *see* Chapter 1. They both probably formed as a result of limited spreading above an oblique subduction zone, which resulted in extension in a zone of episodic transtension and transpression (Fig. 6.23).

6.8.2 Back Arc Basins in a Strike-slip Regime.

Bebien *et al.,* (1980) have postulated a back arc basin model for the "ophiolites" of the Peonias Subzone of the Vardar-Axios Zone (also referred to as the IMHOB). In this model, subduction of the Almopias ocean eastwards under the Paikon Subzone resulted in extension above the subduction zone and the formation of a back arc basin of limited extent. This situation was further complicated by supposed oblique subduction of the Almopias oceanic crust, which would have resulted in significant strike-slip motion within the back arc basins. This model accounts for the calc-alkaline chemistry by suggesting that the spreading resulted from intra-continental extension and never resulted in a wide oceanic area. Continental material was thus intimately involved in the formation of and emplacement of the basic rocks.

6.8.3 Strike-slip Zones

It appears inevitable that strike-slip tectonics must have been important in the geological evolution of the eastern Mediterranean when the relative motions of Gondwana and Eurasia are examined. Strike-slip motion has been invoked by numerous authors (e.g. Livermore and Smith, 1984; Robertson and Dixon, 1984; Smith and Spray, 1984; De Wet, 1989), however, the position, timing and significance of these strike-slip motions are, however, in dispute.

Examples of the arguments between the different strike-slip models are briefly outlined below. Smith and Spray (1984) suggested that the similarities of the east and western ophiolitic belts in Greece could be plausibly explained by strike-slip motion. They suggested that a once continuous, subduction-linked marginal basin and adjacent continent were disrupted by a Middle to Late Jurassic sinistral transcurrent fault which ran along the eastern edge of the Pelagonian zone.

Robertson and Dixon (1984) rejected this model, but proposed "complex oblique convergence" along the northern boundary of the Paleotethys. They believed that this resulted in the formation of a "Rhodope-Pontide Collage Zone". Strike-slip motions are also invoked in the formation of a Turkish "mosaic" during the Jurassic. The initial collision between the Apulian plate and Eurasia plate during the Maastrichtian (Upper Cretaceous) was also dominated by oblique motion.

The lack of consensus regarding the importance and timing of strike-slip faults is partly due to varying interpretations of plate orientations through time. Smith and Spray (1984) orientated the Pelagonian Zone and Apulia margin east-west. They invoked the opening of the Italian ophiolite basins as a driving mechanism for the duplication of the Pelagonian Zone. In contrast, Robertson and Dixon (1984) indicated that the Apulian margin was orientated north-south and invoked straight extension and convergence during the Triassic to Cretaceous. The ultimate resolution of these disputes is hampered by the fact that many of these strike-slip zones probably occurred within oceanic basins and were subsequently destroyed or overprinted.

This study has shown strike-slip tectonics to be the dominant component in the evolution of the study area. The regional significance of the study area is discussed in Section 6.8.4.

6.8.4 Discussion

The following discussion is an attempt to place the conclusions of this work into a regional framework. The initial time-tectonic framework follows the conclusions of De Wet (1989), but is altered or expanded by the interpretations from this study (Fig. 6.23).

1) *Pre-Permian.* (Fig. 6.23a) Consolidation, deformation and metamorphism of the SMM and Subpelagonian Massifs. Available data suggest that this event was Upper Palaeozoic (Chapter 1). In the wake of this event the Palaeotethys opened (or simply widened) between the African and Eurasian plates. A possible site of the Palaeotethys is the western part of the Vardar-Axios zone (Almopias Basin), although this is far from being proven. Evidence presented by De Wet (1989) and in this work suggest that the IMHOB or the Volvi (Thermi-Gomati) Complex cannot be the site of the Palaeotethys. Therefore the site of the Palaeotethys suture may more reasonably lie further to the east possibly through the Istanbul-Strandja Nappe region (Sengor, 1984) or, possibly it is represented by numerous sutured small ocean basins over a wide area which would have

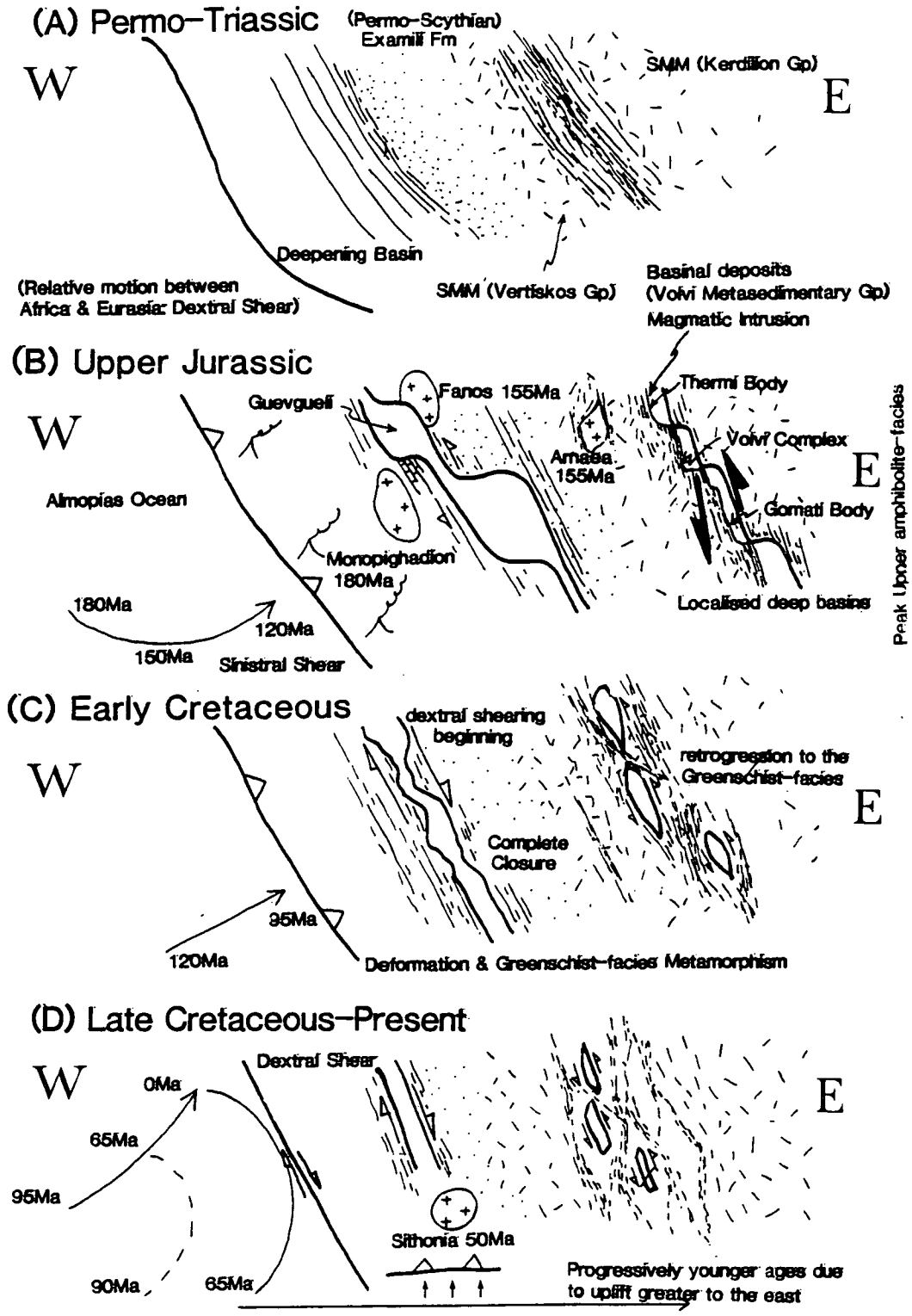

Fig. 6.23: Schematic diagrams showing the evolution of the Innermost Hellenic ophiolite belt and the Volvi-Thermi-Gomati Complexes, from the Precambrian to the present, after De Wet (1989), and this thesis.

accommodated closure of a large ocean without the preservation of a major oceanic terrane.

2) *Permo-Triassic.* (Fig. 6.23b) During the Permo-Triassic, dextral shear occurred between Africa and Eurasia (from palaeomagnetic data reviewed by Robertson and Dixon, 1984). The Almopias ocean may have been spreading at this time following rifting of the SMM from the Pelagonian microcontinent. Gradual subsidence and extension initially resulted in the deposition of clastic sediments and acidic volcanics (Examili Formation) during the Permo-Triassic. Continued subsidence resulted in the deposition of neritic and pelagic sediments in an elongate basin trending NW-SE along the margin of the SMM which may have had a large strike-slip component. The Volvi (Thermi-Gomati) Complex may have started to open in conjunction with the western strike-slip margin, although of only minor extent. However, the Volvi Complex strike-slip basinal regime may represent a failed rift/pull-apart basin either before or after opening of the Peonias Basins. It is possible that some thinning and subsidence may have occurred along the Volvi "line" at this stage in which the "tiger-striped" lithologies were deposited.

3) *Jurassic.* (Fig. 6.24b) Toward the end of the Triassic the relative motion of Africa compared to Eurasia reversed and became sinistral. Oceanic spreading in the Almopias basin continued during the Early and Middle Jurassic but sometime in the Middle Jurassic an east-dipping oblique subduction zone was initiated west of the SMM margin. A volcanic arc formed above the subduction zone, the rocks of which are now preserved in the Paikon Zone. The inferred subduction may have resulted in the formation of marginal or back arc basins in the western parts of the SMM. The present orientation of this margin and the relative motion of Africa favour the formation of sinistral shear. This suggestion contradicts the interpretation of Bebien *et al.*, (1986) who suggested dextral shear. The evidence presented by Bebien *et al.*, (1986) for strike-slip tectonics does not demand a specific sense of shear. However, the sigmoidal shape of the Arnaea granite appears to indicate a sinistral sense of shear. Continual deposition along the NW-SE basin culminated in the deposition of the Svoula Flysch during the middle Jurassic. The Guevgueli ophiolite appears to have been formed at and displaced on to the continental margin around 150 Ma. This may have been initiated by a shift in the displacement direction of the African plate. During this time transpressional-transtensional tectonics were probably operating within the Lake Volvi area. The Volvi Complex was intruded during

the initial dominant phase of transtenion, followed by deformatiom and continued intrusion during a locally variable transtensional-transpressional regime. Burial of the Volvi basin by an overriding restraining bend from along the same strike-slip system resulted in high P conditions being developed. This in turn probably resulted in the synchronous deformation now preserved as complex structures associated with the numerous dyke phases in the Chortiatis Group. The Arnaea Granite was intruded at about this time and supports the interpretation of a transcurrent regime. This study proposes that the Arnaea granite was initiated by crustal anatexis in response to crustal thinning and decompression in conjunction with underplating and intrusion of the crust by mafic and ultramafic rocks.

4) *Late Jurassic-Early Cretaceous.* (Fig. 6.24c) With the closure of the Thessaloniki-Metamorphosis Ocean (which may simply be represented by stringers of pull-apart basins similar to the Volvi area) strike-slip tectonics probably evolved into a more dominant transpressional regime. Continental sinistral rotation of Africa caused dextral shear, which possibly caused the final closure of the Sithonia basin and the formation of northward vergent folds. This event possibly caused the onset of oblique dextral shearing of the Thessaloniki-Metamorphosis ophiolite to occur.

5) *Early Tertiary.* (Fig. 6.24d) According to Robertson and Dixon (1984), around 65 Ma, the Pelagonian promontory impinged on the edge of the SMM. Continued subduction of an ocean remnant under the largely sutured Pelagonian-SMM plate resulted in the intrusion of large calc-alkaline plutons in Sithonia (Sithonia Granitoid, 50 Ma).

6) Final exhumation of the area may have resulted in the development of extensional shear zones, such as the Agios Anastasias shear zone in the Chortiatis series, and south of Lake Volvi. This deformation may also account for the west to east younging of radiogenic ages (Chapter 1; Appendix II) in association with increasing metamorphic grade. The young ages of the rocks outcropping to the east are interpreted as resetting ages caused by heating at depth and presently exposed by isostatic equilibration raising the eastern boundary and causing rapid erosion. This is not well understood.

7) Beginning about 10 Ma ago extension of the Aegean area resulted in the development of E-W graben structures (Chapter 1).

6.9. Future Work

This study has provided a useful new approach to interpreting the structural and metamorphic history for the Lake Volvi area. The main contribution has been the development of a new structural framework based on progressive, heterogeneous strain-partitioned criteria in a ductile anastomosing complex. The interpretation and models which have been developed for the area provide an insight into at least some of the structures and mechanisms of deformation within a deep crustal regime in a strike-slip environment. The field and mineralogical evidence for the up-pressure transition at high T, of locally heated migmatites and sedimentary screens, is explained by invoking the same strike-slip driven process of restraining-bend overthrusting that will almost certainly overtake the Salton Sea area of California. Therefore, the area around Lake Volvi could be effectively used as a type example to show the range and style of structures, and the mechanism of deformation developed within a strike-slip tectonic environment which is presently an area that is poorly understood. It also provides a realistic model for rapid transitions in metamorphic conditions unrelated to orthogonal rift/convergence processes. In addition to the models proposed for the interpretation of deep crustal structures and the resulting comparative studies to similar areas world wide, this project has raised a number of questions about the Lake Volvi area which need to be resolved before more extensive comparisons can be made.

1) More fieldwork is required throughout the SMM, to study and map areas where the detailed geology is still unknown. By applying a similar approach to determining the structural and metamorphic history used in this study, to areas which have yet to be studied it is hoped that the ambiguities between this study and previous work may be resolved. Extrapolation of the structural models and mechanisms of deformation derived during this study could be usefully combined with and extrapolated into areas which have recently been studied in the area to the W of Volvi and in the NW Serbo-Macedoniann Massif (e.g. Kourou, 1991; Sidiropoulos, 1991; Asvesta, 1992). An integrated study in conjunction with this recent work may enable a useful large-scale structural and tectonic model to be produced for the SMM. This particular aspect is important, as the regional metamorphism and structures observed during this study are strongly influenced by the intrusion of the Volvi Complex. It is therefore important in order to understand deep level structures in a strike-slip environment whether the structural and metamorphic framework and the models produced from this study only apply to the area immediately adjacent to the

Volvi Complex, or whether they apply to the entire eastern margin of the SMM. This may be difficult to constrain as rapid changes in structural style occur from N and S of Lake Volvi. The important question is to establish the area of the terrain affected by the inferred low- to high-pressure transition and to establish a wider regional correlation of the deformational events associated with it.

2) This study proposes that the Kerdilion and Vertiskos Groups are essentially analogous. The slight variations in structural style and metamorphic history can easily be accounted for by strike-slip translation and thermal perturbations. The metasedimentary sequences around Lake Volvi are interpreted to be locally developed basin-fill deposits with a lateral NNW-SSE along-strike correlation due to the strike-slip margin. These metasedimentary groups are deposited at similar times and in approximately similar regimes to those of the Svoula Group. Further studies along strike and comparative studies from the west (Svoula Group) to east (Rhodope Massif) should be made in order to clarify and refine the interpretation of this study.

3) From the structural geometries developed along a strike-slip margin there is a strong possibility that en-échelon basin development has occurred and that the Therma-Volvi-Gomati mafic bodies are truly related (arranged along the present Vertiskos-Kerdilion Group "strike-slip" boundary). Therefore, do these mafic bodies show similar structural histories and styles of deformation, or does the eastern margin of the SMM provide an insight into a wide range of rapidly changing mid-crustal structural regimes?

4) By proposing that the Vertiskos and Kerdilion Groups are analogous, a question is raised over the relationship between the eastern margin of the Kerdilion Group (SMM) and the Rhodope Massif. It is therefore necessary to determine the true significance of the Strimon Valley. Does this tectonic discontinuity mark a major terrane boundary and if so what is the relationship between the SMM and Rhodope Massifs?

5) The models proposed in this study invoked rapid loading resulting in a range of metamorphic assemblages. In order to accurately determine the P-T history for the area it is neccessary to undertake detailed thermobarometric studies. Of prime importance is the constraint that the loading-unloading history of the area provides for the model of overthrusting of the basin by the restraining bend. This study has found a range of useful lithologies which can be correlated with similar lithologies exposed along the Thessaloniki to Serres road, and these may

provide further information on the polymetamorphic history of the Volvi Complex and its envelope.

6) This study has correlated the carbonate metasediments in the Kerdilion and Volvi Metasedimentary Groups. Hence, a comparative study on the numerous carbonate bodies throughout the Volvi area (and possibly further afield) is required to attempt to finally determine an origin for these metasediments. In order to make these correlations for the region as a whole, comparisons between the Volvi carbonates with comparable lithologies to both the east (Rhodope) and west (Svoula Group) should also be included.

7) Comprehensive, well-constrained isotopic age determination would be invaluable in constraining the structural and P-T history and evolution within the area. Although data is available at present this is sparse and difficult to correlate. In addition the present array of ages have been applied to a poorly constrained tectonic framework. A prime need is for dates which are close to formation (i.e. magmatic crystallisation) ages of the various melts present, using high closure temperature isotopic systems.

THE END

BIBLIOGRAPHY

ABBEY, S., 1980. Studies in "standard samples" for use in the general analysis of silicate rocks and minerals. *Part 6, 1979 edition of "usable" values. Geol. Surv. Canada,* 80. 30pp.

ALBEE, A.L., 1965. Distribution of Fe, Mg and Mn between garnet and biotite in natural mineral assemblages. *J. Geol.,* 73. p155-164.

ALDERTON, D.H.M., PEARCE. J.A., & POTTS. P.J., 1980. Rare earth element mobility during granite alteration: evidence from Southwest England. *Earth Planet. Sci. Lett.,* 49. p149-165.

ALEKSIC, V., DIMITRIADIS, S., KALENIC, M., STOJANOV, R., & ZAGORCHEV, I., 1984. Precambrian in the Serbo-Macedonian Massif. In: Zoubek, V., (ed). *Precambrian in Younger Fold Belts; European Variscides, the Carpathians and Balcans.* John Wiley & Sons.

ALEKSIC, V., KALENIC, M., PANTIC, N., & HADZI, E., 1974. Historical geology of the evolution of continental, transitional-oceanic and oceanic lithosphere in Serbia and surrounding areas. In: Janjovic, S., (ed). *Metallogeny and Concepts of the Geotectonic Development of Yugoslavia.* Faculty of Mining and Geology, Belgrade Univ., p229-274.

ALTHAUS, E., KARATKE, E., NITSCH, K.-H., & WINKLER, H.G.F., 1970. An experimental re-examination of the upper stability limit of muscovite plus quartz. *N. Jb. Mineral., Mh.* p325-336.

ANCIREV, A., GOROZANIN, O., VELICKOV, D., & BOGOYAVLENSKAYA, O., 1980. About a find of faunistic remains in the metamorphic rocks of the Western Rhodopes. *Geologica Balcanica,* 10. p29-32.

ANOVITZ, L.M., & CHASE, C.G., 1990. Implications of post-thrusting extension and underplating for P-T-t paths in granulite terranes: a Grenville example. *Geology,* 18. p466-469.

ARGAND, E., 1924. La tectonique de l'Asie. *C.R. Congr. Geol. Int., 13e, 1922, Liege.* p169-371.

ARSOVSKI, M., 1961. Bemerkungen zur tektonischen Entwicklung des Pelagonischen Horst - Antiklinoriums und seine Stellung im Rahmen der alpidischen Structur von Makedonien. *Bull. Inst. Geol. Rep. Mac.,* 8. Skopje.

ARTH, J.G., 1976. Behaviour of trace-elements during magmatic processes. A summary of theoretical models and their applications. *US. Geol. Surv. J. Res.,* 4. p41-7.

ASHWORTH, J.R., 1985. Introduction. In: Ashworth, J.R., (ed). *Migmatites.* Glasgow: Blackie & Sons Ltd., p1-35

ASHWORTH, J.R., BIRDI, J.J., & EMMETT, T.F., 1992. A complex corona between olivine and plagioclase from the Jotun Nappe, Norway, and the diffusion modelling of multimineralic layers. *Min. Mag.,* 56. p511-526

ASVESTA, A., 1992. The magmatism and accompanying sedimentation during the first stages of opening of the Axios Ocean basin during the Triassic. *Unpubl. PhD. Thesis Univ. of Thessaloniki.* (In Greek with English Abstract).

AUBOUIN, J., 1959. Contribution à l'étude géologique de la Grèce septentrionale: Les confins de l'Epire et de la Thessalie. *Ann. géol. Pays. Hell.,* 10. p1-483.

AUBOUIN, J., BONNEAU, M., CELET, P., CHARVET, J., CLEMENT, B., DEGARDIN, J.M., DERCOURT, J., FERRIERE, J., FLEURY, J.J., GUERNET, C., MAILLOT, H., MANIA, J.H., MANSY, J.L., TERRY, J., THIEBAULT, P., TSOFLIAS, P., & VERRIEUX, J.J., 1970, Contribution à la géologie des Hellénides; Le Gavrovo, le Pinde et la zone ophiolitique subpélagonienne. *Ann. Soc. géol. Nord,* 90. p277-306.

AUBOUIN, J., Le PICHON, X., WINTERER, E., & BONNEAU, M., 1977. Les Hellénides dans l'optique de la tectonique des plaques. *6th Proc. Colloq. Geol. Aegean Region,* 3. p1333-1354.

AYDIN, A., & NUR, A., 1982. Evolution of pull-apart basins and their scale independence. *Tectonics,* 1. p91-105.

AYDIN, A., & NUR, A., 1984. The types and role of stepovers in strike-slip tectonics. In: Biddle, K.T., & Christie-Blick, N., (eds). *Strike-slip Deformation, Basin Formation and Sedimentation. Spec. Publ. Soc. Econ. Palaeont. Min.,* 37. p35-44.

AYDIN, A., & PAGE, B.M., 1984. Diverse Pliocene-Quaternary tectonics in a transform environment, San Francisco Bay region, California. *Geol. Soc. Am. Bull.,* 95. p1303-1317.

BALDWIN, J.A., & PEARCE, J.A., 1982. Discrimination of productive and nonproductive porphyritic intrusions in the Chilean Andes. *Econ. Geol.,* 77. p664-674.

BAROZ, F., BEBIEN, J., & IKENNE, M., 1987. An example of high-pressure low-temperature metamorphic rocks from an island-arc: the Paikon Series (Innermost Hellenides, Greece). *J. Met. Geol.*, 5. p509-527.

BARROW, G., 1893. On an intrusion of muscovite biotite gneiss in the S.E. Highlands of Scotland and its accompanying metamorphism. *Q. J. Geol. Soc. Lond.*, 49. p330-358.

BARROW, G., 1912. On the geology of lower Deeside and the southern highland border. *Proc. Geol. Assoc.*, 23. p268-284.

BARTON, C.M., 1976. The tectonic vector and emplacement age of an allochthonous basement slice in the Olympus area, NE Greece. *Bull. Soc. géol. France,* 18. p253-258.

BATCHELOR, R.A., & BOWDEN, P., 1985. Petrogenetic interpretation of granitoid rock series using multicationic parameters. *Chem. Geol.*, 48. p43-55.

BEACH, A., 1976. The inter relationsions of fluid transport, deformation, geochemistry, and heat flow in early Proterozoic shear zones in the Lewisian complex. *Phil. Trans. R. Soc. Lond. Ser A,* 280. p569-604.

BEACH, A., 1980. Retrogressive metamorphic processes in shear zones with special reference to the Lewisian complex. *J. Struc. Geol.*, 2. p257-263.

BEBIEN, J., BAROZ, F., CAPEDRI, S., & VENTURELLI, G., 1987. Magmatismes basiques associés à l'ouverture d'un bassin marginal dans les Hellénides Internes au Jurassique. *Ofioliti,* 12. p53-70.

BEBIEN, J., DUBOIS, R., & GAUTHIER, A., 1986. Example of ensialic ophiolites emplaced in a wrench zone: Innermost Hellenic ophiolite belt (Greek Macedonia). *Geology,* 14. p1016-1019.

BEBIEN, J., OHNENSTETTER, D., OHNENSTETTER, M., & VERGELY, P., 1980. Diversity of Greek ophiolites: birth of ocean basins in transcurrent systems. *Ofioliti, Spec. Issue* 2. p129-197.

BELL, T.H., 1978. Progressive deformation and reorientation of fold axes in a ductile mylonite zone: the Woodroffe thrust. *Tectonophysics,* 44. p285-320.

BELL, T.H., 1981. Foliation development: the contribution, geometry and significance of progressive bulk inhomogeneous shortening. *Tectonophysics,* 75. p273-296.

BELL, T.H., 1985. Deformation partitioning and porphyroblast rotation in metamorphic rocks: a radical reinterpretation. *J. Met. Geol.*, 3. p109-118.

BELL, T.H., 1986. Foliation development and refraction in metamorphic rocks: reactivation of earlier foliations and decrenulation due to shifting patterns of deformation partitioning. *J. Met. Geol.*, 4. p421-444.

BELL, T.H., & ETHERIDGE, M.A., 1973. Microstructure of mylonites and their descriptive terminology. *Lithos,* 6. p337-348.

BELL, T.H., FLEMING, P.D., & RUBENACH, M.J., 1986. Porphyroblast nucleation, growth and dissolution in regional metamorphic rocks as a function of deformation partitioning during foliation development. *J. Met. Geol.*, 4. p37-67.

BELL, T.H., & HAMMOND, R.L., 1984. On the internal geometry of mylonite zones. *J. Geol.*, 92. p667-686.

BELL, T.H., & RUBENACH, M.J., 1983. Sequential porphyroblast growth and crenulation cleavage development during progressive deformation. *Tectonophysics,* 92. p171-194.

BERNOULLI, D., & LAUBSCHER, H., 1972. The palinspastic problem of the Hellenides. *Eclogae Geol. Helv.*, 65. p107-118.

BERTHE, D., & BRUN, J.P., 1980. Evolution of folds during progressive shear in the South Armorican Shear Zone, France. *J. Struc. Geol.*, 2. p127-133.

BERTHE, D., CHOUKROUNE, P., & JEGOUZO, P., 1979. Orthogneiss, mylonite and non-coaxial deformation of granites: the example of the South Armorican Shear Zone. *J. Struc. Geol.*, 1. p31-42.

BICKLE, M.J., HAWKESWORTH. C.J., ENGLAND, P.C., & ATHEY, D.R., 1975. A preliminary thermal model for regional metamorphism in the eastern Alps. *Earth Planet. Sci. Lett.*, 26. p13-28.

BLOXAM, T.W., & LEWIS, A.D., 1972. Ti, Zr and Cr in some British pillow lavas and their petrogenetic affinities. *Nature Phys. Sci.*, 237. p134-136.

BOCCALETTI, M., MANETTI, P., & PECCERILLO, A., 1974. The Balkanids as an instance of back-arc thrust belt: Possible relation with the Hellenides: *Geol. Soc. Am. Bull.*, 85. p1077-1084.

BOHLEN, S.R., 1987. Pressure-temperature-time paths and tectonic model for the evolution of granulites. *J. Geol.*, 95. p617-632.

BOHLEN, S.R., 1991. On the formation of granulites. *J. Met. Geol.*, 9. p223-229

BOHLEN, S.R., WALL, V.J., & BOETTCHER, A.L., 1983. Experimental investigations and geological applications of equilibria in the system FeO-TiO_2-Al_2O_3-SiO_2-H_2O. *Am. Mineral.*, 68. p1049-1058.

BONCEV, E., 1978. Geotectonic position of the Balkanides. *Geologica Balcanica*, 8. p23-40.

BONCEV, E., 1987. Main ideas in the tectonic synthesis of the Balkans, I. The lithospheric plates and the collision space between them. *Geologica Balcanica*, 17. p9-20.

BONCEV, E., 1988a. Main ideas in the tectonic synthesis of the Balkans, II. The Balkan-Carpathian arc and the Kraistide structural zone. *Geologica Balcanica*, 18. p15-35.

BONCEV, E., 1988b. Notes sur la tectonique alpine des Balkans. *Bull. Soc. géol. France*, 8. p241-249.

BORSI, S., FERRARA, G., & MERCIER, J., 1965. Détermination de l'âge des séries métamorphiques du massif Serbo-Macédonien au nord-est de Thessalonique (Grèce) par les méthodes Rb/Sr et K/Ar. *Ann. Soc. géol. du Nord*, 84. p223-225.

BOWEN, N.L., 1940. Progressive metamorphism of siliceous limestones and dolomite. *J. Geol.*, 48. p225-274.

BOYANOV, I., & KOZHOUKHAROV, D., 1968. Stroer ie i blokovoe razclenenije Rhodopskogo massiva (Structure and block subdivision of the Rhodope Massif). *Isv. Geol. Inst., Ser. Getect, Stratigr, i. litol.*, 17. p199-226.

BOYANOV, I., RUSEVA, M., & DIMITROVA, E., 1982. First find of Upper Cretaceous foraminiferas in East Rhodopes: *Geologica Balcanica*, 12. p20.

BRADLEY, D.A., 1982. Subsidence in Late Paleozoic basins in the Northern Appalachians. *Tectonics*, 1. p107-123.

BRUN, J.P., & CHOUKROUNE, P., 1981. Déformation progressive et structures crustales. *Rév. Geogr. Phys. Géol. dyn. Paris*, 23. p177-193.

BRUNN, J.H., 1956. Contribution a l'étude géologique du Pinde septentrional et d'une partie de la Macédoine occidentale. *Ann. géol. Pays. Hell.*, 7. 358p.

BRUNN, J.H., CLEMENT, B., & DERCOURT, J., 1977. Histoire des recherches géologiques dans les Hellénides. *6th Colloq. Aegean Geol.*, 1977, 1. p21-60.

BULLARD, E.C., EVERETT, J.E., & SMITH, A.G., 1965. Fit of the continents around the Atlantic. In: Blackett, P.M.S., Bullard, E.C., & Runcorn, S.K., (eds). *A Symposium on Continental Drift. Phil. Trans. R. Soc. Lond., Ser. A*, 258. p41-75.

BUMA, G., FREY, F.A., & WONES, D.R., 1971. New England granites: trace element evidence regarding their origin and differentiation. *Contrib. Mineral. Petrol.*, 31. p300.

BURG, J.P., IVANOV, Z., RICOU, L.E., DIMOR, D., & KLAIN, L., 1990. Implications of shear-sense criteria for the tectonic evolution of the Central Rhodope massif, southern Bulgaria. *Geology*, 18. p451-454.

BURGATH, K., KOCKEL, F., MOHR, F., RASCHKA, H., JUNG, D., & MUSSALLAM, K., 1979. A complex of sheeted dykes and pillow lavas in the southern part of the Chalkidiki peninsula, Greece. *2nd Int. Ophiolite Sympos. Abstracts.* p20.

BURGATH, K., & LAUER, J.P., 1984. Palaeomagnetic data from Tertiary units of the north Aegean zone. In: Dixon, J.E., & Robertson, A.H.F., (eds). *The Geological Evolution of the Eastern Mediterranean. Spec. Publ. Geol. Soc. Lond.*, 17. p681-686.

BUTLER, R.W.H., 1982. A structural analysis of the Moine Thrust zone between Loch Eriboll and Foinaven, N.W. Scotland. *J. Struc. Geol.*, 4. p19-29.

CANN, J.R., 1969. Spilites from the Carlsberg ridge, Indian Ocean. *J. Petrol.*, 10. p1-19.

CANN, J.R., 1970. Rb, Sr, Y, Zr and Nb in some ocean floor basaltic rocks. *Earth Planet. Sci. Lett.*, 10. p7-11.

CASTRO, A., 1986. Structural pattern and ascent model in the Central Estremadura Batholith, Hercynian Belt, Spain. *J. Struc. Geol.*, 8. p633-645.

CELET, P., CLEMENT, B., & FERRIERE, J., 1976. La zone béotienne en Grèce: Implications paleogéographiques et structurales. *Eclog. Geol. Helv.*, 69. p577-599.

CHADWICK, B., 1968. Deformation and metamorphism in the Lukmanier region, central Switzerland. *Bull. Geol. Soc. Am.*, 79. p1123-1150.

CHAPPELL, B.W., & WHITE, A.J.R., 1974. Two contrasting granite types. *Pacif. Geol.*, 8. p173-174.

CHAPPELL, B.W., & WHITE, A.J.R., 1977. Ultrametamorphism and granitoid genesis. *Tectonophysics*, 43. p7-22.

CHATTERJEE, N.D., & JOHANNES, W., 1974. Thermal stability and standard thermodynamic properties of synthetic $2M_1$-muscovite $KAl_2(AlSi_3O_{10}(OH)_2)$. *Contrib. Mineral. Petrol.*, 48. p89-114.

CHATZIDIMITRIADIS, E.A., & KILIAS, A., 1984. Paleozoisch-Mesozoische Faltungs - phasen im Gebiet oestlich von Thessaloniki/Nord Griechenland. (Ein Beitrag zur Geologie der inneren Helleniden-Zone. *N. Jb. Geol. Paleont. Mh.*, 4. p193-203.

CHOUKROUNE, P., & GAPAIS, D., 1983. Strain pattern in the Aar granite (central Alps): orthogneiss developed by bulk homogeneous flattening. *J. Struc. Geol.*, 5. p411-418.

CHRISTIE-BLICK, N., & BIDDLE, K.T., 1985. Deformation and basin formation along strike-slip faults. In: Biddle, K.T., & Christie-Blick, N., (eds). *Strike-slip Deformation, Basin Formation and Sedimentation. Spec. Publ. Soc. Econ. Paleont. Miner.*, 37. p1-34.

CHRISTOFIDES, G., D'AMICO, C., DEL MORO, A., ELEFTHERIADIS, G., & KYRIAKOPOULOS, C., 1986. A Rb/Sr study of the granitoids of the Sithonia Peninsula (Northern Greece). *Abstract I.C.O.G.*, Camb.

CLIFF, R.A., 1985. Isotopic dating in metamorphic belts. *J. Geol. Soc. Lond.*, 142. p97-110.

COBBOLD, P.R., & QUINQUIS, H., 1980. Development of sheath folds in shear regimes. *J. Struc. Geol.*, 2. p119-126.

COWARD, M.P., 1976. Strain within ductile shear zones. *Tectonophysics*, 34. p181-197.

COWARD, M.P., & POTTS, G.J., 1983. Complex strain patterns developed at the frontal and lateral tips to shear zones and thrust zones. *J. Struc. Geol.*, 5. p383-399.

COX, F.C., 1969. Inclusion in garnets: discussion and suggested mechanism of growth for syn-tectonic garnets. *Geol. Mag.*, 106. p57-62.

COX, K.G., BELL, J.D., & PANKHURST, R.J., 1979. *The Interpretation of Igneous Rocks.* George Allen and Unwin, London.

CROWELL, J.C., 1974. Sedimentation along the San Andreas Fault. In: Dott, R.H., (ed). *Modern and Ancient Geosynclinal Sedimentation. Spec. Publ. Soc. Econ. Paleontol. Mineral., Tulsa*, 19. p292-303.

CROWELL, J.C., 1975. The San Gabriel fault and Ridge Basin, southern California. In: Crowell, J.C., (ed). *San Andreas Fault in Southern California. Spec. Rep. Calif. Div. Mines. Geol.*, 118. p208-233.

CROWELL, J.C., & SYLVESTER, A.G., 1979. Introduction to the San Andreas-Salton Trough Juncture. In: Crowell, J.C., & Sylvester, A.G., (eds). *Tectonics of the Juncture between the San Andreas Fault System and the Salton Trough South-eastern California. A Guidebook.* Univ. Calif. Santa Barbara. p1-13.

CVIJIC, J., 1908. Grundlinien der Geographie und Geologie von Mazedonien und Altserbien (Basic lines in geography and geology of Macedonian and old Serbia). *Peterm. Mitt., Erganz.*, 162. p1-392.

DAVIDSON, A., 1984. Identification of ductile shear zones in the southwestern Grenville Province of the Canadian Shield. In: Kröner, A., & Greiling, R., (eds). *Precambrian Tectonics Illustrated.* p263-279. Schweizerbart., Stuttgart.

DAVIS, G.H., & CONEY, P.J., 1979. Geologic development of the Cordilleran metamorphic core complexes. *Geology*, 7. p120-124.

de la ROCHE, H., LETERRIER, J., GRANDCLAUDE, P., & MARCHAL, M., 1980. A classification of volcanic and plutonic rocks using R1-R2 diagrams and major element analyses-its relationships with current nomenclature. *Chem. Geol.*, 29. p183-210.

DERCOURT, J., ZONENSHAIN, L.P., RICOU, L.E., KAZMIN, V.G., Le PICHON, X., KNIPPER, A.L., GRANDJACQUET, C., SBORTSHIKOV, I.M., GEYSSANT, J.,

LEPVRIER, C., PECHERSKY, D.H., BOULIN, J., SIBUET, J.-C., SAVOSTIN, L.A., SOROKHTIN, O., WESTPHAL, M., BAZHENOV, M.L., LAUER, J.P., & BIJU-DUVAL, B., 1986. Geological evolution of the Tethys Belt from the Atlantic to the Pamirs since the Lias. *Tectonophysics,* 123. p241-315.

De WET, A.P., 1989. Geology of part of the Chalkidiki Peninsula, Northern Greece. *Unpubl. PhD Thesis Camb. Univ.*

De WET, A.P., & MILLER, J.A., 1987. ^{40}Ar-^{39}Ar data from some of the granitoids of the Chalkidiki peninsula, Northern Greece : *Abstract, Terra Cognita. E.U.G.,* 7. p107.

De WET, A.P., MILLER, J.A., BICKLE, M.J., & CHAPMAN, H.J. 1989. Geology and geochronology of the Arnaea, Sithonia and Ouranopolis intrusions, Chalkidiki Peninsula, Northern Greece. *Tectonophysics,* 161. p65-79.

DEWEY, J.F., 1978. Origin of long transform-short ridge systems. *Geol. Soc. Am., Abstr. Programs,* 10. p388.

DEWEY, J.F., 1982. Plate tectonics and the evolution of the British Isles. *J. Geol. Soc. Lond.,* 139. p371-412.

DEWEY, J.F., HEMPTON, M.R., KIDD, W.S.F., SAROGLU, F., & SENGÖR, A.M.C., 1986. Shortening of continental lithosphere: The neotectonics of Eastern Anatolia - A young collision zone. In: Coward, M.P., & Ries, A.C., (eds). *Collision Tectonics. Geol. Soc. Lond. Spec. Publ.,* 19. p3-36,

DEWEY, J.F., PITMAN, III, W.C., RYAN, W.B.F., & BONIN, J., 1973. Plate tectonics and the evolution of the Alpine system. *Geol. Soc. Am. Bull.,* 84. p3137-3180.

de YOREO, J.J., LUX, D.R., & GUIDOTTI, C.V., 1989. The role of crustal anatexis and magma migration in the thermal evolution of regions of thickened continental crust. In: Daly, J.S., Cliff, R.A., & Yardley, B.W.D. (eds). *Evolution of Metamorphic Belts. Geol. Soc. Lond. Spec. Publ.,* 48. p187-202.

DIETRICH, V.J, & OBERHANSLI, R., 1976. Die Gabbro der Jufer-Horen (Avers, GR). *Schweiz. Mineral. Petrogr. Mitt.,* 56. p481-500.

DIMITRIADIS, S., 1974. Petrological study of the migmatitic gneisses and amphibolites of Rendina-Asprovalta-Stavros-Olympias. *Unpubl. PhD Thesis Univ. of Thessaloniki.*

DIMITRIADIS, S., 1980. A possible palaeomargin evolution of the southern most part of Serbo-Macedonian Massif: *Abstact. Proc 26th Int. Geol: Congr.,* 1. p335.

DIMITRIADIS, S., & GODELITSAS, A., 1991. Evidence for high pressure metamorphism in the Vertiskos Group of the Serbomacedonian Massif. The eclogite of Nea Roda, Chalkidiki. *Bull. Geol. Soc. Greece,* 25. p67-80.

DIMITRIJEVIC, M.D., 1963. Sur l'âge du métamorphisme et des plissements dans la masse Serbo-Macédonienne. *Proc. VI Congr. Carp. Balk. Geol. Assoc.,* p339-347.

DIMITRIJEVIC, M.D., & CIRIC, B., 1967. Essai sur l'évolution de la masse Serbo-Macédoniene. *Acta. Geol. Acad. Sci. Hung.,* 11. p35-47.

DINTER, D.A., & ROYDEN, L., 1993. Late Cenozoic extension in northeastern Greece: Strymon Valley detachment system and Rhodope metamorphic core complex. *Geology,* 21. p45-48.

DIPPLE, G.M., BUCHER-NURMINEN, K., & AUSTREIM, H., 1990. Fluid controlled eclogitization of granulites in deep crustal shear zones, Bergen Arcs, western Norway. *Contrib. Mineral. Petrol.,* 104. p184-193.

DIXON, J.E., & DIMITRIADIS, S., 1982. Metamorphosed ophiolitic rocks from the Serbo-Macedonian Zone, Lake Volvi, Greece. In: Dixon, J.E., & Robertson, A.H.F., (eds). *The Geological Evolution of the Eastern Mediterranean, Abstracts, Edinburgh.* p32.

DIXON, J.E., & DIMITRIADIS, S., 1984. Metamorphosed ophiolitic rocks from the Serbo-Macedonian Massif, near Lake Volvi, North-east Greece. In: Dixon, J.E., & Robertson, A.H.F., (eds). *The Geological Evolution of the Eastern Mediterranean. Geol. Soc. Spec. Publ.,* 17. p603-618.

DIXON, J.E., & DIMITRIADIS, S., 1989. The geochemistry of the Volvi body: An in-situ Mesozoic within-plate ophiolite, northeast Greece. *Abstracts, Terra Cognita EUG V.* p165.

DURR, St, ALTHERR, R., KELLER, J., OKRUSCH, M., & SEIDEL, E., 1976. The median Aegean crystalline belt: stratigraphy, structure, metamorphism, magmatism. In: Closs, H.,

Roeder, D., & Schmidt, K., (eds). *Alps, Apennines and Hellenides.* Springer-Verlag, Stuttgart.

EATON, G.P., 1979. Regional geophysics, Cenozoic tectonics, and geologic resources. In: Newman, G.W., & Goode, H.D., (eds). *Basin and Range Symposium. Rocky Mtn. Assoc. Geol.,* p11-39

ECHTLER, H., 1985. Large southeastward ductile thrusting in the Alpine Serbo-Macedonian belt: Abstract, *Terra Cognita. EUG.* 7. p106.

EINSELE, G., 1985. Basaltic sill-sediment complexes in young spreading centres: genesis and significance. *Geology,* 13. p317-338.

EINSELE, G., 1986. Interaction between sediments and basalt injections in young Gulf of California-type spreading centres. *Geol. Rund.,* 75. p197-208.

El BOUSEILY, A.M., & El SOKKARY, A.A., 1975. The relation between Rb, Ba and Sr in granitic rocks. *Chem. Geol.,* 16. p207-219.

ELLIOTT, D., & JOHNSON, M.R.W., 1980. Structural evolution in the northern part of the Moine thrust belt, NW Scotland. *Trans. R. Soc. Edinb. Earth Sci.,* 71. p69-96.

ELLIOT, R.B., 1973. The chemistry of Gabbro/Amphibolite transitions in south Norway. *Contrib. Mineral. Petrol.,* 38. p71-79.

ELLIS, D.J., 1987. Origin and evolution of granulites in normal and thickened crusts. *Geology,* 15. p167-170.

ELLIS, D.J., SHERATON, J.W., ENGLAND, R.N., & DALLWITZ, W.B., 1980. Osumilite-sapphirine-quartz granulites from Enderby Land Antarctica - mineral assemblages and reactions. *Contrib. Mineral. Petrol.,* 72. p123-143.

ELLIS, M., & WATKINSON, A.J., 1987. Orogen-parallel extension and oblique tectonics: The relation between stretching lineations and relative plate motions. *Geology,* 15. p1022-1026.

ENGEL, A.E.J., & ENGEL, C.G., 1962. Hornblende formed during progressive metamorphism of amphibolites, northwest Adirondack Mountains, NewYork. *Geol. Soc. Am. Bull.,* 73. p1499-1514.

ENGLAND, P.C., 1987. Diffuse continental deformation: length scales, rates and metamorphic evolution. *Phil. Trans. R. Soc. Lond., Ser. A.,* 321. p3-22.

ENGLAND, P.C., & HOUSEMAN, G.A., 1988. The mechanics of the Tibetan Plateau. *Phil. Trans. R. Soc. Lond., Ser. A.,* 326. p301-320.

ENGLAND, P.C., & HOUSEMAN, G.A., 1989. Extension during continental convergence, with application to the Tibetan Plateau. *J. Geophys. Res.,* 94. p17561-17579.

ENGLAND, P.C., & RICHARDSON, S.W., 1977. The influence of erosion upon the mineral facies of rocks from different metamorphic environments. *J. Geol. Soc. Lond.,* 134. p201-213.

ENGLAND, P.C., & THOMPSON, A.B., 1984. Pressure-temperature-time paths of regional metamorphism I. Heat transfer during the evolution of regions of thickened continental crust. *J. Petrol.,* 25. p894-928.

ENGLAND, P.C., & THOMPSON, A.B., 1986. Some thermal and tectonic models for crustal melting in continental collision zones. In: Coward, M.P., & Ries, A.C., (eds). *Collision Tectonics. Geol. Soc. Lond. Spec. Publ.,* 19. p83-94.

FERRARA, G., INNOCENTI, F., RICCI, C.A., & SERRI, G., 1976. Ocean floor affinity of basalts from north Apennine ophiolites: geochemical evidence. *Chem. Geol.,* 17. p101-111.

FERRIERE, J., 1982. Paleogéographies et tectoniques superposées dans les Héllénides internes au niveau de l'Othrys et du Pélion (Grèce). *Soc. géol. du Nord.,* 8. p1-970.

FIELD, D., & ELLIOT, R.B., 1974. The chemistry of Gabbro/Amphibolite transitions in south Norway: trace elements. *Contrib. Mineral. Pertrol.,* 47. p63-76.

FISHER, M.A., PATTON, W.M.Jr., THOR, D.R., HOLMES, M.L., SCOTT, E.W., NELSON, C.H., & WILSON, C.L., 1979. The Norton Basin of Alaska. *Oil and Gas Jour.,* 77. p96-98.

FITTON, J.G., & DUNLOP, H.M., 1985. The Cameroon line, West Africa, and its bearing on the origin of oceanic and continental alkali basalts. *Earth Planet. Sci. Lett.,* 72. p23-38.

FITTON, J.G., JAMES, D.J., KEMPTON, P.D., ORMEROD, D.S., & LEEMAN, W.P., 1988. The role of lithospheric mantle in the generation of Late Cenozoic basic magmas in the Western United States. *J. Petrol., Spec. Lith. Issue.* p331-349.

FITTON, J.G., JAMES, D.J., & LEEMAN, W.P., 1991. Basic magmatism associated with Late Cenozoic extension in the Western United States: Compositional variations in space and time. *J. Geophys. Res.*, 96. p693-713.

FITZSIMONS, I.C.W., 1991. The metamorphic histories of some Proterozoic Granulites from East Antarctica. *Unpubl. PhD. Thesis Univ. of Edinburgh.*

FLINN, D., 1962. On folding during three-dimensional progressive deformation. *J. Geol. Soc. Lond.*, 118. p385-433.

FLOYD, P.A., & WINCHESTER, J.A., 1975. Magma type and tectonic setting discrimination using immobile elements. *Earth Planet. Sci. Lett.*, 27. p211-218.

FLOYD, P.A., & WINCHESTER, J.A., 1978. Identification and discrimination of altered and metamorphosed volcanic rocks using immobile elements. *Chem. Geol.*, 21. p291-306.

FOUNTAIN, D.M., HURICH, C.A., & SMITHSON, S.B., 1984. Seismic reflectivity of mylonite zones in the crust. *Geology*, 12. p195-198.

FOUNTOULIS, D., 1980. Etude néotectonique et seismotectonique du basin de Langadha (Macédoine, Grece). *These 3e cycle, Univ. de Paris-Sud, Paris.*

FREUND, R., 1971. Kinematics of transform and transcurrent faults. *Tectonophysics*, 21. p93-134.

FREY, F.A., HASKIN, M.A., POETZ, J.A., & HASKIN L.A., 1968. Rare-earth abundances in some basic rocks. *J. Geophys. Res.*, 73. p6085-6098.

FUIS, G.S., MOONET, W.D., HEALEY, J.H., McMECHAN, G.A., & LUTTER, W.J., 1982. Crustal structure of the Imperial Valley region. In: *The Imperial Valley, California, earthquake of October 15, 1979. U.S. Geol. Surv. Prof. Paper*, 1254. p25-49.

GANGULY, J., 1972. Staurolite stability and related parageneses; theory, experiments and applications. *J. Petrol.*, 13, p335-365.

GARDNER, P.M., & ROBINS, B., 1974. The olivine-plagioclase reaction: geological evidence from the Seiland petrographic province, Northern Norway. *Contrib. Mineral. Petrol.*, 44. p149-156.

GASS, I.G., & SMEWING, J.D., 1974. Intrusion, extrusion and metamorphism at constructive margins: Evidence from the Troodos Massif, Cyprus. *Nature*, 242. p26-29.

GHOSH, S.K., & SENGUPTA, S., 1987. Progressive development of structures in a ductile shear zone. *J. Struc.Geol.*, 9. p277-287.

GRANT, S.M., 1988. Diffusion models for corona formation in metagabbros from the Western Grenville Province, Canada. *Contrib. Mineral. Petrol.*, 98. p49-63.

GRAHAM, C.M., & ENGLAND, P.C., 1976. Thermal regimes and regional metamorphism in the vicinity of overthust faults: an example of shear heating and inverted metamorphic zonation from southern California. *Earth Planet. Sci. Lett.*, 31. p142-152.

GRAHAM, C.M., & POWELL, R., 1984. A garnet-hornblende geothermometer: calibration, testing and application to the Pelona Schist, southern California. *J. Met. Geol.*, 2. p13-31.

GREEN, D.H., & HIBBERSON, W., 1970. The instability of plagioclase in peridotite at high pressure. *Lithos*, 3. p209-221.

GREEN, D.H., & RINGWOOD, A.E., 1967. An experimental investigation of the gabbro to eclogite transition and its petrological applications. *Geochim. Cosmochim. Acta.*, 31. p767-833.

GREEN, H.W., GRIGGS, D.T., & CHRISTIE, J.M., 1970. Syntectonic and annealing recrystallisation and fine-grained quartz aggregates. In: Paulitsch, P., (ed). *Experimental and Natural Rock Deformation.* Springer, Berlin-Heidelberg.

GREEN, T.H., 1980. Island arc and continent-building magmatism: a review of petrogenetic models based on experimental petrology and geochemistry. *Tectonophysics*, 63. p367-388.

GREIVE, R.A.F., & GITTINS, J., 1975. Composition and formation of coronas in the Hadlington Gabbro, Ontario, Canada. *Can. J. Earth Sci.*, 12. p289-299.

GRIFFIN, W.L., 1971. Genesis of coronas in anorthosites of the upper Jotun Nappe, Indre Sogn, Norway. *J.Petrol.*, 12. p219-243.

GRIFFIN, W.L., & HEIER, K.S., 1973. Petrological implications of some corona structures. *Lithos*, 6. p315-335.

GROCOTT, J., 1977. The relationship between Precambrian shear belts and modern fault systems. *J. Geol. Soc. Lond.*, 133. p257-262.

GRUBIC, A., 1980. Yugoslavie. In: Dercourt, J., & others (eds). *Géologie des Pays Européens. Bordas and 26th Int. Geol. Congr. Paris, France.* p291-342.

GUIDOTTI, C.V., 1974. Transition from staurolite to sillimanite zone, Rangeley Quadrangle, Maine. *Geol. Soc. Am. Bull.,* 85. p475-490.

GUNN, B.M., 1966. Modal and element variations in Antarctic tholeiites. *Geochim. Cosmochim. Acta,* 30. p881-920.

HADZI, E., PANTIC, N., ALEKSIC, V., & KALENIC, M., 1974. The Alpides of southeastern Europe in the light of plate tectonics. In: *Metallogeny and Concepts of the Geotectonic Development of Jugoslavia,* Belgrade. p277-310.

HALL, C.A.Jr., 1981. San Luis Obispo Transform Fault and middle Miocene rotation of the western Transverse Ranges, California. *J. Geophys. Res.,* 86. p1015-1031.

HAMILTON, W., 1982. Structural evolution of the Big Maria Mountains, northeastern Riverside Country, southeastern California. In: Frost, E.G., & Martin, D.L., (eds). *Mesozoic-Cenozoic Tectonic Evolution of the Colorado River Region, California, Arizona and Nevada.* p1-28 Cordilleran Publishers, San Diego.

HAMILTON, W., 1987. Crustal extension in the Basin and Range Province southwestern United States. In: Coward, M.P., Dewey, J.F., & Hancock, P.L., (eds). *Continental Extensional Tectonics. Geol. Soc. Spec. Publ.,* 28. p155-176.

HANCOCK, P.L., & ATIYA, M.S., 1979. Tectonic significance of mega-fracture systems associated with the Lebanese segment of the Dead Sea transform fault. *J. Struc. Geol.,* 1. p143-154.

HANMER, S., 1988. Great Slave Lake Shear Zone, Canadian Shield: reconstructed vertical profile of a crustal-scale fault zone. *Tectonophysics,* 149. p245-264.

HANMER, S., & LUCAS, S.B., 1985. Anatomy of a ductile transcurrent shear: the Great Slave Lake Shear Zone; District of MacKenzie, N.W.T. (Preliminary Report). *Curr. Res. Geol. Surv. Pap. Can.,* 85-1B. p7-22.

HANMER, S., BOWRING, S., van BREEMEN, O., & PARRISH, R., 1992. Great Slave Lake Shear Zone. NW Canada: mylonitic record of early Proterozoic continental convergence, collision and indentation. *J. Struc. Geol.,* 14. p757-773.

HANSON, G.N., 1978. The application of trace elements to the petrogenesis of igneous rocks of granitic composition. *Earth Planet. Sci. Lett.,* 38. p26-43.

HANSON, G.N., & GOLDICH, S.S., 1972. Early Precambrian rocks in the Saganaga Lake - Northern Light Lake Area, Minnesota-Ontario, II. Petrogenesis. *Geol. Soc. Am. Mem.,* 135. p179.

HANSON, G.N., SIMMONS, K.R., & BENCE, A.E., 1975. $^{40}Ar/^{39}Ar$ spectrum ages for biotite, hornblende and muscovite in a contact metamorphic zone. *Geochem. Cosmochim. Acta.,* 39. p1269-1277.

HARDING, T.P., 1983. Divergent wrench fault and negative flower structure, Andaman Sea. In: Bally, A.W., (ed). *Seismic Expression of Structural Style. Am. Ass. Petrol. Geol.,* 4. p201-208.

HARDING, T.P., 1985. Seismic characteristics and identification of negative flower structures, positive flower structures and positive structural inversion. *Bull. Am. Ass. Petrol. Geol.,* 69. p582-600.

HARPUM, J.R., 1963. Petrographic classification of granitic rocks in Tanganyika by partial chemical analysis: Tanganyika. *Geol. Surv. Rec.,* 10. p80-88.

HARLAND, W.B., 1971. Tectonic transpression in Caledonian Spitsbergen. *Geol. Mag.,* 108. p27-42.

HARLEY, S.L., 1989. The origins of granulites: a metamorphic perspective. *Geol. Mag.,* 126. p215-247.

HARRE, W., KOCKEL, F., KREUZER, H., LENZ, H., MULLER, P., & WALTHER, H.W., 1968. Uber rejuvenation im Serbo-Macedonischen Massiv (Deutung radiometrischer Altersbestimmungen): *Proc. 23rd Int. Geol. Congr. Prague,* 6. p223-236.

HARRIS, L., 1985. Progressive and polyphase deformation of the Schistes Lustrées in Cap Corse, Alpine Corsica. *J. Struc. Geol.,* 7. p637-650.

HARRIS, N.B.W., 1981. The role of fluorine and chlorine in the petrogenesis of a peralkaline complex from Saudi Arabia. *Chem. Geol.,* 31. p303-310.

HARRIS, N.B.W., DUYVERMAN, H.J., & ALMOND, D.C., 1983. The trace element and isotope geochemistry of the Sabaloka Igneous Complex, Sudan. *J. Geol. Soc. Lond.*, 140. p245-256.

HARRIS, N.B.W., & MARINER, G.F., 1980. Geochemistry and petrogenesis of a peralkaline granite complex from the Midian Mountains, Saudi Arabia. *Lithos*, 13. p325-37.

HART, S.R., 1970. Chemical exchange between sea water and deep ocean basalts. *Earth Planet. Sci. Lett.*, 9. p269-279.

HART, S.R., ERLANK, A.J., & KABLE, E.J.D., 1974. Sea-floor basalt alteration: some chemical and Sr isotopic effects. *Contrib. Mineral. Petrol.*, 44. p219

HARTE, B., & HUDSON, N.F.C., 1979. Pelite facies series and the temperatures and pressures of Dalradian metamorphism in E. Scotland. In: Harris, A.L., Holland, C.H., & Leake, B.E., (eds). *The Caledonides of the British Isles - Reviewed. Geol. Soc. Lond. Spec. Publ.*, 8. p 323-337.

HERRMANN, A.G., POTTS, M.J., & KNAKE, D., 1974. Geochemistry of the rare earth elements in spilites from the oceanic and continental crust. *Contrib. Mineral. Petrol.*, 44. p266-275.

HIGGINS, M.W., 1971. Cataclastic rocks. *Prof. Paper U.S. Geol. Surv.*, 637. p1-97

HILDRETH, W., 1981. Gradients of siliceous magma chambers: implications for lithospheric magmatism. *J. Geophys. Res.*, 86. p10153-10192.

HILL, M., MORRIS, J., & WHELAN, J., 1981. Hybrid granodiorites intruding the accretionary prism, Kodiak, Shumagin and Sanak Islands, SW Alaska. *L. Geophys. Res., B.* 86. p10569-90.

HIRSCHBERG, A., & WINKLER, H.G.F., 1968. Stabilitaetsbeziehungen zwischen Chlorit, Cordierit und Almandin bei der Metamorphose. *Contrib. Mineral. Petrol.*, 18. p17-42.

HOBBS, B.E., MEANS, W.D., & WILLIAMS, P.F., 1976. *An Outline of Structural Geology.* New York: John Wiley & Sons. 571pp.

HODGES, K.V., le FORT, P., PECHER, A., 1988. Possible thermal buffering by crustal anatexis in collisional orogens: thermobarometric evidence from the Nepalese Himalaya. *Geology*, 16. p707-710.

HOLDAWAY, M.J., 1971. Stability of andalusite and the aluminosilicate phase diagrams. *Am. J. Sci.*, 271. p97-131

HOLDAWAY, M.J., & LEE, S.M., 1977. Fe-Mg cordierite stability in high grade pelitic rocks based on experimental, theoretical and natural observations. *Contrib. Mineral. Petrol.*, 63. p175-198.

HOLDSWORTH, R.E., & STRACHAN, R.A., 1991. Interlinked system of ductile strike-slip and thrusting formed by Caledonian sinistral strike-slip and thrusting formed by Caledonian sinistral transpression in northeastern Greenland. *Geology*, 19. p510-513.

HOFFMANN, P.F., 1987. Continental transform tectonics: Great Slave Lake Shear Zone (ca. 1.9 Ga), northwest Canada. *Geology*, 15. p785-788.

HOSCHEK, G., 1969. The stability of staurolite and chloritoid and their significance in metamorphism of pelitic rocks. *Contrib. Mineral. Petrol.*, 22. p208-232.

HOUSEMAN, G.A., McKENZIE, D.P., & MOLNAR, P., 1981. Convective instability of a thickened boundary layer and its relevance for the thermal evolution of continental convergent belts. *J. Geophys. Res.*, 86. p6115-6132.

HSU, K., NACHEV, I.K., & VUCHEV, V.I., 1977. Geologic evolution of Bulgaria in light of plate tectonics. *Tectonophysics*, 40. p245-256.

HUDSON, T., & ARTH, J.G., 1983. Tin granites of the Seward peninsula, Alaska. *Bull. Geol. Soc. Am.*, 94. p768-90.

HYNES, A.J., NISBET, E.G., SMITH, A.G., WELLAND. M.J.P., & REX, D.C., 1972. Spreading and emplacement ages of some ophiolites in the Orthris region, eastern central Greece. (Proc. 4th Aegean Symposium, Hannover). *Z. Dtsch. Geol. Ges.*, 123. p455-468.

INSTITUTE OF GEOLOGICAL AND MINERAL EXPLORATION (I.G.M.E.), 1970. Sitochorion Sheet, 1: 50 000 scale. Athens.

INSTITUTE OF GEOLOGICAL AND MINERAL EXPLORATION (I.G.M.E.), 1978. Stavros Sheet 1: 50 000 scale. Athens.

INSTITUTE OF GEOLOGICAL AND MINERAL EXPLORATION (I.G.M.E.), 1978. Vasiliki Sheet, 1: 50 000 scale. Athens.

INSTITUTE OF GEOLOGICAL AND MINERAL EXPLORATION (I.G.M.E.), 1978. Zangliverion Sheet 1: 50 000 scale. Athens

INSTITUTE OF GEOLOGICAL AND MINERAL EXPLORATION (I.G.M.E.), 1979. Sochos Sheet 1: 50 000 scale. Athens.

INSTITUTE OF GEOLOGICAL AND MINERAL EXPLORATION (I.G.M.E.), 1983. Geological Map of Greece. 1: 500 000 scale. Athens.

IRVINE, T.N., & BARAGAR, W.R.A., 1971. A guide to the chemical classification of the common volcanic rocks. *Can. J. Earth Sci.,* 8. p523-548.

IRVING, A.J., & GREEN, D.H., 1970. Experimental duplication of mineral assemblages in basic inclusions of the Delegate breccia pipes. *Phys. Earth. Planet. Int.,* 3. p385-389.

IVANOV, R., 1981. The deep-seated Central-Rhodope Nappe and the interference tectonics of the Rhodope crystalline basement. *Geologica Balcanica,* 11. p.47-66.

IVANOV, Z., MOSKOVSKI, S., & KOLCHEVA, K., 1979. Basic features in the structure of the central parts of the Rhodope Massif. *Geologica Balcanica,* 9. p.3-50.

IVANOV, Z., MOSKOVSKI, S., & SIRAKOV, N., 1978. Olistostomes in the Paleogene of Hvoina basin. *Annuare Univ. Sofia.* Fac. Geol. Geogr., 70. p17-52.

IVANOV, Z., 1988. Apercu générale sur l'évolution géologique et structurale du massif des Rhodopes dans le cadre des Balkanides: *Bull. Soc. géol. France.,*8. p227-240.

IVANOV, Z., MOSKOVSKI, S., DIMOV, D., & KOLCHEVA, K., 1980. Lithostratigraphic division of the metamorphic rocks from the autochthonous complex of the Central Rhodopes between the upper course of the Cepelarska river and the Vâca valley. *Geologica Balcanica,* 10. p3-30 (in Russian).

IVANOV, Z., MOSKOVSKI, S., KOLCEVA, K., DIMOV, D., & KLAIN, L., 1984. Geological structure of the Central Rhodopes I: Lithostratigraphic subdivision and features of the section of metamorphic rocks in the northern parts of central Rhodopes. *Geologica Balcanica,* 14. p3-42 (in Russian with English abstract).

IVANOV, Z., MOSKOVSKI, S., DIMOV, D., KOLCEVA, K., & KLAIN, L., 1985. Geological structure of the central Rhodopes. II: Structural sequences in the synmetamorphic evolution of the central Rhodopes metamorphic group: *Geologica Balcanica,* 15. p3-32 (in Russian).

JACOBSHAGEN, V., DURR, St., KOCKEL, F., KOPP, K.-O., KOWALCYK, G., with contrib. BERCKHEMER, H., & BUTTNER, D., 1978. Structure and geodynamic evolution of the Aegean region. In: Cloos, H., Roeder, D., & Schmidt, K., (eds). *Alps, Apennines, Hellenides. Geodynamic investigation along geotraverses by an international group of geoscientists. I.U.G.S. Rep.,* 38. p.537-564.

JACOBSHAGEN, V., RISCH, H., & ROEDER, D., 1976. Die Eohellenische phase, definition und interpretation. *Z. Dutsch. Geol. Gest.,* 127. p133-145.

JAMES, S.D., 1987. Volcanism in sedimentary basins and its implications for mineralization. *Unpubl. PhD. Thesis Univ. Newcastle-Upon-Tyne.*

JAMTVEIT, B., BUCHER-NURMINEN, K., & AUSTREIM, H., 1990. Fluid controlled eclogitization of granulites in deep crustal shear zones, Bergen Arcs, Western Norway. *Contrib. Mineral. Petrol.,* 104. p184-193.

JANEV, S., TENCHOV, J., & ILIEVA, H., 1979. Stratigrafia na mladija paleozoi ot Lozenskata planina i Vakarelskija rid (Stratigraphy of the Late Palaeozoic in Lozen Mountain and Vakarel ridge). *Geofond, Geol. Inst.*

JARANOFF, D., 1938. La géologie du massif des Rhodopes et son importance à propos de la tectonique de la peninsule Balkanique. *Rev. Géogr. Phys. Géol. Dyn.,* 11. p131-142.

JARANOFF, D., 1960. Tektonika na Balgaria (Tectonics of Bulgaria). *Sofia, Technika.* p283.

JOHNSON, C.D., & CARLSON, W.D., 1990. The origin of olivine-plagioclase coronas in metagabbros from the Adirondack Mountains, New York. *J. Met. Geol.,* 8. p697-717.

JONES, D.G., SILBERLING, N.J., & HILLHOUSE, J., 1977. Wrangellia - A displaced terrane in northwestern North America. *Can. J. Earth Sci.,* 14. p2565-2577.

JONES, T., & NUR, A., 1984. The nature of seismic reflections from deep crustal fault zones. *J. Geophys. Res.,* 89. p3153-3171.

JUNG, D., MUSSALLAM, K., BURGATH, K., KOCKEL, F., MOHR, M., & RASCHKA., 1981. Ultramafic and related rocks of Chalkidiki, (Northern greece). *Proc. Int. Symp. Metal. Maf. Ultramaf. Complexes* (Athens), 3. p24-42.

JUNGER, A., 1976. Tectonics of the Southern California borderland. In: Howell, D.G., (ed). *Aspects of the Geologic History of the California Continental Borderland. Misc. Publ. Am. Petrol. Geol. Pac. Sect.*, 24. p486-498.

KALENIC, M., 1966. Pervaja nahodka niznego kembrija vo Vostocnoj Serbiji (First find of Lower Cambrian in East Serbia). *Spis. Bulg. geol. druzestvo.* 27. p219-220.

KARAMATA, S., 1974. Dynamo-thermal metamorphism related to the emplacement of ultramafics from the Dinarides. *Ann. Soc. Geol. Belgique,* 1. p197-207.

KARAMATA, S., MAJER, V., & PAMIC, J., 1980. Ophiolites of Yugoslavia. *Ofioliti,* 1. p27-46.

KARIG, D.E., 1982. Accreted terranes in the northernmost part of the Phillipine Archipelago. *Tectonics,* 2. p211-236

KARISTINEOS, N., & SOTIRIADIS, L., 1987. Contribution to the East Mediterranean-Tethys evolution. The Rhodope-Serbomacedonian Massifs boundary. *Abstracts Terra Cognita, EUG.*, 7. p107.

KASSOLI-FOURNARAKI, A., 1981. Contribution to the mineralogical and petrological study of amphibolitic rocks of the Serbo-Macedonian Massif. *Unpubl. PhD Thesis Univ. of Thessaloniki.*

KAUFFMANN, G., KOCKEL, F., & MOLLAT, H., 1976. Notes on the stratigraphic and palaeogeographic position of the Svoula Formation in the Innermost zone of the Hellenides (Northern Greece). *Bull. Soc. géol. France.*, 18. p225-230.

KAY, R., HUBBARD, N.J., & GAST, P.W., 1970. Chemical characteristics and origin of oceanic ridge volcanic rocks. *J. Geophys. Res.*, 75. p1585-1614.

KELTS, K., 1981. A comparison of some aspects of sedimentation and transitional tectonics from the Gulf of California and the Mesozoic Tethys, northern Penninic margin. *Eclogae Geol. Helv.*, 74. p317-338.

KILIAS, A., 1980. Geologische und tectonische Untersuchung des Gebietes von ostlichen Varnopus (NW Makedonien). *Unpubl. PhD. Thesis Univ. of Thessaloniki.*

KINGMA, J.T., 1958. Possible origin of piercement structures, local unconformities and secondary basins in the Eastern Geosyncline, New Zealand. *N.Z. J. Geol. Geophys.*, 1. p269-274.

KLIGFIELD, R., CRESPI, J., NARUK, S., & DAVIS, G.H., 1984. Displacement and strain patterns of extensional orogens. *Tectonics,* 3. p557-609.

KNIPE, R.J., & NEEDHAM, D.T., 1985. Deformation processes in accretionary wedges - examples from the southwestern margin of the Southern Uplands, Scotland. In: Coward, M.P., & Ries, A.C. (eds). *Collision Tectonics. Spec. Publ. Geol. Soc. Lond.*, 19. p51-67.

KNIPE, R.J., & WINTSCH, R.P., 1985. Heterogeneous deformation, foliation development, and metamorphic processes in a polyphase mylonite. In: Thompson, A.B., & Rubie, D.C., (eds). *Advances in Physical Geochemistry, 4, Metamorphic Reactions.* Springer-Verlag, New York.

KOBER, L., 1929. Die grossgliederung der Dinariden. *Zentralbl. Min. Geol.*, 10. p426-437.

KOCKEL, F., MOLLAT, H., 1976. Untersuchungen an den Magnesitvererzungen in der Westlichen Chalkidiki (N-Griechenland). *Geol. Jb.*, 16. p29-54.

KOCKEL, F., MOLLAT, H., & WALTHER, H.W., 1971. Geologie des Serbo-Macedonischen Massivs und seines mesozoischen Rahmens (Nord griechenland). (Geology of the Serbo-Macedonian Massif and its Mesozoic framework, Northern Greece): *Geol. Jb.*, 89. p529-551.

KOCKEL, F., MOLLAT, H., & WALTHER, H.W., 1977. Erläuterungen zur geologischen Karte der Chalkidiki und agrenzender Gebiete 1: 100 000 (Nord-Griechenland): (Explanations to the geological map of Chalkidiki and the adjacent areas, 1: 100 000, Nord-Griechenland). *Bundesanstalt für Geowissenschaften und Rohstoffe, Hannover,* 119pp.

KOCKEL, F., & WALTHER, H.W., 1965. Die Strimonlinie als Grenze zwischen Serbo-Macedonischen und Rila-Rhodope-Massiv in Ost-Mazedonien (The Strimon line as a boundary between the Serbo-Macedonian and the Rila-Rhodope Massifs in East Macedonia), *Geol. Jb.*, 83. p573-602.

KOCKEL, F., & WALTHER, H.W., 1968. Zur geologischen Entwicklung des Sudlichen Serbo-Macedonischen Massivs (On the geological development of the Serbo-Macedonian Massif in Northern Greece). *Bull. Geol. Inst., Ser. Geotect., Stratigr. Lithol.*, 17. p133-142.

KOIDE, H., & BHATTACHARJI, S., 1977. Geometric patterns of active strike-slip faults and their significance as indicators for areas of energy release. In: Saxena, S.K., (ed). *Energetics of Geological Processes.* New York, Springer Verlag. p46-66.

KOKKINAKIS, A., 1977. Das Intrusivgebiet des Symvolon - Gebirges und von Kavala in Ost-Makedonien, Griechenland. (The intrusive region of Symvolon Mountain and Kavala, Greece). *Unpubl. PhD.Thesis Univ. of Munchen.*

KONDOPOULOU, D., 1982. Paléomagnétisme et déformations néogènes du Nord de la Mer Egée. *Thèse 3eme Cycle, Univ. L. Pasteur, Strasbourg.* pp123.

KONDOPOULOU, D., & LAUER, J.D., 1984. Palaeomagnetic data from Tertiary units of the north Aegean zone. In: Dixon., J.E., & Robertson, A.H.F., (eds). *The Geological Evolution of the Eastern Mediterranean. Spec. Publ. Geol. Soc. Lond.*, 17. p681-686.

KONDOPOULOU, D., & WESTPHAL, M., 1986. Paleomagnetism of the Tertiary intrusives from Chalkidiki (N. Greece). *J. Geophysics*, 59. p62-66.

KOSSMAT, F., 1924. Geologie der Zentral Balkanhalbinsel, Die Kriesgsschauplatz 1914-1918. *Geologisch Dargestellt*, 13. 198pp., Berlin.

KOSTOPOULOS, D., 1989. Geochemistry and tectonic setting of the Pindos ophiolite, northwestern Greece. *Unpubl. PhD. Thesis Univ. Newcastle-Upon-Tyne.*

KOUKOUZAS, K., 1972. Le chevauchement de Strymon dans la région de la frontière Gréco-Bulgare. *Z. Deutsch. Geol. Ges.*, 123. p343-347.

KOUROU, A., 1991. Lithology, tectonism, geochemistry and metamorphism of part of the west part of the Vertiskos Group. The area NE of Lake Agios Vasilios (Koronia). *Unpubl. PhD. Thesis Univ. of Thessaloniki.* (In Greek with English abstract).

KOZHOUKHAROV, D., 1968. Proterozoiski compleks (The Proterozoic Complex). *Strat. na Bâlgaria, Sofia, Nauka i iskustvo.* p25-62.

KOZHOUKHAROV, D., 1978. Principles of the stratigraphic division of the Precambrian. In: Zoubek, V., (ed). *The Precambrian in Bulgaria. Materials of IGCP Project 22*, p6-15.

KOZHOUKHAROV, D., KOZHOUKHAROV, E., & ZAGORCHEV, I., 1978. The Precambrian in Bulgaria. In: Zoubek, V., (ed). *Materials of IGCP Project, 22.* p65.

KOZHOUKHAROV, D., & TIMOFEEV, B., 1980. Pervie nahodki nukrofitofasili v dokembru Rodopskogo massiva (First finds of microphytofossils in the Precambrian of the Rhodope massif). In: Zoubek, V., (ed). *The Precambrian in Bulgaria. Materials of IGCP Project 22, p27-32.*

KOZHOUKHAROV, D., YANEV, S., & BELOV, A., 1980. Geologiceskie i isotopnie dannie o tektoniceskom polozenii Rodopskogo massiva v pozdnem Paleozoe (Geological and isotopic data on the tectonic position of the Rhodope massif during the Late Palaeozoic). *Geologica Balcanica*, 10. p91-107.

KRONBERG, P., 1966. Petrographie und Tektonik im Rhodopen-Kristallins des Tsal Dag, Simvolon und ost. Pangaon (Grieschen-Makedonien). (Petrography and tectonics of the Rhodope Crystalline of Tsal Dag, Simvolon, and east Pangaon, Greek Macedonia). *N. Jb. Geol. Palaont.*, 7. p410-424.

KRONBERG, P., 1969. Gliederung, Petrographie und Tektogenese des Rhodopen Kristallins im Tsal-Dag, Simvolon und Ost-Pangäon im Griechisch Mazedonien. (Subdivision, petrography and tectonogenesis of the Rhodope Crystalline in Greek Macedonia). *Geotekt. Forsch.*, 31. p1-49.

KRONBERG, P., MEYER, W., & PILGER, A., 1970. Geologie der Rila-Rhodope Masse zwischen Strimon und Nestos (Nord-Griechenland): *Beitr. Geol. Jb.*, 88. p133-180.

KRONBERG, P., & RAITH, M., 1977. Tectonics and metamorphism of the Rhodope Crystalline Complex in Eastern Greek Macedonia and parts of Western Thrace. *N. Jb. Geol. Palaont.*, 11. p697-704.

KUSHIRO, I., & YODER, H.S., 1966. Anorthite-forsterite and anorthite-enstatite reactions and their bearing on the basalt-eclogite transformation. *J. Petrol.*, 5. p195-218.

LAGARDE, J.L., & MICHARD, A., 1986. Stretching normal to the regional thrust displacement in a thrust-wrench shear zone, Rehamna Massif, Morocco. *J. Struc. Geol.*, 8. p483-492.

LAIRD, J., & ALBEE, A.L., 1981. Pressure, temperature, and time indicators in mafic schist: their application to reconstructing the polymetamorphic history of Vermont. *Am. J. Sci.*, 281. p127-175.

LANPHERE, M.A., 1976. Identification of excess ^{40}Ar by $^{40}Ar/^{39}Ar$ spectrum technique. *Earth Planet. Sci. Lett.*, 32. p141-148.

LANPHERE, M.A., & DALRYMPLE, G.B., 1971. A test of the $^{40}Ar/^{39}Ar$ age spectrum technique on some terrestrial materials. *Earth Planet. Sci. Lett.*, 12. p359-372.

LANPHERE, M.A., COLEMAN, R,G., KARAMATA, S., & PAMIC, J., 1975. Age of amphibolites associated with Alpine peridotites in the Dinaride ophiolite zone, Yugoslavia. *Earth Planet. Sci. Lett.*, 26. p271-276.

LAPWORTH, C., 1885. The Highland controversy in British History: Its causes, course, and consequences. *Nature*, 32. p558-559.

LATIN, D.M., DIXON, J.E., & FITTON, J.G., 1989. Rift-related magmatism in the North Sea Basin. In: Blundell, D.J., & Gibbs, A.D., (eds). *Tectonic Evolution of the North Sea Rifts:* Oxford, England.

LEAKE, B.E., 1964. The chemical distinction between ortho- and para-amphibolites. *J. Petrol.*, 5. p238-254.

Le FORT, P., 1981. Manaslu leucogranite: a collision signature of the Himalaya: a model for its genesis and emplacement. *J. Geophys. Res.*, 86. p10545-68.

LEGGET, J.K., 1982. Controls on structural style in accretionary fore-arcs: evidence from modern and ancient (abstract). *Int. Geol. Congr.*, 26. p1346.

LILOV, P., 1981. Potassium-argon dating of the Struma diorite formation north of the town of Stanke Dimitrov. *Geologica Balcanica*, 11. p27-31.

LIOU, J.G., 1971. Synthesis and stability relations of prehnite, $Ca_3Al_2Si_3O_{10}(OH)_2$. *Am Min.*, 56. p507-531.

LISTER, G.S., ETHERIDGE, M.A., & SYMONDS, P.A., 1986. Detachment faulting and the evolution of passive continental margins. *Geology*, 14. p246-250.

LISTER, G.S., & WILLIAMS, P.F., 1983. The partitioning of deformation in flowing rock masses. *Tectonophysics*, 92. p1-33.

LIVERMORE, R.A., & SMITH, A.G., 1984. Some boundary conditions for the evolution of the Mediterranean region. In: Stanley, D.J., & Wezel, F.-C., (eds). *Geological Evolution of the Mediterranean Basin.* Springer. p83-110.

LOGAN, J.M., 1979. Brittle phenomena. *Rev. Geophys. & Space Phys.*, 17. p1121-1132.

LOOSVELD, R.J.H., & ETHERIDGE, M.A., 1990. A model for low-pressure facies metamorphism during crustal thickening. *J. Met. Geol.*, 8. p257-267.

LOWELL, J.D., 1972. Spitsbergen Tertiary orogenic belt and the Spitsbergen fracture zone. *Geol. Soc. Am. Bull.*, 83. p3091-3102

LUTH, W.D., JAHNS, R.H., & TUTTLE, O.F., 1964. The granite system at pressures of 4 to 10 kilobars. *J. Geophys. Res.*, 69. p659-773.

LYBERIS, N., 1984. Tectonic evolution of the Northern Aegean trough. In: Dixon, J.E., & Robertson, A.H.F., (eds). *The Geological Evolution of the Eastern Mediterranean. Geol Soc. Lond. Spec. Publ.*, 17. p709-725.

MACGREGOR, I.D., 1970. The effect of CaO, Cr_2O_3, Fe_2O_3 and Al_2O_3 on the stability of spinel and garnet peridotites. *Phys. Earth Planet. Int.*, 3. p372-377.

MANN, P., HEMPTON, M.R., BRADLEY, D.C., & BURKE, K., 1983. Development of pull-apart basins. *J. Geol.*, 91. p529-554.

MARAKIS, G., 1969. Geochronology studies of some granites from Macedonia. *Ann. géol. Pays. Hell.*, 21. p121-152.

MARATOS, G., & ANDRONOPOULOS, B., 1964. Contribution à la détermination de l'âge d'un horizon dans le cristallophylien du Rhodope. *Bull. Soc. géol. Greece*, 6. p25-35.

MATHEWS, D.H., 1971. Weathered basalts from Swallow Bank, an abyssal hill in the NE Atlantic. *Phils. Trans. R. Soc. Lond., Ser. A.*, 268. p551-571.

McKENZIE, D.P., 1978. Some remarks on the development of sedimentary basins. *Earth Planet. Sci. Lett.*, 40. p25-32.

McKENZIE, D.P., & BICKLE, M.J., 1988. The volume and composition of melt generated by extension of the lthosphere. *J. Petrol.*, 29. p625-679.

McKENZIE, D.P., & O'NIONS, R.K., 1991. Partial melt distributions from inversion of rare earth element concentrations. *J.Petrol.*, 32. p1021-1091.

MCLAY, K., 1987. *The Mapping of Geological Structures.* Halstead Press: John Wiley & Sons, Inc., New York.

McLELLAND, J.M., & WHITNEY, P.R., 1980. Compositional controls on spinel clouding and garnet formation in plagioclase of olivine metagabbros, Adirondack Mountains, New York. *Contrib. Mineral. Petrol.*, 73. p243-251.

MEANS, W.D., 1976. *Stress and Strain. Basic Concepts of Continuum Mechanics for Geologists.* Springer, New York.

MEANS, W.D., HOBBS, B.E., & WILLIAMS, P.F., 1980. Vorticity and non-coaxiallity in progressive deformation. *J. Struc. Geol.*, 2. p 371-378.

MEHNERT, K.R., 1968. *Migmatites and the Origin of Granitic Rocks.* Amsterdam: Elsevier, 393pp.

MELSON, W.G., 1978. Chemical stratigraphy of Leg 45 basalts: electron probe analyses of glasses. In: Melson, W.G., & Rabinowitz, P.O., (eds). *Initial Rep. Deep. Sea. Drill. Proj.*, 45. p507-12.

MELSON, W.G., & Van ANDEL, Tj.H., 1966. Metamorphism in the Mid-Atlantic Ridge, 22°N Latitude. *Mar. Geol.*, 4. p165-186.

MERCIER, J., 1960. Zone Pélagonienne et zone du Vardar en Macédoine Grècque. *Bull. Soc. géol. France*, 7. p435-449.

MERCIER, J., 1966. Paléogéographie, orogenèse, métamorphisme et magmatisme des zones internes des Hellénides en Macédoine (Grèce): vue d'ensemble. *Bull. Soc. géol. France*, 8. p1020-1049.

MERCIER, J., 1966a. Mouvements orogéniques et magmatisme d'âge Jurassique supérieur-Eocretacé dans les zones internes des Héllénides (Macédoine, Grèce). *Rev. Geogr. Phys. Géol. dyn.*, 2. p265-278.

MERCIER, J., 1973a. Etude géologique des zones internes des Héllénides en Macédoine centrale (Grèce). *Ann. géol. Pays. Hell.*, 20. p1-792.

MERCIER, J., 1973b. Plissements synmétamorphiques d'échelle kilométrique d'âge Jurassique supérieur-Eocrétacé dans les Hellénides internes (Macédoine, Grèce). *C. r. Acad, Sci., Paris*, 276. p2249-2252.

MERCIER, J.L, 1981. Extensional-compressional tectonics associated with the Aegean Arc: comparison with the Andean Cordillera of south Peru-North Bolivia. *Phil. Trans. R. Soc. Lond., Ser. A*, 300. p337-355.

MERCIER, J.L., CAREY-GAILHARDIS, E., MOUYARIS, N., St-MEAKIS, K., & ANGHELIDHIS, CH., 1983. Structural analysis of recent and active faults and regional state of stress in the epicentral area of the 1978 Thessaloniki earthquakes. (N. Greece). *Tectonics*, 2. p577-600.

MERCIER, J.L., MOUYARIS, N., SIMEAKIS, C., ROUNDOYANNIS, & ANGELIDHIS, C., 1979. Intraplate deformation: a quantitative study of the faults activated by the 1978 - Thessaloniki earthquakes. *Nature*, 278. p45-48.

MERCIER, J.L., SOREL, D., VERGELY, P., & SIMEAKIS, K., 1988. Extensional tectonic regimes in the Aegean basins during the Cenozoic. *Basin Research*, 2. p49-71

MERCIER, J.L, VERGELY, P., & BEBIEN, J., 1975. Les ophiolites Helléniques "obductées" au Jurassique supérieur sont-elles les vestiges d'un océan Téthysien ou d'une mer marginale péri-européene? *C. r. Soc. éeol. de France.* p108-112.

MERRILL, R.B., ROBERTSON, J.K., & WYLLIE, P.J., 1970. Melting reactions in the system $NaAlSi_3O_8$-$KAlSi_3O_8$-SiO_2-H_2O to 20 kilobars compared with other feldspar-quartz-H_2O and rock-H_2O systems. *J. Geol.*, 78. p558-569.

MESCHEDE, M., 1986. A method of discriminating between different types of mid-ocean ridge basalts and continental tholeiites with the Nb-Zr-Y diagram. *Chem. Geol.*, 56. p207-18.

MEYER, W., 1969. Die faltenachsen im Rhodopen-Kristallin ostlich des Strimon (Nordost-Griechenland): *Geotektonische Forchungen,* 31. p86-96.

MEYER, W., & PILGER, A., 1963. Zur Geologie des Gebietes zwischen Strymon und Nestos. (Rhodopen Massiv in Griechisch Mazedonien (On the geology of the area between Strymon and Nestos, Rhodope Massif in Greek Macedonia). *N. Jb. Geol. Pal., Abh.* 118. p272-280.

MILLER, E., GANS, P.B., GARING, J., 1983. The Snake Range decollement: an exhumed mid-Tertiary ductile-brittle transition. *Tectonics,* 2. p239-263.

MIYASHIRO, A., 1961. Evolution of Metamorphic Belts. *J. Petrol.,* 2. p277-311.

MOLNAR, P., & TAPPONNIER, P., 1975. Cenozoic tectonics of Asia: effects of a continental collision. *Science,* 189. p419-426.

MOLNAR, P., & TAPPONNIER, P., 1978. Active tectonics of Tibet. *J. Geophys. Res.,* 83. p5361-5375.

MOORE, D.G., 1973. Plate-edge deformation and crustal growth, Gulf of California structural province. *Geol. Soc. Am. Bull.,* 84. p1883-1906.

MOUNTRAKIS, D., 1984. Structural evolution of the Pelagonian Zone in Northwest Macedonia, Greece. In: Dixon, J.E., & Robertson, A.H.F., (eds). *The Geological Evolution of the Eastern Mediterranean. Spec. Publ. Geol. Soc. Lond.,* 17. p581-590.

MOUNTRAKIS, D., 1986. The Pelagonian Zone in Greece: a polyphase-deformed fragment of the Cimmerian continent and its role in the geotectonic evolution of the Mediterranean. *J. Geol.,* 94. p335-347.

MUSSALLAM, K., & JUNG, D., 1986. Petrology and geotectonic significance of sialic rocks preceding ophiolites in the eastern Vardar Zone, Greece. *Tschermaks. Min. Pet. Mitt.,* 35. p217-242.

NAMSON, J.S., & DAVIS, T.L., 1988. Seismically active fold and thrust belt in the San Joaquin Valley, Central California. *Bull. Geol. Soc. Am.,* 100. p257-273.

NAYLOR, M.A., MANDL, G., & SIJPESTEIJN, C. H.K., 1986. Fault geometries in basement-induced wrench faulting under different initial stress states. *J. Struc. Geol.,* 8. p737-752.

NEUBAUER, W.H., 1957. Die Suedgrenze der Rhodopen. Ein Betrag zur stratigraphischen Auf losung des Kristallins auf der Halbinsel Chalkidiki (The southern boundary of the Rhodopes. A contribution to the stratigraphic problems of the crystalline on Chalkidiki Peninsula), *Sitz. Ber. Oesterr. Akad. Wiss. Math. Natur.,* Kl. 1. p166, 1-18.

NICOLAS, A., & POIRIER, J.P., 1976. *Crystalline Plasticity and Solid State Flow in Metamorphic Rocks.* Wiley, New York.

NIGGLI, P., 1954. *Rocks and Mineral Deposits. (translated by R.L. Parker).* W.H. Freeman & Sons, San Francisco.

NITSCH, K.-H., 1970. Experimentelle Bestimmung der oberen Stabilitätsgrenze von Stilpnomelan (Experimental determination of the stability limit of stilpnomelane) [Abstract]. *Fortschr. Mineral.,* 47. p48-49.

NORRISH, K., & HUTTON, J.T., 1969. An accurate X-Ray spectrographic method for the analysis of a wide range of geochemical samples. *Geochim. Cosmochim. Acta.,* 33. p431-453.

O'HARA, K., 1988. Fluid flow and volume loss during mylonitzation: an origin for phyllonite in an overthrust setting, North Carolina, U.S.A. *Tectonophysics,* 156. p21-36.

OKRUSCH, M., SEIDEL, E. KREUZER, H., & HARRE, W., 1978. Jurassic age of metamorphism at the base of the Brezovica peridotite (Yugoslavia). *Earth Planet. Sci. Lett.,* 39. p291-297.

OLESEN, N.O., 1978. Distinguishing between inter-kinematic and syn-kinematic porphyroblasts. *Geol. Rundsch.,* 67. p278-287.

OSSWALD, K., 1938. Geologische Geschichte Von Griechisch-Nordmakedonien. *Denkschr. Geol. Land. Griechen.,* 3. *Athen.*

OXBURGH, E.R., 1990. Some thermal aspects of granulite history. In: Vielzeuf, D., & Vidal, Ph., (eds). *Granulites and Crustal Evolution.* Dordrecht: Kluwer Academic Publishers. p569-580.

OXBURGH, E.R., & TURCOTTE, D.L., 1971. Origin of paired metamorphic belts and crustal dilation in island arc regions. *J. Geophys. Res.,* 76. p1315-1327.

OXBURGH, E.R., & TURCOTTE, D.L., 1974. Thermal gradients and regional metamorphism in overthrust terrains with special reference to the Eastern Alps. *Schweiz. Mineral. Petrogr. Mt.*, 54. p641-662.

PALLISTER, J.S., 1981. Structure of the sheeted dyke complex of the Semail ophiolite near Ibra, Oman. *J. Geophys. Res.*, 86. p2661-2672.

PALLISTER, J.S., & HOPSON, C.A., 1981. Semail ophiolitic plutonic suite: field relations, phase variation, cryptic variation and layering, and a model of a spreading ridge magma chamber. *J. Geophys. Res.*, 86. p2593-2644.

PAPADAKIS, A., 1971. On the age of the granitic intrusion near Stratonion, Chalkidiki (Greece). (In Greek with English Summary). *Ann. géol. Pays. Hell.*, 23. p297-300.

PAPADOPOULOS, C., & KILIAS, A., 1985. Altersbeziehungen zwischen metamorphose und deformation im zentralen teil des Serbo-Macedonischen massivs (Vertiskos Gebirge, Nord-Griechenland). *Geol. Rundsch.*,74. p77-85.

PAPANIKOLAOU, D., & PANAGOPOULOS, A., 1981. On the structural style of Southern Rhodopes, Greece. *Geologica Balcanica*, 13. p13-22.

PAPANIKOLAOU, D., SASSI, F.P., & SKARPELIS, N., 1982. Outlines of the Pre-Alpine metamorphisms in Greece. In: Sassi, F.P., (ed). *ICGP Project 5, Newsletter*, 4. p56-62.

PARK, R.G., 1969. Structural correlation in metamorphic belts. *Tectonophysics*, 7. p323-338.

PARSONS, B., & McKENZIE, D.P., 1978. Mantle convection and the thermal structure of the plates. *J.Geophys. Res.*, 83. p4485-4496.

PASSCHIER, C.W., 1982. Pseudotachylite and the development of ultramylonite bands in the Saint-Barthélemy Massif, French Pyrenees. *J. Struc. Geol.*, 4. p69-79.

PATERSON, S.R., TOBISCH, O.T., & RADLOFF. J.K., 1987. Post-Nevadan deformation along the Bear Mountains fault zone: Implications for the Foothills terrane, central Sierra Nevada, California. *Geology*, 15. p513-516.

PATRAS. D., KILIAS, A., CHATZIDIMITRIADIS, E., & MOUNTRAKIS, D., 1989. Structural analysis of deformation episodes and correlation with metamorphic events in the Rhodope Massif and the Phyllitic series of Alexandroupolis area, North Greece: *Geologica Rhodopica*, 1. p37-46.

PAVLIDES, S., 1985. Neotectonic evolution of the Florina-Vegoritis-Ptolemais basin (W. Macedonia, Greece). *Unpubl. PhD. Thesis Univ. Thessaloniki.*

PAVLIDES, S., & KILIAS, A., 1987. Neotectonic and active faults along the Serbomacedonian Zone (SE Chalkidiki, N. Greece). *Ann. Tectonicae*, 1. p97-104.

PEACOCK, S.M., 1989. Thermal modeling of metamorphic pressure-temperature-time paths: A forward approach. In: Spear, F.S., & Peacock, S.M., (eds). *Metamorphic Pressure-Temperature-time Paths. 28th Int. Geol. Congr.*

PEARCE, J.A., 1975. Basalt geochemistry used to investigate past tectonic environment on Cyprus. *Tectonophysics*, 25. p41-67.

PEARCE, J.A., 1980. Geochemical evidence for the genesis and eruptive setting of lavas from Tethyan ophiolites. In: Panayiotou, A., (ed). *Proceedings of the International Ophiolite Symposium, Cyprus, 1979*, p261-272.

PEARCE, J.A., 1982. Trace element characteristics of lavas from destructive plate boundaries. In: Thorpe, R. S., (ed). *Andesites.* J. Wiley & Sons Ltd. p525-548.

PEARCE, J.A., 1983. Role of the sub-continental lithosphere in magma genesis at active continental margins. In: Hawkesworth, C.J., & Norry, M.J., (eds). *Continental Basalts and Mantle Xenoliths*, Nantwich: Shiva. p230-249.

PEARCE, J.A., 1984. A "users' guide" to basalt discrimination diagrams. *Unpubl. Manuscript.*

PEARCE, J.A., 1988. Interpretation of trace element patterns in basalts using linear programming. *Chem. Geol.*, 70. p154.

PEARCE, J.A., & CANN, J.R., 1971. Ophiolite origin investigated by discriminant analysis using Ti, Zr and Y. *Earth Planet. Sci. Lett.*, 12. p339-349.

PEARCE, J.A., & CANN, J.R., 1973. Tectonic setting of basic volcanic rocks determined using trace element analyses. *Earth Planet. Sci. Lett.*, 19. p290-300.

PEARCE, J.A., & GALE, G.H., 1977. Identification of ore-deposition environment from trace-element geochemistry of associated igneous host rocks. In: Anonymous (ed). *Volcanic Processes in Ore Genesis. Spec. Publ. Geol. Soc. Lond.*, 7. p14-24.

PEARCE, J.A., HARRIS, N.B.W., & TINDLE, A.G., 1984. Trace-element discrimination diagrams for the tectonic interpretation of granitic rocks. *J. Petrol.*, 25. p956-983.

PEARCE, J.A., & NORRY, M.J., 1979. Petrogenetic implications of Ti, Zr, Y, and Nb variations in Volcanic rocks. *Contrib. Mineral. Petrol.*, 69. p33-47.

PEARCE, T.H., GORMAN, B.E., & BIRKETT, T.C., 1975. The TiO_2-K_2O-P_2O_5 diagram: A method of discrimination between oceanic and non-oceanic basalts. *Earth Planet. Sci. Lett.*, 24. p419-426.

PEARCE, T.H., GORMAN, B.E., & BIRKETT, T.C., 1977. The relationship between major element chemistry and tectonic environment of basic and intermediate volcanic rocks. *Earth Planet. Sci. Lett.*, 36. p121-132.

PERFIT, M.R., BRUECKER, H., LAWRENCE, J.R., & KAY, R.W., 1980. Trace element and isotopic variations in a zoned pluton and associated volcanic rocks, Unalaska island: Alaska: a model for fractionation in the Aleutian calc-alkaline suite. *Contrib. Mineral. Petrol.*, 73. p69-87.

PERKINS, D., & NEWTON, R.C., 1981. Charnockite geobarometers based on coexisting garnet-pyroxene-plagioclase-quartz. *Nature*, 292. p144-146.

PHILPOTTS, J.A., 1964. Origin of pseudotachylytes. *Am. J. Sci.*, 262. p1008-1035.

PHILPOTTS, J.A., SCHNETZLER, C.C., & HART, S.R., 1969. Submarine basalts: Some K, Rb, Sr, Ba, rare-earth, H_2O and CO_2 data bearing on their alteration, modification by plagioclase, and possible source materials. *Earth Planet. Sci. Lett.*, 7. p293.

PICHON, J.F., 1979. Une transversale dans la zone pélagonienne depuis les collines de Krapa (SW) jusqu'au massif du Vermion (NE): les premières séries transgressives sur les ophiolites. *6th Coll. Aegean Region*, Athens, 1977. p163-171.

PITCHER, W.S., 1979. The nature, ascent and emplacement of granite magmas. *J. Geol. Soc. Lond.*, 136. p627-662.

PITCHER, W.S., 1983. Granite type and tectonic environment. In: Hsü, K., (ed). *Mountain Building Processes. Acad. Press, Lond.*, p19-40.

PLATT, J.P., & BEHRMANN, J.H., 1986. Structures and fabrics in a crustal scale shear zone, Betic Cordillera, SE Spain. *J. Struc. Geol.*, 8. p15-23.

POWELL, C.McA., 1974. Timing of slaty cleavage during folding of Precambrian rocks, Northwest Tasmania. *Bull. Geol. Soc. Am.*, 85. p1043-1060.

POWELL, C.McA., 1979. A morphological classification of rock cleavage. *Tectonophysics*, 58. p21-34.

POWELL, C.McA., & VERNON, R.H., 1979. Growth and rotation history of garnet porphyroblasts with inclusion spirals in a Karakoram schist. *Tectonophysics*, 54. p25-43.

POWELL, D., & TREAGUS, J.E., 1970. Rotational fabrics in metamorphic minerals. *Min. Mag.*, 37. p801-814.

PSILOVIKOS, A.A., 1977. Palaeogeographical evolution of the Mygdonia basin and lake (Langada-Volvi). *Unpubl. PhD. Thesis Univ. Thessaloniki.* (In Greek with an English abstract).

PSILOVIKOS, A.A., 1984. Geomorphological and structural modification of the Serbomacedonian Massif during the Neotectonic stage. *Tectonophysics*, 110. p27-45.

RAMSEY, J.G., 1962. The geometry and mechanics of formation of similar type folds. *J. Geol.*, 79. p309-327.

RAMSEY, J.G., 1967. *Folding and fracturing of rocks.* McGraw Hill. New York. 568pp.

RAMSEY, J.G., & GRAHAM, R.H., 1970. Strain variation in shear belts. *Can. J. Earth Sci.*, 7. p786-813.

RAO, B.B., & JOHANNES, W., 1979. Further data on the stability of staurolite. *N. Jb. Min.*, 1979. p437-447.

READING, H.G., 1980. Characteristics and recognition of strike-slip faults. In: Balance, P.F., & Reading, H.G., (eds). *Sedimentation in Oblique-slip Mobile Zones. Spec. Publ. Int. Ass. Sed.*, 4. p7-26.

RENZ, C., 1955. Die vorneogene Stratigraphie der normalsedimentaren Formation, Griechenlands. *Inst. Geol. Subs. Res.*, 1. (Athens).

RICHARD, P., & ALLEGRE, C.J.,1980. Neodymium and strontium isotope study of ophiolite and orogenic lherzolite petrogenesis. *Earth Planet. Sci. Lett.*, 47. p65-74.

RICHARDSON, S.W., 1968. Staurolite stability in a part of the system Fe-Al-Si-O-H. *J. Petrol.*, 9. p467-488.

RICHARDSON, S.W., & POWELL, R., 1976. Thermal causes of the Dalradian metamorphism in the central Highlands of Scotland. *Scot. J. Geol.*, 12. p237-268.

RICOU, L.-E., 1965. Contribution a l'étude géologique de la bordure sud-ouest du Massif serbo-Macédonien aux environs de Salonique. *Thèse, 3 eme Cycle, Univ. de Paris.*

ROBERTSON, A.H.F., CLIFT, P.D., DEGNAN, P.J., & JONES, G., 1991. Palaeogeographic and palaeotectonic evolution of the Eastern Mediterranean Neotethys. *Palaeogeo. Palaeoclim. Palaeoecol.*, 87. p289-343.

ROBERTSON, A.H.F., & DIXON, J.E., 1984. Introduction: Aspects of the geological evolution of the Eastern Mediterranean. In: Dixon, J.E., & Robertson, A.H.F., (eds). *The Geological Evolution of the Eastern Mediterranean. Geol. Soc. Lond. Spec. Publ.*, 17. p1-74.

ROBIN, P.-Y.F., 1979. Theory of metamorphic segregation and related processes. *Geochim. Cosmochim. Acta*, 43. p1587-1600.

RODDICK, J.C., CAMERON, N.E., & SMITH, A.G., 1979. Permo-Triassic $^{40}Ar/^{39}Ar$ ages from Greek ophiolites and associated rocks. *Nature*, 279. p788-790.

RODDICK, J.C., CLIFF, R.D., & REX, D.C., 1980. The evolution of excess argon in Alpine biotites - a $^{40}Ar/^{39}Ar$ analysis. *Earth Planet. Sci. Lett.*, 48. p185-208.

RODGERS, D.A., 1980. Analysis of pull-apart basin development produced by en echelon strike-slip faults. *Spec. Publ. Int. Assoc. Sed.*, 4. p27-41.

RON, H., NUR, A., & HOFSTETTER, A., 1990. Late Cenozoic and Recent strike-slip tectonics in Mt. Carmel Northern Israel. *Annales Tectonicae*, 4. p70-80.

ROUSOS, N., & LYSSIMACHOU, T., 1988. An active deformation in the North Aegean. *BSRG/TSG meeting on the Structural and Sedimentary Evolution of the Aegean Basins (abstract).*

ROYDEN, L.H., HORVATH, F., & BURCHFIEL, B.C., 1982. Transform faulting, extension, and subduction in the Carpathian Pannonian region. *Geol. Soc. Am. Bull.*, 93. p717-725.

SAKELLARIOU, D.Th., 1988. Deformation and metamorphism of the Serbo-Madcedonian Massif in N.E. Chalkidiki (Northern Greece): *Abstract Unpubl. Ph.D Thesis Univ. Maniz.*

SAKELLARIOU, D.Th., 1990. Deformation and metamorphism of the Serbo-Madcedonian Massif in N.E. Chalkidiki (Northern Greece): *Unpubl. Ph.D Thesis Univ. of Mainz.*

SANDERSON, D.J., & MARCHINI, W.R.D., 1984. Transpression. *J. Struc. Geol.*, 6. p449-458.

SANDIFORD, M., 1989a. Horizontal structures in granulite terrains: a record of mountain building or mountain collapse? *Geology*, 17. p449-452.

SANDIFORD, M., 1989b. Secular trends in the thermal evolution of metamorphic terrains. *Earth Planet. Sci. Lett.*, 95. p85-96.

SANDIFORD, M., & POWELL, R., 1986. Deep crustal metamorphism during continental extension: modern and ancient examples. *Earth Planet. Sci. Lett.*, 79. p151-158.

SANDIFORD, M., & POWELL, R., 1990. Some isostatic and thermal consequences of the vertical strain geometry in convergent orogens. *Earth Planet. Sci. Lett.*, 98. p154-165.

SANDIFORD, M., & POWELL, R., 1991. Some remarks on high-temperature - low-pressure metamorphism in convergent orogens. *J. Met. Geol.*, 9. p333-340.

SAPOUNTZIS, E., KASSOLI-FOURNARAKI, A., & CHRISTOFIDES, G., 1990. Amphibolites from the Serbo-Macedonian Massif (northern Greece). *Geologica Balcanica*, 20. p3-17.

SAPOUNTZIS, I.S., 1969. Petrographische und geologische Stellung der grunen Gneise von Thessaloniki. *Unpubl. PhD. Thesis Univ. Thessaloniki.*

SAPOUNTZIS, I.S., 1980. On the age of the ophiolitic sequences in the southwestern part to the Axios (Vardar) Zone (North greece). *N. Jb. Mineral. Abh.*, 138. p39-48.

SAXENA, S.K., & ERIKSSON, G., 1985. Anhydrous phase equilibria in Earth's upper mantle. *J. Petrol.*, 26. p378-390.

SCHENK, P.F., 1970. Geologie des westlichen Pangaion in Griechischen - Ost-Makedonien (Geology of west Pangaion in Greek East Macedonia). *Beih. Geol. Jb.*, 88. p81-132.

SCHERMER, E.R., HOWELL, D.G., & JONES, D.L., 1984. The origin of allochthonous terranes: perspectives on the growth and shaping of continents. *Ann. Rev. Earth Planet. Sci.*, 12. p107-131.

SCHIFFMANN, P., & LIOU, J.G., 1980. Synthesis and stability relations of Mg-Al pumpellyite, $Ca_4Al_5MgSi_6O_{21}(OH)_7$. *J. Petrol.*, 21. p441-474.

SCHIFFMANN, P., & LIOU, J.G., 1983. Synthesis of pumpellyite and its stability relations with epidote. *J. Met. Geol.*, 1. p91-101.

SCHONEVELD, C., 1977. A study of some typical inclusion patterns in strongly paracrystalline rotated garnets. *Tectonophysics*, 39. p453-471.

SCHUMACHER, R., SCHENK, V., RAASE, P., & VITANAGE, P.W., 1990. Granulite facies metamorphism of metabasic and intermediate rocks in the Highland series of Sri Lanka. In: Ashworth, J.R., & Brown, M., (eds). *High-temperature Metamorphism and Crustal Anatexis.* London: Unwin Hyman Ltd. p235-271.

SCHUNEMANN, M., 1985. Contributions to the geology, geochemistry and tectonics of the Chortiatis Series metamorphic calc-alkaline suite, Chalkidiki, Northern Greece. *Diss. Hamburg.*

SCOTT, J.S., & DREVER, H.I., 1953. Frictional fusion along a Himalayan thrust. *Proc. R. Soc. Edinb., Ser. B.*, 65. p121-40.

SELVERSTONE, J., MORTEANI, G., & STAUDE, J.-M., 1991. Fluid channelling during ductile shearing: transformation of granodiorite into aluminous schist in the Tauern window, Eastern Alps. *J. Met. Geol.*, 9. p419-431.

SENGOR, A.M.C., 1984. The Cimmeride orogenic system and the tectonics of Eurasia. *Geol. Soc. Am. Spec. Paper*, 195. pp65

SENGOR, A.M.C., YILMAZ, Y., & KETIN, I., 1980. Remnants of a pre-Late Jurassic ocean in northern Turkey: fragments of Permian-Triassic Palaeo-Tethys? *Bull. Geol. Soc. Am.*, 91. p599-609.

SENGOR, A.M.C., YILMAZ, Y., & SUNGURLU, O., 1984. Tectonics of the Mediterranean Cimmerides: nature and evolution of the western termination of Palaeo-tethys. In: Dixon, J.E., & Robertson A.H.F., (eds). *The Geological Evolution of the Eastern Mediterranean. Spec. Publ. Geol. Soc. Lond.*, 17. p77-112.

SERVAS, S., 1975. Age detremination by the ^{87}Rb-^{87}Sr method of some pegmatites in the area of Langadha (Macedonia, Greece). *Ann. géol. Pays. Hell.*, 27. p143-153.

SHARRY, J., LANGAN, R.T., JOVANOVICH, D.B., JONES, G.M., HILL, N.R., & GUIGISH, T.M., 1986. Enhanced imaging of the COCORP seismic line, Wind River Mountains. *Am. Geophys. Union Geodyn. Ser.*, 13. p223-236.

SIBSON, R.H., 1975. Generation of pseudotachylyte by ancient seismic faulting. *Geophys. J. Royal. Astr. Soc.*, 43. p775-94.

SIBSON, R.H., 1977. Fault rocks and fault mechanisms. *J. Geol. Soc. Lond.*, 133. p191-213.

SIBSON, R.H., 1983. Continental fault structure and the shallow earthquake source. *J. Geol. Soc. Lond.*, 140. p741-767.

SIBSON, R.H., ROBERT, F., & POULSON, K.H., 1988. High-angle reverse faults, fluid-pressure cycling and mesothermal gold-quartz deposits. *Geology*, 16. p551-555.

SIDIROPOULOS, N., 1991. Lithology, geochemistry, tectonism and metamorphism of the NW part of the Vertiskos Group. The area of Disors Mountain (Kroussia), west of Kilkis. *Unpubl. PhD. Thesis Univ. of Thessaloniki.* (In Greek with an English abstract).

SIDIROPOULOS, N., & DIMITRIADIS, S., 1989. Extension and melting of continental crust during intracontinental emplacement of the Guevgueli ophiolite, eastern Vardar Zone. *Abstracts, Terra EUG V.* p57.

SIMPSON, C., 1982. Strain and shape fabric variations associated with ductile shear zones. *J. Struc. Geol.*, 5. p61-72.

SIMPSON, C., & WINTSCH, R.P., 1989. Evidence for deformation-induced K-feldspar replacement by myrmekite. *J. Met. Geol.*, 7. p261-275.

SMITH, A.G., 1971. Alpine deformation and the oceanic areas of the Tethys, Mediterranean and Atlantic. *Bull. Geol. Soc. Am.*, 82. p2039-2070.

SMITH, A.G., & BRIDEN, J.C., 1977. *Mesozoic and Cenozoic Paleocontinental Maps.* Camb. Univ. Press. pp63.

SMITH, A.G., HYNES, A.J., MENZIES, M., NISBET, E.G., PRICE, I., WELLAND, M.J., & FERRIERE, J., 1975. The stratigraphy of the Othris Mountains, eastern central Greece: a deformed Mesozoic continental margin sequence. *Eclog. Géol. Helv.*, 68. p463-481.

SMITH, A,G., & MOORES, E.M., 1974. The Hellenides. In: Spencer, A.M., (ed). *Mesozoic and Cenozoic Orogenic belts. Geol. Soc. Spec. Publ. Lond.*, 4. p159-186.

SMITH, A.G., & SPRAY, J.G., 1984. A half-ridge transform model for the Hellenic-Dinaric ophiolites. In: Dixon, J.E., & Robertson, A.H.F., (eds). *The Geological Evolution of the Eastern Mediterranean. Spec. Publ. Geol. Soc. Lond.*, 17. p629-644.

SMITH, A.G., & WOODCOCK, N.H., 1982. Tectonic synthesis of the Alpine-Mediterranean region: a review. In: Berkheimer, H., *et al.*, (eds). *Alpine-Mediterranean geodynamics. Geodynamics Series*, 7. p15-38.

SMITH, A.G., WOODCOCK, N.H., & NAYLOR, M.A., 1979. The structural evolution of a Mesozoic continental margin. *J. Geol. Soc. Lond.*, 136. p589-603.

SMITH, R.B., & BRUHN, R.L., 1984. Intraplate extensional tectonics of the eastern Basin-range: Inferences on structural style from seismic reflection data, regional tectonics and thermal-mechanical models of brittle/ductile deformation. *J. Geophys. Res.*, 89. p5733-5762.

SMITH, R.E., & SMITH, S.E., 1976. Comments on the use of Ti, Zr, Y, Sr, K, P and Nb in classification of basaltic magmas. *Earth Planet. Sci. Lett.*, 32. p114-120.

SOLDATOS, K.T., & CHRISTOFIDES, G., 1986. Rb-Sr geochronology and origin of the Elatia pluton, central Rhodope, North Greece. *Geologica Balcanica*, 16. p15-23.

SONDER, L.J., ENGLAND, P.C., WERNICKE, B.P., & CHRISTIANSEN, R.L., 1987. A physical model for Cenozoic extension of western North America. In: Coward, M.P., Dewey, J.F., & Hancock, P.L., (eds). *Continental Extensional Tectonics. Geol. Soc. Spec. Publ. Lond.*, 28. p449-452.

SOPTRAJANOVA, G., 1967. Pers. comm. in Spray *et al.*, 1984.

SPEAR, F.S., 1980. NaSi = CaAl exchange equilibrium between plagioclase and amphibole. An empirical model. *Contrib. Mineral. Petrol.*, 72. p33-41.

SPEAR, F.S., & SELVERSTONE, J., 1983. Quantitative P-T paths from zoned minerals: theory and tectonic applications. *Contrib. Mineral Petrol.*, 83. p348-357.

SPEAR, F.S., & SELVERSTONE, J., HICKMOTT, D., CROWLEY, P., & HODGES, K.V., 1984. P-T paths from garnet zoning: a new technique for deciphering tectonic processes in crystalline terranes. *Geology*, 12. p87-90.

SPRAY, J.G., & RODDICK, J.C., 1980. Petrology and $^{40}Ar/^{39}Ar$ geochronology of some Hellenic subophiolitic metamorphic rocks. *Contrib. Mineral. Petrol.*, 72. p43-55.

SPRAY, J.G., BEBIEN, J., REX, D.C., & RODDICK, J.C., 1984. Age constraints on the igneous and metamorphic evolution of the Hellenic-Dinaric ophiolites. In: Dixon, J.E., & Robertson, A.H.F., (eds). *The Geological Evolution of the Eastern Mediterranean. Spec. Publ. Geol. Soc. Lond.*, 17. p619-627.

SPRY, A., 1969. *Metamorphic Textures.* Pergamon Press Ltd., Oxford.

STEIGER, R.H., & JAGER, E., 1977. Subcommission on geochronology convention on the use of decay constants in geo- and cosmochronology. *Earth Planet. Sci. Lett.*, 36. p359-362.

SUN, S.-S., & NESBITT, R. W., 1977. Chemical heterogeneiity of the Archaean mantle, composition of the earth and mantle evolution. *Earth Planet. Sci. Lett.*, 35. p429.

SYLVESTER, A.G., 1988. Strike-slip faults. *Bull. Geol. Soc. Am.*, 100. p1666-1703.

SYLVESTER, A.G., & SMITH, R.R., 1976. Tectonic transpression and basement-controlled deformation in the San Andreas fault zone, Salton Trough, California. *Am. Assoc. Petrol. Geol. Bull.*, 60. p2081-2102.

TARNEY, J., SAUNDERS, A.D., & WEAVER, S.D., 1977. Geochemistry of volcanic rocks from the island arcs and marginal basins of the Scotia Arc Region. In: Talwani, M., & Pitman III, W.C., (eds). *Island arcs, deep-sea trenches and back-arc basins.* American Geophysical Union, Washington D.C., p367-377.

TAPPONIER, P., MERCIER, J.L., ARMIJO, R., Han TONGLIN., & ZHOU, JI., 1981. Field evidence for active normal faulting in Tibet. *Nature,* 294. p410-414.

TAPPONIER, P., PELTZER, G., Le DAIN, A.Y., ARMIJO, R., & COBBOLD, P., 1982. Propagating extension tectonics in Asia: New insights from simple experiments in plasticene. *Geology,* 10. p611-616.

TAYLOR, S.R., & WHITE, A.J.R., 1966. Trace element abundances in andesites. *Bull. Volc.,* 29. p177-194.

TCHALENKO, J.S., & AMBRASEYS, N.N., 1970. Structural analysis of the Dasht-e Bayaz (Iran) earthquake fractures. *Geol. Soc. Am. Bull.,* 81. p41-60.

THIRLWALL, M.F., & JONES, N.W., 1983. Isotope geochemistry and contamination mechanics of Tertiary lavas from Skye, Northwest Scotland. In: Hawkesworth, C.J., & Norry, M.J., (eds). *Continental Basalts and Mantle Xenoliths.* Nantwich: Shiva Publications. p186-208.

THOMPSON, A.B., 1982. Dehydration melting of pelitic rocks and the generation of H_2O undersaturated granitic liqiuds. *Am J. Sci.,* 282. p1567-1595.

THOMPSON, A.B., & ENGLAND, P.C., 1984. Pressure-temperature-time paths of regional metamorphism II. Their inference and interpretation using assemblages in metamorphic rocks. *J. Petrol.,* 25. p929-955.

THOMPSON, A.B., & TRACEY, R.J., 1979. Model systems for anatexis of pelitic rocks, II. Facies series melting and reactions in the system $CaO\text{-}KAlO_2\text{-}NaAlO_2\text{-}Al_2O_3\text{-}SiO_2\text{-}H_2O$. *Contrib. Mineral. Petrol.,* 70. p429-438.

THOMPSON, G., 1973. A geochemical study of the low-temperature interaction of sea-water and oceanic in igneous rocks. *Trans. Am. Geophys. Union,* 54. p1015.

THOMPSON, J.B., 1955. The thermodynamic basis for the mineral facies concept. *Am. J. Sci.,* 753. p65-103.

THOMPSON, R.N., DICKIN, A.P., GIBSON, I.L., & MORRISON, M.A., 1982. Elemental fingerprints of isotopic contamination of Hebridean Palaeocene mantle-derived magmas by Archaean sial. *Contrib. Mineral. Petrol.,* 79. p159-68.

THUIZAT, R., WHITECHURCH, H., MONTIGNY, R., & JUTEAU, T., 1981. K/Ar dating of some intra-ophiolitic metamorphic soles from the Eastern Mediterranean: new evidence from oceanic thrustings before obduction. *Earth Planet. Sci. Lett.,* 52. p302-310.

TINDLE, A.G., & PEARCE, J.A., 1983. Assimilation and partial melting of continental crust: evidence from the mineralogy and geochemistry of autoliths and xenoliths. *Lithos,* 16. p185-202.

TOBISCH, O.T., & PATERSON, S.R., 1988. Analysis and interpretation of composite foliations in areas of progressive deformation. *J. Struc. Geol.,* 10. p745-754.

TULLIS, J.A., SNOKE, A.W., & TODD, V.R., 1982. Penrose Conference report: significance and petrogenesis of mylonitic rocks. *Geology,* 10. p227-230.

TURNER, F.J., & WEISS, L.E., 1963. *Structural Analysis of Metamorphic Tectonites.* McGraw-hill, New York.

TURNER, S.P., & STUWE, K., 1992. Low-pressure corona textures between olivine and plagioclase in unmetamorphosed gabbros from Black Hill, South Australia. *Min. Mag.,* 56. p503-511.

TUTTLE, O.F., & BOWEN, N.L., 1958. Origin of granite in light of experimental studies. *Geol. Soc. Am. Memoir,* 74.

Van de KAMP, P.C., 1969. Origin of amphibolites in the Beartooth Mountains, Wyoming and Montana: new data and interpretation. *Geol. Soc. Am. Bull.,* 81. p1127-1136.

Van LAMOEN, H., 1979. Coronas in olivine gabbros and iron ores from Susimaki and Riuttamaa, Finland. *Contrib. Mineral. Petrol.,* 68. p259-268.

VEILZEUF, D., CLEMENS, J.D., PIN, C., & MOINET, E., 1990. Granites, granulites and crustal differentiation. In: Vielzeuf, D., & Vidal, Ph. (eds). *Granulites and Crustal evolution.* Dordrecht: Kluwer Academic Publishers. p59-85.

VERGELY, P., 1976. Chevauchement vers l'Ouest et rétrocharriage vers l'Est des ophiolites: deux phases tectoniques au cours du Jurassique supéreur-Éocrétacé dans les Hellénides Internes. *Bull. Soc. géol. France,* 7. p233-246.

VERGELY, P., 1977. Discussion of the paleogeographic significance of rocks beneath the Vourinos ophiolite, Northern Greece. *J. Geol. Soc. Lond.,* 133. p505-507.

VERGELY, P., 1984. Tectoniques des ophiolites dans les Héllénides internes. Conséquences sur l'évolution des régions Téthysiennes occidentales. *Unpubl. PhD. Thesis Univ. Paris-sud, Orsay.*

VERNON, R.H., 1974. Controls of mylonitic compositional layering during non-cataclastic ductile deformation. *Geol. Mag.*, 111. p121-123.

VERNON, R.H., & FLOOD, R.H., 1988. Contrasting deformation of S- and I-type granitoids in the Lachlan fold belt, eastern Australia. *Tectonophysics*, 147. p127-143.

VERNON, R.H., WILLIAMS, V.A., & D'ARCY, W.F., 1983. Grain size reduction and foliation development in a deformed granite batholitih. *Tectonophysics*, 92. p123-146.

VOCKE, R.D.Jr., HANSON, G.N., & GRUNENFELDER, M., 1987. Rare earth element mobility in the Roffna Gneiss, Switzerland. *Contrib. Mineral. Petrol.*, 95. p145-154.

VOGEL, D.E., 1975. Precambrian weathering in acid metavolcanic rocks from the Superior Province, Villebon Township, South-Central Quebec. *Can. J. Earth Sci.*, 12. p2080-2085.

WAKEFIELD, J., 1977. Mylonitization in the Lethakane shear zone, eastern Botswana. *J. Geol. Soc. Lond.*, 133. p262-275.

WATERS, D.J., 1986. Metamorphic history of sapphirine-bearing and related magnesian gneisses from Namaqualand, South Africa. *J. Petrol.*, 27. p541-565.

WATTERSON, J., 1975. Mechanism for the persistence of tectonic lineaments. *Nature*, 253. p520-521.

WATTS, M.J., & WILLIAMS, G.D., 1979. Fault rocks as indicators of progressive shear deformation in the Guingamp region of Brittany. *J. Struc. Geol.*, 1. p323-332.

WELLS, P.R.A., 1980. Thermal models for the magmatic accretion and subsequent metamorphism of continental crust. *Earth Planet. Sci. Lett.*, 46. p253-265.

WEGENER, A., 1924. *The origin of continents and oceans.* Methuen, Lond., 212pp. (English translation of third German edition, 1922).

WENK, H.R., 1978. Are pseudotachylites products of fracture or fusion? *Geology*, 6. p507-511.

WERNICKE, B., 1981. Low-angle normal faults in the Basin and Range Province: Nappe tectonics in an extending orogen. *Nature*, 291. p645-648.

WERNICKE, B., 1985. Uniform-sense normal simple shear of the continental lithosphere. *Can. J. Earth Sci.*, 22. p108-125.

WHITE, S.H., 1975. Tectonic deformation and recrystallisation of plagioclase. *Contrib. Mineral. Petrol.*, 50. p287-304.

WHITE, S.H., 1976. The effects of strain on the microstructures, fabrics and deformation mechanisms in quartzite. *Phil. Trans. R. Soc. Lond., Ser A*, 283. p69-86.

WHITE, S.H., 1977. Geological significance of recovery and recrystallisation processes in quartz. In: Lister, G.S., Williams, P.F., Weber, K., & Zwart, H.J., (eds). *The Effect of Deformation on Rocks. Tectonophysics*, 39. p143-170

WHITE, S.H., BURROWS, S.E., CARRERAS, J., SHAW, N.D., & HUMPHREYS, F.J., 1980. On mylonites in ductile shear zones. *J. Struc. Geol.*, 2. p175-187.

WHITNEY, P.R., & McLELLAND, J.M., 1973. Origin of coronas in metagabbros of the Adirondack Mts., N.Y. *Contrib. Mineral. Petrol.*, 39. p81-98.

WICKHAM, S.M., & OXBURGH, E.R., 1985. Continental rifts as a setting for regional metamorphism. *Nature*, 318. p330-333.

WILCOX, R.E., HARDING, T.P., & SEELY, D.R., 1973. Basic wrench tectonics. *Am. Assoc. Petrol. Geol. Bull.*, 57. p74-96.

WILLIAMS, P.F., 1985. Multiply deformed terrains - problems of correlation. *J. Struc. Geol.*, 7. p269-280.

WILLIAMS, P.F., & COMPAGNONI, R., 1983. Deformation and metamorphism in the Bard area of the Seisia Lanzo zone, western Alps, during subduction and uplift. *J. Met. Geol.*, 1. p117-140.

WILLIAMS, P.F., & SCHONEVELD, C., 1981. Garnet rotation and the development of axial plane crenulation cleavage. *Tectonophysics*, 78. p307-334.

WILLIAMS, P.F., & ZWART, H.J., 1977. A model for the development of the Seve-Koli Caledonian nappe complex. In: Saxena, S.K., & Bhattacharji, S. (eds). *Energetics of Geological Processes.* Springer, New York. p169-187.

WILSON, M.R., 1971. On syntectonic porphyroblast growth. *Tectonophysics,* 11. p239-260.

WINCHESTER, J.A., & FLOYD, P.A., 1976. Geochemical magma type discriminations: application to altered and metamorphosed basic igneous rocks. *Earth Planet. Sci. Lett.,* 28. p459-469.

WINCHESTER, J.A., & FLOYD, P.A., 1977. Geochemical discrimination of different magma series and their differentiation products using immobile elements. *Chem. Geol.,* 20. p325-343.

WINCHESTER, J.A., & MAX, M.D., 1984. Element mobility associated with syn-metamorphic shear zones near Scotchport, NW Mayo, Ireland. *J. Met. Geol.,* 2. p1-11.

WINKLER, H.G.F., 1979. *Petrogenesis of Metamorphic Rocks.* Springer-Verlag, New York. 348pp.

WISE, D.U., DUNN, D.E., ENGELDER, J.T., GEISER, P.A., HATCHER, R.D., KISH, S.A., ODOM, A.L., & SCHAMEL, S., 1984. Fault rocks: Suggestions for terminology. *Geology,* 12. p391-394.

WOODCOCK, N.H., 1986. The role of the strike-slip fault systems at plate boundaries. *Phil. Trans. R. Soc. Lond., Ser. A.,* 317. p13-29.

WOODCOCK, N.H., & FISCHER, M., 1986. Strike-slip duplexes. *J. Struc. Geol.,* 8. p725-735.

WU, F.T., BLATTER, L., & ROBERTSON, H., 1975. Clay gouges in the San Andreas Fault System and their possible implication. *Pageophysics,* 113. p87-95.

YARDLEY, B.W.D., 1981. A note on the composition and stability of Fe-staurolite. *N. Jb. Min.,* 1981. p127-132.

YARDLEY, B.W.D., 1989. *An Introduction to Metamorphic Petrology.* Longman Scientific and Technical: Harlow. 248pp.

YARDLEY, B.W.D., MacKENZIE, W.S., & GUILDFORD, C., 1990. *Atlas of Metamorphic Rocks and Textures.* Longman: John Wiley & Sons Inc., New York.

YARWOOD, G.A., & AFTALION, M., 1976. Field relations and U-Pb geochronology of a granite from the Pelagonian Zone of the Hellenides (High Pieria, Greece). *Bull. Soc. géol. France,* 7. p259-264.

YARWOOD, G.A., & DIXON, J.E., 1979. Lower Cretaceous and younger thrusting in the Pelagonian rocks of the High Pieria, Greece. *Vth Colloq. Reg. Egeenes,* (Athens, 1977). p269-280.

YODER, H.S., & TILLEY, C.E., 1962. Origin of basaltic magmas: an experimental study of natural and synthetic rock systems. *J. Petrol.,* 3. p342.

ZAGORCHEV, I.S., 1974. On the Precambrian Tectonics of Bulgaria. *Precamb. Res.,* 1. p139-156.

ZAGORCHEV, I., & MOORBATH, S., 1986. Problems of the metamorphism in the central Rhodope mountains in the light of Rb-Sr isotope data: *Geologica Balcanica,* 16. p61-78 (in Russian).

ZECK, H.P., 1974. Cataclasites, hemiclasites, holoclasites, blasto-ditto and myloblastites-cataclastitic rocks. *Am. J. Sci.,* 274. p1064-1073.

ZEN, E-an., 1966. Construction of pressure-temperature diagrams for multi-component systems after the method of Schreinemakers - a geometrical approach. *U.S. Geol. Surv. Bull.,* 1225.

APPENDIX I

GEOCHEMICAL ANALYSES USING X-RAY FLUORESCENCE TECHNIQUES

Whole rock geochemical analysis was undertaken on a range of samples, representing basic and acidic intrusives and probable intrusives from the Lake Volvi region, N.E. Greece. The main data set concentrated on a suite of basic dykes and amphibolites, and an acidic suite of granites and associated gneisses. The basic data set has subsequently been compared to that of Dixon and Dimitriadis (pers. comm.), which was based predominantly on samples from within the main body of the Volvi Complex and also a number of samples from the country rock. The locations of samples analysed during this study can be found on the Inserts, Maps B to H.

Major and trace element data from the initial 1988 field season were analysed on a Philips PW 1450/20 (Rh-tube) sequential automatic X-ray spectrometer. However, major and trace element data analysed after the 1989 and 1990 field seasons were analysed using separate machines. Major elements were analysed on a new Philips PW 1480 (Cr-tube) spectrometer, while the trace elements were analysed on the original Philips PW 1450/20 (W-tube) spectrometer.

Major elements were analysed from fused glass discs. These were prepared by the addition of a measured quantity of Lithium flux (Johnson-Mathey Spectroflux) and ignited to 1100°C, following the method of Fitton and Dunlop (1985), itself based on the original procedure of Norrish and Hutton (1969). Trace elements were determined from pressed powder pellets.

In order to process the data it was necessary for interference and matrix corrections to be applied. Interference corrections were calculated from a range of synthetic in-house glass standards, and matrix corrections were calculated for every sample from major element analyses (for accuracy see Fitton and Dunlop, 1985). Both the major and trace element analyses were calibrated using USGS and CRPG International standards (as recommended by Abbey, 1980).

To assess the consistency of the methods and techniques used in processing the discs for analyses, a standard sample from the area was prepared six times and analysed for both major and trace elements. The mean and standard deviations are shown in Table A1. Tables A2 and A3 show the normalising values which have been used for producing multi-element diagrams during the course of this study.

Table A1: Mean and Standard deviation of six analyses, Sample: VAM 19B. To show the degree of error which is incured during the preparation of both fused glass discs (major elements), and pressed powder pellets (trace elements).

	X		1σ
SiO_2	53.11	±	0.38
Al_2O_3	15.59	±	0.12
Fe_2O_3	9.34	±	0.08
MgO	6.68	±	0.06
CaO	8.75	±	0.05
Na_2O	2.88	±	0.02
K_2O	1.04	±	0.007
TiO_2	1.62	±	0.02
MnO	0.17	±	0.005
P_2O_5	0.28	±	0.004
L.O.I.	0.76	±	0.12
TOTAL.	99.47	±	0.7
V	264.83	±	0.9
Ba	171.33	±	6.87
Sc	49.17	±	1.07
La	11.5	±	0.76
Nd	17.67	±	0.94
Ce	32.83	±	1.46
Cr	326	±	6.98
Ni	39.5	±	1.61
Cu	16	±	1
Zn	131.33	±	0.94
Pb	10.5	±	0.76
Th	3.5	±	0.76
Rb	18.67	±	0.47
Sr	171.5	±	0.76
Y	33.17	±	0.37
Zr	169.17	±	5.3
Nb	10.67	±	0.75

Table A2: MORB normalising values for use on multi-element diagrams. Values from Pearce, (1980, 1983); Kostopoulos, (1989); * Tarney (1977).

Ba	÷	20 ppm	Zr	÷	90 ppm	(Hf	÷	2.4 ppm)
Sr	÷	120 ppm	(Sm	÷	3.3 ppm)	TiO_2	÷	1.5 wt %
K_2O	÷	0.15 wt %	Y	÷	30 ppm	(Yb	÷	3.4 ppm)
Rb	÷	2 ppm	Sc	÷	40 ppm	Cr	÷	250 ppm
Th	÷	0.2 ppm	La	÷	3 ppm.*	Ni	÷	138 ppm *
Nd	÷	8 ppm	(Ta	÷	0.18 ppm.	Nb	÷	3.5 ppm
Ce	÷	10 ppm	P_2O_5.	÷	0.12 wt %			

Table A3: ORG normalising values for use on multi-element diagrams, after Pearce *et al.*, (1984).

K_2O	÷	0.1 wt %	Y	÷	30 ppm	(Yb	÷	3.4 ppm)
Ce	÷	10 ppm	Zr	÷	90 ppm	(Hf	÷	2.4 ppm)
Rb	÷	1.0 ppm	Ba	÷	12.5 ppm	Th	÷	0.2 ppm
Nd	÷	3 ppm	(Sm	÷	3.3 ppm)	(Ta	÷	0.2 ppm)

Amphibolites (filled squares)

	ASK 1	ASK 1A	ASK 2	ASK 9A	ASK 11	ASK 11A	ASK 11B	ASK 11C	ASK11D	ASK 13	ASK 18A	ASK 18B	EAF 9A	EAF 9B	EAF 9C	EAF 9D	EAF 19A	EAF 19B
SiO2	54.28	59.36	54.48	50.12	49.86	59.44	49.9	51.54	50.85	55.37	57.89	52.2	46.92	49.66	51.32	48.72	56.61	50.39
Al2O3	15.49	15.16	14.61	15.74	16.51	15.4	13.78	16.27	15.44	14.94	15.04	15.82	14.33	15.81	16.04	16.1	15.9	16.54
Fe2O3	8.86	3.6	7.93	9.73	9.18	6.21	9.97	8.62	11.03	10.46	8.79	11.26	12.9	10.85	9.28	10.7	4.84	11.29
MgO	6.44	5.44	8.53	7	8.39	5.73	11.53	7.86	7.24	5.04	4.94	6.31	11.04	8.62	6.58	7.67	7.25	5.17
CaO	7.9	10.41	7.35	8.45	9.26	6.26	10.18	9.21	7.41	6.17	5.66	7.19	10.4	9.02	9.62	10.13	8.3	7.39
Na2O	3.02	3.56	2.83	2.37	2.06	5.24	3.17	4.24	3.87	3.7	2.94	2.75	1.82	3.1	3.75	3.27	4.55	4.17
K2O	1.35	0.2	1.93	2.69	1.58	0.29	0.56	0.57	0.42	1.11	1.57	1.23	0.5	0.3	0.51	0.44	0.8	1.49
TiO2	1.38	1.28	1.17	1.52	1.2	0.85	0.93	1.25	1.63	2.01	1.53	2.06	1.33	1.5	1.9	1.82	0.79	2.09
MnO	0.13	0.04	0.09	0.17	0.15	0.11	0.2	0.16	0.19	0.18	0.1	0.14	0.2	0.16	0.16	0.18	0.07	0.21
P2O5	0.15	0.14	0.13	0.25	0.13	0.1	0.03	0.15	0.18	0.36	0.26	0.39	0.08	0.18	0.24	0.29	0.09	0.4
L.O.I.	1.24	0.9	1.23	1.74	1.96	0.6	0.7	0.82	1.73	1	1.37	1.3	1.21	1.14	1.01	1.25	0.86	1.48
Total	100.2	100.09	100.3	99.78	100.28	100.23	100.95	100.69	99.99	100.34	100.09	100.65	100.73	100.34	100.41	100.57	100.06	100.62
V	214.3	168.3	179	238.7	202.1	144.3	193.5	207.3	272.5	243.4	217.3	297.4	287.2	280.4	286.6	269.4	137.6	247.8
Ba	173.9	58.9	137.4	385	204.1	33.3	27.5	85.1	35.8	300.7	283	222.8	51.3	30.8	36.4	65.1	85.5	211.2
Sc	38.6	31.7	38.8	39.5	37.4	30	28	38.9	47.5	46	33.5	47.4	51.9	46.2	54.2	40.8	31.3	46.1
La	13.3	12.5	7	10.7	2.8	12.2	5.7	6.3	8.9	21.1	19.5	18.5	4.7	2.7	9.5	6.3	12.1	28.9
Nd	13.4	26.2	10.3	18.5	10.7	14.7	6.6	14.9	12.7	31.6	30.1	31.7	7.9	10.4	19	14.1	14.8	37.4
Ce	24.3	46.9	12.4	29.3	15.5	36	12.5	25.7	20.2	54.5	57	59.6	15.8	15.8	30.5	18.2	29.5	66
Cr	151.1	133	271	239	284.2	189.9	214.7	248.1	108.7	177.4	179.6	235.7	318.3	353.9	620.8	222.6	236	168.7
Ni	45.7	30.7	81.5	64.9	87	67.7	54.3	74.2	45.1	43.1	56.5	60.5	112.4	116	67.5	91.9	98	39.3
Cu	11.3	-2.1	-1.7	13.2	42.7	-0.9	-0.8	18.7	-0.2	0.5	4.5	-0.7	-1.5	56.2	12.3	52.5	-0.8	21
Zn	60.6	11.8	35.2	83.1	79	46.5	138.7	92.3	67.1	86.8	68.3	87.5	105.5	81.2	66.6	82.1	30.7	109.5
Pb	2.8	4.9	0	5.9	4.8	6.4	6.2	7.6	2.7	4.8	5.5	5.4	0	3.3	4.4	5.2	2.4	9.4
Th	5.7	2.9	2.9	2.2	1.8	13.8	5	3.7	0.7	6.3	12	6	-0.4	-1.8	0.5	-1	6.2	6.8
Rb	69.3	4.5	135.6	115.7	64.9	8.4	16.5	13.3	12	39.1	54.8	41.7	14.1	5.2	16.2	14.2	37.2	58.5
Sr	179.5	274.3	207.3	190.9	172.2	177.7	154.3	216.3	163	215.7	202.7	189.4	126.5	308	417.2	377.1	214.9	270.2
Y	32.9	32.9	32.6	34.4	26.1	26.1	24.1	27.6	32.3	53.8	41.6	50.9	30.2	30.9	44.1	32.5	24.8	68
Zr	133.8	132.9	100.5	151.8	104.9	109.2	106.2	120.5	127	329.5	153.9	172.1	109.5	126.2	265.1	149.1	88.4	412.1
Nb	7.5	7.9	6.4	8.2	5.6	7.7	6.4	6.2	6.8	13.1	19	25.6	4.9	5.2	8.2	5.7	6.4	18.8

Dykes (open squares)

	ASK 7	ASK 7B	ASK 8	ASK15	ASK18A	ASK 21C	ASK 21E	ASK 28	ASK29C	ASK 29 D	ASK 33	ASK 33A	ASK34	ASK40	ASK 41C	L 33	L 45	L48	L 53	L 76
SiO2	48.25	48.70	51.04	55.99	57.89	47.75	48.43	51.03	53.07	49.6	52.77	52.4	54.04	49.76	51.78	49.18	49.07	47.97	47.15	46.87
Al2O3	14.5	16.52	16.10	14.62	15.04	16.67	16.27	14.21	14.24	15.01	14.68	14.75	14.22	14.63	14.52	17.17	16.05	16.54	16.99	16.09
Fe2O3	13.54	10.36	9.42	10	8.79	9.43	10.28	13.86	13.11	11.4	13.61	13.42	13.8	15.14	12.84	8.87	10.94	12.75	11.70	12.52
MgO	6.49	8.99	7.51	4.97	4.94	9.27	8.26	5.2	4.42	7.48	5.46	5.51	4.65	4.41	5.46	8.62	6.97	7.29	7.28	9.22
CaO	7.82	8.12	7.43	6.12	5.66	10.02	10.08	6.34	6.38	8.44	7.1	6.74	5.13	6.95	6.56	10.36	9.43	9.06	9.48	9.04
Na2O	0.18	3.07	2.82	3.24	2.94	2.61	3.05	3.04	3.3	3.39	2.9	2.72	2.62	3.62	2.61	3.20	3.23	2.43	2.87	2.15
K2O	1.24	1.00	2.37	1.03	1.57	1.30	0.57	0.60	0.86	0.56	0.43	0.35	0.3	0.62	0.96	0.33	0.95	0.41	0.85	0.58
TiO2	2.67	1.41	1.49	1.88	1.53	1.36	1.57	2.90	2.92	2.02	2.79	2.81	3.13	3.77	2.59	1.22	1.91	1.91	2.06	1.42
MnO	0.21	0.16	0.15	0.17	0.1	0.16	0.17	0.29	0.28	0.25	0.27	0.24	0.37	0.23	0.19	0.17	0.16	0.17	0.21	0.20
P2O5	0.53	0.13	0.25	0.34	0.26	0.12	0.18	0.39	0.56	0.27	0.42	0.44	0.54	0.6	0.33	0.16	0.25	0.21	0.26	0.08
L.O.I.	4.32	2.05	1.96	1.27	1.37	1.45	1.31	1.25	0.76	0.99	0.53	0.89	1.09	N/A	1.93	N/A	N/A	N/A	N/A	N/A
Total	99.75	100.51	100.54	99.63	100.09	100.14	100.17	99.11	99.9	99.41	100.96	100.27	99.89	99.73	99.77	99.28	98.96	98.74	98.85	98.17
V	330.9	230.6	241.5	222.7	217.3	228.9	255.4	365.1	318.5	310.1	368	343.1	326.4	427.3	348.3	189.7	276.1	322.6	288.5	295.6
Ba	181.3	182.9	316.7	255	283	293.7	92.5	174.3	129.3	39.7	52.6	24.4	32.5	162.5	271.2	52.6	161.9	33.7	129.6	37.2
Sc	37.7	42.8	43.8	42.4	33.5	43.5	45.6	49	42.1	47.7	49.2	48.6	45.3	54.3	53.3	31	42.7	46.8	43.2	49.2
La	18.8	5.4	12.1	19.1	19.5	2	3.2	12.9	21.3	32.5	16.9	17.1	18.3	22.3	13	3.2	8.7	7.7	13.7	8.1
Nd	32.3	7.3	21.3	29.1	30.1	7.6	9.3	23.5	34	16.3	26.9	27.1	33	35.5	22.1	14.6	15.1	12.9	15.5	11.6
Ce	50.7	7.9	30.4	51.6	57	9	15.8	41	64.5	28.4	48.3	48.1	57.9	64.2	39.2	15.7	20.7	19.8	26	9.1
Cr	118	394.1	313.8	163.6	179.6	328.6	204.3	31.5	28	250.9	46.6	45.4	19.1	49.7	64.4	321.2	283.2	294.2	300.3	322.2
Ni	33.7	151.6	82	38.9	56.5	114.8	81	16	15.9	84.8	19.8	19.4	17.5	23.3	21.8	125.4	63.7	89.9	77.1	115.4
Cu	-3	-0.4	20.9	9.3	4.5	3.4	-2.8	3.1	23	6.5	2.4	3.7	5.9	82.7	1.2	4.8	86.3	5.4	7.6	5
Zn	165.2	98.9	82.7	88	68.3	70.1	85.1	181.2	127.6	104.6	172.9	180.5	115.9	131.6	120.4	95.5	97.5	231.5	229.8	108.5
Pb	26.2	-1.1	2	4.6	5.5	9.1	8.8	7.2	21.8	14.3	13.2	13.9	11.7	14.6	17.8	17.1	17	13.2	15.3	13.2
Th	3.7	43.7	2	5.7	12	-0.3	-1.1	4.5	6.6	0.4	6	4.4	7.4	4.4	5.5	-0.5	0.3	-1	0.3	3
Rb	70.8	231.2	116.3	40.3	54.8	42.8	15.2	14.4	27.8	12.5	15.5	11.1	11.9	12.9	31.2	7.3	38.7	11.7	28.2	21.7
Sr	301.4	25.8	214	236	202.7	321.5	226.3	182.7	193.7	212.2	162.4	157	117.6	216.6	225.6	293.5	212.7	105.4	145.7	100.9
Y	65.2	108.6	35.8	51	41.6	24.9	27.5	49.4	55.4	40.7	51.9	50.9	58.6	61.3	42.2	22.1	34.9	35.5	37.5	28.1
Zr	356.5	3	152.5	332	153.9	106.9	121.1	250.8	308.6	171.2	273	274	334.6	315.7	219.1	115.8	165.3	128.8	171	93.7
Nb	15.7	8.6	8.1	11.2	19	4	5.8	11.8	15.7	13.7	11.6	26.4	14.9	15.7	10	3.9	6.6	6.5	7.5	5.4

Amphibolites (open triangles)

	L 78-1	L 78-2	L 78-3	L 86	L 87	L 87C	L 88	L 113A	L 119-2	L 119-3	EAF 1	EAF 6	EAF 12	EAF 16	EMV 1	EMV 2	EMV 8	EMV 11	EMV 15	EMV16	EMV23E	EMV 23F
SiO2	47.60	51.55	49.60	49.2	49.37	50.61	49.7	46.81	51.41	49.36	49.77	48.38	49.84	44.5	50.3	47.7	48.38	47.57	44.25	45.78	51.7	41.89
Al2O3	15.24	15.06	17.05	14.2	14.39	14.26	14.3	14.06	14.84	13.54	16.04	16.25	12.87	15.8	15.74	16.29	15.08	15.5	13.56	14.32	17.41	15.54
Fe2O3	13.39	12.12	11.93	13.9	13.79	14.27	13.8	9.94	11.15	11.60	11.72	12.21	13.97	16.07	10.42	9.78	12.28	11.22	9.16	11.28	10.56	17.1
MgO	7.02	6.83	6.70	6.52	5.97	5.91	6.10	6.64	5.17	5.69	7.09	7.99	7.62	5.71	7.05	9.54	7.83	8.76	6.24	5.93	4.52	7.01
CaO	9.18	9.05	8.66	8.79	9.06	7.98	9.52	11.78	8.90	9.89	8.87	8.23	9.35	8.12	9.2	10.85	9.58	9.64	10.2	6.4	10.13	11.05
Na2O	2.81	2.94	2.34	2.36	2.06	2.32	3.41	3.89	4.14	3.91	2.95	1.9	1.28	3.32	3.73	2.89	3.08	2.6	-0.14	0.82	2.53	1.24
K2O	0.58	0.46	1.22	0.58	0.74	0.48	0.43	0.24	0.68	0.55	0.26	0.68	0.24	0.36	0.7	0.3	0.85	1.04	4.01	2.96	0.47	0.71
TiO2	1.78	1.71	2.45	2.43	2.46	2.62	2.45	1.80	2.10	2.62	2.23	2.54	3.15	4.56	1.79	1.23	1.76	1.56	1.36	2.2	1.45	3.61
MnO	0.20	0.21	0.20	0.24	0.21	0.22	0.22	0.21	0.17	0.23	0.17	0.15	0.38	0.48	0.13	0.16	0.2	0.17	0.16	0.17	0.16	0.53
P2O5	0.30	0.21	0.51	0.27	0.28	0.30	0.28	0.22	0.34	0.32	0.24	0.38	0.36	0.6	0.13	0.09	0.16	0.16	0.16	0.34	0.16	0.39
L.O.I.	N/A	N/A	N/A	N/A	N/A	N/A	N/A	N/A	N/A	N/A	0.81	1.67	0.86	0.75	1.26	0.77	0.98	2.1	10.82	9.54	0.66	1.03
Total	98.1	100.1	100.7	98.5	98.33	98.97	100	95.59	98.9	97.71	100.2	100.38	99.92	100.27	100.45	99.6	100.18	100.32	99.78	99.74	99.75	100.1
V	388.6	299.3	257	350	353.7	352	350	275.8	274.3	340.8	283.3	297.4	436.8	421.8	240.1	226.3	297.5	277.8	239.7	46.8	172.3	439.3
Ba	170.5	427.5	292.9	73.6	104.8	20.6	82.5	51.8	90.3	81	5.4	85.1	29.4	66.6	67.9	38.6	99.1	121.7	231.8	238.9	156.9	56.2
Sc	47.8	43.6	25.8	47.2	47.6	48.8	47.7	36.9	39.7	47.4	48	47.2	55	59.1	44.1	46.5	50.8	50.9	39.5	285.2	50.4	58.9
La	2.8	13.5	25.5	15.8	15.5	19	15	8	7.9	12	12.4	9.6	10.7	24.7	9.5	1.4	5.8	6.9	6.6	12.2	-2.5	5.5
Nd	15.2	15.9	27.5	19	19.5	27	26.2	14.4	16.9	18.7	19	18.6	22.2	40.3	16.5	9.9	10.9	10.4	10.7	31.6	9.4	18.6
Ce	21.6	25.5	49	34.1	33.3	45.6	40.9	22.1	15.6	24	31.7	31.4	32.1	69.1	28.7	8.9	17.7	16.2	17.7	21.6	8.5	29.9
Cr	140.3	187.6	178.4	105	109.1	86.6	104	231	223.7	202.4	431.1	218.5	26.6	31.5	258.5	332.9	250.5	255.9	269.7	43.4	266.9	81.4
Ni	52	58.9	109.8	27.5	33.9	31.9	31	68.2	70.5	40.8	136.7	93	27.1	29.4	52.4	154.2	64.4	70.9	90.4	25.9	87.9	22.8
Cu	26.3	83.3	57.4	34.3	44.9	11.4	40.2	30.1	16.1	9.6	6.3	0.7	264.8	2.2	2	7.7	96.6	66.5	52.9	12.8	108.9	93.9
Zn	168.9	144.1	118	137	123.9	170.2	132	69.2	112.3	94.1	88	814.2	206.9	136.5	51.3	57.8	106.1	92	82.3	449.5	257.2	132.1
Pb	17.8	10.5	12.3	14.5	14.8	12.1	13.5	9.8	13.2	10.4	16.5	195	5	12	0.7	2.8	1.9	7.6	28.3	33.5	55.5	4.7
Th	0.3	0.7	0.2	1.4	0	-0.4	-0.7	-3.5	-0.8	-1.1	7	5.5	-0.9	2.8	12.9	-1.3	0.3	-0.7	2.2	0.8	0.2	-2.8
Rb	16.2	10.4	36.8	16.3	27.9	20.2	5.3	1.3	9.5	11.3	1.8	41.8	1.3	6.9	16.8	2.9	20.1	40	214.1	113.9	13.5	21.5
Sr	233.3	193.2	250.3	96.8	127.7	90.4	112	677	454.9	303.6	340.3	58.8	84.3	232.6	216.6	249.2	158.2	205.6	194.6	130.8	491.5	77.7
Y	41.1	37.7	32.4	41.6	42.6	45.5	42.9	27.8	40.5	40.4	37.3	34	63.1	52.8	44.2	26	33.6	25.4	26.2	32.1	31.6	69.8
Zr	132.9	161.3	242.4	184	193.7	220.1	194	155.6	234.7	210.5	186	178	213.7	357.8	243.2	74.1	125.7	104.4	103.8	207.7	103.9	198.8
Nb	10	9.2	36.3	7.9	8.4	10.8	8	4.8	7.8	9.6	16	13.7	10.7	24.6	10.3	4.6	11.2	9.5	5	13.2	3.6	24.9

	Amphibolites (filled diamonds)						Amphibolites (open circles)													
	LIMN 2	LIMN 3	LIMN 4	LIMN 5	LIMN 6	LIMN 7	LEF7	LEF8	LEF9A	LEF9B	LEF10	LEF10E	LEF16A	LEF16B	LEF16C	LEF23-1	LEF 25	LEF 25A	LEF 25B	LEF 25C
SiO2	48.88	54.22	50.70	50.34	44.21	51.65	51.04	50.14	50.82	51.32	50.55	49.18	51.15	51.04	50.46	48.33	52.8	50.60	51.18	51.79
Al2O3	16.1	16.14	16.65	14.29	16.90	14.83	15.23	15.5	15.84	15.8	14.25	14.02	15.16	15.19	17.91	17.2	16.03	15.15	17.08	16.84
Fe2O3	11.55	7.75	9.57	10.17	11.96	12.89	10.26	10.56	11.08	11.84	14.42	14.86	11.24	13.1	6.79	10.31	6.80	11.42	8.95	7.23
MgO	8.07	5.25	5.01	7.25	6.94	5.62	7.48	7.23	6.36	6.38	5.96	6.66	7.11	6.43	9.25	8.19	9.26	7.63	9.01	10.64
CaO	8.36	9.60	10.28	13.21	15.00	7.49	9.6	9.39	9.56	9.25	9.06	9.36	9.42	8.92	11.27	9.95	11.01	9.84	8.99	10.59
Na2O	3.93	4.48	4.62	2.11	1.46	4.85	2.83	2.91	3.31	2.9	3.39	2.85	2.93	2.88	2.24	2.2	2.16	2.57	2.42	2.17
K2O	0.19	0.19	0.10	0.26	0.14	0.13	0.75	0.77	0.63	0.54	0.34	0.35	0.41	0.24	0.5	0.3	0.50	0.44	0.28	0.29
TiO2	1.56	1.18	1.09	1.53	1.62	2.01	1.4	1.9	2.1	1.98	2.5	2.54	1.88	2.25	0.52	1.47	0.52	1.55	0.86	0.43
MnO	0.25	0.13	0.16	0.18	0.19	0.23	0.15	0.18	0.18	0.21	0.24	0.25	0.2	0.22	0.13	0.16	0.14	0.22	0.15	0.14
P2O5	0.14	0.07	0.10	0.18	0.15	0.19	0.14	0.23	0.33	0.31	0.25	0.23	0.1	0.21	0.03	0.15	0.04	0.14	0.02	0.03
L.O.I.	1.29	0.74	0.78	1.05	1.73	0.54	1.41	0.91	0.39	-0.16	-0.39	-0.13	0.8	0.34	1.5	2.1	1.26	0.56	1.56	0.19
Total	100.32	99.75	99.06	100.57	100.3	100.43	100.3	99.72	100.6	100.37	100.57	100.17	100.4	100.82	100.6	100.36	100.52	100.12	100.5	100.34
V	336.6	295.2	311.1	312.2	383.5	388.4	301.9	272	289.6	300.9	396.4	425.2	381.7	372.3	181.5	42.1	198.6	295.4	192.3	169.6
Ba	17.6	18.7	-1.5	12.1	6.7	31.1	165.7	186.2	220.1	299.3	277	137.6	89.6	151.9	103.6	158.5	64.9	152.4	58.2	126.7
Sc	50.7	51.7	46.8	50.9	51.3	44.3	56.4	45.4	45.2	48.7	50.1	59	60.9	48.4	46.1	243.5	49.2	57.6	44.7	39.9
La	4.5	2.8	2.7	2.1	3	5.7	6.2	13.1	17.6	14.1	8.3	6.9	11.2	10.9	-1	2.3	4.4	6.5	5.2	1.5
Nd	8	6.2	6.2	7.4	7.7	12.5	10.5	21.1	24.3	25.3	22.3	15.4	16	18.6	3.7	18.4	9.8	14	7.6	4.3
Ce	7.5	6.7	8.3	11	7.2	15	21.6	38.2	41.5	42.5	36.2	25.7	24	30.7	2.5	15.3	14.3	23.5	15.8	6.8
Cr	128.6	318.5	260.5	261.1	95.4	80.5	199.8	255	164.2	207	45.1	41.1	116.6	106.8	791	269.4	1117.2	97	422.6	550.3
Ni	49.8	64.4	74.5	81.7	61.9	35.8	29.4	73.3	39.7	33.4	31.7	17.1	28.1	25.2	80.4	94	70.1	19.1	116.4	74.1
Cu	21.9	4.6	37.4	31.4	43.1	8.2	10.3	19.8	25	19.7	15.9	9.2	7.7	47.1	23.8	19.3	-2	11	24.4	33.8
Zn	641.9	56.9	69.6	87.8	111	58.9	96	100.9	93.3	119.5	140.6	130.8	86.7	121.4	49	147	64.4	98.4	105.7	48
Pb	3.8	4.3	1.1	1.6	-0.2	0.5	17.7	8.6	5.4	2.8	2.4	0.7	2.8	3.2	2.5	9.8	5	3.6	4.2	1.5
Th	1.3	0.7	-0.4	-1.1	-2.6	-0.1	0.4	-0.2	-0.6	-0.9	-1.7	-0.3	-1.5	0	-0.6	0.3	5.4	0.4	0.4	1.3
Rb	0.6	2.6	-0.4	4.7	1.1	0.3	20.6	14.7	5.3	4.5	-0.01	4.3	7.1	1.9	10	5.6	9.8	4.7	1.3	3.7
Sr	140	137.5	80.7	159.4	226	112.1	207.6	221.1	255.9	244.5	190.3	194	237.9	207.8	202	203.1	189.5	200.8	192.7	196.9
Y	34.9	21.6	26.6	31.9	35.2	39.6	27	34	36.9	36.7	43.7	42.5	32.2	38.1	11.6	28.4	18.6	30.5	18.7	10.2
Zr	105.1	64.9	59.7	108.3	104.1	117.2	100.1	131.1	218.9	390.1	175.1	153.6	107.1	156.8	31.4	98.4	42.6	92.4	40.7	31
Nb	4.2	3	3.3	6.4	5.8	4.9	4.2	9.5	12.8	11.7	7.4	8.7	8.1	8.5	2.4	4.2	3.1	5.6	2.3	2.3

	Dykes (filled circles)										Amphibolites (open diamonds)								
	LEF 25D	LEF 25F	LEF25GA	LEF 11	LEF19	LEF 20	LEF 21A	LEF 21B	LEF 21C	LEF 23	STAV-3	STAV-5	STAV-7	STAV-8	MOD-7	MOD-8	MOD-9	MOD-10	MOD-11
SiO2	51.76	51.88	51.76	48.69	49.91	50.2	49.61	49.19	49.95	51.89	48.48	59.99	46.91	50.11	49.6	49.44	47.93	51.8	44.66
Al2O3	16.85	15.95	16.63	14.71	14.17	14.84	15.39	15.19	15.19	15.80	15.34	14.29	16.82	9.06	15.2	15.88	16.02	14.57	14.18
Fe2O3	7.17	8.09	8.51	13.86	13.78	13.01	12.70	12.64	12.99	10.79	10.75	5.75	14.08	8.99	11.42	10.78	10.96	11.08	11.27
MgO	9.79	10.37	9	6.87	7.94	6.59	7.15	6.88	6.98	6.53	7.61	7.19	5.33	15.4	6.76	6.31	7	6.37	8.63
CaO	11.15	10.76	10.42	9.12	9.48	8.84	10.13	9.98	9.91	8.93	11.32	8.28	8.93	11.65	8.02	9.08	9.77	7.96	6.4
Na2O	2.29	2.22	2.42	2.79	1.16	3.06	2.62	2.96	1.93	2.83	2.56	3.25	3.94	1.54	4.19	4.26	2.88	4.14	0.95
K2O	0.30	0.37	0.37	0.42	0.32	0.55	0.52	0.48	0.88	0.83	0.66	0.29	0.51	0.32	0.33	0.32	0.73	0.3	0.99
TiO2	0.44	0.69	0.48	2.39	2.45	2.11	2.17	2.19	2.21	1.91	1.37	0.43	2.36	0.47	1.97	2.19	0.99	1.99	1.52
MnO	0.13	0.16	0.17	0.25	0.21	0.19	0.23	0.22	0.24	0.19	0.22	0.1	0.24	0.18	0.15	0.14	0.15	0.15	0.11
P2O5	0.03	0.09	0.05	0.24	0.47	0.22	0.22	0.23	0.23	0.28	0.19	0.04	0.12	0.04	0.27	0.23	0.29	0.3	0.2
L.O.I.	0.49	0.12	0.21	0.84	0.15	0.49	0.24	0.18	0.14	0.21	0.84	1.11	0.42	2.13	1.4	1.07	2.08	1.67	10.49
Total	100.4	100.7	100.02	100.18	100.04	100.1	100.98	100.14	100.65	100.19	99.34	100.72	99.66	99.89	99.31	99.7	98.8	100.33	99.4
V	182.7	200.2	236.4	378	338.8	356.6	329.6	333.5	342.7	267.4	44.8	35.1	55.4	66.2	45.5	43.9	43.9	44.9	28.7
Ba	94	195.9	106.7	107.5	57.8	317.5	124.5	129.1	225.9	219.3	71.7	22	37.4	6.2	20.2	27.6	122.5	37.9	77.4
Sc	44.8	44.2	57.7	57.3	55.8	52.4	52.9	54.6	55.8	45.9	287.6	131.6	662.6	217	286.2	287.7	279.5	328.8	228.2
La	2.5	3.6	3.2	8.4	15.8	8	7.2	6	7.4	14.1	2.7	6.3	6.1	4.2	14.9	11.8	8.4	10.9	8.7
Nd	4.5	8.6	5.9	17.5	28.8	14.8	14.9	15.4	16.7	25.2	10.4	23.8	31.7	5.1	41.2	30.3	34.4	33.4	26.7
Ce	4.3	15.5	10.3	27.9	49	25.2	21	23.4	23.70	43.7	10.3	15.4	18.9	6.8	26.9	20.3	17.8	20.5	16.8
Cr	488.9	495.4	475.5	87.7	164.7	142	161.8	166.7	170.2	230.7	362	540.8	45.1	2286.3	249.3	249.5	221	334.9	177.6
Ni	61.9	73.6	66.4	30.4	45.5	22.8	47.5	41	46.3	48.3	100	106.7	12.6	213.7	88.4	64.6	80.7	46.2	135.7
Cu	19.5	36.9	7.4	32.1	57.3	18	32.7	35.3	42.2	24.5	15.1	5.3	25.4	13.9	74.2	42.5	24.6	33	29.8
Zn	51.3	55.7	78.5	107.2	181.2	200.5	111.8	104.1	111.7	93.6	107.7	33.6	117.2	131.1	105.7	88.2	96.9	97.7	103.2
Pb	0.5	1.6	2.6	3.5	3.2	7	6.9	3.9	3.8	4.7	11	5.8	25.2	4.8	9.8	10.3	4.8	5.1	5.5
Th	-0.2	-1.4	-1.4	-1.3	-2	-3.1	0.4	-2.6	-0.9	-1.1	0.4	2.2	1.1	-0.6	1.1	0.7	1.3	1.8	1.8
Rb	3.2	3.9	5.6	5.2	1.1	10.6	10.8	7.6	25.4	10.3	13.4	4.3	3.6	3.9	8.6	2.9	26.9	7.8	64.8
Sr	196	185.3	222.8	193.4	77.7	273	218	224.6	189.8	224.8	141.4	159.3	217.8	42.7	267.1	245.6	246.3	205.7	171.4
Y	13.3	16.6	17.2	39.7	44.9	37.6	36.7	37.3	36.2	36.5	32.8	38.7	42.9	10.3	41.5	44.7	42	41.1	26.1
Zr	41	59.2	31.8	151.7	92.6	153.5	155.2	156	154.6	168.1	91.5	213.8	120.4	27.5	169.6	171.4	167.6	154.8	122.9
Nb	2.4	3.2	2.2	8.4	12.5	8.1	7.1	5.5	7.5	10.4	5.1	2.4	4.2	1.9	9.3	10.4	9	9.5	7.1

Amphibolites (filled triangles)

	MOD-13	MOD-28	MOD-29	NMAD3	VAM18-3	VAMRX	VAM 1	VAM 2B	VAM 11	VAM19A	VAM19B	VAM21A	VAM21B	VR 1	VR 2	VAMR7	VAMR9	VAMR14
SiO2	52.43	49.88	45.19	47.83	52.04	48.29	48.33	49.88	50.93	47.35	53.06	47.15	49.43	49.82	49.02	48.36	51.1	48.07
Al2O3	17.42	15.05	13.52	14.42	15.92	14.92	14.80	14.67	15.99	16.67	15.52	17.79	15.12	15.75	15.38	15.85	16.58	17.25
Fe2O3	10.19	11.62	14.52	10.79	10.94	9.67	10.06	9.32	7.37	9.84	9.33	8.63	11.2	8.77	9.79	11.6	10.65	9.18
MgO	3.54	5.99	9.19	8.98	7.06	7.09	7.79	7.03	9.96	8.79	6.63	10.87	8.5	6.98	7.67	7.38	7.39	8.45
CaO	8.24	8.44	9.36	10.59	7.89	11.38	12.43	11.97	9.13	11.22	8.74	9.45	9.02	10.74	11.38	9.91	7.72	10.55
Na2O	5.6	3.19	2.74	2.31	2.39	3.46	2.90	3.29	3.45	2.93	2.85	2.16	2.35	4.71	3.46	1.94	2.68	2.64
K2O	0.78	0.48	0.48	0.92	0.49	0.39	0.23	0.53	0.75	0.46	1.04	0.66	0.71	0.62	0.35	0.58	0.58	0.52
TiO2	1.12	2.15	2.13	1.41	1.66	1.71	1.85	2.11	0.88	1.49	1.62	0.99	2.44	1.57	1.77	1.28	1.15	1.25
MnO	0.2	0.15	0.17	0.17	0.15	0.17	0.16	0.17	0.13	0.17	0.17	0.15	0.20	0.19	0.18	0.18	0.14	0.14
P2O5	0.37	0.31	0.19	0.39	0.16	0.26	0.19	0.33	0.32	0.15	0.28	0.09	0.18	0.24	0.27	0.15	0.13	0.13
L.O.I.	0.9	2.1	2.33	1.67	1.41	2.52	0.76	1.38	1.42	1.38	0.71	2.55	1.20	1.07	0.73	2.35	1.56	1.94
Total	100.79	99.36	99.82	99.48	100.11	99.86	99.5	100.68	100.33	100.45	99.95	100.49	100.35	100.46	100	99.58	99.68	100.12
V	42.8	40.8	42.8	45.4	38.3	36.6	290.4	290.8	197.4	233.7	264.1	150.9	235.1	215.2	259.7	48.1	27.1	36.2
Ba	46.4	96.9	101.6	50.2	234.9	72.5	59.5	84.4	47.4	76.6	163	364	244.7	196.2	73.8	69.3	386.7	140.7
Sc	270.6	306.7	349.6	272.4	215.2	260.7	47.3	46.6	37.1	46.2	49	37.3	59.7	38.5	41.3	307	181.8	217.1
La	2.2	11.9	5.6	4	16.5	10.6	5.4	3.6	27.6	2.1	10.6	3.2	11.5	9	4.3	3.9	14.6	-3.5
Nd	17.6	37.6	29.6	28.1	31.8	28	12.5	16.1	27.6	8.3	17	9.4	17.8	15.8	13.9	17.4	34	11.9
Ce	12	23.6	16	17.8	24.5	16.2	19.2	20.8	63.6	12.4	32.1	12.4	34.2	28.7	22.4	8.3	13	6.5
Cr	208.1	232.2	256	356.6	219.8	316.9	281.6	207.9	424.5	331.5	325.1	496.5	297.2	239.8	311.2	315	336.3	355.7
Ni	50.4	58.8	83.3	85.4	71.8	84.6	89.5	61.8	192.6	108.3	38.3	172.7	115	36	92.3	51.3	76.7	129.6
Cu	25.9	37.4	22.1	74.2	69.2	10.4	-3.1	-2.3	18.1	44.2	16.1	72.1	39.1	40.8	0.2	35.7	51.7	44.2
Zn	64.5	107	138.7	107.8	114	64.8	64	39.1	62.8	72.4	131.2	57	96.9	71.3	60.9	177.3	136.5	87.2
Pb	4.6	6.9	4.4	8.4	8.4	2.8	0.7	1.6	9.4	4.5	10.2	2.6	5.3	-2.4	0.8	8.1	9.8	6
Th	0.9	1.7	2.5	1.6	1.1	1.6	-1.6	-0.4	10.5	-1.5	2.9	-0.8	2	1.6	-2.3	0.3	0	0.3
Rb	9	13.6	14.8	37.7	8.7	12.8	4.5	11.7	26.5	7	17.5	19.6	11	7.2	9.3	13.8	12.3	16.9
Sr	126.4	339.7	131.7	200.6	188.7	479.4	566	450.8	381.2	240.4	171.2	315.4	210	624.6	448	154	220.4	236
Y	22.6	43.7	36	26.9	34.7	30.8	31.5	33.3	19.6	24.6	33.9	18.3	30.3	37.8	27.5	39.1	28.3	24.2
Zr	88.4	166.6	1301.7	100.8	77.1	138.1	149	183.6	187.8	113.7	161	94.4	137	228.3	144.5	100.9	114.1	93.7
Nb	3	10	25.1	9.5	11.4	8.2	6.3	9.2	9.2	3.8	10.9	3.5	11.4	8.7	5	6.1	7	3.5

	VAMR21	VAMR22	VAMR23	VAMR29	VAMR35	VAMR36	VAMR38	VAMR39	VAMR41	VAMR46	VAMR51	VAMR52	VAMR57	VAMR61	VAMR65	VAMR80
SiO2	50.65	48.06	47.51	52.64	50.65	49.62	51.02	45.01	53.23	49.74	49.53	54.25	50.12	49.15	48.87	51.04
Al2O3	14.96	17.68	16.08	14.7	17.11	17.47	17.24	16.97	17.75	16.64	15.91	16.6	16.61	15.69	14.75	17.89
Fe2O3	10.92	8.09	11.4	13.52	7.83	7.92	8.32	14.01	9.64	11.09	12.8	11.11	9.22	11.51	10.25	7.6
MgO	7.55	9.47	5.2	5	7.85	8.13	8.09	6.87	6.39	7.11	6.36	5.38	7.1	6.23	7.09	7.67
CaO	7.43	9.89	8.17	7.22	9.42	8.9	9.03	10.26	7.73	8.5	8.25	5.45	9.71	9.9	9.29	7.48
Na2O	2.49	3.02	2.8	1.04	3.46	3.13	3.03	1.18	2.08	1.89	1.95	2.68	2.74	3.3	1.01	2.94
K2O	0.96	0.6	1.06	0.76	1.07	1.33	1.12	0.46	0.52	0.78	0.95	0.57	0.93	0.96	0.9	1.8
TiO2	1.41	0.75	1.68	2.79	0.95	1.02	0.68	2.31	0.79	1.73	1.62	1.4	0.94	1.85	1.74	0.89
MnO	0.16	0.11	0.17	0.21	0.12	0.12	0.11	0.24	0.22	0.22	0.28	0.2	0.18	0.18	0.11	0.11
P2O5	0.17	0.08	0.2	0.44	0.11	0.11	0.1	0.35	0.11	0.42	0.28	0.28	0.11	0.22	0.2	0.14
L.O.I.	2.08	2.13	5.53	1.39	1.01	2.18	1.82	2.61	1.65	1.71	1.82	1.33	2.09	1.87	5.19	2.01
Total	98.78	99.88	99.8	99.71	99.58	99.93	100.56	100.27	100.11	99.83	99.75	99.25	99.75	100.86	99.4	99.57
V	52.8	34.3	34.7	41.9	34.8	28.9	31.1	35.2	32.6	32.3	44.2	32.9	53	46.2	49	27
Ba	365.1	60.4	203.1	497.6	148.2	177.1	186.5	180.7	218.7	336.6	264.8	596.3	154.5	115.7	162	371.4
Sc	270.4	139.3	255.2	350.3	166.1	162.1	136.6	311.5	243.3	277.2	321.1	258.7	290.3	312.1	302.9	135.3
La	16.5	-1.5	2.5	33.9	11.9	11.2	5.7	12.7	10.9	13.9	6.9	27.3	10.9	8.3	-4.6	6.3
Nd	41.4	10.9	24.7	84	38.6	18.1	28.3	48.5	52.6	47.4	36.2	62.8	17.6	36.2	25.3	40
Ce	24.1	2.2	16.2	53.8	20	19.5	11.6	21	23.9	28.4	23.7	26.1	10.8	15.3	20.3	25.9
Cr	285.2	433.3	140	69.5	329.4	240.6	359.7	131.4	306.8	284.4	183.2	207.2	206.8	138.9	254.7	168.5
Ni	111.9	159.8	47.9	22	127.6	163.7	165.9	85	122.9	114.6	64.4	46.5	18.5	38.1	53	127
Cu	62.6	8.7	35.2	39.9	46	47.3	38.7	12.6	38	40.6	83.9	73.4	11.2	43.7	149.5	45.1
Zn	96.9	72.6	98.8	222.6	56.1	60.9	63.2	174.4	95.9	148.2	149.1	124.6	99.1	102.9	205.5	56.3
Pb	5.4	6.7	7.4	1.5	6.1	3.3	5.4	9.4	10.8	7.6	6.4	8.2	11	5.3	5	7.9
Th	3.1	0.4	3.1	4	7.1	5.4	6.1	2.3	2.4	2.7	1.8	8.6	1.2	-0.1	1.5	6.9
Rb	20.7	11.8	50.6	36.5	33.6	51.4	40.2	21.5	17.2	19.2	27.3	14.9	29.6	40	42	71.6
Sr	224.1	263.3	272.4	99.1	209.9	219.5	197.2	318.5	242.8	275.7	171.9	287.5	249.7	190.1	196.4	232.2
Y	32	14.5	24.6	65	24.4	24	19.3	37.9	24	32.1	36.9	40.7	26.5	35.8	31.7	26.5
Zr	138.9	54.2	81.4	424.1	122	121.7	103.3	184.9	89.6	158.5	120.6	206.1	71.9	153.6	124	147.7
Nb	11.3	2.9	5.8	20.8	5.1	3.9	5.2	23.1	3.6	17.6	13	13.6	5.3	6.4	4.9	4.2

	VAMR82	VAMR83	VAMR84	VAMR85.1	VAMR87	VAMR89	VAMR96	VAMR98	VAMR99	VAMR101.1	VAMR102
SiO2	55.66	56.18	46.47	47.2	48.72	46.53	49.2	49.5	49.06	51.31	50.54
Al2O3	17.97	17.33	17.71	17.31	15.41	16.18	16.16	15.84	15.5	17.01	17.79
Fe2O3	7.7	7.33	10.63	9.58	10.33	11.94	11.59	12.17	11.82	9.11	7.23
MgO	5.29	4.78	8.45	10.41	9.2	8.87	6.87	6.36	6.36	5.69	6.97
CaO	6.22	6.84	8.29	10.25	8.76	10.4	8.84	9.66	9.57	6.96	10.47
Na2O	3.33	3.94	2.46	2.46	2.61	2.47	2.31	2.26	2.41	3.41	2.82
K2O	1.54	0.96	0.98	0.27	1.24	0.42	0.59	0.4	0.65	1.82	0.99
TiO2	0.84	1.07	1.53	1.16	1.06	2.01	2.19	2.32	2.25	1.1	0.95
MnO	0.12	0.12	0.16	0.14	0.16	0.12	0.18	0.19	0.18	0.14	0.12
P2O5	0.16	0.17	0.12	0.1	0.14	0.19	0.37	0.4	0.37	0.23	0.12
L.O.I.	0.98	1.2	2.45	0.75	1.94	0.94	1.98	0.5	1.83	2.29	1.5
Total	99.81	99.92	99.25	99.63	99.57	100.07	100.28	99.6	100	99.07	99.5
Sc	19.6	33.1	29.1	29.9	30.1	42.5	45	43.1	42.6	25	40.2
Ba	271.3	216.1	178	84.4	207.5	67.6	405.4	325.5	259.4	576.1	267.3
V	145.3	194.4	211.1	184.7	179.3	281.3	305.7	314.5	310.7	152.9	208.4
La	15.4	13.3	0.4	-4.9	6.8	5.5	15.3	14.9	17.4	39.3	8.3
Ce	16.7	28.7	7.5	15.3	16.5	17.1	45.9	52.5	49.1	65.3	21.5
Nd	6.3	16.3	7.8	10.1	11.2	5.5	32	28.4	32.7	35.9	8.7
Cr	273.9	157.4	158.7	550.1	399.3	412.2	307.3	277.4	302.6	253.6	539
Ni	50.8	72.2	146.4	309.1	206.4	210.3	58.1	54.5	58.1	96.7	45.7
Cu	33.9	30.9	81.7	89.3	31.2	49.2	61.3	56.8	48.9	40.4	21.4
Zn	99.2	65.1	89.5	70.6	85.7	96.8	122.7	112.5	109.8	107.1	63.8
Pb	6.8	10.1	4.1	0.9	6.4	1.6	5.6	5.9	6.3	15.1	8.8
Th	3	4.4	0.9	-0.4	5.4	0	-0.5	0.9	2.6	1.8	1.2
Rb	55	25.8	38.3	7.3	40.3	12.3	16.5	7.5	15.7	57.2	28.8
Sr	225.5	264.1	226.6	209	171.1	191.9	220.3	229.2	228.8	183.4	261.5
Y	16.3	31.4	24.3	21.7	25.8	36.6	47.1	50.8	46.1	31.6	18.8
Zr	56.8	123.8	104.5	79.5	124.8	139.9	179.6	224.7	167.4	332.5	83.6
Nb	7.9	7.7	3	2.7	5.9	3.9	12.2	13.3	12.3	11.3	6.1

Analyses which failed the screening criteria: Dykes & Amphibolites

	ASK5A	ASK5B	ASK5C	ASK5D	ASK7A	ASK16	ASK19	ASK21	ASK21A	ASK21B	ASK21D	ASK24A	ASK24B	ASK25B	ASK26	ASK27	ASK29A	ASK29B	ASK30
SiO2	62.76	60.51	27.28	60.21	55.26	60.15	61.53	52.8	58.82	61.19	53.26	60.84	62.21	64.19	48.54	64.97	58.36	54.24	54.51
Al2O3	13.95	13.97	20.67	13.63	2.44	14.33	15.65	13.32	14.63	16.15	12.99	14.6	14.42	13.89	18.64	15.18	14.22	13.16	14.07
Fe2O3	8.47	9.45	28.6	9.53	6.68	9.52	7.46	14.28	10.24	6.28	15.43	9.03	8.86	7.35	12.5	6.52	10.36	13.34	13.04
MgO	2.24	2.41	14.27	3.04	20.52	3.01	4.43	3.95	2.96	3.67	3.36	3.53	3.02	2.27	8.86	3.25	3.49	3.42	3.8
CaO	3.62	3.81	0.18	4.06	11.64	4	1.34	5.76	4.46	5.77	5.94	4.08	4.18	2.31	1.55	1.2	4.16	5.77	6.39
Na2O	6	5.79	0.29	6.2	0.27	4.08	2.11	3.98	4.96	4.65	3.46	3.13	3.26	4.97	2.24	1.2	3.36	2.82	3.56
K2O	0.15	0.23	0.01	0.26	0.05	1.5	3.28	0.37	0.33	0.49	0.1	1.61	1.49	0.47	2.05	3.21	1.34	0.97	0.59
TiO2	1.55	1.67	0.06	1.88	0.04	1.65	1.38	3.2	2.18	1.04	3.38	1.82	1.7	1.46	2.09	0.89	2.17	2.88	3.12
MnO	0.14	0.14	0.5	0.23	0.24	0.2	0.09	0.38	0.19	0.12	0.13	0.14	0.14	0.11	0.1	0.11	0.19	0.25	0.23
P2O5	0.48	0.51	0.03	0.46	0.01	0.49	0.29	0.72	0.66	0.24	0.7	0.47	0.47	0.44	0.06	0.14	0.38	0.75	0.54
L.O.I.	0.08	0.57	8.71	0.4	2.25	0.86	2.6	1.69	0.75	0.56	1.88	1.18	0.51	1.72	3.92	3.36	1.45	2.04	0.53
Total	99.44	99.06	100.6	99.9	99.4	99.79	100.16	100.45	100.18	100.16	100.63	100.43	100.26	99.18	100.55	100.03	99.48	99.64	100.38
V	105.9	111.7	198.2	154.4	52.7	105	168.6	276.2	159.1	149.8	271.6	204.8	157.2	104.4	168.8	20	242.4	284.1	338.9
Ba	1.5	9.8	6	13.8	9.4	361.5	522.9	53.2	67.2	84.7	13.2	424.5	499.9	88.3	369.6	707.7	486.2	153.7	150.4
Sc	26.7	29.2	2.1	31.5	26.9	31	24.9	48.6	29.4	26.7	36.6	31.5	29.7	24	38.9	121.4	34	38	43.3
La	34.6	33.3	2.9	28.4	1.9	27.3	35.9	22.6	36.5	47.3	23.6	30.7	31.9	42.1	8.4	28.5	25.2	22.6	23.4
Nd	45	48.3	-7.6	42.2	2.4	43.1	38.1	42.2	54.4	44.6	41.8	43.3	42.9	49.8	8.5	70.2	34.7	35.8	33.8
Ce	91.7	86.8	-8.7	80	-3.1	77.8	86.9	71.5	96.8	102.8	64.7	82.9	85.7	97.7	14.6	31.7	67.8	60.2	62
Cr	18.8	20.1	24.5	43.6	1821	56.7	111.4	19.2	9.2	102.4	25.4	46	39.3	23.5	220.9	124.8	45.5	5.6	16.7
Ni	12.4	12.3	38.7	19.8	1323.4	23.4	47.5	14.5	13.3	48.5	15	18.6	16.7	20.6	143.4	56.2	19.1	12.1	13.5
Cu	2.3	1.4	-1.6	3.8	0	1.4	7	6	3.2	5.7	8.6	45.1	41.4	1.2	7.8	56	5.8	34.7	34
Zn	37	28	261.8	62.3	62.4	114.7	80.8	479.4	98.8	76.1	163.3	112.8	144.8	95.3	139.1	57.1	138.1	150.5	114.4
Pb	5.4	5.9	-1.4	3.8	3.3	5.4	4.3	2.4	5.9	7.9	10.3	22.7	22.7	13.9	9.8	9.4	39.4	19.6	11.9
Th	12.5	11.3	-2.2	10.5	0.6	9.7	19.4	5.6	11	21.5	5.5	12	13	14.4	2	11.8	8.7	6.9	7.2
Rb	0	1.4	0.3	1.8	0	56.4	136.1	7.4	10.1	13.5	2.8	80.6	96.7	16.9	93.2	107.4	42.2	34.9	14
Sr	167.4	200	14.9	108.8	14.3	158.5	107.9	123.7	191	258.1	238.6	167.9	166.8	125.2	160.7	126.9	190.6	172.2	238.3
Y	72.5	72	4.6	66.5	10.8	74	40.7	81.7	93.3	37.6	81.7	60.8	66.9	73.1	17.1	29.6	57.4	60.9	59.2
Zr	479	486.3	23.5	422.8	2.1	466.2	195.8	536.8	533.9	240.6	551.7	458	452.9	481.8	148.8	191.1	458.7	319.2	330.7
Nb	16.3	17.1	0.4	14.8	2	17.2	19	20	19	15.5	19.9	12.7	16.3	17.8	13.2	13.8	15.9	15.3	15

Analyses which failed the screening criteria: Dykes & Amphibolites

	ASK31	ASK32	ASK35	ASK36	ASK37	ASK41B	ASK43	L8	L10	L13	L27	L30	L31	L83	L84	L107	L113-2	EAF4	EAF13	EAF14	EAF17A
SiO2	55.56	54.19	55.38	60.52	52.15	55.35	61.72	52.58	55.19	60.04	53.3	57.71	52.05	53.27	53.8	62.06	59.79	56.88	55.99	56.39	53.21
Al2O3	13.6	14.03	13.67	14.84	13.3	13.94	13.77	14.33	13.73	15.2	13.75	15.37	14.41	14.04	14.07	16.33	13.6	14.11	13.14	12.9	23.81
Fe2O3	13.08	13.92	12.53	8.6	14.71	12.4	8.83	14.91	14.15	9.56	13.44	9.68	14.19	14.44	12.85	6.74	9.27	11.79	13.54	15.94	7.5
MgO	3.89	3.77	3.25	2.48	3	3.43	2.25	3.95	3.66	2.78	3.49	3.26	3.66	3.78	3.9	2.88	3.61	2.82	3.15	1.97	1.88
CaO	5.91	6.78	5.14	4.51	6.2	3.95	5.08	6.59	6.65	4.04	6.97	6.45	6.73	6.56	6.92	2.7	5.64	5.43	5.78	4.2	0.55
Na2O	3.01	2.8	2.81	6.01	1.25	3.01	4.59	2.4	2.26	4	2.33	4.65	2.47	2.52	4	4.04	4.59	4.48	3.98	4.52	1.83
K2O	0.39	0.26	1.33	0.18	3.71	1.25	0.19	0.7	0.26	1.59	0.34	0.37	1.18	0.54	0.38	2.75	0.3	0.56	0.35	0.33	6.59
TiO2	3.2	3.36	2.41	1.72	2.68	2.98	1.66	3.4	3.18	1.7	3.15	1.75	3.32	3.3	2.66	0.84	1.73	2.11	2.71	1.89	1.02
MnO	0.23	0.26	0.23	0.16	0.28	0.39	0.1	0.21	0.33	0.23	0.21	0.16	0.27	0.22	0.23	0.14	0.13	0.24	0.26	0.12	0.09
P2O5	0.54	0.64	0.87	0.46	1.3	0.51	0.64	0.52	0.56	0.5	0.57	0.46	0.57	0.54	0.78	0.24	0.4	0.52	0.77	0.81	0.13
L.O.I.	0.61	0.26	1.85	0.26	1.49	2.61	0.38	N/A	N/A	N/A	N/A	N/A	N/A	N/A	N/A	N/A	N/A	0.76	1.11	0.73	3.01
Total	100.02	100.27	99.47	99.74	100.07	99.82	99.21	99.59	99.97	99.64	97.55	99.86	98.85	99.21	99.59	98.72	99.06	99.7	100.78	99.8	99.62
V	329.1	359.1	141.4	154.7	159.1	302.7	107.8	449.7	359.2	165.5	410.9	186.6	431.1	426.1	268.8	116.3	167.6	158	202.3	50.2	125.2
Ba	53.5	28.8	217.7	4.4	1252.5	546.2	35.4	152.7	43.5	185.5	93	113.2	236.3	109.8	56.5	734.1	53.3	424.8	117.6	70.1	927.4
Sc	44.5	44.3	32	23.8	38.6	45.2	30	51.2	39.1	23.9	42.3	29.6	45.9	44.8	35.8	11.7	30.2	33.1	38.1	42.1	21.8
La	28.6	24.6	29.4	30.7	23.9	23.3	38.7	27.6	28.4	40.6	28.9	24.3	19.7	30.4	25.5	21.4	28.3	31	28	41.1	46.4
Nd	35.7	39.9	44.6	43.7	46.4	37.1	57.6	39.6	37.3	49.9	43.3	41.9	37.3	33.7	37.2	23	41	41.5	47.5	62.5	41.1
Ce	64.1	69.4	72.2	85.3	72.5	65.7	105.7	69.9	62.4	91.7	75.4	68	66.3	64.5	61.1	43.8	78	76.7	76.2	110.5	108.3
Cr	11.5	10.9	22.3	14.8	10.4	20.5	4.6	36	32.8	34.8	32.9	81.6	36.4	36.6	40.9	35	104.3	30.3	14	6.7	116.8
Ni	13.5	14.2	11.5	12.1	11	14	9.4	13	11.6	17.5	11.8	28.4	10.3	13.7	20.3	12.4	22.9	15.5	11.2	11.1	49.8
Cu	27.6	8.5	39	14.7	4.4	20.2	5.7	10.3	7.9	2.8	6.7	21.8	35.2	8.2	37.5	17.8	20.8	60.8	34.5	11.6	33.8
Zn	128.8	138.8	120.3	58.3	148.3	153.8	41.5	207.8	161.2	171.7	156.4	97.6	150	186.8	215.1	95.7	89.1	146.6	143.9	156.4	72.8
Pb	13.8	15	8.2	5.5	12.1	21.3	3.3	22.1	18.7	29.5	17.5	14.9	29	20.6	26.1	10.2	6.7	18.1	9.2	9.8	9.5
Th	7.3	6	8.6	16.7	1.5	8.3	12.9	5.3	6.2	12.6	6.9	7.8	6.8	4.4	5.4	5.6	7.1	7.8	6.1	9.5	21.4
Rb	12.8	5.2	55.5	0.7	198.7	75.1	2.3	33.5	9.6	98.6	10.1	8.7	51.1	17.3	9.5	98.1	6	15	9.1	10.8	215.4
Sr	182.7	265.6	205.2	183.6	123.1	206.1	309.3	75.1	63.6	98.5	105.7	148.4	202.7	116.6	112.2	113	226.7	139.3	162.2	157.7	98.4
Y	57.8	62	84.1	65.5	79.9	57.9	83	59.4	54.1	85	51.7	65.4	59.1	55.7	74.9	38.3	73.6	73	83.1	103.8	36.2
Zr	323.3	359.9	471.8	410.7	501.8	318.6	911.5	313	305.7	497.5	309.6	426.3	330.3	305.5	357.9	281	491.2	541.1	648.8	1486.3	133
Nb	14.6	16.1	16.5	14.6	15.1	14.2	17.5	14.2	12.9	14.3	13.7	11.4	14.1	16.1	11.6	5	13.7	17.9	19.9	27.2	19.9

Analyses which failed the screening criteria: Dykes & Amphibolites

	EAF17B	EAF18	EAF18A	EMV3A	EMV 3B	LEF1	LEF4	LEF10A	LEF10B	LEF10C	LEF10D	LEF12	LEF 15	LEF 16D	LEF23A	LEF23B	LEF23C	LEF23F	LEF25GB	LEF25G
SiO2	52.41	61.39	58.03	45.71	47.64	58.42	39.17	59.12	53.26	48.52	53.43	51.12	48.72	51.70	57.69	45.11	45.81	52.89	45.72	47.26
Al2O3	14.01	13.95	14.55	11.16	14	18.75	0.51	17.88	17.79	18.22	17.84	18.28	17.55	13.78	2.04	15.4	8.95	12.88	18.07	17.4
Fe2O3	14.75	9.43	10.68	9.28	8.89	7.09	9.12	8.33	11.54	7.82	11.51	6.44	9.53	7.81	6.06	11.93	9.54	16.28	19.94	18.34
MgO	3.35	2.17	2.97	12.2	11.44	2.79	39.54	0.6	1.85	9.93	1.85	9.02	9.76	11.14	27.81	13.74	26.15	3.07	2.99	3.8
CaO	5.54	4.25	5.11	14.36	11.22	4.45	1.9	2.72	5.85	11.74	5.86	10.55	1.73	11.24	0.64	5.84	2	7.06	8.26	8.23
Na2O	3.54	3.9	3.35	0.9	1.72	4.19	-0.27	4.16	3.78	2.38	3.73	2.49	1.87	1.51	-0.19	1.77	-0.07	1.95	2.1	2.25
K2O	0.84	1.56	0.72	1.06	1.73	2.54	0	5.85	3.42	0.15	3.44	0.31	0.12	0.35	0.01	0.38	0.03	0.5	0.27	0.32
TiO2	3.03	1.6	2.36	1.04	1.22	1.52	0.03	0.96	1.76	1.08	1.76	0.42	1.24	0.61	0.04	1.11	0.59	3.79	2.64	2.388
MnO	0.25	1.3	0.21	0.21	0.16	0.08	0.1	0.19	0.23	0.13	0.23	0.1	0.17	0.16	0.05	0.18	0.11	0.25	0.34	0.29
P2O5	0.96	0.57	0.56	0.14	0.15	0.1	0.01	0.24	0.42	0.1	0.43	0.02	0.09	0.03	.01	0.06	0.05	0.81	0.76	0.57
L.O.I.	1.14	1.36	1.03	3.31	2.08	0.04	9.13	0	-0.41	0.12	-0.33	1.25	-0.06	1.64	4.88	4.38	6.64	N/A	-0.84	-0.11
Total	99.82	101.5	99.57	99.37	100.25	99.97	99.24	100.05	99.49	100.19	99.75	100	90.72	99.97	99.04	99.9	99.8	99.48	100.25	100.738
V	235.2	84.3	226.9	191.2	200	21.9	20.1	25.9	136.3	176.4	24.6	177.9	227.5	270.7	81.9	185.8	138	343.2	160.8	226.5
Ba	257.1	401.4	150.7	124	223.1	820.1	185.2	955.2	2800.8	298.2	1937.2	43.4	42.7	46.5	13.6	216.2	9.6	463.3	218.5	246.9
Sc	42.8	25.4	31.4	32	37.3	139.2	2.8	31.9	40.9	41	28.3	46.9	46.2	62	9.4	29.5	19.6	60.2	65.1	54.3
La	30.3	32.4	35.3	4.1	1.7	150.9	0.1	15.3	15	0.4	16.9	0.4	0.6	1.4	0.5	31.8	8.8	53.3	26.6	18.9
Nd	51.5	45.8	49.7	6.9	9.6	324.3	0	24.2	32.6	11.2	29.7	4.3	8.2	4.5	2.9	22.3	7.4	79.6	41.4	34.8
Ce	85	83.9	91.2	6.5	11.4	156.7	2.3	38.8	40.9	10.8	48.2	6.7	7.9	7.5	4	61.5	19.5	147	70.5	59.8
Cr	12.8	17.7	19.5	772.8	861.9	37.3	2087.8	7.8	19.9	505.1	7.9	444.4	369.6	396.4	2918.2	248.9	1448.7	6	16.7	25.9
Ni	12.9	11.3	15.7	289	316.8	16	3032.3	8.4	14.3	150.4	9.7	80.3	92.2	69.5	2067.1	212.5	1000.2	13.4	22.9	19.1
Cu	17.7	25.6	16.3	-2.8	-2	15.2	6.6	2.5	11.1	43.3	16.3	14.2	28.5	37.9	7.6	34.6	11.9	23.9	31.2	33
Zn	210.6	78.2	123.3	85	87.4	104.4	79.4	94.3	111.5	50.8	95.1	43.2	64.7	54.8	100.3	122.1	108.4	168.4	121.4	157.1
Pb	16.7	21	12.7	21.2	23.4	22.1	1.9	10	4.9	0	10.4	1.5	0.2	2.5	2.7	8.6	0.6	5.4	1.9	2
Th	6.4	10.6	11	-1.1	-0.3	71.3	3.8	1.1	-1.8	-1.3	-2.6	0.3	-2	0.6	3.6	2.5	2.8	0	-1.6	-3.2
Rb	42.7	66	30.2	24.5	55.1	37.7	-1.3	48	31.1	2.2	47.6	3.8	0.5	5.4	-1.1	5.3	-0.9	4.7	6.6	6.9
Sr	168	225.7	180.9	287.3	365.1	301.9	10.9	77.6	197.7	245.9	115.9	235.3	209.7	125.5	11.3	186.9	6.7	159.4	261.7	290.3
Y	88.6	83.7	89.5	19.1	23.4	27.2	0.6	32.5	39.9	21.2	39.2	10.2	23	14.9	3.2	24.9	11.6	95	50	47.1
Zr	683.3	525.6	518.1	89.1	98.8	295.6	1	1636.5	706.6	98	1815.2	34.6	86.9	46.3	0.3	409.8	218.2	590.5	740.6	633.1
Nb	19.2	18.4	19.6	5.8	5.4	17.6	1.5	10.6	13.7	2.1	13.8	0.5	3.5	2.40	1.8	11	5.4	28.3	8.7	7.4

Analyses which failed the screening criteria: Dykes & Amphibolites

	VAMR1	VAMR2	VAMR3	VAM3A	VAM4	VAMR10	VAMR11	VAMR12	VAMR13	VAM17-1	VAM19-1	VAM19-2	VAMR28	VAMR30	VAMR33	VAMR34	VAMR34A
SiO2	40.6	43.87	33.56	40.31	41.87	49.51	49.97	48.61	48.66	59.93	45.36	58.46	52.93	54.56	57.07	65.9	64.63
Al2O3	15.15	12.5	17.74	14.22	18.98	20.97	19.63	20.24	19.75	14.23	30.21	14.52	16.47	16.53	18.78	14.52	14.97
Fe2O3	9.85	8.81	10.42	13.01	8.56	6	6.76	6.86	6.72	8.35	14.74	11.82	14.4	13.76	5.78	5.55	5.16
MgO	21.23	17.13	15.64	2.25	3.3	5.94	7.95	6.99	7.55	2.68	5.03	1.63	2.89	3.73	4.2	2.52	2.45
CaO	7.66	9.83	10.15	27.27	23.55	10.12	11.41	10.73	10.6	3.68	1.11	4.62	6.23	3.95	6.35	3.34	4.36
Na2O	0.57	1.4	0.34	0.04	0.28	2.65	2.15	3.44	3.53	2.65	0.16	1.85	2.05	2.05	3.78	2.6	3.03
K2O	0.23	0.57	0.51	0	0.01	1.14	0.36	0.48	0.63	2.56	0.69	3.62	0.23	0.83	1.66	3.14	2.58
TiO2	0.07	0.11	0.08	0.46	0.81	0.9	0.55	0.71	0.55	1.52	1.56	1.57	3.19	2.55	0.51	0.97	0.9
MnO	0.12	0.12	0.1	0.5	0.31	0.09	0.11	0.11	0.1	0.12	0.29	0.17	0.33	0.21	0.1	0.08	0.09
P2O5	0.02	0.03	0.02	0.09	0.14	0.11	0.06	0.16	0.06	0.34	0.03	0.52	0.66	0.43	0.55	0.19	0.2
L.O.I.	4.38	5.73	11.39	1.99	2.37	1.78	1.74	1.63	1.72	4.19	0.66	0.99	0.7	1.01	1.32	0.93	1.14
Total	99.88	100.1	99.95	100.14	100.18	99.21	100.69	99.96	99.87	100.25	99.84	99.77	100.08	99.61	100.1	99.74	99.51
V	45.8	40.9	47.4	128.5	128.7	161.6	146	140.3	141.4	167.6	237	76.5	134.4	266.6	102.2	108.3	97.2
Ba	34.7	48	206.9	8.9	2.9	356.4	189.2	176.6	143.8	484	145.4	1033.2	133.6	113	360.9	477.2	391.5
Sc	5.6	7.2	5.4	6.8	19.2	23.9	35.2	21.6	28.4	24.8	14.4	33.6	34	43.4	16.1	20.7	16.2
La	2	9.5	5.5	13.3	37.5	4.2	4.7	10.2	4.2	24.6	20.2	31.7	22.1	32.6	11	39.6	34.9
Nd	-1.8	8.2	-1.3	31.3	29.6	16.5	7.2	13.9	3.1	36.2	15.6	66.1	53.7	46.8	24.8	52.7	48.2
Ce	0.4	9.9	1.8	37.8	86.3	29	6.3	26.6	10.7	77.6	40.8	102.1	87	99.7	48.5	102.8	96.6
Cr	935.7	674.5	813	68.7	119.3	238.1	452.9	217.7	370.4	56.1	239.1	11.2	53	73.4	321.5	87	68.2
Ni	415.9	316.1	425.3	32.8	53.5	68.6	68.1	58.8	62.5	18.7	85.2	5.1	17.1	24.2	28.8	30.4	35
Cu	17	290.6	22.3	20	13.6	58.8	37.3	32.7	35	25.2	84.8	26.4	46.4	31.1	10.8	27.1	18.9
Zn	78.5	36.2	115.4	36.4	51.9	56.9	57.8	53.8	63	66.5	139.3	135.3	88.7	114.7	75	57.4	44.9
Pb	0.1	2.5	1.3	1	0.5	2.8	2.5	4.2	6.3	11.9	3.9	18.6	8.5	4.8	7	17.5	17.4
Th	-0.2	2.1	-0.9	8	14.5	1.9	1.2	0.9	1.2	9.6	8.5	6	4.7	4.3	6.6	28.4	26.8
Rb	6.4	20	25.7	0.1	-1.2	41	7.4	7.4	9.1	125.3	31.8	97.6	7.9	43.2	60.2	136.3	108.2
Sr	70	75.7	113.7	553.4	1785.1	293.7	227.6	244.2	249.2	130	24.2	185.6	215.4	195.4	248.3	124.6	145.6
Y	1.5	11.1	1.2	18.6	32.2	17	15.6	18.6	15.1	51.3	12.6	75.6	63.6	65.3	29.7	46.2	43.9
Zr	4.2	13.7	6.8	78.7	163.2	92.6	55.5	71.6	56.2	369.4	193.2	462.3	364.1	365.7	41.4	240.6	241.1
Nb	2.1	4.2	2.1	6.6	16.8	5.7	3.4	5	4.4	16.2	24.7	26.4	20.7	24.3	5.1	18	16

	VAMR37	VAMR40	VAMR42	VAM42-2	VAMR43	VAMR48	VAMR58	VAMR58A	VAMR58C	VAMR81	VAMR85.2	VAMR86	VAMR88	VAMR90	VAMR93	VAMR94
SiO2	47.77	56.62	56.07	62.14	50.64	54.92	62.82	61.72	60.91	53.48	44.96	47.6	47.9	48.87	47.46	52.67
Al2O3	19.36	15.4	15.32	14.6	21.06	16.78	15.53	15.98	15.93	18.62	15.26	18.08	19.39	25.68	19.78	14.85
Fe2O3	7.92	11.72	13.99	9.26	11.62	10.95	5.06	5.99	5.55	10.03	10.32	8.72	8.28	11.58	12.86	15.04
MgO	9.27	2.27	2.33	1.78	4.42	5.18	3.88	3.92	4.8	3.96	13.6	9.4	9.51	4.57	4.76	2.45
CaO	10.96	5.41	5.92	3.61	3.19	4.69	4.12	4.53	4.41	4.63	8.63	9.27	10.67	1.47	4.35	6.32
Na2O	2.67	3.17	2.24	2.37	4.12	2.64	3.08	3.18	2.95	4.02	1.57	2.66	2.63	2.05	2.55	2.52
K2O	0.2	1.24	0.82	2.96	1.46	1.46	3.37	2.6	3.21	1.18	0.41	0.49	0.18	2.54	2.75	1.58
TiO2	0.98	1.99	2.07	1.53	1.55	1.23	0.75	0.88	0.49	1.36	0.84	1.09	0.98	1.44	1.68	2.08
MnO	0.12	0.18	0.2	0.12	0.32	0.19	0.08	0.1	0.1	0.15	0.15	0.14	0.12	0.45	0.16	0.22
P2O5	0.09	0.63	0.74	0.49	0.07	0.21	0.16	0.18	0.12	0.1	0.08	0.11	0.09	0.08	0.16	0.77
L.O.I.	0.75	0.97	0.29	0.92	1.87	1.71	0.85	0.94	1.14	2.04	3.72	2.29	0.82	2.27	3.33	1.2
Total	100.09	99.6	99.99	99.78	100.32	99.96	99.7	100.02	99.61	99.57	99.54	99.85	100.57	101	99.84	99.7
V	155.5	116.4	117.1	92.4	263	216.2	98	106.8	80.9	219.6	144	162.5	149.9	220.3	247.7	111.6
Ba	67.8	249.9	268.4	542	400.2	800.5	428.7	356.6	475.7	409.2	72	141.8	56.1	914.2	814.1	866.1
Sc	23.7	36.5	36.1	28.8	37.3	28.2	14.7	18.4	15.2	35.3	23.7	27.7	23.5	27.1	32.8	41.7
La	4.4	34.2	27	61.5	49.9	20	48.3	23.2	29.5	9.6	11	0.4	3.9	46.8	25.5	27.2
Nd	12.7	57.1	43.6	75.4	37.9	27.9	34.8	23.1	31.5	13.9	8.9	15.6	4.8	50	26.6	51.4
Ce	18	97.6	75.5	146.5	99.7	52.3	101	51.4	58.5	34.2	13.1	18.1	12.9	126.8	54.4	90.3
Cr	290.3	21.7	18.8	14.8	191.5	195.5	113.4	123.1	149.4	131.3	636.7	312	269.5	225.4	192.4	17.9
Ni	192.3	5.2	5.3	8.9	78	73.2	65.5	61.2	137.7	71.3	401.5	223	192.4	82.4	66	5.5
Cu	62	24.9	45.7	24.1	20.8	58.3	28.4	30.9	52.9	53.7	71.7	67.6	62.4	41	49.4	31.3
Zn	52.4	125	143.6	108.2	226.2	139.1	50.6	54.9	49.5	127.6	71.7	61.4	54.4	206	154.2	146.6
Pb	0.3	11.7	12.3	14	17.5	10.5	18.9	15.3	16.7	10.9	1.6	1.2	1.5	9.3	16.4	9.8
Th	0.6	7	2.8	36	8.9	5	28.2	19.1	26.1	3.4	0.1	0.7	1.1	21	9.7	6.3
Rb	4.6	46.5	23.7	181.6	48.6	44.4	124.3	121	103	40.8	12.3	15.8	3.6	72.1	126.9	43.8
Sr	240	218.4	240.1	166.5	299.4	289.5	160.5	154.1	172	394.1	154.1	245.9	240.3	186.6	213	226.5
Y	17.6	56.4	50.9	70.3	32.4	41.2	31.1	30.9	28.4	17.8	15.2	19.9	17.3	55.2	33.6	70.7
Zr	65.1	567	102.7	331	137.8	180.2	181.6	155.6	195.5	277.7	57.4	81.4	67.9	178.3	267.3	259.6
Nb	1.9	26.4	14.6	25.4	21.3	12.9	11.1	13.7	7.9	12.8	3.3	2.5	2.1	21.7	19.3	21.7

	VAMR97	VAMR103	VAMR104	VAMR112	VAMRU	VAMRV1	VAMRV2	VAMRY	VAMRZ
SiO2	48.68	51.62	50.12	48.67	56.65	55.57	55.58	54.51	44.82
Al2O3	20.01	15.11	20.46	13.19	14.23	17.53	15.38	14.63	18.28
Fe2O3	9.12	13.01	6.21	13.46	4.7	3.64	5.83	4.68	7.76
MgO	7.27	2.9	5.87	8.93	3.8	2.3	3.53	3.8	4.07
CaO	8.36	6.84	8.64	8.77	12.36	8.94	11.88	11.6	20.7
Na2O	2.53	3.26	2.84	1.62	4.88	6.15	4.78	5.08	1.26
K2O	0.72	1.65	2.03	0.64	0.12	0.47	0.19	0.36	0.09
TiO2	1.19	2.62	0.94	1.33	2.02	0.64	0.72	2.13	0.83
MnO	0.15	0.21	0.1	0.18	0.12	0.09	0.17	0.13	0.12
P2O5	0.16	0.87	0.13	0.2	0.28	0.11	0.1	0.32	0.18
L.O.I.	1.68	1.09	2.55	2.77	0.74	5.15	1.3	2.67	1.67
Total	99.87	99.18	99.89	99.76	99.9	100.59	99.46	99.91	99.78
V	216.8	229.8	141	379.1	246.2	100.7	100	256.6	200.1
Ba	218.5	942.8	419.9	285	35.2	119.3	67.9	87.9	8.4
Sc	27.7	43.6	20.4	45.6	34.3	17.4	14.2	40.3	27.2
La	13.4	37.7	13.9	2.8	15.2	24.6	30.6	22.9	35
Nd	11.6	73.4	15.6	9.4	22.2	25.4	32.7	33.2	36.5
Ce	27.2	118.8	27.9	16.7	38.6	54.6	62.1	58	82.7
Cr	428.8	27.4	119.4	274.4	93.7	118.5	98.3	103.1	148.4
Ni	111.3	11	56.6	85.8	14.5	21.6	41.1	20.8	73.3
Cu	92.7	35.6	31.5	57.8	16.3	3.2	10.2	8.3	34.7
Zn	100.5	149.1	59	235.9	20.9	21	25.3	27.3	15.3
Pb	6.8	11.5	7.3	5.7	2.2	2.3	2.5	0.6	5
Th	-1.4	6.9	2.7	0.1	8.5	8.4	12.1	5.4	14.4
Rb	21.2	37.6	85.5	9.8	2.2	17.6	4.5	10.3	3.3
Sr	237.2	235.9	307.1	86.6	698.4	877.6	905	688.6	998
Y	18	88.6	20.3	31.9	45	28.1	27.3	52.4	36.5
Zr	76.2	647.6	124.4	82.2	239.9	120.6	139.3	238.4	148.2
Nb	5.9	32.1	7.2	8.7	12.4	9.1	13.7	12.3	8.4

Ultramafic lithologies which failed the screening criteria

	EAF20A	EAF20B	EAF21	VAM2A	VAM9	VAM9A	VAM9B	VAM10	UM1	UMHT1	UMHT2	UMHT3
SiO2	38.77	37.27	30.62	43.97	40.17	39.17	39.38	39.68	39.61	38.9	39.53	42.12
Al2O3	3.28	3.41	17.65	15.01	0.18	0.33	0.3	0.36	0.83	0.52	1.36	2.15
Fe2O3	10.31	13.57	10.82	11.6	7.57	7.45	7.86	8.22	10.8	12.08	10.54	9.9
MgO	33.75	31.51	28.76	4.36	39.02	38.66	38.49	38.83	37.26	37.11	37.4	34.61
CaO	0.11	0.06	0.11	23	0.42	0.88	0.71	0.2	0.02	0.03	0.03	1.54
Na2O	-0.19	-0.17	-0.18	0.32	-0.19	-0.21	-0.25	-0.24	-0.12	-0.24	-0.17	-0.16
K2O	0.01	0.01	0	0	0	0	0	0	0	0	0	0
TiO2	0.14	0.17	0.49	0.6	0.02	0.02	0.01	0.02	0.04	0.05	0.1	0.08
MnO	0.05	0.07	0.14	0.26	0.06	0.08	0.07	0.11	0.06	0.14	0.1	0.13
P2O5	0.04	0.04	0.05	0.07	0.01	0.01	0.01	0.01	0.01	0.01	0.02	0.02
L.O.I.	10.09	9.56	11.4	0.89	12.55	12.98	N/A	12.07	11.15	11	11.14	9.95
Total	96.36	95.5	99.86	100.08	99.81	99.37	86.58	99.26	99.66	99.6	100.05	100.34
Sc	36	44.3	65.3	109	19.3	21.8	27.5	26.8	14.5	20	27.7	71.5
Ba	46.9	58.3	13.1	9.4	-1	1.2	8	5.4	-4.1	6.9	5	-2.5
V	4.1	3.8	11.2	14.3	6	6	8.1	7.2	0.6	-0.8	1.5	3.5
La	0.3	6.2	12.6	28.5	-2	0.5	-0.5	1.6	2.8	1.7	1.3	2.4
Ce	7.4	10	0.9	38.9	0.1	-0.4	0	-0.4	-0.4	-0.3	-0.4	-0.2
Nd	6.8	10.1	-0.1	72.6	0.2	-1.5	2.3	0.1	-1.8	0.7	-2.3	0.1
Cr	14103.6	20246.5	5103.6	57.6	1877.5	2232	2296.4	2323.9	2708.3	3489.2	2344.7	1156.4
Ni	2427.5	2625.7	1384	41	2458.7	2298.4	2424.3	2273.9	2756.1	2645.8	1421.5	1944.6
Cu	1.6	3.4	26.3	-2	13.3	10.2	17.3	13.9	14.8	34.9	15.4	111
Zn	64.7	115	217.3	32.6	29.6	34.9	33.2	33	40.5	80	67.3	60.7
Pb	4.7	40.4	1.7	-1.1	2.8	1.2	1.5	1.6	3	2.5	1.4	2.9
Th	4.1	6.3	0.5	11.1	2.8	1.8	1.7	1.4	3.6	2.8	2.7	2.1
Rb	-1.1	-1	-1.9	-2.4	-1.7	-1.4	-1.2	-1.3	-1.6	-1	-0.4	-1.1
Sr	3.6	5.2	4.8	1092.2	7.2	17.1	7.5	3.1	2.3	2.2	2.5	4.3
Y	3.1	16.7	1.3	56.5	0.4	1	-0.2	0.8	0.9	1	1.2	0.9
Zr	2.3	2.8	3.8	249.8	-0.3	0.4	-0.8	-0.1	-0.2	0.3	0.2	0.7
Nb	3.4	5.7	7.6	16.2	1.6	1.3	0.6	1.9	1.6	1.3	1.5	1.4

Melts from the Vamvakia River

	VAM11-1	VAM11-2	VAM20	VAMRW	VAMR34A	VAMR34	VAMR58	VAMR58A	VAMR58C	VAMR95A	VAMR95	VAMR101-2	VAMR111	VAMR111C	VAMR44	VAMR45	VAMR60
SiO2	74.72	67.37	69.96	69.56	64.63	65.9	62.82	61.72	60.91	74.97	74.07	66.49	67.34	65.12	62.22	64.29	73
Al2O3	13.12	15.26	14.53	11.1	14.97	14.52	15.53	15.98	15.93	13.83	13.6	14.5	14.62	16.5	16.33	16.43	13.43
Fe2O3	1.62	4.02	3.17	2.83	5.16	5.55	5.06	5.99	5.55	3.6	4	3.21	4.13	4.14	7.21	5.37	1.7
MgO	0.42	1.8	1	2.04	2.45	2.52	3.88	3.92	4.8	0.8	0.96	1.52	2.01	1.91	3.15	2.15	0.45
CaO	0.69	2.23	1.58	3.53	4.36	3.34	4.12	4.53	4.41	0.39	0.38	4.97	3.88	4.51	1.62	3.97	1.25
Na2O	3.46	3.61	3.1	0.04	3.03	2.6	3.08	3.18	2.95	0.11	-0.05	3.98	4.21	4.92	2.69	4.65	2.69
K2O	4.48	3.24	5.14	2.18	2.58	3.14	3.37	2.6	3.21	2	1.84	0.92	0.59	0.59	2.84	0.79	6.16
TiO2	0.28	0.57	0.56	0.33	0.9	0.97	0.75	0.88	0.49	0.25	0.19	1.13	0.92	0.86	1.02	0.66	0.34
MnO	0.02	0.05	0.03	0.04	0.09	0.08	0.08	0.1	0.1	0.03	0.03	0.05	0.07	0.08	0.08	0.09	0.03
P2O5	0.11	0.23	0.16	0.12	0.2	0.19	0.16	0.18	0.12	0.2	0.18	0.31	0.13	0.18	0.12	0.2	0.07
L.O.I.	1.22	1.81	1.16	7.74	1.14	0.93	0.85	0.94	1.14	3.25	4.36	2.92	2.17	1.04	2.37	1.15	0.92
Total	98.9	98.4	99.24	91.78	98.45	98.81	98.84	99.08	98.48	96.16	95.19	97.09	97.9	98.8	97.29	98.58	99.11
V	5.3	10.2	9	4.1	16.2	20.7	14.7	18.4	15.2	8.7	7	15.6	16.5	24.2	19.6	17	1.3
Ba	382.2	723.5	599	665.8	391.5	477.2	428.7	356.6	475.7	62	55.9	702.6	619.1	599.9	889.5	477.8	1197.5
Sc	16.7	82	38.7	33.9	97.2	108.3	98	106.8	80.9	25.2	15.3	53	100.3	105.5	153.5	95.9	21.5
La	33.7	30.6	24.9	22.5	34.9	39.6	48.3	23.2	29.5	11.9	13.6	39.5	19.7	17.5	43.3	36	9
Nd	72.4	73.9	63.3	54.6	96.6	102.8	101	51.4	58.5	253.7	154.6	96.4	40.5	26.2	95.7	87.2	33.8
Ce	31.9	30.1	29.8	27.9	48.2	52.7	34.8	23.1	31.5	1.9	17.7	51.3	16.7	8.6	42	42.6	14.3
Cr	5.7	50.5	22.4	19.6	68.2	87	113.4	123.1	149.4	7.4	8.3	54.9	16.3	15.1	135.6	46.2	8
Ni	3.2	18.5	6.7	17.2	35	30.4	65.5	61.2	137.7	4.8	2.8	38.3	5.4	5	56.9	15	3.9
Cu	4	15.9	10	30.7	18.9	27.1	28.4	30.9	52.9	3.9	3.3	61.9	35.6	23.8	47.1	19.2	5.8
Zn	21	65.6	45.3	20.6	44.9	57.4	50.6	54.9	49.5	19.1	20.4	33.3	38.5	36.8	120.5	85.6	14.4
Pb	20.9	23.1	23.4	4.3	17.4	17.5	18.9	15.3	16.7	5.5	0.9	16	15	18.7	21.8	16.5	14.2
Th	20.4	14.5	16.4	11.2	26.8	28.4	28.2	19.1	26.1	4.6	6.5	6.2	1.1	-0.2	16	10.6	4.9
Rb	148.7	100.4	200.8	58.3	108.2	136.3	124.3	121	103	65.8	60.8	30.3	14.6	14.4	92	14.2	107.8
Sr	60.6	231.4	79.7	59.7	145.6	124.6	160.5	154.1	172	13.9	10.4	248.1	416.3	474.4	258.7	428.8	141.2
Y	31.5	21.9	30.3	30.4	43.9	46.2	31.1	30.9	28.4	16.3	15.7	26.4	10.8	13.2	27.4	27.2	9
Zr	144.2	147.3	337.2	124.2	241.1	240.6	181.6	155.6	195.5	62.5	60.5	584.7	74.8	61.3	269.7	215	186.3
Nb	10.3	12.6	14.6	8.1	16	18	11.1	13.7	7.9	8.7	8.1	20.6	9.5	9	16	13	5.7
R1	2652	2332	2263	4028	0	0	0	0	0	0	0	0	0	0	0	0	0
R2	352	627	504	697	0	0	0	0	0	0	0	0	0	0	0	0	0

Askos Granites& Granitic Gneisses

	ASK1-1	ASK1-2	ASK1-3	ASK1-4	ASK1-5	ASK3	ASK3-B	ASK4	ASK4-1	ASK5A	ASK7	ASK7A	ASK9A	ASK10	ASK10A	ASK14	ASK20	ASK33
SiO2	75.02	74.99	78.75	78.22	76.68	75.18	77.4	78.18	78.42	70.18	76.62	78.14	73.16	75.43	76.1	65.66	72.51	71.7
Al2O3	12.53	12.5	11.87	12.17	12.32	12.76	12.25	12.56	12.17	14.21	11.58	12.51	12.79	13.49	14.22	15.76	15.18	13.76
Fe2O3	1.92	1.65	0.72	0.8	0.75	2.08	0.81	1.11	0.74	3.87	1.88	0.97	2.47	1.33	0.38	5.17	1.36	4.33
MgO	0.48	0.45	0.23	0.26	0.57	0.42	0.17	0.31	0.24	1.54	0.41	0.39	0.5	0.75	0.4	2.36	0.75	1.77
CaO	1.06	0.78	1.75	1.62	2.56	0.73	0.31	0.84	1.1	1.45	0.55	0.86	1.18	0.6	0.84	2.42	1.3	0.88
Na2O	3.17	3.09	5.4	5.39	5.04	2.91	3.36	4.64	6.37	4.15	2.63	6.16	2.72	6.92	7.3	4.76	7.23	1.62
K2O	4.68	5.3	0.2	0.22	0.45	5.08	5.09	1.47	0.14	2.34	5.33	0.16	4.8	0.21	0.33	2.08	0.31	2.42
TiO2	0.32	0.29	0.18	0.18	0.23	0.32	0.1	0.22	0.22	0.5	0.3	0.15	0.38	0.35	0.28	0.73	0.48	0.61
MnO	0.01	0.01	0.01	0.01	0.01	0.02	0.01	0	0.01	0.04	0.01	0.01	0.02	0.01	0.01	0.06	0.02	0.07
P2O5	0.07	0.07	0.03	0.03	0.06	0.08	0.02	0.04	0.04	0.24	0.07	0.03	0.11	0.11	0.06	0.24	0.14	0.14
L.O.I.	1.01	1	0.8	0.95	1.32	1.17	0.68	1.25	0.84	1.56	0.73	1.05	2.04	1.04	0.8		0.99	2.34
TOTAL	99.26	99.12	99.15	98.89	98.67	99.57	99.52	98.38	99.43	98.53	99.37	99.37	98.15	99.2	99.9	99.24	99.28	97.3
V	4	3.4	1.7	3.5	3.1	5.1	2.5	3.3	4	7.8	1.9	3.2	7.9	4.9	3.6	15	7	14.2
Ba	403.4	289.7	45.1	44.3	76.3	235.6	34.5	250	11.9	397	247.9	39.5	467.7	12.4	32.8	513	70.3	721.8
Sc	15.3	15	8.3	9.1	23.5	17.4	2.8	15.5	13.2	54.2	19	17.1	25.5	25.9	17.6	89	26.5	86.4
La	52.2	48.4	40.5	37.7	31.2	44.1	40.1	46	43.8	18.9	41.7	28.2	44.2	44.4	5.6	35	78.5	39.2
Nd	108.5	110.9	95.2	86.1	72.9	112	82.2	86.7	78	55	94.1	67.6	86	86.3	30.3	76	147.2	78.7
Ce	54.6	51.8	38.4	33.6	32.2	42.8	40.2	32.8	30.2	26.6	43.7	27.5	41.1	33.9	16.5	33	59.9	31.7
Cr	5.3	6.3	0.6	0.5	6.7	3.9	0.3	3.9	2.6	46.8	6.2	4.7	6.2	8.8	4.2	79	8.7	70.5
Ni	3	6.2	1.9	1.5	4.6	4.1	1.6	1.6	3	21.6	3.8	2.7	5.4	6.1	2.5	41	7.6	27.4
Cu	4.9	3.8	-1	0.8	1.9	7.9	1.8	0.1	-1.4	12	3.2	15.2	7.7	-0.5	-2.5	30	-0.2	29.3
Zn	12.2	16.7	0.2	-0.5	3.2	33.3	8	1.3	-0.4	39.8	27.7	5.9	24	11.9	0.6	47	13	68.5
Pb	10.4	13.9	2.7	1.6	4.6	18.9	18	3.7	1.1	14.9	19.5	7.5	19.9	3.5	3.7	9	6	17.7
Th	23.2	24.1	46.7	42.2	30.7	28.3	38	39	37.4	10.6	23.7	24	25.2	40.7	28.3	16	31.3	13.1
Rb	129	187.4	9.8	9.8	24.3	195.3	213.4	72.5	2.1	88.2	192.5	4.8	141.5	8.5	17.1	86	9.1	67.7
Sr	74.9	75.9	161.4	171.4	187.6	34.9	13.1	58.3	109.8	177.5	33.4	127.8	75.9	59.4	93.4	223	128	141.5
Y	56.4	37.2	28.5	26.6	27.7	55.2	58.36	28.4	33.4	27.2	33.7	28.2	43.5	32	25.4	33	28.5	24.5
Zr	275.1	237.9	116.9	120.1	126.7	247.6	111.9	129	130.8	160.8	215.2	87.6	212.9	233.6	140.5	205	334.5	210.4
Nb	18.1	16.4	9.3	8.8	9.8	18.8	18.4	12	10.5	10.6	15.8	5.6	14.2	12	9.5	13	14.4	12.5
R1	0	0	0	0	0	0	0	0	0	0	0	0	0	0	0	0	0	0
R2	0	0	0	0	0	0	0	0	0	0	0	0	0	0	0	0	0	0

	Arnaea Granites														Kerdilion Granitoids					
	ASK36	ASK38	ASK39	ASK42	EAF1B	EAF14A	ARN1	ARN2	ARN3	ARN4	ARN5	ARN7	ARN8	ARN T.	VAM14	VAM15	STAV-1	STAV-2	STAV-4	STAV-6
SiO2	74.49	76.94	78.68	77.9	70.25	80.04	78.42	77.31	68.36	78.09	79.04	76.94	77.87	74.17	70.37	72.56	68.06	70.61	72.64	75.53
Al2O3	12.47	11.47	12.38	12.29	14.31	11.71	12.74	11.96	17.09	11.8	12.41	12.11	12.01	13.04	15.64	14.97	12.53	11.39	14.85	13.59
Fe2O3	1.88	0.89	1.14	1.57	5.13	1.13	0.45	1.26	3.55	1.25	0.31	1.18	1.23	1.73	2.6	1.63	4.99	4.07	1.08	2.41
MgO	0.4	0.22	0.34	0.37	0.52	0.16	0.09	0.22	0.04	0.2	0.03	0.17	0.14	0.34	0.85	0.72	3.04	2.34	0.37	0.29
CaO	0.97	0.07	0.3	0.25	0.5	0.62	0.66	0.36	1.4	0.24	0.94	0.38	0.58	0.73	2.12	2.73	5.4	5.42	1.36	1.6
Na2O	3.37	0.92	3.93	4.94	5.71	6.08	5.23	3	9.07	3.28	6.5	2.95	3.13	3.22	3.92	4.29	1.77	1.12	3.91	5.82
K2O	4.59	8.56	2.08	1.57	1.82	0.14	2.47	5.28	0.09	4.54	0.13	5.34	4.98	5.63	3.39	1.64	1.64	2.57	4.58	0.68
TiO2	0.29	0.12	0.13	0.2	0.52	0.12	0.15	0.17	0.05	0.19	0.13	0.18	0.18	0.26	0.32	0.21	0.76	0.59	0.17	0.21
MnO	0.02	0	0.01	0.02	0.02	0.01	0	0	0.01	0	0	0.01	0	0.03	0.05	0.02	0.1	0.06	0.02	0.02
P2O5	0.07	0.03	0.03	0.04	0.1	0.02	0.03	0.4	0.03	0.05	0.02	0.04	0.05	0.07	0.11	0.12	0.15	0.14	0.08	0.05
L.O.I.	1.07	0.88	1.43	1.41	1.75	0.67	0.41	0.71	0.75	0.81	0.65	0.55	0.53	1.09	0.89	1.21	1.25	1.59	0.51	0.3
TOTAL	98.55	99.2	99.01	99.16	98.88	100.02	100.24	99.6	99.68	99.62	99.5	99.31	100.17	99.23	99.38	98.91	98.44	98.2	99.08	100.2
V	3.5	3.7	3.1	8.2	11.7	2.9	2.2	5.2	-0.1	2.7	1.1	5.2	1	2.6	4.8	4.8	16.7	11.4	0.8	8.8
Ba	278.8	712.6	687.7	325.1	299.9	50	52.7	88	6.9	99.5	3.7	84.8	106.5	411.9	521.4	399.7	252	503.6	427.5	215.3
Sc	17.5	3.9	7	13.1	7.8	5.1	1.5	5	6.4	6.1	-0.4	5.2	7.2	14.5	28.3	33.6	106.8	79.1	10.3	-0.4
La	53.7	47.8	34.1	35.9	39.8	34.1	57.5	38.2	56.9	74.6	11.7	62.4	47	52.2	31.9	11.8	27.1	33.2	22.4	8.7
Nd	128.8	102.4	102.2	89.4	117.9	89.4	102.5	72.7	121.5	75.7	33.6	126.7	97.6	104.2	66.4	42.3	55.5	61.4	46.2	29.8
Ce	55	56	32.7	41.7	62.5	32.2	44.3	38.7	49.6	72.3	16.4	62.3	42.3	48.2	27.7	20.8	30.3	26.4	22.5	20.4
Cr	3.9	2.8	-0.5	1.3	2.2	-1.4	-1	2.7	1.6	2.6	-0.6	2.6	1.5	4.8	5.2	8.8	146.8	122.7	3.1	0
Ni	4.4	2.3	2.9	1.9	2.8	2.4	2.2	3	1.5	2.1	2.5	1.9	2.5	3.8	4	5.2	58.7	54.3	4	1.2
Cu	4.6	4.8	0.8	4.8	18.3	-0.7	1.7	1.1	1.4	2	-0.8	4.1	4.7	4.8	6.4	4.9	14.3	27.4	4.3	6.4
Zn	24.2	4.9	15.1	7.9	37.4	3.7	3.1	23	-2.6	24.5	-2	27.2	12.8	11	43.3	26.9	88.3	69.2	37.1	13
Pb	16.8	6.1	19	-0.5	5.9	1	7.4	21.5	0.7	22.5	1.7	20.8	23.1	4.8	20.7	23.2	12.1	14.6	45.8	11
Th	27.5	27.7	30.9	19.5	18.2	27.2	25.8	28.5	43.4	28.2	34.3	29.2	27.9	23.7	12.7	10.2	9.6	9.7	15.7	3.8
Rb	126.6	201.8	48.9	42.4	46.9	3.2	93.6	252.4	5	199.8	3.3	283.7	236.4	134.7	122.1	52.1	75.4	119.8	238.9	18.7
Sr	55.8	31.8	36.2	26.2	107.4	57.6	64.6	19.2	192.6	42.5	101.4	17.2	36.8	66.9	125.7	255.5	145	172.9	187.5	106.5
Y	55.5	48.7	52.4	43.2	84.1	43.3	39	38.7	15.7	41.7	50.7	59.8	49.4	45.2	25.6	15.2	29.3	19.1	6.7	53.8
Zr	219	137.9	154.8	220.5	1138.5	110.5	123.9	147.7	274.1	154.3	209.7	164.5	147.6	195.4	165.4	110	176.7	173.2	84.2	197.3
Nb	16.9	15	19	16.7	26.7	11.8	16.2	15.7	1.8	16.3	14.6	17.8	16.1	14.3	12.7	5.2	18.2	13.9	10.9	5.2
R1	0	0	0	0	0	0	0	0	0	0	0	0	0	0	0	0	0	0	0	0
R2	0	0	0	0	0	0	0	0	0	0	0	0	0	0	0	0	0	0	0	0

	Modhi Granitoids												Lefkoudha Granitoids			
	MOD 1	MOD14	MOD15	MOD16	MOD17	MOD18	MOD19	MOD20	MOD21	MOD22	MOD23	MOD24	LEF23-2	LEF18	LEF 21 A	LEF 21B
SiO2	74.48	77.48	71.43	87.02	86.69	79.7	74.7	77.42	74.81	76.13	72.85	69.23	64.49	71.47	75.59	74.93
Al2O3	14.1	12.1	16.09	6.63	7.33	10.98	13.53	11.92	13.21	12.56	14.12	14.36	21.12	14.56	14.67	13.96
Fe2O3	1.55	1.35	1.75	0.44	0.42	1.13	1.91	1.49	1.72	2.01	2.28	4.31	1.37	1.42	0.85	1.2
MgO	0.44	0.47	0.7	0.14	0.22	0.47	0.71	0.4	0.53	0.67	0.84	1.26	0.4	0.41	0.27	0.41
CaO	0.29	0.24	0.36	0.11	0.15	0.24	0.33	0.52	0.36	0.72	0.65	1.42	4.16	1.25	1.14	1.5
Na2O	4.76	3.48	5.16	0.78	2.03	3.21	3.92	4.59	4.83	5.8	5.51	5.31	7.45	2.6	3.93	4.91
K2O	2.94	3.24	2.91	4.04	2.32	2.54	2.87	2.22	2.86	0.91	2.29	2.17	0.42	7.14	3.14	1.9
TiO2	0.36	0.26	0.34	0.17	0.2	0.26	0.34	0.27	0.33	0.3	0.35	0.49	0.42	0.37	0.11	0.15
MnO	0.01	0.01	0.01	0.01	0	0.01	0.01	0.02	0.02	0.02	0.03	0.04	0.03	0.02	0.02	0.02
P2O5	0.14	0.1	0.15	0.08	0.09	0.011	0.14	0.11	0.13	0.117	0.14	0.18	0.07	0.09	0.18	0.14
L.O.I.	1.37	1.53	1.59	1.03	0.66	1.45	1.61	0.98	1.68	0.76	0.6	1.37	0.91	1.05	1.08	0.81
TOTAL	99.1	99.73	98.9	99.41	99.45	98.64	98.45	98.96	98.89	99.22	99.06	98.77	99.94	99.35	99.91	99.15
V	7.2	4.2	5.3	2.2	4.3	1.7	6.4	6.1	5.6	5.2	5.3	8.5	3.1	0.5	0.8	3.7
Ba	396	371.9	269.1	607.2	306.6	322.4	341.6	344.9	466.9	362.9	417	243.1	386.6	567.6	201.8	369.6
Sc	19.5	16.9	26.4	6.7	5.9	12	23.1	15.7	17.1	24.6	22.3	42.2	23.6	11.3	6.4	18.5
La	33	25	37.8	19.3	24.2	20.3	44.3	97.5	18	49.5	28.3	53.2	20	55.2	6.3	7.5
Nd	67.6	60.9	82.9	45.5	48.8	40.5	84.6	272.6	47.2	99.1	63.1	91.9	31.3	102	9.8	25.6
Ce	32.8	27.7	37.2	17.3	17.7	15.2	38	64.1	21.9	43.4	26.6	48.4	14.3	40.3	1.8	9.8
Cr	6.4	5.9	8.1	3.5	4.5	5.8	8.4	8.5	6.6	5.6	9.5	12.6	8.7	10.7	2.9	4.8
Ni	5.5	2.1	3.3	2.2	2.1	2.7	3.6	4.2	4.8	3.3	4.5	7.5	5	5.5	2.9	6.8
Cu	1.8	2.9	2.3	2	2.1	2.7	3.3	2.8	1.9	4.8	5.7	46.6	7.1	6.4	2.7	5.8
Zn	20.3	18.9	24.9	3.2	3.4	15.6	33.9	21.5	27.8	24.5	41.9	64.4	13.7	18.6	15.4	12.5
Pb	11.8	15.5	12.6	30.7	13.1	13.4	16	19.6	20.1	15	26.4	40.8	23.2	21.8	31	25.6
Th	21.6	16.5	22	9.1	11.7	14.7	23	18.4	21.5	19.3	22.5	32.6	0.7	9.3	3.5	8.5
Rb	118.8	118.4	133.9	100.9	70.6	96.1	123	63.6	76.5	25.5	68.9	84.9	6.3	99.8	112.7	62.5
Sr	37.3	48.8	39.9	63	31.9	32.1	39.5	67.4	70.7	82.7	67.5	99.5	388.2	115.4	70.5	175.4
Y	36	32.4	43.4	17	22.6	21.5	38	31	28.1	43.5	29.3	54.2	10.7	11.6	12.2	19.9
Zr	194.3	143.9	190.6	90.4	110.7	144.3	195.2	151.9	187.7	165.4	195	273.2	438.3	233.5	26.5	64.1
Nb	13.3	10.6	13.6	7.2	7.9	9.2	11.9	10.5	11.1	11.3	12.2	15.9	8	6.4	9.3	10.9
R1	0	0	0	0	0	0	0	0	0	0	0	0	0	0	0	0
R2	0	0	0	0	0	0	0	0	0	0	0	0	0	0	0	0

	JED DATA-Granitic Melts and Leuco Dykes											GRANITE.	
	DD106A	DD103	DD158A	DD247B	MYRP11BM	MYRP11BW	ANMP2	ZN25	BGK1	DDBAM	DD114E	EMV13	EMV17
SiO2	78.5	75.3	69.76	74.16	62.54	68.62	63.17	63.77	59.22	63.35	62.86	77.91	76.76
Al2O3	11.96	12.85	14.9	15.43	16.02	17.65	16.35	16.27	16.8	18.47	16.01	12	12.23
Fe2O3	1.16	2.3	3.21	0.76	5.93	1.4	3.53	5.21	5.08	2.41	3.21	1.39	1.7
MgO	0.08	0.13	1.16	0.46	1.37	0.33	2.18	1.43	4.19	1.23	2.12	0.06	0.11
CaO	0.21	0.62	1.58	1.02	6.07	3.24	5.68	3.79	6.58	5.89	6.94	0.15	0.27
Na2O	4.22	3.93	4.48	7.21	5.7	7.59	5.82	4.61	5.07	6.66	6.71	4	3.9
K2O	3.72	4.74	4.19	0.24	0.35	0.19	0.66	3.08	0.74	0.34	0.56	4.5	4.53
TiO2	0.07	0.15	0.35	0.08	1.14	0.45	1.36	0.86	1.25	0.92	1.09	0.08	0.11
MnO	0.01	0.03	0.06	0.01	0.08	0.02	0.04	0.06	0.08	0.04	0.06	0	0.01
P2O5	0	0.012	0.03	0.04	0.25	0.07	0.34	0.17	0.23	0.22	0.24	0.01	0.02
L.O.I.	0.3	0.2	0.5	0.7	0.5	0.3	0.9	1.2	1.2	0.5	0.4	0.41	0.34
TOTAL	100.23	100.262	100.22	100.11	99.95	99.86	100.03	100.45	100.44	100.03	100.2	100.11	99.64
V	0.1	2.3	31.7	12.1	29.1	14.7	93.7	133.4	134.6	58	66.3	1.7	0.3
Ba	40.4	128.6	365	35.2	53.4	42.4	27.3	449.7	135	104	15.2	44.1	57.3
Sc	-1.7	0.5	1.5	-2.3	22.8	9.5	18	6.6	17.5	12.3	14.1	1.6	2.6
La	25.1	62.9	20	-2.7	44.7	12.9	22.5	22.5	6.7	34	12.7	28.4	55.1
Nd	45.1	63.2	22.1	5.7	47.5	21.5	49.8	29.5	19.7	48.3	39	77	119.8
Ce	86.4	156.2	54.6	14	106.9	50.5	93.8	67.2	29	100.8	63.1	42.3	56.7
Cr	-1	-0.3	23.7	2.3	12.9	-0.1	39.1	17.9	97.3	17.8	41.6	1.5	5.1
Ni	2.8	2.5	13.9	5.8	7.8	3.1	17.6	18	46.5	17.8	13.1	2.1	3.4
Cu	0.3	1.2	20	1.7	7.1	1	0.2	6.2	7.6	6.9	0.2	2.4	1.5
Zn	9	11.7	29.6	4.4	22.1	4.2	4.2	36.2	37.7	8.1	3.6	-0.1	22.5
Pb	7	5.3	7.9	4.4	5.7	3.9	5	9.4	7.5	0.9	1.6	2	7.7
Th	24.1	24.8	29.4	4.6	7.7	9.4	17.8	25.1	17.5	28.6	15.7	22.2	21.7
Rb	162.3	98.9	99	5.8	0.2	-0.6	24.6	75.7	22.1	1.5	20.7	107.5	180.2
Sr	17.1	33.7	84.3	1.7	373.2	353.2	399.6	272.1	262.5	679	323.3	16.3	22.7
Y	97.1	76.1	16.9	4.3	66.6	26.7	96.3	40.3	42.4	88.3	92.5	69.7	89.5
Zr	275.6	320.7	222.8	20.5	501.8	865.8	939.3	760.4	816.4	866.3	847.1	225.8	262.8
Nb	23.2	23.1	4	3.1	14.9	6.5	18.7	6.8	8.5	20.1	17.2	30.4	24
R1	0	0	0	0	0	0	0	0	0	0	0	0	0
R2	0	0	0	0	0	0	0	0	0	0	0	0	0

APPENDIX II

RADIOMETRIC AGE DATA FOR THE INTERNAL HELLENIDES

PART I: Granitoids and related rocks

Reference	Description	Locality	Sample No.	Sample Type	Analytical Technique	Age (1) (Ma)	Age (2) (Ma)	Latitude	Longitude
Rhodope Massif									
Harre et al., 1968	Mesolakkia Hbl-granitoid	3.5 km N of Ofrinion 2.2 km WSW of Mesaolakkia	302	Biotite	K-Ar	15.0 ± 0.3 13.8 ± 0.2	15.4 14.1	40°49′20 40.8222	23°54′17 23.9047
Marakis 1968	Vrontou granite	50 km NW of Drama	24.1 24.2 24.3 24.4 24.5 24.6	Biotite Biotite Biotite Biotite Biotite Biotite	K-Ar K-Ar K-Ar K-Ar K-Ar K-Ar	29 ± 1 29 ± 1 30 ± 2 30 ± 1 31 ± 1 33 ± 2	30 30 31 31 32 34	41°16′22 41.2727	23°36′47 23.6131
(in) Durr et al., 1976	Vrontou granitoid-granite	50 km NW of Drama	*	Biotite	K-Ar	30 ± 3	31	41°16′22 41.2727	23°36′47 23.6131
	Panorama granitoid	30 km NW of Drama	*	Biotite	K-Ar	26.8 ± 0.5	27.5	41°16′22 41.2727	23°46′47 23.7798
	Granitis granitoid	25 km NW of Drama	*	Biotite	K-Ar	28.2 ± 0.5	28.9	41°17′44 41.2955	23°55′00 23.9167
	Thalos pegmatite	25 km E of Drama	*	Musc	K-Ar	38.3 ± 1.1	39.2	41°06′49 41.1136	24°31′05 24.5179
	Xanthi granitoid	55 km E of Drama	*	Biotite	K-Ar	27.1 ± 0.4 27.9 ± 0.5	27.8 28.6	41°09′33 41.1591	24°56′47 24.9464
Kronberg 1966	Krinidhes granitoid	12 km S Drama	*	Biotite	K-Ar	26.0 ± 0.5		41°04′06 41.06882	24°17′51 24.2976
Serbomacedonian Massif									
De Wet et al., 1989	Arnaea granite	SE of Paleohora	AD 84134	Phlog	Ar-Ar	136.5 ± 1.5		40°30′00 40.5000	23°30′32 23.5089
De Wet & Miller (unpubl)	Arnaea granite	E of Paleokastron	AD 8493	Musc	Ar-Ar TF	122.6 ± 51		40°27′51 40.4642	23°32′58 23.5328
De Wet et al., 1989	Arnaea granite	Various	128/ 304	W/R	Rb-Sr	155 ± 11 153 ± 3 144 ± 1		40°30′ 40.50	23°30′ 23.50
De Wet et al., 1989	Ouranopolis granite	0.5 km S of Ouranopolis	AD 84314	Musc Biotite	Ar-Ar Ar-Ar	44.5 ± 1 47.2 ± 0.7		40°19′26 40.3239	23°59′14 23.9872
Papadakis 1971	Stratoni granite	0.5 km N of Stratoni	*	Biotite	K-Ar	29.6 ± 1.4		40°31′28 40.5244	23°49′49 23.8303
Harre et al., 1968	Pegmatite in Vertiskos	11 km NE of Langadhas	305/G10	Musc	K-Ar	191 ± 3 135 ± 2	195 ± 3 138 ± 2	40°49′35 40.8264	23°09′17 23.1547
	Musc-Bi-granitoid in Kerdilion	3 km SE of Dafni	114/G5	Biotite	K-Ar Rb-Sr	39.0 ± 0.8 43.2 ± 3.1	40.0 ± 0.8 44.7 ± 3.1	40°49′52 40.8311	23°40′34 23.6761
	Pegmatite in Kerdilion	3 km WNW of Stavros	117/G9	Musc	K-Ar Rb-Sr	36.8 ± 0.8 48.0 ± 2	37.7 ± 0.8 49.7 ± 2	40°40′34 40.6761	23°39′17 23.6547
	Pegmatite in Kerdilion	7.5 km NE of Asprovalta	115/G6	Biotite	K-Ar Rb-Sr	32.9 0.6 31.3 ± 0.6 39.0 ± 2.8	33.7 ± 0.6 32.1 ± 0.6 40.4 ± 2.8	40°40′21	23°46′04
Marakis 1968	Rendina Granite	Rendina WNW of Stavros	25.1 25.2 25.2	Biotite Musc Musc	K-Ar K-Ar K-Ar	36 ± 1 41 ± 2 42 ± 1	37 ± 1 42 ± 2 42 ± 1	40°41′ 40.68	23°39′ 23.65
Servas 1975	Pegmatite in Vertiskos	Langadas	*	W/R	Rb-Sr isochron	152 ± 26	155 ± 26	40°40 40.67′	23°09′ 23.15
Marakis 1969	Pegmatitite in Vertiskos	Langadas	27.1 27.1	Biotite	K-Ar	140 ± 3 139 ±3	143 ± 3 142 ± 3	40°40′ 40.67	23°09′ 23.15

Reference	Description	Locality	Sample No.	Sample Type	Analytical Technique	Age (1) (Ma)	Age (2) (Ma)	Latitude	Longitude
Vardar Zone									
Soptrajanova 1967 in Spray 1984	Furka granite	S Yugoslavia	*	Biotite	Rb-Sr	168 ± 7	171 ± 7		
	Stip granite	SYugoslavia	*	Biotite	Rb-Sr	156 ± 3	159 ± 3		
Mercier 1968/1973	Furka granite	S Yugoslavia	*	?	?	156 6	159 ± 6		
					K-Ar	167	171		
					Rb-Sr	156	160		
	Stip granite	S Yugoslavia	*	?		150	153		
					?	167			
Borsi et al., 1966	Fanos granite	Reka Valendi Leka	26.1 EB	Biotite	Rb-Sr	148	151	44°01′06	22°27′20
								44.0183	22.4556
			27.1 EB	Biotite	Rb-Sr	151	154	44°01′11	22°28′02
								44.0197	22.4672
			28.1 EB	Biotite	Rb-Sr	153	156	44°01′20	22°28′20
					K-Ar	150	153	44.0222	22.4722
			29.1 EB	Biotite	Rb-Sr	152	155	44°01′34	22°28′38
								44.0261	22.4772
			28 EB	Biotite	Rb-Sr	149	153	44°02′08	22°28′38
								44.0356	22.4772
		Kodza Dere	85 EA	Biotite	Rb-Sr	151	154	44°02′08	22°27′33
								44.0356	22.4592
		Kour Dere	15 EC	Biotite	Rb-Sr	153	156	44°02′31	22°29′01
								44.0419	22.4836
		Plaghia	44 EC	Biotite	Rb-Sr	147	150	44°05′02	22°29′31
								44.0839	22.4919
Marakis 1968	Fanos granite	N of Thessaloniki	21.5	Biotite	K-Ar	113 ± 3	116 ± 3	41°05′	22°29′
			21.5	Biotite	K-Ar	113 ± 3	116 ± 3	41.08	22.48
			21.7	Biotite	K-Ar	132 ± 4	135 ± 4		
			21.7	Biotite	K-Ar	134 ± 4	137 ± 4		
			21.1	Biotite	K-Ar	146 ± 3	149 ± 3		
			21.2	Biotite	K-Ar	148 ± 4	151 ± 4		
			21.3	Biotite	K-Ar	148 ± 4	151 ± 4		
			21.6	Biotite	K-Ar	148 ± 4	151 ± 4		
Ricou 1965	Monopigadhon granite	Monopigadhon village	*	Biotite	K-Ar	180		40°26′	23°07′
								40.44	23.12
Mercier 1968	Karathodhoro gneiss	E of Fanos	*	Biotite	Rb-Sr	146 ± 20	149 ± 20	41°03′49	22°36′31
	granite-aplite		*	Biotite	Rb-Sr	156 ± 5	159 ± 5	41.0636	22.6086
			*	Biotite	Rb-Sr	156 ± 5	159 ± 5		
			*	Biotite	Rb-Sr	157 ±5	161 ± 5		
			*	Biotite	Rb-Sr	157 ± 5	161 ± 5		
Spray et al., 1984	Fanos granite	*	*	Biotite (Igneous)	K-Ar		148 ± 3	41°05′	22°29′
								41.08	22.48
Kreuzer pers. comm. in Mussallam et al.,1986	Monopigadhon granite	*	*	Biotite?	K-Ar		149	40°26′	23°07′
								40.44	23.12
	pegmatite in Chalkidiki Ophiolite	*		Musc	K-Ar		156		
Kreuzer pers. comm. in Burgath, 1980	Pegmatite in Chalkidiki Ophiolite	*	*	Musc	K-Ar		155.6 ± 1.1 154.2 ± 2.5 125 ± 1.4		

Reference	Description	Locality	Sample No.	Sample Type	Analytical Technique	Age (1) (Ma)	Age (2) (Ma)	Latitude	Longitude
De Wet et al., 1989	Sithonia granitoid	Sarti	AD84189	Biotite	Ar-Ar		42.6 ± 0.4	40°05′58 40.0994	24°58′50 24.9806
	Sithonia pegmatite		AD84167	Musc	Ar-Ar			40°10′52 40.1811	23°42′18 23.7050
			AD84169	Musc	Ar-Ar			40°10′18 40.1717	23°43′20 23.7222
Christofides et al., 1986	Sithonia gt 2 mica granite	N Intrusion	*	W/R	Rb-Sr isochron	50.9 ± 0.5 i.r.=0.7072 ± 1			
	2 mica granite	N Intrusion	*	Musc Biotite	Rb-Sr Rb-Sr	54.5 ± 3.1 to 45.6 ± 1.3 47.7 ± 0.8 to 28.9 ± 1.1			
	granodiorite	S Intrusion	*	Biotite	Rb-Sr	46.5 ± 0.9 to 41.3 ± 0.7			
Kondopoulou et al., 1984	Sithonia granitoid	S near Sarti	*	Biotite	K-Ar		40 ±1.5	40°05′58 40.0994	24°58′50 24.9806
Vergeley 1984	Sithonia granite	*	*	W/R Musc W/R Biotite	Rb-Sr W/R-min pairs Rb-Sr W/R-min pairs		38 ± 2.3 40 ± 2.4	40°10′ 40.17	23°50′ 23.83
Pelagonian Zone									
Marakis 1969	Florina granite	W of Florina	19.4	Biotite?	K-Ar	217 ± 6	222 ± 6	40°46′ 40.77	21°13′ 21.22
			19.1		K-Ar	228 ± 6	233 ± 6		
			19.2		K-Ar	238 ± 6	243 ± 6		
			19.3		K-Ar	258 ± 7	263 ± 7		
			19.5		K-Ar	268 ± 7	273 ± 7		
			19.6		K-Ar	461 ± 12	469 ± 12		
			19.6		K-Ar	465 ± 12	473 ± 12		
Kilias 1980	Florina granite	W of Florina	*	Biotite?	K-Ar		468 ± 14 526 ± 16	40°51′ 40.85 40°48′ 40.80	21°19′ 21.32 21°18′ 21.30
Mountrakis 1984	Kastoria granite	2.5 km S of Mt Vitsi	*	Zircon	U-Pb		302.4 ± 5/15	40°38′ 40.63	21°21′ 21.35
Yarwood & Aftalion 1976	Piera granite	W of Katerini	RC998	Zircon	U-Pb		302 ± 5	40°15′57 40.2658	22°08′39 22.1442

Radiometric age data: Part 2: Ophiolites, metamorphic soles and related rocks of Greece and Yugoslavia

Reference	Description	Locality	Sample No.	Sample Type	Analytical Technique	Age (1) (Ma)	Age (2) (Ma)	Latitude	Longitude
Yugoslavia									
Okrush et al., 1978	Brezovica metamorphic sole	*	B65-79	Musc	K-Ar		161.5 ± 1.6	44°45′	17°40′
			B65-82	Musc	K-Ar		162.8 ± 1.9	44.75	17.67
			B65-77	Hbl	K-Ar		169.0 ± 3.2		
			B65-80	Hbl	K-Ar		162.6 ± 3.4		
Karamata et al., 1978	Brezovica Ophiolite (amphibolite)		98210	Hbl	K-Ar	172 ± 8	176 ± 8	44°45′	17°40′
								44.75	17.67
	(amphibolite)		98211	Hbl	K-Ar	172 ± 9	176 ± 9		
	(amphibolite)		98212	Hbl	K-Ar	176 ± 6	180 ± 6		
	(amphibolite)		98213	Hbl	K-Ar	161 ± 9	165 ± 9		
	(amphibolite)		98231	Hbl	K-Ar		171 ± 6		
	(metapelite)		98233	Biotite	K-Ar		168 ± 5		
	(amphibolite)		98232	Musc	K-Ar		161 ± 5		
				Hbl	K-Ar		172 ± 8		
	(amphibolite)		98237	Musc	K-Ar		159 ± 5		
				Hbl	K-Ar		161 ± 5		
Lanphere et al., 1975	Krivaja-Konjuh (met. sole, amph.)	near Vares	YUG-1-71	Parg	K-Ar	157 ± 4	161 ± 4	44°20′	18°35′
								44.33	18.35
	Zlatibor (met. sole, amph.)	1 km N of Bistrica	72YUG-1	Amph	K-Ar	174 ± 14	178 ± 14	43°29′	19°39′
						168 ± 8	172 ± 8	43.48	19.65
		1.25 km N of Bistrica	72YUG-3	Parg	K-Ar	170 ± 11	174 ± 11		
Subpelagonian Zone									
Thuizat et al., 1981	Pindos Ophiolite (met. sole, amph.)	*	Pin II-4	Hbl	K-Ar	172 ± 5	176 ± 5	39°58′20	21°09′32
								39.9722	21.1589
Roddick et al., 1979	Pindos Ophiolite (met. sole, amph.)	Avominsta valley, Perivoli	B76-24 (123656)	Hbl	Ar-Ar		182 ± 4	39°58′20	21°09′32
							173 ± 3	39.9722	21.1589
							169 ± 5		
Spray et al., 1980	Pindos Ophiolite (met. sole, amph.)	Kiatra Fourka Mt. 3 km SW Perivolvi	124659	Hbl	Ar-Ar	172 ± 3 (plat)	165 ± 3	39°57′30	21°05′45
								39.9583	21.0958
Spray et al., 1984	Pindos Ophiolite (dolerite sill)	Moschophyton	TG389	Kaers	K-Ar		163 ± 5		
Roddick et al., 1979	Pindos Ophiolite (wehrlite, ig)	2 km W of Andinitsa Othris Mts.	G-16R (108185)	Hbl (ig)	Ar-Ar		251 ± 5	39°00′	22°35′
								39.00	22.59
	Othris area (dacite, ig)	3 km SE Dhomokos Othris Mts	G-18 (108201)	Hbl (ig)	Ar-Ar		245 ± 5	39°06′33	22°19′11
								39.1092	22.3197
Hynes et al., 1972	Othris Group Agrilia Fm. (spilitised oph dol)	W-central Othris	OH275c	W/R	K-Ar	156 ± 6	160 ± 6	38°57′	22°25′10
								38.95	22.4195
	(rhyolite)		EGN-106	W/R	K-Ar	181 ± 7	185 ± 7	39°59′44	22°34′29
								39.9955	22.5747
	Mirna Group (spilite)	W Othris	OH165	W/R	K-Ar	125 ± 5	128 ± 5	38°57′49	22°22′04
			ETCS53	W/R	K-Ar	127 ± 5	130 ± 5	38.9636	22.3678
	(dolerite) (porphyritic rhyo)	N of Stilis	EGN101	W/R	K-Ar	97 ± 4	99 ± 4	39°59′44	22°34′29
								39.9955	22.5747
	(basalt)	Anavra	AGS-69-10	W/R	K-Ar	87 ± 4	89 ± 4	39°04′55	22°31′02
								39.0818	22.5172
	(porphyritic rhyo)	Moskhokaria	AJH-71-1202A	W/R	K-Ar	78 ± 4	80 ± 4	39°00′16	22°13′48
								39.0045	22.2299
	(spilite)	Anavra	AGS-69-18	W/R	K-Ar	65 ± 10	67 ± 10	39°03′16	22°33′27
								39.0545	22.5575
	(dolerite)	Moskhokaria	ETCS54	W/R	K-Ar	61 ± 2	62 ± 2	39°01′06	22°13′48
								39.0182	22.2299
Smith et al., 1975	Mirna Group (amphibolites)	W of Othris	*	Hbl	K-Ar	162 ± 10	166 ± 10		
				Hbl	K-Ar	152 ± 15	152 ± 15		

Reference	Description	Locality	Sample No.	Sample Type	Analytical Technique	Age (1) (Ma)	Age (2) (Ma)	Latitude	Longitude
Ferriere 1982	Lavas of the	N of Lamia	OT1	W/R	K-Ar		90.0 ± 8.1		
	Unite de Fourca		OT3	W/R	K-Ar		71.9 ± 7.1		
	(lavas of Maria-		OT4	W/R	K-Ar		156.4 ± 9.4		
	Magdalena)		OT2b	W/R	K-Ar		83 ± 9		
			OT6	W/R	K-Ar		147.6 ± 9.5		
	possible Unite		OT16	W/R	K-Ar		134.2 ± 9.9		
	de Fourca		OT18	W/R	K-Ar		114 ± 19		
	Lavas of the		OT21	W/R	K-Ar		184 ± 21		
	Unite de Fourca		OT11b	W/R	K-Ar		164.0 ± 21.4		
			OT12	W/R	K-Ar		187.1 ± 23.1		
			OT14	W/R	K-Ar		178.1 ± 24.3		
Spray et al., 1980	Othris ophiolite (met. sole, amph)	2 km SW of Lamia	124748	Hbl	Ar-Ar	177 ± 4	169 ± 4	38°53'48 38.8967	22°25'40 22.4278
	Euboea (met. sole)	SW Prokopion near Kandilion Mt	124765	Hbl	Ar-Ar		180 ± 5	38°42'15 38.7042	23°28'15 23.4708
	Vourinos (met. sole, amph)	5 km NW of Chromion	124699	Hbl	Ar-Ar	179 ± 4	171 ± 4		
Richard & Allegre 1980	Vourinos gabbro & lava	*	*	W/R	Sm-Nd		approx 150		
Vardar Zone									
Spray et al., 1984	Guevgueli diorite (matrix to breccias)	(from eastern unit)	GV854	Biotite (ig)	K-Ar		154 ± 3	41°03'	22°33'
				Hbl (ig)	K-Ar		163± 3	41.05	22.55
	Guevgueli gabbro		GV801	Hbl (ig)	K-Ar		149 ± 3		
Sapountzis 1969	Chalkidiki Oph hypersthene gabbro	Panorama	?	W/R	K-Ar	1400-1300	1405-1307		
Sapountzis 1980	Chalkidiki Oph gabbro	Vasiliks-Galatista	IVG	W/R	K-Ar		132 ± 25	40°29' 40.48	23°12' 23.20
	gabbro	Vavdos	2MV	W/R	K-Ar		225 ± 30	40°24' 40.40	23°18' 23.30
	gabbro	Gerakini	3V	W/R	K-Ar		42 ± 8	40°16' 40.27	23°30' 23.50
	gabbro	Metamorphosis	4M	W/R	K-Ar		311 ± 30	40°14' 40.23	23°34' 23.57
Kreuzer pers comm in Jung et al., 1980	Chalkidiki Oph youngest unit	*	*	Hbl	K-Ar		approx 160		
Kreuzer pers comm in Burgath 1980	Chalkidiki Oph gabbro dyke in dunite	*	*	Hbl (ig)	K-Ar		172 ± 4		
Kreuzer pers comm in Mussallam et al., 1986	Chalkidiki Oph Hbl gabbro dyke	*	*	Hbl	K-Ar		172 ± 5		
	Perigranitic peg	*	*	Musc			156		
Kreuzer pers comm in Burgath 1980	pegmatite in Chalkidiki Oph	*	*	Musc	K-Ar		156.6 ± 1.1 154.2 ± 2.5 125.3 ± 1.4		
De Wet & Miller in De Wet 1989	Chalkidiki Oph Vavdos amphibolite	Vavdos	451	Hbl	Ar-Ar		723 ± 11 390 ± 7	40°24'44 40.4122	23°19'28 23.3244
	Chalkidiki oph	Vavdos	53	Hbl	Ar-Ar TF		314 ± 33	40°24'44	23°19'28
			53a				215 ± 8	40.4122	23.3244
			55	Hbl	Ar-Ar TF		333 ± 24	40°24'44	23°19'28
			60	Hbl	Ar-Ar TF		235 ± 7	40.4122	23.3244
			60a				226 ± 10		
	Peg in ophiolite	SW of Vavdos	92	Musc	Ar-Ar TF		117 ± 2		

Reference	Description	Locality	Sample No.	Sample Type	Analytical Technique	Age (1) (Ma)	Age (2) (Ma)	Latitude	Longitude
Serbo-Macedonian Massif									
Borsi et al., 1965	Vertiskos Pegmatite	Megali Rema, 2.5 km SSW of Lipsidhion	77-HA	Musc	Rb-Sr	275 ± 30	285 ± 30	40°54'03 40.9008	22°56'47 22.9464
	Vertiskos Pegmatite	Kouro Rema, 1.5 km W of Krithia	44-IHA	Musc	Rb-Sr	278 ± 30	288 ± 30	40°50'41 40.8447	22°58'04 22.9678
	Vertiskos Pegmatite	Kouro Rema, 1.5 km W of Krithia	45-IHA	Musc	Rb-Sr	296 ± 15	306 ± 15	40°50'41 40.8447	22°58'04 22.9678
	Vertiskos Pegmatite	Kouro Rema, 1.5 km W of Krithia	46-IHA	Musc	Rb-Sr	291 ± 15	301 ± 15	40°50'41 40.8447	22°58'04 22.9678
	Vertiskos pegmatite	1 km E of Kartiera	102 HA	Musc	Rb-Sr	316 ± 15	327 ± 15	40°54'31 40.9086	23°06'04 23.1011
	Vertiskos mica-schist	Megali Rema, 2.5 km SSW of Lipsidhion	81-2HA	Musc	K-Ar	300 ± 10	306 ± 10	40°54'03 40.9008	22°56'47 22.9464
Harre et al., 1968	Vertiskos pegmatoid	11 km NE Langadhas	305/G10	Musc	K-Ar	191 ± 3 135 ± 2	195 ± 3 138 ± 2	40°49'35 40.8264	23°09'17 23.1547
	Vertiskos pegmatoid	2.5 km WNW of Triandfilia	116/G8	Musc	K-Ar Rb-Sr	107 ± 1.6 22.8 ± 6.2	109 ± 1.6 23.6 ± 6.2	41°00' 41.00	23°19'17 23.1547
	Vertiskos amphibolite	1.5 km E of Xiropotamos	209/W350d	Hbl	K-Ar	109 ± 3 114 ± 3 108 ± 3	111 ± 3 117 ± 3 111 ± 3	40°46'13 40.7703	23°30'32 23.5089
	Vertiskos amphibolite	4 km SSE of Arethousa	208/W181c	Hbl	K-Ar	111 ± 3 110 ± 2	114 ± 2 113 ± 2	40°42'19 40.7053	23°36'26 23.6072
	Kerdilia plag-micro-granite	0.5 km SSW Oreskia	113/G4	Musc Biotite	K-Ar Rb-Sr K-Ar	41.8 ± 0.8 55.8 ± 4 37.7 ± 0.6	42.8 ± 0.8 57.9 ± 4 38.5 ± 0.6	40°50'58 40.8494	23°38'13 23.6369
	Kerdilia musc-biotite-granitoid	3 km SE of Dafni	114/G5	Biotite	K-Ar Rb-Sr K-Ar	39.0 ± 0.8 43.2 ± 3.1 36.8 ± 0.8	39.9 ± 0.8 44.7 ± 3.1 37.7 ± 0.8	40°49'34 40.8311	23°40'34 23.6761
	Kerdilia pegmatoid	3 km WNW of Stavros	117/G9	Musc	Rb-Sr	48.0 ± 2	49.7 ± 2	40°40'34 40.6761	23°39'17 23.6547
	Kerdilia amphibolite	Kiani Akti 8 km NNE of Asprovalta	304/G11	Hbl	K-Ar	78.0 ± 2	79.9 ± 2	40°45'49 40.7636	23°45'00 23.7500
	Kerdilia biotite gneiss	Kiani Akti 7.5 km NE of Asprovalta	303/G12	Biotite	K-Ar	32.8 ± 0.5 33.6 ± 0.4	33.6 ± 0.5 34.4 ± 0.4	40°46'21 40.7725	23°46'04 23.7678
	Kerdilia pegmatoid	Kiani Akti 7.5 km NE Asprovalta	115/G6	Biotite Rb-Sr	K-Ar	32.9 ± 0.6 31.3 ± 0.6 39.0 ± 2.8	33.7 ± 0.6 32.1 ± 0.6 40.4 ± 2.8	40°46'21 40.7725	23°46'04 23.7678
	Kerdilia plag-micro granite	Kara Bair 4 km E of Amfipolis	112/G2	Musc Biotite	K-Ar K-Ar Rb-Sr	35.0 ± 0.5 33.9 ±0.7 39.3 ± 2.4	35.8 ± 0.5 34.7 ± 0.7 40.7 ± 2.4	40°48'47 40.8131	23°52'43 23.8786

Reference	Description	Locality	Sample No.	Sample Type	Analytical Technique	Age (1) (Ma)	Age (2) (Ma)	Latitude	Longitude
Papadopoulos & Kilias 1985	Mica schist "Bunte Series"	4 km E of Megali Volvi	RA1	Musc	K-Ar		91 ± 4.5 90 ± 5.0	40°41'58 40.6994	23°28'15 23.4708
	Vertiskos garnet mica schist	1 km NW of Megali Volvi	RA2	Musc	K-Ar		116.2 ± 5.3	40°42'16 40.7044	23°25'15 23.4208
	Augen Gneiss (Arnaea granite)	1 km W of Vaiohorion	RA4	Musc Biotite	K-Ar Rb-Sr K-Ar Rb-Sr		108 ± 4.7 131 ± 10 124 ± 5.2 102 ± 10	40°42'16 40.7128	23°22'23 23.3731
	Vertiskos musc-biotite-schist	1.5 km NE of Vaiohorion	RA5	Musc Biotite	K-Ar K-Ar		123 ± 5.5 114.6 ± 5.4	40°43'21 40.7225 40°43'21	23°23'38 23.3939 23°23'38
	Vertiskos quartz-paragneiss	1.5 km NE of Vaiohorion	RA7	Musc	K-Ar		120 ± 5	40.7225	23.3939
	Vertiskos amphi in paragneiss	1.5 km NE of Vaiohorion	RA8	Hbl	K-Ar		93.0 ± 5.3	40°43'21 40.7225	23°23'38 23.3939
	Vertiskos biotite-orthogneiss	Megali Volvi	RA10	Musc Biotite	K-Ar Rb-Sr K-Ar Rb-Sr		110 ± 4.6 145.7 ± 15 87.8 ± 4.2 78.2 ± 10	40°42'26 40.7072	23°26'26 23.4406
	amphibolite in "Bunte Series"	3 km NNE of Megali Volvi	RA11	Hbl	K-Ar		122.8 ± 8	40°43'13 40.7203	23°26'34 23.4428
	Vertiskos orthogneiss	1 km NE of Megali Volvi	RA12	Musc	K-Ar		114 ± 5.5	40°42'11 40.7031	23°25'58 23.4328
	Vertiskos Musc-plag-gneiss	2 km NE of Vaiohorion	RA13	Musc	K-Ar Rb-Sr		125 ± 5.6 172.7 ± 31	40°43'21 40.7225	23°24'23 23.4064
	Vertiskos chl-Musc-biotite-gneiss	Koryphi Avraam	RA14	Musc	K-Ar		116.2 ± 4.8	40°43'50 40.7306	23°24'17 23.4047
	SMM Volvi Complex	Lake Volvi		Hbl	K-Ar		1370 ± 76	40°42'11 40.7031	23°31'15 23.5208
Dixon pers comm in De Wet 1989	SMM Vertiskos-Volvi biotite-gabbro	Lake Volvi	*	Biotite (ig)	K-Ar		approx 190	40°42' 40.70	23°33' 23/.55
Servas et al., 1975	SMM Vertiskos pegmatite	Langadhas	*	W/R	Rb-Sr isochron	152 ± 26		40°40' 40.67	23°09' 23.15
Marakis 1969	SMM Vertiskos pegmatite?	Langadhas	*	Biotite	K-Ar	140 ± 3 139 ± 3		40°40' 40.67	23°09' 23.15
Stip-Axios Unit/ Vardar Zone									
De Wet & Miller pers comm in De Wet 1989	SAZ biot-gar-gneiss	SW of Vavdos	AD84161	Biotite	Ar-Ar		160 ± 1.7	40°23'27 40.3908	23°16'47 23.2797
	Peonias Zone Svoula flysch (phyllite)	N of Poligiros	AD8442 AD84101	W/R W/R	Ar-Ar TF Ar-Ar TF		108 ± 2 109 ± 2		
Sapountzis 1969	Peonias Zone Chortiatis Mag. Suite	Evangelistria, Thessaloniki	M0882	Musc	K-Ar	113 ± 4	116 ± 4		
Mercier 168/1973	Peonias Zone pegmatite of Balteika Topani & Filios	W of Melissochori	50HB 56HB 62HB	Musc Musc Musc	Rb-Sr Rb-Sr Rb-Sr	289 247 289	299 256 299		

Reference	Description	Locality	Sample No.	Sample Type	Analytical Technique	Age (1) (Ma)	Age (2) (Ma)	Latitude	Longitude
Pelagonian Massif									
Mercier 1968	Kajmaktchalan Massif	N Pelagonian Massif	12TL	Musc	Rb-Sr	140	145	40°58′38 40.9772	21°52′52 21.8811
			13 TC	Musc	Rb-Sr	133.5	138.2	40°58′38 40.9772	21°52′52 21.8811
			147T	Biotite	Rb-Sr	134	139	40°58′38 40.9772	21°52′52 21.8811
			37TC(1)	Biotite	Rb-Sr	101 ± 7	105 ± 7	40°55′	21°52′52
			37TC(2)	Biotite		98	101	40.92	21.8811
	Vardar Loutra		6TC	Musc	Rb-Sr	101	105	41°00′ 41.00	21°48′ 21.80
	Pozar Unit-quartzite		8TC	Musc	Rb-Sr	63	65	41°00′ 41.00	21°48′ 21.80
Barton 1976	Olympus area mylonite	S of Mt Olympus	*	W/R	Rb-Sr	141 ± 80 128 ± 26		39°59′ 39.98	22°25′ 22.42
			301	W/R Musc W/R	Rb-Sr WR-min pairs Rb-Sr	125.2 ± 10.7 126.6 ± 1.2			
	Olympus area phyllonites	N of Mt Olympus	307 *	Musc W/R	WR-min pairs Rb-Sr	40.0 ± 1.2		40°09′ 40.15	22°18′ 22.30
Yarwood & Dixon 1979	Kataphygion gt (foliated)	N of Livadi	*	?	Rb-Sr		122 ± 3	40°25′ 40.25	22°09′ 22.15
	Lower Mavroneri augen schist	S margin of Piera allochthon	*	?	Rb-Sr		103 ± 2		
Smith et al., 1975	Pteleon Fm. (basement seds.)	E Othris	*	Musc Musc Musc	K-Ar K-Ar K-Ar	94 ± 4 83 ± 3 74 ± 3	96 ± 4 85 ± 3 76 ± 3	39°04′13 39.0702	22°26′19 22.4386
Hynes et al 1972	Basement schist	E Othris	M944 M137 M136	W/R W/R W/R	K-Ar K-Ar K-Ar	138 ± 4 73 ± 4 72 ± 4	141 ± 4 75 ± 4 74 ± 4	39°04′ 39.07	22°26′ 22.44

Map A

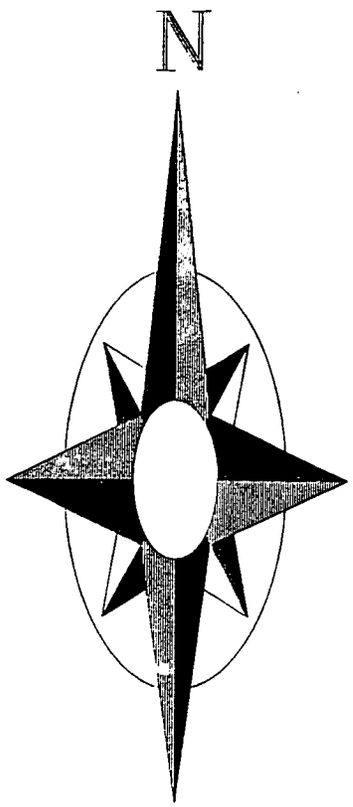

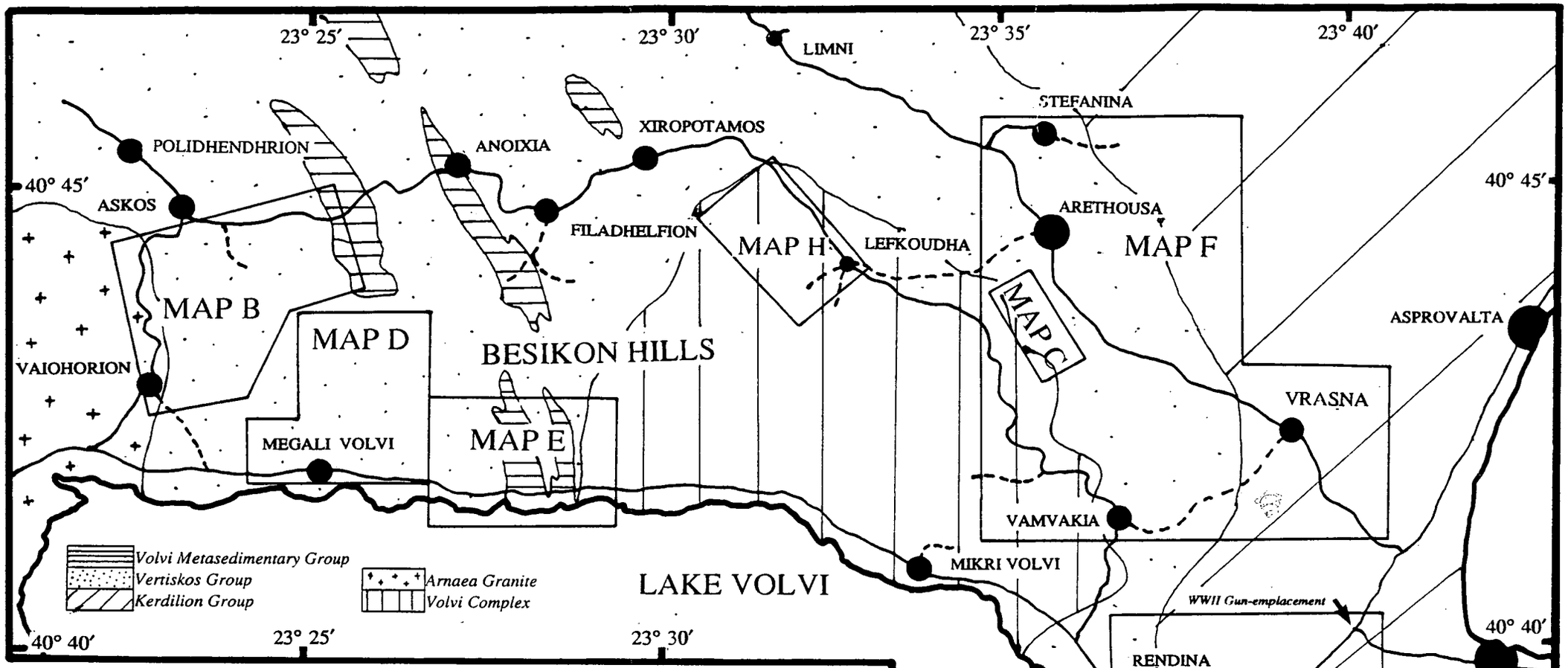

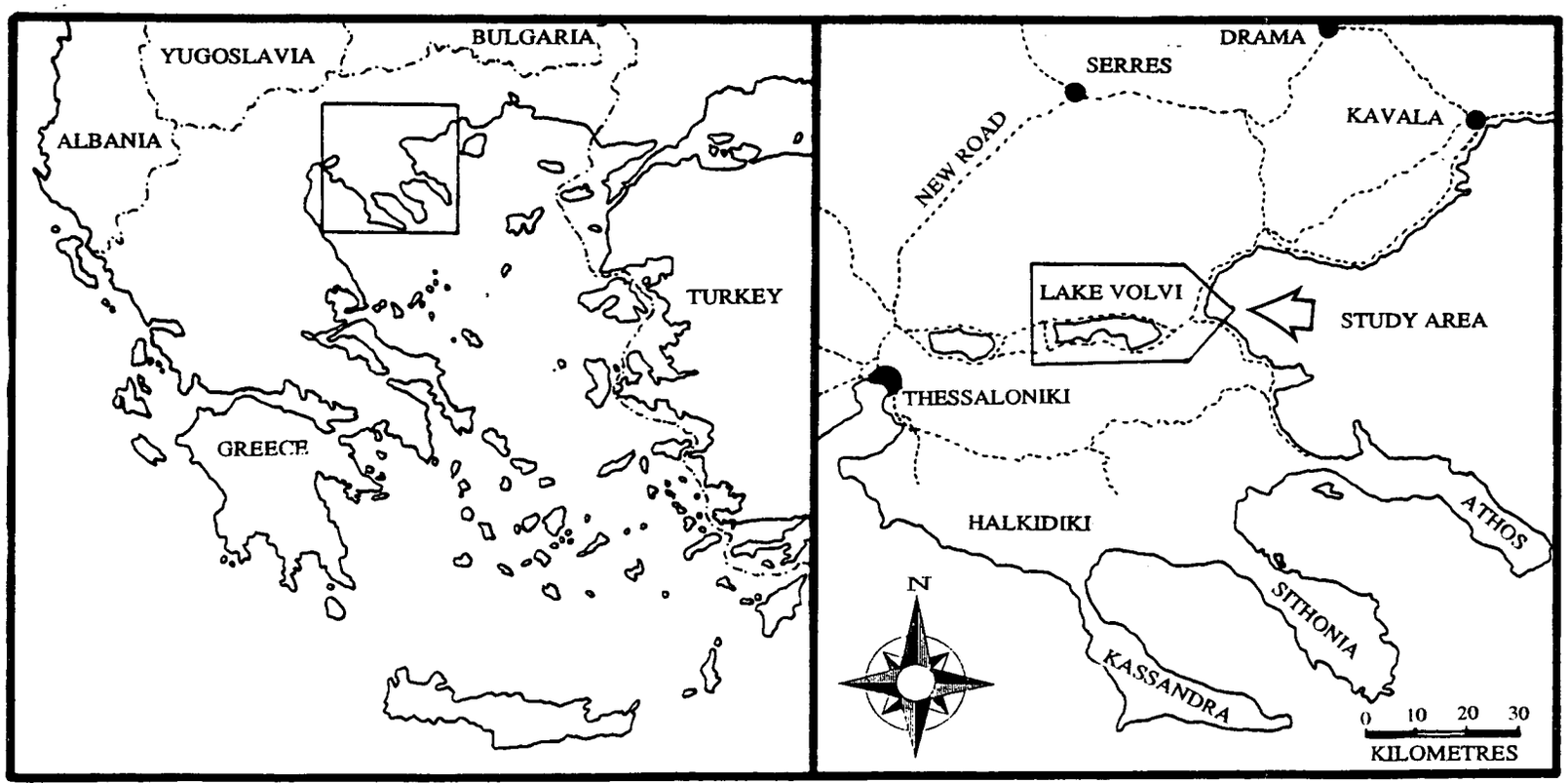

MAP A: Regional locality maps for the study area in NE Greece and an outline of the area showing the villages and towns referred to in the text. Boxed areas represent areas mapped in greater detail (*see* large-scale Maps, B to H).
Mapping was undertaken by S.D. Batty during 1988, 1989, 1990 as part of a PhD thesis at Edinburgh University. Reference has also been made to Sakellariou (1990) and to the 1:50 000 geological maps of northern Greece:
Stavros Sheet (IGME, 1978); Sitochorion Sheet (IGME, 1970)
Zangliverion Sheet (IGME, 1978); Sochos Sheet (IGME, 1979)

23°23′ 23°24′ 40°45′ 23°25′ 40°44′ 40°43′ 40°42′

To Askos

To Lake Volvi

VAIOHORION

Sheared Augen Pod "ASK BOUDIN"

Ultramafic Pods (0.5-3m diameter)

Kilometres

0 1 2

N

MAP B

RECENT

Alluvium

VOLVI METASEDIMENTARY GROUP

Megali Volvi Marble Formation (Section 2.4.5)

- Pure, white, crystalline Marble Member
- Impure Carbonate Member

VERTISKOS GROUP

- Askos Garnet Mica Schist Formation (Section 2.3.3.5)
- Askos Garnet Mica Paragneiss Formation (Section 2.3.3.4)
- Askos Feldspar Mica Schist Formation (Section 2.3.3.3)
- Askos Augen Paragneiss Formation (Section 2.3.3.2)

IGNEOUS INTRUSIONS/INTERCALATION

- Askos Marginal Amphibolite Formation (Section 2.3.3.1)
- Volvi Ultramafic Formation (Section 2.3.3.6)
- Askos Augen Orthogneiss Member (Section 2.6.3)
- Arnaea Granite (Section 2.6.3)

EAF9 Sample Locality

A–A′ Locality of Cross-sections

Boundaries and Contacts (Observed, Inferred)

S_2 Foliations

Early-, Pre-S_2 Foliations

F_2 Antiform , Synform

F_3 Synform

Shear Zones (observed, inferred)

Lineation

Minor F_2 Fold Axial Plane

Minor F_2 Fold Plunge

Faults

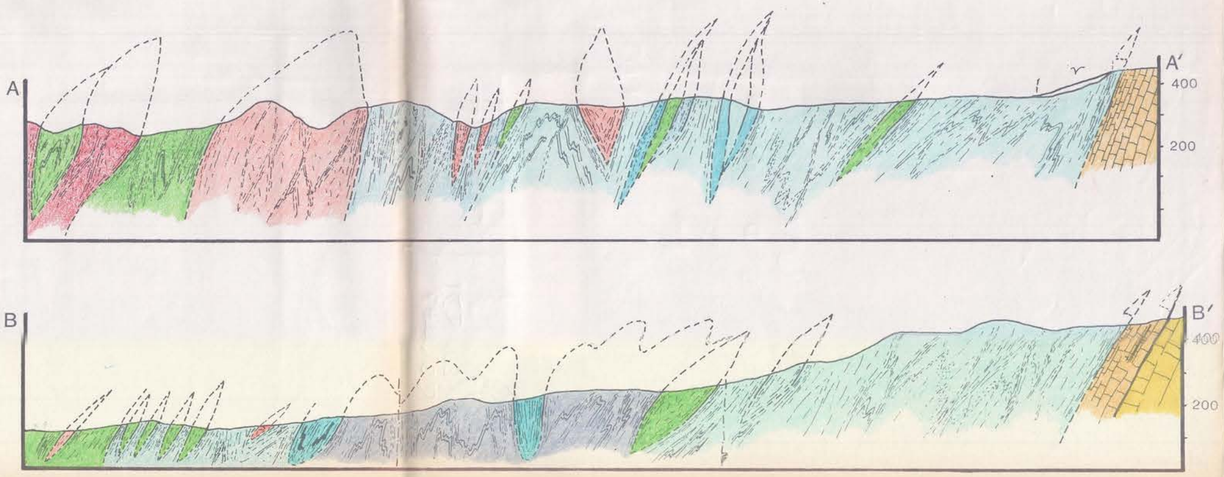

MAP C: THE VAMVAKIA RIVER (Northern Section)

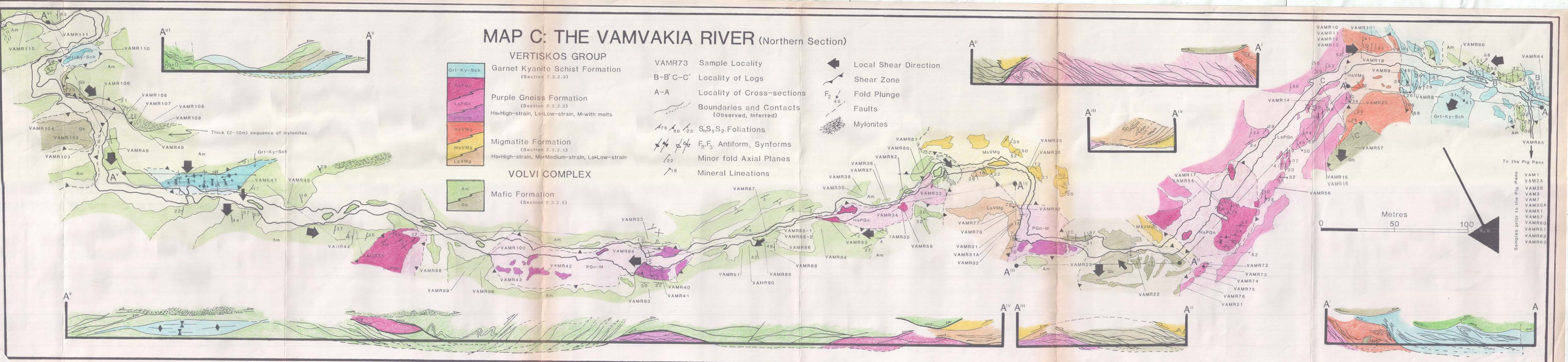

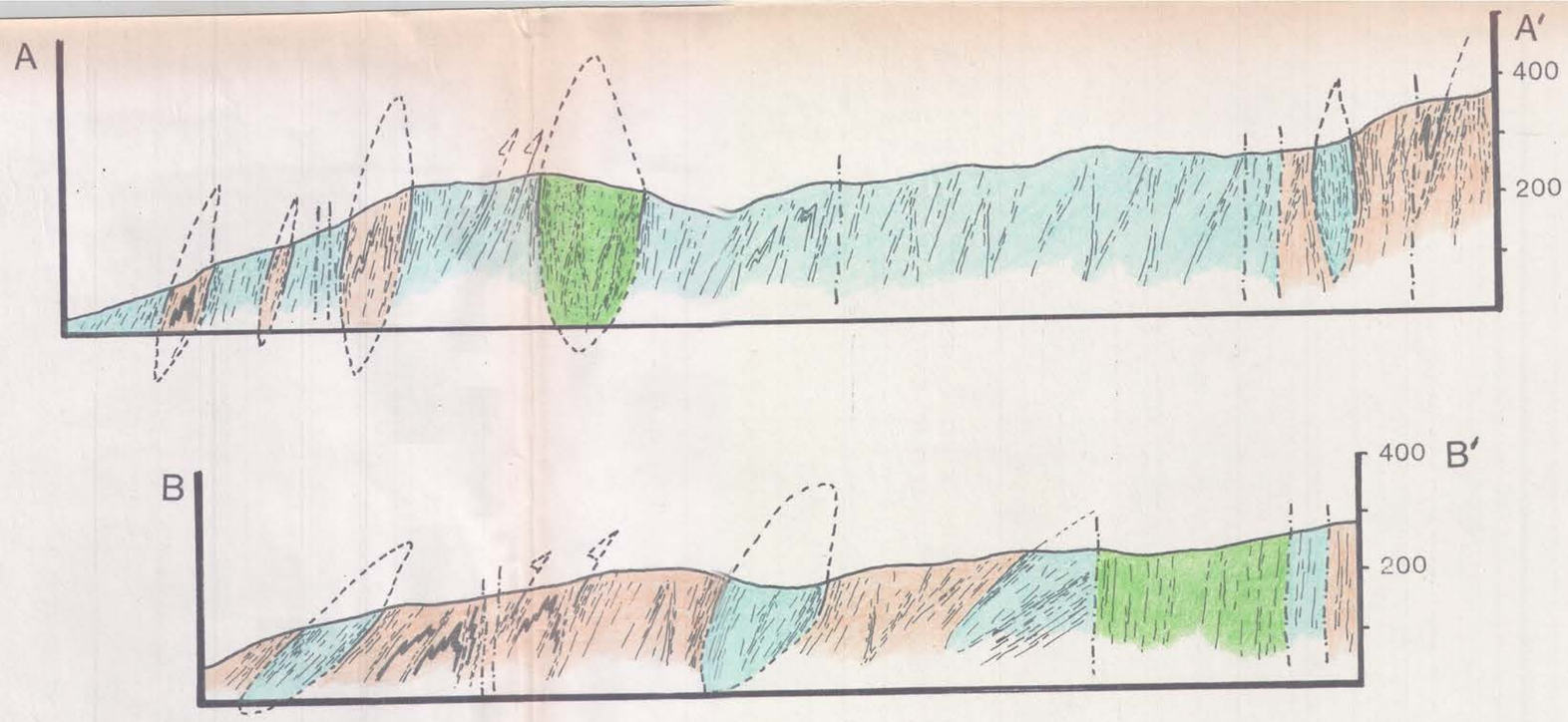

RECENT

Alluvium

VOLVI METASEDIMENTARY GROUP

MVQG — Megali Volvi Quartzofeldspathic Gneiss Formation (Section 2.4.4)

IGNEOUS INTRUSIONS/INTERCALATIONS

AAOGn — Askos Augen Orthogneiss Formation (Section 2.6.3)

VERTISKOS GROUP

AGt-Sch — Askos Garnet Mica Schist Formation (Section 2.3.3.5)

AF-Sch — Askos Feldspar Mica Schist Formation (Section 2.3.3.3)

AA-PGn — Askos Augen Paragneiss Formation (Section 2.3.3.2)

AMAm — Askos Marginal Amphibolite Formation (Section 2.3.3.1)

L7 — Sample Locality

A–A′ — Locality of Cross-sections

Boundaries and Contacts (Observed, Inferred)

78 — S_2 Foliations

76 — Early-, Pre-S_2 Foliations

F_2 Antiforms, Synforms

F_3 Antiforms, Synforms

19 — Minor F_2 Fold Axial Plane

9 — Minor F_2 Fold Plunge

12 — Lineation

Shear Zone

Faults

0 Kilometres 2

N

MAP D

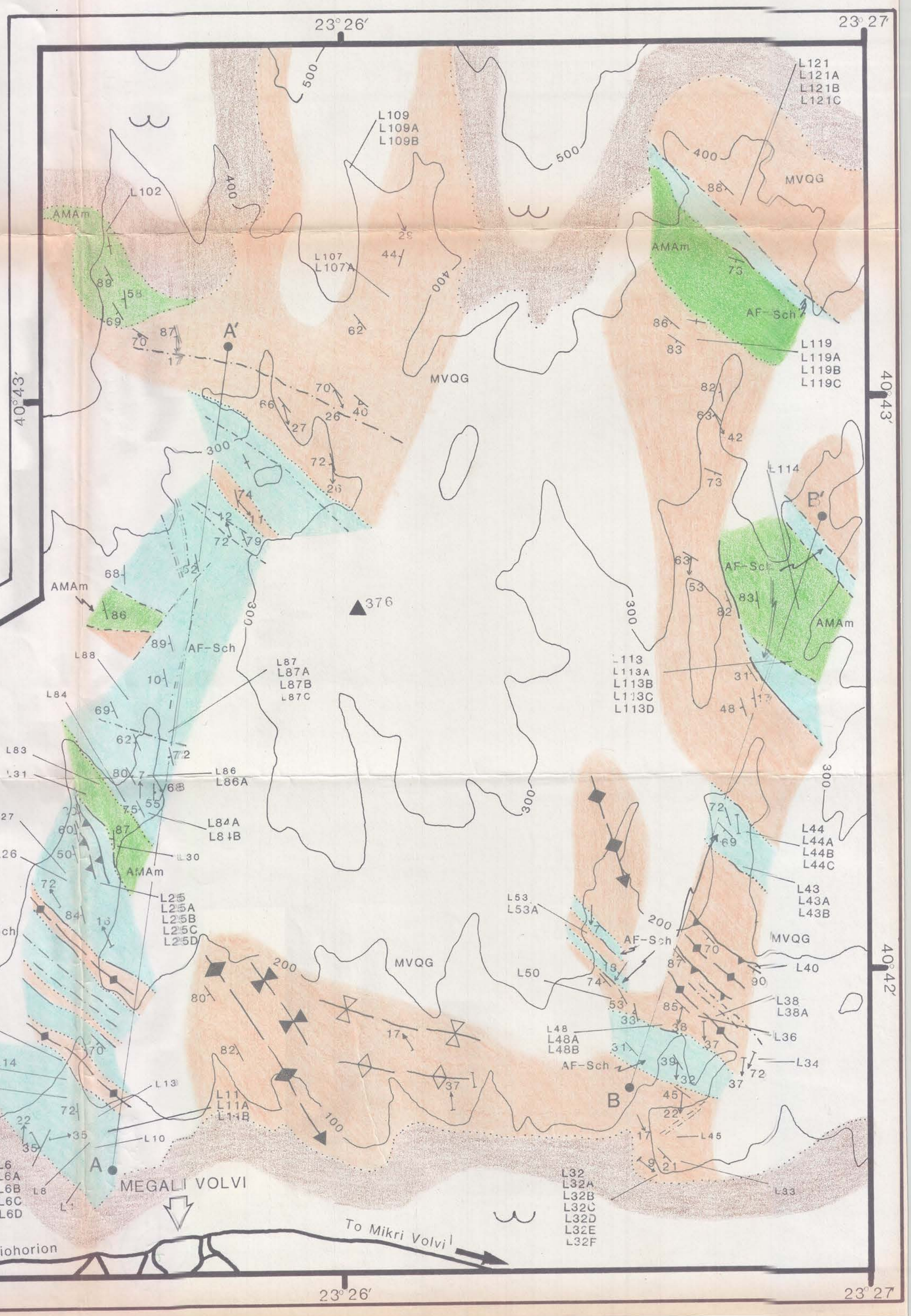

EMV12 Sample Locality

A–A Locality of Cross-section

Boundaries and Contacts (Observed, Inferred)

S_2 Foliations

Early–, Pre–S_2 Foliations

Lineation

Minor F_2 Fold Plunge

Minor F_2 Fold Axial Plane

Shear Zone

Faults

Kilometres

0 1 2

N

MAP E

A A′ B B′

400 200

23°28′ 23°29′ 23°30′

40°42′ 40°41′

L81 L81A L81B L81C ▲458 A′ PMVMb EMV16 500 600 ▲563 VCAm EMV2 EMV1 EMV3A EMV3B

L65 L65A L65B EMV23 MVQG IMVMb EMV9 EMV9A EMV9B L78 L78A L78B B′ AGt-Sch AF-Sch

L76 L76A B MVGG-Sch VCAm L75 L75A L75B EMV10 EMV20 EMV20A EMV20B EMV8 EMV7 EMV14

EMV21 EMV11 L69 L61 A L70 EMV18 EMV6 L67 L67A L68 L68A EMV13 EMV12 VCAm

To Megali Volvi

To Mikri Volvi

LAKE VOLVI

RECENT

Alluvium

VOLVI METASEDIMENTARY GROUP

IMVMb Impure Member

PMVMb Pure, white, Member

Megali Volvi Marble Formation (Section 2.4.5)

MVQG Megali Volvi Quartzofeldspathic Gneiss Formation (Section 2.4.4)

MVGG-Sch Megali Volvi Garnet Graphite Schist Formation

VERTISKOS GROUP

AGt-Sch Askos Garnet Mica Schist Formation (Section 2..3.3.5)

AF-Sch Askos Feldspar Mica Schist Formation (Section 2.3.3.3)

Undifferentiated

VOLVI COMPLEX

VCAm Amphibolites (Section 2.5)

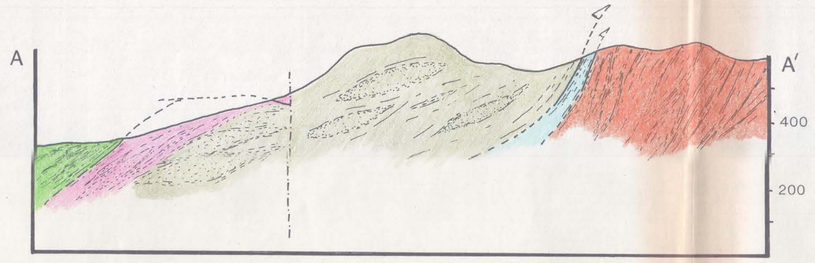

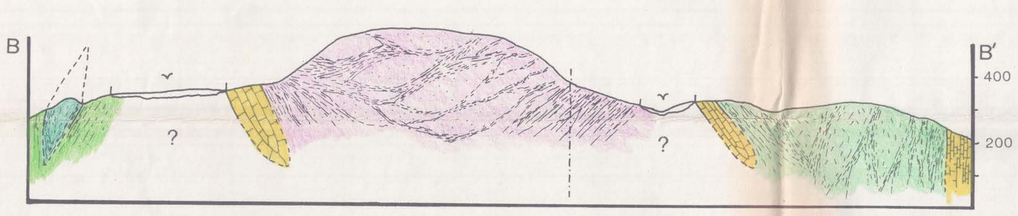

RECENT

- River Deposits
- Alluvium

VOLVI METASEDIMENTARY GROUP

- SMb — Stefanina Marble Formation (Section 2.2.5.2)
- VMb — Vrasna Marble Formation (Section 2.2.4.3)
- VST — Vamvakia Siberian Tiger Formation (Section 2.3.2.4)

KERDILION–VERTISKOS GROUPS

- Gt-Ky-Sch — Vamvakia Garnet Kyanite Schist Formation (Section 2.3.2.3)
- PGn — Vamvakia Purple Gneiss Formation (Section 2.3.2.2)
- VFGn — Vrasna Feldspathic Gneiss Formation (Section 2.2.4.2)

IGNEOUS INTRUSIONS/ INTERCALATIONS

- SAm — Stefanina Amphibolite Formation (Section 2.2.5.1)
- VAm — Vrasna Amphibolite Formation (Section 2.2.4.1)
- Am — Amphibolites (Section 2.3.2.5)
- Gb — Gabbros (Section 2.3.2.5)
- AU — Arethousa Ultramafic Member (Section 2.3.3.6)

] VOLVI COMPLEX

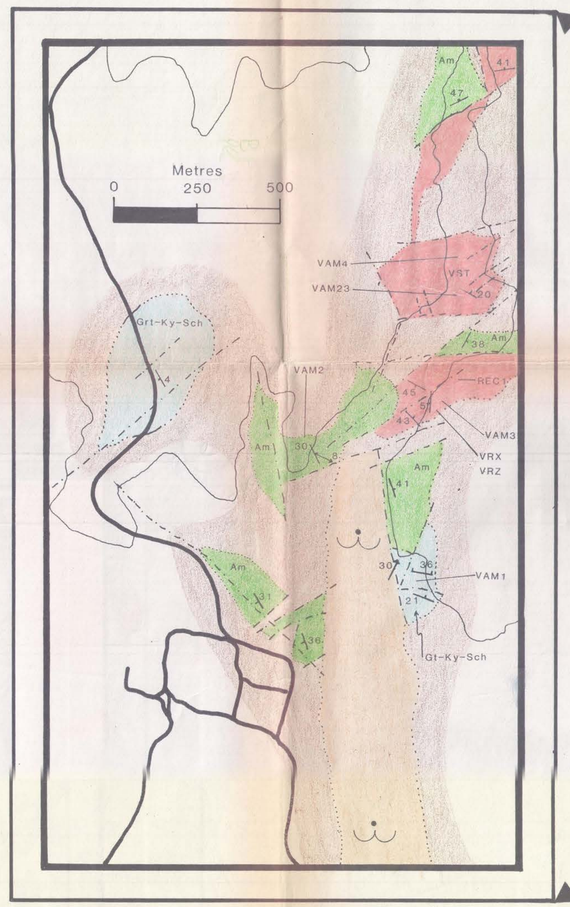

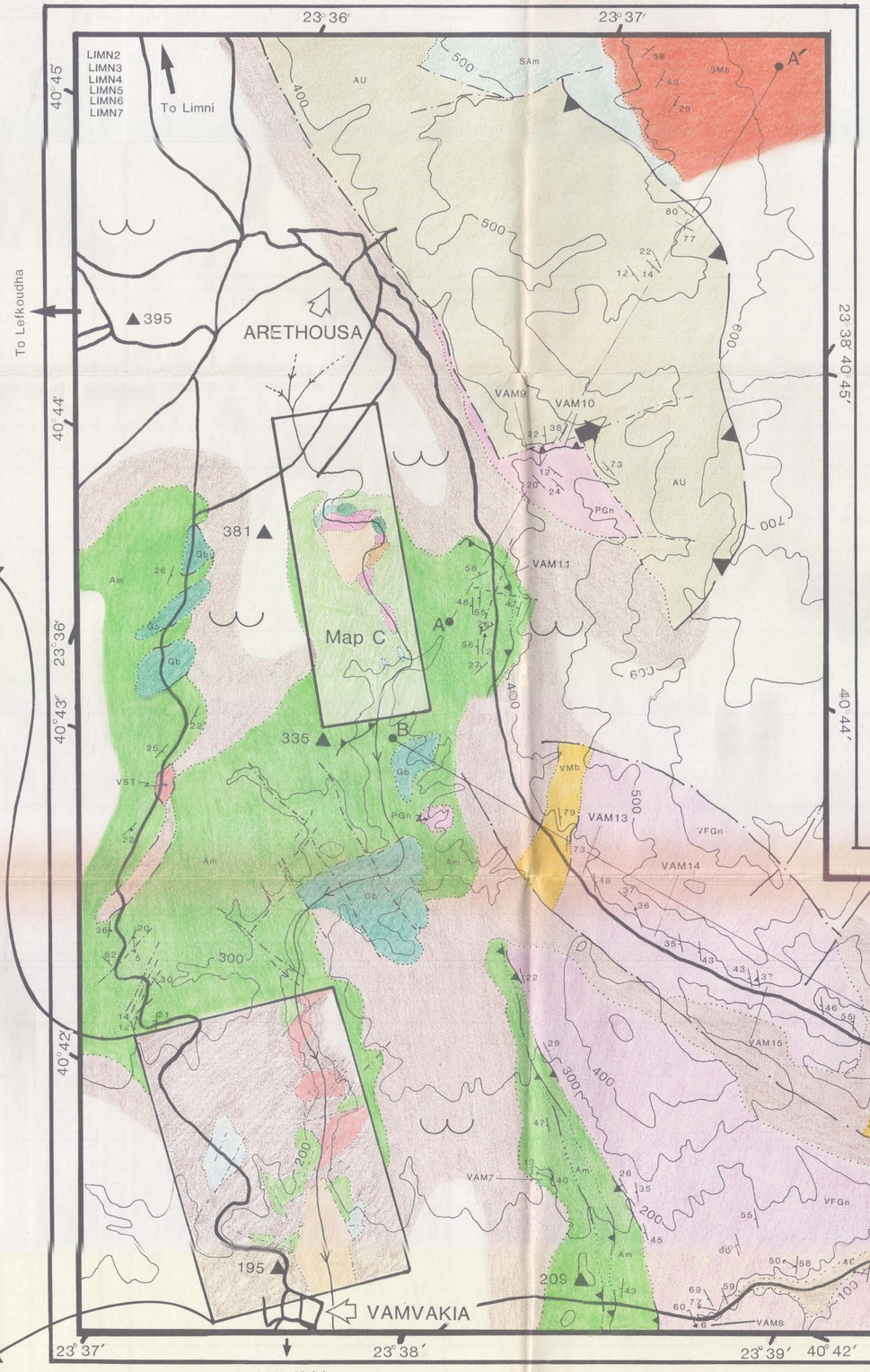

MAP F

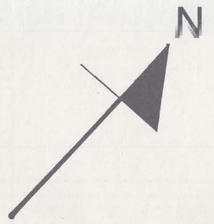

Kilometres

0 1 2

- VAM15 — Sample Locality
- A–A′ — Locality of Cross-Sections
- Boundaries and Contacts (Observed, Inferred)
- 16 — S_2 Foliations
- 22 — Minor Fold Axial Planes
- 50 — Fold Plunge
- 12 — Lineations
- Shear Zone
- Faults

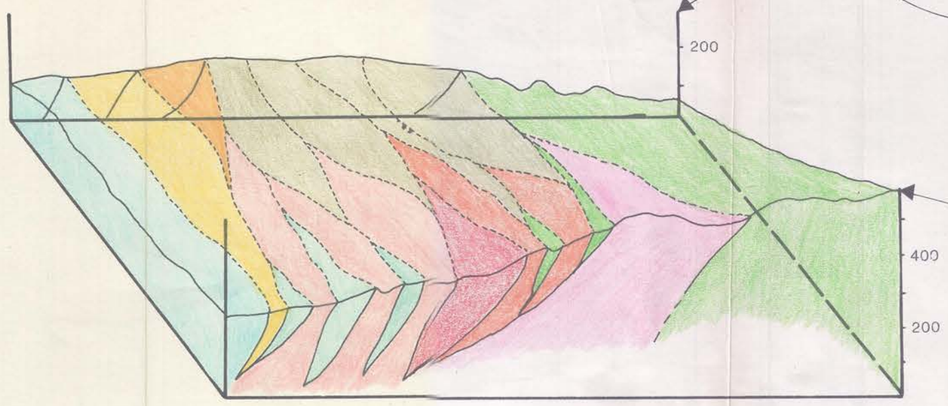

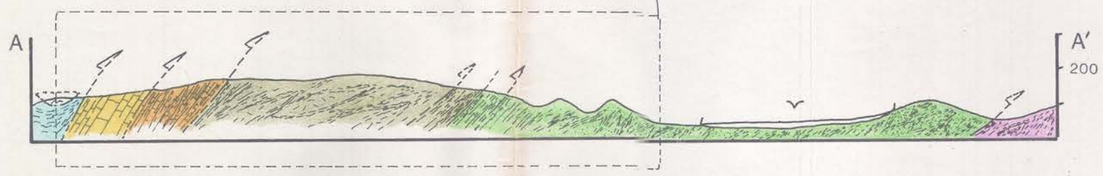

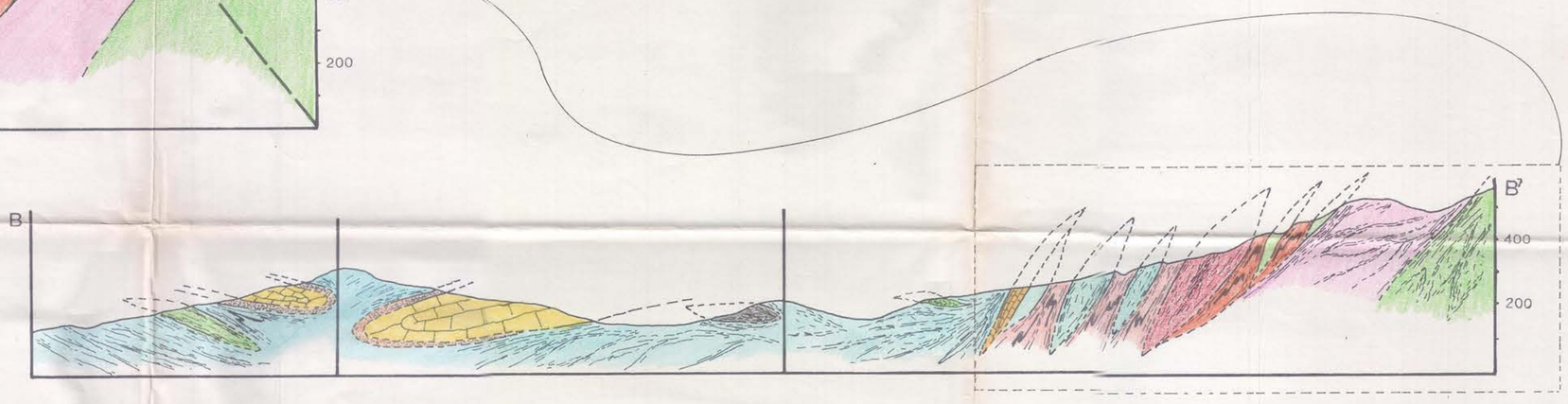

RECENT

- Alluvium

VOLVI METASEDIMENTARY GROUP

- WMMb — West Member
- EMMb — East Member

Modhi Marble Formation (Section 2.2.3.3)

- PRMb — Pure, white coarse-crystalline Member
- IRMb — Impure, Grey Member

Rendina Marble Formation (Section 2.2.2.5)

- RBGn — Rendina Ruins Banded Gneiss Formation (Section 2.2.2.4)
- MVGG-Sch — Megali Volvi Garnet Graphite Schist Formation (Section 2.4.3)
- MCGn — Modhi Coloured Gneiss Formation (Section 2.4.2)

VERTISKOS /KERDILION GROUP

- NM-PGn — Nea Madhitos Paragneiss Formation (Section 2.3.4.3)
- NM-LGn — Nea Madhitos Leucocratic Gneiss Formation (Section 2.3.4.2)

Undifferentiated

- MLGn — Modhi Leucocratic Gneiss Formation (Section 2.2.3.2)
- GGn — Gun-emplacement Gneiss Formation (Section 2.2.2.1)

IGNEOUS INTRUSIONS/INTERCALATIONS

- NMAm — Nea Madhitos Amphibolite Formation (Section 2.3.4.1)
- WMAm — West Member
- EMAm — East Member

Modhi Amphibolite Formation (Section 2.2.3.1)

- RAm — Rendina Amphibolite Formation (Section 2.2.2.3)
- MGd — Modhi Granitoid Formation (Section 2.6.4)

MOD16 — Sample Locality

A–A′ — Locality of Cross-section

Boundaries and Contacts (Observed, Inferred)

S_2 Foliations

Early, or Pre-S_2 Foliations

Lineation

F_2 Antiforms, Synforms

F_3 Antiforms, Synforms

Minor F_2 Fold Axial Plane

Minor F_2 Fold Plunge

Shear Zones

Faults

N

MAP G

Area briefly studied, modified after Sakellariou (1990)

LEF7 Sample Locality

A–A Locality of Cross-section

Boundaries and Contacts

55 S_2 Foliations

38 Early–, or Pre–S_2 Foliations

27 Lineation

38 Minor F_2 Fold Plunge

39 Minor F_2 Fold Axial Planes

Shear Zone

Fault

Kilometres

0 1 2

RECENT

Alluvium

VERTISKOS GROUP

VGrt–(Ky)–Sch Vamvakia Garnet (Kyanite) Schist Formation

VPGn Vamvakia Purple Gneiss Formation

VOLVI COMPLEX

BiAm Biotite–rich Member

FdsAm Banded Feldspar–rich Member

Amphibolites

Dol Dolerite

Gb Gabbro

Gd Granite

N

A

400

200

B

B′

400

200

MAP H

23° 31′ 23° 32′ 40° 45′

To Arethousa

To Xiropotamos

LEFKOUDHA

A

A′

B

B′

LEF1 LEF2 LEF4 LEF7 LEF8 LEF9A LEF9B LEF10 LEF10A LEF10B LEF10C LEF10D LEF10E LEF11 LEF12 LEF15 LEF16A LEF16B LEF16C LEF16D LEF18 LEF19 LEF20 LEF21A LEF21B LEF21C LEF23 LEF23A LEF23B LEF23C LEF23D LEF23F LEF25 LEF25A LEF25B LEF25C LEF25D LEF25F LEF25G LEF25GA LEF25GB

VGrt–(Ky)–Sch

Dol

Gb

Gd

BiAm

FdsAm

FdsAM

Sheeted Dyke Complex?

▲485

▲577

Into the Besikon Hills

Into the Besikon Hills

40° 45′

40° 44′

23° 30′

23° 31′

40° 44′

23° 32′